Intermodulation Distortion Performance Enhancement of Microwave Power Amplifiers

A thesis submitted to the Faculty of Technology in Candidacy for the Degree of Doctor of Philosophy

by

Modeste MBABELE

Brunel University

Department of Electronic and Computer Engineering

Uxbridge, Middlesex, UB8 3PH

May 2000

For the attention of candidates who have completed Part A

i) Attention is drawn to the fact that the copyright of a thesis rests with its author.

ii) A copy of a candidate's thesis is supplied to the Library on condition that anyone who consults it is understood to recognise that its copyright rests with its author and that no quotation from the thesis and no information derived from it may be published without the prior written consent of the author or the University, as appropriate.

Requests for such permission should be addressed in the first instance to the Head of Library Services.

Intermodulation Distortion Performance Enhancement of Microwave Power Amplifiers

A thesis submitted to the Faculty of Technology in Candidacy for the Degree of Doctor of Philosophy

by

Modeste MBABELE

Brunel University

Department of Electronic and Computer Engineering

Uxbridge, Middlesex, UB8 3PH

May 2000

Abstract

This thesis reports the author's investigation of the effects of the injection of specific signals on the intermodulation distortion performance of microwave power amplifiers. Theory, simulation and practical results are presented, analysed and compared.

The thesis gives the reader background knowledge of power amplifiers and their nonlinearities and go on to analyse the phenomena of intermodulation distortion product generation in power amplifiers. The analysis is based on a three-tone test since this highlights a second kind of third order intermodulation distortion (IMD3), which are in general higher in amplitude than the first kind of IMD3 found in a two-tone test.

A mathematical analysis and a simulation of a MESFET amplifier are performed. It enables the comparison of the performance of IMD cancellation by injection of signals whose frequencies are chosen to be first, the second harmonic of the fundamental signals, second, the sum of the fundamental signal frequencies and finally the difference frequencies of the fundamental signals.

A practical implementation of the difference frequency technique is then presented and practical results are compared to the other two techniques of second harmonic injection and the injection of the sum of fundamental frequencies. It is further shown that in practise these two techniques may be considered as a single technique.

Acknowledgements

First of all, I would like to express my gratitude to my supervisors, Prof. Colin S. Aictchison and Dr. Michael Berwick.

I thank Prof. C. S. Aictchison for his advice, guidance and suggestions, which have proved invaluable in the early stages of this work. I am grateful to him for always finding the time to talk me and show a lot of interest in this work. I would like to equally thank Dr. M. Berwick for his advice and guidance in the completion of my work. I am indebted to him for helpful suggestions in organising the thesis and for detailed critiques of the chapters.

I thank my friends of the Communication Research group at Brunel University for their fruitful comments and suggestions as well as discussions both work and non-work related. I also thank Dr. Reza Moazzam for his advice and suggestions. I also would like to thank Mrs Valerie Hayes for her help with all administrative related matters.

Last but not least, I would like to thank my family, with whom I had spent some wonderful years. I am grateful to my mum and dad for their love, encouragement and support during my years of studies. My deepest thanks go to all of them.

TABLE OF CONTENTS

LIST OF FIGURES

LIST OF TABLES

Abreviations

ACI	Adjacent channel interference
ACP	Adjacent channel power
ACPR	Adjacent channel power ratio
AM-PM	Amplitude modulation to phase modulation
AM	Amplitude modulation
ACI	Adjacent channel interference
BPSK	Binary phase shift keying
BPF	Band pass filter
CAD	Computer aided design
CDMA	Code division multiplex access
C/I	Carriers to inband intermodulation distortion ratio
DSP	Digital signal processing
DUT	Device under a test
FM	Frequency modulation
FF	Feedforward

GSM	Global system of mobile communications
GaAs FET	Gallium arsenide field effect transistor
gcp	gain compression point
HBT	Heterojunction bipolar transistor
HEMT	High electron mobility transistor
HPA	High power amplifier
IMD	Intermodulation distortion
IMD2	Second order intermodulation distortion
IMD3	Third order IMD product
InGaAs/GaAs	Indium gallium arsenide/ gallium arsenide
InAlAs/GaAs	Indium aluminium arsenide/ Gallium Arsenide
InP	Indium phosphide
IP3	Third order intercept
LINC	Linear amplification with nonlinear components
LMDS	Local multipoint distributed system
LPF	Low pass filter
MCPA	Multicarrier power amplifier
MDS	Microwave design system software
MESFET	Metal semiconductor field effect transistor
MMIC	Monolithic microwave integrated circuits
MOSFET	Metal-oxide semiconductor field effect transistor
MPA	Microwave power amplifiers
PA	Power amplifiers

PAE Power Added efficiency

PCN Personal communications networks

PCS Personal communications systems

PD predistortion

QPSK Quadrature phase shift keying

SSPA Solid state power amplifier

SCPA Single channel power amplifier

S/N Signal to noise ratio

WLL wireless local loop

Symbols

b	Channel thickness
Cgs	MESFET gate-source capacitance
Cds	MESFET drain-source capacitance
Cgd	MESFET gate-drain capacitance
Dgs	Schottky-barrier junctions at the source of the channel
Dgd	Schottky-barrier junctions at the drain of the channel
g_m	MESFET transconductance
g_{01}	First derivative of the conductance
g_{02}	Second derivative of the conductance
g_{03}	Third derivative of the conductance
$h(u)$	Impulse response of the linear system
I_{ds}	Drain current
L_g	Gate inductance
L_d	Drain inductance
L_s	Source inductance
L	Length of the gate
n	Ideality factor for good diodes

R_c MESFET gate-source resistance

R_{ds} MESFET drain-source resistance

R_g Gate resistance

R_d Drain resistance

R_{ds} Drain-source resistance

R_i Input resistance

R_s Source resistance

P_{out} Power delivered to the load

P_{dc} DC input power

P_{in} Input power

$S21$ Forward transmission coefficient of two-port network

$S11$ Input reflection coefficient of two-port network

$S22$ Output reflection coefficient of two-port network

$S12$ Reverse transmission coefficient of two-port network

T Junction temperature

V_G Bias applied to the metal side of the diode

V_{bi} Build in voltage of the diode

V_{gs} Gate-source voltage

V_{ds} Drain-source voltage

V_{gd} Gate-drain voltage

V_T Pinch-off voltage parameter

V_{po} Pinch-off voltage

V_{sat} Electrons velocity saturation

V_{to} Threshold voltage of an ideal FET

W Channel width of MESFET

β Transconductance

η Drain collector efficiency

ϕ Circuit phase shifter parameter

λ Channel lenght modulation parameter

ε_0 Permittivity of insulator

CHAPTER 1.

INTRODUCTION

1.1 Introduction

The information handling capacity of current communication systems is limited by nonlinearities in microwave power amplifiers (MPA) used in systems such as satellite transponders.

A nonlinear system can be described as a system in which the output signals vary with respect to the phase and amplitude of one or more input vector signals. The variation of the signals cannot be described by a simple linear system and therefore requires the use of complex nonlinear structures. A typical solid state power amplifier output when plotted against the input power is fairly linear in the low signal region, and becomes highly nonlinear as the solid state power amplifier (SSPA) is driven to saturation in the high signal region.

Solid state microwave components are all nonlinear. In communication amplifiers, any nonlinearity in the phase and the amplitude of the voltage transfer function must be minimised to preserve the shape and spectrum of the signal. Nonlinearities of the microwave transmitter amplifier limit the performance of communication systems through undesirable effects such as noise, phase ambiguities, intermodulation distortion (IMD) and sideband regrowth resulting in channel interference and reduced spectral efficiency.

There is a necessity in telecommunication systems for the use of amplifiers capable of providing large carrier to inband intermodulation distortion ratios (C/I). With

the growth of subscribers in wireless personal communications systems (PCS) and wireless local loop (WLL), has come the demand for highly efficient, linear amplification of complex modulated signals. System designers have to upgrade their systems to avoid a violation of the interference standards or a degradation of the system performance.

Digital modulation for example, relies on accurate transmission of a complex vector or symbol. The nonlinearities in the transmitter due to nonlinear elements distort these symbols and in turn the emitted signal is disturbed and as a result, information may be lost.

In certain microwave applications, there is a need to obtain high output power with low IMD, for example in multicarrier systems, modulated transmitting systems and digital systems. A way to achieve this is to use the amplifier at a level far below its maximum output capability. Amplifiers are therefore usually backed off several dBs from saturation level to ensure a more linear operation. This may be impractical in many cases since it leads to poor efficiency, increased running cost and reduced handling capacity.

The fact that most components such as limiting amplifiers, oscillators, doublers and mixers rely on the device nonlinearities for their operations, makes IMD an important problem and a real challenge for the designer. The designer's aim is to achieve as near ideal operation as possible in the realised device or circuit. Hence, IMD needs to be understood and in theory may be eliminated for perfect operation of the devices. One such approach to cancel the IMD is to use linearisation techniques.

Complete circuit analysis of the components requires a nonlinear device model and analytic means to extract the circuit behaviour and the cause of the nonlinearities

and their effects. A frequency description of the linear circuit is particularly advantageous at microwave frequencies as elements such as capacitors simply map a phasor into a different magnitude and angle.

The modelling of different devices and their study have shown that the nonlinear effects are generally associated with active elements in the circuit. One such element contributing to the effects of nonlinearities in the microwave power amplifier (MPA) is the Field Effect Transistor (FET).

1.2 Aims and Objectives of the Research

In wireless applications such as the global system of mobile communications (GSM), personal communications networks (PCN), wireless local loop (WLL) and the local multipoint distributed system (LMDS), the system operators have had to upgrade their networks from using such architectures as the single channel power amplifier (SCPA) of figure 1.1 to the use of multicarrier power amplifier (MCPA) of figure 1.2. This upgrading has been introduce to overcome problems such as the increase in capacity overload and dropped calls. The approach enables multiple channels or different modulation scheme to be processed simultaneously.

The use of the MCPA, mentioned above requires a power amplifier (PA) capable of providing high linearity. This has led to the devising of a number of techniques for improving the amplifier's nonlinear characteristics. This report reviews existing techniques and develops new ones.

It deals with a research project investigating the effects of the injection of multiple signals of different frequencies on the intermodulation distortion performance of

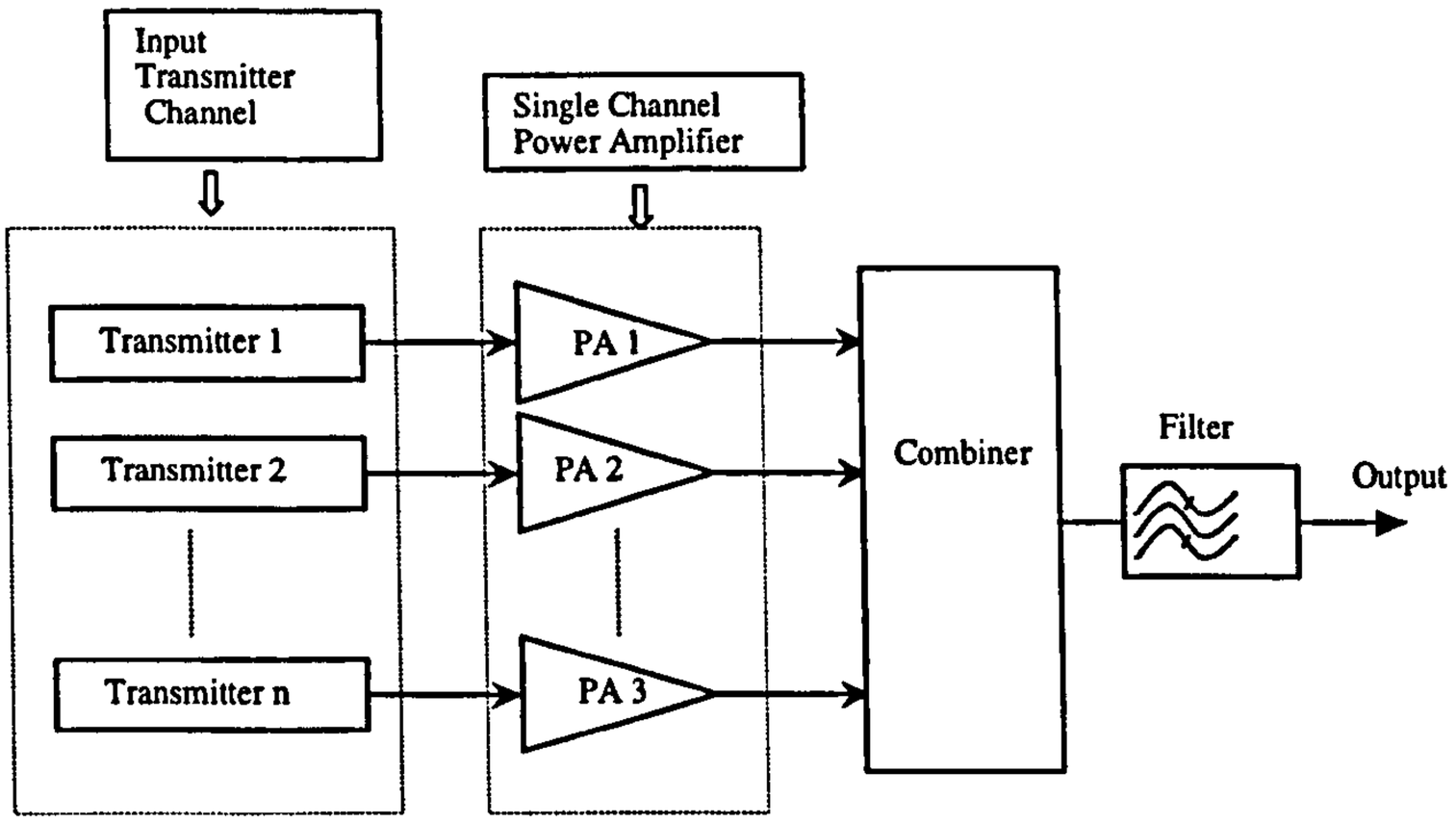

Figure 1..1: **Single carrier power amplifier schematic for base stations.**

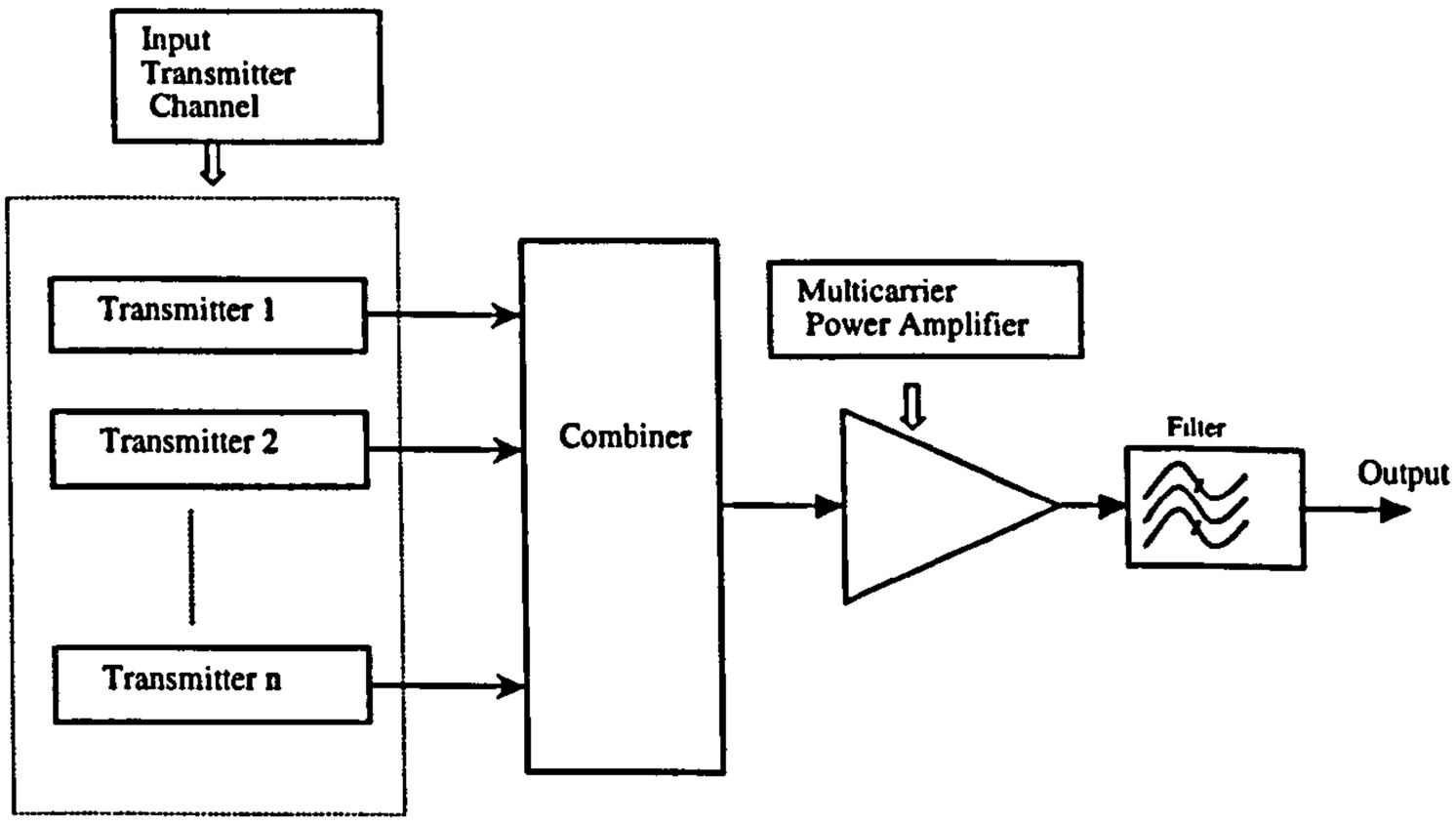

Figure 1..2: **Multicarrier power amplifier schematic for base stations.**

microwave amplifiers and its applications to multicarrier amplifier linearisation. The concept of frequency injection into an amplifier is first analysed mathematically and then the effects of the injected signals on intermodulation performance are analysed and presented. The results of the study then enable the implementation of the concept in order to eliminate the intermodulation distortion in power amplifiers.

A clear objective of this report is to first enable the reader to become familiar with the nonlinearities of devices and therefore understand the problems of intermodulation distortion and their generation mechanisms as well as the various ways by which these are presently eliminated. New techniques are then introduced to the reader. Analysis and practical performance are compared to existing techniques. A predistorter circuit is then designed and its practical performance is presented.

1.3 Thesis Structure

Chapter 1 discusses the ever-growing need for efficient power amplifiers for the various systems used around the world, which have brought high requirements on the linearity of the amplifier.

The second chapter deals with the problem of device nonlinearities. It first presents the power amplifier and describes briefly its use before outlining the source of nonlinearities. The nonlinear behaviour of the elements in the device, which are the main causes of IMD in circuit and how these are modelled for nonlinear circuits analysis, is also presented.

Chapter 3 introduces the concept of intermodulation. A power series expansion analysis of the intermodulation distortion terms is presented. Other mathematical

methods used to calculate the IMD are briefly presented and discussed. The techniques used for IMD elimination are discussed in chapter 3, with a detailed emphasis on circuit design techniques and their effectiveness.

A study of the second harmonic injection technique is presented in chapter 4, where the concept is introduced and analysis results are discussed. A low frequency injection technique is introduced and investigated in chapter 4, in the same manner as the second harmonic. The effects of the second harmonic and the difference frequency injection on multicarrier microwave power amplifiers are compared. Investigation into the effects of the injection of a signal, the frequencies of which are the sum of the fundamental frequencies is also analysed in this chapter. The IMD reduction performance of all the above mentioned techniques on a power amplifier are presented and compared.

In chapter 5, a practical implementation of the difference frequency technique is described. A new circuit implementation of the difference frequency technique is presented and tested. Experimental results using the second harmonic technique are also introduced and discussed. The difference frequency circuit techniques can also be used for the second harmonic technique.

In chapter 6, conclusions are drawn on the overall work. Chapter 6 further discusses the investigated technique advantages and disadvantages and outlines various others method of implementing the difference frequency technique. Further work that is relevant to the implementation of the technique for radio frequency and microwave frequency communication systems is also highlighted.

CHAPTER 2.

AMPLIFIER NONLINEARITIES & CIRCUIT CHARACTERIZATION

2.1 Introduction

The goal of this chapter is to present an introduction to the microwave power amplifier and therefore provide an understanding of the issue of power amplifier device characterization and modeling. The nonlinear elements associated with the power amplifier active devices and their nonlinear behavior are described.

Although the chapter is centered on the Gallium Arsenide Field effect transistor (GaAs FET), as is most of the thesis, other devices are presented, because most of the techniques apply equally well to the various types of power devices currently being developed with appropriate modifications.

2.2 High Power Amplifiers

Power amplifiers (PAs) are used in the transmitting chain of a wireless radio system. They are required for amplification in order to provide sufficient power for transmission. The amount of output power is dependent on the application ranging from milliWatts to Watts.

The first reported prototype Gallium Arsenide Field effect transistor was reported by Mead in 1966 [43]. In the middle of the 1970's, the first available GaAs FET appeared offering usable gain for amplification up to the X-band ($8GHz - 12GHz$). This was first use for small signal devices and then for power amplification. The first announcements of high power GaAs FETs were made simultaneously by Fukula et al [2] and Napoli et al [3]. The focus of development shifted to higher power added efficiency

and improved distortion qualities as well as to operating frequency and output power. A new FET structure was developed by Mimura et al [4], called the High electron mobility transistor (HEMT) with superior high frequency characteristics. High power amplifiers using HEMT have been designed and reported [5]. Other devices using semiconductor heterojunctions, with superior noise figures and gain characteristics, such as the hetero-junction bipolar transistor (HBT) have also been reported [6,7]. GaAs FET have been enhanced by incorporating heterojunctions in some architecture areas such as indium gallium arsenide/ gallium arsenide (InGaAs/GaAs), heterojunction, indium aluminum arsenide/ Gallium Arsenide (InAlAs/GaAs) heterojunction, indium phosphide (InP), etc.

Today, GaAs FETs and their derivatives, such as high electron mobility transistors (HEMTs), have completely replaced diodes in small signal and low noise applications. Discrete power GaAs FETs with power outputs ranging from $25W$ at $4GHz$ to $1W$ at $20GHz$ and beyond are readily commercially available [44,45].

Research on GaAs Monolithic Microwave Integrated Circuits (MMIC) has offered advantages such as increased reliability and decreased size and achieves high uniformity of performance between samples. Impressive results have been achieved from MMIC power amplifiers [1]. Distributed power amplifiers [9,10] have become popular with the availability of good quality microwave GaAs FETs, although distributed techniques have been used in the design of very broadband amplifiers since 1940.

The PA is the primary consumer of power in the RF portion of the transceiver unit in a wireless system. PAs are characterised by various factors of which the two most important are efficiency and linearity. The efficiency is defined by two metrics.

The drain collector efficiency, η, is equal to the power delivered by the load at the fundamental frequency, divided by the power drawn from the supply. The power added efficiency (PAE) is the difference between the input and output powers divided by the supply power. Expressions for efficiency and PAE are:

$$\eta = \frac{P_{out}}{P_{DC}} \tag{2..1}$$

$$PAE = \left(1 - \frac{1}{G}\right) \frac{P_{out}}{P_{DC}} = \frac{P_{out} - P_{in}}{P_{DC}} \tag{2..2}$$

Where G, is the gain.

P_{out} is the power delivered to the load.

P_{dc} is the dc input power.

P_{in} is the input power.

If the PA has a large gain, then $\eta = PAE$. These factors have to satisfy the relevant wireless standards.

One of the primary considerations in the design of PAs involves trade-offs of efficiency and linearity. Power amplifiers are categorised by mode of operation under many classes: A, B, C, D, E, F, etc [11,12]. In class A amplifiers, the PA devices operate continuously for all of the carrier cycle. For class B operation, the power device operates for half the time. Class AB is between class A and class B PA. In class C operation, the power device is on for less than half the carrier period so as to improve the efficiency. Higher class PAs are distinguished by how often the power device is turned on [13-15], which affects the efficiency or by how hard they are driven.

2.3 MESFET Principle, Operation and Characterisation

The GaAs MESFET performs a number of functions, such as amplification and switching, for microwave devices, such as low-noise amplifiers, power amplifiers and switches [16]. In typical applications, models are used to predict or estimate the performance information that is not available or easily obtainable by direct measurement.

The equations describing these models are usually modifications of some analytical formulae for the device. The constants in the equations and the values of model elements are extracted from the dc pulsed and small signal S-parameter measurements. There are clearly two types of models: the numerical and the analytical (an equivalent circuit)[17].

The numerical models can be made much more accurate than the analytical models whose parameters are adjusted to match the terminal behaviour of the device. There is often a lack of direct correlation between the model parameters and physical parameters.

Numerical models are based on the computer solution of the nonlinear equations describing the device physics. The accuracy of these devices is often compromised because of the amount of detailed information required on the physics of the device and the speed of computation. When these models are applied in the design of MMICs, the simulations required large computer resources. They are mainly used by the device physicists. The equations are formulated under specific assumptions.

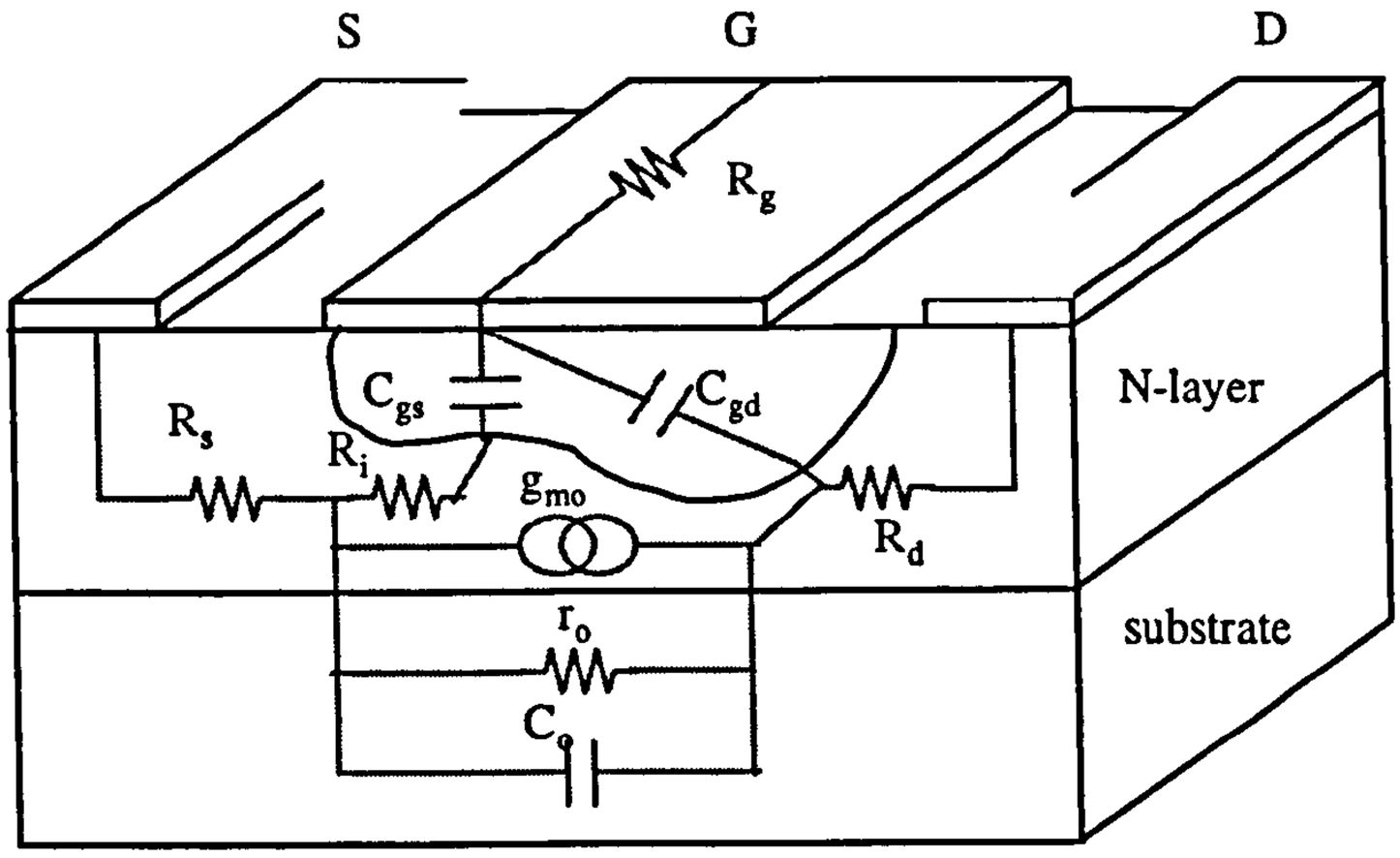

Figure 2..1: **Cross section of a MESFET showing the origin of the small signal elements. (symbol key: Co, Cgs, Cgd = output, gate-source & gate-drain capacitances , Rg, Rd, Rs, Ro, Ri =gate, drain, source, output & input resistance, g_{mo}=transconductance)**

2.3.1 Principles and Operation

The MESFET is a three-terminal device. It consists of two ohmic electrodes named the source (S) and drain (D) and an intermediate control called the gate (G). The gate of the MESFET is of the Schottky type that is in intimate contact without the interfacial dielectric between the metal and the semiconductor. The structure consists of a perfectly insulating medium surmounted by an n-type semiconductor active layer with uniform doping (figure 2.1) [48]. A Schottky gate is placed between the two ohmic surfaces of the active layer.

When a voltage is applied in the direction to reverse bias the junction between the gate and the source, the source and drain are forward biased. The electrons flow in the n-type epitaxial layer from the source electrode, through the channel beneath

the gate, to the drain. This will then cause a voltage drop along the channel length causing the Schottky barrier to become more reversed biased at the drain end. A charge depletion region is created in the channel and will pinch-off the channel against the substrate towards the drain end. The height of the charge depletion region will increase as the source and gate reverse bias increases. The decrease of the channel height in the non-pinched-off region will increase the channel resistance and therefore enables the modulation of the drain current I_{ds} by the gate voltage.

2.3.2 Equivalent Circuit

The equivalent circuit or analytical model is a simplified and abstract representation of the device, which allows the engineer to be able to manage and control the design of the circuit.

The elements in the equivalent circuit are intended to represent the electrical behaviour of the physical structure of the device. The elements in the physical structure of figure 2.1 showed the origin of the equivalent circuit elements.

2.3.2.1 Small Signal Equivalent Circuit

A small signal FET equivalent circuit (figure 2.2) is a subset of the large signal FET equivalent circuit, simply because a large signal that is biased at a specific point in the I/V range of operation of the device will operate as an accurate small signal model [19-22].

A small signal equivalent circuit for the MESFET can be represented by lumped elements up to $12GHz$ for the extrisinc FET and up to $14GHz$ for the intrinsic FET. The lumped elements: the gate inductance (L_g), the drain inductance (Ld), the source

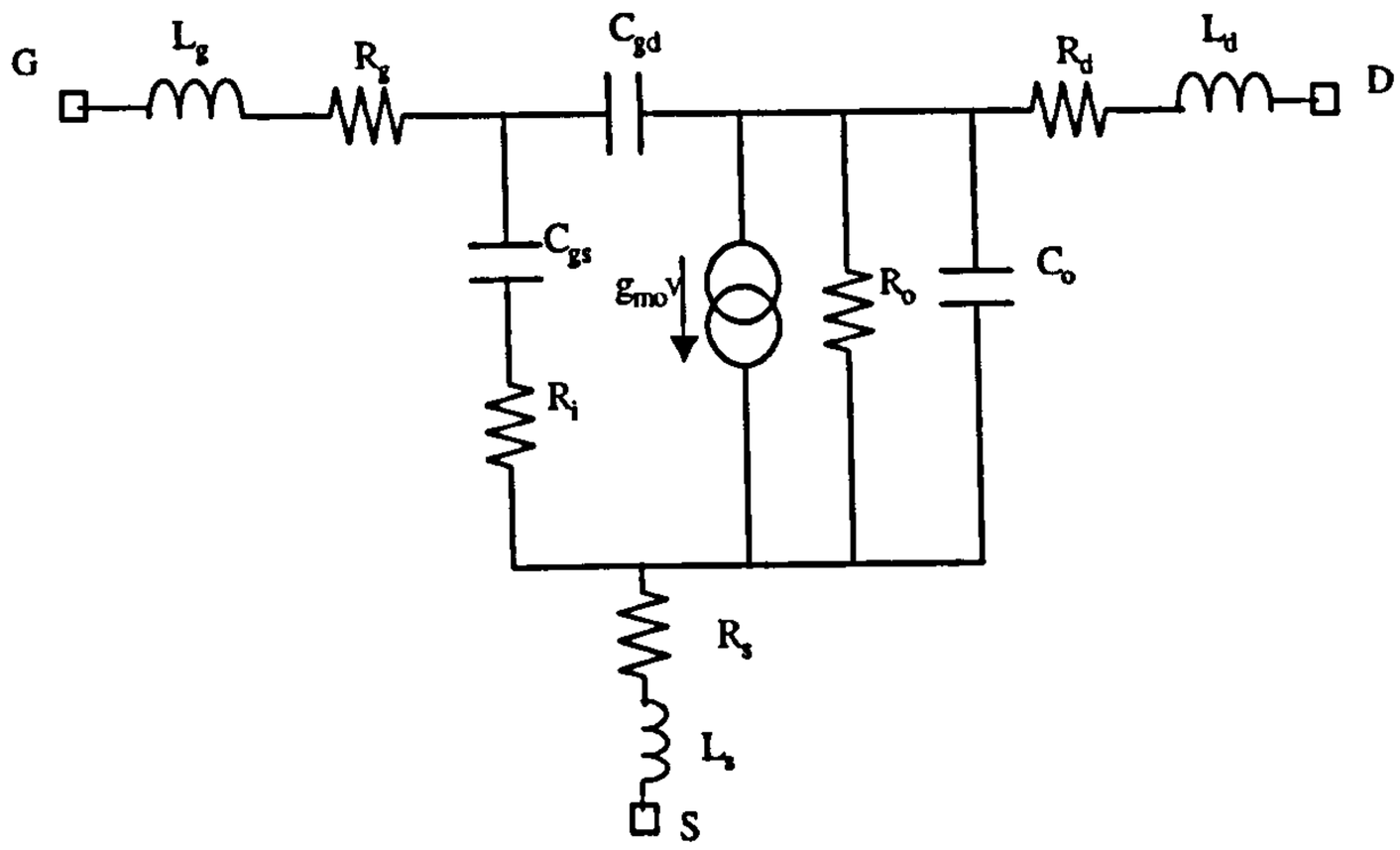

Figure 2..2: **Small signal equivalent circuit of the MESFET.(symbol key : L_s, L_d, Lg = source, drain & gate inductances, R_d, R_s= drain & source resistances)**

inductance (L_s), the gate resistance (Rg), the drain resistance (R_d) and the source resistance (R_s) represent the extrinsic elements. The activity of the FET is determined by its maximum frequency of oscillation where the FET becomes passive.

2.3.2.2 Large Signal Equivalent Circuit

A large signal refers to the situation where the voltage across the depletion capacitance has increased and become a significant fraction of the applied DC gate-source voltage [23]. The effect of this is that the relationship between the voltage and the amount of output power is broken. Large signal effects can occur in low output power FETs when driven hard.

Large signal operation is usually associated with such undesirable effects as gain compression, the generation of harmonics and intermodulation products and amplitude modulation to phase modulation (AM-PM).

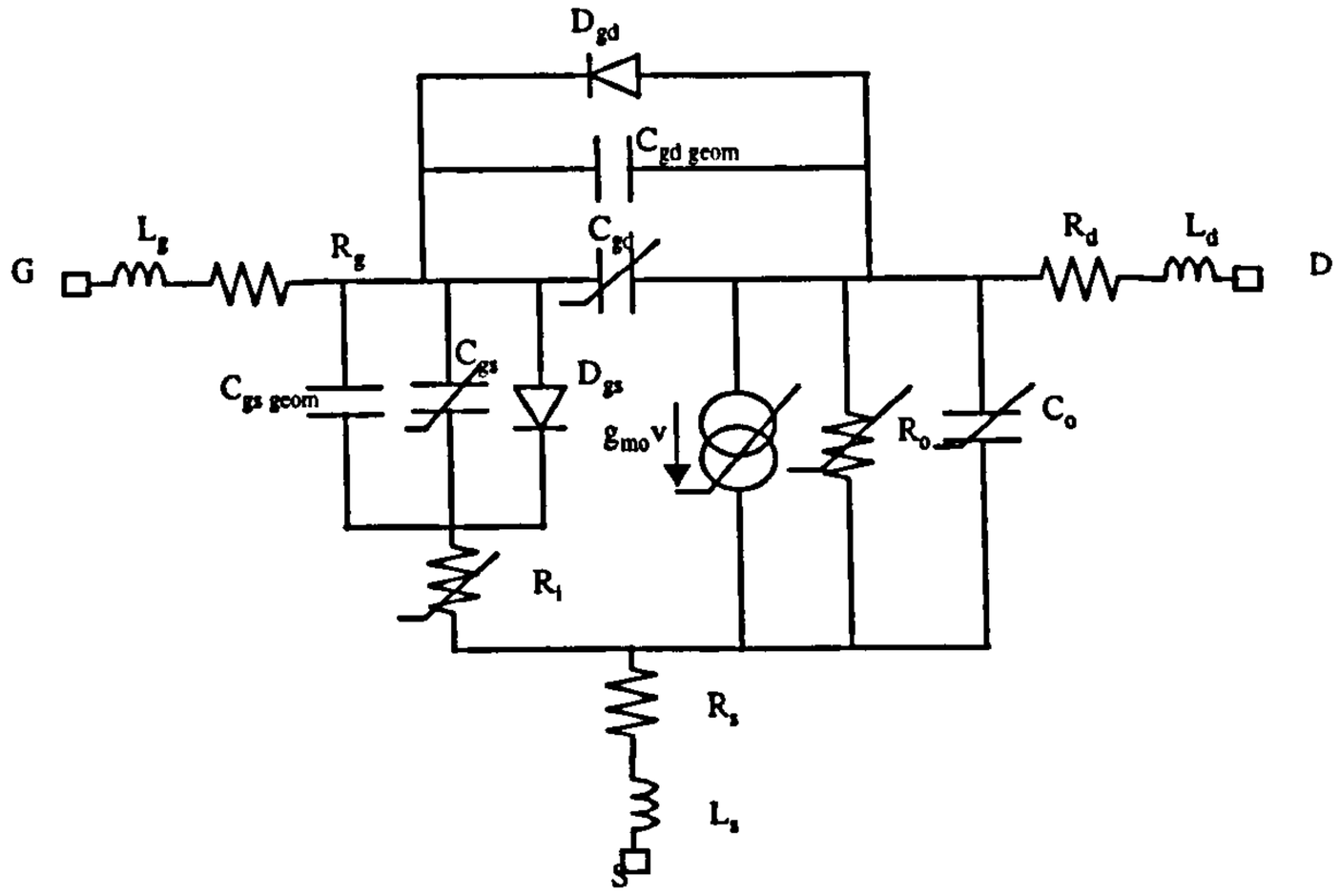

Figure 2..3: **Large signal equivalent circuit of the MESFET.**

The effects of the large signal will depend on the bias point and the signal level. It is well documented that some of the nonlinear elements can be ignored in the simulation without affecting the accuracy significantly. A very commonly used large signal circuit is represented in figure 2.3 [159].

The diodes are included in the model to account for the effect of forward gate-source current and gate-drain avalanching, which has to be considered in order to obtain accurate simulation.

The large-signal MESFET models used for circuit design and analysis are empirical models that incorporate analytical functions to represent the FET nonlinearity dependence on the gate-source voltage and the drain-source voltage. These analytical expressions do not however have a very close relevance to the physical behaviour of the device.

The transconductance (g_m), the drain-gate conductance (Cgd), drain-source con-

ductance (Cds), the gate-source conductance (Cgs), the drain-source resistance (rds) and the input resistance (r_i) are all nonlinear elements. The elements not found in the small signal circuit are the nonlinear gate-source capacitance and the gate-drain capacitance, which model the forward bias junction conduction.

The element g_m is a highly nonlinear element in the FET and is important in the generation of harmonics and intermodulation products. The values of these elements in the model are determined by various methods [24-27].

2.3.3 Linear Elements

The linear elements within the model which are considered not to change with the bias are:

a) The series lead inductances: L_s, L_d and L_g.

The parasitic inductance models the metal contact pads deposited on the device surface. In modern short gate length devices, the gate inductance is usually the largest of all. The values of the inductance depends on the type of surface and the feature, and therefore change very little under any practical conditions.

b) The series resistances:R_s, R_d, and R_g.

The gate resistance, Rg, results from the metallization resistance of the Schottky contact. The other resistances are included to account for the contact resistance of the ohmic contacts and the bulk resistance leading to the active channel. These resistances are considered constant due to the fact that their resistance dependence on the bias voltage is small.

c) The drain-source fringing capacitance C_{ds}

The drain-capacitance accounts for the geometric capacitance effects between the source and the drain electrodes. C_{ds} is not considered bias dependant for the purpose of device modelling, as its variation is very small.

2.3.4 Nonlinear Elements

Every element of the device depends on various effects. Some have greater effect on the device behaviour than others. The nonlinear behaviour is however associated with a certain number of elements that have some very important effects that need to be taken into consideration when analysing the nonlinear behaviour of devices. The six nonlinear elements of the model depend on three internal voltages: the gate-source voltage (V_{gs}), the drain-source voltage (V_{ds}) and the gate-drain voltage (Vgd) [28]. In order to accurately simulate the device for large signal nonlinear analysis a number of points have to be taken into account which include the drain-source current characteristic (I_{ds}) as it contributes to great distortion. Its pinch-off and saturation effects have to be known as well as the forward current of the gate-source Schottky-barrier junction. The transconductance and output conductance at microwave frequencies have to be determined. The terminal impedance over the bandwidth of interest and the gate-drain breakdown voltage have to be known.

2.3.4.1The Nonlinear Current Source

The nonlinear current source $I_{ds}(v_d, v_g)$ describe the DC I/V characteristics of the MESFET. It is seen as the principal nonlinear element within the MESFET [29-31]. It simulates the control of the channel current by voltages applied to the device terminals. The I/V characteristics are symmetric about the $V_{ds} = 0$ origin. The linearity of the

device occurs over a limited range of the drain source voltage.

The current source and the other important elements such as the bias point, the pinch-off and the saturation of the device describe the dc characteristics of the MESFET.

In the linear region of the device a good approximation of the I/V characteristics of the current can be modelled by the equation (2.3)

$$I_{D,sat} = \beta \left(2 \left[V_{gs} - V_T\right] - V_{ds}\right) \left(1 + \lambda V_{ds}\right) \qquad (2..3)$$

Where β is the transconductance.

V_{gs} is the gate-source voltage.

$V_T$is the pinch-off voltage parameter.

λ is the channel length modulation parameter.

It is demonstrated that a square law drain current to gate voltage fits the measured characteristics of a long gate length FET quite well without being strongly affected by the doping profile [32,33].

In the saturation region the value of I_{ds} is approximately equal to the square of the pinch-off voltage. The equation for the drain current modelling the saturation region is therefore defined as:

$$I_{D,sat} = \beta \left(V_{gs} - V_T\right)^2 \left(1 + \lambda V_{ds}\right) \qquad (2..4)$$

The term $(V_{gs} - V_T)$ is known as the pinch-off voltage (Vp).

$$V_P = V_{gs} - V_T \qquad (2..5)$$

The pinch-off voltage defines the transition from the linear to the saturation region of the device. It is the Drain-Source voltage that extends the depletion layer across the channel at the drain end of the gate by removing all free electrons from the channel. When $V_{gs} = 0V$, then the pinch-off voltage corresponds to $Vp = -V_T$.

The constant λ is a measure of the leakage current that causes the I/V characteristics to be highly nonlinear in the saturation region. A high value of λ corresponds to high output conductance and poor saturation.

The constant β is the transconductance and is proportional to the ratio of the width over the length of the device and is dependent on the electron mobility.

Since β is proportional to the width, W, and inversely proportional to the length of the device, L, the current I_{ds} is also proportional to these quantities and dependant on the electron mobility, μ_n [34].

$$I_{d,sat} = \mu_n \frac{W}{L} \tag{2..6}$$

The equation 2.4 is commonly used as the basis for a simulation of the operation of the current model. It illustrates the dependence of the drain current on both the drift mobility and saturated drift velocity.

By introducing equation 2.6 in equation 2.4, it can be seen that the drain current is changing nonlinearly with the gate length, L. For long L, the second term becomes dominant and I_d varies as $1/L$. For shorter gate length the current increases rapidly as L is reduced rapidly.

2.3.4.2 The Transconductance

The transconductance nonlinearity is principally determined by the gate voltage, which

controls the depth of depletion in the MESFET.

Shur et al [34] defined the transconductance to be

$$\beta = \frac{2\varepsilon_s \mu_n V_{sat} W}{b(\mu_n V_{PO} + 3V_{sat} L)} \tag{2..7}$$

The terms in the equation represent:

V_{po} , the pinch-off voltage.

b, the channel thickness.

L, the length of the gate.

W, the channel width.

V_{sat}, the electrons velocity saturation.

ε_s, is the permittivity of the insulator.

This equation defined the transconductance according to the physical structure of the device. A simple analytic expression is used in the equivalent circuit for circuit simulation. This is defined according to the source current on which it is dependent.

The transconductance in association with the source current can predict the gain of the device. The transconductance, g_m, is of importance for the MESFET, it is defined as

$$g_m = \left[\frac{\delta I_d}{\delta V_{gs}}\right]_{V_{ds}=\text{constant}} \tag{2..8}$$

The transconductance is significant because it relates to the increase in I_d to an increase in V_{gs}, the control voltage of the FET. It is therefore closely related to the gain of the device.

The power series form can represent the voltage dependency of these elements:

$$I_d = g_{m1} V_{gs} + g_{m2} V_{gs}^2 + g_{m3} V_{gs}^3 + \cdots \tag{2..9}$$

The terms $g_{m1}=\frac{dI_d}{dV_g}$, represent the first derivative of the transconductance in respect to the gate-source voltage. $g_{m2}=\frac{d^2I_d}{dV_g^2}$ and $g_{m3}=\frac{d^3I_d}{dV_g^3}$, are the second and third derivatives.

2.3.4.3 The Output Conductance

The output conductance is in general a function of the drain current and the drain-to-source voltage over the saturation region of the bias characteristics. It can be analysed as two-dimensional, no-memory nonlinearity.

$$g_o = f(I_d, V_{ds}) \tag{2..10}$$

The expression of the term g_o can be represented by a simple expression over the range for which it depends on the drain voltage alone. This dependency occurs in the saturation region of the device and for gate voltages corresponding to the high gain amplifier bias conditions. The output conductance of a MESFET in saturation is mainly due to three phenomena, which can vary with different models:

(*i*)The channel length modulation, which gives a positive conductance that increases with the channel current [16].

(*ii*)-Leakage current due to electrons being injected into the substrate [34,36]

(*iii*)-High field dipole domains formed near the drain, which decreases the output conductance.

The expression of the output conductance takes the simple form:

$$g_o = \left[\frac{\delta I_d}{\delta V_{ds}}\right]_{V_{gs}=\text{constant}} \tag{2..11}$$

The dependence of the conductance on drain current in the saturation region is not so strong. The contribution of the nonlinearity to intermodulation is rather small.

If the above equation 2.11 is solved for I_d, the current I_d can be expressed in terms of V_{ds}. Expanding the characteristic to a power series form, gives

$$I_d = g_{o1}V_{gs} + g_{o2}V_{gs}^2 + g_{o3}V_{gs}^3 + \cdots \tag{2..12}$$

The terms g_{o1}, g_{o2}, g_{o3} again represent the first, the second and third derivative of the conductance.

2.3.4.4 Schottky-Barrier Junctions

The two components D_{gs} and D_{gd} of figure 2.3 represent Schottky-barrier junctions at the source and drain of the channel. The Schottky-barrier junction at the source is primarily dependent on the voltage V_{gs}. The Schottky barrier junction at the drain on the other hand is dependent on both the voltage V_{gd} and the current source I_{ds}.

In Schottky diode contact also known as rectifying, the I/V characteristics depends on the polarity of the potential applied.

The current through the contact is given by the relationship [37]:

$$I_G = AT^2LW \exp\left(q\frac{V_{bi}}{KT}\right) \exp\left(\frac{qV_g}{nKT}\right) \tag{2..13}$$

With A being the effective Richardson's constant.

T is the junction temperature in Kelvin.

L is the contact length.

W is the contact width.

V_G is the bias applied to the metal side of the diode.

V_{bi} is the build in voltage of the diode and depends on the material used.

n is the ideality factor (in the range 1.1 -1.2 for good diodes).

q is the electron charge.

The equation is very often simplified to

$$I_G \simeq I_s \exp\left(\frac{qV_G}{KT}\right) \tag{2..14}$$

The current Is is the saturation current and indicates the magnitude of the gate leakage current under reverse bias conditions.

In small signal analysis, where it is assumed that the voltage V_{gd} is much larger than the breakdown voltage, the reverse biased diode (D_{gs} and D_{gd}) effects are assumed to be negligible, and are therefore omitted. This enables the device to be considered as linear at a particular point.

2.3.4.5 Nonlinear Capacitors

The nonlinear capacitor, C_{gs}, associated with the voltage V_g, represents the depletion layer at the source. The capacitor C_{gd}, associated with the voltage V_{gd} represents the fringing capacitances associated with the drain ends of the channel. Unlike the drain-source capacitor C_{ds}, these capacitors are considered nonlinear because of their great dependence on the bias conditions.

These capacitors, C_{gs} and C_{gd}, model the change in the depletion charge with respect to the gate-source and the gate-drain voltages, respectively. The gate source capacitance is normally larger in quantity than the other capacitances because of the fluctuations in the gate-source voltage.

2.3.4.6 Parasitic Resistors

The source and drain resistances are known as the nonlinear elements. The resistor R_s (figure 2.3) corresponds to the undepleted part of the channel under the gate through which the gate-source capacitor charges. The gate and source are separated by an ungated channel (as opposed to the drain and source which are separated by the gate channel), a doubly implanted region under the source contact and the contact interface and metal. This only contributes to the undesired excess resistance. This is a non-ideal element that needs to be considered in the design and analysis of the device. This phenomenon can be very important and causes a surface potential, which will bend the bands up and deplete part of the surface of the free electrons.

The presence of this resistor has the effect of reducing the applied gate to source voltage, V_{gs}. The effective voltage applied across the source and gate will then be:

$$V_{gs,i} = V_{gs,i} - I_D R_s \tag{2..15}$$

This resistance causes similar effects on the Transconductance, g_m. If $g_{m,e}$ is defined as the transconductance available outside the circuit and the intrinsic internal transconductance is defined as $g_{m,i}$, then it can be shown that:

$$g_{m,e} = g_{m,i}\left(\frac{1}{1+g_{m,i}R_s}\right) \tag{2..16}$$

The effects on the conductance will be such that the effective conductance outside the device will be:

$$g_{o,e} = g_{o,i}\left(\frac{1}{1+g_{m,i}R_s+g_{o,i}R_s}\right) \tag{2..17}$$

The drain resistance R_d, which corresponds to the undepleted portion of the channel under the gate which the gate-drain capacitor charges, produces similar effects.

The effects associated with this resistance are minimised by increasing the doping level in the source and drain regions [38,39] or by recessing the gate in the centre of the channel in order to thicken the source and drain regions.

2.4 Device Modelling for Simulation

The drain current, I_{ds}, is one of the elements that contribute most to the non-linearities of the devices. I_{ds} is controlled by the gate-source voltage V_{gs} and the drain-source voltage V_{ds} .

Various models for the FET have been implemented and are available for the simulation of the complex behaviour of the physical device [37-40]. Each one is an approximation of the behaviour of the different elements that contribute to the overall device. Since the modelling of the changes in the device to the dc supply of the system cannot be exact, each model will approximate some parameters more accurately than other models.

The next sections will describe some of the popular models available to the designer. The modelling expressions and the advantages of the devices such as the Curtice model used in circuit simulation in the work presented in this thesis will be described.

2.4.1 The Curtice Model

The Curtice model was first proposed by Van Tuyl et al [42]. The model was then simplified by Curtice [39]. Originally the nonlinear elements represented in the Curtice model were the drain source current and the gate -source capacitance. The drain-source current is a function of the drain-source and the gate source voltage.

The expression for the drain-source current is:

$$I_{ds}\left(V_{gs}, V_{ds}\right) = \beta\left(V_{gs} - V_{T0}\right)^2 \left(1 + \lambda V_{ds}\right) \tanh\left(\alpha V_{ds}\right) \tag{2..18}$$

Where α is a time constant, which represents the electron transit time under the gate.

The first element of the equation 2.18, $\beta\left(V_{gs} - V_{T0}\right)^2$, is used to model the square law behaviour of the drain current in respect to the gate-source voltage. The second element is used to model the device output conductance, which is the slope of the drain-source current with respect to the drain source voltage. The final element of the equation is the hyperbolic tangent used to approximate the drain-current to drain-source voltage characteristics observed in the FET [39]. The hyperbolic tangent is used because it approximates the $(I_{ds} - V_{ds})$ characteristics observed in MESFETs and the graph of $\tanh\left(\alpha V_{ds}\right)$ versus the drain-source voltage illustrates clearly that rapid current saturation can be modelled by increasing the coefficient α. Thus giving a more consistent numerical analysis of the device.

For accurate simulation of the FET, the various behaviours of the elements (transconductance, output conductance, capacitors, etc.) must be represented by different equations. This enables more accurate modelling of the physical structure.

The gate-source conductance is a function of the intrinsic gate source voltage. Differentiating the drain-source current with respect to the voltage V_{gs} and V_{ds} directly derives the small signal transconductance and the output conductance.

For the transconductance,

$$g_m = \frac{\delta I_{ds}}{\delta V_{gs}} = I_{ds}\left[\frac{2}{V_{gs} - V_{T0}}\right] \tag{2..19}$$

For the conductance,

$$g_0 = \frac{\delta I_{ds}}{\delta V_{ds}} = \beta \left(V_{gs} - V_{T0}\right)^2 (1 + \lambda V_{ds}) \frac{\alpha}{\left[\cosh^2(\alpha V_{ds})\right]} + \beta \left(V_{gs} - V_{T0}\right)^2 \tanh\left(\alpha V_{ds}\right) \tag{2..20}$$

The Curtice model consists primarily of the voltage controlled current source I_{ds}, the gate-source capacitance C_{gs}, the gate-drain capacitance C_{gd}, the drain source capacitance C_{ds} and the diode D_{gs}.

Gate-source capacitance and the gate-drain capacitance are included as nonlinear elements in the simulation because they are sources of highly nonlinear characteristics. The term C_{gd} is considered to be a function of the intrinsic gate-source voltage. The Curtice model uses the capacitance expression derived from the first order semiconductor junction theory applied to a two terminal Schottky diode.

The expression used for both capacitances is

$$C_{gs,gd} = C_{gs0,gd0} \left(1 - \frac{V_{applied}}{V_{bi}}\right)^{-\frac{1}{2}} \tag{2..21}$$

V_{bi} is the built-in voltage (typical value is $0.8V$).

Some alternative models to the original Curtice model have evolved to provide for the elements ignored in the previous model or in most cases to enable a better modelling of the device for better simulation and design.

The Curtice-Ettenberg model, known as the Curtice cubic model, uses a third order polynomial to describe the I/V characteristic of the device [37].

The drain current source is represented by

$$I_d = \left(A_0 + A_1 V_i + A_2 V_i^2 + A_3 V_i^3\right) \tanh\left(\alpha V_{ds}\right) \tag{2..22}$$

With

$$V_i = V_{gs}\left[1 + \beta_2 \left(V_{ds0} - V_{ds}\right)\right] \quad \text{for } V_{ds} \geq 0 \tag{2..23}$$

Where the voltage V_{ds0} represents, the voltage at which the coefficients A_0, A_1, A_2 and A_3 are calculated.

α is the internal time delay parameter.

β_2 is a coefficient for pinchoff change as a function of V_{ds}.

A_0, A_1, A_2 and A_3 are coefficients in the cubic equation.

The cubic relationship can result in a pinchoff voltage that make either the transconductance or the current to be zero. The analysis must therefore include the phenomenon of pinch off voltage increase due to V_{ds} changes. Since I_{ds} cannot be pinched off at large V_{ds} due to the gate current produced by the breakdown voltage. The following constraint are applied in this model [37]:

For the I_{dg}

$$I_{dg=}\begin{cases} \frac{Vdg(t)-V_B}{R_B}, & V_{dg} > V_B \\ \\ 0 & V_{dg} > V_B \end{cases} \tag{2..24}$$

where V_B is the breakdown voltage and R_B is the breakdown resistance.

For I_{gs} ,

$$I_{gs} = \begin{cases} \frac{Vi(t)-Vbi}{RF}, & V_i \geq V_{bi} \\ \\ 0 & V_{in} < V_{bi} \end{cases} \tag{2..25}$$

where V_{bi} is the built in voltage.

2.4.2 The Statz Model

The Statz model was originally proposed in 1975 for MOSFET device modelling. It offered an improved analytic dc I/V formulation and an improved charge model representation of C_{gs} and C_{gd} as functions of the gate-source voltage and the drain-source voltage [38].

The simple Statz I/V dc model is represented by

$$I_{ds}\left(V_{gs}, V_{ds}\right) = \left[\frac{\beta(V_{gs}-V_{T0})^2}{1+b(V_{gs}+|V_P|)}\right]\left(1+\lambda V_{ds}\right)\tanh\left(\alpha V_{ds}\right) \qquad (2..26)$$

with b, the channel thickness.

V_p, the pinch-off voltage.

α and γ are the model parameters.

2.4.3 The Marteka Model

The Marteka and Kacprzak model uses a very simple but quite accurate formula to describe the dc I/V characteristic of the device [40]

$$I_{ds}\left(V_{gs}, V_{ds}\right) = I_{ds}\left(\frac{1+V_{gs}}{V_t}\right)\tanh\left(\alpha\frac{V_{ds}}{V_{gs}+V_t}\right) \qquad (2..27)$$

With

$$V_{gs} = V_{t0} + \gamma V_{ds} \qquad (2..28)$$

where V_t is the effective threshold voltage.

where I_{ds} is the saturation current.

α and γ are the model parameters.

V_{t0} is the threshold voltage of an ideal FET.

2.5 Conclusions

Each MESFET model has some specific constraints and inaccuracies, but additionally, there are more general limitations related to the fact that equivalent circuit models are only convenient approximations of the much more complicated physical reality.

Their uses, even though they do not provide complete accuracy, give an understanding of the physical device and a solution to circuit design problems such as intermodulation distortion. They will be used in the next chapters.

CHAPTER 3.

INTERMODULATION ANALYSIS & CANCELLATION TECHNIQUES

3.1 Introduction

A perfectly linear amplifier would simply amplify the signals at its input. However perfectly linear amplifiers do not exist, and nonlinearities will result in additional output signals that are the result of mixing phenomena in the amplifier as demonstrated in this chapter.

The characterisation of signal distortion is very important in a communication system since the range of signals that can be processed with very high quality determines its usefulness. This is dictated by its noise figure or its sensitivity for the lower input power limit and by its acceptable level of signal distortion at the upper power limit. The means by which the IMD components are characterised and measured, are shown in this chapter as well as the various existing techniques devised to reduce the effects of these distortions to improve system performance.

3.2 Intermodulation Distortion Analysis

Intermodulation distortion occurs in communication systems when the amplitude and phase components of a transfer function are frequency dependent functions, i.e. it may be written as $|H(j\omega)|exp[(j\omega)]$. Intermodulation describes the process by which power at one frequency, or a group of frequencies, is transferred to power at other frequencies. This process engenders the sum and difference frequency of the original signals at the output.

If the system possesses nonlinear elements, the system cannot be described by

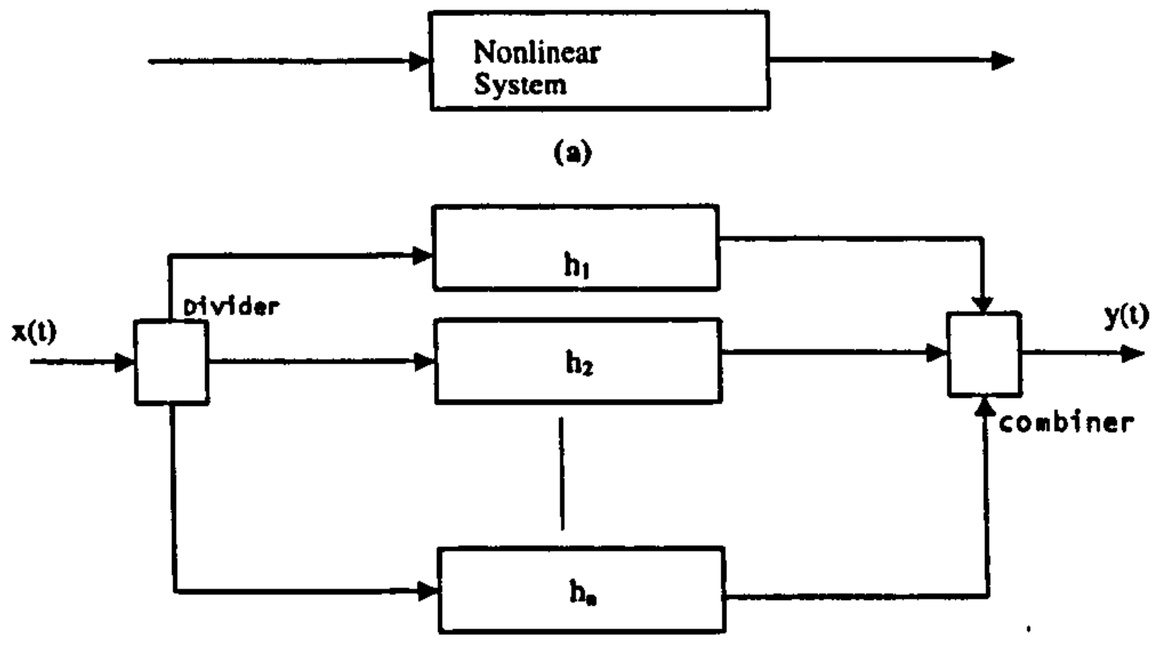

Figure 3..1: **Diagram of a nonlinear system (a) and its functional expansion representation (b).**

a single transfer function as in the linear case. Instead the output is often expressed as a nonlinear function of the input.

The subject of nonlinear functions is one of the more complex domains of mathematics and circuit theory. Various methods are used in the nonlinear analysis of circuits with applications to the study of amplifier intermodulation. Amongst these methods are the Volterra series [50-59], power series [60-64] and Taylor series [64,66]. These methods, known as frequency domain nonlinear analysis techniques solve the steady state response of a nonlinear circuit by operating entirely in the frequency domain. They can be used to analyse intermodulation distortions for strongly nonlinear systems with multi-tone excitations. Time domains techniques [67] are also used, as well as hybrid techniques known as harmonic balance techniques [68-72] which have been implemented for computer simulation of nonlinear circuits with multiple inputs.

The Volterra series, which is an extension of the theorem of convolution from linear to nonlinear systems, is used to analyse weakly nonlinear systems with memory. A system is said to have memory when the output at the time t depends upon the

value prior to that time. In a nonlinear system, the relationship between the input and the output cannot be defined by a single function but by a series of functions called functionals. The use of the functionals is to extend the analysis for the linear systems to nonlinear systems in the frequency domain [65]. The nonlinear system is represented by various functions as in Figure 3.1. The nonlinear effects are reflected in the variations of the value of the describing function gain with the amplitude of the input signal [55].

When the Volterra series is used, the time-dependent output of a linear system is defined by:

$$y(t) = \int_{-\infty}^{\infty} h(u)x(t-u)du \tag{3..1}$$

where $h(u)$ is the impulse response of the linear system.

In a nonlinear system, the output is defined by a series of functions

$$\begin{aligned} y(t) &= \int_{-\infty}^{\infty} h(u_1)x(t-u_1)du_1 \\ &+ \int_{-\infty}^{\infty}\int_{-\infty}^{\infty} h(u_1,u_2)x(t-u_1)x(t-u_2)du_1du_2 \\ &+ \int_{-\infty}^{\infty}\int_{-\infty}^{\infty}\int_{-\infty}^{\infty} h(u_1,u_2,u_3)x(t-u_1)x(t-u_2)x(t-u_3)du_1du_2du_3 \\ &+\cdots+\int_{-\infty}^{\infty}\int_{-\infty}^{\infty}\cdots\int_{-\infty}^{\infty} h(u_1,u_2,\cdots,u_n)x(t-u_1)x(t-u_2)\cdots x(t-u_n)du_1du_2\cdots du_n \end{aligned} \tag{3..2}$$

Where the n^{th} transfer function $y_n(t)$ is defined as

$$y_n(t) = \int_{-\infty}^{\infty}\int_{-\infty}^{\infty}\cdots\int_{-\infty}^{\infty} h(u_1,u_2\cdots u_n)x(t-u_1)x(t-u_2)\cdots x(t-u_n)du_1du_2\cdots du_n \tag{3..3}$$

The output of equation 3.2 can be rewritten as

$$y(t) = \sum_{n=1}^{\infty} y_n(t) \tag{3..4}$$

The usefulness of the Volterra series is seen when the nonlinear effects of a system with an input signal made up of a sum of sinusoidal signals can be predicted [55]. If the input is the sum of sinusoidal signals, it can be expressed using Euler's theorem as:

$$x(t) = \sum_{k=1}^{\infty} A_k \exp(j\omega_k t) \tag{3..5}$$

where A_k is the amplitude of the k signal.

f_k is the frequency of the k signal with $\omega_k = 2\pi f_k$.

Putting equation 3.5 into equation 3.4, the system output becomes

$$\begin{aligned} y(t) &= \int_{-\infty}^{\infty}\int_{-\infty}^{\infty}\cdots\int_{-\infty}^{\infty} h(u_1, u_2 \cdots u_n) \sum_{k=1}^{p} A_k \exp\left[j\omega_k(t-u_1)\right] du_1 \\ &\times \sum_{k=1}^{p} A_k \exp\left[j\omega_k(t-u_2)\right] du_2 \cdots \times \sum_{k=1}^{p} A_k \exp\left[j\omega_k(t-u_n)\right] du_n \end{aligned} \tag{3..6}$$

$$= \int_{-\infty}^{\infty}\int_{-\infty}^{\infty}\cdots\int_{-\infty}^{\infty} h_n(u_1, u_2, \cdots, u_n) \prod_{i=1}^{n}\sum_{k=1}^{p} A_k \exp\left[j\omega_k(t-u_i)\right] du_i$$

and then

$$\begin{aligned} y(t) = &\sum_{k_1=1}^{p}\sum_{k_2=1}^{p}\cdots\sum_{k_n=1}^{p}\prod_{i=1}^{n} A_k \exp\left[j\omega_k t\right] \\ &\times \int_{-\infty}^{\infty}\int_{-\infty}^{\infty}\cdots\int_{-\infty}^{\infty} h_n(u_1, u_2, \cdots, u_n) \prod_{i=1}^{n} A_k \exp\left[j\omega_k(-u_i)\right] du_i \end{aligned} \tag{3..7}$$

The nth dimensional Fourier transform of the nth order impulse response is given by

$$H_n(\omega_1,\omega_2,\cdots,\omega_n) = \int_{-\infty}^{\infty}\int_{-\infty}^{\infty}\cdots\int_{-\infty}^{\infty} h_n(u_1,u_2,\cdots,u_n) \times \exp\left[j\left(\omega_1 u_1+\omega_2 u_2+\cdots+\omega_n u_n\right)\right] du_1 du_2\cdots du_n \quad (3..8)$$

Using equation 3.3, the system output for the nth order response becomes

$$y_n(t) = \sum_{k_1=1}^{p}\sum_{k_2=1}^{p}\cdots\sum_{k_n=1}^{p}\left[\prod_{i=1}^{n} A_{k_i}\exp\left[j\omega_k t\right]\right] H_n(j\omega_{k_1}, j\omega_{k_2},\cdots,j\omega_{k_n})$$

$$\sum_{k_1=1}^{p}\sum_{k_2=1}^{p}\cdots\sum_{k_n=1}^{p}\left[\prod_{i=1}^{n} A_{k_i}\right] H_n(j\omega_{k_1}, j\omega_{k_2},\cdots,j\omega_{k_n}) \times \exp\left[j\left(\omega_{k_1}+\omega_{k_2}+\cdots+\omega_{k_n}\right)\right] \quad (3..9)$$

Calculation of equation 3.9 gives all the relevant components at the output of the system. The nonlinear effects of many communication systems can be predicted with an analysis using up to three different frequencies. The use of Volterra series to solve the nonlinearity problem of MPA systems is very cumbersome but can be simplified by the use of the power series. The next chapter of this report will concentrate on the use of the power series to deduce the necessary information to analyse the different IMD products of a nonlinear MESFET device.

In this section, the nonlinearity arising in a system without memory (memoryless system), which has its output as an instantaneous response of the input, is investigated. In such a case, amplitude and phase nonlinearities can be represented by polynomial series to a certain extent. Because the input signals have different frequencies and the device behaviour is different at each frequency, there will be a different phase response associated with the different frequencies.

The Volterra series has been described as a power series but with memory and can best represent the nonlinearity analysis [52,65]. It is generally used as an extension of the power series and is well suited to represent the frequency dependent nonlinearities. However, since phase and amplitude can be evaluated in weakly nonlinear systems, then for simplicity, this analysis uses a polynomial series to evaluate the IMD products. Power series expansion analysis of a nonlinear system is a straightforward and easy way to solve nonlinear phenomena in sinusoidally excited nonlinear circuits.

In the power series, the output relation to the input is represented by a polynomial function such that the output is expressed as

$$\begin{aligned} y(t) &= \sum_{n=1}^{N} k_n x^n(t) H_n \\ &= k_1 x(t) + k_2 \left(x(t)\right)^2 + k_3 \left(x(t)\right)^3 + \cdots + k_1 \left(x(t)\right)^N \end{aligned} \tag{3..10}$$

The first term in the power series is generalised by the first order kernel $h_1(u_1)$ of the first order impulse response in the Volterra series. Similarly, the second term is generalised by the second order kernel $h_2(u_1, u_2)$ of the second order impulse response $y_2(t)$ of the system. The nth term in the power series is thus generalised by the nth-order kernel associated with an nth input system of equation 3.2.

In order to represent the system output spectrum, the harmonic input system must be considered . The input signal $x(t)$ is a sum of sinusoids such that

$$x(t) = \sum_{q=1}^{p} A_q \cos(\omega_q + \theta_q) \tag{3..11}$$

Where A_q is a complex amplitude coefficient.

p is the number of the input sinusoid.

θ_q is the phase of the q^{th} sinusoid.

ω_q is the input frequency of the q^{th} sinusoid with $\omega_q = 2\pi f_q$.

Using exponential functions, the input becomes

$$x(t) = \sum_{q=1}^{p} \frac{1}{2} \left[A_q \exp\left(j(\omega_q t + \theta_q)\right) + A_q^* \exp\left(-j(\omega_q t + \theta_q)\right) \right] \tag{3..12}$$

By defining $A_{-q} = A_q^*$ and $\omega_{-q} = -\omega_q$.

If $\theta_q = 0$ then, $A_q = |A_q| \exp\left(j\theta_q\right)$.

The input signal can be written as

$$x(t) = \sum_{q=-p}^{p} \frac{1}{2} \left[A_q \exp\left(j\omega_q t\right) \right] \tag{3..13}$$

The intermodulation components at the output of the system are found by inserting a number of input signals into equation 3.10. Inserting equation 3.13 into equation 3.10 gives

$$y(t) = \sum_{n=1}^{N} k_n \left(\frac{1}{2} \sum_{q=-p}^{p} A_q \exp\left(j\omega_q t\right) \right)^n \tag{3..14}$$

The nth term in the output series can be calculated as

$$\begin{aligned} x^n(t) = & \left(\tfrac{1}{2} \sum_{q_1=-p}^{p} A_{q_1} \exp\left(j\omega_{q_1} t\right) \right) \\ & \times \left(\tfrac{1}{2} \sum_{q_2=-p}^{p} A_{q_2} \exp\left(j\omega_{q_2} t\right) \right) \cdots \left(\tfrac{1}{2} \sum_{q_n=-p}^{p} A_{q_N} \exp\left(j\omega_{q_N} t\right) \right) \end{aligned} \tag{3..15}$$

Interchanging the order of the summation and the multiplication in equation

3.15, it becomes

$$x^n(t) = \frac{1}{2^n} \sum_{q_1=-p}^{p} \sum_{q_2=-p}^{p} \cdots \sum_{q_n=-p}^{p} [A_{q_1}, A_{q_2}, \cdots, A_{q_N}] \exp [j (\omega_{q_1} + \omega_{q_1} + \cdots + \omega_{q_N}) t] \tag{3..16}$$

This equation facilitates the calculation of the IMD components associated with each order of the nonlinear systems. The overall system output components can be found by inserting equation 3.16 into equation 3.10. The output is then

$$y(t) = \sum_{n=1}^{N} k_n \left(\begin{array}{c} \frac{1}{2^n} \sum_{q_1=-p}^{p} \sum_{q_2=-p}^{p} \cdots \sum_{q_n=-p}^{p} [A_{q_1}, A_{q_2}, \cdots, A_{q_N}] \\ \times \exp [j (\omega_{q_1} + \omega_{q_1} + \cdots + \omega_{q_N}) t] \end{array} \right) \tag{3..17}$$

The system output of equation 3.17 is a simplified version of equation 3.9. The coefficients in equation 3.17 are complex numbers whereas the coefficients in equation 3.9 obtained through a Volterra series expansion are frequency dependent coefficients.

The phenomena of IMD generation occur when more than one signal is present at the input of a nonlinear system. Applying a single input signal to the nonlinear device will generate harmonic signals at the output of a nonlinear system. The transfer signal is represented by an infinite power series. However, for simplicity in circuit analysis, the transfer function of the device is in general written as an expression of the input signal to the cubic power. The level of the fifth order IMD are relatively small compare to the third order in the calculation and are therefore neglected, it therefore reduces the computing power requirements to simulate a three tone test system.

If the input signal $x(t)$ is a single sinusoid such that

$$x(t) = \sum_{q=-1}^{1} \frac{1}{2} [A_q \exp (j\omega_q t)] \tag{3..18}$$

The system output is expressed using equation 3.10, as

$$y(t) = \sum_{n=1}^{N} k_n \left(\sum_{q=-1}^{1} \tfrac{1}{2} \left[A_q \exp\left(j\omega_q t\right) \right] \right)^n$$

$$= \tfrac{1}{2} \left[\begin{array}{c} k_1 \left(A_1 \exp\left(-j\omega_1 t\right) + A_1 \exp\left(j\omega_1 t\right) \right) + k_2 \left(A_1 \exp\left(-j\omega_2 t\right) + A_1 \exp\left(j\omega_2 t\right) \right)^2 \\ + \cdots + k_n \left(A_1 \exp\left(-j\omega_1 t\right) + A_1 \exp\left(j\omega_1 t\right) \right)^N \end{array} \right] \tag{3..19}$$

and gives

$$y(t) = \frac{1}{2} \left[\begin{array}{c} k_1 A_1 \exp\left(-j\omega_1 t\right) + k_1 A_1 \exp\left(j\omega_1 t\right) + k_2 A_1^2 \exp\left(-j2\omega_1 t\right) \\ + k_2 A_1^2 \exp\left(j2\omega_1 t\right) + \cdots + k_n A_1^n \exp\left(-jN\omega_1 t\right) + k_N A_1^N \exp\left(jN\omega_1 t\right) \end{array} \right] \tag{3..20}$$

The equation 3.20 shows that when a single frequency sinusoidal signal excites a nonlinear circuit, the output response consists of not only the fundamental signal at the frequency ω_1 and the dc, but also of the harmonic signal at the harmonic frequencies $(2\omega_1)$, $(3\omega_1)$, $(4\omega_1)$ up to the nth harmonic frequency $(n\omega_1)$. In practise, the power level of the harmonics will be such that it is negligible at higher orders. Looking at the above equation, it is clear that the power level of the harmonic is decreasing with higher harmonic order. It shows that an infinite number of signals are generated by nonlinear systems.

Note that using Euler's formula

$$Cos(\omega_q t + \theta_q) = \frac{1}{2} \left[A_q \exp\left(j(\omega_q t + \theta_q)\right) + A_q \exp\left(-j(\omega_q t + \theta_q)\right) \right] \tag{3..21}$$

with $\theta_q = 0$, equation 3.20 can be rewritten as

$$y(t) = \frac{1}{2^{n-1}} \left[k_1 A_1 \cos(\omega_1 t) + 2k_2 A_1^2 \cos(2\omega_1 t) + \cdots + k_N A_1^N \cos(N\omega_1 t) \right] \qquad (3..22)$$

The process is even more complex when the input includes more than one sinusoid. Two-tone and three-tone intermodulation distortion tests are cases where the input consists of two and three input sinusoidal signals respectively.

Considering, the input signal $x(t)$ is a sinusoid ,consisting of equi-amplitude tones (A_q) at the frequencies (ω_q) with zero phase, such that

$$x(t) = \sum_{q=-2}^{2} \frac{1}{2} \left[A_q \exp(j\omega_q t) \right] \qquad (3..23)$$

The output is calculated as

$$y(t) = \sum_{n=1}^{N} k_n \left(\sum_{q=-2}^{2} \frac{1}{2} \left[A_q \exp(j\omega_q t) \right] \right)^n \qquad (3..24)$$

Evaluation of equation 3.24 and collection of the terms up to the third order, gives

$$y(t) = k_1 A_1 \exp(-j\omega_1 t) + k_1 A_1 \exp(j\omega_1 t) + \tfrac{1}{2} k_1 A_2 \exp(-j\omega_2 t) + \tfrac{1}{2} k_1 A_2 \exp(-j\omega_2 t)$$

$$+\tfrac{1}{2} k_2 A_1^2 + \tfrac{1}{2} k_2 A_1^2 \exp(-j2\omega_1 t) + \tfrac{1}{2} k_2 A_1^2 \exp(j2\omega_1 t) + k_2 A_1 A_2 \exp(-j(\omega_1 - \omega_2) t)$$

$$+k_2 A_1 A_2 \exp(j(\omega_1 - \omega_2) t) + k_2 A_1 A_2 \exp(-j(\omega_1 + \omega_2) t) + k_2 A_1 A_2 \exp(j(\omega_1 + \omega_2) t)$$

$$+\tfrac{1}{2} k_2 A_2^2 \exp(-j2\omega_2 t) + \tfrac{1}{2} k_2 A_2^2 \exp(j2\omega_2 t) + \tfrac{1}{2} k_2 A_2^2 + \tfrac{3}{4} k_3 A_1^3 \exp(-j\omega_1 t)$$

$$+\tfrac{3}{4} k_3 A_1^3 \exp(j\omega_1 t) + k_3 A_1^3 \exp(-j3\omega_1 t) + k_3 A_1^3 \exp(j3\omega_1 t)$$

$$+\tfrac{3}{4} k_3 A_1^2 A_2 \exp(-j(2\omega_1 - \omega_2) t) + \tfrac{3}{4} k_3 A_1^2 A_2 \exp(j(2\omega_1 - \omega_2) t) + \tfrac{3}{2} k_3 A_1^2 A_2 \exp(-j\omega_2 t)$$

$$+\tfrac{3}{2} k_3 A_1^2 A_2 \exp(j\omega_2 t) + \tfrac{3}{4} k_3 A_1^2 A_2 \exp(-j(2\omega_1 + \omega_2) t) + \tfrac{3}{4} k_3 A_1^2 A_2 \exp(j(2\omega_1 + \omega_2) t)$$

$$+\tfrac{3}{2} k_3 A_1 A_2^2 \exp(-j\omega_1 t) + \tfrac{3}{2} k_3 A_1 A_2^2 \exp(j\omega_1 t) + \tfrac{3}{4} k_3 A_1 A_2^2 \exp(-j(2\omega_2 - \omega_1) t)$$

$$+\tfrac{3}{4} k_3 A_1 A_2^2 \exp(j(2\omega_2 - \omega_1) t) + \tfrac{3}{4} k_3 A_1 A_2^2 \exp(-j(2\omega_2 + \omega_1) t)$$

$$+\tfrac{3}{4} k_3 A_1 A_2^2 \exp(j(2\omega_2 + \omega_1) t) + \tfrac{3}{4} k_3 A_2^3 \exp(-j\omega_2 t) + \tfrac{3}{4} k_3 A_2^3 \exp(j\omega_2 t)$$

$$+k_3 A_2^3 \exp(-j\omega_2 t) + k_3 A_2^3 \exp(j\omega_2 t) \qquad (3..25)$$

The output signal consists of the components at the dc, the fundamental frequencies (ω_1), (ω_2), the second harmonics $(2\omega_1)$, $(2\omega_2)$ and the third harmonics products $(3\omega_1)$, $(3\omega_2)$. The output includes also intermodulation products of third order $(2\omega_1 + \omega_2)$, $(2\omega_1 - \omega_2)$, $(2\omega_2 + \omega_1)$ and $(2\omega_2 - \omega_1)$. The output spectrum is illustrated in figure 3.2

The order of the harmonic and the intermodulation is determined by the sum of the coefficient of the different frequencies. The sum of the magnitude of the coefficients is the order of the signal. For example a signal at the frequency $(2\omega_2 - \omega_1)$ is of the order $2 + |-1| = 3$.

Each term in the expression of the third order component is made up of terms

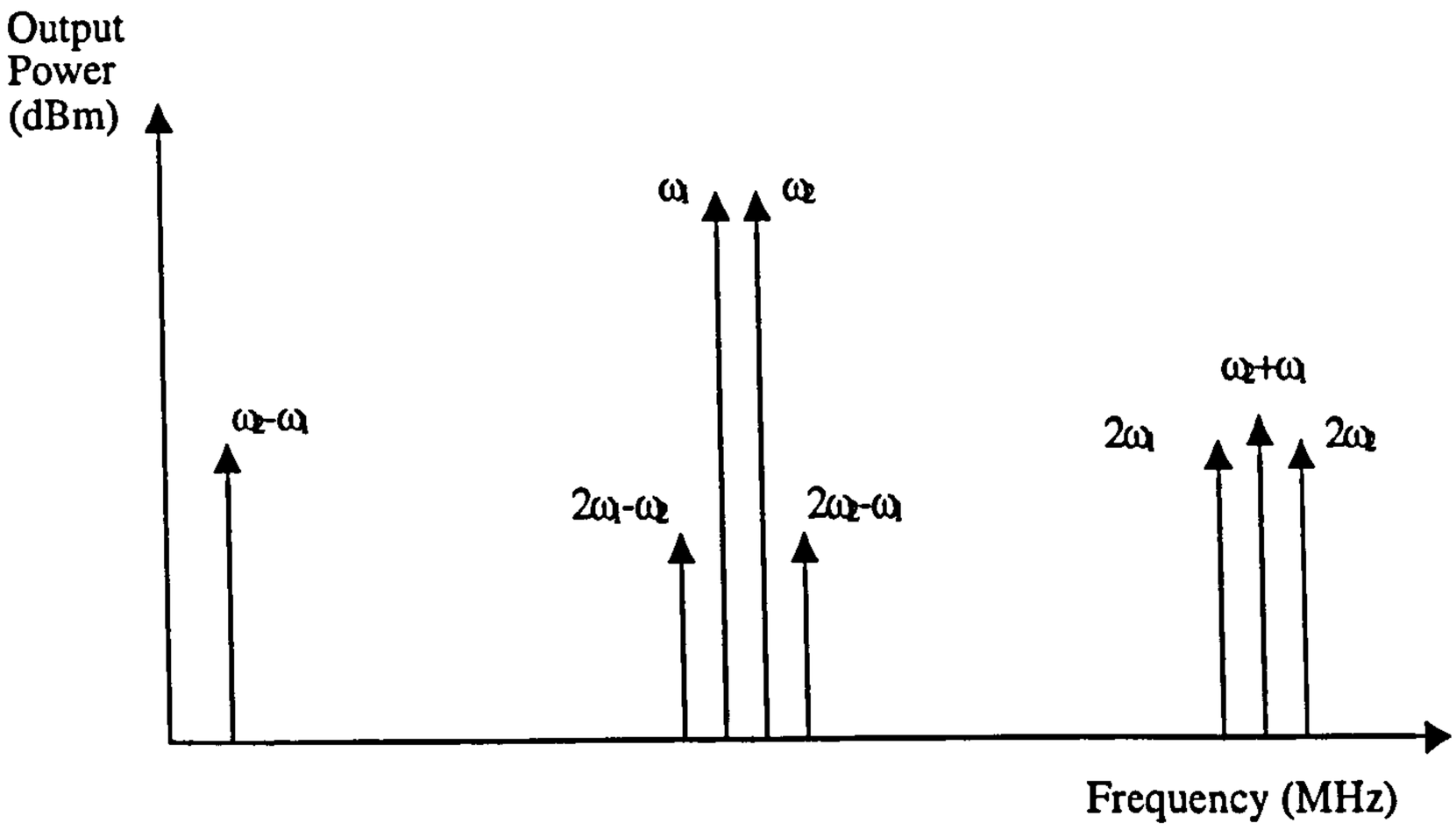

Figure 3..2: **Output spectrum of a two-tone test showing the fundamental signals, as well as the second and third order intermodulation distortion products.**

whose magnitudes are proportional to V_{in}^3. The third order signal generated is proportional to the cube of the input signal (Figure 3.3). The slope of the curve of the third order signal will therefore be 3 when the input signal is 1 in the same axis.

The most important of the IMD products is the third order IMD product (IMD3) resulting from the combination of a second order product of one signal with the first order product of another to give the signals at the frequencies $(2\omega_1 - \omega_2)$ and $(2\omega_2 - \omega_1)$. The IMD3 components are close to the original signal frequencies and are large in amplitude compared to other intermodulation products (Figure 3.2). The second order intermodulation products are not very close to the fundamental signal and therefore do not cause distortion.

For a three-tone test, the input is expressed as

$$x(t) = \sum_{q=-3}^{3} \frac{1}{2} \left[A_q \exp\left(j\omega_q t\right) \right] \tag{3..26}$$

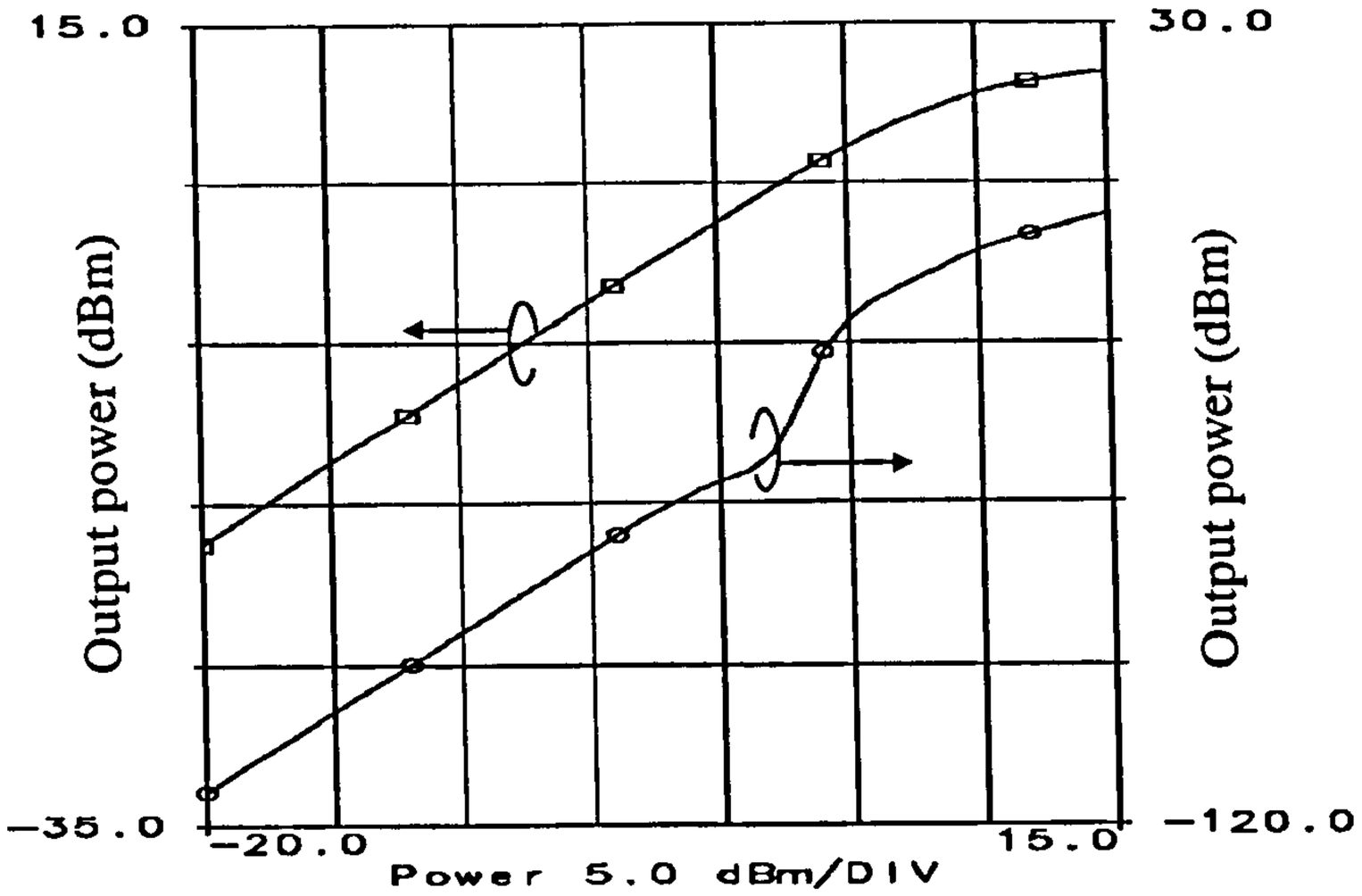

Figure 3..3: **Output power Vs input powers of fundamental and third order intermodulation distortion in a power amplifier.**

The output is calculated as

$$y(t) = \sum_{n=1}^{N} k_n \left(\sum_{q=-3}^{3} \frac{1}{2} \left[A_q \exp\left(j\omega_q t\right) \right] \right)^n \tag{3..27}$$

Evaluation of equation 3.27 is best simplified by calculating terms up to the third order as these intermodulations cause greater distortions. The output equation to be evaluated is therefore

$$y(t) = \frac{1}{2^3} \sum_{n=1}^{3} k_n \left(\sum_{q=1}^{3} \left[A_q \exp\left(j\omega_q t\right) \right] \right)^3 \tag{3..28}$$

The overall output voltage expression at the dc and the fundamental frequencies

is

$$
\begin{aligned}
y_{dc+fund}(t) &= \tfrac{1}{2}\left(k_2A_1^2 + k_2A_2^2 + k_2A_3^2\right) \\
&+ \left(\tfrac{1}{2}k_1A_1 + \tfrac{3}{8}k_3A_1^3 + \tfrac{3}{4}k_3A_1A_2^2 + \tfrac{3}{4}k_3A_1A_3^2\right)\left[\exp\left(-j\omega_1 t\right) + \exp\left(j\omega_1 t\right)\right] \\
&+ \left(\tfrac{1}{2}k_1A_2 + \tfrac{3}{4}k_3A_1^2A_2 + \tfrac{3}{8}k_3A_2^3 + \tfrac{3}{4}k_3A_2A_3^2\right)\left[\exp\left(-j\omega_2 t\right) + \exp\left(j\omega_2 t\right)\right] \\
&+ \left(\tfrac{1}{2}k_1A_3 + \tfrac{3}{4}k_3A_1^2A_3 + \tfrac{3}{4}k_3A_2^2A_3 + \tfrac{3}{8}k_3A_3^3\right)\left[\exp\left(-j\omega_3 t\right) + \exp\left(j\omega_3 t\right)\right]
\end{aligned}
\tag{3..29}
$$

Similarly for all second and third order harmonics products, the expression is

$$
\begin{aligned}
y_{har}(t) &= \tfrac{1}{4}k_2A_1^2\exp\left(-j2\omega_1 t\right) + \tfrac{1}{4}k_2A_1^2\exp\left(j2\omega_1 t\right) \\
&+ \tfrac{1}{4}k_2A_2^2\exp\left(-j2\omega_2 t\right) + \tfrac{1}{4}k_2A_2^2\exp\left(j2\omega_2 t\right) \\
&+ \tfrac{1}{4}k_2A_3^2\exp\left(-j2\omega_3 t\right) + \tfrac{1}{4}k_2A_3^2\exp\left(j2\omega_3 t\right) \\
&+ \tfrac{1}{8}k_3A_1^3\exp\left(-j3\omega_1 t\right) + \tfrac{1}{8}k_3A_1^3\exp\left(j3\omega_1 t\right) \\
&+ \tfrac{1}{8}k_3A_2^3\exp\left(-j3\omega_2 t\right) + \tfrac{1}{8}k_3A_2^3\exp\left(j3\omega_2 t\right) \\
&+ \tfrac{1}{8}k_3A_2^3\exp\left(-j3\omega_2 t\right) + \tfrac{1}{8}k_3A_2^3\exp\left(j3\omega_2 t\right)
\end{aligned}
\tag{3..30}
$$

For all second order IMD products, the output expression is

$$
\begin{aligned}
y_{IMD2}(t) &= \tfrac{1}{4}k_2A_1A_2\left(\exp\left[-j\left(\omega_1 t + \omega_2 t\right)\right] + \exp\left[j\left(\omega_1 t + \omega_2 t\right)\right]\right) \\
&+ \tfrac{1}{4}k_2A_1A_2\left(\exp\left[-j\left(\omega_1 t - \omega_2 t\right)\right] + \exp\left[j\left(\omega_1 t - \omega_2 t\right)\right]\right) \\
&+ \tfrac{1}{4}k_2A_1A_3\left(\exp\left[-j\left(\omega_1 t + \omega_3 t\right)\right] + \exp\left[j\left(\omega_1 t + \omega_3 t\right)\right]\right) \\
&+ \tfrac{1}{4}k_2A_1A_3\left(\exp\left[-j\left(\omega_1 t - \omega_3 t\right)\right] + \exp\left[j\left(\omega_1 t - \omega_3 t\right)\right]\right) \\
&+ \tfrac{1}{4}k_2A_2A_3\left(\exp\left[-j\left(\omega_2 t + \omega_3 t\right)\right] + \exp\left[j\left(\omega_2 t + \omega_3 t\right)\right]\right) \\
&+ \tfrac{1}{4}k_2A_2A_3\left(\exp\left[-j\left(\omega_2 t - \omega_3 t\right)\right] + \exp\left[j\left(\omega_2 t - \omega_3 t\right)\right]\right)
\end{aligned}
\tag{3..31}
$$

The expression for all third order IMD products is

$$
\begin{aligned}
y_{IMD3}(t) = {} & \tfrac{3}{8}k_3A_1^2A_2\left(\exp\left[-j\left(2\omega_1t+\omega_2t\right)\right]+\exp\left[j\left(2\omega_1t+\omega_2t\right)\right]\right) \\
& +\tfrac{3}{8}k_3A_1^2A_2\left(\exp\left[-j\left(2\omega_1t-\omega_2t\right)\right]+\exp\left[j\left(2\omega_1t-\omega_2t\right)\right]\right) \\
& +\tfrac{3}{8}k_3A_1A_2^2\left(\exp\left[-j\left(2\omega_2t+\omega_1t\right)\right]+\exp\left[j\left(2\omega_2t+\omega_1t\right)\right]\right) \\
& +\tfrac{3}{8}k_3A_1A_2^2\left(\exp\left[-j\left(2\omega_2t-\omega_1t\right)\right]+\exp\left[j\left(2\omega_2t-\omega_1t\right)\right]\right) \\
& +\tfrac{3}{8}k_3A_1^2A_3\left(\exp\left[-j\left(2\omega_1t+\omega_3t\right)\right]+\exp\left[j\left(2\omega_1t+\omega_3t\right)\right]\right) \\
& +\tfrac{3}{8}k_3A_1^2A_3\left(\exp\left[-j\left(2\omega_1t-\omega_3t\right)\right]+\exp\left[j\left(2\omega_1t-\omega_3t\right)\right]\right) \\
& +\tfrac{3}{8}k_3A_2^2A_3\left(\exp\left[-j\left(2\omega_2t+\omega_3t\right)\right]+\exp\left[j\left(2\omega_2t+\omega_3t\right)\right]\right) \\
& +\tfrac{3}{8}k_3A_2^2A_3\left(\exp\left[-j\left(2\omega_2t-\omega_3t\right)\right]+\exp\left[j\left(2\omega_2t-\omega_3t\right)\right]\right) \\
& +\tfrac{3}{8}k_3A_1A_3^2\left(\exp\left[-j\left(2\omega_3t+\omega_1t\right)\right]+\exp\left[j\left(2\omega_3t+\omega_1t\right)\right]\right) \\
& +\tfrac{3}{8}k_3A_1A_3^2\left(\exp\left[-j\left(2\omega_3t-\omega_1t\right)\right]+\exp\left[j\left(2\omega_3t-\omega_1t\right)\right]\right) \\
& +\tfrac{3}{8}k_3A_2A_3^2\left(\exp\left[-j\left(2\omega_3t+\omega_2t\right)\right]+\exp\left[j\left(2\omega_3t+\omega_2t\right)\right]\right) \\
& +\tfrac{3}{8}k_3A_2A_3^2\left(\exp\left[-j\left(2\omega_3t-\omega_2t\right)\right]+\exp\left[j\left(2\omega_3t-\omega_2t\right)\right]\right) \\
& +\tfrac{3}{8}k_3A_1A_2A_3\left(\exp\left[-j\left(\omega_1t+\omega_2t-\omega_3t\right)\right]+\exp\left[j\left(\omega_1t+\omega_2t-\omega_3t\right)\right]\right) \\
& +\tfrac{3}{8}k_3A_1A_2A_3\left(\exp\left[-j\left(\omega_1t-\omega_2t+\omega_3t\right)\right]+\exp\left[j\left(\omega_1t-\omega_2t+\omega_3t\right)\right]\right) \\
& +\tfrac{3}{8}k_3A_1A_2A_3\left(\exp\left[-j\left(\omega_3t+\omega_2t-\omega_1t\right)\right]+\exp\left[j\left(\omega_3t+\omega_2t-\omega_1t\right)\right]\right) \\
& +\tfrac{3}{8}k_3A_1A_2A_3\left(\exp\left[-j\left(\omega_1t+\omega_2t+\omega_3t\right)\right]+\exp\left[j\left(\omega_1t+\omega_2t+\omega_3t\right)\right]\right)
\end{aligned}
\tag{3..32}
$$

The output signal as shown in the above equations is made up of the fundamental and the dc as well as the harmonic signals at the frequencies $(2\omega_1)$, $(2\omega_2)$, $(2\omega_3)$, $(3\omega_1)$, $(3\omega_2)$ and $(3\omega_3)$. It also comprises the second order intermodulation products $(\omega1 \pm \omega2)$, $(\omega1 \pm \omega3)$ and $(\omega2 \pm \omega3)$. It also has the third order intermodulation products $(2\omega_1 \pm \omega_2)$, $(2\omega_1 \pm \omega_3)$, $(2\omega_2 \pm \omega_3)$, $(2\omega_2 \pm \omega_1)$, $(2\omega_3 \pm \omega_1)$ and $(2\omega_3 \pm \omega_2)$, which are known as the first kind of third order intermodulation products and the second kind

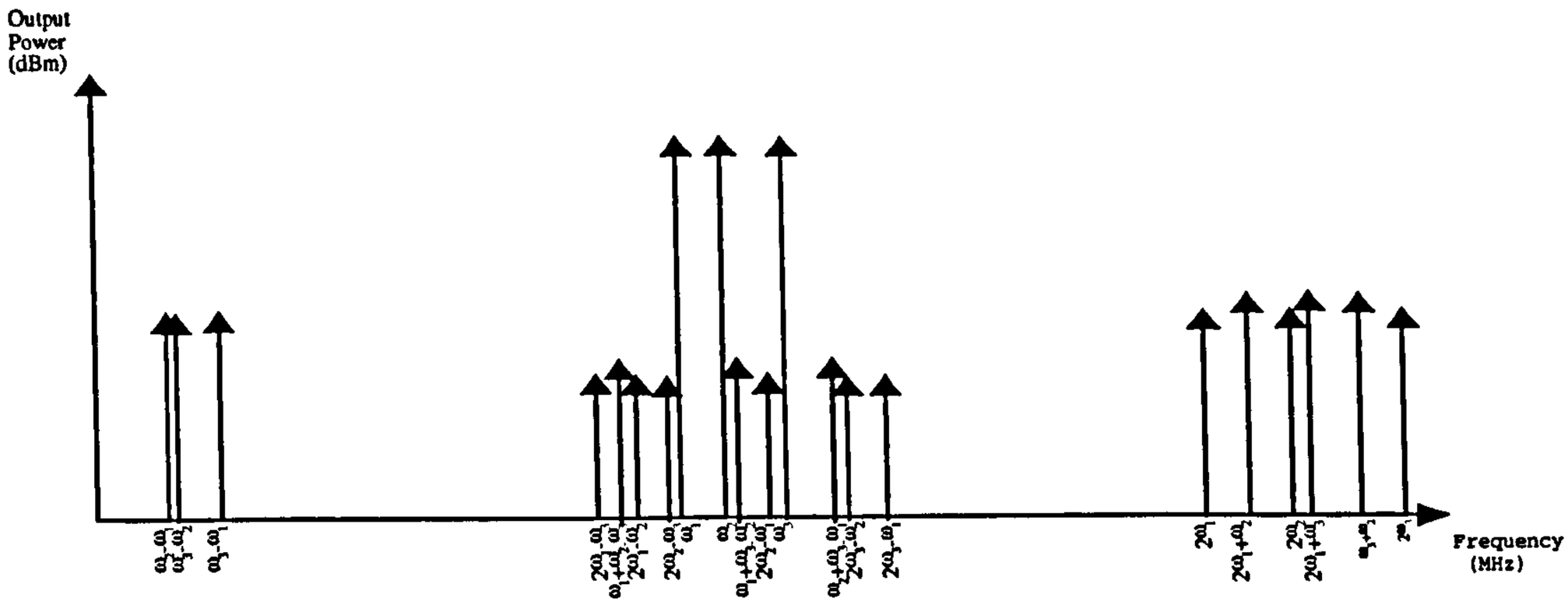

Figure 3..4: **Output spectrum of a three-tone test showing the fundamental signal and second harmonics as well as the second and third order (first kind and second kind) intermodulation distortion products.**

of third order intermodulation products are given by $(\omega_1 + \omega_2 - \omega_3)$, $(\omega_1 - \omega_2 + \omega_3)$, $(\omega_2 + \omega_3 - \omega_1)$ and $(\omega_1 + \omega_2 + \omega_3)$.

The most important of the IMD products, as mentioned earlier, are the third order IMD products (IMD3) resulting from the combination of a second order product of one signal with the first order product of another at the frequencies $(2\omega_1 - \omega_2)$ and $(2\omega_2 - \omega_1)$, etc. The IMD3 are close to the original signal frequencies and large in amplitude compared to other products.

The third order intermodulation products are very important because they not only fall into the band of interest but have a higher amplitude compared to other intermodulation products as shown in Figure 3.4.

By looking at the coefficients in the power series analysis of the three input signals test, it can be seen that the second kind of third order intermodulations generated are higher in amplitude than the first kind. They are therefore of greater importance

when analysing the effects of the intermodulation in an amplifier.

The amplitude of the first kind of IMD3 is $(3A^3k_3)/8$ and of the power levels in the second kind of IMD3 is $(3A^3k_3)/4$ with $A_1 = A_2 = A_3 = A$.

Changing the expression of the amplitude into dBW, the expression of 1st Kind of IMD3

$$P1_{IMD3} = 20\log\left(3A^3\right) + 20\log\left(k_3\right) - 20\log\left(8\right) \tag{3..33}$$

For the 2nd Kind of IMD3

$$P2_{IMD3} = 20\log\left(3A^3\right) + 20\log\left(k_3\right) - 20\log\left(4\right) \tag{3..34}$$

Since A and k have the same value for both first and second kinds of IMD3, equation 3.33 of the 1st kind of IMD3 can be rewritten as

$$P1_{IMD3} = 20\log\left(3A^3\right) + 20\log\left(k_3\right) - 20\log\left(4\right) - 20\log\left(2\right) \tag{3..35}$$

By comparing equation 3.34 and equation 3.35, it can be seen that the 2nd kind of IMD3 is larger in magnitude than the 1st kind of IMD. There is a 6dB difference between the 1st and 2nd kinds of IMD3.

Two-tone tests have been widely used for measuring IMD levels in amplifiers and other devices because it is a very simple technique to implement and only two inband third order IMDs are generated. The power level of the third order intermodulations for a multicarrier system can not be determined by a two-tone test since only the first kind of IMD3 is generated.

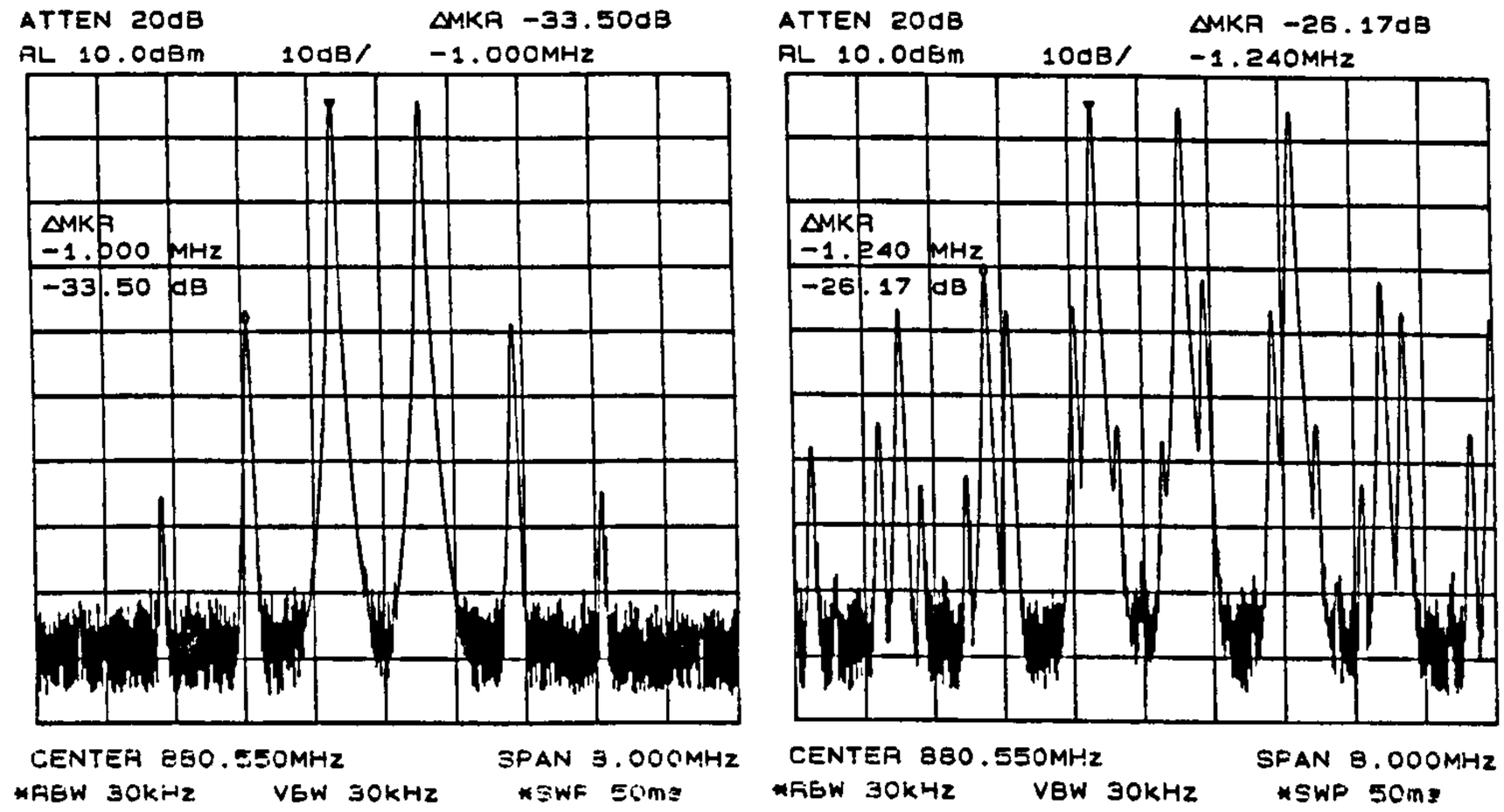

Figure 3..5: Measured output spectrum of an amplifier showing the difference in intermodulation level of for a two tone (a) and three tone (b) test at the same input power level.

It is clear that the use of more than two tones is needed for a correct measurement of the intermodulation levels in an amplifier as shown in figure 3.5. The reduction of third order intermodulations in amplifiers requires the reduction of not just the first kinds of IMD3 but both kinds of IMD3. This requires a three-tone analysis of the amplifier in order to analyse both the first and second kinds of the third order IMD. The analysis will concentrate on both kinds of third order IMD and the evaluation of the techniques effects on both third order intermodulation products in two-tone and three-tone tests.

3.3 IMD Measurement Techniques

As stated above, intermodulation distortions are very important because they occur as a result of mixing of the fundamental signals and fall within the bandwidth of

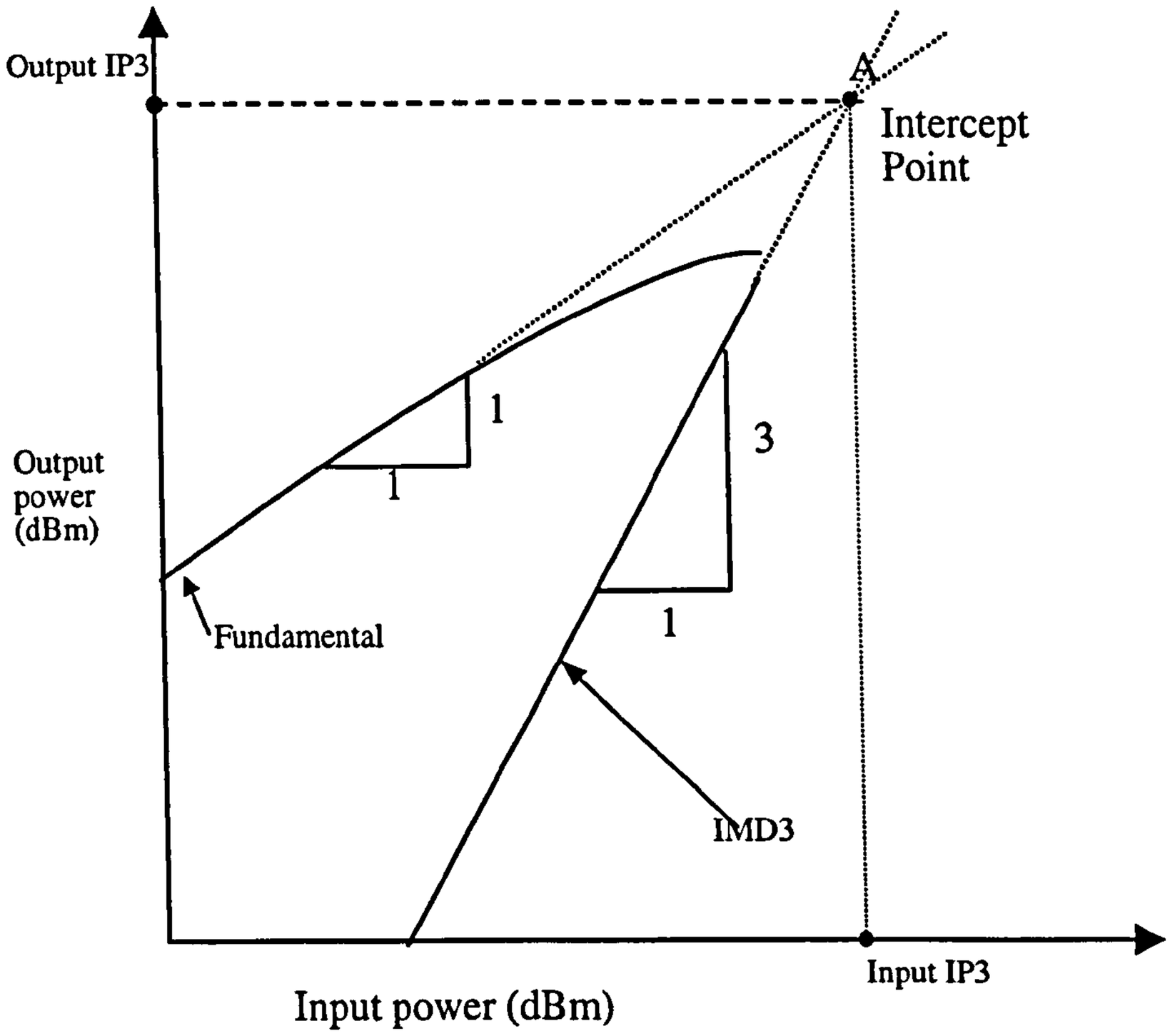

Figure 3..6: **Definition of the intercept point.**

interest but are also large in magnitude. They are very difficult to filter since they are close to the fundamentals. There are various means by which IMDs are measured.

The intercept point is defined as the output power level at which the output power $P_{2\omega_2-\omega_1}$ of the third order intermodulation at the frequency $(2\omega_1 - \omega_2)$ would intercept the output power of the input signal at the frequency (ω_1). Linear operation is taken into account for the measurement and extrapolated into higher power regions as shown in fig 3.6. The intercept point is a figure of merit for IMD3 suppression. A high intercept point clearly means a better suppression of IMD3 in the device.

The intercept point for a single stage amplifier can be approximated as [12]

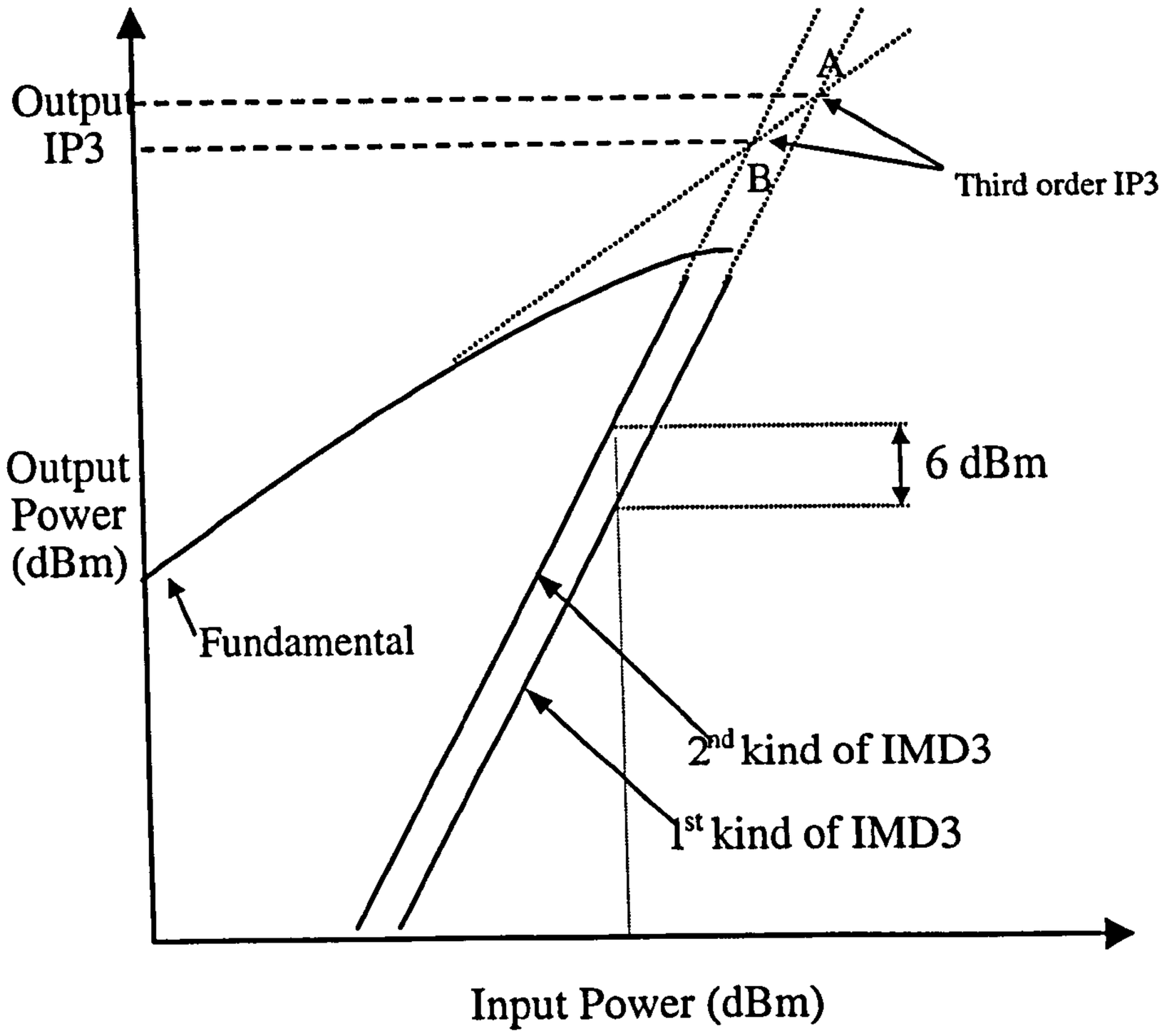

Figure 3..7: **Intercept point measurement difference between the first and second kind of IMD3.**

$$IP3 = \sqrt{\frac{4}{3}\frac{g_{m1}}{g_{m3}}} \tag{3..36}$$

With g_{m1} and g_{m3}, the device tranconductance first and third derivative respectively.

For a multistage amplifier (two stages), it is defined as

$$IP3 = \sqrt{\frac{4}{3}\frac{g_{m1a}g_{m1b}}{g_{m3a}g_{m1b} + 2g_{m1a}g_{m2a}g_{m2a} + (g_{m1a})^3 g_{m3b}}} \tag{3..37}$$

With g_{m1a}, g_{m2a}, g_{m3a}, g_{m1b}, g_{m2b}, g_{m3b}, the tranconductance first, second and third derivative for the first device denoted (a) and the second device denoted (b)

respectively.

The intercept point can be can also be calculated from the signal level in the two-tone output spectrum and approximate as [12]:

$$IP3 = \frac{1}{2}\Delta P + P_{in} \tag{3..38}$$

Where ΔP is the difference between the output power of the fundamental signal (P_{fund}) and the output power of a third order signal (P_{IMD3}) in dB.

P_{in} is the input power level at which the output value is calculated in dB.

By applying equation 3.39 to a three-tone test with the fundamental frequencies (ω_1), (ω_2) and (ω_3) of equal amplitude and using the second kind of IMD at the frequency ($\omega_1 - \omega_2 + \omega_3$), the intercept point can be calculated as

$$IP3 = \frac{P_{\omega_1} - P_{\omega_1 - \omega_2 + \omega_3}}{2} + P_{in} \tag{3..39}$$

Since from equation 3.36, the second kind of IMD3 are 6 dB higher than the first kind. Equation 3.40 then becomes

$$IP3 = \frac{P_{\omega_1} - P_{2\omega_1 - \omega_2}}{2} + P_{in} - \frac{6}{2} \tag{3..40}$$

It is shown in this analysis, that the intercept point is degraded by 3dB in a three-tone system by the existence of the second kind of IMD3. This is illustrated in figure 3.7.

A well-defined method for measuring the IMD power level is shown in figure 3.8. Two signals are adjusted to have the same power level and combined before being

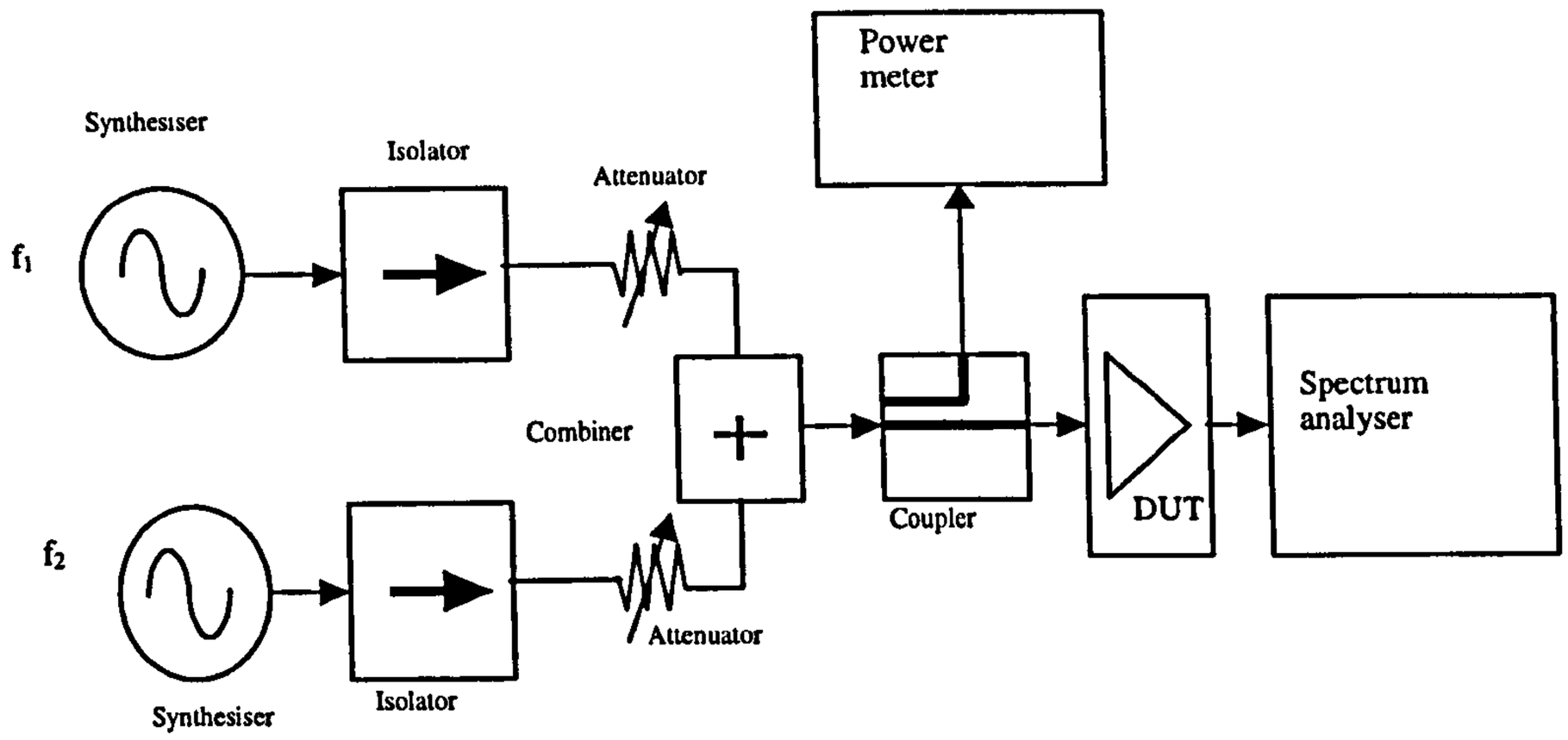

Figure 3..8: **Two-tone intermodulation distortion measurement set-up.**

passed through the device under test (DUT). The resulting output signals are detected and measured using a spectrum analyser.

If the transmitted signal has a fluctuating envelope as in a digitally modulated carrier with for example binary phase shift keying (BPSK) or quadrature phase shift keying (QPSK) as used in CDMA systems, then The amplifier nonlinear output distortion is specified in term of the adjacent channel power ratio (ACPR). The adjacent channel power (ACP) as illustrated in figure 3.9 is defined as the summation of the IMDs terms in the adjacent channel. ACPR is calculated as the power in the adjacent channel divided by the power in the channel carrying the modulated signal. The maximum allowable adjacent channel interference (ACI) levels are defined by a specified power spectral density masks as specify by the relevant international bodies [160] In section 4.10, the techniques developed in this work are shown to significantly improve the ACPR (see fig 4.60 on page 153).

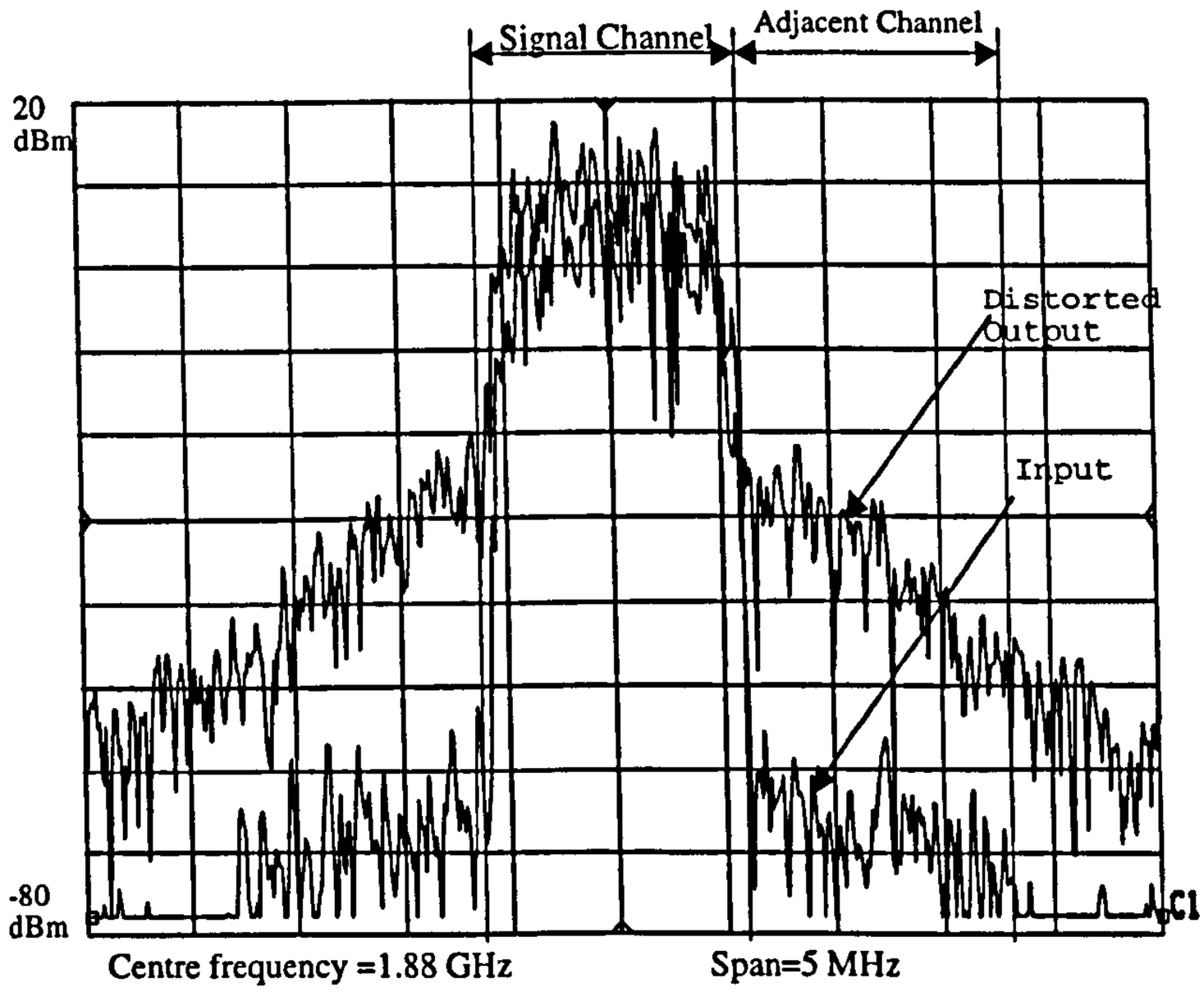

Figure 3..9: **Simulated input and output spectrum of an amplifier with a code division multiple access input signal at** $1.88GHz$.

3.4 Techniques of IMD Reduction

The amplifier is a nonlinear device, as it basically comprises nonlinear elements, which are the cause of the nonlinear effects of the device [76,77]. The use of this device in the amplification of multiple signals leads to a number of undesirable effects as mentioned earlier, such as intermodulation distortion (IMD), reduced S/N ratio, etc. The characteristic of an MPA can be modified to be more linear with various techniques.

In order to reduce the nonlinear effects in the MPA, often the operating point is backed off several dBs relative to the saturation point hence reducing its efficiency. Although the amplifier operates far below its capacity, the improvements on the nonlinear behaviour of the device permit to obtain a better output response. This is proven to

be an easy and effective way of reducing the intermodulation level in power amplifiers.

The biasing of the amplifier is important for good operation and affects the intermodulation behaviour of the device. As mentioned in chapter 2, the nonlinear terms in the active device are bias dependent. The choice of a dynamic biasing can lead to a reduction in the nonlinear performance of a device and therefore more linear operation [78,79]. The FET linearity degrades as the transconductance decreases, so correct gate or drain bias can improve the linearity, and therefore the IMD level.

A linearizer may be used in order to improve the linear behaviour of the MPA. A linearizer has to be able to compensate both the amplitude and phase nonlinearity, which are sources of distortion. With a linearizer, the efficiency of the MPA can be increased since the carrier to IM noise ratio (C/I) can be met at a higher operating point. Higher output power level with a low IMD level is desirable.

There are various ways of improving the linearity of MPAs and these techniques can be implemented at different levels of system design, from the device fabrication to the circuit and system design.

3.4.1 Device Fabrication

3.4.1.1 Ion Implantation

Detailed studies have been done on the ion implantation process, which show its various applications [80]. Ion implantation is widely used throughout industry as part of the technology for fabricating electronic devices and integrated circuits. Its use is due to several advantages it has over other techniques [80].

The technique of ion implantation entails the bombardment of a material with high velocity, positively charged ions produced in a source held at a high dc potential. After extraction from the source, the beam is mass analysed and allowed to accelerate to the target, which is at earth potential. The ions impinge on the target, penetrate some distance and come to rest at a point. This is a function of the ion energy and the mass and atomic number of the ion and the target atoms. The application of the process to the device is to achieve a high dose for the ohmic contact or a low dose to produce the channel of the FET. Further applications of active ion implantation are to form resistors and the doped region of the Schottky barrier diode.

The use of ion implantation in the design process of the device enables the device to perform better and therefore be more linear [81,82]. The technique is commonly used in industry to fabricate highly linear devices for MPA applications.

The technique and the process related to it, are beyond the scope of this thesis. The devices fabricated under such process will give a more linear process and better IMD levels. This work is more concerned with the circuit design techniques that are used for the reduction of IMD, rather than the device fabrication itself.

3.4.2 Linearizer Techniques

There are various methods by which the MPA characteristic can be improved to a more linear characteristic. The ever-growing need for highly linear power amplifiers has brought a large number of techniques. Power amplifiers constitute a very important part of the transmitter and therefore are very critical for the linear operation of communication systems.

Linearisation techniques are divided into various groups. The most widely known techniques are presented below. The need for linear amplifiers has brought on the application of the linearisation techniques on the overall transmitter with the use of digital signal processing (DSP) equipment to control the linearisation process. These techniques are briefly introduced in the next sections with appropriate references for further reading.

3.4.2.1 Predistortion Linearizer

This technique was developed in the early 1970s [83]. The principle is the compensation of the amplitude and the phase nonlinearities by distorting the input signals with the inverse of the amplitude and phase of the original amplifier response. A basic circuit can be seen in figure 3.10(a).

The linearizer is required to generate both the amplitude and phase inverse nonlinearities of the input because the nonlinearities are caused by these two elements, which are orthogonal.

Two approaches are used in the design of the predistortion (PD) circuit. The first one uses a single path with an active device, designed such that its amplitude and phase characteristics are the opposite of the main amplifier [85-87]. A signal passing through a PD will have a phase and amplitude distortion as shown in figure 3.10(b), which will be compensated in the main amplifier and therefore cancel the nonlinearities of the overall amplifier [148].

The second approach relies on the use of two distinctive paths that are combined to provide an inverse signal characteristic at the input of the amplifier [84] as shown in

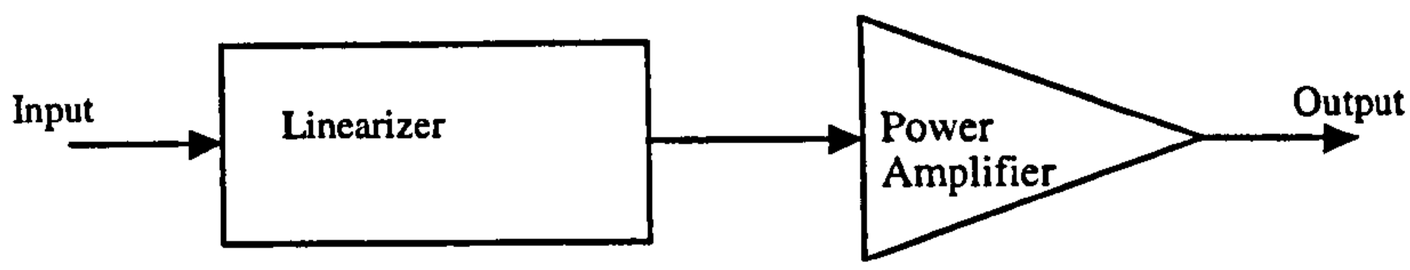

(a)

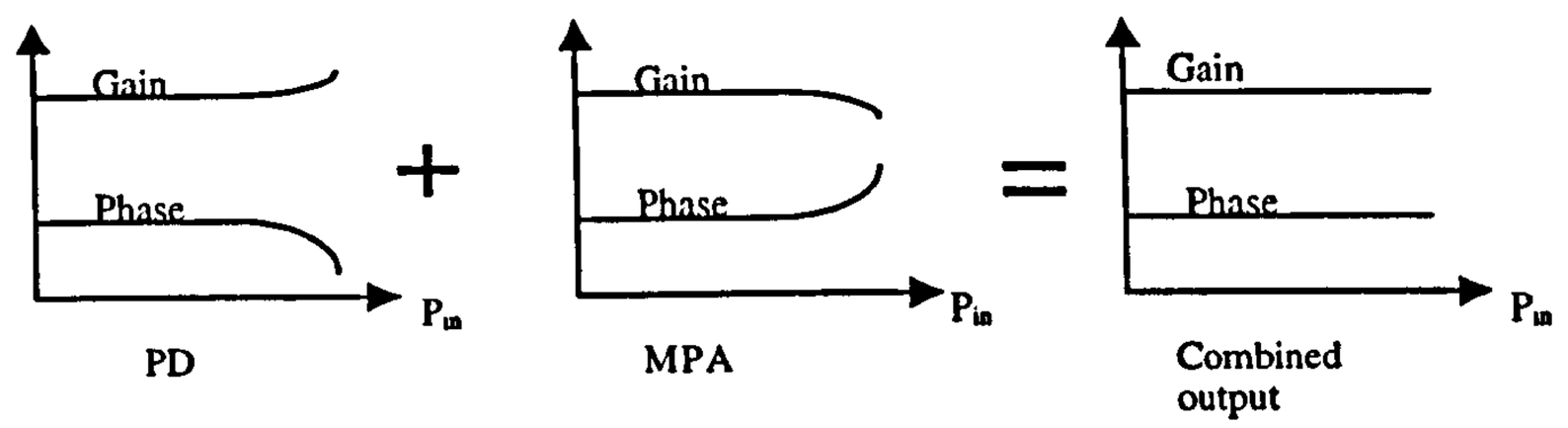

(b)

Figure 3..10: **Basic predistortion linearizer circuit diagram (a) and the corresponding phase and amplitude characteristics of the predistorter circuit and the amplifier with the output signal characteristic (b).**

figure 3.11. The input signal is divided into two paths: a linear path and a distortion path. The distortion path comprises a nonlinear device to generate the distortion and an attenuator and phase shifter to adjust the signal amplitude and phase so as to cancel the IMD component. The amplitude and phase changes of the signal through that path must be correctly adjusted. The configuration has to be suitable for adjustment in order to obtain a high signal component isolation. The signals generated are adjusted to compensate the third order IMD. The frequencies of the signal to be fed into the HPA are mostly chosen to be those of the first kind of IMD3 in the order of $(2f_1 - f_2)$ and $(2f_2 - f_1)$ for a two-tone test. This can lead to the undesired injection of the original signals, which are closed to the injected distorted signals therefore increasing the level of distortion at the output or reducing the amplifier gain. The design of the circuit requires that the frequencies of the injected signals be determined for a clear

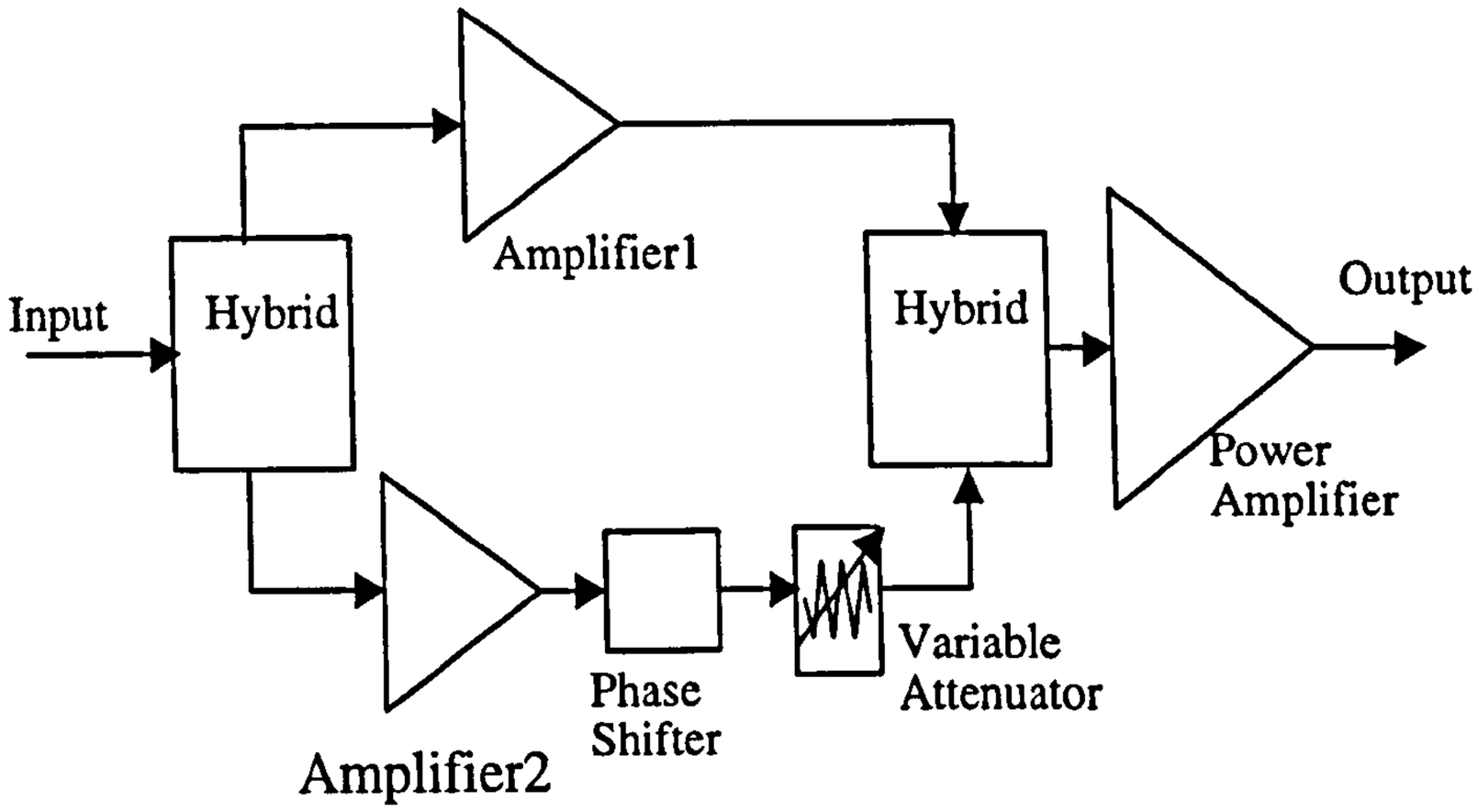

Figure 3..11: **Schematic of an active predistortion circuit with phase and amplitude equaliser.**

understanding of the requirements for IMD cancellation [150].

The predistortion linearizer scheme provides broad frequency and wide dynamic range. Many linearizers use Schottky diodes as intermodulation generators [88-92], that prove simple and compact and provide a large bandwidth with low thermal sensitivity. Schottky diodes are commonly used because they require low forward voltage hence low drive requirements. The amplitude and phase adjustment can be controlled by a dc bias to reduce the IMD. The use of a Schottky diode as an intermodulation generator and the varactor diode as a phase shifter has been investigated with successful IMD level reduction. The advance in MIC technology brought circuits using MESFETs and varactor diodes [93,94], more recently with more complex elements such as shifters and attenuators being implemented [95-100]. A linearizer circuit using an amplifier for the generation of the distortion is shown in figure 3.11 where a phase shifter is added to account for the phase distortion of the amplifier [149].

The desired linearizer gain expansion and phase advance can be achieved by a suitable choice of amplitude and phase of the predistorter component. The optimisation of the linearizer depends enormously on the transfer characteristic of the PD device but improvement will depend on the value selected for optimisation. The system has been shown to achieve an IM reduction of up to $20dB$ over a $300MHz$ bandwidth and over a wide range of temperatures from 0^o - 50^o [117]. Toshio et al [102] showed that $10dB$ reduction could be achieved using a cuber linearizer technique. This predistortion linearizer relies on the use of a cuber circuit in the distortion path of the amplifier. Kumar et al presented a PD using a dual gate FET to generate nonlinearities; a $12dB$ IMD reduction was achieved at saturation [100]. In summary, the PD provides broadband amplification with IM reduction of between $10dB$ to $25dB$.

3.4.2.2 Feedforward Linearizer

This technique uses two MPAs operating in parallel. The main MPA provides most of the power [101]. The auxiliary MPA, with a low power, provides the correction needed for linear operation of the combined device. Feedforward error control techniques [103,104] are the basis of this technique. Error is detected, amplified and injected after a proper time delay in the forward time stream of the amplifier. This enables the cancellation of the distortion over the band of interest. Because the circuit requires another MPA, this reduces the efficiency of the system and makes the system more complex and costly [105,154].

A schematic of the linearizer circuit is shown in figure 3.12. A1 is the main power amplifier, A2 is the error amplifier, C1, C2, C3 and C4 are directional couplers

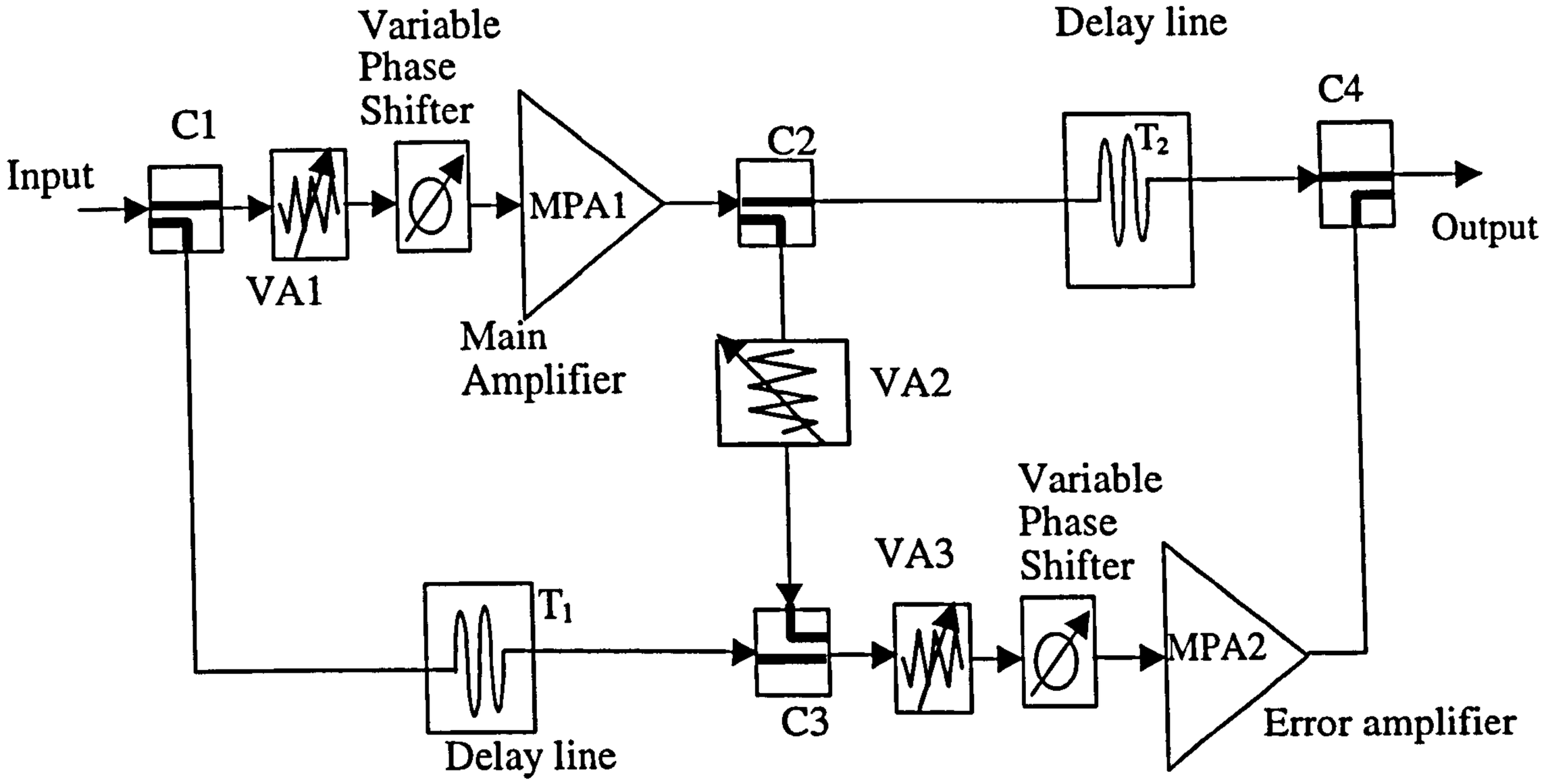

Figure 3..12: **Schematic of Feedforward linearizer using the signal cancellation loop and the error cancellation loop for the cancellation of IMD. (VA1, VA2 & VA3 are variable amplifiers, C1, C2, C3 & C4 are couplers).**

and T1 and T2 are delay lines to compensate for the phase shift of A1 and A2.

Amplifiers A1 and A2 need not be identical amplifiers with flat gain characteristics. The circuit works in the following manner: The input signal is first divided into two paths at C1. The coupler C2 samples the output from the main amplifier A1. The sample containing the distortion and noise generated by A1 is fed into the coupler C3 where the original signal is cancelled out, leaving only the distortion and noise.

The delay line T1 has to match the amplifier A1 delay in order to achieve a perfect cancellation of the fundamental signal at the coupler C3. The attenuator A enables the signal from C2 to be equalised such that a perfect cancellation is obtained at C3.

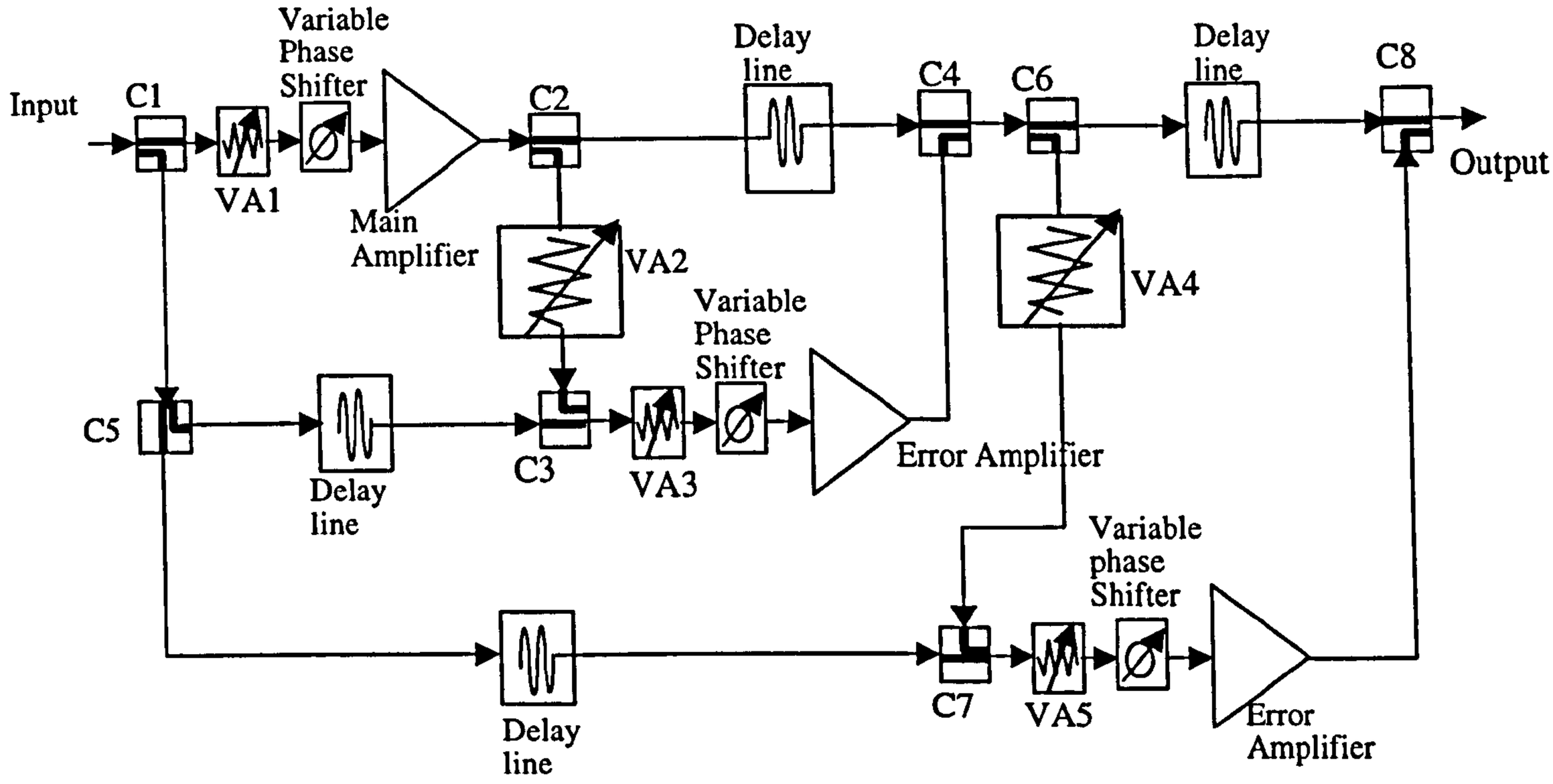

Figure 3..13: **Schematic of a dual loop feedforward amplifier.**

Once the fundamental signal has been cancelled, the remaining signals, the distortion and the noise generated by the various components will be amplified in the second amplifier A2 (error amplifier). The signal is amplified back to its normal level and fed into the coupler C4 to be coupled with the signal coming from the amplifier A1 which has been delayed by the delay line T2 that matches the delay of A2. The result of combining the signal at C4 will create a signal with no distortion or noise.

The technique is rather interesting since it gives total freedom over the transit time limitation. It is in a way similar at the previous PD since a distorted signal is required to cancel the amplifier distortion. The MPA2 only amplifies the error signal, which contains the intermodulation products and the remains of the signals. Hence,it requires less power than the main one(MPA1). The power of MPA2 needs to be such that it does not lead to distortion within the device, hence , its transfer characteristic

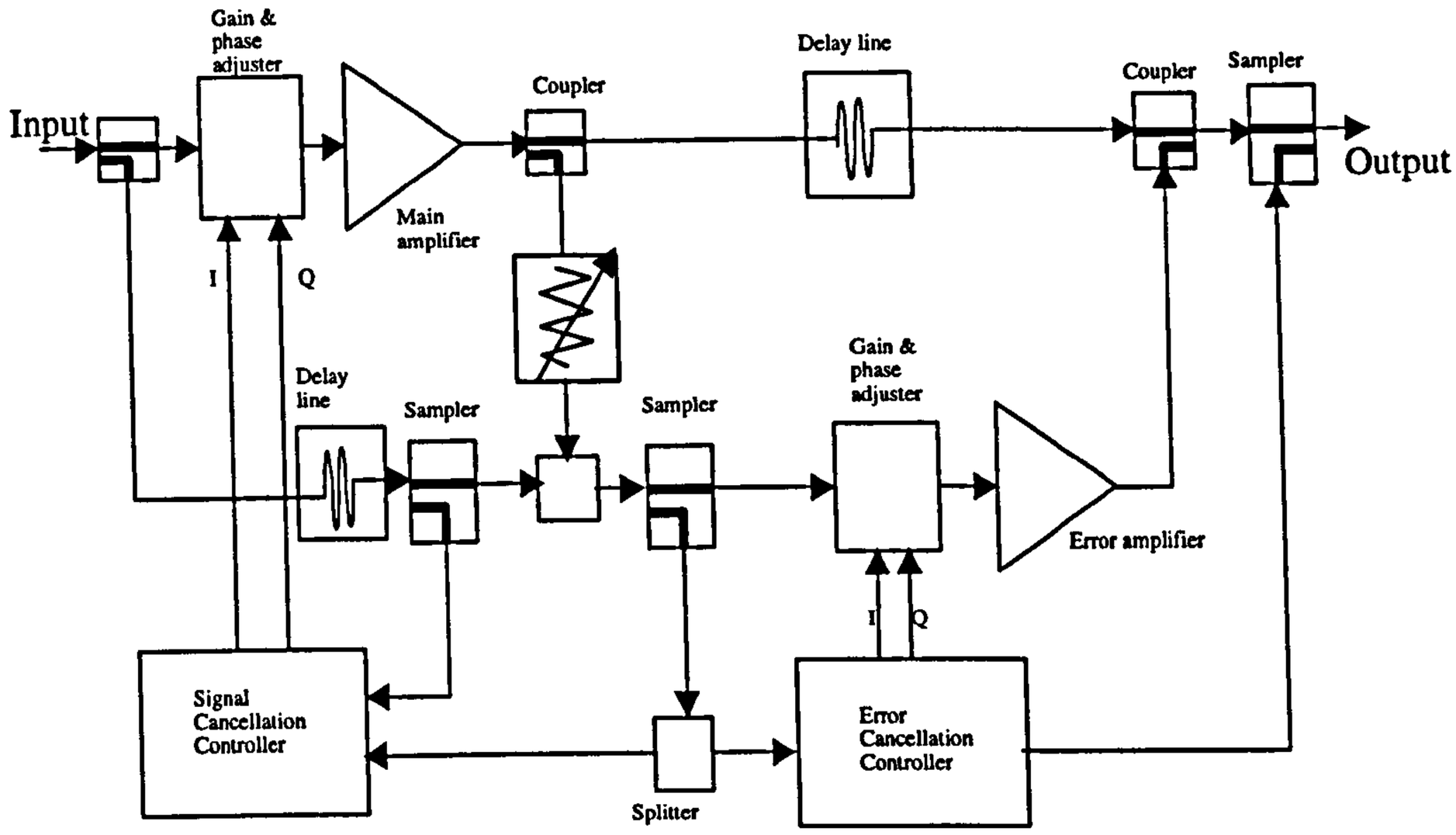

Figure 3..14: **Circuit schematic of an adaptive feedforward linearizer.**

is linear [152].

The operation of the circuit depends enormously on the cancellation at the couplers C3 and C4 as well as the perfect match in the delay lines [110]. A large number of problems can occur with this technique, particularly the loss of gain, if the cancellation of the fundamentals is not done properly at C3. At the coupler C4, there will be a reduction in the fundamentals and therefore a reduction in the gain. The amplification of the distortion signal in the amplifier A2 can result in more distortion, in particular if large distortions are created in A1 and C2 before being amplified and fed into the auxiliary amplifier A2. This is an effective technique that has shown a great reduction in the amplifier nonlinearity effects. It is used in such applications as the phase array antenna [106] and mobile communication systems [107-109].

The feedforward technique requires control of the error phase [111,112]. An

important advantage is its independence from the amplitude and phase delay of the MPA, which exist in general. The gain bandwidth of the device is consumed within the band of interest [113]. The feedforward system in its early conception was shown to reduce IMD levels by over $20dB$ over $20MHz$ [101-103] and could reach up to $40dB$ with a multistage system as in figure 3.13.

Although multistage feedforward systems are being implemented [114], thermal noise in the system can become a major problem. The multistage system requires the use of an additional MPA with the increase in complexity, weight and cost. This increases the output loss of the system and the static phase difference of the MPA.

Improvement to the system linearity can be achieved by the use of complex gain and phase adjuster circuits controlled by a signal and error cancellation controller [114-115] as shown in figure 3.14. This is known as an adaptive feedforward linearizer. The controllers use fast and robust DSP algorithms to adjust the signal in both the signal cancellation and error cancellation for maximum cancellation. The adaptive feedforward technique shows greater linearity improvement than conventional feedforward systems.

3.4.2.3 Feedback System

Feedback is one of the easiest methods of reducing IMD [116]. Feedback requires the output to be fedback via an appropriate feedback loop. There are requirements for the treatment of time delay and bandwidth involved since the time delay required for the technique involves a reduction in the bandwidth. There are different types of feedback circuits, varying from the passive feedback [117,118] to the active feedback circuit [120-

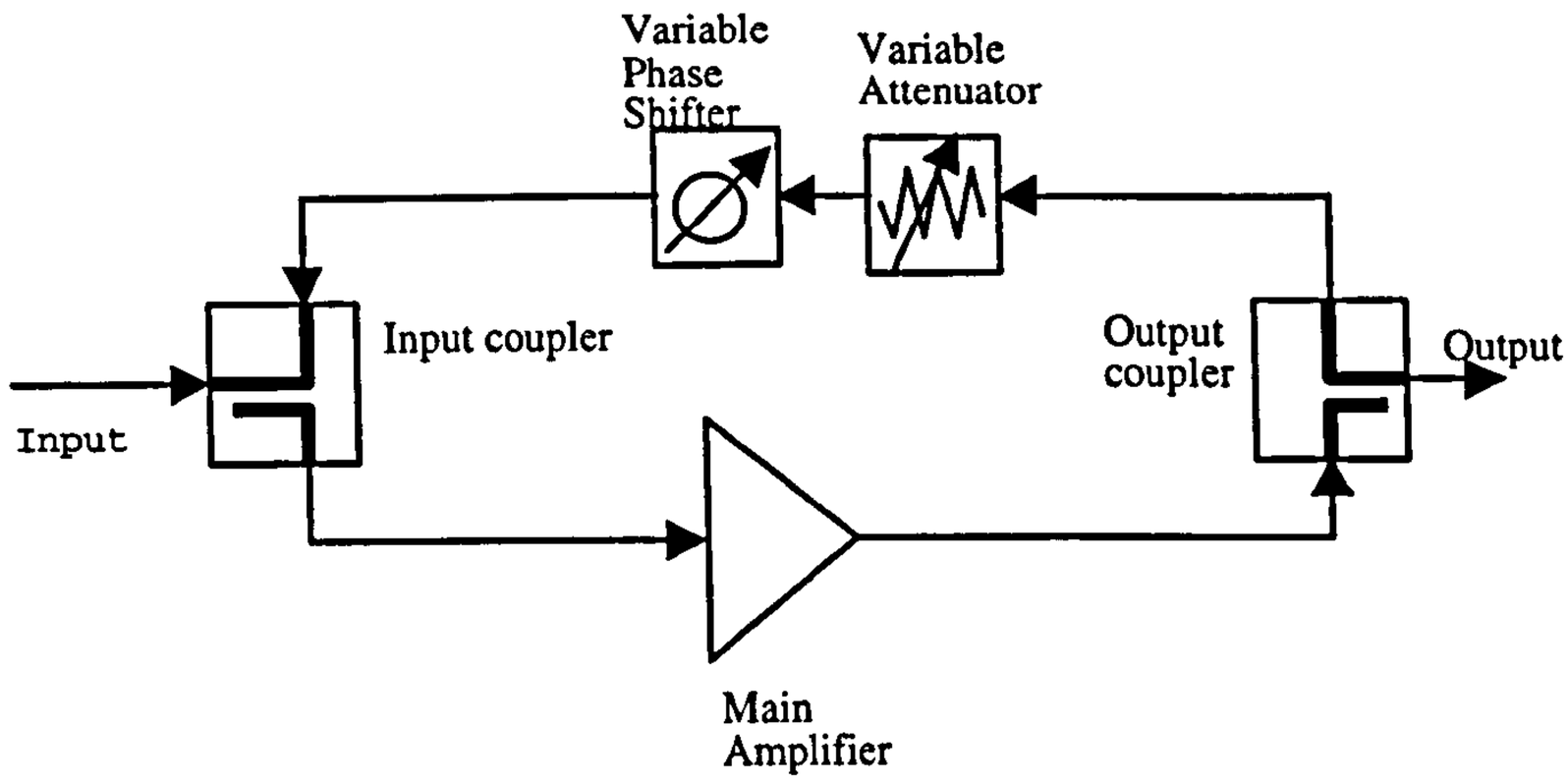

Figure 3..15: **Circuit schematic of a basic lossy feedback linearizer.**

123].

In early passive circuits, the output is fedback via a simple network of couplers. Investigations into the technique have shown that negative feedback produces an IMD reduction equal to the amplifier loop gain [116,125]. Feedback circuits are easy to implement and use a less complex circuit than other techniques. The intermodulation products are fed back via a coupler to the input to obtain a cancellation (figure 3.15). There is a need to add an appropriate phase shift to the feedback signal in order to achieve the desired effects.

If many stages were to be cascaded, this obviously increases the overall gain of the amplifier but reduces the bandwidth of the circuit and the phase change will increase dramatically.

A feedback of the output signals containing the fundamental and the IMD frequencies can cause a reduction in the third order IM distortion, but also a reduction of the fundamental signal, therefore reducing the overall amplifier gain. By removing the

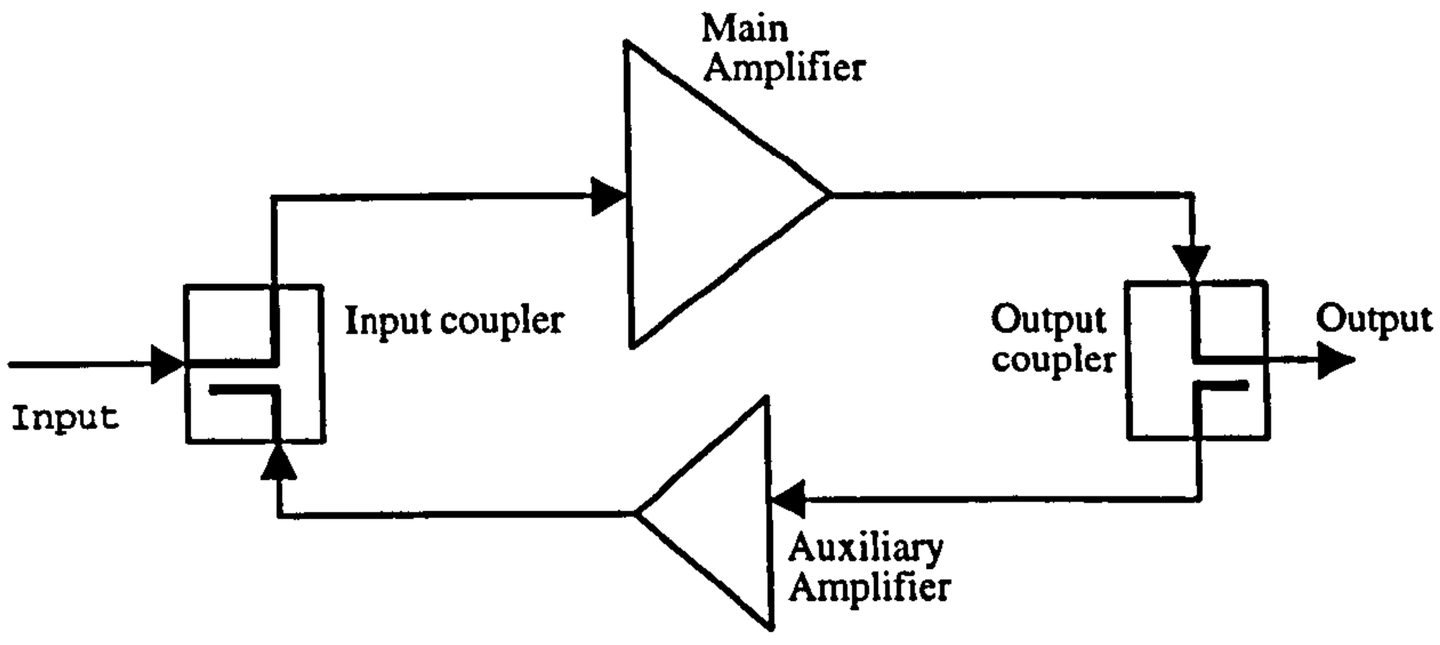

Figure 3..16: **Circuit schematic of an active feedback amplifier using an active feedback circuitry.**

fundamentals from the feedback loop, only the IMD3 will be reduced by the feedback at the intermodulation frequencies. The gain of the amplifier will remain unchanged since the fundamentals are not fedback.

Active feedback uses an auxiliary amplifier to feed the signal into the main amplifier [122]. It can be compared to the reinjection amplifier [121] or passive feedback system [118]. The operations of active feedback circuits are quite similar to those of the active predistortion system because of the use of an auxiliary amplifier. The active feedback circuit provides a low gain loss and better stability of the system. The Ballesterros et al active feedback design [121] uses two amplifiers and provides a C/I of $40dB$ and an increase of about 55% in the efficiency. The auxiliary amplifier was shown to use less power than an auxiliary amplifier used in a feedforward system. A low frequency feedback with the correct amplitude and phase adjustment showed that a $12dB$ reduction was achieved in practise with a mixer circuit [120]. An adaptive feedback circuit which make use of a voltage controlled phase shifter for predistortion purpose, shows that the control of the phase and gain can further improve the performance of

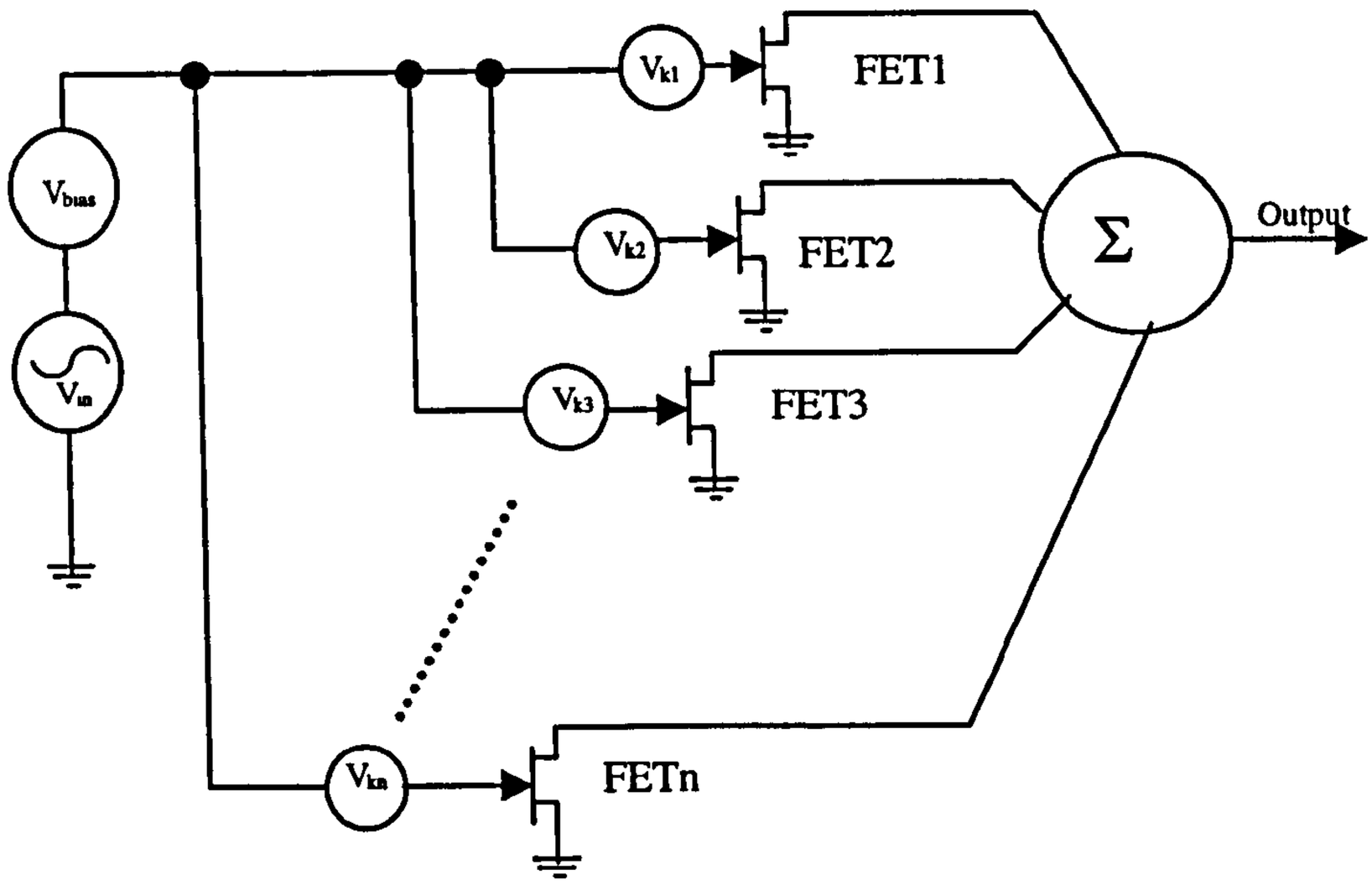

Figure 3..17: **Circuit schematic of derivative superposition with FETs of different width, scaled by the factor k_i and offset voltage v_{ki}.**

feedback circuit [155].

When the signal is fedback, although the gain of the amplifier is not reduced, the IM produced by the amplifier is fedback at the same time and can cause problems [156,157]. The technique is most suited to narrow band applications because the changes in the phase shift of the system with the frequency causes a reduction in the bandwidth.

3.4.2.4 Derivative Superposition

Derivative superposition is a linearisation technique, which combines the derivative effects of a number of devices biased at different points to give less distortion at the output [126,127].

Introduced by Parker et al [126], it consists of connecting a number of FETs in parallel as shown in figure 3.17 with different gate lengths and each one operating at a

bias point such that the overall linearity of the circuit can be controlled. Webster et al [128,129] showed a 10dB to 20dB reduction on small signal third order intermodulation for a HEMT amplifier. The application of the technique to power amplifiers was showed [130-132] to achieved low distortion with an improved overall efficiency.

3.4.3 Transmitter Linearisation

Linearised multicarrier power amplifiers are required within the transmitter for perfect transmission. Since mixing phenomena in other transmitter elements such as mixers and up converters, generate IMD, these can deteriorate the overall IMD performance of the power amplifier and therefore the transmitter. One approach to solving this problem is the linearisation of the power amplifier and the transmitter elements. Transmitter linearisation techniques provide a reduction in the level of distortion in the transmitted signal. These techniques are briefly presented below.

These techniques fall within two categories: those that are derived from the conventional technique described above but make use of modulated signal on the I and Q channel to control the process of linearisation. The second type provide a means by which an information signal is divided and processed in different paths (amplitude, phase, envelope, etc) before been amplified. A less distorted amplified version of the signal is reconstructed at the output.

3.4.3.1 Cartesian Feedback

The Cartesian feedback linearizer [133] shown in Figure 3.18 takes baseband signals in I and Q form and converts these directly into RF signals. The output is converted first into baseband frequency, which is filter and adjusted before injection at the input

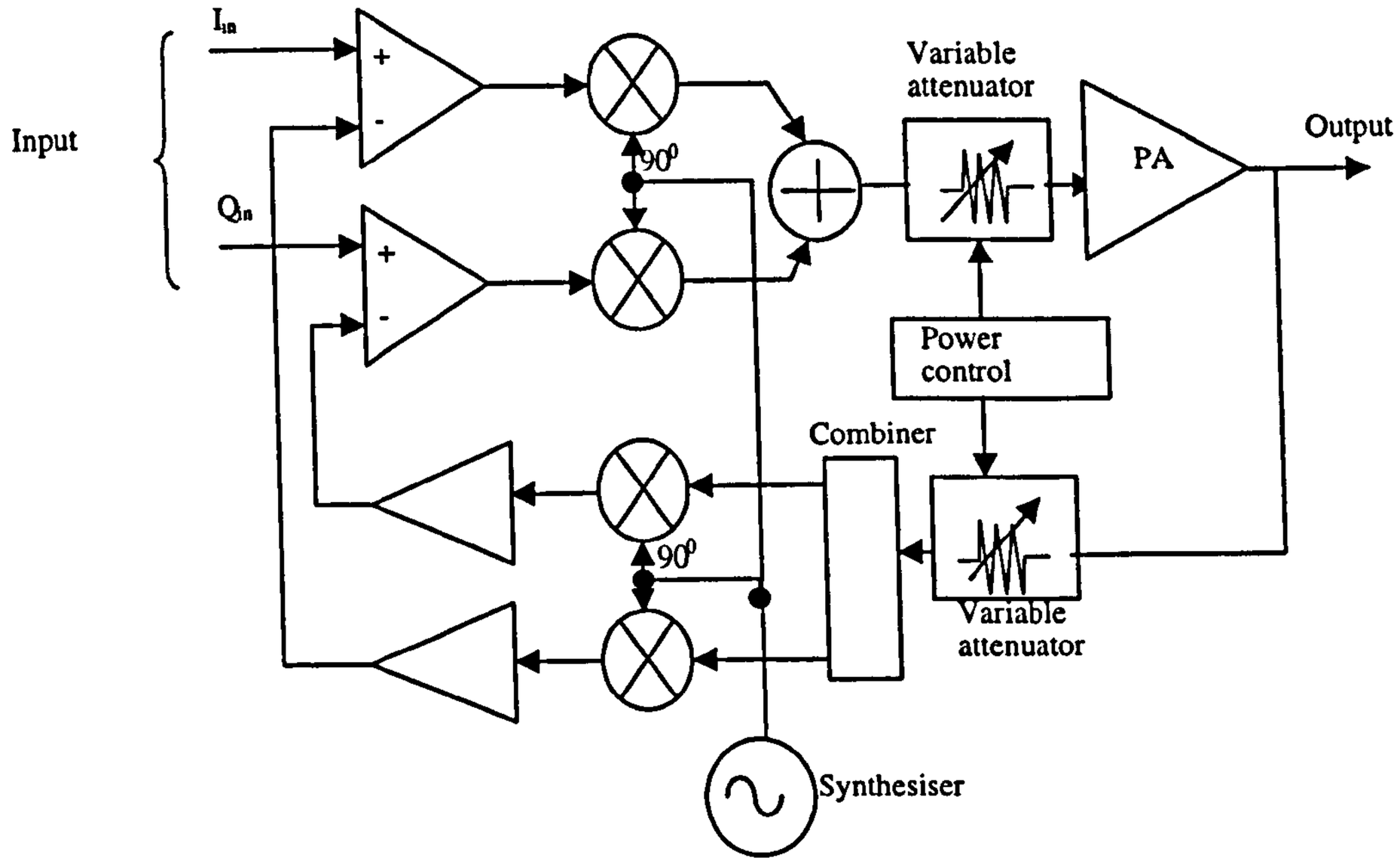

Figure 3..18: **Circuit diagram of a cartesian feedback amplifier.**

as baseband signals I_{fb} and Q_{fb}. The conversion of the signal into RF at the input, enable the transmitter to be designed such that the distortions caused by the local oscillator and up converting processes are minimised. The input signals I_{in} and Q_{in} and the feedback signals are compared. The signals are then adjusted for optimum IMD reduction. An increase in the loop gain causes an increase in the IMD performance of the technique but can cause degradation in the loop stability. The stability of the loop is a problem in feedback system and therefore limits the performance of the system. The delay around the loop can cause a reduction in the IMD improvement and the overall bandwidth. Various cartesian feedback transmitters have been implemented and have shown an improvement of up to $30dB$ in the linearity [134-136].

The cartesian feedback [133] technique is a robust version of the polar transmitter introduced by Petrovic et al [137]. Both techniques achieve reduction in the

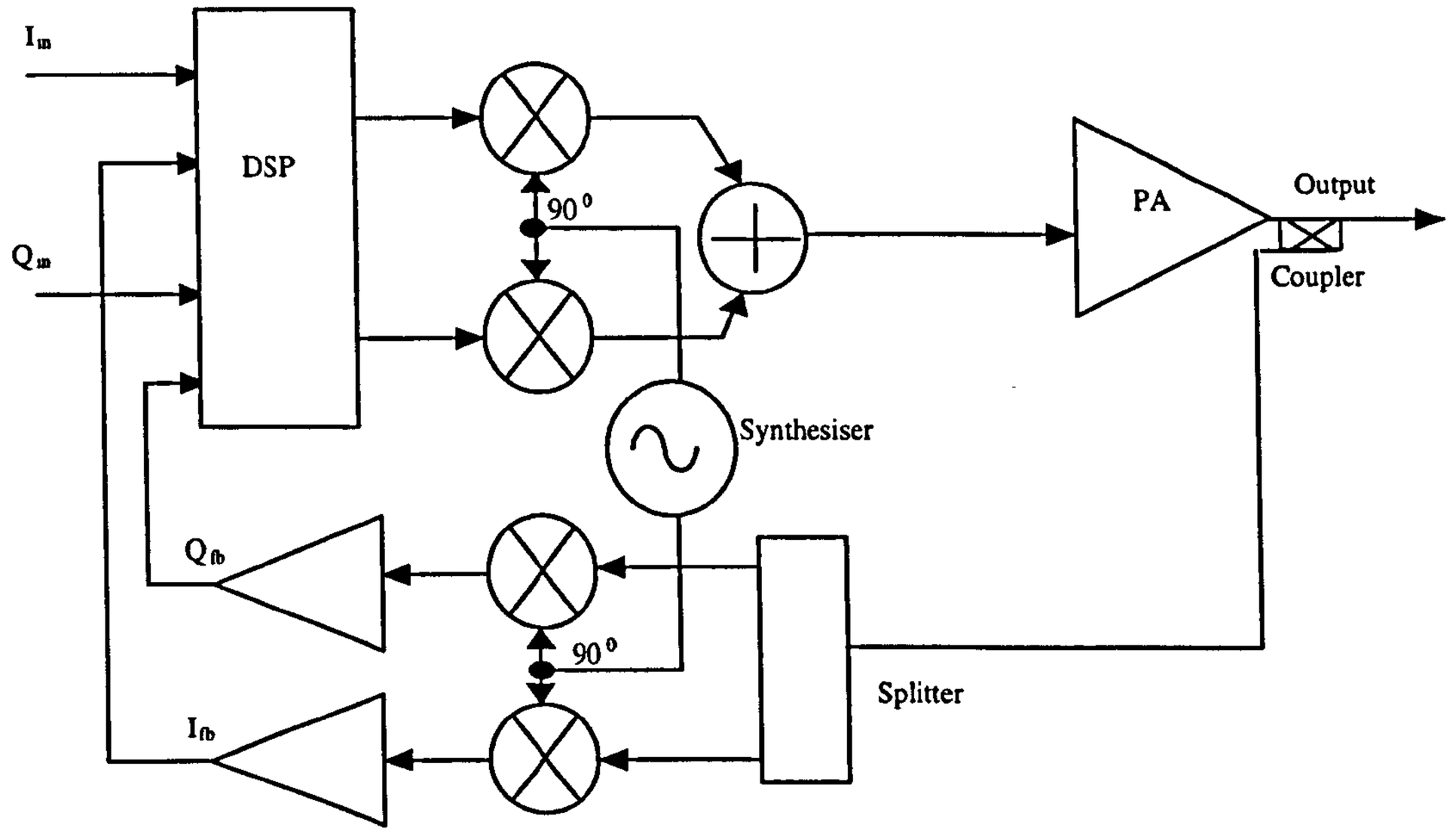

Figure 3..19: **Circuit diagram of an adaptive predistortion linearizer.**

intermodulation by means of modulation feedback. The polar loop transmitter uses an amplitude and phase correction as opposed to the I and Q quadrature information used in the cartesian feedback transmitter.

3.4.3.2 Adaptive Predistortion

The adaptive predistortion technique [138-140] as shown in figure 3.19, generates a predistorted baseband signal. This operation requires knowledge of the predistorter circuit. The distortion can be characterised during a sequence, which sends the baseband signal through a transmitter and then demodulates the RF signal down to the baseband frequency. From the feedback information, a predistorted baseband signal is generated for the corrected RF amplifier output [141]. The predistortion elements can be implemented using the DSP circuits that generate the transmit signal.

Predistortion circuits can be implemented in baseband by storing the predistor-

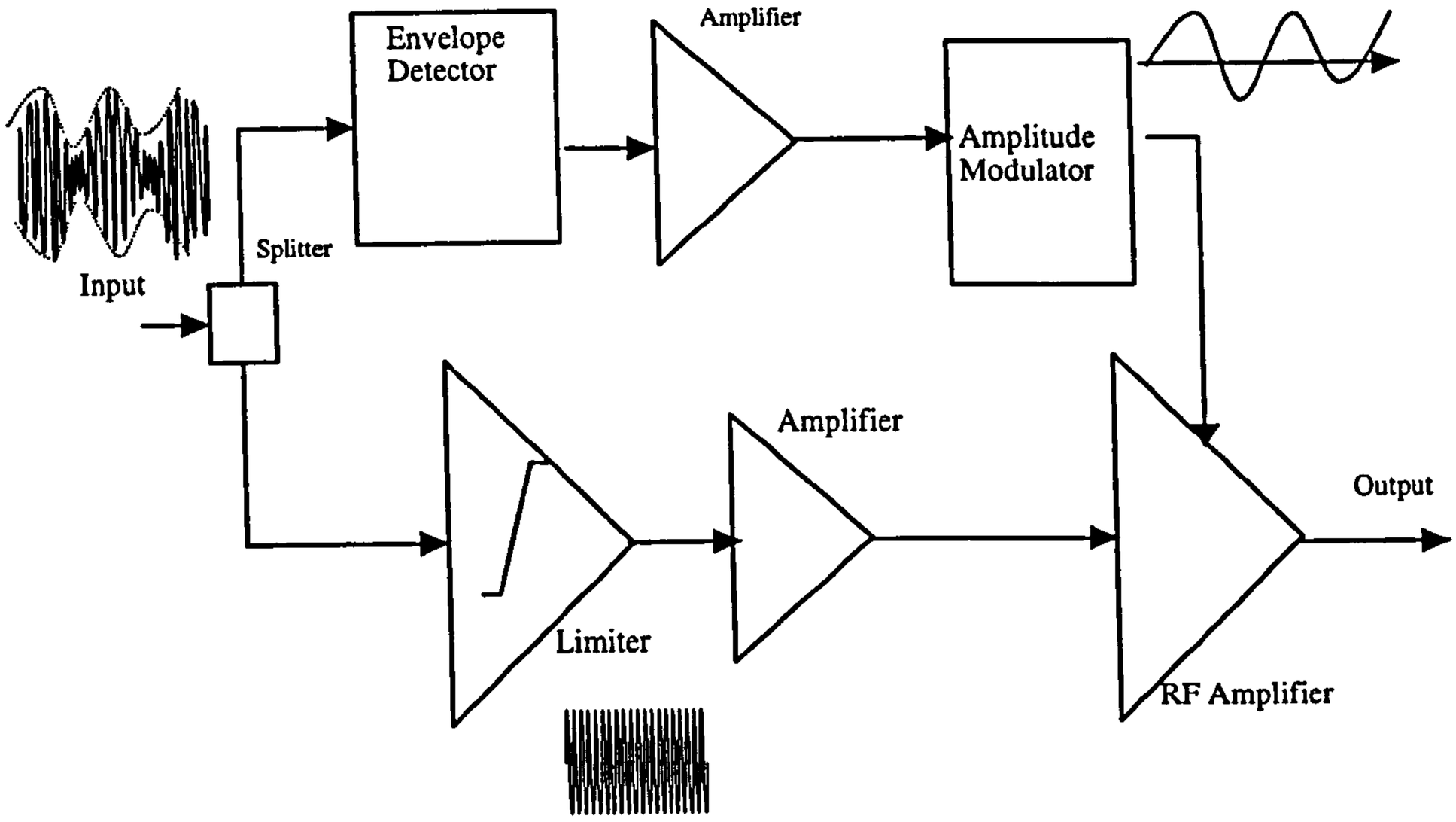

Figure 3..20: **Circuit diagram of the envelope elimination and restoration technique also called the Khan technique.**

tion elements using DSP circuits in order to predistort the input stage of the PA. An improvement of between $15dB$ to $25dB$ was demonstrated in an adaptive predistortion system [142,143]. The technique clearly requires a robust signal-processing algorithm to improve on the IMD reduction.

3.4.3.3 Envelope Elimination and Restoration

Introduced by Khan [144,145], the technique is independent of amplifier type. The modulated input signal is divided into two paths consisting of the phase and amplitude or envelope information as shown in figure 3.20. The phase modulation information is obtained by limiting the signal in a limiter, which enables the proper phase modulation of the original signal to be obtained. This signal is amplified in a class C, D, E or F amplifier with low distortion. In the other path, the signal envelope is detected, amplified and then processed by a modulator. The resulting signal is then used to

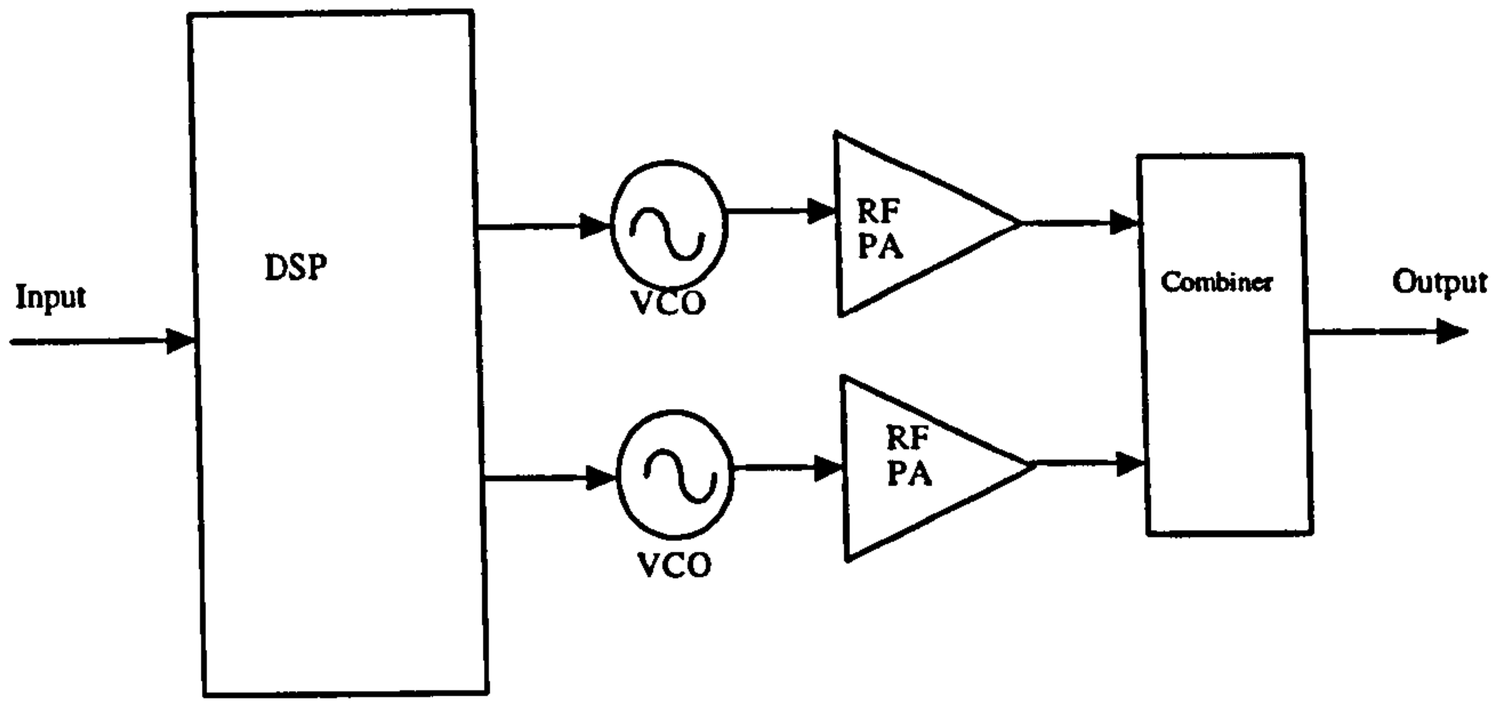

Figure 3..21: **Circuit diagram for a linear amplification using nonlinear amplifier transmitter (VCO=Voltage controlled Oscillator).**

modulate the amplified phase modulated component. The result of this is that a less distorted amplified version of the signal is obtained at the output. The scheme allows for the amplifiers to be used in saturation as both amplitude and phase information are amplified separately.

Although first implemented over half a century ago, the technique is becoming popular and can be implemented for use in a wide range of applications. Raab et al [146] have shown recently that intermodulation of -40 dBc can be achieved at saturation level with an efficiency of up to 56%.

3.4.3.4 Linear Amplification with Nonlinear Components

The linear amplification with nonlinear components (LINC) technique [147] provides a bandpass amplification with nonlinear components. A simple implementation of the technique is shown in Figure 3.21. The bandpass input signal is separated into two constant amplitude, phase modulated signals which are then amplified using high efficiency switching amplifiers (Class C, D, E or F) and the output of the two paths

are then combined to give an amplified replica of the input signal. The distortions engendered in both paths are made to be out of phase and therefore will cancel out. The signal component separator used at the input is a complex process that is required to produce a constant envelope signal and maintaining the phase and amplitude balance.

3.5 Discussion

A different approach for the reduction of IMD level in solid state power amplifiers (SSPA) is to combine the different existing techniques described in order to create a new and perhaps more powerful linearizer. The different techniques described earlier have various advantages and disadvantages discussed above, which depend on the application.

The techniques can be tailored and combined in stages for various applications with reduced IMD levels. McRory et al [117] have shown a combined feedback and feedforward circuit, although not classified as such, in which IMD level was reduced by an amount equal to the loop gain of the circuit. The reduction was in the order of $20dB$. The undesirable effects of one technique can be reduced or cancelled by another technique. Increases in some of these undesirable effects can occur as well.

The choice of a carefully tailored device and its use in a particular system will result in better performance overall. The careful study of the concentration of the channel doping profile was made as well as a careful selection of the bias point, which resulted in good overall performance on the IMD as the circuit was proven to be more linear than conventional circuits [79].

A dynamic bias on the drain with an envelope feedback on the gain was realised

and improvement of the intermodulation products was achieved [78]. However, there is clearly a need for further investigation into these techniques.

3.6 Conclusions

With the existing techniques discussed, the amplifier's nonlinear operations are improved, the effects of the nonlinearities although reduced, are still present and are causing the effects described above. The use of a good linearizer is important to the operation of communication systems. IMD needs to be cancelled by the use of linearizer. The design of the linearizer has to be done with consideration of the complexity of the circuit, which can only add to the cost.

The cancellation of IMD is generally achieved using the techniques presented by the interaction between the IMD signals in the MPA with an IMD signal generated. A new technique will be analysed which works with signals at higher frequencies (harmonic signals) as opposed to the techniques working in the vicinity of the IMD3 frequencies. An extension of the technique to the use of the difference frequency will be introduced, analysed and its performance evaluated.

In general, the use of a nonlinear device in the overall circuit is engendering harmonic and intermodulation products, which obviously need to be controlled. Most of the techniques rely on feeding signals at intermodulation frequencies with an inverse phase and the same amplitude into the amplifier in order to reduce the existing intermodulation.

CHAPTER 4.

SIGNAL INJECTION EFFECTS ON POWER AMPLIFIER IMD PERFORMANCE

4.1 Introduction

A system for the reduction of IMD in high frequency amplifiers is described. The technique uses the fundamental nonlinearity of the amplifier to generate the second harmonic of the original signal in order to cancel the existing IMD [73,74]. The second harmonic is injected into the device in order to cancel the third order IMD. In theory both second harmonics of the original signals at the frequencies $2f_1$ and $2f_2$ are injected into the amplifier together with the fundamental signals at the frequencies f_1 and f_2 for a two input system. The injection of the second harmonic with the appropriate phase and amplitude will in theory enable the cancellation of the third order IMD.

The technique was reported in the literature by Aichitson et al [73]. The technique was shown to reduce the IMD3 by $20dB$ in a two-tone test system with a MESFET Power amplifier. The analysis of the technique is extended to a multi-tone system in this report. It shows the limitation of the technique as it does not reduce all IMD3 in a multi-tone system. Generation of the second harmonic signal at the output of the amplifier is accompanied by other harmonics and intermodulation of the second order. Since intermodulation was reduced by a second order distortion (second harmonic signals), the technique is then further extended to the injection of new signals whose frequency is the sum of or the difference between the pair of fundamental signals. The present work shows that the new technique of difference frequency injection provides

better performance than the second harmonic injection technique (second order IMD). The combination of the second harmonic and the sum of the fundamental frequencies also provides adequate performance for IMD reduction. The analysis and simulated performances of all the techniques are presented in this chapter.

4.2 Theoretical Analysis of the Injection Techniques

Intermodulation can be attributed to the device's strong or mild nonlinearities. In the first case, the input and output signals are such that the waveform is clearly distorted by the high curvature of the I/V characteristics, and a high IMD is observed. In the second case, the signal is so low that the strong nonlinearities cannot be reached, and low level IMDs are generated. For small-signal intermodulation distortion behaviour, the MESFET I_{ds} current source is generally modelled as a third degree bi-dimensional power series, that should include terms dependent on V_{gs} and V_{ds} as well as cross terms. Usually in the analysis of intermodulation, the cross terms are considered to be zero in order to simplify the analysis. This simplification leads to only two separate nonlinear sources of IMD, one of which only dependent on V_{gs} and the other on V_{ds} [79,82].

In terms of the required Ids (Vgs, Vds) model extraction procedure, its parameter set is sometimes adjusted to match the I_{ds} which is measured at dc [34]. Its derivatives are more commonly adjusted by a least square polynomial to fit the ac measured transconductance for several values of V_{gs} and V_{ds}, dependent on the output conductance. I_{ds} is by far the most significant element of the FET circuit model that contributes to the nonlinear behaviour of the device.

In computer aided design (CAD) of circuits, the drain current needs to be mod-

elled by a mathematical equation which is simultaneously controlled by the intrinsic gate-source and drain-source voltages, V_{gs} and V_{ds}, respectively.

$$I_{ds} = f\left(V_{gs}, V_{ds}\right) \tag{4..1}$$

The nonlinearities of the device are often expressed by a power series in which the nonlinear element I_{ds} is considered dependent on two nonlinearities. Nonlinear elements such as the transconductance and the output conductance are associated with the change in drain-source current, which is a function of the gate-source voltage and the drain-source voltage.

For simplicity in the analysis, a single nonlinear element is used to model the IMD. The use of power series representation of the system gives a better characteristic of the system output. The power series is very often extended to the third order so as to derive the square law nonlinearity and the cubic law nonlinearities of the system.

4.2.1 Second Harmonic Injection Technique

Considering the two-tone case where the input signal, V_{in}, is a sum of two distinct sinusoid at the frequencies ω_1 and ω_2 with amplitudes A_{ω_1} and A_{ω_2} respectively, the input is expressed as

$$V_{in} = \sum_{n=1}^{2} \left(A_{\omega_n} \cos\left(\omega_n t\right)\right) = A_{\omega_1} \cos\left(\omega_1 t\right) + A_{\omega_2} \cos\left(\omega_2 t\right) \tag{4..2}$$

If the amplifier is modelled by the third order power series with the transconductance as the nonlinear element. The amplifier output can be expressed as

$$V_{out} = \sum_{k=1}^{3} g_{mk} V_{in}^{k} \tag{4..3}$$

In general $g_{mo} = 0$

The resulting signal at the output of the amplifier is given by

$$V_{out} = g_{m1}\left(A_{\omega_1}\cos(\omega_1 t) + A_{\omega_2}\cos(\omega_2 t)\right) + g_{m2}\left(A_{\omega_1}\cos(\omega_1 t) + A_{\omega_2}\cos(\omega_2 t)\right)^2$$
$$+ g_{m3}\left(A_{\omega_1}\cos(\omega_1 t) + A_{\omega_2}\cos(\omega_2 t)\right)^3 \tag{4..4}$$

The third order intermodulation term in the overall output expression at the frequency $(2\omega_1 - \omega_2)$ is

$$V_{out} = \tfrac{3}{4} g_{m3} A_{\omega_1}^2 A_{\omega_2}\cos(2\omega_1 - \omega_2)\, t \tag{4..5}$$

Similarly, at the frequency $(2\omega_2 - \omega_1)$, the signal is

$$V_{2\omega_2-\omega_1} = \tfrac{3}{4} g_{m3} A_{\omega_1} A_{\omega_2}^2\cos(2\omega_2 - \omega_1)\, t \tag{4..6}$$

The intermodulation signals at the frequencies $(2\omega_1 + \omega_2)$ and $(2\omega_2 + \omega_1)$ fall outside the band of interest and can easily be filtered out. These IM distortions will therefore be omitted from the analysis.

The injection of the second harmonic of the original fundamental signals is performed with the use of a multiplier, for harmonic generation, and a coupler, for injection into the PA. The second harmonic signal can be represented at the frequency $(2\omega_1)$ by the following expression

$$V_{2\omega_1} = A_{2\omega_1}\cos\left(2\omega_1 t + \phi_{2\omega_1}\right) \tag{4..7}$$

Where $A_{2\omega_1}$ is the amplitude of the sinusoid and $\phi_{2\omega_1}$ is the phase of the signal.

Similarly at the frequency $(2\omega_2)$, the second harmonic is defined by the following expression

$$V_{2\omega_1} = A_{2\omega_2}\cos\left(2\omega_2 t + \phi_{2\omega_2}\right) \tag{4..8}$$

Where $A_{2\omega_2}$ is the amplitude of the sinusoid and $\phi_{2\omega_2}$ is the phase of the signal.

The second harmonics of the signals are injected into the amplifier together with the fundamental signals. The input signal of the amplifier is then

$$V_{in} = \sum_{n=1}^{2} \left(A_{\omega_n} \cos\left(\omega_n t\right)\right) + \sum_{n=1}^{2} \left(A_{2\omega_n} \cos\left(2\omega_n t + \phi_{2\omega_n}\right)\right) \tag{4..9}$$

The output consists of a large number of signals at various frequencies. The interaction of the fundamental signals and the injected signals within the device through the electron mobility results in the generation of more signals at harmonic and intermodulation frequencies.

Amongst the signals generated by the injection of the second harmonic, the third order intermodulation at the frequencies $(2\omega_1 - \omega_2)$ and $(2\omega_2 - \omega_1)$ are of particular interest. At the frequency $(2\omega_1 - \omega_2)$, the signal is

$$\begin{aligned} V_{2\omega_1-\omega_2} = {} & \tfrac{3}{4} g_{m3} A_{\omega_1}^2 A_{\omega_2} \cos\left(2\omega_1 t - \omega_2 t\right) + g_{m2} A_{2\omega_1} A_{\omega_2} \cos\left(2\omega_1 t - \omega_2 t + \phi_{2\omega_1}\right) \\ & + \tfrac{3}{2} g_{m3} A_{\omega_2} A_{2\omega_1} A_{2\omega_2} \cos\left(2\omega_1 t - \omega_2 t + \phi_{2\omega_1} - \phi_{2\omega_2}\right) \end{aligned} \tag{4..10}$$

At the frequency $(2\omega_2 - \omega_1)$, the signal is:

$$\begin{aligned} V_{2\omega_2-\omega_1} = {} & \tfrac{3}{4} g_{m3} A_{\omega_1} A_{\omega_2}^2 \cos\left(2\omega_2 t - \omega_1 t\right) + g_{m2} A_{\omega_1} A_{2\omega_2} \cos\left(2\omega_2 t - \omega_1 t + \phi_{2\omega_2}\right) \\ & + \tfrac{3}{2} g_{m3} A_{\omega_1} A_{2\omega_1} A_{2\omega_2} \cos\left(2\omega_2 t - \omega_1 t + \phi_{2\omega_2} - \phi_{2\omega_1}\right) \end{aligned} \tag{4..11}$$

For cancellation of the intermodulation terms, the expression of the signals at the frequencies $(2\omega_1 - \omega_2)$ and $(2\omega_2 - \omega_1)$ must be equal to zero. This implies that for a two input system with a second harmonic injection, equation 4.10 and equation 4.11 must be zero.

For cancellation of the third order intermodulation at $(2\omega_2 - \omega_1)$, the following equation must be solved

$$\begin{aligned} &\tfrac{3}{4} g_{m3} A_{\omega_1} A_{\omega_2}^2 \cos(2\omega_2 t - \omega_1 t) + g_{m2} A_{\omega_1} A_{2\omega_2} \cos(2\omega_2 t - \omega_1 t + \phi_{2\omega_2}) \\ &+ \tfrac{3}{2} g_{m3} A_{\omega_1} A_{2\omega_1} A_{2\omega_2} \cos(2\omega_2 t - \omega_1 t + \phi_{2\omega_2} - \phi_{2\omega_1}) = 0 \end{aligned} \tag{4..12}$$

The above equation can be simplified by the fact that the third term in the equation is very small in comparison to the other terms and can therefore be omitted. The above equation then simplifies to

$$\tfrac{3}{4} g_{m3} A_{\omega_1} A_{\omega_2}^2 \cos(2\omega_2 t - \omega_1 t) + g_{m2} A_{\omega_1} A_{2\omega_2} \cos(2\omega_2 t - \omega_1 t + \phi_{2\omega_2}) = 0 \tag{4..13}$$

Which translates into the following conditions

$$A_{2\omega_2} = \tfrac{3}{4} \frac{A_{\omega_2}^2 g_{m3}}{g_{m2}} \qquad |\phi_{2\omega_2}| = 180^\circ \tag{4..14}$$

In a similar manner to the above, the conditions for the cancellations of the IMD at the frequency $(2\omega_1 - \omega_2)$ are found to be;

$$A_{2\omega_1} = \tfrac{3}{4} \frac{A_{\omega_1}^2 g_{m3}}{g_{m2}} \qquad |\phi_{2\omega_1}| = 180^\circ \tag{4..15}$$

These conditions will allow a reduction in the level of third order IMD. This can be achieved if the phase $\phi_{2\omega_1}$ and $\phi_{2\omega_2}$ and the amplitude $A_{2\omega_1}$ and $A_{2\omega_1}$ of the second harmonic are appropriately chosen.

For an two tone test with input signal power of $1W$ and assuming that $g_{m2} \simeq 0.06$ and $g_{m3} \simeq 0.016$ for the device use, the second order harmonic signal power will be $112.5mW$ which is $9.5dB$ down on the main signal.

In a three-tone case, the input signal consists of three distinct sinusoidal signals

at the frequencies ω_1, ω_2 and ω_3 of amplitude $A\omega_1$, $A\omega_2$ and $A\omega_3$, respectively.

$$V_{in} = \sum_{n=1}^{3} (A_{\omega_n} \cos(\omega_n t)) = A_{\omega_1} \cos(\omega_1 t) + A_{\omega_2} \cos(\omega_2 t) + A_{\omega_3} \cos(\omega_3 t) \qquad (4..16)$$

Substitution of equation (4.16) into equation (4.3) gives all the relevant frequency components at the output of the amplifier. The number of intermodulation products of the first kind (product of form $(2\omega_m \pm \omega_n)$, with n and m integers representing the different frequencies at the input) has risen to 6. These products generated by the interaction between the fundamental frequencies ω_1, ω_2 and ω_3, are.

$$V_{2\omega_m \pm \omega_n} = \tfrac{3}{4} g_{m3} \left(\begin{array}{l} A_{\omega_1}^2 A_{\omega_2} \cos(2\omega_1 - \omega_2)\, t + A_{\omega_1}^2 A_{\omega_2} \cos(2\omega_1 + \omega_2)\, t \\ + A_{\omega_1} A_{\omega_2}^2 \cos(2\omega_2 - \omega_1)\, t + A_{\omega_1} A_{\omega_2}^2 \cos(2\omega_2 + \omega_1)\, t \\ + A_{\omega_1}^2 A_{\omega_3} \cos(2\omega_1 - \omega_3)\, t + A_{\omega_1}^2 A_{\omega_3} \cos(2\omega_1 + \omega_3)\, t \\ + A_{\omega_1} A_{\omega_3}^2 \cos(2\omega_3 - \omega_1)\, t + A_{\omega_1} A_{\omega_3}^2 \cos(2\omega_3 + \omega_1)\, t \\ + A_{\omega_2}^2 A_{\omega_3} \cos(2\omega_2 - \omega_3)\, t + A_{\omega_2}^2 A_{\omega_3} \cos(2\omega_2 + \omega_3)\, t \\ + A_{\omega_2} A_{\omega_3}^2 \cos(2\omega_3 - \omega_2)\, t + A_{\omega_2} A_{\omega_3}^2 \cos(2\omega_3 + \omega_2)\, t \end{array} \right) \qquad (4..17)$$

The frequencies of the form $(2\omega_m + \omega_n)$ are not of interest as these intermodulation products fall outside the band of interest and can be filtered if the difference frequency of the input tone is large (valid for less than one octave bandwidth). The analysis concentrates on the inband IMD3 product of the form $(2\omega_m - \omega_n)$. The expression of the signal at the frequency $(2\omega_1 - \omega_2)$ is

$$V_{2\omega_1 - \omega_2} = \tfrac{3}{4} g_{m3} A_{\omega_1}^2 A_{\omega_2} \cos(2\omega_1 - \omega_2)\, t \qquad (4..18)$$

At the frequency $(2\omega_1 - \omega_3)$, the signal is

$$V_{2\omega_1 - \omega_3} = \tfrac{3}{4} g_{m3} A_{\omega_1}^2 A_{\omega_3} \cos(2\omega_1 - \omega_3)\, t \qquad (4..19)$$

Similarly the expression for the other IMD products $(2\omega_2 - \omega_1)$, $(2\omega_2 - \omega_3)$, $(2\omega_3 - \omega_1)$ and $(2\omega_3 - \omega_2)$ are of the same form.

The use of three input signals also generates (as previously mentioned in chapter 3) a second kind of IMD (product of the form $(\omega_m + \omega_n - \omega_q)$, with m, n and q integers representing the different frequencies at the input). These are very different from the first kind. The expression of the second kinds of IMD3 generated is

$$V_{\omega_m \pm \omega_n \pm \omega_q} = \frac{3}{2} g_{m3} \left(\begin{array}{c} A_{\omega_1} A_{\omega_2} A_{\omega_3} \cos(\omega_3 + \omega_2 - \omega_1)\, t + A_{\omega_1} A_{\omega_2} A_{\omega_3} \cos(\omega_1 + \omega_2 - \omega_3)\, t \\ + A_{\omega_1} A_{\omega_2} A_{\omega_3} \cos(\omega_1 - \omega_2 + \omega_3)\, t + A_{\omega_1} A_{\omega_2} A_{\omega_3} \cos(\omega_1 + \omega_2 + \omega_3)\, t \end{array} \right) \tag{4..20}$$

The third order signal at the frequencies $(\omega_1 + \omega_2 - \omega_3)$, $(\omega_1 - \omega_2 + \omega_3)$, and $(\omega_2 - \omega_1 + \omega_3)$ fall in the amplifier operating bandwidth and can not be filtered. The signal at the frequency $(\omega_1 + \omega_2 + \omega_3)$ falls outside the bandwidth of interest and can be easily filtered. It is therefore omitted from the analysis.

The expression of the signal associated with the second kind of IMD at the frequency $(\omega_1 + \omega_2 - \omega_3)$, is

$$V_{\omega_1 + \omega_2 - \omega_3} = \frac{3}{2} g_{m3} \left(A_{\omega_1} A_{\omega_2} A_{\omega_3} \cos(\omega_1 + \omega_2 - \omega_3)\, t \right) \tag{4..21}$$

The expressions associated with the other IMD3 products $(\omega_1 - \omega_2 + \omega_3)$ and $(\omega_3 + \omega_2 - \omega_1)$ are similar.

The system is injected with the second harmonic of the fundamental signals $(2\omega_1)$, $(2\omega_2)$ and $(2\omega_3)$ with phases $\phi_{2\omega_1}, \phi_{2\omega_2}$and $\phi_{2\omega_3}$ and amplitude $A_{2\omega_1}, A_{2\omega_2}$ and $A_{2\omega_3}$ respectively, together with the fundamental signals ω_1, ω_2 and ω_3.

The input signal of the system is

$$V_{in} = \sum_{n=1}^{3} \left(A_{\omega_n} \cos\left(\omega_n t\right)\right) + \sum_{n=1}^{3} \left(A_{2\omega_n} \cos\left(2\omega_n t + \phi_{2\omega_n}\right)\right) \qquad (4..22)$$

Substitution of equation (4.22) into equation (4.3) gives all the relevant frequency components at the output of the amplifier. The injection of the second harmonic has generated additional signals at the same frequencies as those of equation 4.17.

The output expression of the IMD3 at the frequency $(2\omega_1 - \omega_2)$, is

$$\begin{aligned} V_{2\omega_1-\omega_2} = {} & g_{m2} A_{2\omega_1} A_{\omega_2} \cos\left(2\omega_1 t - \omega_2 t + \phi_{2\omega_1}\right) + \tfrac{3}{4} g_{m3} A_{\omega_1}^2 A_{\omega_2} \cos\left(2\omega_1 t - \omega_2 t\right) \\ & + \tfrac{3}{2} g_{m3} A_{\omega_2} A_{2\omega_1} A_{2\omega_2} \cos\left(2\omega_1 t - \omega_2 t + \phi_{2\omega_1} - \phi_{2\omega_2}\right) \end{aligned} \qquad (4..23)$$

The output expression of the IMD3 at the frequency $(2\omega_2 - \omega_1)$, is

$$\begin{aligned} V_{2\omega_2-\omega_1} = {} & g_{m2} A_{\omega_1} A_{2\omega_2} \cos\left(2\omega_2 t - \omega_1 t + \phi_{2\omega_2}\right) + \tfrac{3}{4} g_{m3} A_{\omega_1} A_{\omega_2}^2 \cos\left(2\omega_2 t - \omega_1 t\right) \\ & + \tfrac{3}{2} g_{m3} A_{\omega_1} A_{2\omega_1} A_{2\omega_2} \cos\left(2\omega_2 t - \omega_1 t + \phi_{2\omega_2} - \phi_{2\omega_1}\right) \end{aligned} \qquad (4..24)$$

The output expression of the IMD3 at these frequencies is the same as previously calculated in the two-tone case. This implies that if the phase and amplitude of the second harmonic signals were appropriately chosen, it would result in a cancellation of the IMD3 products. Similar expressions are found for the other first kind of IMDs.

For the cancellation of third order intermodulation, the second kind of third order IMD generated by the three input signals, needs to be investigated. The output of the system at these frequencies does not change and no other signals are generated at these frequencies.

The expression of the signal at the frequency $(\omega_1 + \omega_2 - \omega_3)$, is:

$$V_{\omega_1+\omega_2-\omega_3} = \tfrac{3}{2} g_{m3\omega_1} A_{\omega_1} A_{\omega_2} A_{\omega_3} \cos(\omega_1 + \omega_2 - \omega_3)\, t \qquad (4..25)$$

This is the same as observed in equation 4.21, without the injection of the second harmonic signals. The expression also remains unchanged for the other second kind of IMDs at the frequencies $(\omega_1 - \omega_2 + \omega_3)$ and $(\omega_3 + \omega_2 - \omega_1)$.

This suggests that the injection of the second harmonic does not introduce additional signals, and therefore will not result in the cancellation of the second kind of third order IMDs. The study of the third order IMD product cancellation by the injection of the second harmonic using the simplified method of power series in a three-tone system gives a better understanding of the IM behaviour of the system. From the above analytical results, it is clear that the injection of the second harmonic will not introduce a reduction in the second kind of IMD3 amplitude level but only in the amplitude of the first kind of IMD3.

The cancellation of IMD3 in the amplifier is provided by the mechanism of interaction between the injected signals and the original signals. The above analysis shows that the injection of the second harmonic signal $(2\omega_1)$ into the amplifier interact with the fundamental signals ω_1 and ω_2 and causes the generation of extra IMD terms at the frequencies $(2\omega_1 - \omega_2)$ and $(2\omega_1 - \omega_3)$, through a power series expansion of the second order term. The injected second harmonic signal $(2\omega_2)$ interacts with the fundamental signals ω_1 and ω_3 and generates of extra IMD terms at the frequencies $(2\omega_2 - \omega_1)$ and $(2\omega_2 - \omega_3)$. The signal $(2\omega_1)$ behaves in a similar way and generates extra terms at the frequencies $(2\omega_3 - \omega_1)$ and $(2\omega_3 - \omega_1)$. This analysis clearly shows that the

cancellation of all first kind of IMD3 requires the injection of all second harmonics of the original signals. The cancellation of the second kind of IMD3 can not occur since no extra terms are generated at the frequencies $(\omega_1 + \omega_2 - \omega_3)$, $(\omega_1 - \omega_2 + \omega_3)$ and $(\omega_3 + \omega_2 - \omega_1)$.

The evaluation of the IMD products in a two input system predicts the IMD behaviour of the system and gives some hints to the system performance. However, it does not fully enable a clear understanding of the overall effect of the IMD for multitone input signals. The use of more than two input signals generates a lot more IMD products at different frequencies with different amplitudes and gives rise to a more complex behaviour.

In order to understand and appreciate the process of cancellation and see the difference between the effects in the two-tone and the three-tone systems, simulations of both type of systems need to be performed and compared. The first kind and the second kind of third order IMDs are not of the same amplitude and do not behave in the same manner and therefore need to be analysed differently.

4.2.2 Difference Frequency Injection Technique

The work presented here is an extension of the previous method and is based on the injection of signals, whose frequency is the difference in frequency between a pair of fundamental signals. In order to analyse the system performance, the difference frequency signal is injected into the system together with the fundamental signals.

In a two-tone test, the input of the amplifier is made up of the injected signal at the frequency $(\omega_2 - \omega_1)$ with amplitude $A_{\omega_{21}}$ and phase, $\phi_{\omega_{21}}$, as well as the fundamental

signals ω_2, and ω_1 with amplitudes A_{ω_1} and A_{ω_2}, respectively. The input signal of the amplifier is expressed as

$$V_{in} = \sum_{n=1}^{2} \left(A_{\omega_n} \cos\left(\omega_n t\right)\right) + A_{\omega_{21}} \cos\left(\omega_2 t - \omega_1 t + \phi_{\omega_{21}}\right) \qquad (4..26)$$

Substitution of equation 4.26 into equation 4.3 gives all the relevant frequency components at the output of the amplifier.

The interactions between the original signals and the difference frequency signal injected result in additional signals at the output. Amongst the signals generated by the injection of the difference frequency, the third order intermodulation at the frequencies of $(2\omega_1 - \omega_2)$ and $(2\omega_2 - \omega_1)$ are of interest. The expression for all third order IMD of the form $(2\omega_m \pm \omega_n)$ is

$$\begin{aligned} V_{2\omega_m \pm \omega_n} = {} & g_{m2} A_{\omega_1} A_{\omega_{21}} \cos\left(2\omega_1 t - \omega_2 t - \phi_{\omega_{21}}\right) + g_{m2} A_{\omega_2} A_{\omega_{21}} \cos\left(2\omega_2 t - \omega_1 t + \phi_{\omega_{21}}\right) \\ & + \tfrac{3}{4} g_{m3} A_{\omega_1}^2 A_{\omega_2} \cos\left(2\omega_1 t - \omega_2 t\right) + \tfrac{3}{4} g_{m3} A_{\omega_1}^2 A_{\omega_2} \cos\left(2\omega_1 t + \omega_2 t\right) \\ & + \tfrac{3}{4} g_{m3} A_{\omega_1} A_{\omega_2}^2 \cos\left(2\omega_2 t - \omega_1 t\right) + \tfrac{3}{4} g_{m3} A_{\omega_1} A_{\omega_2}^2 \cos\left(2\omega_2 t + \omega_1 t\right) \\ & + \tfrac{3}{4} g_{m3} A_{\omega_1} A_{\omega_{21}}^2 \cos\left(2\omega_2 t - \omega_1 t + 2\phi_{\omega_{21}}\right) + \tfrac{3}{4} g_{m3} A_{\omega_2} A_{\omega_{21}}^2 \cos\left(2\omega_1 t - \omega_2 t + 2\phi_{\omega_{21}}\right) \end{aligned} \qquad (4..27)$$

From the above equation, the signal at the frequency $(2\omega_1 - \omega_2)$, is expressed as

$$\begin{aligned} V_{2\omega_1 - \omega_2} = {} & g_{m2} A_{\omega_1} A_{\omega_{21}} \cos\left(2\omega_1 t - \omega_2 t - \phi_{\omega_{21}}\right) + \tfrac{3}{4} g_{m3} A_{\omega_1}^2 A_{\omega_2} \cos\left(2\omega_1 t - \omega_2 t\right) \\ & + \tfrac{3}{4} g_{m3} A_{\omega_2} A_{\omega_{21}}^2 \cos\left(2\omega_1 t - \omega_2 t + 2\phi_{\omega_{21}}\right) \end{aligned} \qquad (4..28)$$

At the frequency $(2\omega_2 - \omega_1)$, the expression is:

$$\begin{aligned} V_{2\omega_2 - \omega_1} = {} & g_{m2} A_{\omega_2} A_{\omega_{21}} \cos\left(2\omega_2 t - \omega_1 t + \phi_{\omega_{21}}\right) + \tfrac{3}{4} g_{m3} A_{\omega_1} A_{\omega_2}^2 \cos\left(2\omega_2 t - \omega_1 t\right) \\ & + \tfrac{3}{4} g_{m3} A_{\omega_1} A_{\omega_{21}}^2 \cos\left(2\omega_2 t - \omega_1 t + 2\phi_{\omega_{21}}\right) \end{aligned} \qquad (4..29)$$

For complete cancellation of the intermodulation terms, the expression of the signals at the frequencies $(2\omega_1 - \omega_2)$ and $(2\omega_2 - \omega_1)$ must be equal to zero. This implies that for a two input system with an injection of the difference frequency, the expression of the third order IM of equation 4.28 and equation 4.29 must be zero.

At the frequency $(2\omega_2 - \omega_1)$, the following equation is obtained

$$\begin{aligned} & g_{m2} A_{\omega 2} A_{\omega 21} \cos\left(2\omega_2 t - \omega_1 t + \phi_{\omega 21}\right) + \tfrac{3}{4} g_{m3} A_{\omega 1} A_{\omega 2}^2 \cos\left(2\omega_2 t - \omega_1 t\right) \\ & + \tfrac{3}{4} g_{m3} A_{\omega 1} A_{\omega 21}^2 \cos\left(2\omega_2 t - \omega_1 t + 2\phi_{\omega 21}\right) = 0 \end{aligned} \tag{4..30}$$

The function exhibits a minimum for particular values of $A_{2\omega_1}$ and $\phi_{2\omega_1}$ of the injected signals. This implies that an appropriate choice of phase and amplitude of the injected signals will reduce the third order intermodulations. Similar conditions are found for the cancellation of the other IMD3 at the frequency $(2\omega_1 - \omega_2)$

Consider a three tone input signal consisting of three distinct sinusoidal signals at the frequencies ω_1, ω_2 and ω_3 of amplitudes A_{ω_1}, A_{ω_2} and A_{ω_3} respectively. The system is injected with signals whose frequencies are the difference in frequencies of the pairs of fundamental signals. The injected signals are at the frequencies $(\omega_2 - \omega_1)$, $(\omega_3 - \omega_2)$ and $(\omega_3 - \omega_1)$ with different phases $\phi_{\omega_{21}}$, $\phi_{\omega_{32}}$ and $\phi_{\omega_{31}}$ and amplitudes $A_{\omega_{21}}$, $A_{\omega_{32}}$ and $A_{\omega_{31}}$, respectively.

The input signal of the system is

$$\begin{aligned} V_{in} = & \sum_{n=1} \left(A_{\omega_n} \cos\left(\omega_n t\right)\right) + A_{\omega_{21}} \cos\left(\omega_2 t - \omega_1 t + \phi_{\omega_{21}}\right) \\ & + A_{\omega_{32}} \cos\left(\omega_3 t - \omega_2 t + \phi_{\omega 32}\right) + A_{\omega_{31}} \cos\left(\omega_3 t - \omega_1 t + \phi_{\omega_{31}}\right) \end{aligned} \tag{4..31}$$

Substitution of equation 4.31 into equation 4.3 gives all the relevant frequency components at the output of the amplifier. The injection of the second harmonic has generated additional IMD3 signals at the same frequencies as those of equation 4.17.

The output signal at the frequency $(2\omega_1 - \omega_2)$ is

$$\begin{aligned} V_{2\omega_1-\omega_2} &= g_{m2}A_{\omega_1}A_{\omega_{21}}\cos\left(2\omega_1 t - \omega_2 t + \phi_{\omega_{21}}\right) \\ &+\tfrac{3}{4}g_{m3}A_{\omega_1}^2 A_{\omega_2}\cos\left(2\omega_1 t - \omega_2 t\right) \\ &+\tfrac{3}{4}g_{m3}A_{\omega_2}A_{\omega_{21}}\cos\left(2\omega_1 t - \omega_2 t + 2\phi_{\omega_{21}}\right) \\ &+\tfrac{3}{2}g_{m3}A_{\omega_3}A_{\omega_{21}}A_{\omega_{31}}\cos\left(2\omega_1 t - \omega_2 t - \phi_{\omega_{21}} - \phi_{\omega_{31}}\right) \\ &+\tfrac{3}{2}g_{m3}A_{\omega_1}A_{\omega_{31}}A_{\omega_{32}}\cos\left(2\omega_1 t - \omega_2 t - \phi_{\omega_{31}} + \phi_{\omega_{32}}\right) \end{aligned} \tag{4..32}$$

Similarly, the output signal at the frequency $(2\omega_2 - \omega_1)$ is

$$\begin{aligned} V_{2\omega_2-\omega_1} &= g_{m2}A_{\omega_2}A_{\omega_{21}}\cos\left(2\omega_2 t - \omega_1 t + \phi_{\omega_{21}}\right) \\ &+\tfrac{3}{4}g_{m3}A_{\omega_1}A_{\omega_2}^2\cos\left(2\omega_2 t - \omega_1 t\right) \\ &+\tfrac{3}{4}g_{m3}A_{\omega_1}A_{\omega_{21}}\cos\left(2\omega_2 t - \omega_1 t + 2\phi_{\omega_{21}}\right) \\ &+\tfrac{3}{2}g_{m3}A_{\omega_3}A_{\omega_{21}}A_{\omega_{32}}\cos\left(2\omega_2 t - \omega_1 t + \phi_{\omega_{21}} - \phi_{\omega_{32}}\right) \\ &+\tfrac{3}{2}g_{m3}A_{\omega_2}A_{\omega_{31}}A_{\omega_{32}}\cos\left(2\omega_2 t - \omega_1 t + \phi_{\omega_{21}} - \phi_{\omega_{32}}\right) \end{aligned} \tag{4..33}$$

The expression of the signal at the frequency $(2\omega_1 - \omega_2)$ in equation 4.32 shows that four additional terms are generated by the injection of the difference frequency. The phase and amplitude of the injected difference frequencies determine the amplitude and the phase of these new terms. If the phases and amplitudes of the injected difference frequency signals were appropriately chosen, it will result in a cancellation of the IMD products. A correct choice of phase and amplitude causes the expression of the third order IMDs in equation 4.32 and equation 4.33 to cancel each other. The cancellation of the other IMD signals at the frequencies $(2\omega_2 - \omega_1)$, $(2\omega_2 - \omega_3)$, $(2\omega_1 - \omega_3)$, $(2\omega_3 - \omega_2)$ and $(2\omega_3 - \omega_1)$ will occur in a similar manner as for the signal at the frequency $(2\omega_1 - \omega_2)$.

The injection of the difference frequency signals generates additional IMD3 terms of the second kind.

The expression of the signal at the frequency $(\omega_1 + \omega_2 - \omega_3)$, is

$$V_{\omega_1+\omega_2-\omega_3} = g_{m2}A_{\omega_2}A_{\omega_{31}}\cos\left(\omega_1 t + \omega_2 t - \omega_3 t - \phi_{\omega_{31}}\right)$$

$$+g_{m2}A_{\omega_1}A_{\omega_{32}}\cos\left(\omega_1 t + \omega_2 t - \omega_3 t - \phi_{\omega_{32}}\right)$$

$$+\tfrac{3}{2}g_{m3}A_{\omega_1}A_{\omega_2}A_{\omega_3}\cos\left(\omega_1 t + \omega_2 t - \omega_3 t\right)$$

$$+\tfrac{3}{2}g_{m3}A_{\omega_1}A_{\omega_{21}}A_{\omega_{31}}\cos\left(\omega_1 t + \omega_2 t - \omega_3 t + \phi_{\omega_{21}} + \phi_{\omega_{31}}\right)$$

$$+\tfrac{3}{2}g_{m3}A_{\omega_2}A_{\omega_{21}}A_{\omega_{32}}\cos\left(\omega_1 t + \omega_2 t - \omega_3 t - \phi_{\omega_{21}} - \phi_{\omega_{32}}\right)$$

$$+\tfrac{3}{2}g_{m3}A_{\omega_3}A_{\omega_{31}}A_{\omega_{32}}\cos\left(\omega_1 t + \omega_2 t - \omega_3 t + \phi_{\omega_{31}} - \phi_{\omega_{32}}\right) \quad (4..34)$$

The expression of the signal at the frequency $(\omega_1 - \omega_2 + \omega_3)$, is

$$V_{\omega_1-\omega_2+\omega_3} = g_{m2}A_{\omega_3}A_{\omega_{21}}\cos\left(\omega_1 t - \omega_2 t + \omega_3 t - \phi_{\omega_{21}}\right)$$

$$+g_{m2}A_{\omega_1}A_{\omega_{32}}\cos\left(\omega_1 t - \omega_2 t + \omega_3 t - \phi_{\omega_{32}}\right)$$

$$+\tfrac{3}{2}g_{m3}A_{\omega_1}A_{\omega_2}A_{\omega_3}\cos\left(\omega_1 t - \omega_2 t + \omega_3 t\right)$$

$$+\tfrac{3}{2}g_{m3}A_{\omega_1}A_{\omega_{21}}A_{\omega_{31}}\cos\left(\omega_1 t - \omega_2 t + \omega_3 t - \phi_{\omega_{21}} + \phi_{\omega_{31}}\right)$$

$$+\tfrac{3}{2}g_{m3}A_{\omega_2}A_{\omega_{21}}A_{\omega_{32}}\cos\left(\omega_1 t - \omega_2 t + \omega_3 t - \phi_{\omega_{21}} + \phi_{\omega_{32}}\right)$$

$$+\tfrac{3}{2}g_{m3}A_{\omega_3}A_{\omega_{31}}A_{\omega_{32}}\cos\left(\omega_1 t - \omega_2 t + \omega_3 t - \phi_{\omega_{31}} + \phi_{\omega_{32}}\right) \quad (4..35)$$

The expression of the signal at the frequency $(\omega_3 + \omega_2 - \omega_1)$, is

$$V_{\omega_3+\omega_2-\omega_1} = g_{m2}A_{\omega_3}A_{\omega_{21}}\cos\left(\omega_3 t + \omega_2 t - \omega_1 t + \phi_{\omega_{21}}\right)$$

$$+g_{m2}A_{\omega_2}A_{\omega_{31}}\cos\left(\omega_3 t + \omega_2 t - \omega_1 t + \phi_{\omega_{31}}\right)$$

$$+\tfrac{3}{2}g_{m3}A_{\omega_1}A_{\omega_2}A_{\omega_3}\cos\left(\omega_3 t + \omega_2 t - \omega_1 t\right)$$

$$+\tfrac{3}{2}g_{m3}A_{\omega_1}A_{\omega_{21}}A_{\omega_{31}}\cos\left(\omega_3 t + \omega_2 t - \omega_1 t + \phi_{\omega_{21}} + \phi_{\omega_{31}}\right)$$

$$+\tfrac{3}{2}g_{m3}A_{\omega_2}A_{\omega_{21}}A_{\omega_{32}}\cos\left(\omega_3 t + \omega_2 t - \omega_1 t + \phi_{\omega_{21}} + \phi_{\omega_{32}}\right)$$

$$+\tfrac{3}{2}g_{m3}A_{\omega_3}A_{\omega_{31}}A_{\omega_{32}}\cos\left(\omega_3 t + \omega_2 t - \omega_1 t - \phi_{\omega_{31}} - \phi_{\omega_{32}}\right) \quad (4..36)$$

The injection of the difference frequency signals at the frequencies $(\omega_1 - \omega_2)$, $(\omega_1 - \omega_2)$ and $(\omega_1 - \omega_2)$ leads to interaction with the fundamental signals ω_1, ω_2 and ω_3 to generate extra IMD3 terms at the frequencies $(2\omega_2 - \omega_1)$, $(2\omega_1 - \omega_2)$, $(2\omega_2 - \omega_3)$, $(2\omega_1 - \omega_3)$, $(2\omega_3 - \omega_2)$ and $(2\omega_3 - \omega_1)$ resulting in the reduction of the first kind of IMD3. The technique does also generate extra IMD3 terms at the frequencies $(\omega_1 - \omega_2 + \omega_3)$, $(\omega_1 - \omega_3 + \omega_2)$ and $(\omega_3 - \omega_1 + \omega_2)$. A careful choice of the amplitudes $A\omega_{21}$, $A\omega_{32}$ and $A\omega_{31}$ and phases $\phi\omega_{21}$, $\phi\omega_{32}$ and $\phi\omega_{31}$ of the injected signals in equation 4.31 will result in the cancellation of all third order intermodulations. Equation 4.34, equation 4.35 and equation 4.36 shows that it exhibits a minimum for specific values of the injected signal amplitudes $A\omega_{21}$, $A\omega_{32}$ and $A\omega_{31}$ and phases $\phi\omega_{21}$, $\phi\omega_{32}$ and $\phi\omega_{31}$. If the input tone are of the same amplitude and same phase ($A\omega_{21} = A\omega_{32} = A\omega_{31}$ and $\phi\omega_{21} = \phi\omega_{32} = \phi\omega_{31}$), equation 4.34, equation 4.35 and equation 4.36 have two variables instead of six and the evaluation of these equations shows that they exhibit a minimum for specific value of amplitude and phase. This is demonstrated by the simulated results obtained in section 4.6.

In the two-tone test, the reduction in the third order intermodulation is performed on the first kind of IMD3. In a multicarrier system the second kind of IMD will be present. The technique of difference frequency injection reduces both kinds of IMD.

The above analysis shows that the injection of the difference frequency signal $(\omega_2 - \omega_1)$ into the amplifier interact with the fundamental signals ω_1 and ω_2 and generates extra IMD terms at the frequencies $(2\omega_1 - \omega_2)$ and $(2\omega_2 - \omega_1)$, through a power series expansion of the second and third order term. The injected second harmonic signal $(\omega_3 - \omega_1)$ interacts with the fundamental signals ω_1 and ω_3 and generates of extra

IMD terms at the frequencies $(2\omega_1 - \omega_3)$ and $(2\omega_3 - \omega_1)$. Similarly, the injection of the signal $(\omega_3 - \omega_2)$ generates extra terms at the frequencies $(2\omega_3 - \omega_2)$ and $(2\omega_2 - \omega_3)$. Again, it is demonstrated that the cancellation of all first kind of IMD3 by the injection of the difference frequency signals, requires the injection of all signals whose frequencies are the difference in frequency of the pairs of fundamental signals.

The injection of the difference frequency signal $(\omega_2 - \omega_1)$ into the amplifier, generates extra IMD terms at the frequencies $(\omega_2 - \omega_1 + \omega_3)$ and $(\omega_1 - \omega_2 + \omega_3)$ by interaction with the fundamental signals ω_3, through a second order power series expansion. Similarly, the injection of the difference frequency signal $(\omega_3 - \omega_1)$ into the amplifier, also generates extra IMD terms at the frequencies $(\omega_3 - \omega_1 + \omega_2)$ and $(\omega_1 - \omega_3 + \omega_2)$ by interaction with the fundamental signals ω_2. The interaction of the difference frequency signal $(\omega_3 - \omega_2)$ and the fundamental signals ω_1 generates extra IMD terms at the frequencies $(\omega_3 - \omega_2 + \omega_1)$ and $(\omega_2 - \omega_3 + \omega_1)$. These results demonstrate that the cancellation of all first and second kind of IMD3 necessitate the injection of all difference frequency signals.

4.2.3 Frequency Summation Injection Technique

The work presented in this section looks at the effects of the injection of signals whose frequency is the sum of the pair of the fundamental signals. These signals are very close to the second harmonic signals and are causing some effects on the IMD performance of the amplifier. In order to analyse the system performance, signals, whose frequencies are the sum of the pair of fundamentals frequencies are injected into the amplifier together with the fundamental signals.

The input signal of the amplifier for a two-tone input system comprises the injected signal at the frequency $(\omega_2 + \omega_1)$ with amplitude $A_{\omega_{21}}$ and phase $\phi_{\omega_{21}}$, and the fundamentals signals ω_2 and ω_1 with amplitudes A_{ω_1} and A_{ω_2}, respectively. The expression for the input is

$$V_{in} = \sum_{n=1}^{2} \left(A_{\omega_n} \cos\left(\omega_n t\right)\right) + A_{\omega_{21}} \cos\left(\omega_2 t + \omega_1 t + \phi_{\omega_{21}}\right) \tag{4..37}$$

A substitution of equation 4.37 into equation 4.3 gives all the relevant frequency components at the output of the amplifier.

The interactions between the original signals and the injected sum of the fundamental frequencies result in additional signals at the output. The overall expression for third order IMD of the form $(2\omega_m \pm \omega_n)$ is

$$\begin{aligned} V_{2\omega_m \pm \omega_n} = {} & g_{m2} A_{\omega_1} A_{\omega_{21}} \cos\left(2\omega_1 t + \omega_2 t + \phi_{\omega_{21}}\right) + g_{m2} A_{\omega_2} A_{\omega_{21}} \cos\left(2\omega_2 t + \omega_1 t + \phi_{\omega_{21}}\right) \\ & + \tfrac{3}{4} g_{m3} A_{\omega_1}^2 A_{\omega_2} \cos\left(2\omega_1 t - \omega_2 t\right) + \tfrac{3}{4} g_{m3} A_{\omega_1}^2 A_{\omega_2} \cos\left(2\omega_1 t + \omega_2 t\right) \\ & + \tfrac{3}{4} g_{m3} A_{\omega_1} A_{\omega_2}^2 \cos\left(2\omega_2 t - \omega_1 t\right) + \tfrac{3}{4} g_{m3} A_{\omega_1} A_{\omega_2}^2 \cos\left(2\omega_2 t + \omega_1 t\right) \\ & + \tfrac{3}{4} g_{m3} A_{\omega_1} A_{\omega_{21}}^2 \cos\left(2\omega_2 t + \omega_1 t + 2\phi_{\omega_{21}}\right) + \tfrac{3}{4} g_{m3} A_{\omega_2} A_{\omega_{21}}^2 \cos\left(2\omega_1 t + \omega_2 t + 2\phi_{\omega_{21}}\right) \end{aligned} \tag{4..38}$$

From the above equation at the frequency $(2\omega_1 - \omega_2)$, the signal is

$$V_{2\omega_1 - \omega_2} = \tfrac{3}{4} g_{m3} A_{\omega_1}^2 A_{\omega_2} \cos\left(2\omega_1 t - \omega_2 t\right) \tag{4..39}$$

At the frequency $(2\omega_2 - \omega_1)$, the signal is:

$$V_{2\omega_2 - \omega_1} = \tfrac{3}{4} g_{m3} A_{\omega_1} A_{\omega_2}^2 \cos\left(2\omega_2 t - \omega_1 t\right) \tag{4..40}$$

The expression of the third order IMD at the frequencies $(2\omega_1 - \omega_2)$ and $(2\omega_2 - \omega_1)$ are unchanged when compared to the expressions obtained without the injection of the

signals (equation 4.17). This shows that injection of the sum of the fundamental signals will not cause a change in these third order intermodulation components because no additional terms are generated. Cancellation of the intermodulation distortion by adjusting the injected signals (amplitude and phase) will not be possible.

Considering a three-tone input signal consisting of three distinct sinusoidal signals at the frequencies ω_1, ω_2 and ω_3 of amplitudes $A\omega_1$, $A\omega_2$ and $A\omega_3$ respectively.

The system is injected with signals whose frequencies are the sum of the pairs of frequencies of the fundamental signals ω_1, ω_2 and ω_3. The signal are at the frequencies $(\omega_2+\omega_1)$, $(\omega_3+\omega_2)$ and $(\omega_3+\omega_1)$ with different phases $\phi_{\omega 21}$, $\phi_{\omega 32}$ and $\phi_{\omega 31}$ and amplitudes $A_{\omega 21}$, $A_{\omega 32}$ and $A_{\omega 31}$ respectively.

The input signal of the system is

$$V_{in} = \sum_{n=1}^{3} \left(A_{\omega_n} \cos\left(\omega_n t\right)\right) + A_{\omega 21} \cos\left(\omega_2 t + \omega_1 t + \phi_{\omega_{21}}\right) \tag{4..41}$$
$$+A_{\omega 32} \cos\left(\omega_3 t + \omega_2 t + \phi_{\omega 32}\right) + A_{\omega 31} \cos\left(\omega_3 t + \omega_1 t + \phi_{\omega_{31}}\right)$$

Substitution of equation 4.41 into 4.3 gives all the relevant IM components at the output of the amplifier. The injection of the sum of the fundamental frequency signals has generated additional IMD3 terms.

The expression of the output signal at the frequency $(2\omega_1 - \omega_2)$, is

$$V_{2\omega_1-\omega_2} = \tfrac{3}{4} g_{m3} A_{\omega_1}^2 A_{\omega_2} \cos\left(2\omega_1 t - \omega_2 t\right) \tag{4..42}$$
$$+\tfrac{3}{2} g_{m3} A_{\omega_1} A_{\omega 31} A_{\omega 32} \cos\left(2\omega_1 t - \omega_2 t + \phi_{\omega 31} - \phi_{\omega 32}\right)$$

The expression of the output signal at the frequency $(2\omega_2 - \omega_1)$, is

$$V_{2\omega_2-\omega_1} = \tfrac{3}{4} g_{m3} A_{\omega_1} A_{\omega_2}^2 \cos\left(2\omega_2 t - \omega_1 t\right) \tag{4..43}$$
$$+\tfrac{3}{2} g_{m3} A_{\omega_2} A_{\omega 31} A_{\omega 32} \cos\left(2\omega_2 t - \omega_1 t - \phi_{\omega 31} + \phi_{\omega 32}\right)$$

Similar expression are found for the other first kinds of IMD at the frequencies $(2\omega_2 - \omega_3)$, $(2\omega_1 - \omega_3)$, $(2\omega_3 - \omega_2)$ and $(2\omega_3 - \omega_1)$.

The expression in equation 4.42 and 4.43 of the third order IMD at the frequencies $(2\omega_1 - \omega_2)$ and $(2\omega_2 - \omega_1)$, shows that the injection of the sum of the fundamental signals results in the generation of extra terms at those frequencies. This implies that if the phase and amplitude of the injected sum of the frequencies of the fundamental signals were appropriately chosen, it should result in a cancellation of the IMD products.

The injection of the difference frequencies of the fundamental signals has also generated additional IMD terms of the second kind.

The expression of the IMD signal at the frequency $(\omega_1 + \omega_2 - \omega_3)$, is

$$\begin{aligned} V_{\omega_1+\omega_2-\omega_3} &= g_{m2} A_{\omega_3} A_{\omega_{21}} \cos\left(\omega_1 t + \omega_2 t - \omega_3 t + \phi_{\omega_{21}}\right) \\ &+ \tfrac{3}{2} g_{m3} A_{\omega_1} A_{\omega_2} A_{\omega_3} \cos\left(\omega_1 t + \omega_2 t - \omega_3 t\right) \\ &+ \tfrac{3}{2} g_{m3} A_{\omega_1} A_{\omega_{21}} A_{\omega_{31}} \cos\left(\omega_1 t + \omega_2 t - \omega_3 t + \phi_{\omega_{21}} - \phi_{\omega_{31}}\right) \\ &+ \tfrac{3}{2} g_{m3} A_{\omega_2} A_{\omega_{21}} A_{\omega_{32}} \cos\left(\omega_1 t + \omega_2 t - \omega_3 t - \phi_{\omega_{21}} - \phi_{\omega_{32}}\right) \end{aligned} \tag{4..44}$$

The expression of the IMD signal at the frequency at $(\omega_1 - \omega_2 + \omega_3)$, is

$$\begin{aligned} V_{\omega_1-\omega_2+\omega_3} &= g_{m2} A_{\omega_2} A_{\omega_{31}} \cos(\omega_1 t - \omega_2 t + \omega_3 t + \phi_{\omega_{31}}) \\ &+ \tfrac{3}{2} g_{m3} A_{\omega_1} A_{\omega_2} A_{\omega_3} \cos\left(\omega_1 t - \omega_2 t + \omega_3 t\right) \\ &+ \tfrac{3}{2} g_{m3} A_{\omega_1} A_{\omega_{21}} A_{\omega_{31}} \cos(\omega_1 t - \omega_2 t + \omega_3 t - \phi_{\omega_{21}} + \phi_{\omega_{31}}) \\ &+ \tfrac{3}{2} g_{m3} A_{\omega_3} A_{\omega_{31}} A_{\omega_{32}} \cos(\omega_1 t - \omega_2 t + \omega_3 t + \phi_{\omega_{31}} - \phi_{\omega_{32}}) \end{aligned} \tag{4..45}$$

The expression of the IMD signal at the frequency at $(\omega_3 + \omega_2 - \omega_1)$, is

$$\begin{aligned} V_{\omega_3+\omega_2-\omega_1} &= g_{m2} A_{\omega_1} A_{\omega_{32}} \cos\left(\omega_3 t + \omega_2 t - \omega_1 t - \phi_{\omega_{32}}\right) \\ &+ \tfrac{3}{2} g_{m3} A_{\omega_1} A_{\omega_2} A_{\omega_3} \cos\left(\omega_3 t + \omega_2 t - \omega_1 t\right) \\ &+ \tfrac{3}{2} g_{m3} A_{\omega_2} A_{\omega_{21}} A_{\omega_{32}} \cos\left(\omega_3 t + \omega_2 t - \omega_1 t + \phi_{\omega_{21}} - \phi_{\omega_{32}}\right) \\ &+ \tfrac{3}{2} g_{m3} A_{\omega_3} A_{\omega_{31}} A_{\omega_{32}} \cos\left(\omega_3 t + \omega_2 t - \omega_1 t - \phi_{\omega_{31}} + \phi_{\omega_{32}}\right) \end{aligned} \tag{4..46}$$

The generation of extra terms at the frequencies $(\omega_1 - \omega_2 + \omega_3)$, $(\omega_1 - \omega_3 + \omega_2)$ and $(\omega_3 - \omega_1 + \omega_2)$ as expressed in equation 4.44, equation 4.45 and equation 4.46, shows that a careful choice of the phase and amplitude of the injected signals, will result in a cancellation of the IMD3. The injection of the sum of the fundamentals frequencies in a two-tone test shows that there is no reduction on the third order intermodulation. The expression of the first kind of IMD3 does not change before and after the use of the technique, no extra terms are generated in the expressions.

In the three-tone test, the injected signals at the frequency $(\omega_2 - \omega_1)$, $(\omega_3 - \omega_1)$ and $(\omega_3 - \omega_2)$ interact with the fundamental signals ω_1, ω_2 and ω_3 to generate extra IMD3 terms at the frequencies $(\omega_1 - \omega_2 + \omega_3)$, $(\omega_1 - \omega_3 + \omega_2)$ and $(\omega_3 - \omega_1 + \omega_2)$. It results in a reduction of the second kind of IMD3 with an appropriate choice of amplitudes $A\omega_{21}$, $A\omega_{32}$ and $A\omega_{31}$ and phases $\phi\omega_{21}$, $\phi\omega_{32}$ and $\phi\omega_{31}$ of the injected signals.

A cancellation of the first kind of IMD at the frequencies$(2\omega_1 - \omega_2)$, $(2\omega_2 - \omega_1)$, $(2\omega_2 - \omega_3)$, $(2\omega_1 - \omega_3)$, $(2\omega_3 - \omega_2)$ and $(2\omega_3 - \omega_1)$ occurs with the injection of the sum of the fundamental signals. A careful choice of the amplitudes and phases of the injected signals in equation 4.44, equation 4.45 and equation 4.46 results in an overall cancellation of all third order intermodulation. It is clear that the reduction in the IMD will produce satisfactory results if extra terms are generated in the expression of the

IMDs and that these expressions exhibits a minimum for specific values of amplitudes $A_{\omega 21}$, $A_{\omega 32}$ and $A_{\omega 31}$ and phases $\phi_{\omega 21}$, $\phi_{\omega 32}$ and $\phi_{\omega 31}$. Since the input tones are of the same amplitude and phase ($A\omega_{21} = A\omega_{32} = A\omega_{31}$ and $\phi\omega_{21} = \phi\omega_{32} = \phi\omega_{31}$), it can be demonstrated that the equation exhibit a minimum for specific injected signal amplitude and phase, as shown in section 4.6.

It is demonstrated in the above analysis that the cancellation of the first kind of IMD3 by the injection of the frequency summation signals does not occur. On the other hand, the cancellation of the second kind of IMD can be achieved. The injection of the frequency summation signal $(\omega_2 + \omega_1)$ into the amplifier, generates extra IMD terms at the frequencies $(\omega_2 + \omega_1 - \omega_3)$ by interaction with the fundamental signals ω_3, through a second order power series expansion. Similarly, the injection of the frequency summation signal $(\omega_3 + \omega_1)$ into the amplifier, generates extra IMD terms at the frequencies $(\omega_3 + \omega_1 - \omega_2)$ by interaction with the fundamental signals ω_2. The interaction of the frequency summation signal $(\omega_3 + \omega_2)$ and the fundamental signals ω_1 generates extra IMD terms at the frequencies $(\omega_3 + \omega_2 - \omega_1)$. These results demonstrate that the cancellation of the second kind of IMD3 required the injection of all frequency summation signals.

4.3 Amplifier Circuit Characteristic

A simple single stage amplifier is used for the analysis of the intermodulation products. The circuit is used to verify the above theory by injecting it with the original signals, then adding firstly the sum of the fundamentals, next the second harmonics and finally the difference frequency signals. The output signal behaviour at the IMD3

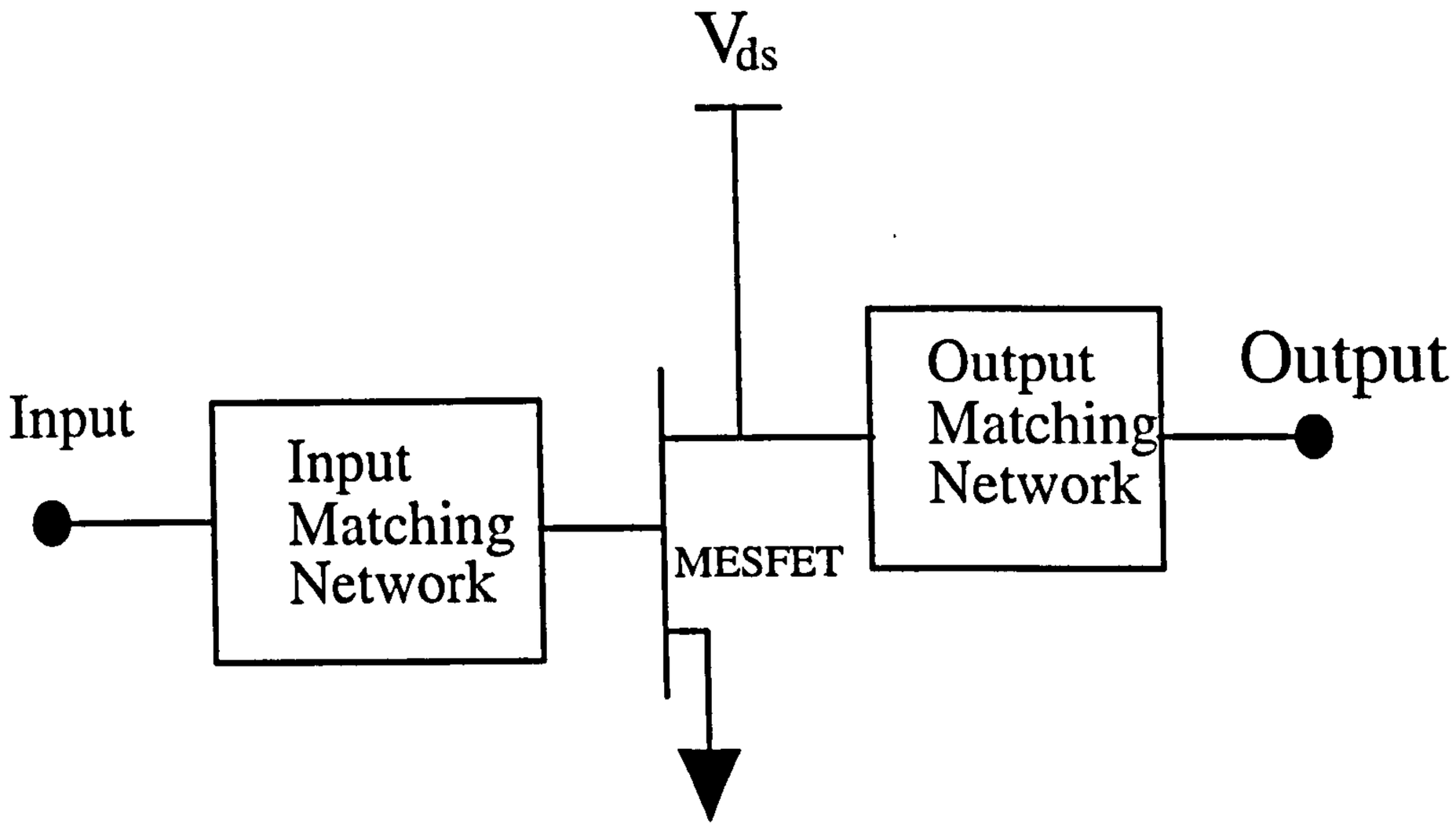

Figure 4..1: **Basic amplifier circuit topology.**

frequencies is presented. The circuit is constructed in a very conventional way which is characteristic of many PA circuit used in communication applications. The basic approach of the circuit design is represented in fig 4.1, where the nonlinear transistor is connected at the input and at the output by matching networks. The device is biased by two dc power supplies at the base and the drain.

The active device model used in this simulation is a MESFET extension of the Curtice cubic model 2 discussed in chapter 2 and is shown in figure 4.2 [49, 124]. The value of the elements describing the model[1] are shown in table 4.1. The equation describing the model is

$$I_{ds} = (A_0 + A_1 V_1 + A_2 V_1^2 + A_3 V_1^3) \tanh\left[\gamma V_{DS}(t)\right] \qquad (4..47)$$

[1] The default values of the Curtice model are used for the other values of the parameters which are not defined in table 4.1.

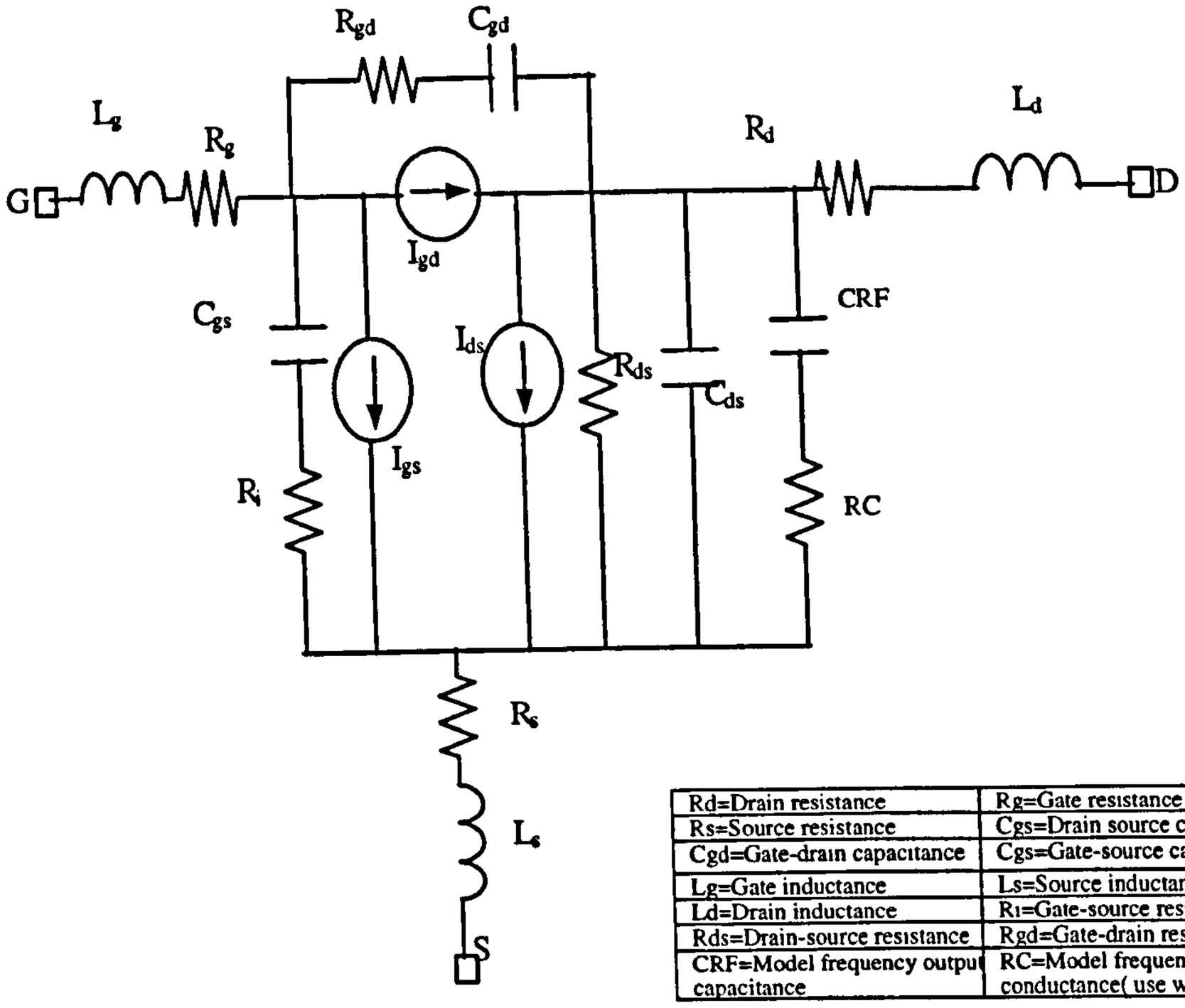

Rd=Drain resistance	Rg=Gate resistance
Rs=Source resistance	Cgs=Drain source capacitance
Cgd=Gate-drain capacitance	Cgs=Gate-source capacitance
Lg=Gate inductance	Ls=Source inductance
Ld=Drain inductance	Ri=Gate-source resistance
Rds=Drain-source resistance	Rgd=Gate-drain resistance
CRF=Model frequency output capacitance	RC=Model frequency output conductance(use with CRF)

Figure 4..2: **Large signal MESFET model used for simulation.**

With

$$I_{ds} = V_{GS}(t-\tau)\left[1+\beta_2\left(V_{DS0}-V_{DS}(t)\right)\right] \tag{4..48}$$

for $V_{DS} \geq 0$

Where β_2 is a coefficient for the pinch-off change as a function of V_{DS}.

V_{DS0} is the value of V_{DS} at which A_0, A_1, A_2 and A_3 are evaluated.

A_0, A_1, A_2 and A_3 are coefficients in the cubic equation.

β_2 is the hyperbolic tangent function parameter.

τ is the internal time delay parameter.

The circuit used for the investigation of the technique is shown in figure 4.3.

The input of the circuit consists of a hybrid T-section and an m-derived half T-section

Name	Meaning	Unit	value
VBI	Built in gate potential	V	0.80
R_D	Drain ohmic resistance	ohm	2.37
R_G	Gate resistance	ohm	2
R_S	Source ohmic resistance	ohm	3.7
C_{gs}	Gate source junction capacitance	pF	0.37
C_{gd}	Drain source junction capacitance	pF	0.37
C_{ds}	Drain source capacitance	pF	0.07
VBR	Gate-drain junction reverse bias breakdown voltage	V	5
IS	gate junction reverse saturation current(diode model)	A	$1.0e-09$
AF	Flicker noise temperature	1	1
R_d	Drain resistance	ohm	2.37
R_{gd}	Gate to drain resistance	ohm	0.001
R_{in}	Gate to source resistance	ohm	0.0001
R_{ds}	drain to source resistance	ohm	1250
$A0$	Cubic fit Ids coefficient	A	007
$A1$	Cubic fit Ids coefficient	A/V	0.12
$A2$	Cubic fit Ids coefficient	$A/V2$	0.06
$A3$	Cubic fit Ids coefficient	$A/V3$	0.009

Table 4..1: **Curtice cubic 30 parameters value and definition.**

(figure 4.4) to provide a wideband match at the input. The input section circuit has a 90° hybrid network to enable the injection of the fundamentals and injected signals. The network is an ideal four-port device that is modelled by the file: hybrid s4p (appendix 1).

The circuit configuration is used so that the input bandwidth does not affect the overall performance of the circuit. At the output, a series resonant circuit and a transformer are used to provide an optimum load for the amplifier. The circuit performances were simulated at various frequencies. The gain and bandwidth of the device, as well as the input and output reflection coefficient characteristic over a frequency range of $5GHz$ were recorded. The gain and $1dB$ gain compression point (gcp) of the amplifier at $2.5GHz$ are shown is fig 4.5. The gain is about $5dB$ over a $5GHz$ bandwidth. Figure 4.6 shows the input (S11) and output (S22) reflection coefficient of the simulated amplifier, as well as the forward (S21) and reverse (S12) coefficient of the amplifier.

The circuit uses a low power device to enable the calculation of IMD in the simulator to be made much more easily and with a lesser computing power requirement.

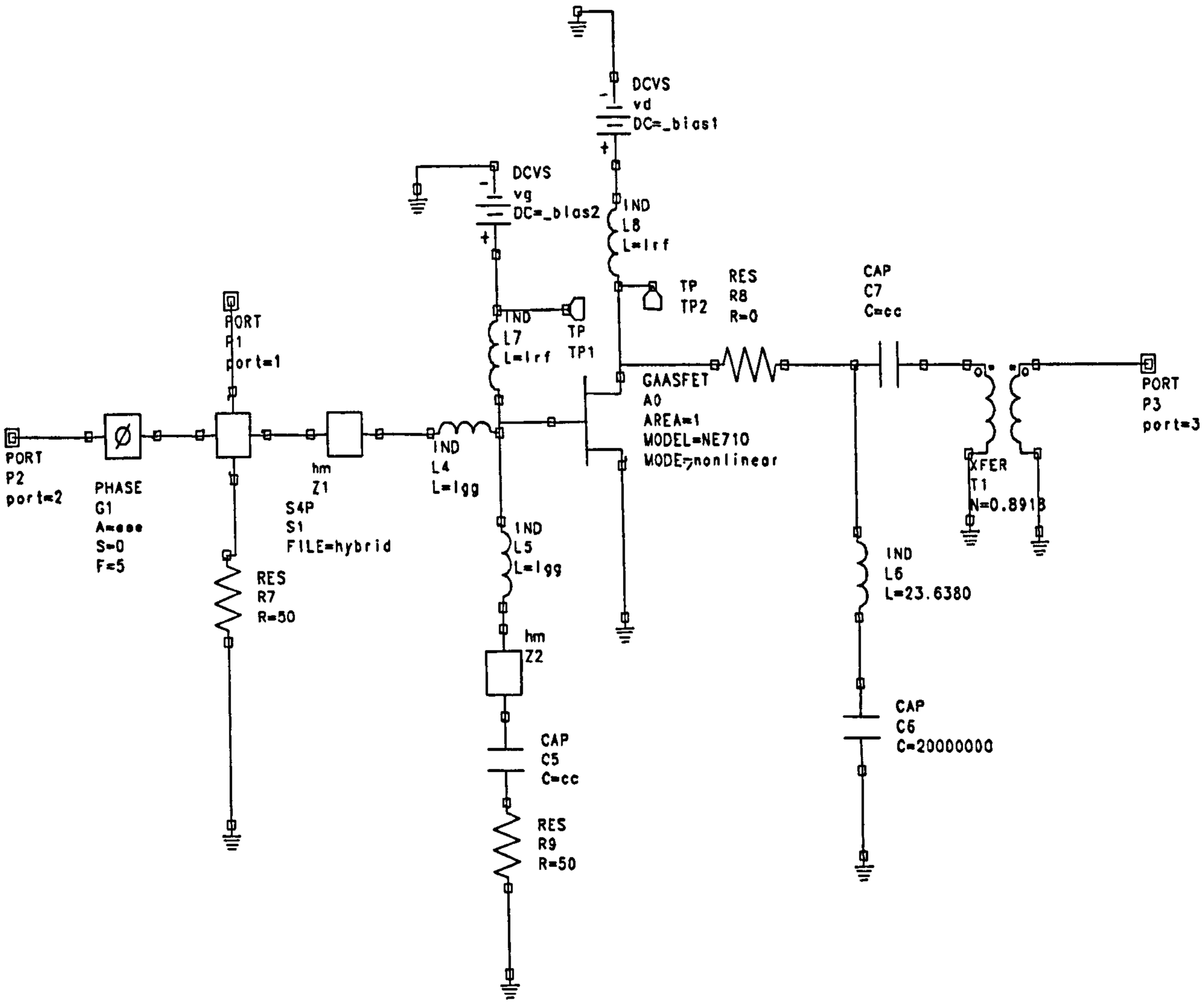

Figure 4..3: **Circuit diagram of the simulated power amplifier.**

The use of a high power device can engender inaccuracies as it requires a great amount of computing power. The results obtained with the circuit give a comprehensible and accurate amplifier response for intermodulation distortion modeling which can be easy to verify experimentally..

A single tone simulation is undertaken to observe the output response of the amplifier to a sinusoidal signal. The intercept point of the amplifier is calculated (for IP measurement technique see section 3.3) and its intermodulation behaviour can be

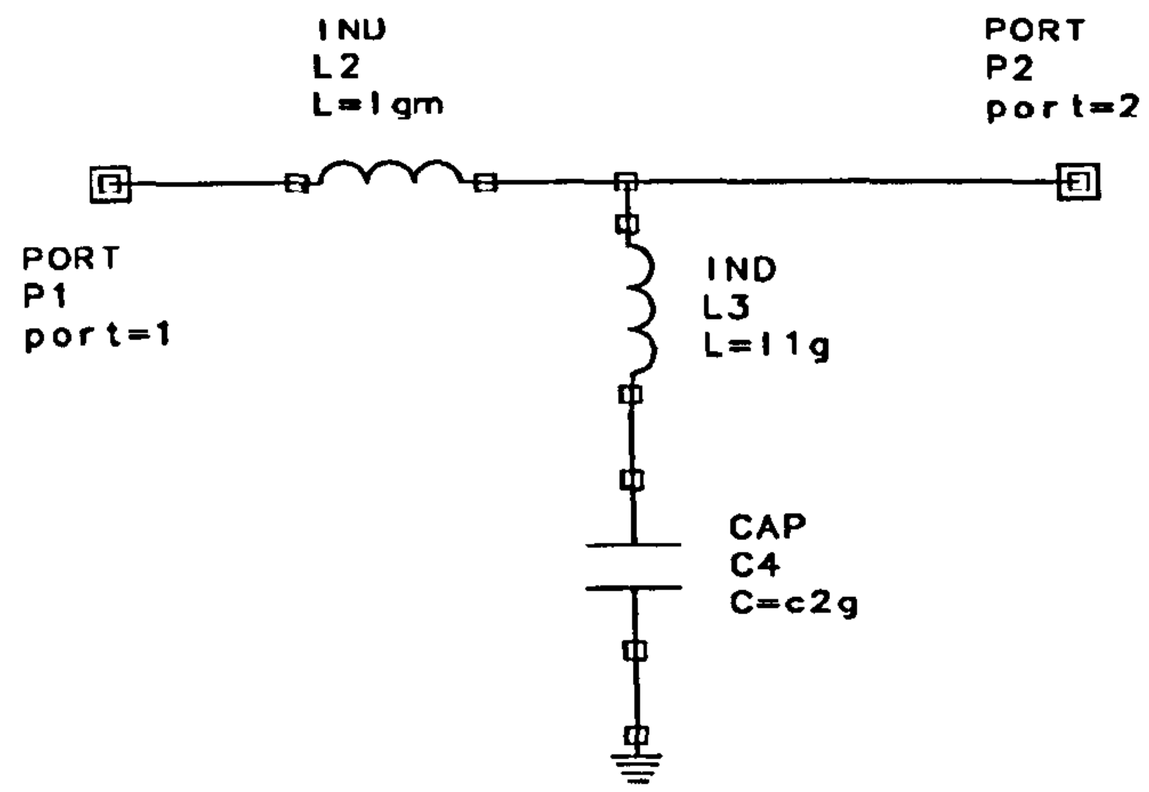

Figure 4..4: **Circuit diagram of the half m derived Hybrid section of the simulated amplifier.**

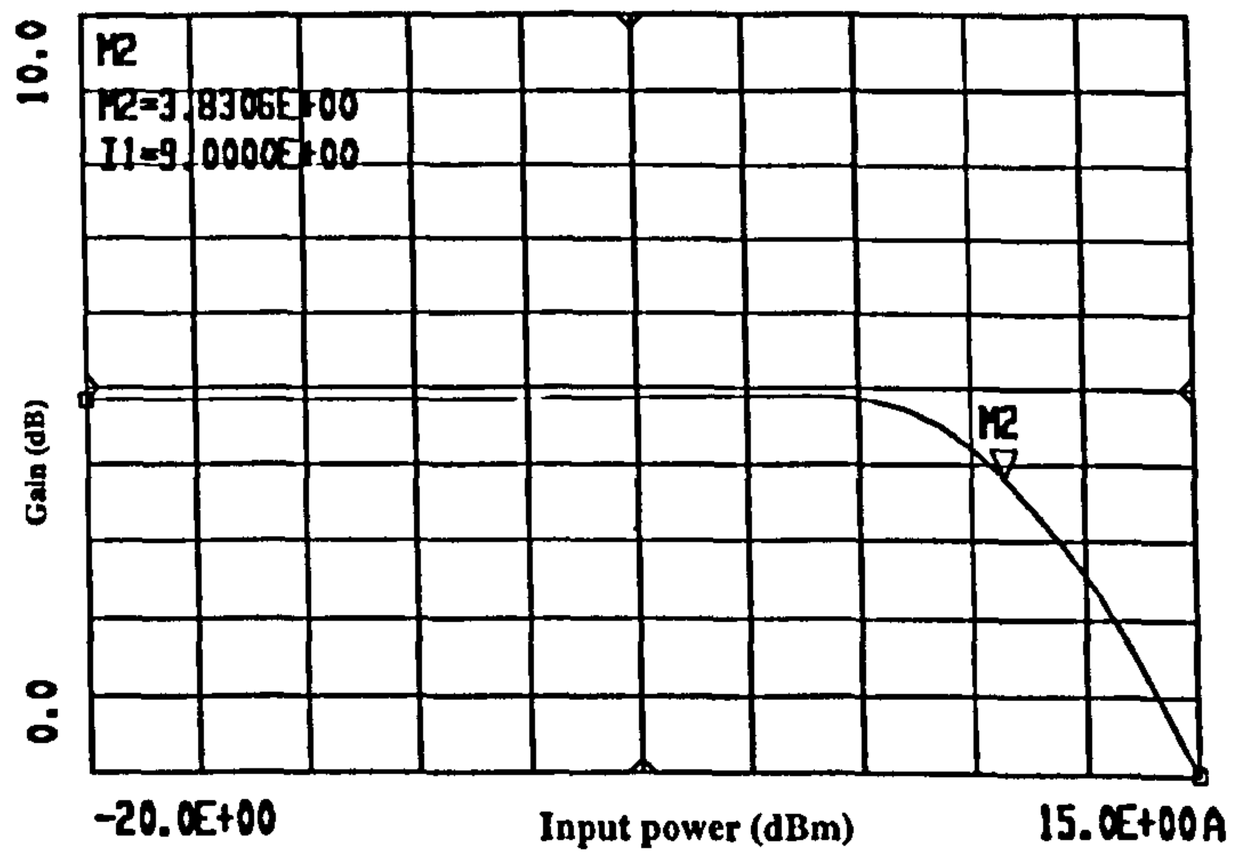

Figure 4..5: **Gain Vs input power of the simulated single stage power amplifier with the marker M2 showing the 1dB compression point.**

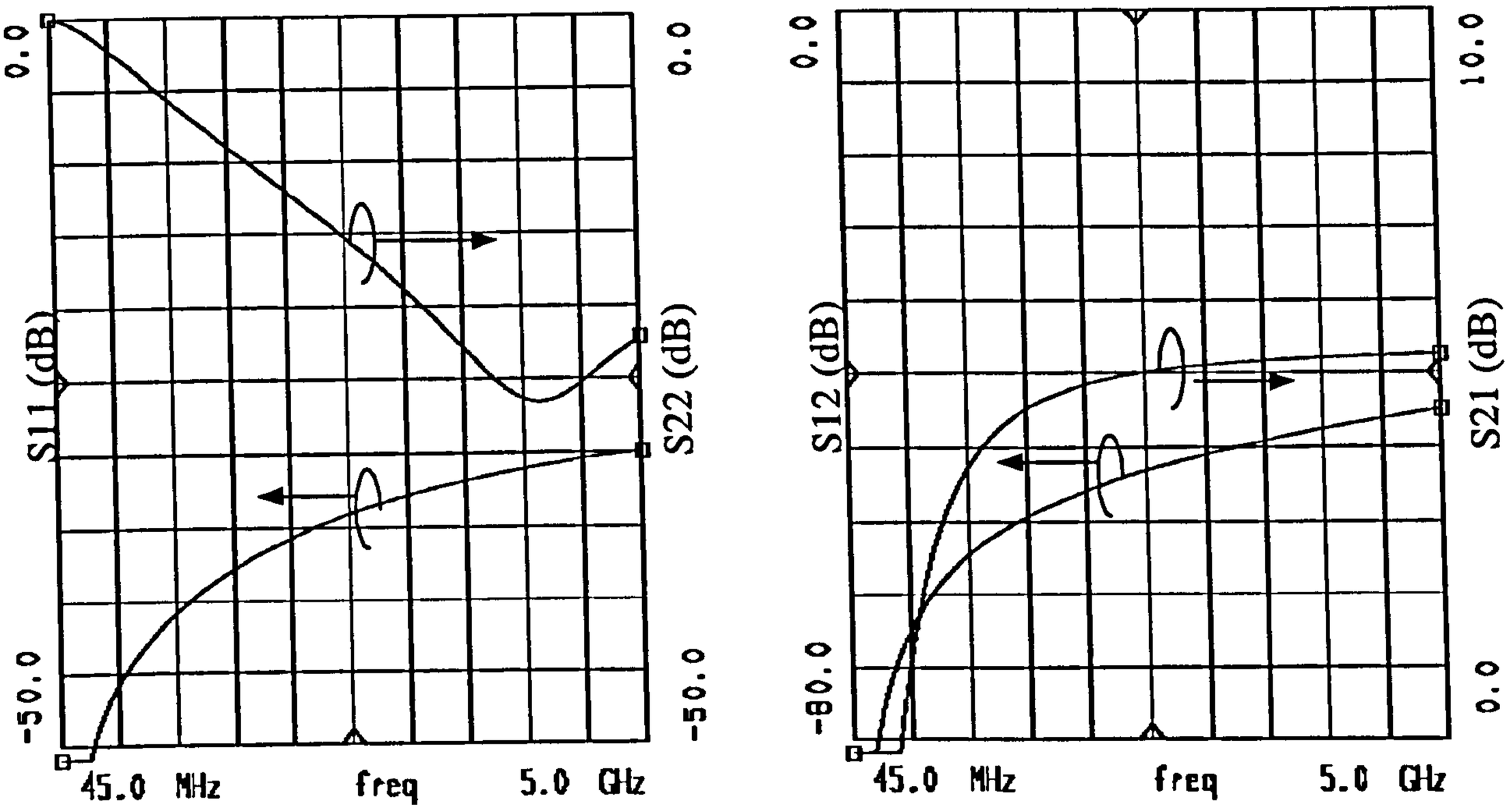

Figure 4..6: **Simulated S-parameters response of the amplifier.**

predicted by using a standard two tone test. Using the configuration of figure 4.7, a single signal in connected to one of the inputs of the hybrid coupler while the other input is terminated in a 50Ω termination. The input power of the amplifier is swept between the value of $-20dBm$ and $15dBm$, this gives the characteristic of figure 4.8. It can be seen that the amplifier characteristic of the fundamental frequency is linear up to the saturation point, at around $10dBm$ power level. For input powers above $10dBm$, the amplifier characteristic reaches saturation and no amplification is obtained. Furthermore a drop in the output power will be noticed at higher input power level.

The output of the amplifier is made up of harmonic signals at various frequencies. The power level of the harmonic signal decreases with the harmonic level. Figure 4.8 also shows the power level of the second, third, fourth and fifth harmonic signals against the input signal.

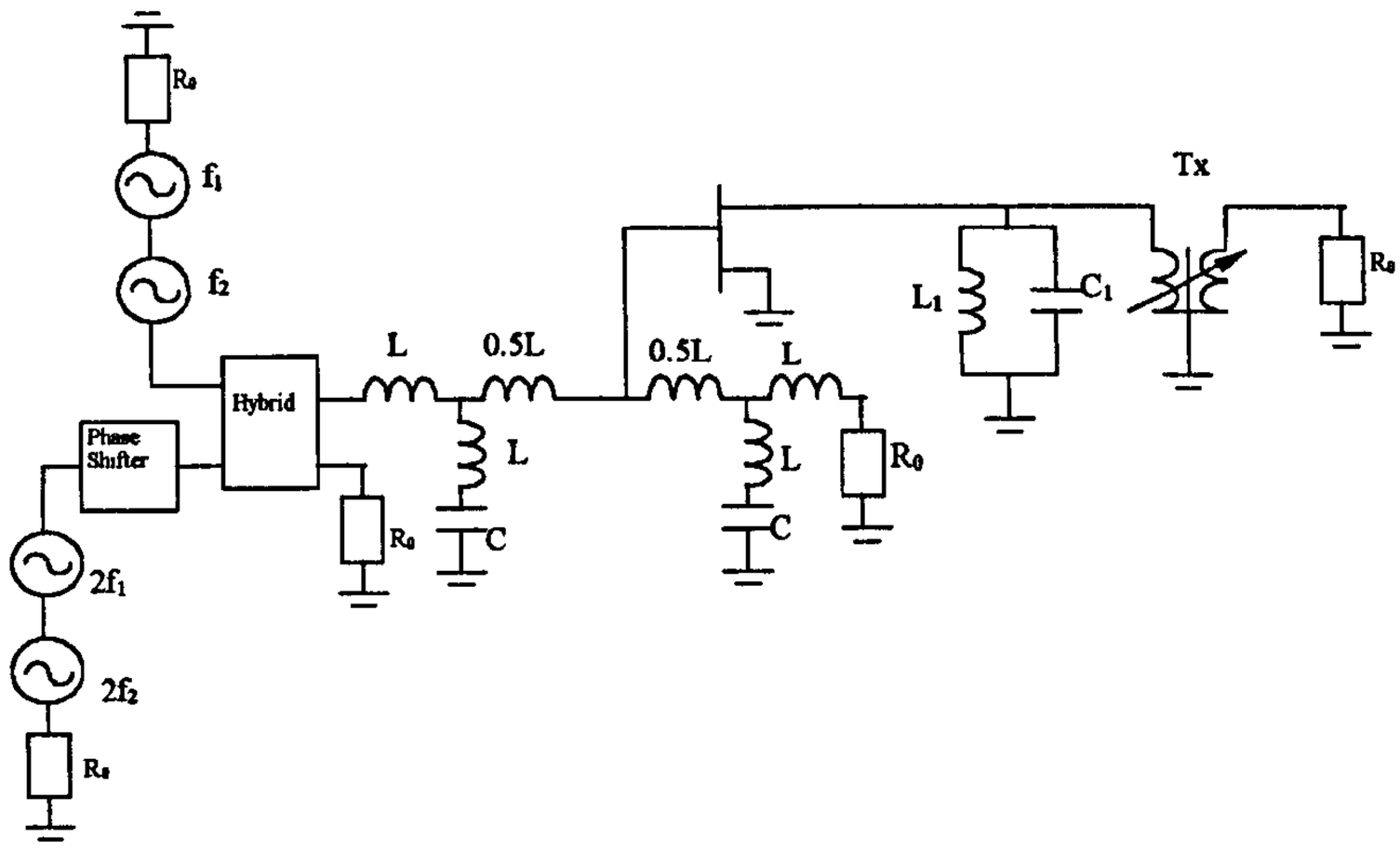

Figure 4..7: **The amplifier schematic diagram showing the fundamentals and injected second harmonics input configuration.**

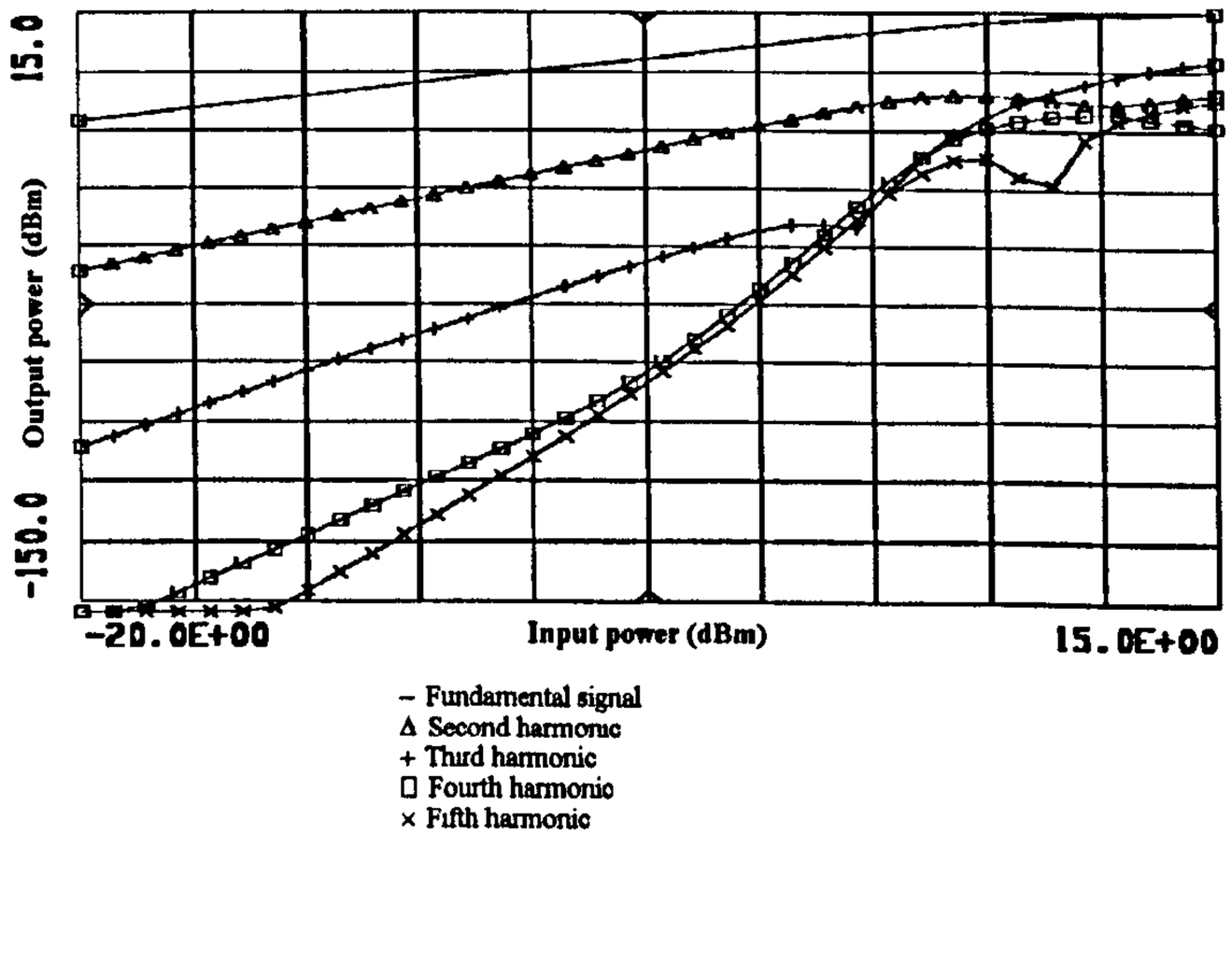

Figure 4..8: **Output Vs input power of fundamental signal and harmonics.**

4.4 Injection Technique Effects in a Simulated Two-Tone Test

A two-tone test is first performed without the injection of the second harmonic signals. The test is performed with two input signals, f_1 and f_2, at the frequencies $2.5GHz$ and $2.51GHz$. The two signals are combined and passed through the amplifier as shown if figure 4.7. The simulation gives the output power shown in figure 4.9 for an equi-tone input power of $-20dBm$. The third order IMD3 components are generated at the frequencies $2.49GHz$ for the signal $(2f_1 - f_2)$ and $2.52GHz$ for $(2f_2 - f_1)$. Signals at various frequencies with variable amplitude and phase are then injected into the amplifier together with the original signals and their effects on the IMD are observed. First the second harmonics of the fundamental signals are injected, then the difference frequency signals (difference frequency technique) and finally, the injection of signals whose frequency is the sum of the pair of the fundamental signals (frequency summation technique).

Although the injection of the sum of the frequencies (at the frequency $5.01GHz$) is realisable in a simulator, it is not however the case in practise as the second harmonics of the input signals fall at the frequencies $5.00GHz$ and $5.02GHz$ and can not be easily separated from the sum of the frequency of the original signals at the frequency $5.01GHz$. If the frequency spacing between the input signals becomes small, it then becomes difficult to distinguish the effects of both sum and second harmonic signals. In practice, the injection of the second harmonic will result in the injection of the sum of the frequency of the fundamental signals and vice versa. Since it was shown that the second harmonic reduces the IMD level in a two-tone system, the study was widened

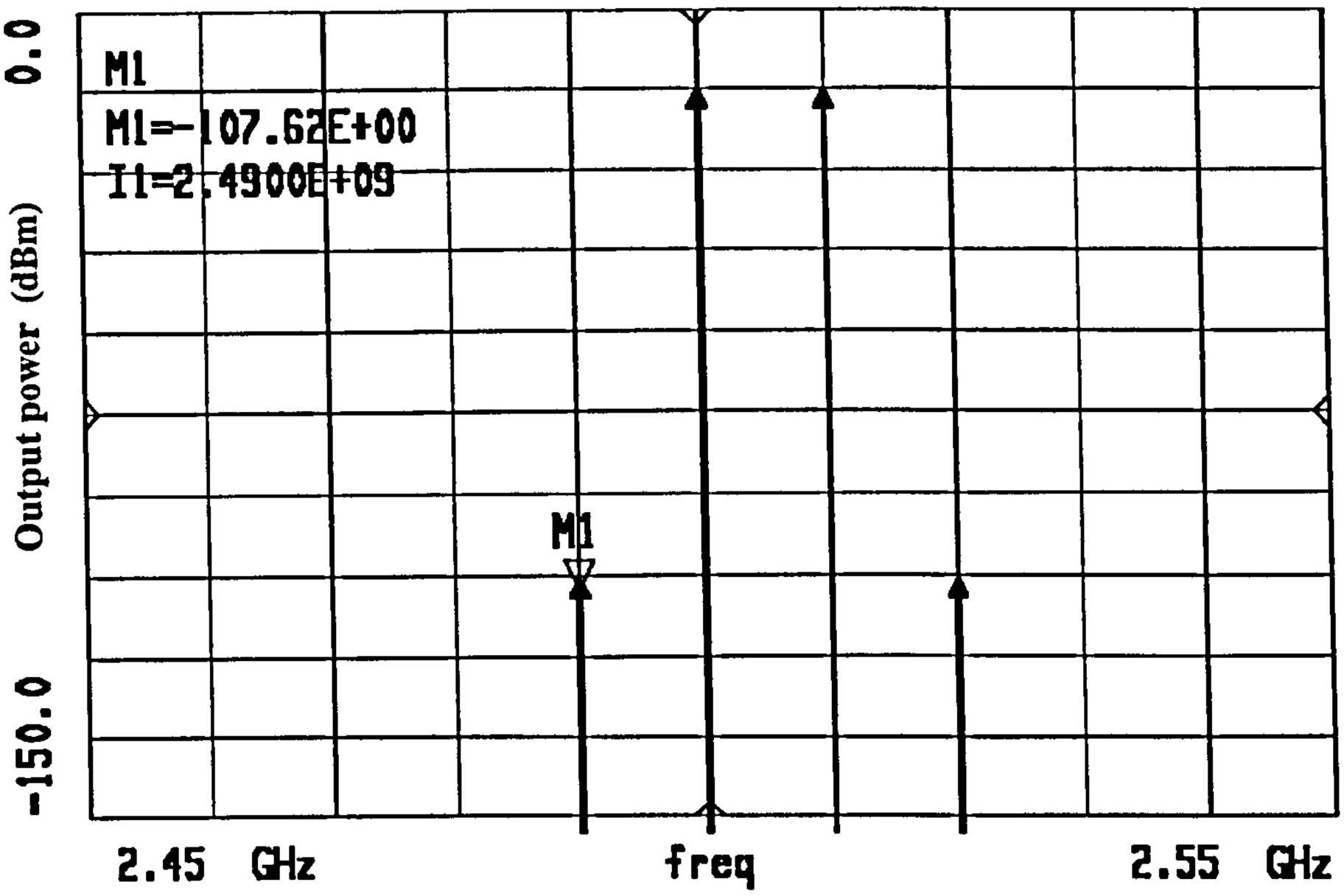

Figure 4..9: **Two-tone simulated output spectrum of amplifier without employing the techniques.**

to include these particular signals. Their effects need to be observed and understood. Although in theory this can be considered and called a frequency summation technique, in practice, the combined effects of both techniques are regarded as one.

When the second harmonics of the input signals with an arbitrary phase and amplitude are injected into the system, a drop in the power level of the IMD3 by about $4dB$ is observed. The optimisation of the circuit phase shifter parameter and the amplitude of the second harmonics is performed for optimum phase and amplitude of the injected signal in order to achieve a reduction of both IMD3 products. This gives the result of figure 4.10. The amplitude of the IMD signals drops by $34dB$ at the input power level of $-20dBm$. This is a significant improvement on the distortion in the amplifier. For a phase shift of about 179.8^{o} and signal amplitude of about $-42dBc$, a

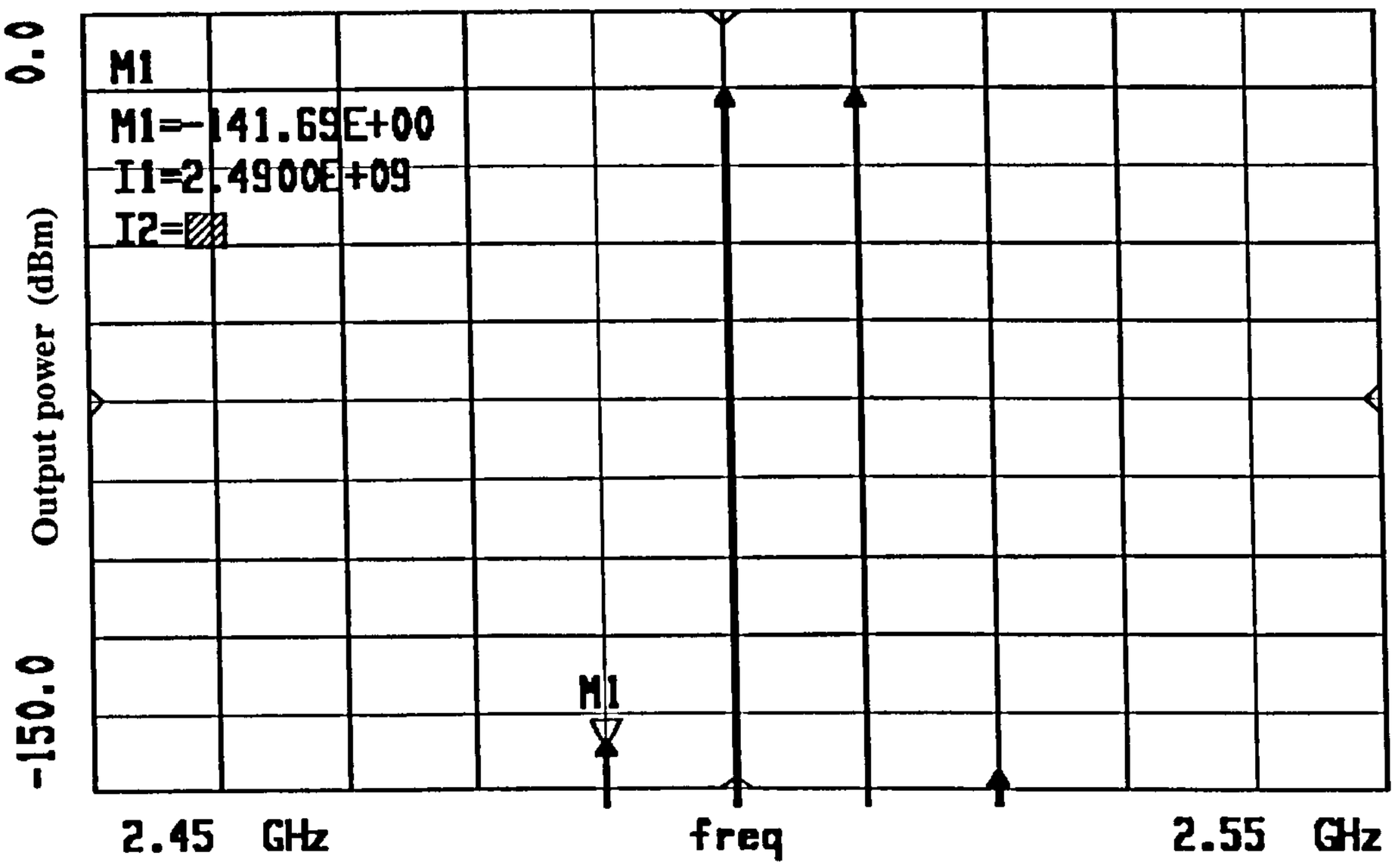

Figure 4..10: **Two-tone simulated output spectrum of amplifier after injection of the second harmonic signals, showing a reduction of IMD3 by more than 30dB.**

reduction of more than $30dB$ is achieved on all IMD3. The use of the second harmonic in a two-tone test required the injection of both the second harmonic $(2f_1)$ of the first signal (f_1) and the second harmonic $(2f_2)$ of the second signal (f_2).

The use of the difference frequency technique on the amplifier required the injection of a single signal into the amplifier at the frequency $(f_2 - f_1)$ as opposed to the second harmonic technique which required the two harmonic signals at the frequencies $(2f_1)$ and $(2f_2)$. The difference frequency signal is injected into the amplifier in a similar way as shown in the circuit of figure 4.8. A decrease of about 3 to $4dBm$ in the level of the IMD3 is clearly noticed. A change in the level of IMD3 occurs instantaneously because these signals were close in phase and amplitude to the optimum value required for IMD3 cancellation. An optimisation is then performed to reduce the IMD3 for opti-

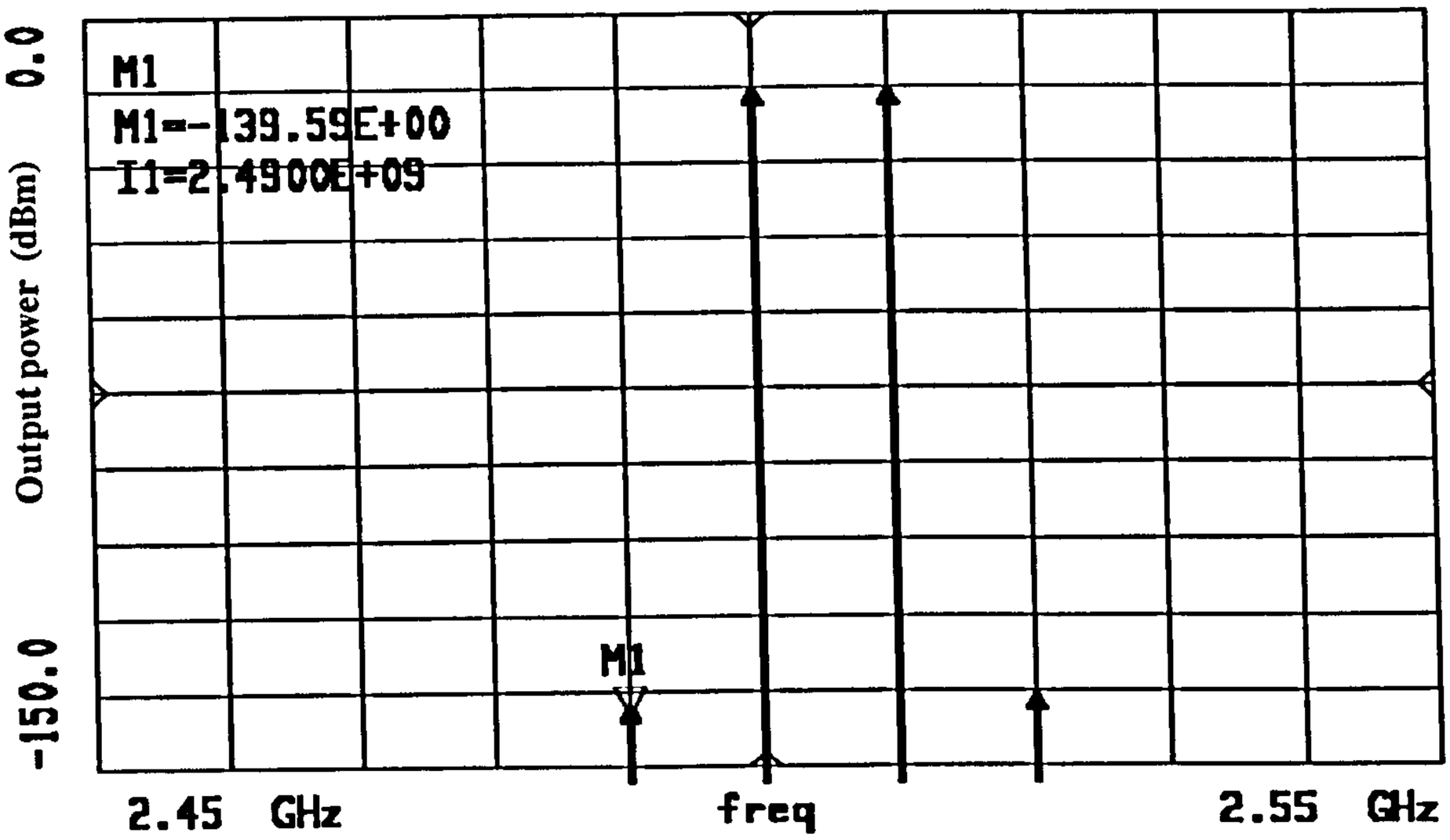

Figure 4..11: **Two-tone simulated output spectrum of amplifier after injection of the difference frequency signal, showing a reduction of IMD3 by more than** $30dB$.

mum amplifier performance. IMD3 are reduced by more than $30dB$ as shown in figure 4.11. This verifies the theory of the IMD reduction by the difference frequency injection technique. After optimisation of both techniques for low intermodulation level, it was found that both techniques reduce the two third order IMD components found in a two tone system as shown in figure 4.10 and figure 4.11.

The injection of the signals whose frequency is the sum of the two fundamental signals results in the injection of a single signal at the frequency $(f_2 + f_1)$. The injection of this signal into the amplifier together with the original signals does not cause a reduction in the third order IM3 level. Since there are no additional terms generated at the third order IM frequencies as observed in the theoretical analysis, there is no improvement on the two intermodulation distortions. This is illustrated in figure 4.12

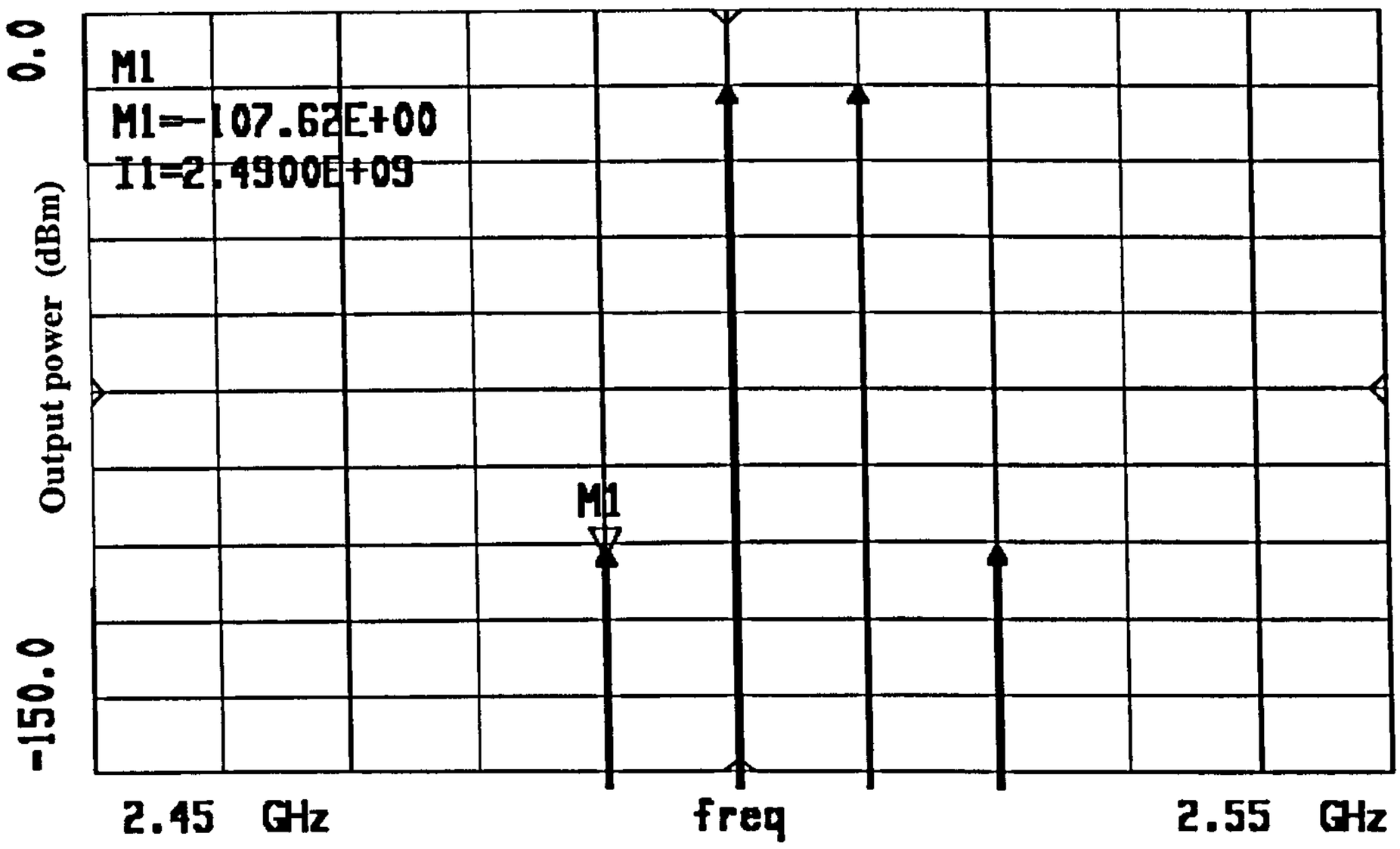

Figure 4..12: **Two-tone simulated output spectrum of amplifier after employing the frequency summation technique, showing no significant reduction on the third order IM.**

where the optimisation at the input power level of $-20dBm$ for a reduction of both IMD3 fails to give an appreciable reduction of their initial value of figure 4.9. A small decrease in the level of the third order IM of less than $1dB$ is noted. The technique does not however reduce the third order intermodulation in a two tone test significantly compared to that observed with the other two techniques.

4.5 Injection Technique Effects in a Simulated Three-Tone Test

A third input signal at the frequency $2.521GHz$ is introduced. The third signal is shifted by $1MHz$ to enable all third order IMD products to be clearly seen as shown in figure 4.14.. The input signals f_1, f_2 and f_3 of the amplifier are at the frequencies $2.5GHz$, $2.51GHz$ and $2.521GHz$ respectively. The simulated test consists of injecting different signals and observing the IMD3 performance of the technique in the amplifier.

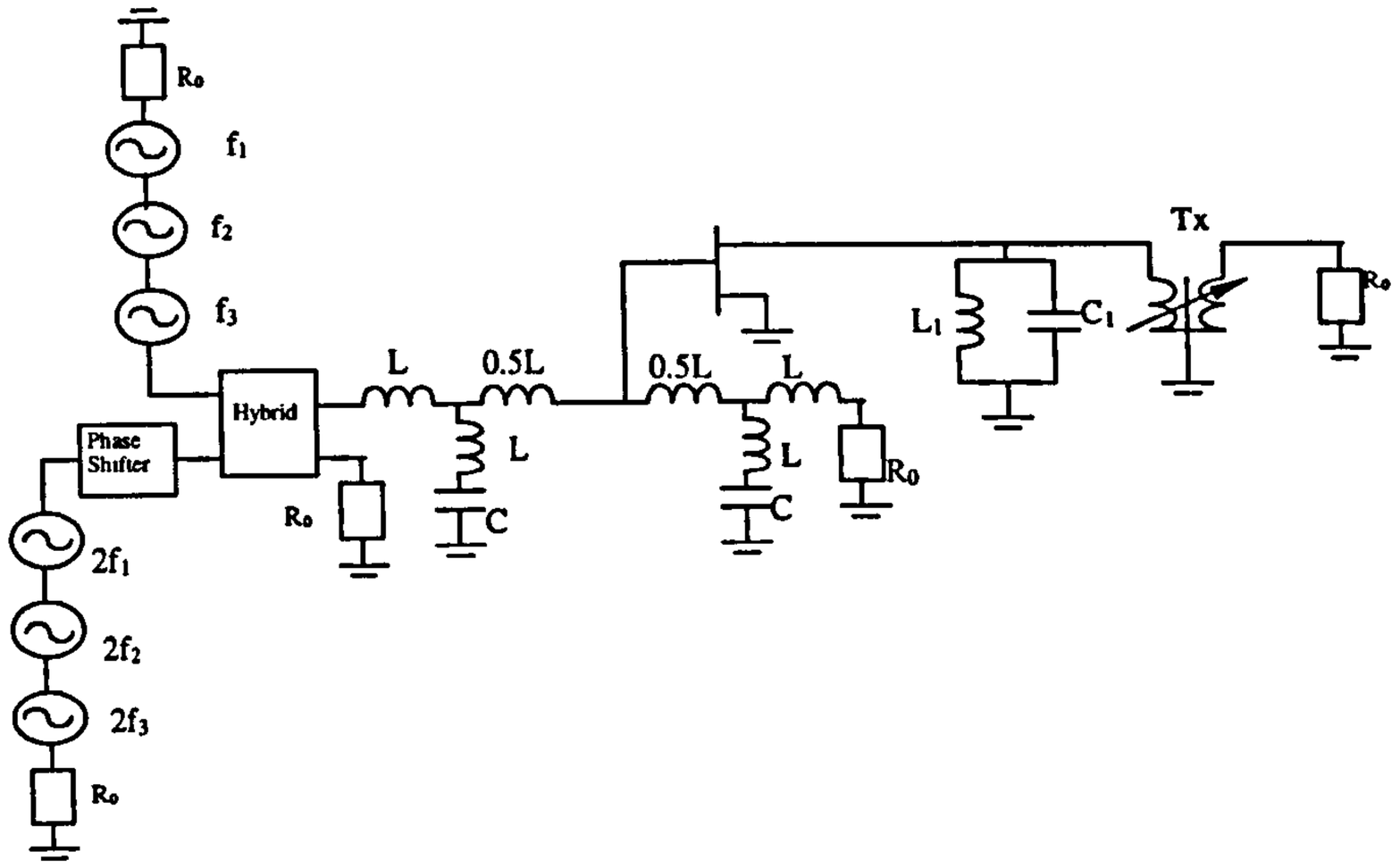

Figure 4..13: **The simulated amplifier schematic diagram(with $R_0 = 50\Omega$, and L and L_1, inductance values, C and C_1, capacitor values).**

The performances of the techniques are then compared.

The three-tone test simulation is performed on the Microwave Design System software[2] (MDS) [49], whereas the previous two-tone simulations were performed on the nonlinear circuit simulator Libra[3] from EESOF, high frequency design solutions [124]. Since the simulator models are identical, the simulation results remain identical. The decision to move from one CAD software to another was prompted by the possibility on the Microwave design software to simulate more than three independent signals.

The input signals f_1, f_2 and f_3 with the same amplitude and phase are fed into the input of the amplifier. The resulting output IMD3 level of the fundamental signals and the third order IMDs at $-20dBm$ input power level are shown in figure 4.14.

Three second harmonics, $2f_1$, $2f_2$ and $2f_3$, of the input signals at the frequencies

[2] The Microwave Design System is Hewlett Packard CAD tool for high frequency (microwave and RF) circuit design and analysis.

[3] Libra is a nonlinear circuit simulator which is part of Hewlett packard EESOF high frequency design solutions.

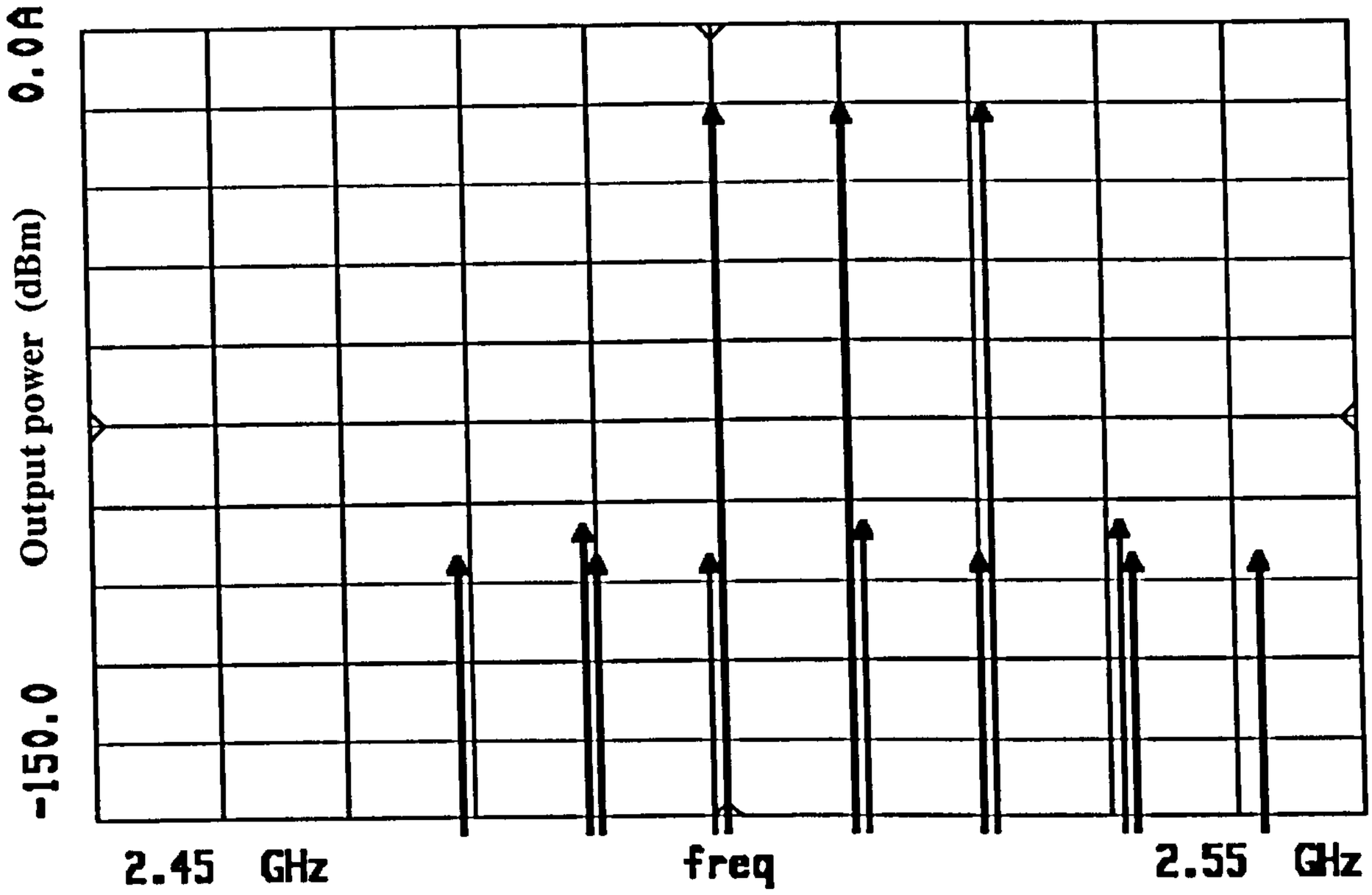

Figure 4..14: **Three-tone simulated output spectrum of amplifier without employing the techniques.**

$5GHz$, $5.02GHz$ and $5.042GHz$ are injected into the system, with the phases ϕ_{2f_1}, ϕ_{2f_2} and ϕ_{2f_3} $(\phi_{2f_1} = \phi_{2f_2} = \phi_{2f_3})$and amplitudes A_{2f_1}, A_{2f_1} and A_{2f_2} $(A_{2f_1} = A_{2f_1} = A_{2f_2})$, respectively. The signals are combined and passed through a phase shifter and attenuator, so as to alter the phase and amplitude of the harmonics in order to achieve a reduction in third order IMD levels. A drop in the power level of the third order IMD is noticed after optimisation of the phase and amplitude of the injected signals for best IMD rejection. The resulting intermodulation signal level after injection can be seen in figure 4.15. There is an improvement of over $35dB$ on the third order IMD in the amplifier but only on the first kind of third order IMDs. For a phase shift of about 181.8^o and amplitude of $-42.4dBc$, a reduction of more than $30dB$ was achieved. The results obtained for the three-tone system are the same as those obtained with the use

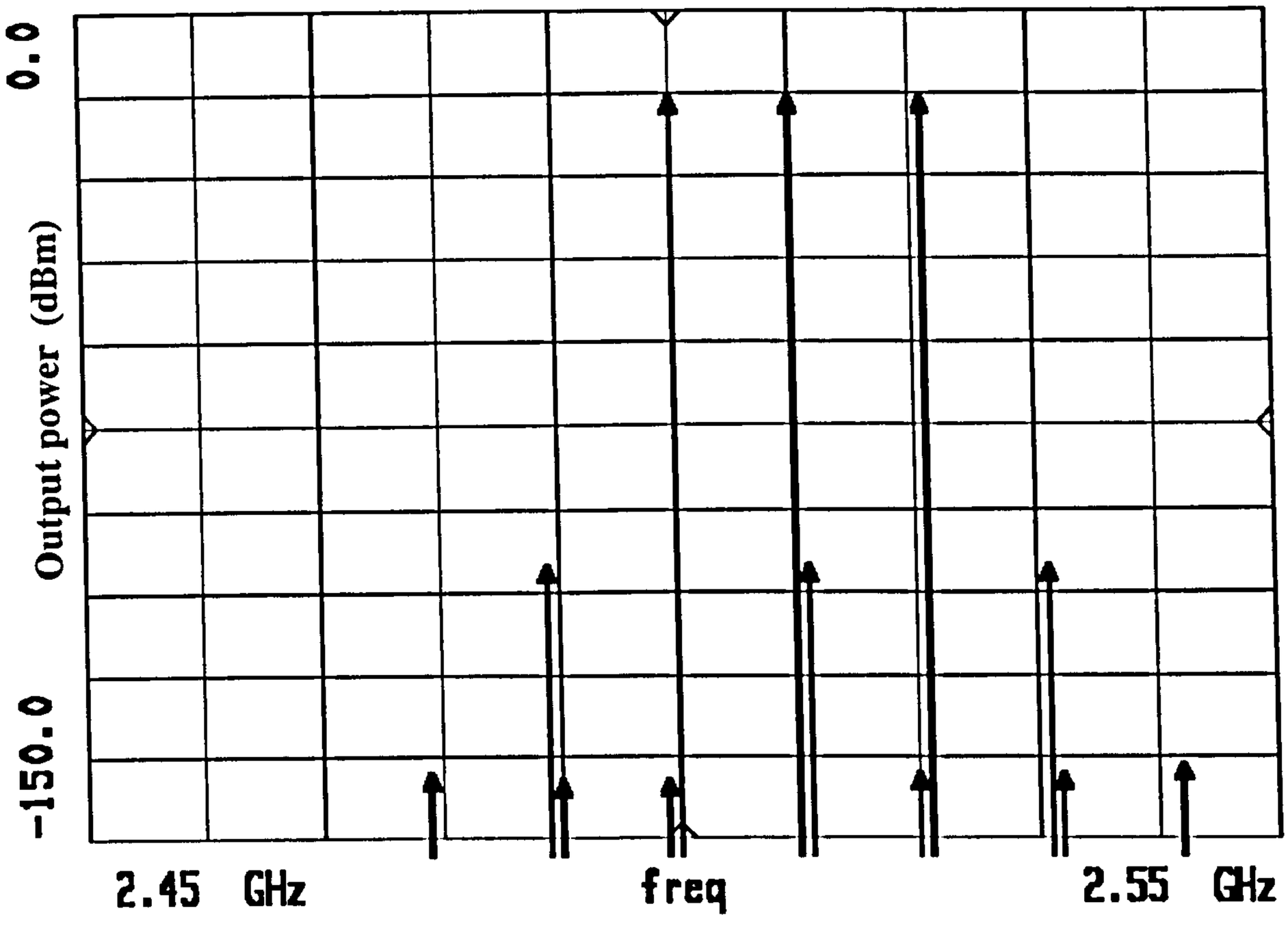

Figure 4..15: **Three-tone simulated output spectrum of amplifier after injection of the second harmonic signals, showing a reduction in the 1st kind of IMD3 of more than 30dB and no reduction in the 2nd kind of IM3.**

of two signals for the first kind of IMD. The second kinds of IMD are not reduced by the injection of the second harmonic signals.

When using the difference technique, the difference frequencies of the input signal $(f_2 - f_1)$, $(f_3 - f_1)$ and $(f_3 - f_2)$ at the frequencies $10MHz$, $11MHz$ and $21MHz$ were injected into the amplifier together with the fundamental signals. The output of the amplifier shows that with the appropriate phase and amplitude of the injected signals, a reduction in the level of IMD3 is achieved. This is shown in figure 4.16 for the third order of IMD with an optimisation at the input power of $-20dBm$. The first and the second kind of IMDs are reduced substantially by the technique. This clearly confirms the theoretical results obtained previously. The first kinds of IMD are reduced by more

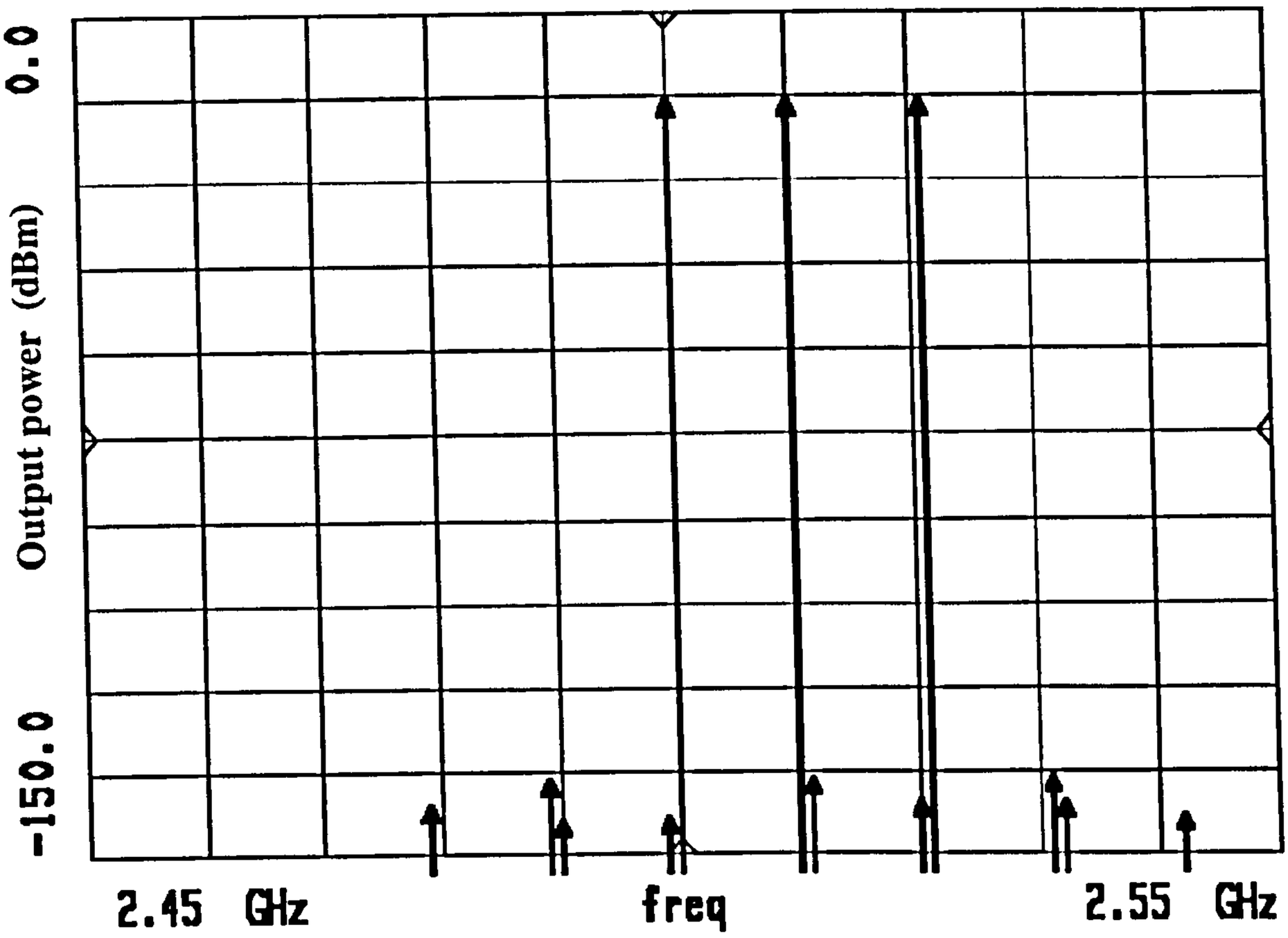

Figure 4..16: **Three-tone simulated output spectrum of amplifier after injection of the difference frequency signals, showing a reduction in the 1st kind of IMD3 and the 2nd kind of IM3 of more than 35 dB.**

than $30dB$ and the second kind by more than $30dB$ as well.

The injection of the signals whose frequencies are the sum of the fundamental signals $(f_2 + f_1)$, $(f_2 + f_3)$ and $(f_3 + f_1)$ at the frequencies $5.01GHz$, $5.031GHz$ and $5.021GHz$, shows that the first kinds of IMD3 are not reduced. On the other hand the second kinds of IMD are reduced by more than $30dB$. The test is performed at the input power of $-20dBm$ (the input signal have the same amplitude and phase)and confirms the theory. Figure 4.17 shows the output spectrum of the system with the fundamental signals with a reduction in the second kind of IMDs and no reduction in the first kind of third order IMDs (see table 4.2).

The reduction of the third order intermodulations by the signal injection does

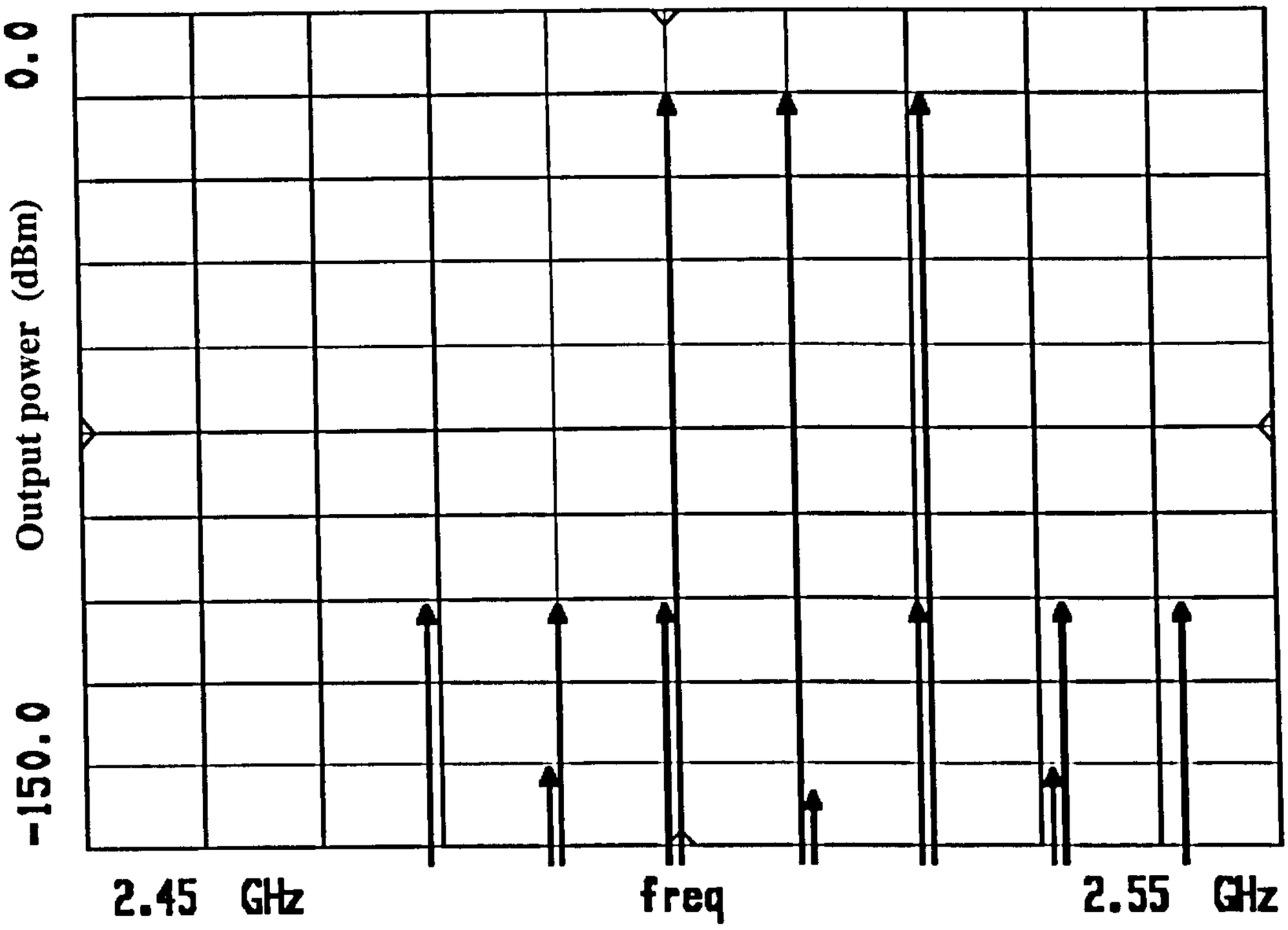

Figure 4..17: **Three-tone simulated output spectrum of amplifier after injection of the sum of the fundamental frequencies, showing a reduction in the first kind of IMD3 of 5dB and a reduction of the second kind of IM3 of more than 35 dB.**

not cause a change in the fundamental signal as shown in figure 4.15 for the second harmonic, figure 4.16 for the difference frequency injection and figure 4.17 for the injection of the sum of fundamental frequencies. Figure 4.18 shows the fundamental signal f_1 before and after applying the second harmonic injection technique. The signal does not change as the technique is applied. Similar results were obtained for the other two fundamental signals f_2 and f_3 and for all three IMD reduction techniques.

The increase in input power causes a decrease in the level of reduction of the intermodulation. This is shown in figure 4.19 where the difference frequency injection technique reduces the first kind of IMD3 components at the frequencies $(2f_1 - f_2)$ and

mathematical expression	frequency (GHz)	IM level without injection (dBm)	IM level with injection of second harmonic (dBm)	IM level with injection of difference frequency (dBm)	IM level with injection of frequency sum (dBm)
ω_1	2.5	-17.164	-17.097	-17.89	-17.099
ω_2	2.51	-17.162	-17.095	-17.087	-17.097
ω_3	2.521	-17.160	-17.093	-17.084	-17.095
$(2\omega_1 t - \omega_3 t)$	2.479	-107.858	-139.061	-141.571	-107.664
$(2\omega_1 t - \omega_2 t)$	2.49	-107.866	-140.707	-144.091	-107.672
$(2\omega_2 t - \omega_3 t)$	2.499	-107.859	-140.431	-143.667	-107.666
$(2\omega_2 t - \omega_1 t)$	2.52	-107.865	-140.268	-142.83	-107.671
$(2\omega_3 t - \omega_2 t)$	2.532	-107.858	-140.161	-142.879	-107.665
$(2\omega_3 t - \omega_1 t)$	2.542	-107.856	-138.581	-145.633	-107.662
$(\omega_2 t + \omega_1 t - \omega_3 t)$	2.489	-101.830	-101.632	-136.792	-136.847
$(\omega_1 t + \omega_3 t - \omega_2 t)$	2.511	-101.834	-101.636	-137.758	-141.747
$(\omega_3 t + \omega_2 t - \omega_1 t)$	2.531	-101.832	-101.634	-138.482	-138.15

Table 4..2: **Fundamental and third order IMD expressions and power levels with and without the techniques for a three-tone test at low power level.**

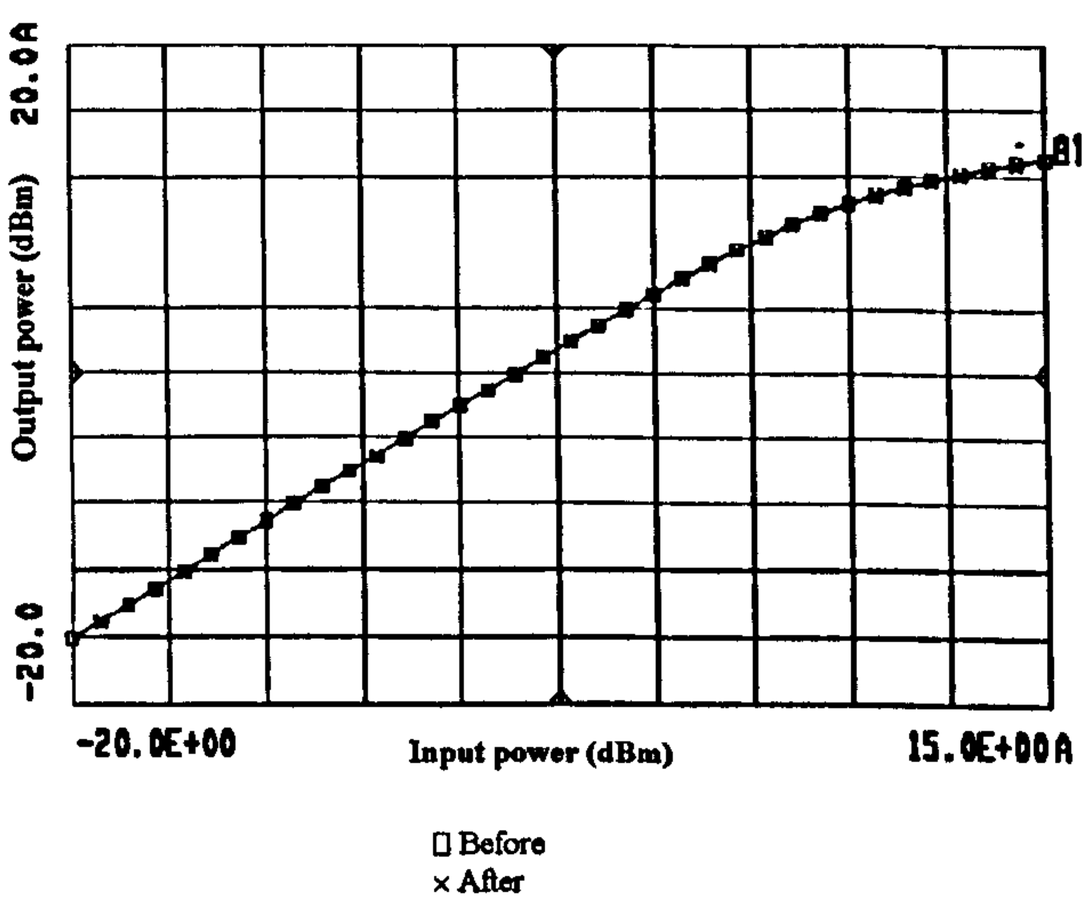

Figure 4..18: **Output Vs input power of the fundamental signal (f_1) at the frequency $2.5GHz$ before and after injection of the difference frequency signals.**

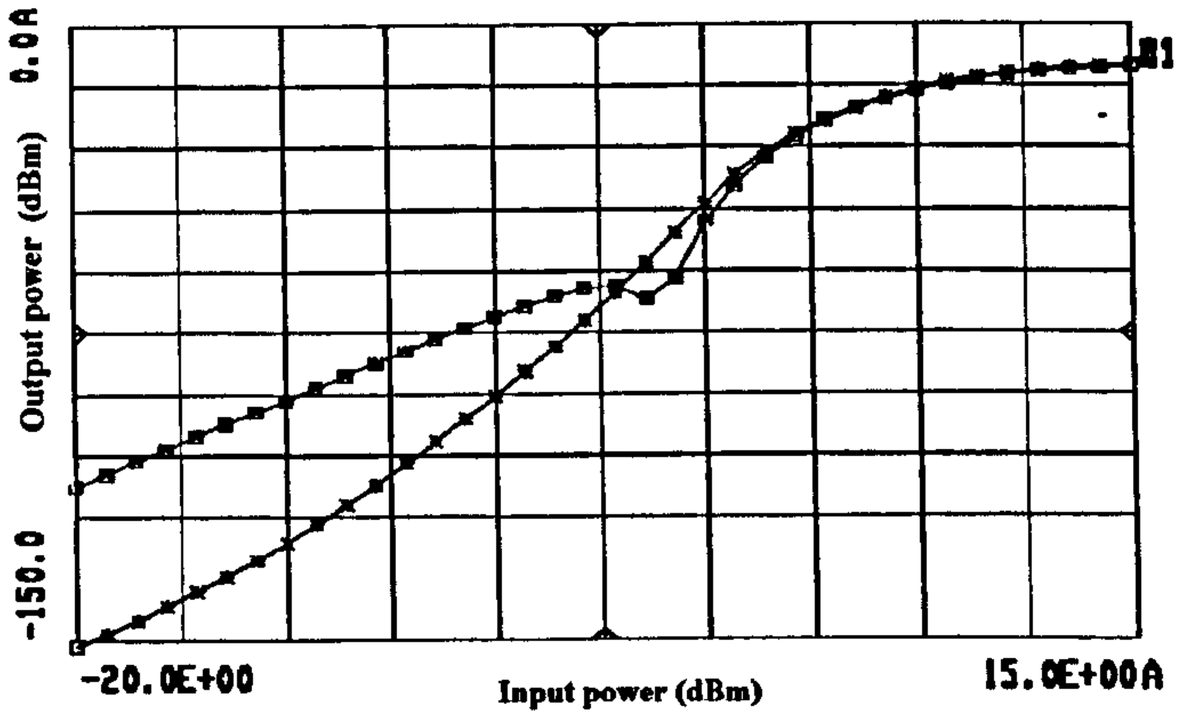

Figure 4..19: **Output Vs input power of the intermodulation signals $(2f_1 - f_2)$ and $(2f_1 - f_3)$ at the frequencies $2.49GHz$ and $2.479GHz$ before and after injection of the difference frequency signals.**

$(2f_1 - f_3)$ by more than $15dB$ for input power below -$10dBm$. Similar results are found for the other first kind of IMD3 components at the frequencies $(2f_3 - f_1)$, $(2f_3 - f_2)$, $(2f_2 - f_1)$ and $(2f_2 - f_3)$ (see appendix c). The reduction of the second kinds of IMD3 is shown in figure 4.20 for the signal $(f_1 - f_2 + f_3)$. Similar results are found for the signals $(f_1 + f_2 - f_3)$ and $(f_3 + f_2 - f_1)$.

The second harmonic injection shows a reduction in the first kind of IMD3 that diminishes with increasing input power level. The reduction in the first kind of IMD3 $(2f_1 - f_2)$ and $(2f_2 - f_1)$ are shown in figure 4.21. The second harmonic injection does not reduce the first kind of IMD as previously demonstrated and it is shown in figure 4.22 for the signals $(f_1 - f_2 + f_3)$. Similar results are found for the signals $(f_1 + f_2 - f_3)$ and $(f_3 + f_2 - f_1)$.

The injection of the sum of the fundamental signal gives similar reduction as the difference frequency technique for the second kind of IMD and no reduction on the

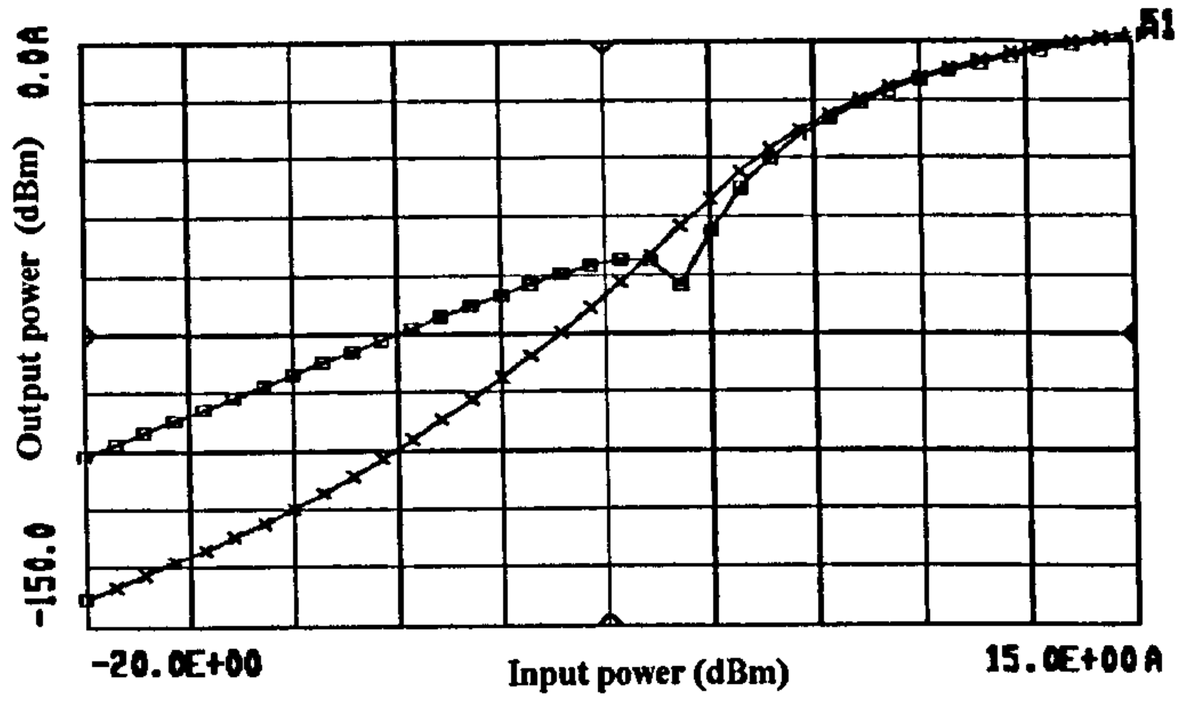

Figure 4..20: **Output Vs input power of the intermodulation signal $(f_1 - f_2 + f_3)$ at the frequency $2.511GHz$ before and after injection of the difference frequency signals.**

first kind of IMD3. The reduction level was further reduced at higher power level.

At $-20dBm$ input power a reduction of $30dB$ was obtained with the use of the difference frequency technique on both kinds of IMD3. The second harmonic gives a $30dB$ reduction on the first kind of IMD3 and the injection of the sum of the fundamental frequencies gives a reduction of $30dB$ on the second kind of IMDs. At $-10dBm$, with the same optimum phase and amplitude, the reduction in IMD3 is smaller ($\simeq 15dB$). At higher power levels, the reduction does not occur since the nonlinearity of the device creates a different phase relation between the input and output signals. This is illustrated in figure 4.23 for the second kinds of IMD3 and figure 4.24 and figure 4.25 for the first kinds of IMD3. The nonlinearity of the amplifier shows that at lower power level, the phase relation between the signal is very close with a difference of less than 1° between the signal at $-20dBm$ input power and $-10dBm$. This difference in phase increases with input power and the linear relation collapses in the high power region

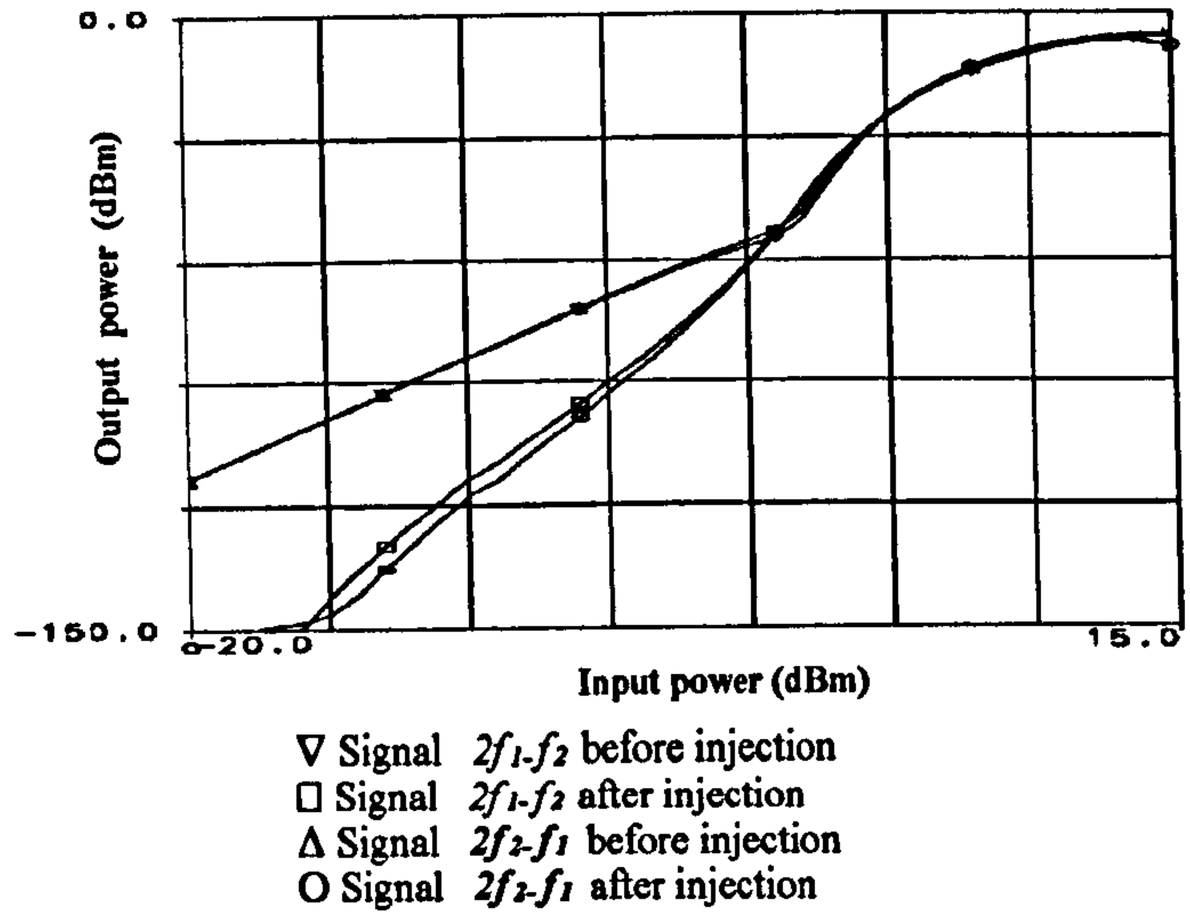

Figure 4..21: **Output Vs input power of the intermodulation signals($2f_1 - f_2$) and ($2f_2 - f_1$) at the frequencies $2.49GHz$ and $2.52GHz$ before and after injection of the second harmonic signals.**

where the change in phase can be up to 180° for an increase of $1dB$ in power.

These results clearly show that although a reduction at $-10dBm$ input power can be reached with the same optimised phase and amplitude as at $-20dBm$ input power, there is a need for a different phase and amplitude adjustment according to power levels. At higher power level, the optimum phase of the injected signals needs to be very different. The use of different phases and amplitudes for each signal injected in the system will therefore give better results. It can be achieved through the careful use of a phase and amplitude control for the injected second harmonic, difference frequency or the sum of the fundamental signals.

Phase nonlinearities in the amplifier change with frequency as shown in figure 4.26. The lowest IMD at the frequency $2.479GHz$ will have a phase that is very different from the phase of the highest third order IMD signals at the frequency $2.542GHz$ at the output of the amplifier. The difference in phase at the output for these two

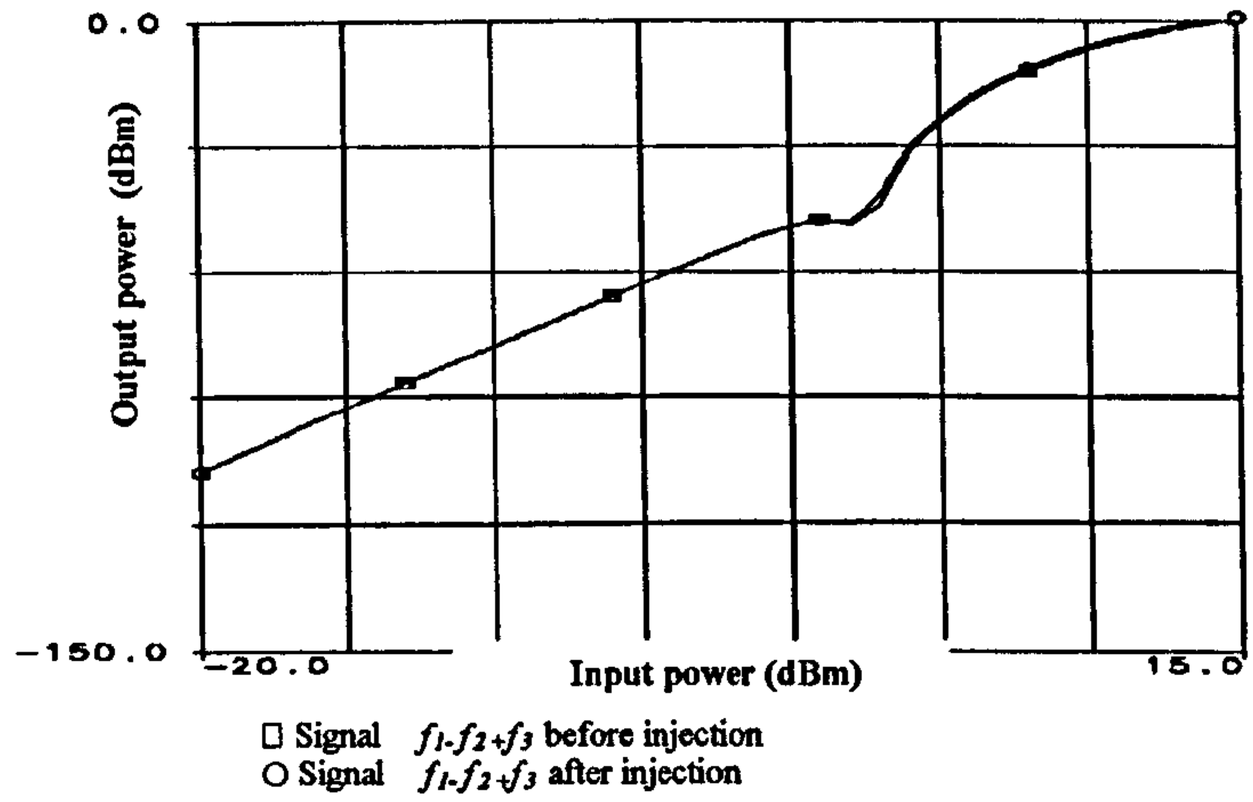

Figure 4..22: **Output Vs input power of the intermodulation signal $(f_1 - f_2 + f_3)$ at the frequency $2.511GHz$ before and after injection of the second harmonic signals.**

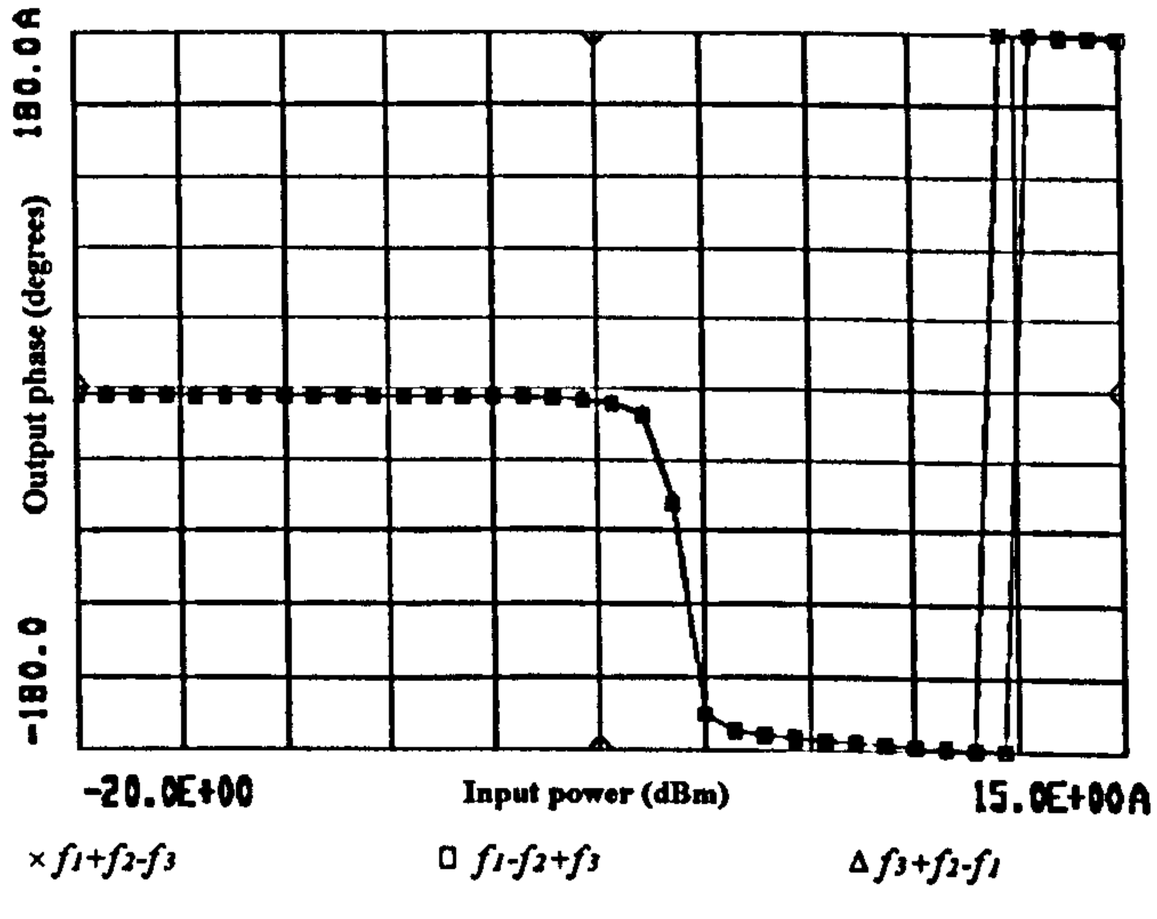

Figure 4..23: **Output phase variation of the IMD signals $(f_1 + f_2 - f_3)$, $(f_1 - f_2 + f_3)$ and $(f_3 + f_2 - f_1)$ at the frequencies $2.489GHz$, $2.511GHz$ and $2.531GHz$ at the output of the amplifier.**

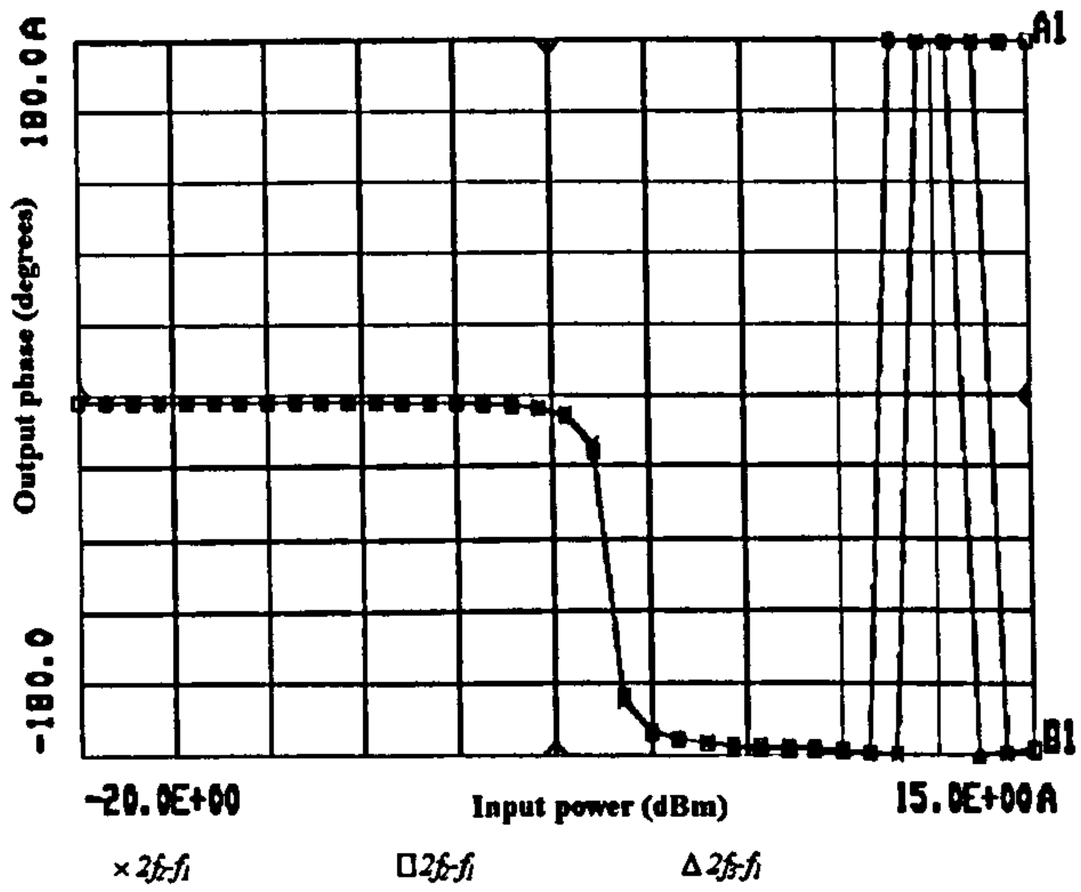

Figure 4..24: **Output phase variation of the IMD signals $(2f_2 - f_1)$, $(2f_2 - f_1)$ and $(2f_3 - f_1)$ at the frequencies $2.49GHz$, $2.52GHz$ and $2.542GHz$ at the output of the amplifier.**

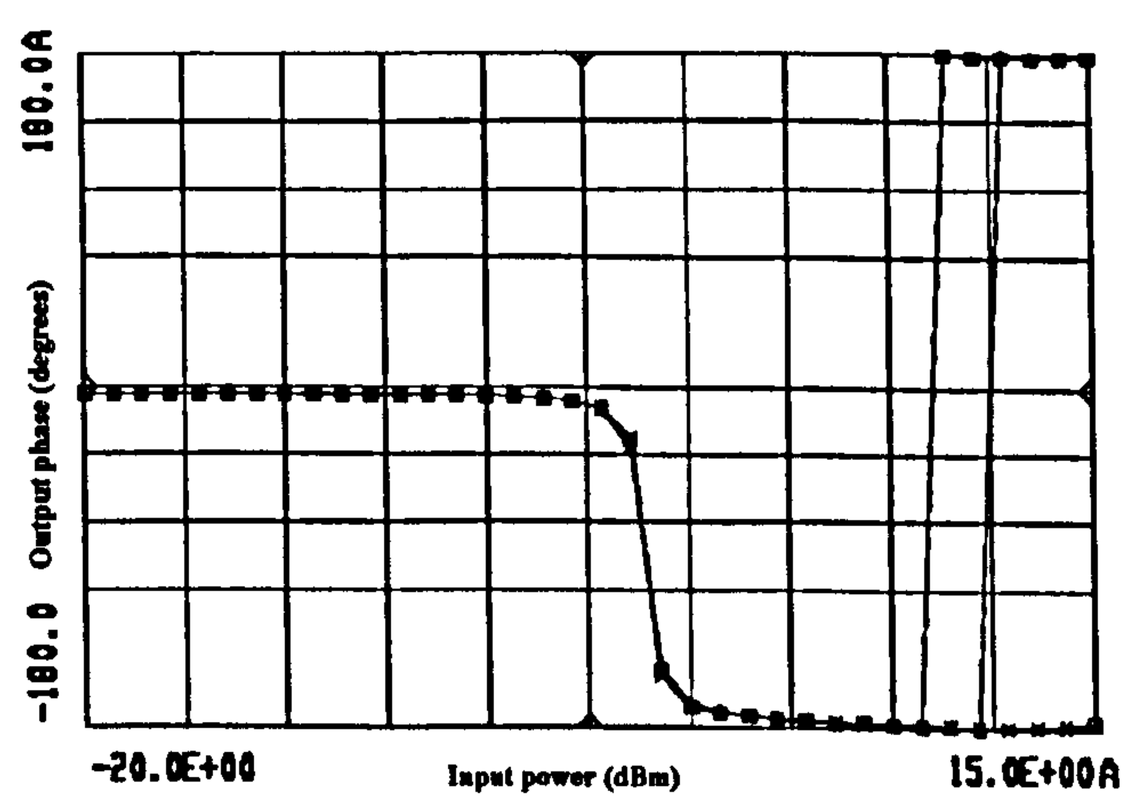

Figure 4..25: **Output phase variation of the IMD signals $(2f_1 - f_3)$, $(2f_2 - f_3)$ and $(2f_3 - f_2)$ at the frequencies $2.479GHz$, $2.499GHz$ and 2.53GHz at the output of the amplifier.**

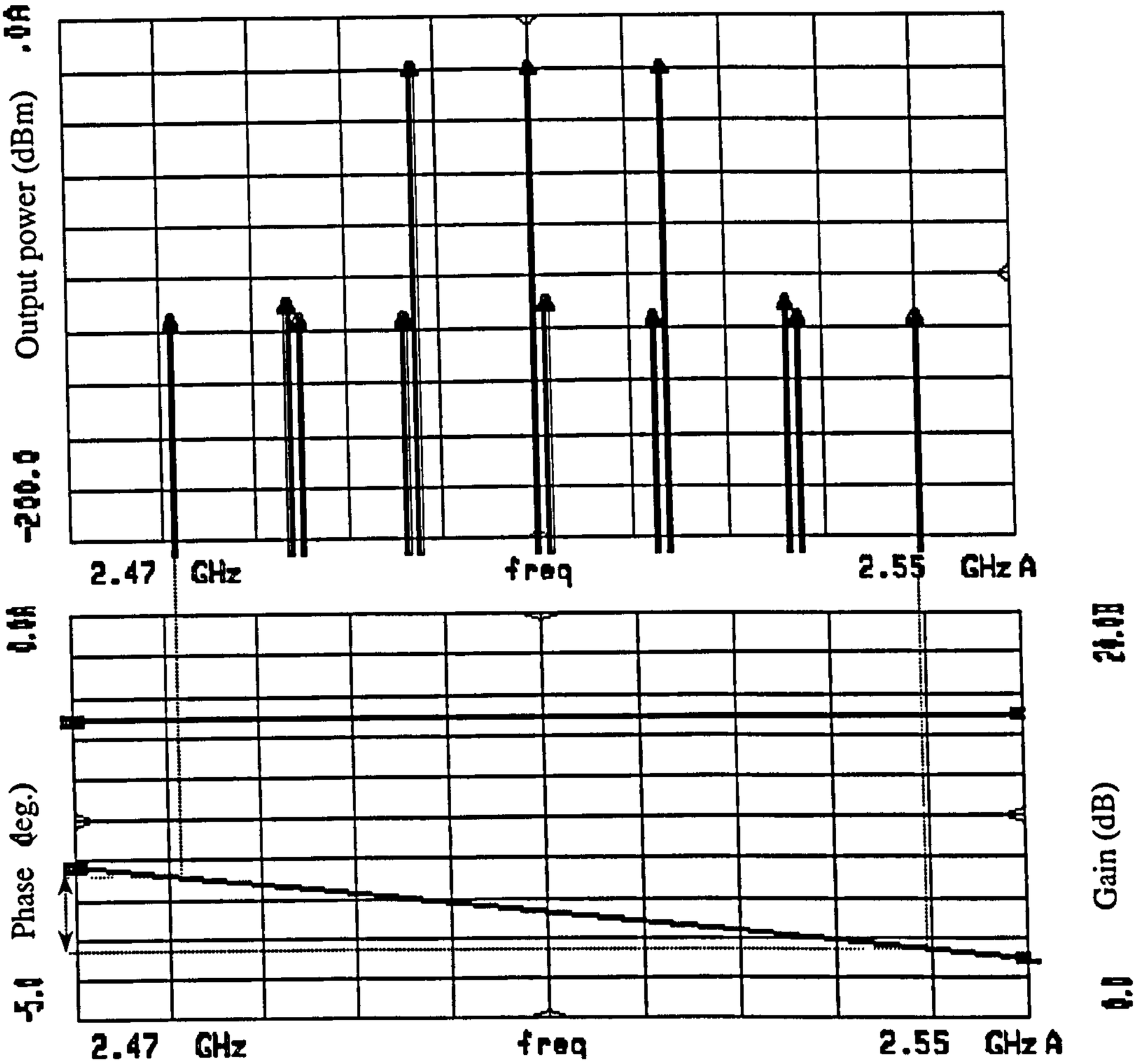

Figure 4..26: **Output spectrum and non-linear phase response of amplifier, showing the different IMD and the correspondings phase informations.**

signals is about 1°. This accounts for the disparities in the reduction in level of the intermodulation products for a fixed phase of the injected signals. It implies that the use of a single phase shifter for the injected signals which provides a similar phase to all injected signals, is not an adequate for the reduction of all IMDs simultaneously since the phase of each signal is different.

The use of different phases for each of the difference frequency signals at the frequencies $(f_2 - f_1)$, $(f_3 - f_1)$ and $(f_3 - f_2)$ shows that the reduction in the IMD

level is further improved on both the first and second kind of third order IMDs. The improvement of the IMD by the use of different phases for each injected signal is related to the fact that the amplifier introduces phase nonlinearities which are frequency dependent. Phase variation between the lowest IMD signals and the highest product is about 5°. The difference between each third order product of about 1° is significant enough to create disparities in the phase requirements for the cancellation of each signal. Ideally, an optimum reduction of the IMD3s is obtained by the use of a different phase and amplitude for each of the injected signals.

4.6 Amplitude and Phase Change Effects on Third Order IMD

The effects of the variation of the phase and amplitude of the injected signals on the IMDs are observed around the above optimised values. The tests give an insight into the phase effect and amplitude effect on IMD3 levels to enable the derivation of the requirements for an effective IMD reduction in the system. A variation of the injected signal phase and amplitude is performed in order to study the effect on the intermodulation performance of the techniques

The second harmonic signals are phase shifted using the phase shifter as shown in the circuit of figure 4.7. The amplitudes and phases of the signals are simultaneously varied. The change in output power of the IMD3 to the amplitude and phase variation as shown in figure 4.27 for the third order IMD at the frequency $(2f_1 - f_3)$, exhibits a minimum around the value of the phase of 181° and amplitude of $-42.5dBc$. This shows that a reduction of more than $30dB$ can be achieved. Similar results were obtained for other first kind of IMDs at the frequencies $(2f_1 - f_2)$, $(2f_2 - f_3)$, $(2f_2 - f_1)$, $(2f_3 - f_1)$

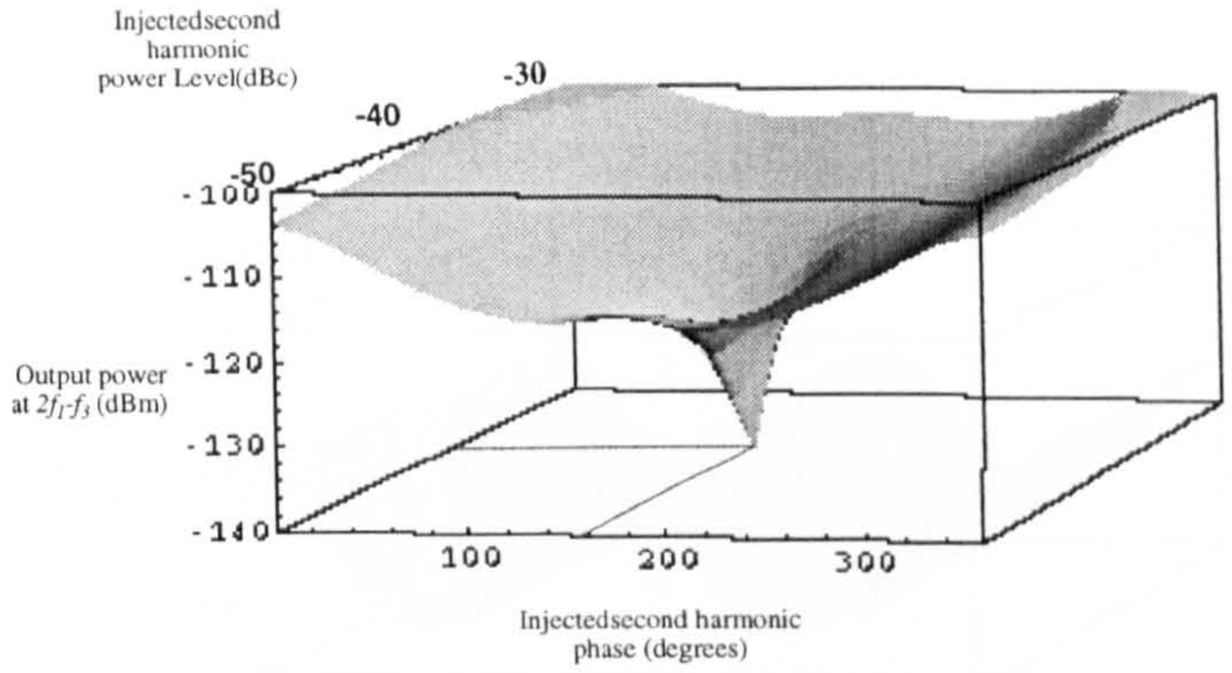

Figure 4..27: **Third order IMD $(2f_1 - f_3)$ amplitude variation as a function of injected second harmonic signal amplitude and phase.**

and $(2f_3 - f_2)$ (see appendix d). The output power level for the fundamental signals f_1, f_2 and f_3 remains constant to within $\pm 1dB$ with variations of the phases and amplitudes of the injected signals. Figure 4.28 shows the amplitude level of the fundamental signal f_1 as a function of phase and amplitude of the injected second harmonic.

The graph showing the change in the second kind of IMD3 power level does not display a single deep minimum, which proves that the second harmonic technique does not significantly reduce the second kind of IMD3. The results of the variation of the amplitude of the signal at the frequency $(f_1 + f_2 - f_3)$ are presented in figure 4.29. Similar results were obtained for the other second kinds of IMD3 at the frequencies $(f_1 - f_2 + f_3)$ and $(f_3 + f_2 - f_1)$.

The first kind of IMDs do not give a significant reduction with the injection of the sum of the fundamental frequencies, since the graph of the variation of the power level of the first kind of IMD does not show a significant reduction in the signal level.

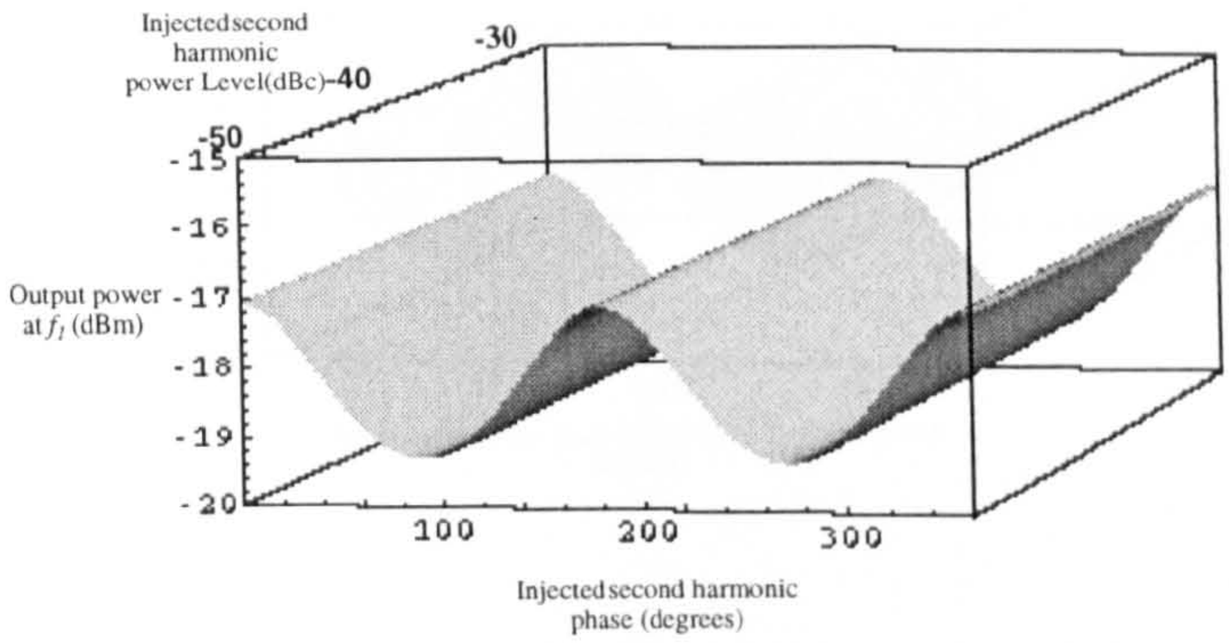

Figure 4..28: **Third order IMD f_1 amplitude variation as a function of injected second harmonic signal amplitude and phase.**

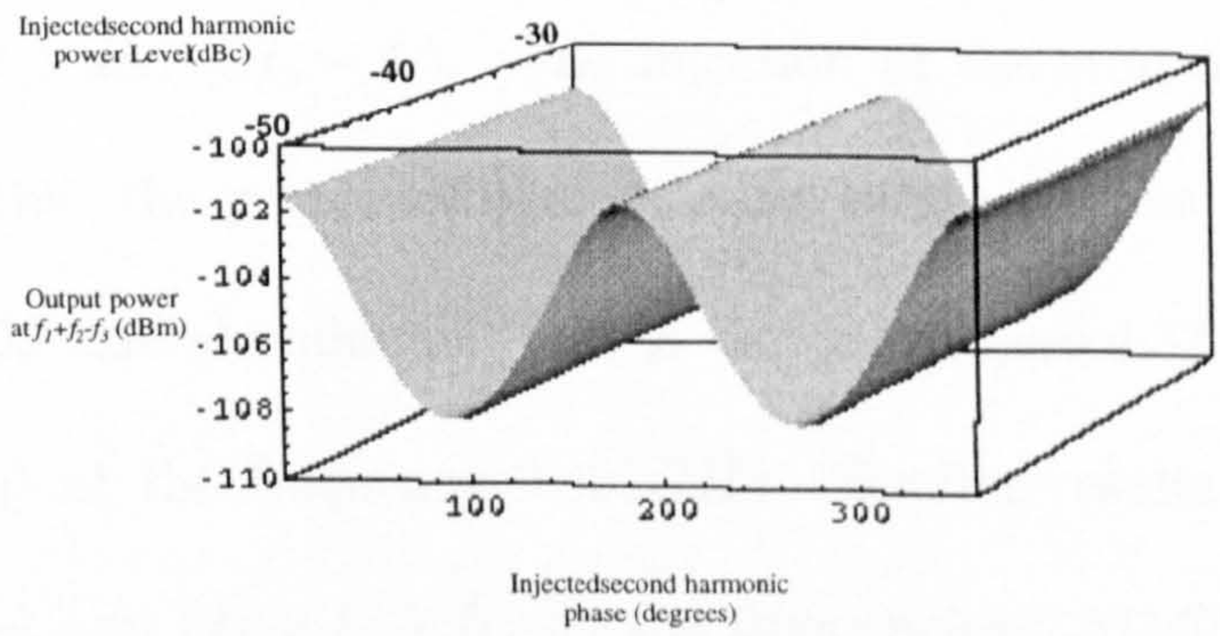

Figure 4..29: **Third order IMD $(f_1 + f_2 - f_3)$ amplitude variation as a function of injected second harmonic signal amplitude and phase.**

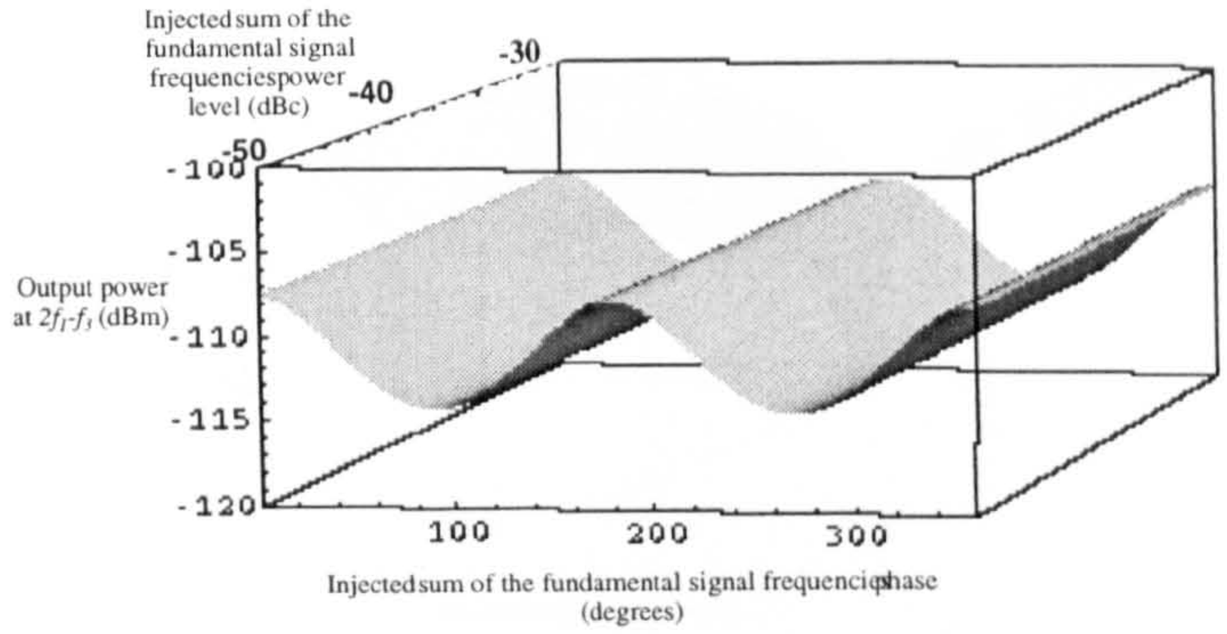

Figure 4..30: **Third order IMD $(2f_1 - f_3)$amplitude variation as a function of injected sum of the fundamental signals amplitude and phase.**

The variation in the signal power level at the frequency $(2f_1 - f_3)$ shown in figure 4.30, shows a slight change as the amplitude and the phase of the sum of the fundamentals signals are varied. A reduction of 10dB can be achieved for a phase of 90° or 270°. Similar results are found for all other first kind of IMD3 signals, $(2f_1 - f_2)$, $(2f_2 - f_3)$, $(2f_2 - f_1)$, $(2f_3 - f_2)$ and $(2f_3 - f_1)$. The injection of the sum of the fundamental frequencies shows that the graphs of the variation of the output power level of the second kind of IMD3 exhibits minima. This is shown in figure 4.31 for the third order signal $(f_1 + f_2 - f_3)$ at the frequency $2.489GHz$. Similar results are found for the signal $(f_1 - f_2 + f_3)$ and $(f_3 + f_2 - f_1)$ at the frequencies $2.511GHz$ and $2.531GHz$ respectively. The graph shows a deep minimum (more than $30dB$ reduction) for a phase of 182° and an amplitude of $-36.3dBc$ of the injected signals.

Results obtained with the injection of the difference frequency shows that for the first kinds of IMD3 and the second kind of IMD3, minima are exhibited as shown

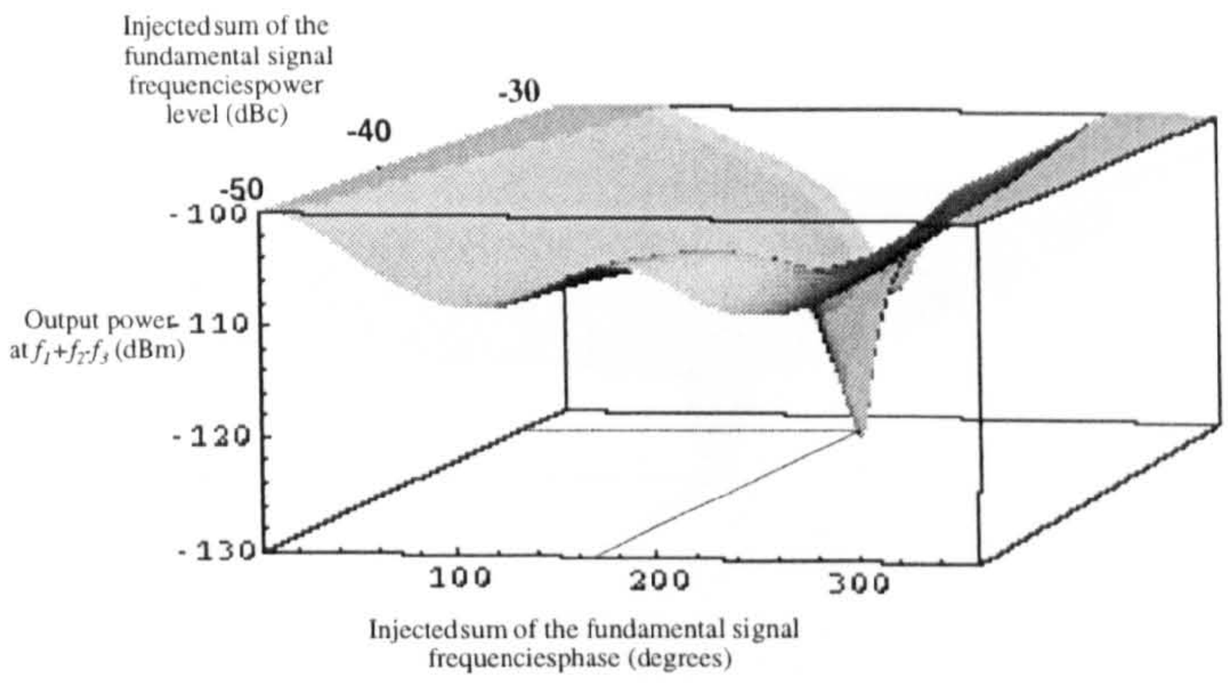

Figure 4..31: **Third order IMD$(f_1 + f_2 - f_3)$ amplitude variation as a function of injected sum of the fundamental signal frequencies amplitude and phase.**

in figure 4.32 and figure 4.33 for the signals $(2f_1 - f_3)$ and $(f_1 + f_2 - f_3)$ respectively. A phase of $181.6°$ and amplitude of $-42.5dBc$ is required to reduce the first kind of IMD3 signals for the signal $(2f_1 - f_3)$ as shown in figure 4.32. The graph shows a region for which the level of the intermodulation drops significantly (more than $30dB$). Similar results are found for other first kind of IMDs. A phase of $181°$ and amplitude of $-42.5dBc$ is required for the reduction of the second kind of IMD3 signal $(f_1 + f_2 - f_3)$ of figure 4.33.

The analysis shows that the signal at the frequency $(f_1 - f_2 + f_3)$ has a complex behaviour as the phase and amplitude of the injected signal changes (figure 4.34). It exhibits various minima. Since the reduction of all other IMD occurs for almost the same phase and amplitude, the value of phase and amplitude required for the cancellation of this signal corresponds to the same value as that required for the cancellation of all other third order IMDs. It is clear that around the phase and amplitude of about

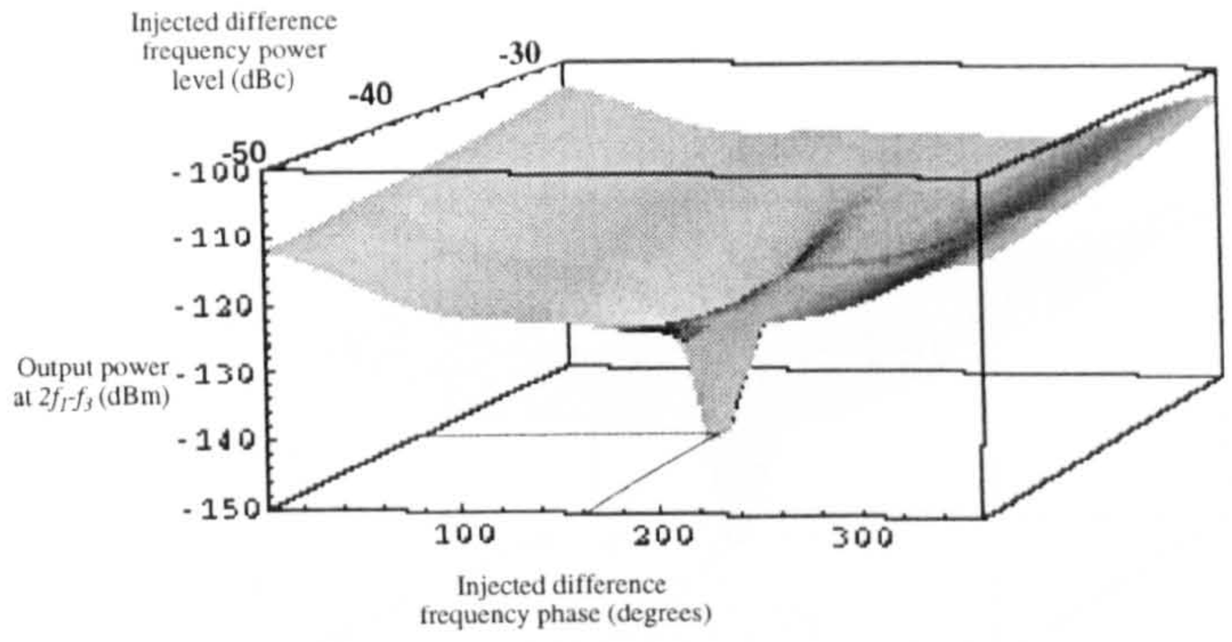

Figure 4..32: **Third order IMD $(2f_1 - f_3)$ amplitude variation as a function of injected difference frequency signal amplitude and phase.**

$180.5°$ and $-42.5dBc$ of the injected signal amplitudes, all third order IMD products are reduced by the injection of the difference frequency signals.

Although there is a reduction in third order IMD, the reduction in the signals does not occur for the same phase and amplitude of the injected signals. The phase and amplitude requirements for the cancellation of each intermodulation is further investigated in the next section. The phase and amplitude required for the cancellation of IMD3 can then be adjusted for better IMD performance with the use of more phase shifters or attenuators. The simulations performed with the different techniques shows that the fundamental signals f_1, f_2 and f_3 remain constant within $\pm 1dB$. The output response of the fundamental signal to the variation of the phase and amplitude of the injected signal is shown in figure 4.28. A similar results is obtained with the fundamental signal for the difference frequency technique and the injection of the summation frequencies.

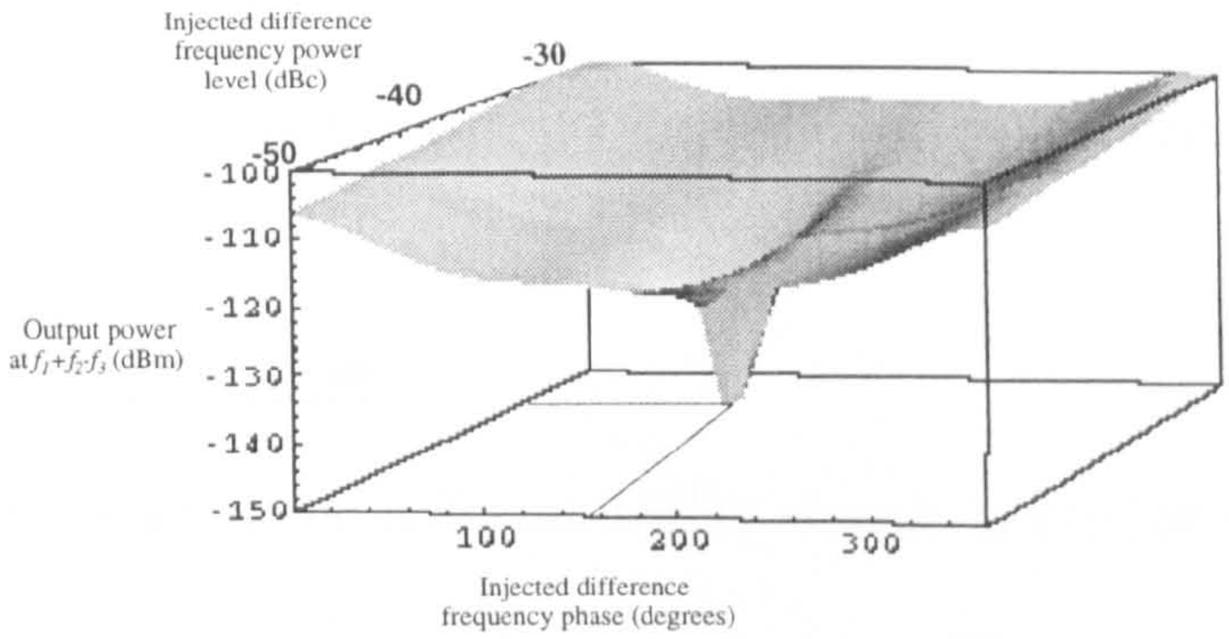

Figure 4..33: **Third order IMD($f_1 + f_2 - f_3$)amplitude variation as a function of injected difference frequency signal amplitude and phase.**

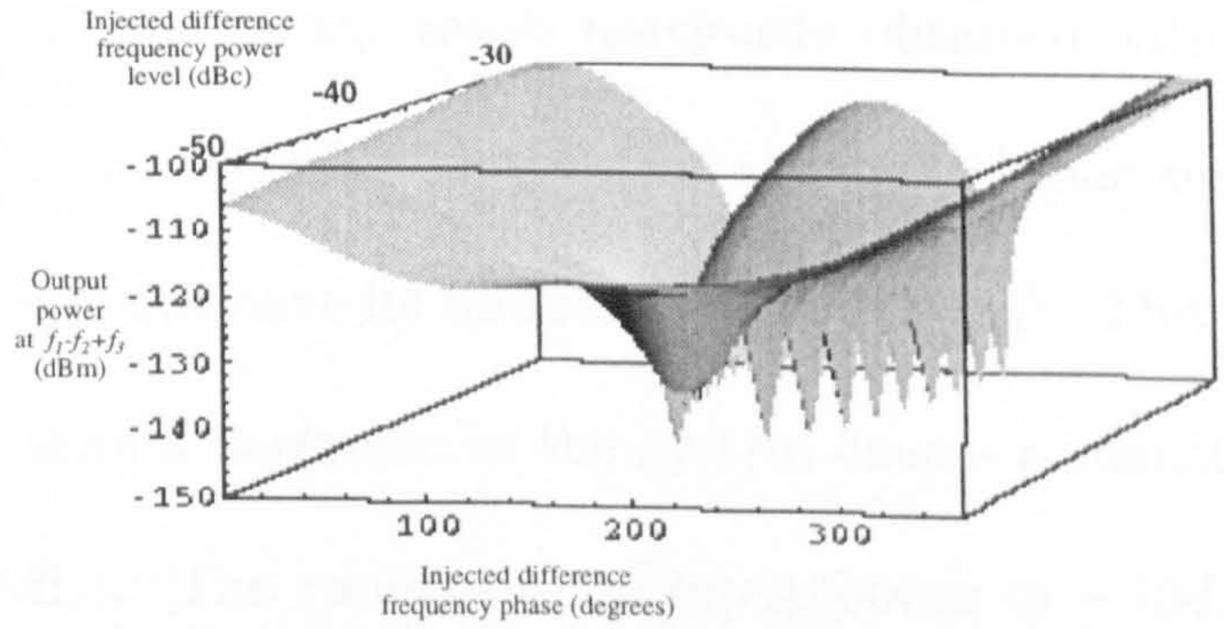

Figure 4..34: **Third order IMD** $(f_1 - f_2 + f_3)$ **amplitude variation as a function of injected difference frequency signal amplitude and phase.**

Fundamental input power (dBm)	Injected second harmonic input power(dBc)	Injected summation frequency input power (dBc)	Injected difference frequency input power (dBc)
0	−8	−6	−3.8
−10	−33.4	−27.4	−31.35
−20	−42.4	−36.2	−40.8

Table 4..3: **Amplitudes of the injected signals for optimum reduction of all IMD3.**

4.6.1 Phase Sensitivity of Systems

The change in power level of the different IMD3 signals is further investigated to determine the optimum phase for a maximum reduction. The tests are performed with constant amplitudes for all injected signals as obtained in section 4.5, after optimum reduction of all IMD3 (see table 4.3 for the amplitudes of injected signals). The injection of the second harmonic with a phase of about 181° causes a drop in the first kind of IMD by more than $30dB$. This is shown in figure 4.35 at the input power of $-20dBm$ for the signal $(2f_1 - f_3)$. Similar results are found for the other second kind os IMD3, $(2f_1 - f_2)$, $(2f_2 - f_3)$, $(2f_2 - f_1)$, $(2f_3 - f_2)$ and $(2f_3 - f_1)$.

This result is similar to the result previously obtained with optimisation. As the phase is changed, the level of IMD will drop slowly and then significantly between 170° and 190°, where it will have its minimum at about 181°. This clearly shows that the injection of the second harmonic in the system causes a reduction in the level of the first kinds of IMDs. The results at the input power of $-10dBm$ are similar to the results at $-20dBm$, showing a reduction in the level of the first kind of IMD by more than $30dB$. As the input power increases into the nonlinear region, the nonlinear effects cause a different behavior whereby the technique does not reduce the first kind of IMDs but reduces the second kind of IMDs as shown in figure 4.35 for the signal

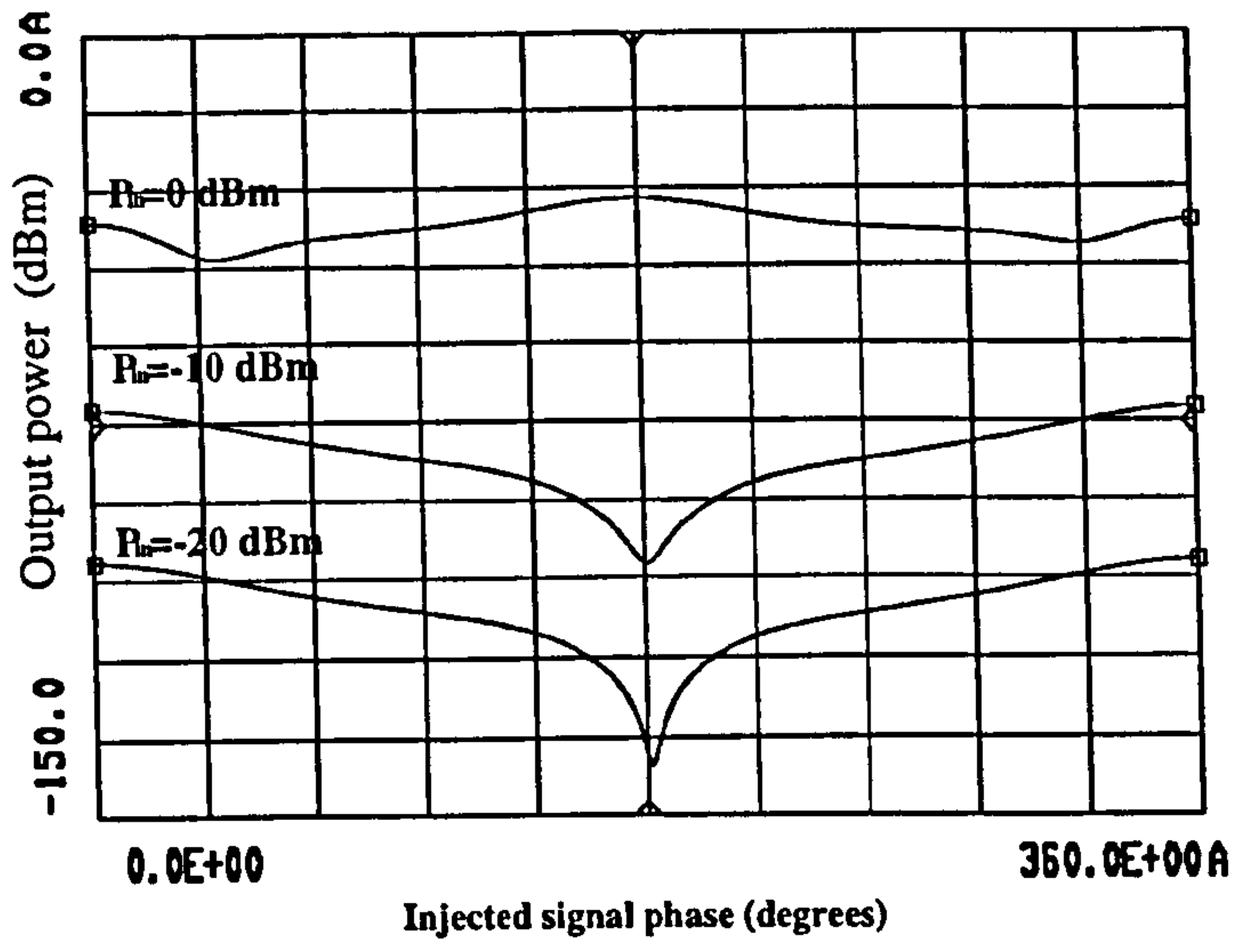

Figure 4..35: **Variations in the amplitude of IM term $(2f_1 - f_3)$ at the frequency $2.479GHz$ as a function of injected second harmonic signals phase for input power levels of $-20dBm$, $-10dBm$ and $0dBm$.**

$(2f_1 - f_3)$. Similar effects are observed for other first kind of IMD products $(2f_1 - f_2)$, $(2f_2 - f_3)$, $(2f_2 - f_1)$, $(2f_3 - f_2)$ and $(2f_3 - f_1)$ (see appendix e).

At input power levels below saturation, as illustrated by the results at input powers of $-20dBm$ and $-10dBm$, the technique of second harmonic injection does not give an appreciable reduction in the level of the second kind of IMD. In figure 4.36, the level of the second kind of IMD $(f_1 + f_2 - f_3)$ vary by $\pm 5dB$ for the entire 360° phase shift. The results of the signal $(f_1 - f_2 + f_3)$ and $(f_3 + f_2 - f_1)$ shows the same effects and there is no significant improvement on the IMD.

The amplitude of the fundamental signals remains constant to within $\pm 1dB$ with the injection of the sum of the pairs of the fundamental signals. The changes in the levels of the fundamentals signal f_1 are shown in figure 4.37 with the second harmonic injection. Similar results are found on the fundamental signal power level with the

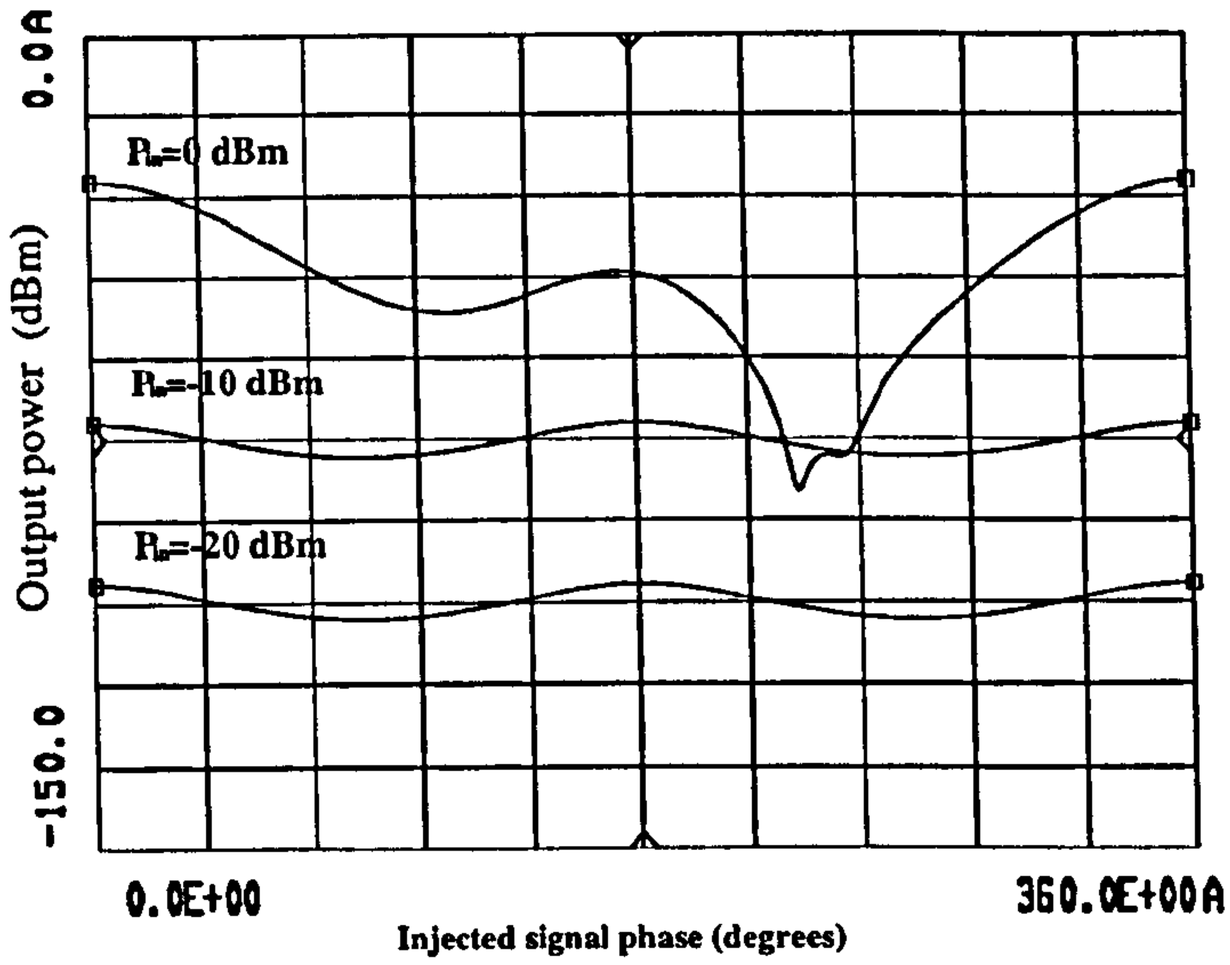

Figure 4..36: **Variations in the amplitude of IM term $(f_1 + f_2 - f_3)$ at the frequency $2.489GHz$ as a function of injected second harmonic signals phase for input power levels of $-20dBm$, $-10dBm$ and $0dBm$.**

injection of the sum of the fundamentals frequencies. The drop in the amplitude of the fundamentals is observed when the phase of the injected signal is at 90° and 270°. No decrease in the fundamental signal level is observed for a phase of between 175° and 185° where greater reduction in IMD3 power levels is achieved.

The injection of the sum of the fundamental signals, together with the original signals, shows results which are the opposite of those obtained using the second harmonic technique. The first kind of IMD3 are not reduced by the technique as shown in figure 4.38 for the signal $(2f_1 - f_3)$. The result of the other signals at the frequencies $(2f_1 - f_2)$, $(2f_2 - f_3)$, $(2f_2 - f_1)$, $(2f_3 - f_1)$ and $(2f_3 - f_2)$ are similar.

The second kind of IMD products $(f_1 + f_2 - f_3)$, $(f_1 - f_2 + f_3)$ and $(f_3 + f_2 - f_1)$ at the frequencies $2.489GHz$, $2511GHz$ and $2.531GHz$ are reduced by the injection of the sum of the fundamental signals frequencies at low power levels. This is shown in fig-

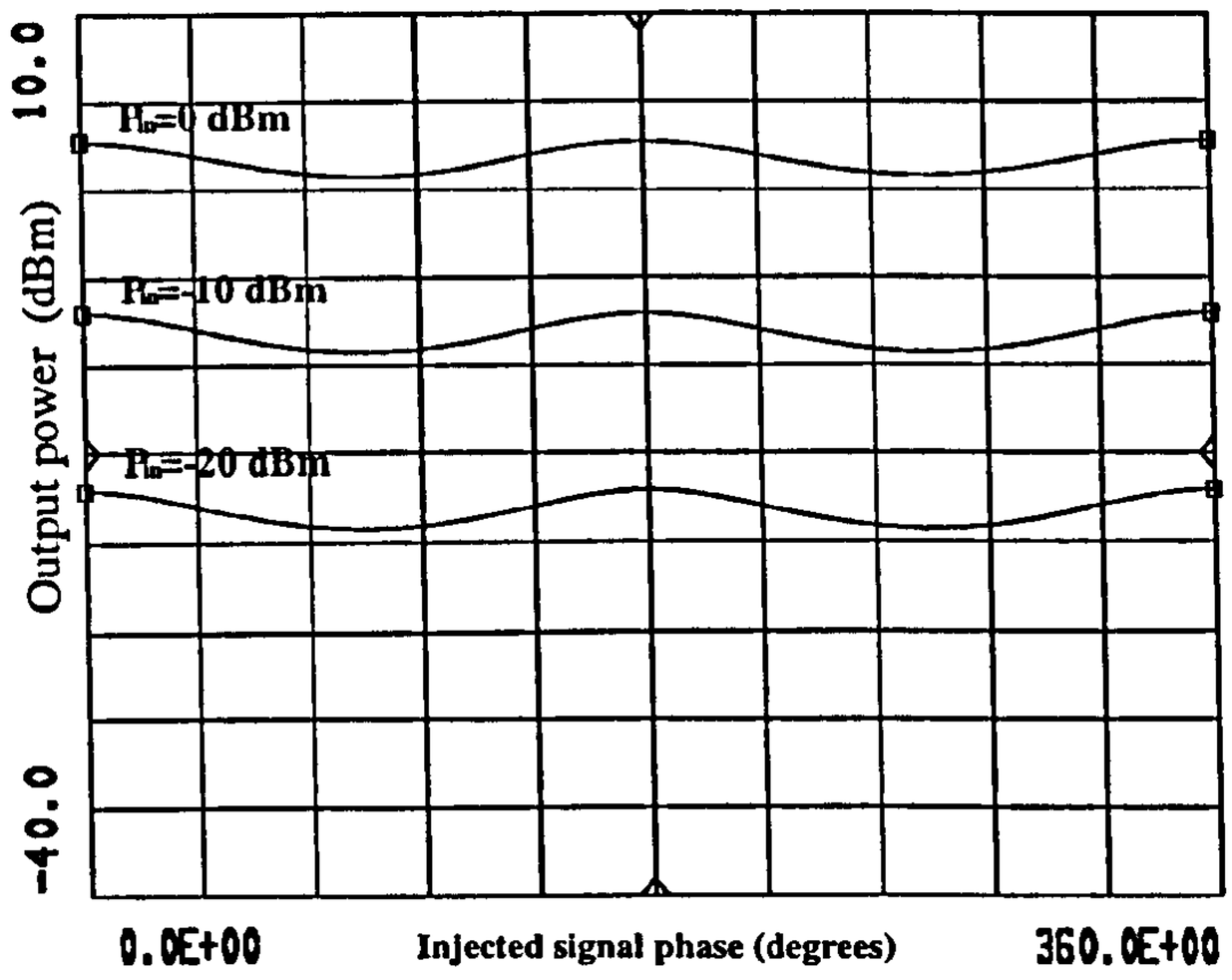

Figure 4..37: **Variations in the amplitude of the fundamental f_1 at the frequency $2.5GHz$ as a function of injected second harmonic signals phase for input power levels of $-20dBm$, $-10dBm$ and $0dBm$.**

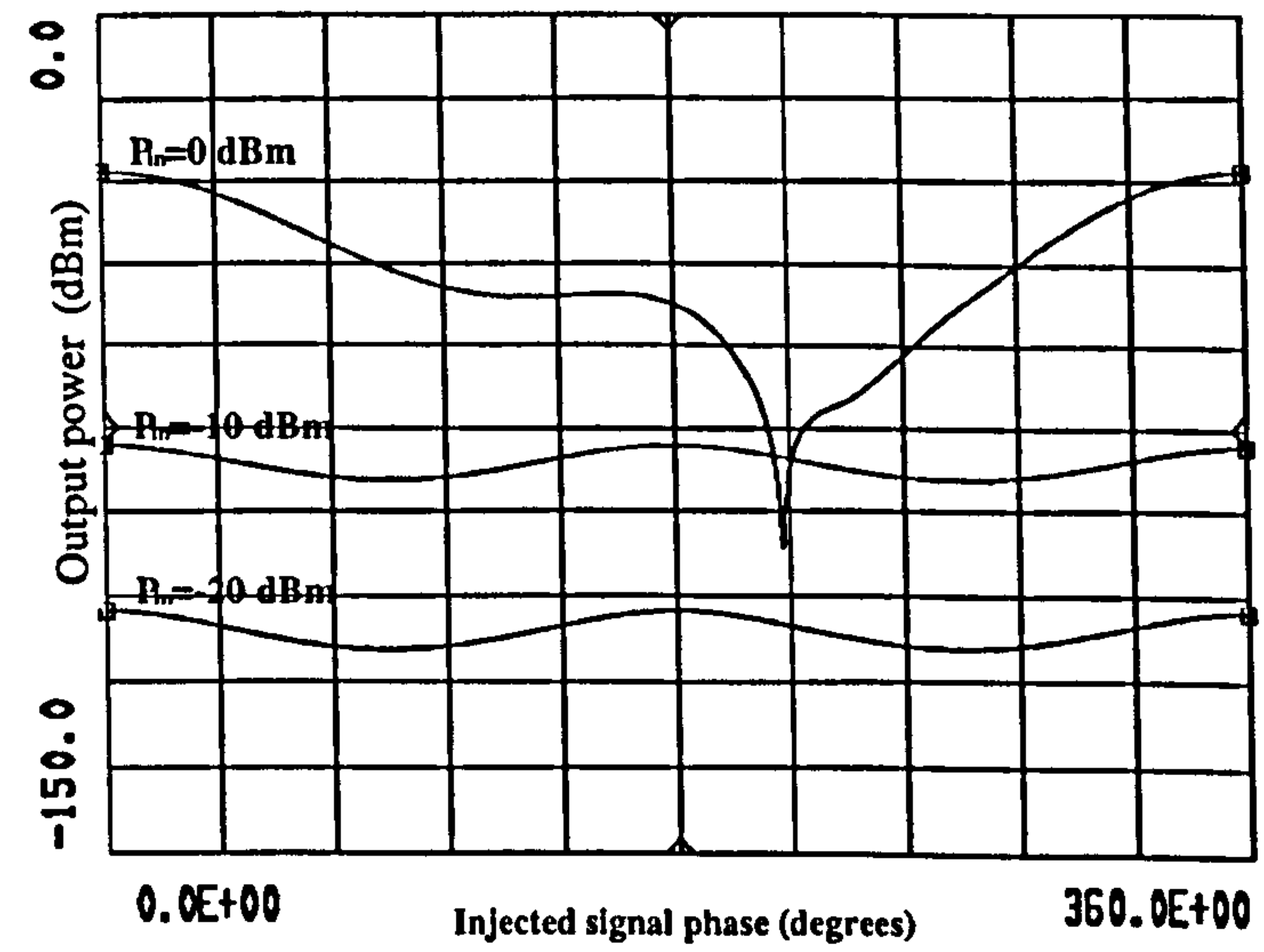

Figure 4..38: **Variations in the amplitude of the IM term $(2f_1 - f_3)$ at the frequency $2.479GHz$ as a function of frequency sum of the fundamental signals phase for input power levels of $-20dBm$, $-10dBm$ and $0dBm$.**

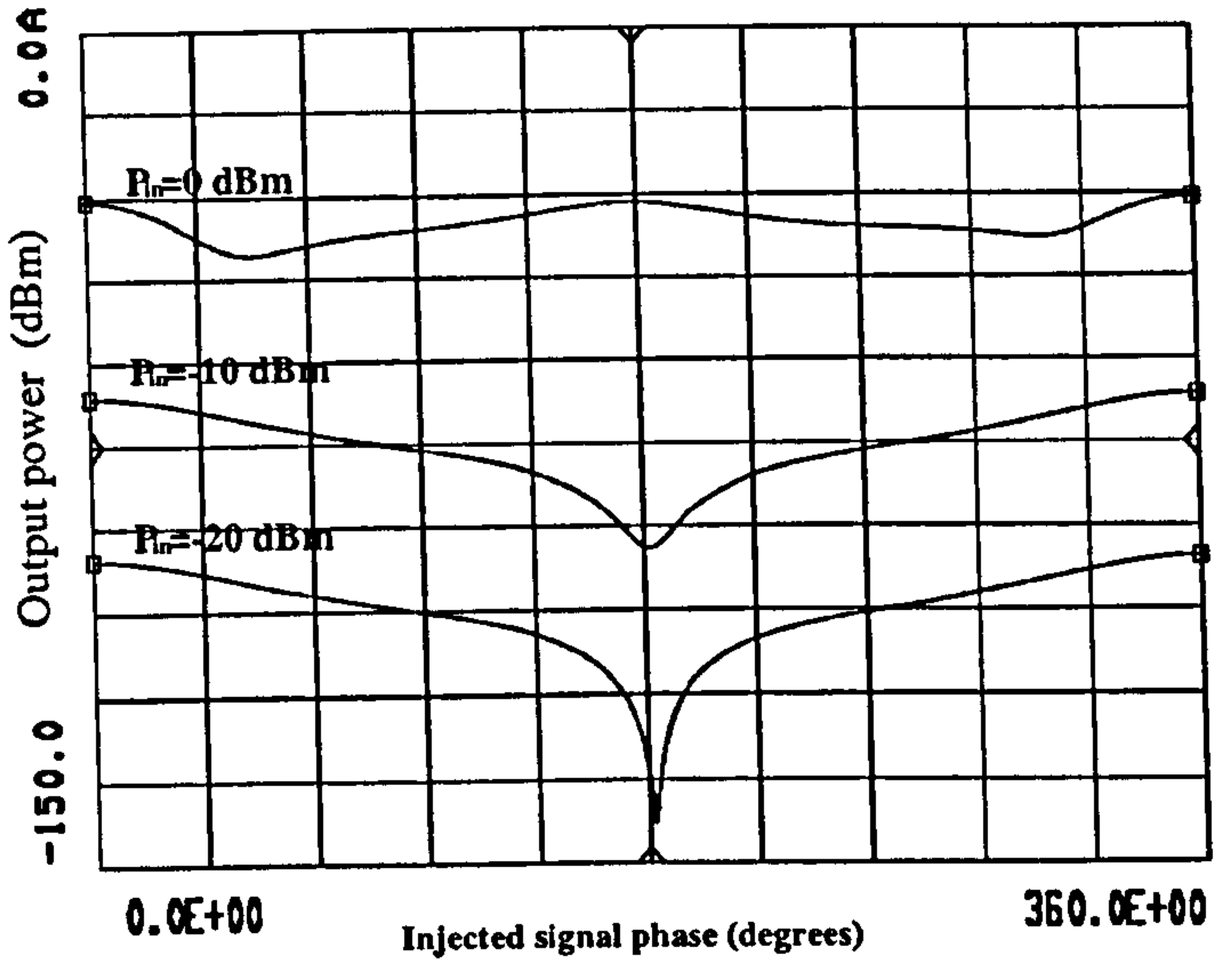

Figure 4..39: **Variations in the amplitude of IM term $(f_1 + f_2 - f_3)$ at the frequency $2.489GHz$ as a function of injected frequency sum of the fundamental signals phase for input power levels of $-20dBm$, $-10dBm$ and$0dBm$.**

ure 4.39 for the signal $(f_1 + f_2 - f_3)$. The increase in input power does create a change in the circuit behaviour, which is illustrated by a slight change in phase required for the injected signals at which the third order IMD are most reduced. At high power levels $(P_{in} = 0dBm)$, the technique of the injection of the sum of the fundamental frequencies is reducing the first kind of IMD3 and not the second kind of IMD. The reduction of more than $65dB$ can be achieved with a phase shift of 230° on the first kind of IMDs as shown in figure 4.38 for the product $(2f_1 - f_3)$. Similar results are observed for all first kind of IMDs. At low power level, The second kind of IMD level drops by only $10dB$ with a phase shift of 50° as shown in figure 4.38 for the first kind of IMD.

From the above results, the combined effects of the injection of the second harmonic and the sum of the fundamental signals can result in the reduction of both the first and second kind of IMDs. As previously mentioned, at saturation level

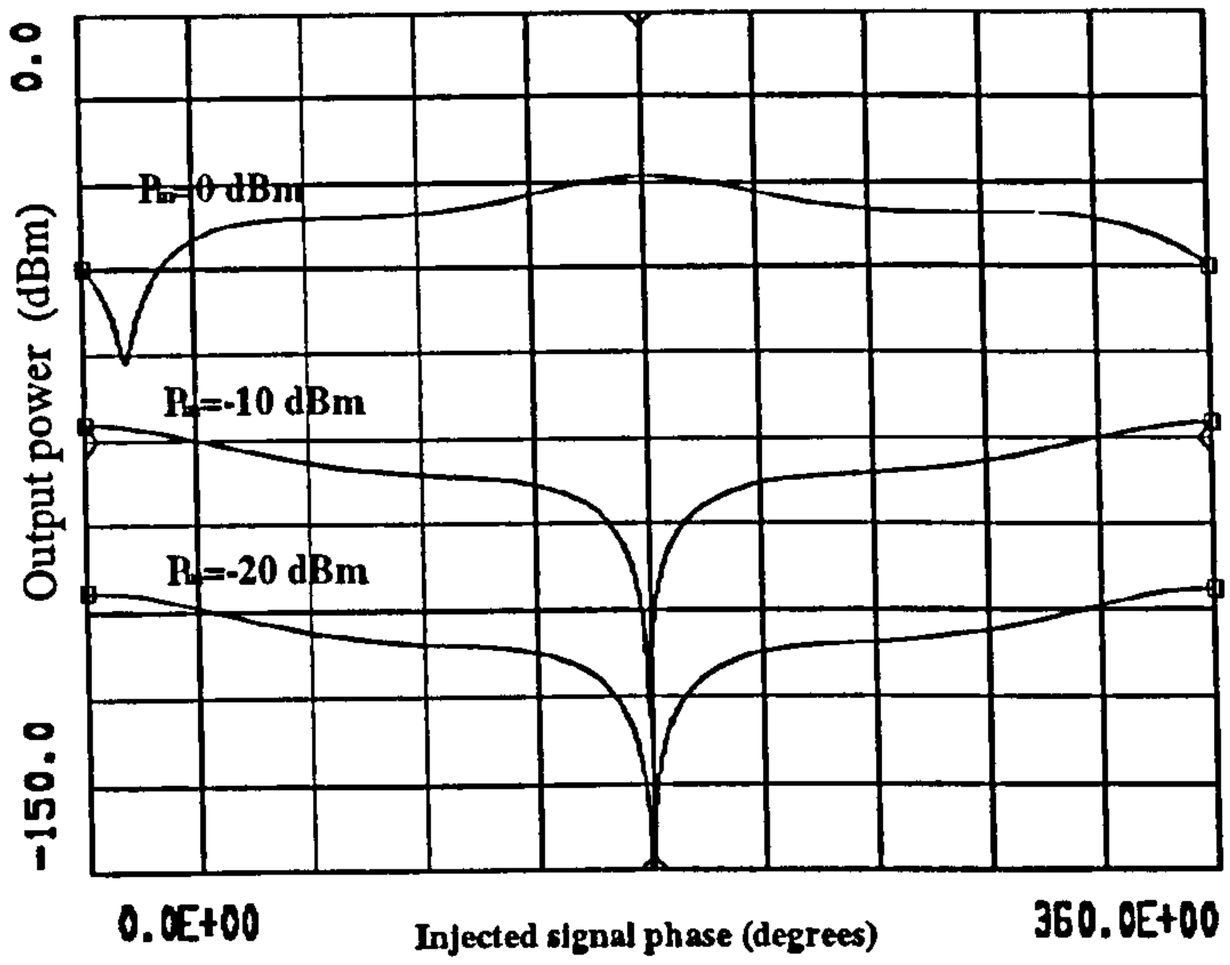

Figure 4..40: **Variations in the amplitude of IM term $(2f_1 - f_3)$ at the frequency $2.479GHz$ as a function of injected difference frequency signals phase for input power levels of $-20dBm$, $-10dBm$ and $0dBm$.**

$(Pin > 0dBm)$ reduction of the second kind of IMD of more than $50dB$ is achieved by the second harmonic technique while more than $60dB$ reduction is achieved on the second kind of IMD by the injection of the sum of the fundamental signal frequencies. A reduction of about $30dB$ is achieved at low power levels. Reduction of both kind of intermodulations can be obtained for the same phase settings at low and high power levels. The close proximity of the second harmonic frequencies and the sum of the fundamentals frequencies, make their separation difficult to achieve in practice. The reduction of IMD by the second harmonic injection as reported in the literature is not solely due to that technique but the injection of both the second harmonics and the sum of the fundamental signals simultaneously.

The injection of the difference frequency gives the result shown in figure 4.40 at the input power of $-20dBm$, $-10dBm$ and $-0dBm$ for the signal at frequencies

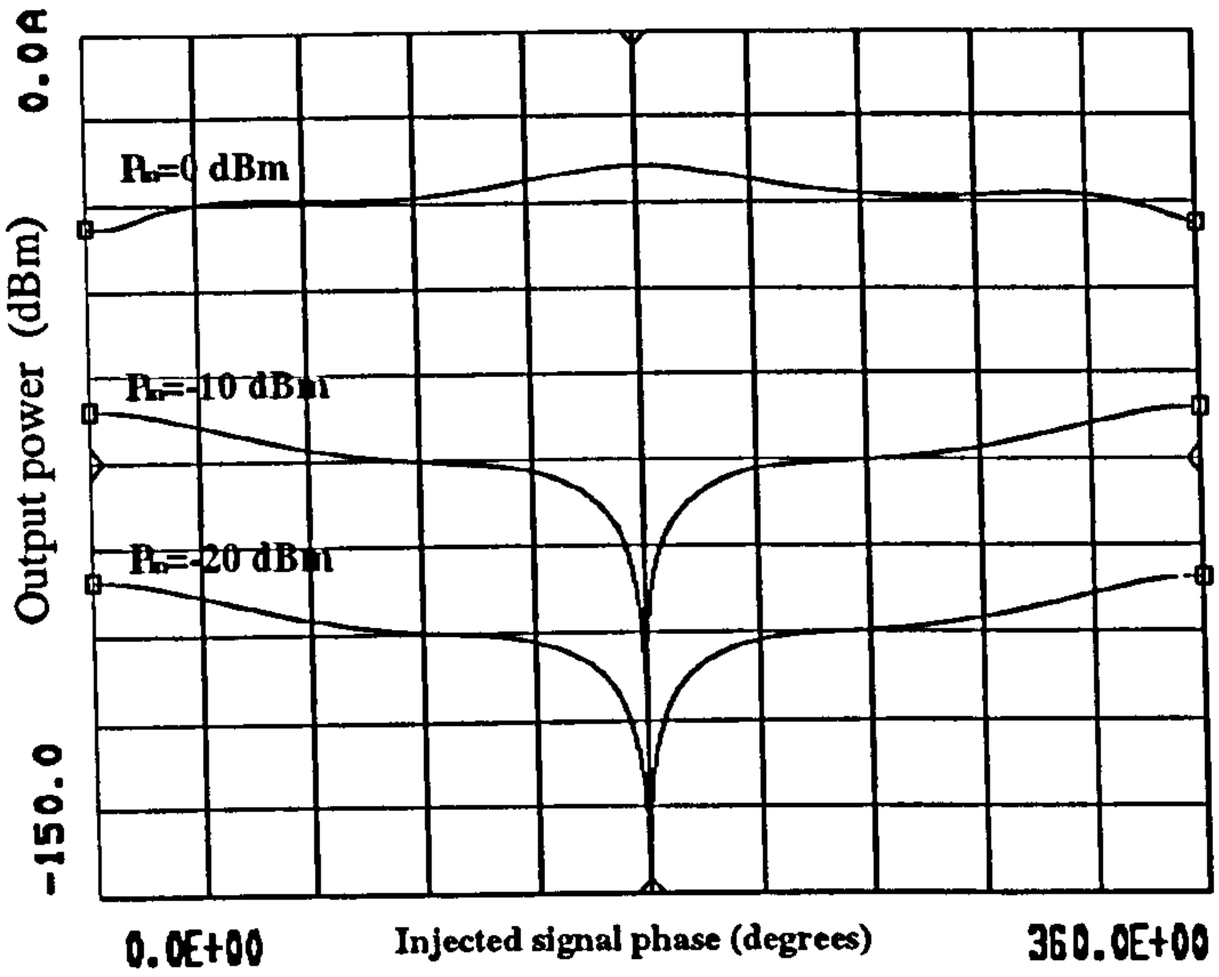

Figure 4..41: **Variations in the amplitude of IM term $(f_1 + f_2 - f_3)$ at the frequency $2.489GHz$ as a function of injected difference frequency signals phase for input power levels of $-20dBm$, $-10dBm$ and $0dBm$.**

$(2f_1 - f_3)$. Similar results are found for the other first kind of IMDs. A reduction of more than $50dB$ at $-20dBm$ input power is achieved. The reduction of the second kind of IMD3 is more than $50dB$ at $-20dBm$ input power as shown in figure 4.41 for the product $(f_1 + f_2 - f_3)$. This shows that a reduction of more than 50dB can be achieved at low power levels on all third order IMD products (both first and second kind of IMD3). The variation in the power level of the second kind of IMD signals as a function of the phase change of the injected signal shows some slight differences between each product. The second kind of IMD3 signals at frequencies $((f_1 + f_2 - f_3)$ and $(f_3 + f_2 - f_1))$ have a small variation and then a great reduction around 180° of more than $60dB$. The middle signal $(f_3 + f_1 - f_2)$ at the frequency $2.511GHz$ will have a constant reduction of more than $50dB$ for a range of phase of between 170° and 190°. This is illustrated in figure 4.42. The nonlinear effects at this particular frequency as

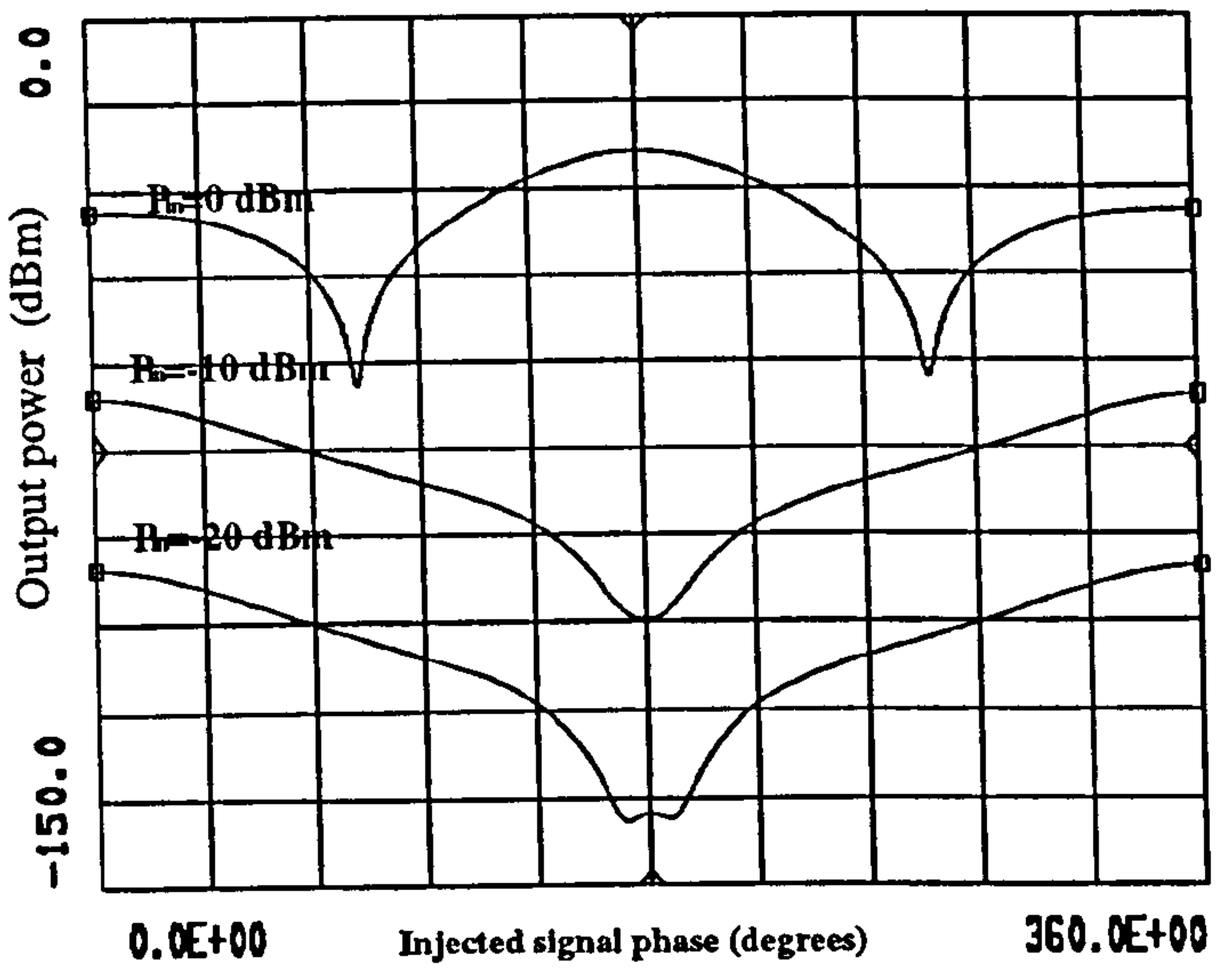

Figure 4..42: **Variations in the amplitude of IM term $(f_1 - f_2 + f_3)$ at the frequency $2.511GHz$ as a function of injected difference frequency signals phase for input power levels of $-20dBm$, $-10dBm$ and $0dBm$.**

observed in figure 4.34 cause this particular behaviour. The signal $(f_3 + f_2 - f_1)$ has a greater reduction of more than $50dB$ at 182°, while the signal $(f_2 + f_1 - f_3)$ will be at about 178°. In theory, the reduction of both kinds of IMD can be achieved with a careful choice of the same phase.

The first kind of intermodulations are reduced by more than $50dB$ with the injection of the difference frequencies. The $50dB$ reduction occurs with the use of a different phase setting of the injected signal. Each IMD3 signal reaches a minimum amplitude at a different phase of the injected signal. However, the close proximity of the phase associated with each signal does enable the use of a single phase shifter for IMD cancellation, producing an adequate reduction in the overall IMD level of the amplifier by up to $40dB$.

At higher output levels (in saturation region), the output behaviour of the IMD

with the technique of difference frequency injection does becomes rather complex. The first kind of IMDs require a completely different phase than the second kind of IMD3 for reduction of IMD. The comparison of the requirement for the first kind of IMD signal $(2f_1 - f_3)$ and the second kind signal $(f_1 + f_2 - f_3)$ in figure 4.40 and figure 4.41 respectively, shows that, the phase shift required to reduce the first kinds of IMDs signal is about 15°. Whereas the phase required for the second kind is of about 345°, because the reduction in the second kind of IMD3 occurred with the injected difference frequency amplitude of $-10dBc$ as oppose to the$-3.8dBc$ used for the graph of figure 4.41. At high power level, with the injected signal amplitude set to $-3.8dBc$, a reduction in the first kind of IMD is obtained. When the injected signal amplitude is set to $-10.5dBc$, a significant reduction in the first kind of IMD was obtained.

The reduction of the signal $(f_1 - f_2 + f_3)$ occurs at two completely different phases than those obtained with the other third order signal as shown in figure 4.42. The phase is completely different to the phase required for the other two second kinds of IMDs $(f_1 + f_2 - f_3)$ and $(f_3 + f_2 - f_1)$. These discrepancies are caused by the phase nonlinearities in the MESFET device. The phase requirements for IMD cancellation will strongly depend on the phase nonlinearity of the device used.

The injection of the difference frequency signals gives better results with an appropriate phase of the injected signal for each individual signals. A reduction of more than $60dB$ for each IMD3 signal can be achieved with the use of different phase settings. The use of a single phase to reduce all IMD does not provide similar results. Although at low power levels, a reduction of about $40dB$ can be achieved, at higher power level, the strong nonlinearity of the device can prevent the technique form being

fully effective. Ideally, the optimum reduction in the level of each IMD3 product requires a different phase.

The signals below the centre frequency of $2.511GHz$ exhibit their minima for a phase of 178.6°, whereas the signals whose frequencies fall above the centre frequency exhibit their minima at around 182° at low power level. If two phase shifters are used, the reduction of the IMD on either side of the centre can exceed $60dB$. The second kind of IMD at the frequency $2.511GHz$ determines the overall reduction level of the IMD since this signal can not be further reduced as shown in figure 4.42.

From the above observation, it is obvious that a change in the phase of the injected signal at the input of the amplifier will result in the degradation of the level at the output. A reduction of $60dB$ can only be obtained for a very small range of phase. The reduction of the signal $(2f_1 - f_3)$ by $60dB$ as seen in figure 4.40 is obtained with a phase of 178.6°. The degradation of the phase by ±0.5° will cause an increase in the IMD by more than $10dB$. A reduction of $30dB$ occurs for a range of phase shifts between 177° and 183°. If the phase is set to 180°, degradation in the phase by ±2.5° can not cause an increase in the level of IMD and a $30dB$ reduction is maintained. Similar results are observed at low power level for the second harmonic technique and the injection of the sum of the fundamental signals.

The use of a simulator enables the variation of the phase in small step of 0.1°. Further reduction in the value of the step used for simulation will show that the reduction of IMD can reach values greater than $100dB$. This is not practicable as it leads to high memory requirements and takes a rather lengthy time to complete. In practice, the phase required for a reduction of more than $60dB$ will require a constant phase and

Fundamental input power (dBm)	Injected second harmonic input phase (deg.)	Injected summation frequency input phase (deg.)	Injected difference frequency input phase (deg.)
0	251	239	9.2
−10	182	182	181
−20	182	182	181

Table 4..4: **Phases of the injected signals for optimum reduction of all IMD3 products.**

needs to be kept to within $\pm 0.01°$ of its value.

The fundamental signals f_1, f_2 and f_3 remain constant to within $\pm 1dB$ with an injection of the difference frequency for a phase change of between 0° to 360°. It does not affect the operation of the amplifier and its IMD performance. The reduction in the fundamental signals levels does not take place at the optimum phase of the IMD3 as illustrated in figure 4.35 with an injection of the difference frequency signals. These results are similar to the results observed with the second harmonic technique and the injection of the sum of fundamental signals.

4.6.2 Amplitude Sensitivity of Systems

The reduction of the IMD by the injection of signals requires the phase and amplitude to be correctly chosen. This section looks at the effects of the amplitude change of the injected signal on the intermodulation level. Simulations are performed with constant injected signal phases which gave optimum reduction of all IMD3 (see table 4.4).

With the injected second harmonic amplitude of the order of $-42.3dBc$, the first kind of IMD3 are reduced by about $20dB$. This is shown in figure 4.43 for the first kind of IMD3 $(2f_1 - f_3)$. Similar results are found for the signals $(2f_1 - f_2)$, $(2f_2 - f_3)$, $(2f_2 - f_1)$, $(2f_3 - f_2)$ and $(2f_3 - f_1)$ (see appendix f). The amplitude of the injected signals, which reduces the IMD, is approximately the same at around $-42.3dBc$ for

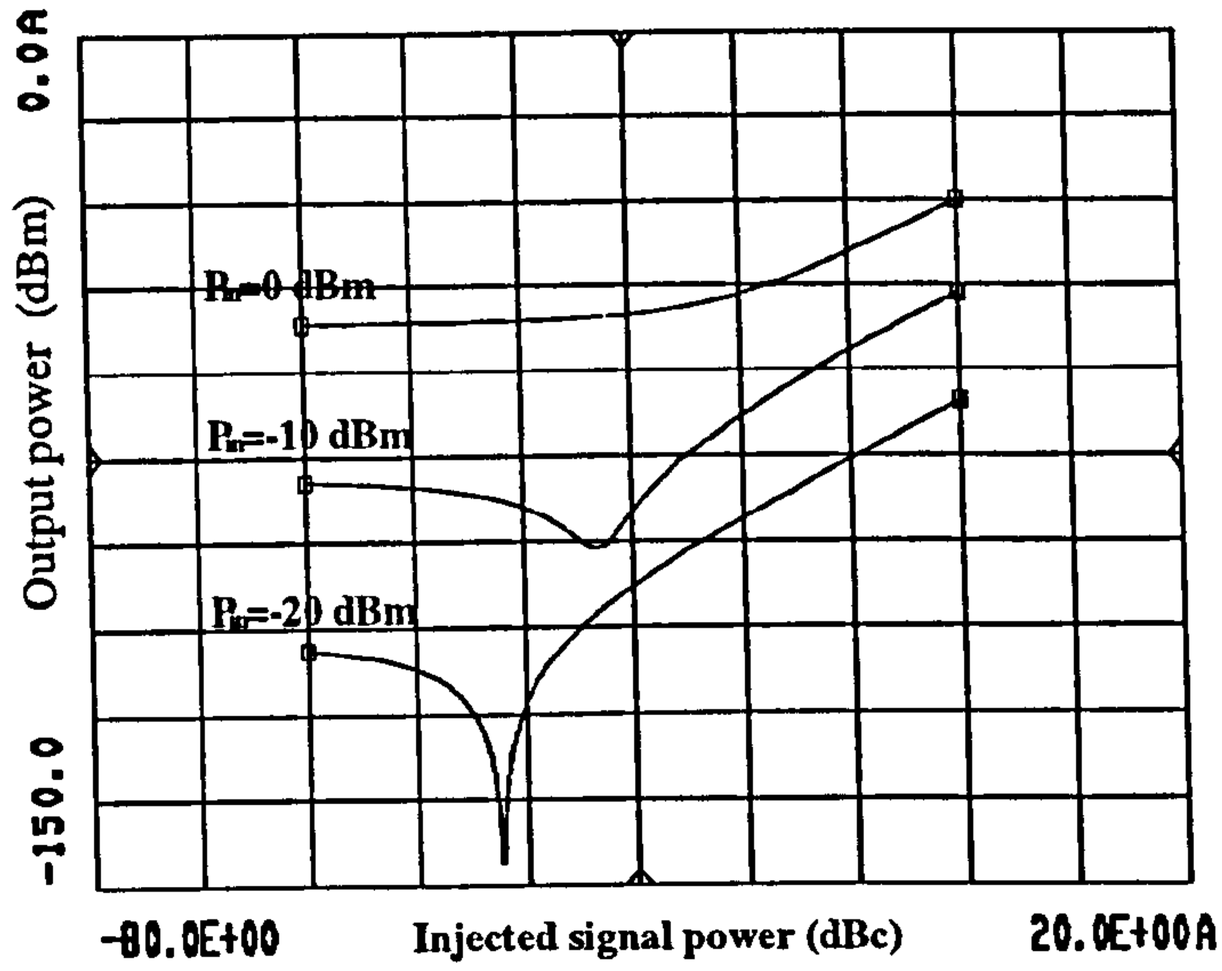

Figure 4..43: **Variations in the amplitude of IM term $(2f_1 - f_3)$as a function of injected second harmonic signals amplitude for input power levels of $-20dBm$, $-10dBm$ and $0dBm$.**

input power of $-20dBm$ and $-33.4dBc$ for input power of $-10dBm$. A reduction of more than $30dB$ is achieved at $-20dBm$ input power. An increase of $10dB$ in the level of fundamental input power required a similar increase of $10dB$ in the level of the injected second harmonic signals. As the power level of the injected signals increases beyond the required amplitude value, the overall IMD3 level will then start to increase. The effects of the injection of the second harmonic signal can be either an increase or a decrease in the IMD3 level of the amplifier. The amplitude of the injected signal needs to be kept low in order not to increase the IMD3 levels.

The second kind of IMD3 however remained unchanged regardless of the amplitude of the injected second harmonic signals. This is illustrated in figure 4.44 for the signal $(f_1 + f_2 - f_3)$. Similar results are found for the signals $(f_1 - f_2 + f_3)$ and $(f_3 + f_2 - f_1)$ respectively at $-20dBm$ and $-10dBm$ input power. As observed previ-

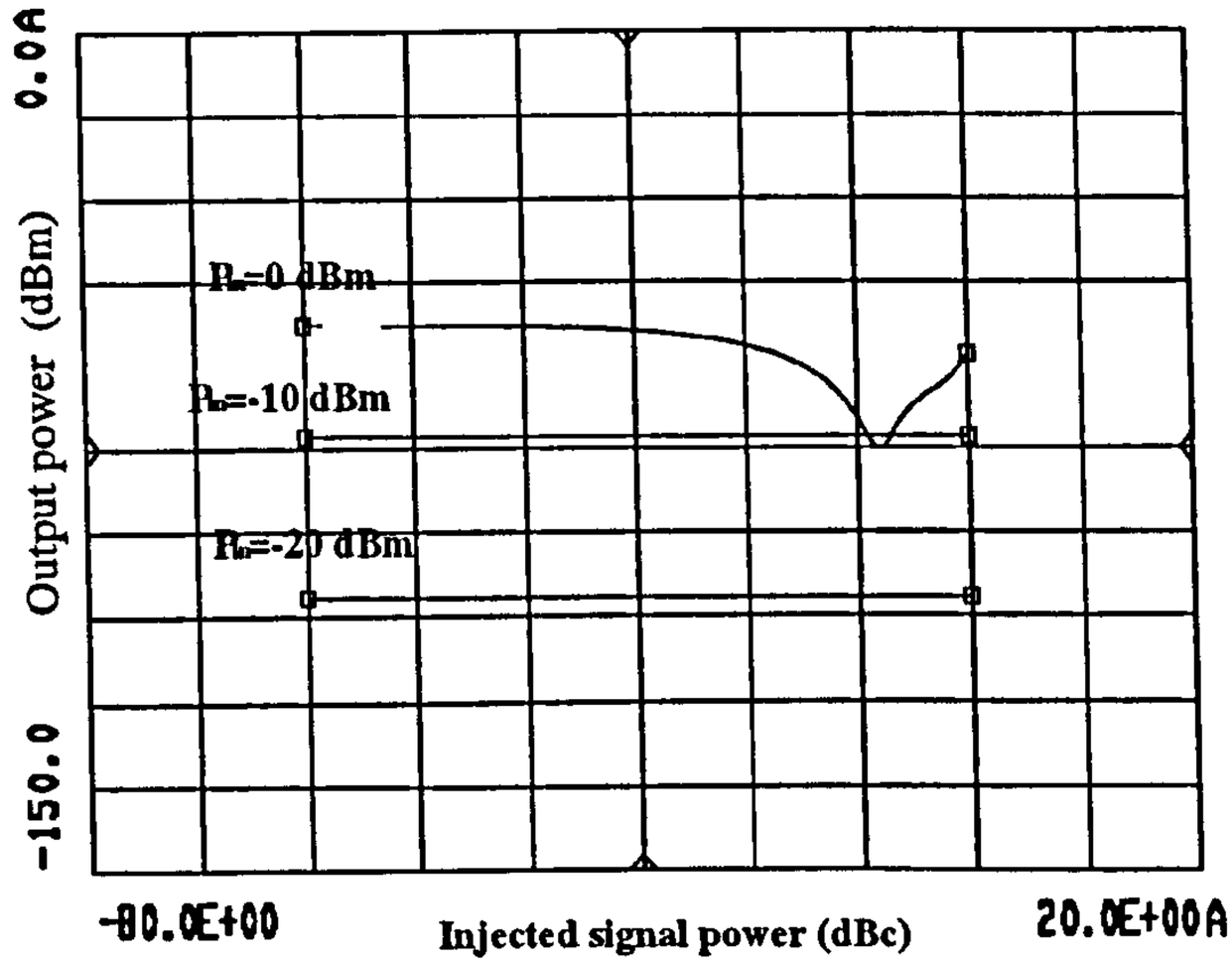

Figure 4..44: **Variations in the amplitude of IM term $(f_1 + f_2 - f_3)$ as a function of injected second harmonic signals amplitude for input power levels of $-20dBm$, $-10dBm$ and $0dBm$.**

ously, the second harmonic injection reduces the second kind of IMD and not the first kinds at high power levels. A reduction of more than $15dB$ is shown in figure 4.44 for the signal $(f_1 + f_2 - f_3)$. A similar result is observed for both signals $(f_1 - f_2 + f_3)$ and $(f_3 + f_2 - f_1)$.

The used of the technique of injection of the sum of the fundamental signals shows that for input powers of $-20dBm$ and $-10dBm$, the reduction in IMD levels only occurs for the second kind of IMD by $25dB$ and $15dB$ respectively (figure 4.45). The reduction in IMD3 occurs for an amplitude of the injected signal of $-36.3dBc$ at $-20dBm$ and for amplitude of $-27.2dBc$ at $-10dBm$ input power. The first kinds of IMD are not reduced by the technique. The levels of all first kind of third order IMDs remain unchanged before increasing as the injected signal levels are further increased above the required optimum reduction value. This is shown in figure 4.46 for the first

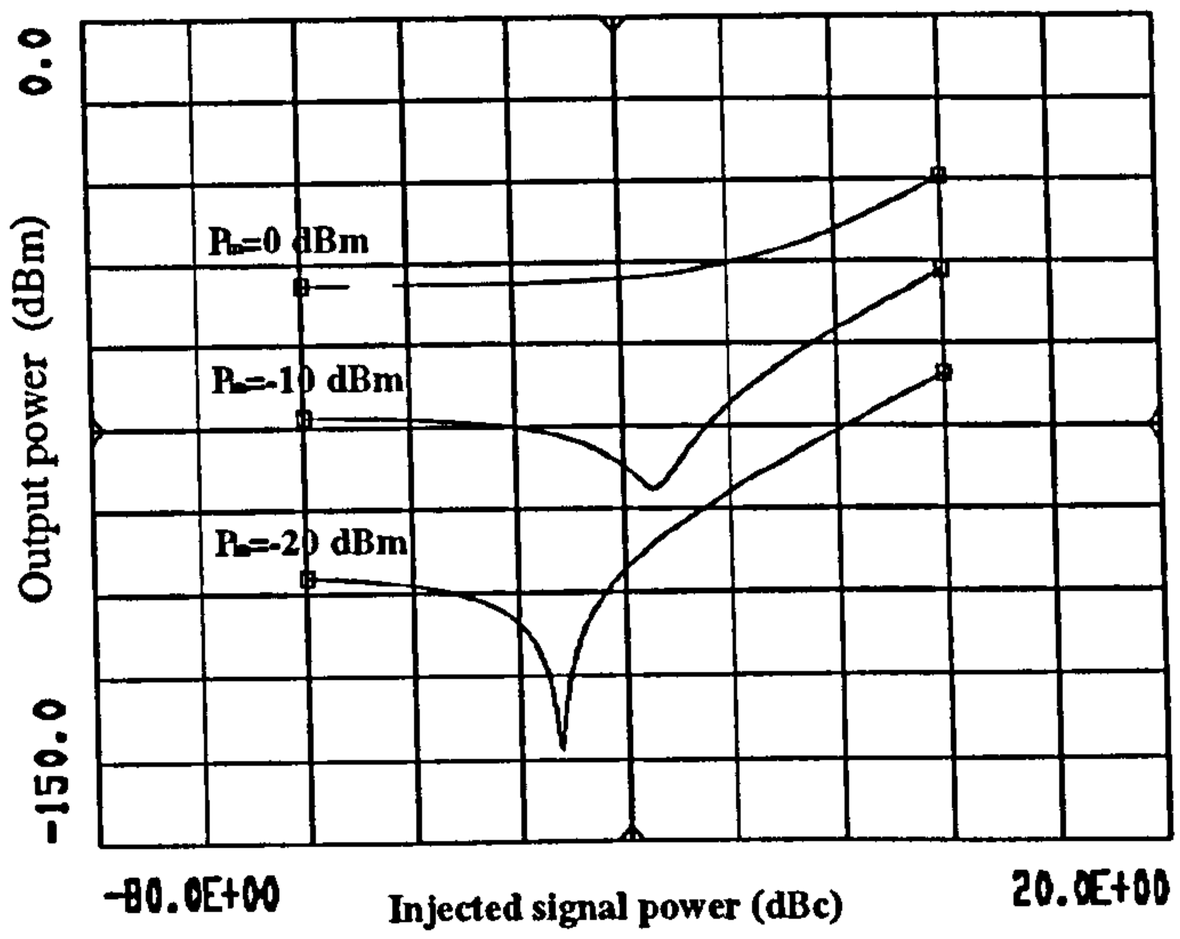

Figure 4..45: **Variations in the amplitude of IM term $(f_1 + f_2 - f_3)$ as a function of the injected frequency sum of the fundamental signals amplitude for input power levels of $-20dBm$, $-10dBm$ and $0dBm$.**

kind of IMD $(2f_1 - f_3)$. Similar results are found for the other first kind of IMD3. At $0dBm$, reduction of the first kind of IMDs takes place and the input power levels of the injected sum of the fundamental signals required for the reduction of the third order signal is of the order of $-5.7dBc$.

This again shows that by injecting both the second harmonic and the sum of the fundamental frequencies at the input of the system, a reduction of all IMD can be achieved at low and high input powers.

The difference frequency injection is more effective in reducing the level of both the first kinds and the second kind for the same amplitude of the injected signals of $-40dBc$ at $-20dBm$ input power and $-31.5dBm$ at $-10dBc$ input power. This can be observed in figure 4.47 for the first kinds of IMDs $(2f_1 - f_3)$. Similar results are found for the other first kind of IMD3. The change in the power level of the second kinds of IMD signal $(f_1 + f_2 - f_3)$ is shown in figure 4.48. The maximum reduction of

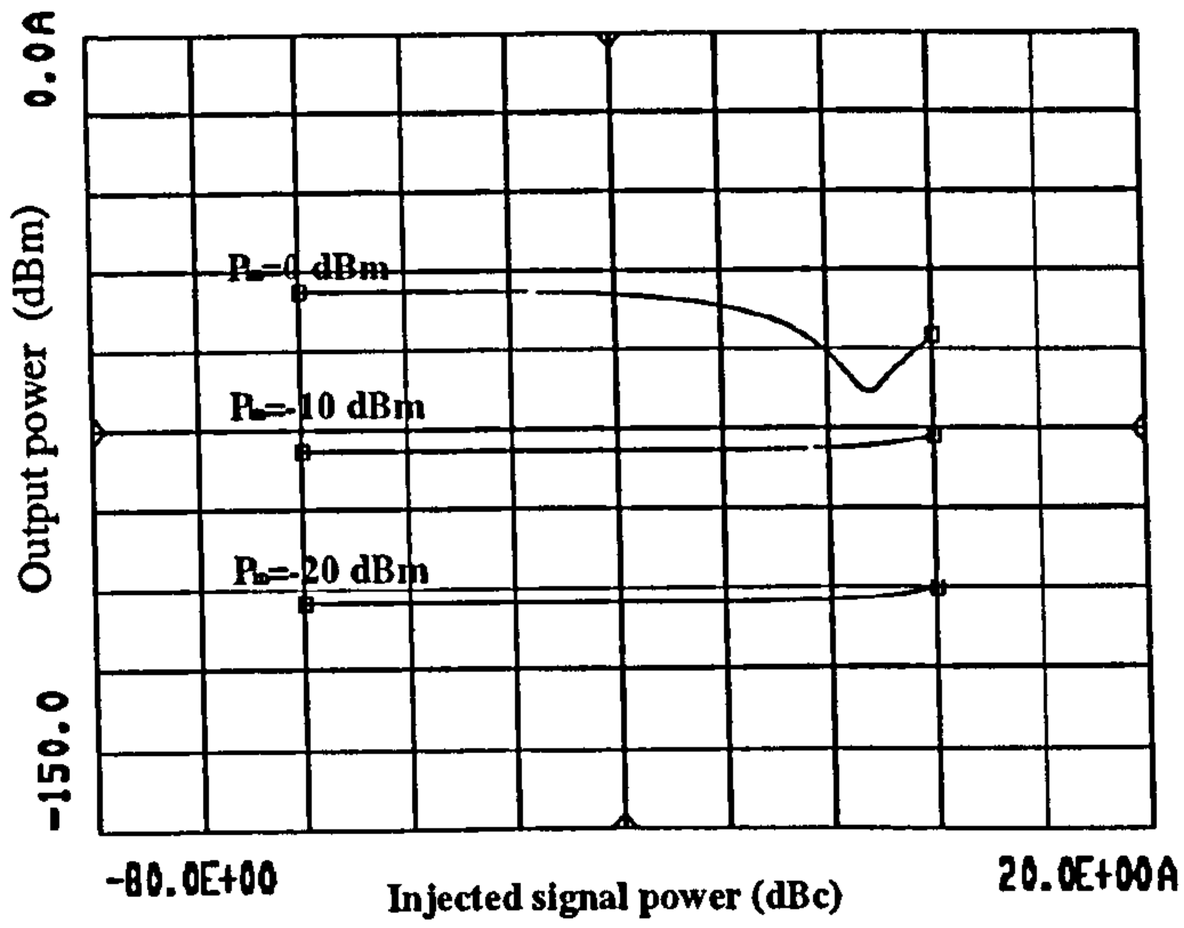

Figure 4..46: **Variations in the amplitude of IM term $(2f_1 - f_3)$ as a function of the injected frequency sum of the fundamental signals amplitude for input power levels of $-20dBm$, $-10dBm$ and $0dBm$.**

all the IMD3 products by the difference frequency injection is greater than $30dB$. At the higher input power of $0dBm$ (close to saturation level) the first kind is reduced by injected signals with an amplitude of $-10.5dBc$ whereas the second kind of third order are reduced by more than $20dB$ with an amplitude of injected difference frequency signals of $-3.4dBc$.

The analysis of the effects of the amplitude of the injected signals on the improvement of the amplifier IMD performance shows clearly, as illustrated in the above results, that reduction in the level of the third order intermodulation signals by the different techniques can occur at the same amplitude of the injected signal. The second harmonic injection technique reduces all first kind of IMD3 at fundamental input power of $-20dBm$, $-10dBm$ and at $0dBm$ for the amplitude of the injected signal of $-42.3dBc$, $-33.4dBc$ and of $-3.4dBc$ respectively. The injection of the difference frequency reduces all IMDs signals at input power of $-20dBm$ and $-10dBm$ for an

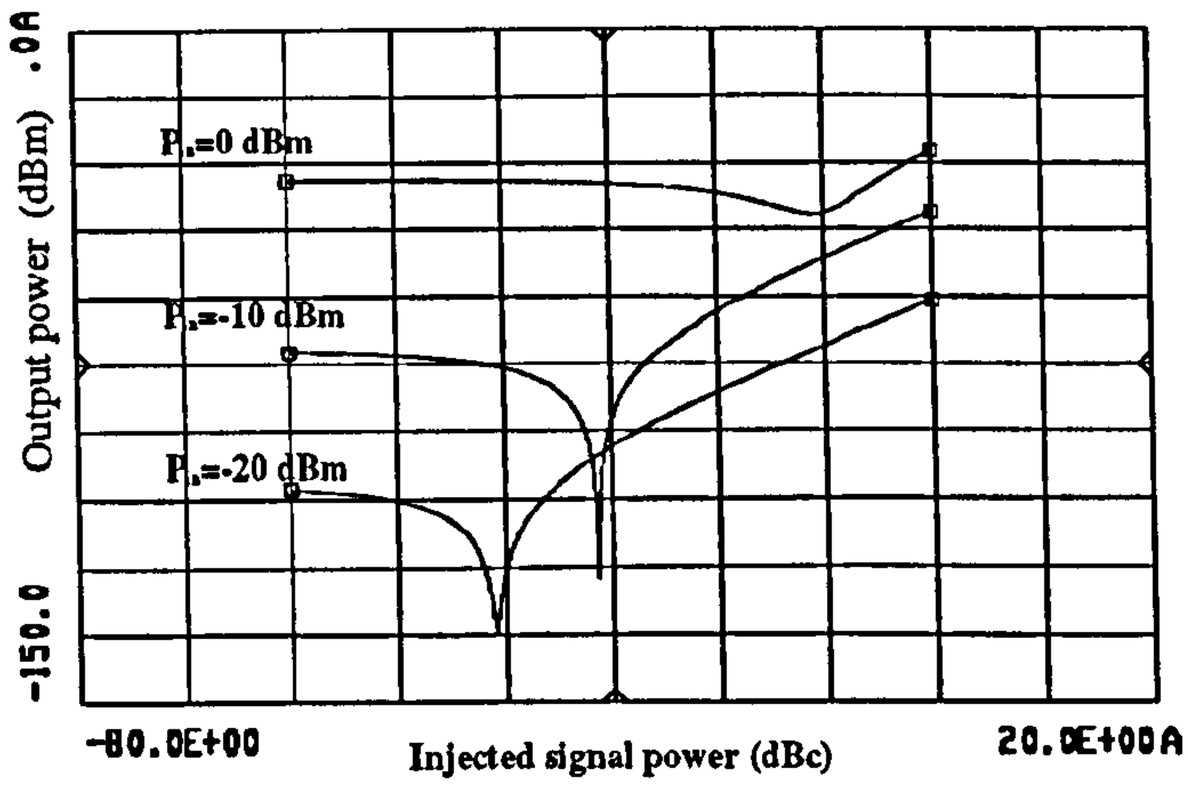

Figure 4..47: **Variations in the amplitude of IM term $(2f_1 - f_3)$ as a function of injected difference frequency signals amplitude for input power levels of $-20dBm$, $-10dBm$ and $0dBm$.**

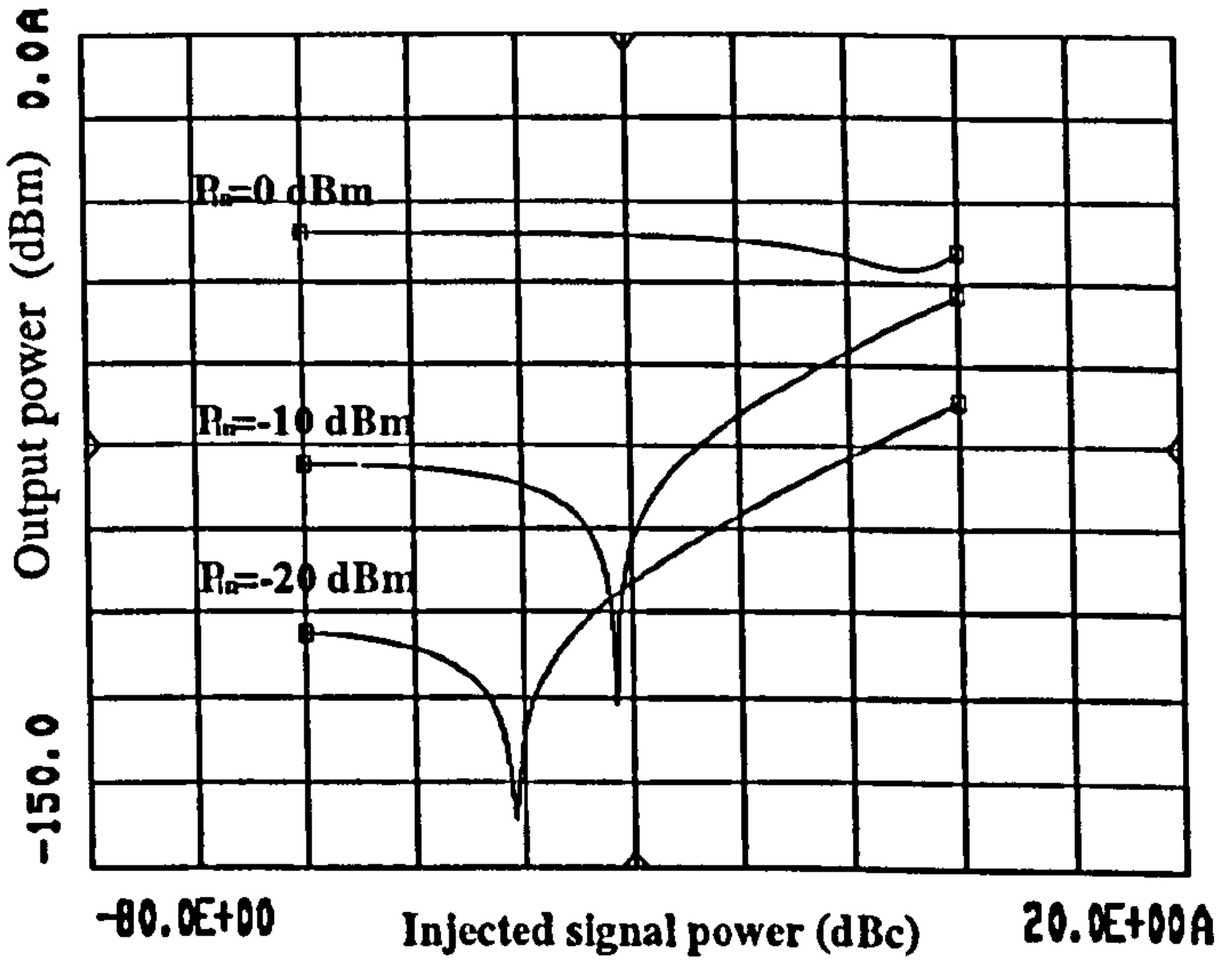

Figure 4..48: **Variations in the amplitude of IM term $(f_1 + f_2 - f_3)$ as a function of injected difference frequency signals amplitude for input power levels of $-20dBm$, $-10dBm$ and $0dBm$.**

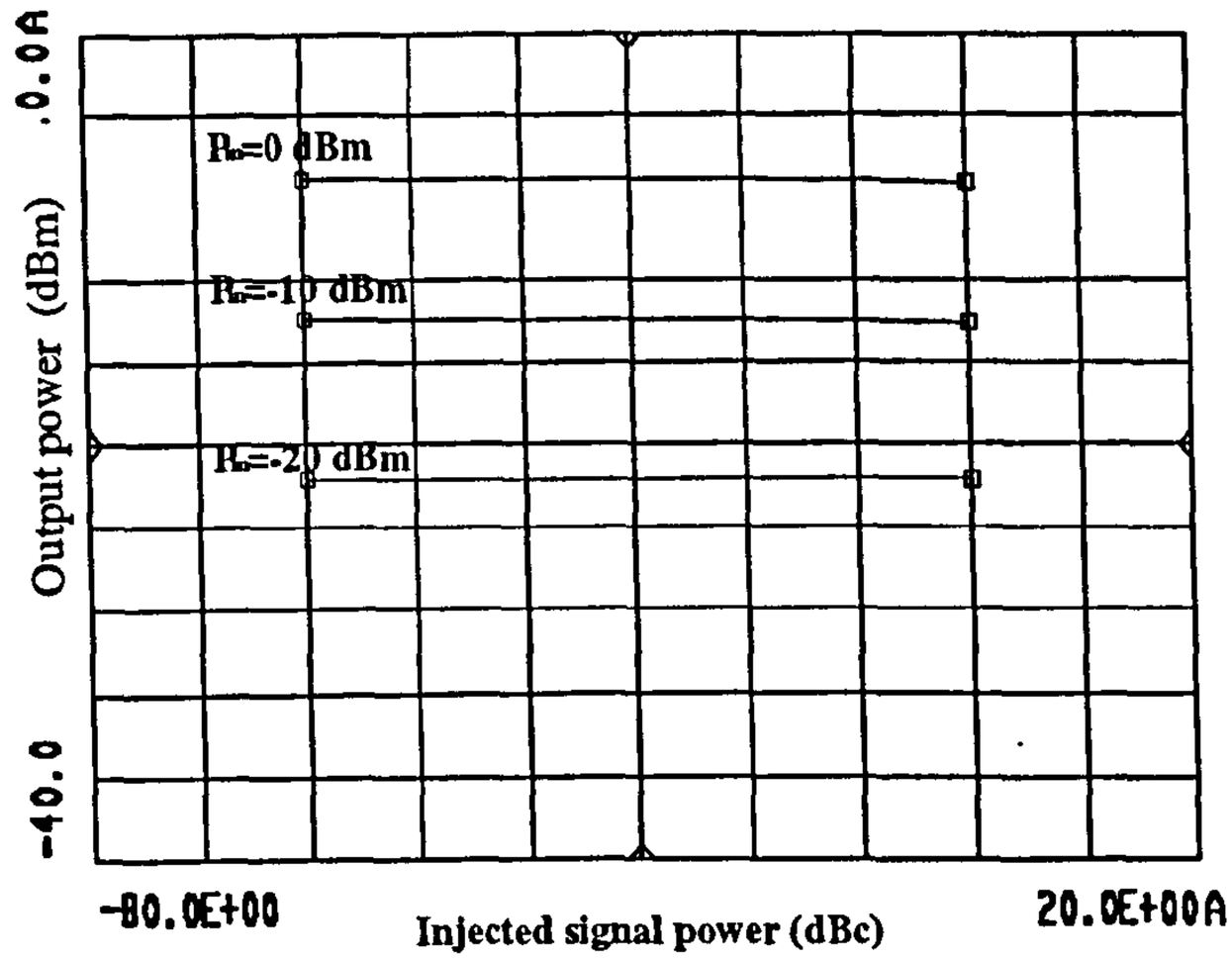

Figure 4..49: **Variations in the amplitude of the fundamental signal f_1 as a function of injected second harmonic signals amplitude for input power levels of $-20dBm$, $-10dBm$ and $0dBm$.**

amplitude of injected signal of $-40.8dBc$ and $-31.5dBc$ respectively. The injection of the sum of frequencies shows that it reduces the second kind of IMDs at input power at $-20dBm$, $-10dBm$ and at $0dBm$ for the same amplitude of the injected signal of $-42.3dBc$, $-33.4dBc$ and of $-3.4dBc$ respectively.

The fundamental signals f_1, f_2 and f_3 at the frequencies $2.50GHz$, $2.51GHz$ and $2.521GHz$ do not change in amplitude. This is shown in figure 4.49 for the signal f_1 with the second harmonic injection technique. Results for the injection of the sum of the fundamental signals and the injection of the sum of the difference frequency produces similar results.

4.7 Frequency Spacing Effect on the Techniques' Performances

Channel spacing in communication systems is defined by various standards. The spacing between tones can change the intermodulation level and contribute to greater

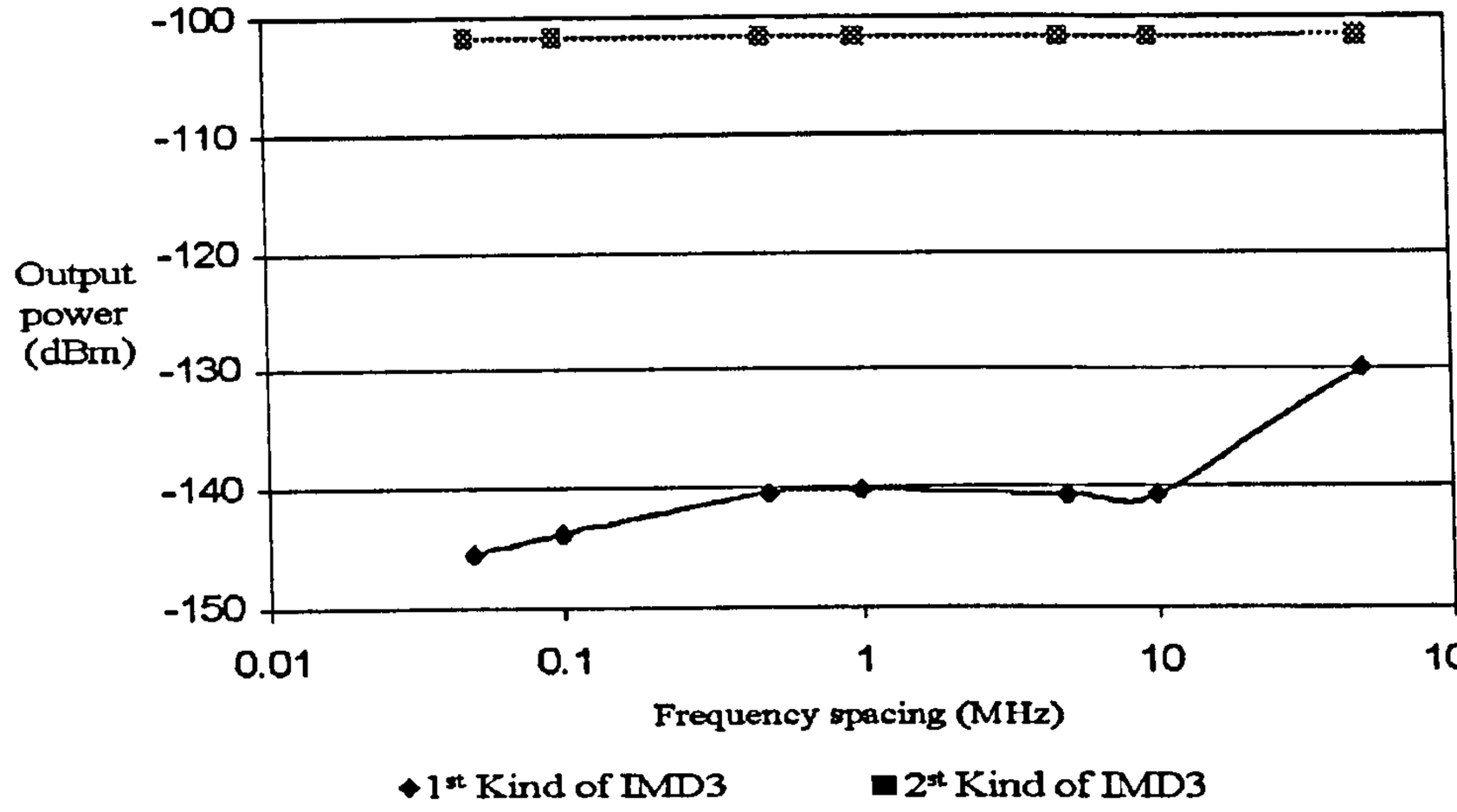

Figure 4..50: **Variation of the IM3 term $(2f_1 - f_2)$ (1st kind) and the IM3 term $(f_2 + f_1 - f_3)$ (2nd kind) power levels as a function of tone spacing in a three-tone test when using the second harmonic technique.**

distortion [8]. The use of the techniques described earlier provides an improvement on the amplifier intermodulation distortion level. The effects of the change in channel spacing are studied in this section. The amplifier IMD performance is tested under different channel spacing conditions. The injected signals phases and amplitudes are kept constant (see table 4.3 and table 4.4 for $-20dBm$ fundamental input power).

In a three-tone test, the improvement on the intermodulation does not change drastically as tone spacing is increased with a constant power level and phase of the injected signals at $-20dBm$ input power. The degradation in the intermodulation performance of the system is very small and almost non-existent until the tone spacing reaches less than $100MHz$. The results obtained with the difference frequency are similar to the second harmonic injection and the injection of the sum of fundamental frequencies. Figure 4.50 shows the change in the level of IMD3 for the first kind of

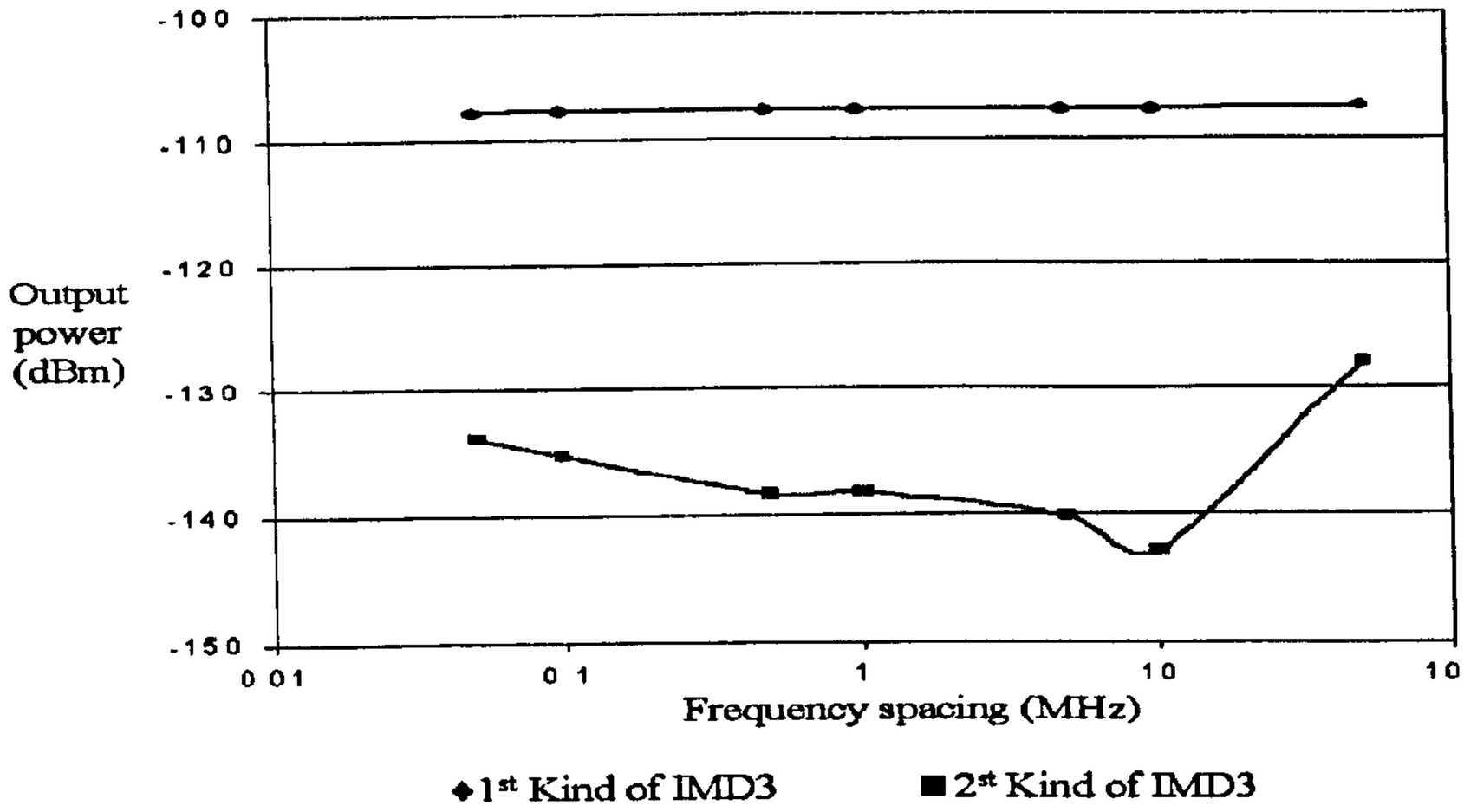

Figure 4..51: **Variation of the IM3 term $(2f_1 - f_2)$ (1st kind) and the IM3 term $(f_2 + f_1 - f_3)$ (2nd kind) power levels as a function of tone spacing in a three-tone test when using the frequency summation technique .**

IMD products $(2f_1 - f_2)$ as the tone spacing is changed. The first kind of IMD3 are reduced from $-107.8dBm$ (without injection , see table 4.2) to less than $-140dBm$ for frequency spacing up to $20MHz$ but increases thereafter. Similar results are found for the other first kinds of IMD3 at the frequencies $(2f_1 - f_3)$, $(2f_2 - f_3)$, $(2f_2 - f_1)$, $(2f_3 - f_1)$ and $(2f_3 - f_2)$. The second kind of IMD remains unchanged since there is no reduction in this signal by the second harmonic injection technique. This is shown in figure 4.50 for the product $(f_1 + f_2 - f_3)$. Similar results were obtained for the other second kinds of IMD3 at the frequencies $(f_1 - f_2 + f_3)$ and $(f_3 + f_2 - f_1)$

The injection of the sum of the fundamental frequencies shows that the second kind of IMDs are reduced from $-101.8dBm$ (without injection, see table 4.2) down to less than $-135dBm$ for frequency spacing below $40MHz$. A reduction of more than $30dB$ is shown in figure 4.51 for the signal at the frequency $(f_1 + f_2 - f_3)$. Since the

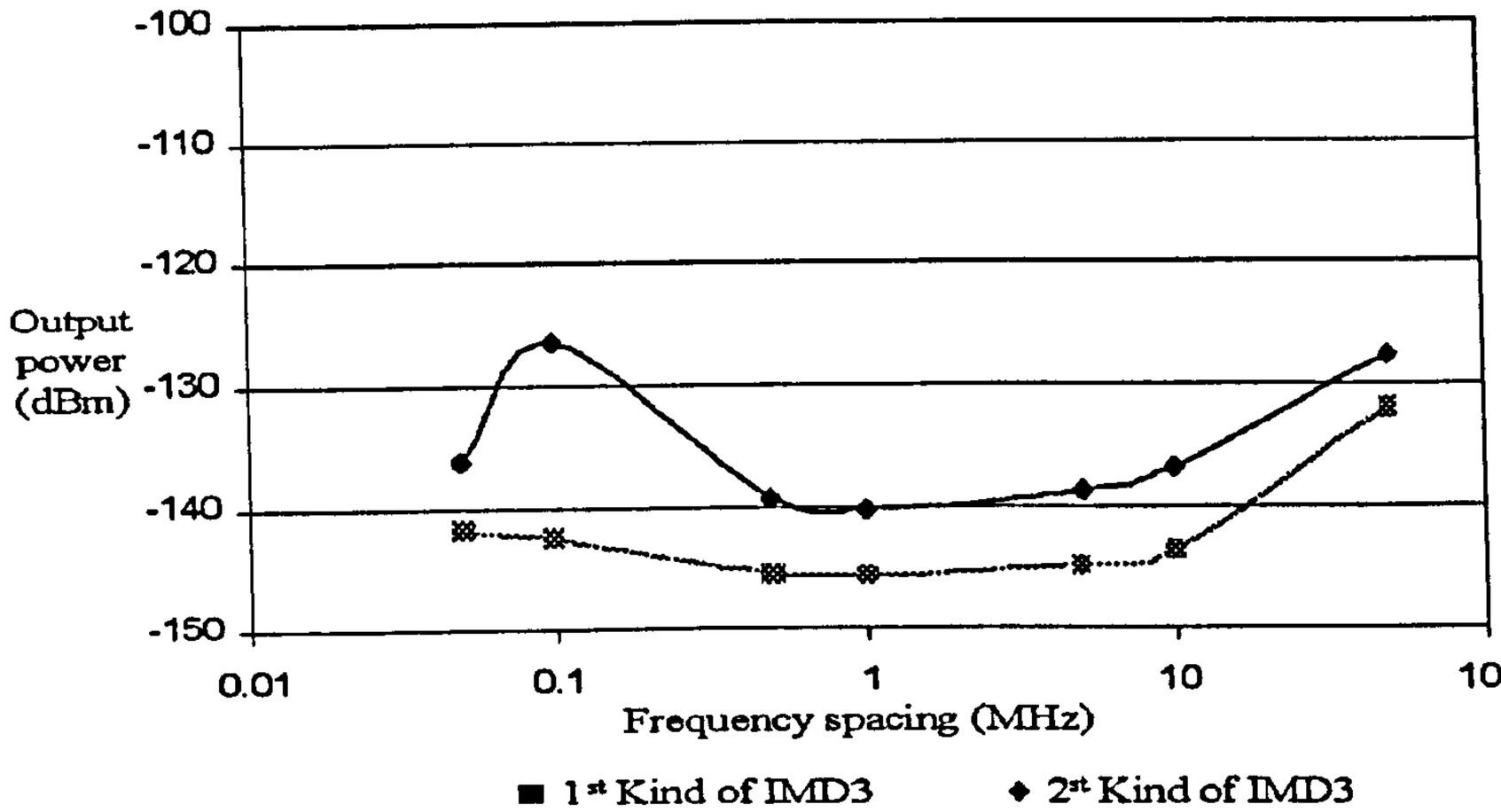

Figure 4..52: **Variation of the IM3 term $(2f_1 - f_2)$ (1st kind) and the IM3 term $(f_2 + f_1 - f_3)$ (2nd kind) power levels as a function of tone spacing in a three-tone test when using the difference frequency technique.**

injection of the sum of the fundamental frequencies does not reduce the first kinds, there is no change to the level of the first kind of IMD as shown in figure 4.51 for the signal $(2f_1 - f_2)$.

The difference frequency reduces both the first and the second kind of IMD and these signals are reduced to below $-135dBm$ for frequency spacings between $0.5MHz$ and $20MHz$. Beyond this frequency range, the increase or decrease in frequency spacing degrades the reduction of IMD. The variation in the level of the first kind of IMD product $(2f_1 - f_2)$ and the second kind $(f_1 + f_2 - f_3)$ are presented in figure 4.52. A $28dB$ reduction of the third order IMD can be achieved for frequency spacing of $20MHz$. Similar results are observed for all other third order IMDs.

This analysis shows that the use of a single phase will provide adequate IMD cancellation for the technique since the same reduction is obtained for two tone with a

difference in frequency of 1MHz or 20MHz. This is particularly useful for systems with more than 3 tones. For example a system with 32 tones and a 1.25MHz tone spacing will have difference frequency spacings of between 1.25MHz (the first two tones) and 40MHz (the first and the last tones), thereby operating within a 40MHz bandwidth. Cancellation of the IMD3 within the system can be obtained with the same phase and amplitude correction settings. Ideally, different settings are required to obtained significant cancellation of the IMDs.

4.8 Effects of Input Power Variations on the Techniques' Performances

The change in the power level of the fundamental signal causes the degradation in the reduction of intermodulation. These changes in fundamental signal amplitude occur with time and can lead to different phase and amplitude requirement of the injected signals for optimum reduction of third order IMD signals. The difference frequency injection technique reduces both kind of IMD3. The reduction performed on IMD results from input signals of the same amplitude. The amplitudes of the injected signals are changed and the difference frequency injection performance on all IMD is then recorded. The test is not performed on the two techniques of second harmonic injection and the injection of the sum of the fundamental frequencies, which do not reduce all third order IMD. As shown in figure 4.53, as one of the signal amplitude increases and decreases by $10dB$, there is a change in the third order improvement for a difference frequency injection technique. It shows that an increase or decrease in two of the fundamental signals by up to $16dB$ does not cause degradation in the reduction of IMD as shown in figure 4.53. The reduction level is constant at $30dB$. As the

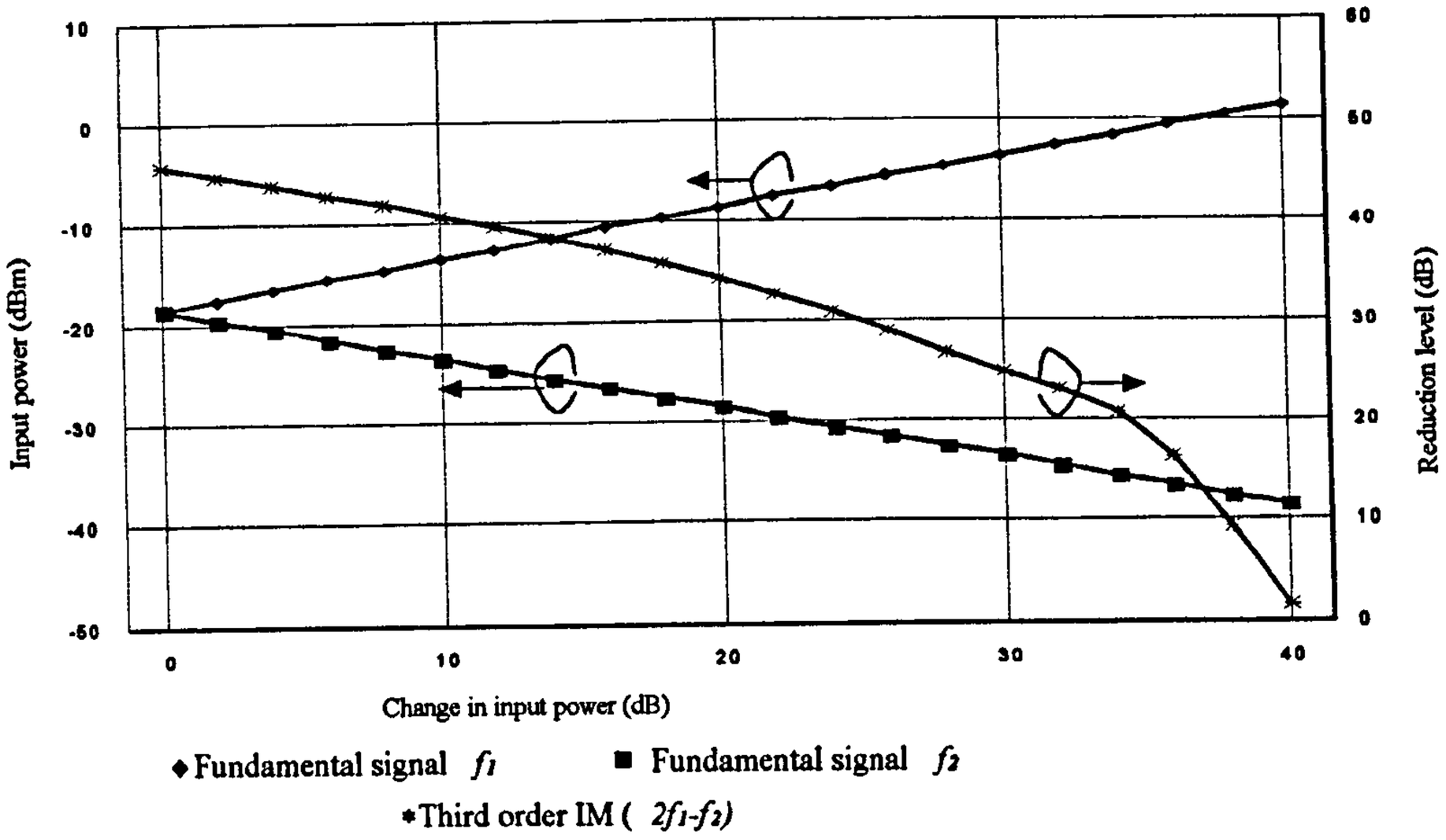

Figure 4..53: **Variation in the intermodulation power level as a function of the input power level for a system using the difference frequency technique.**

amplitude change is further increased, the reduction of the IMD will then be gradually reduced until the difference in the level of the two signals is $30dB$ (two tone test) where the reduction of IMD, then degrades very rapidly. This clearly shows that if the signal amplitude were to be varied by up to $16dB$, while and the total input power is kept constant, the reduction of IMD remains constant. By combining the second harmonic and the sum of fundamental frequencies, similar effects are observed but for a smaller range of fundamental signal amplitude changes.

This clearly demonstrates that the system can be working with the optimum IMD improvement by keeping the total input signal power into the amplifier constant. The changes in power level of a single signal will change the total input power and therefore give a different result. The levels of IMDs are increased significantly and the performance of the system deteriorates.

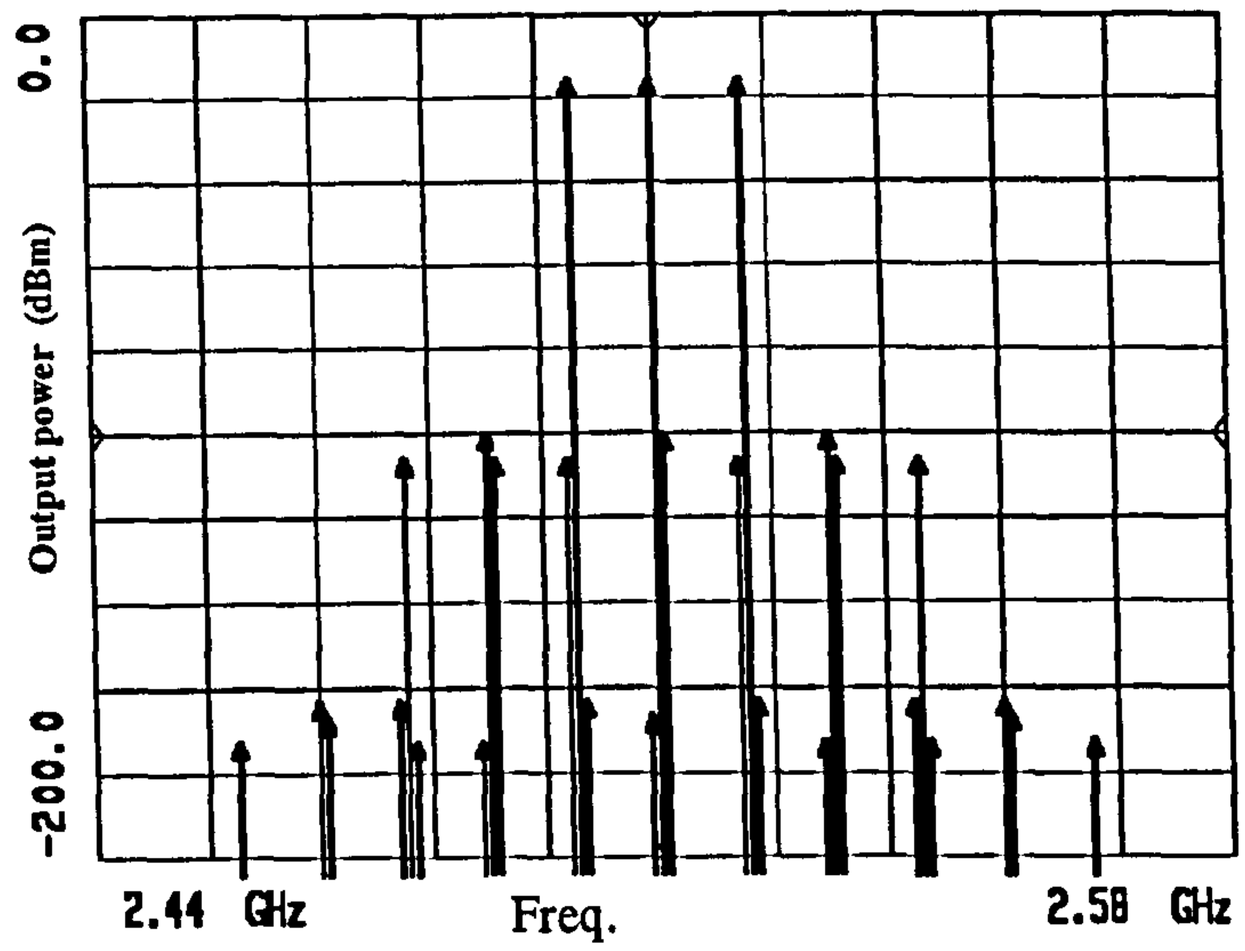

Figure 4..54: **Three-tone simulated output spectrum of amplifier without employing the IMD reduction techniques, showing the third and fifth order intermodulation .**

4.9 Signal Injection Effects on Higher Order IMD Signals

The analysis has concentrated on the third order IMD, because they are higher in amplitude compared to other IMD products and are the most troublesome. The fifth order IMD components also lies within the band of interest and have high amplitude in the large signal region. At low power levels, the fifth order IMD (IMD5) components are very low in amplitude compared to the IMD3. Figure 4.54 shows the amplifier output spectrum with the third and fifth order IMD at $-20dBm$ input power.

The reduction in the third order IMD does not give a similar reduction in the fifth order at the same amplitude and phase of the injected signals. A three-tone test is performed with input signals at the frequencies $2.5GHz$, $2.51GHz$ and $2.521GHz$. The output spectrum of figure 4.55 shows all third order IMD and fifth order IMD at the output of the amplifier after employing the technique of second harmonic injection.

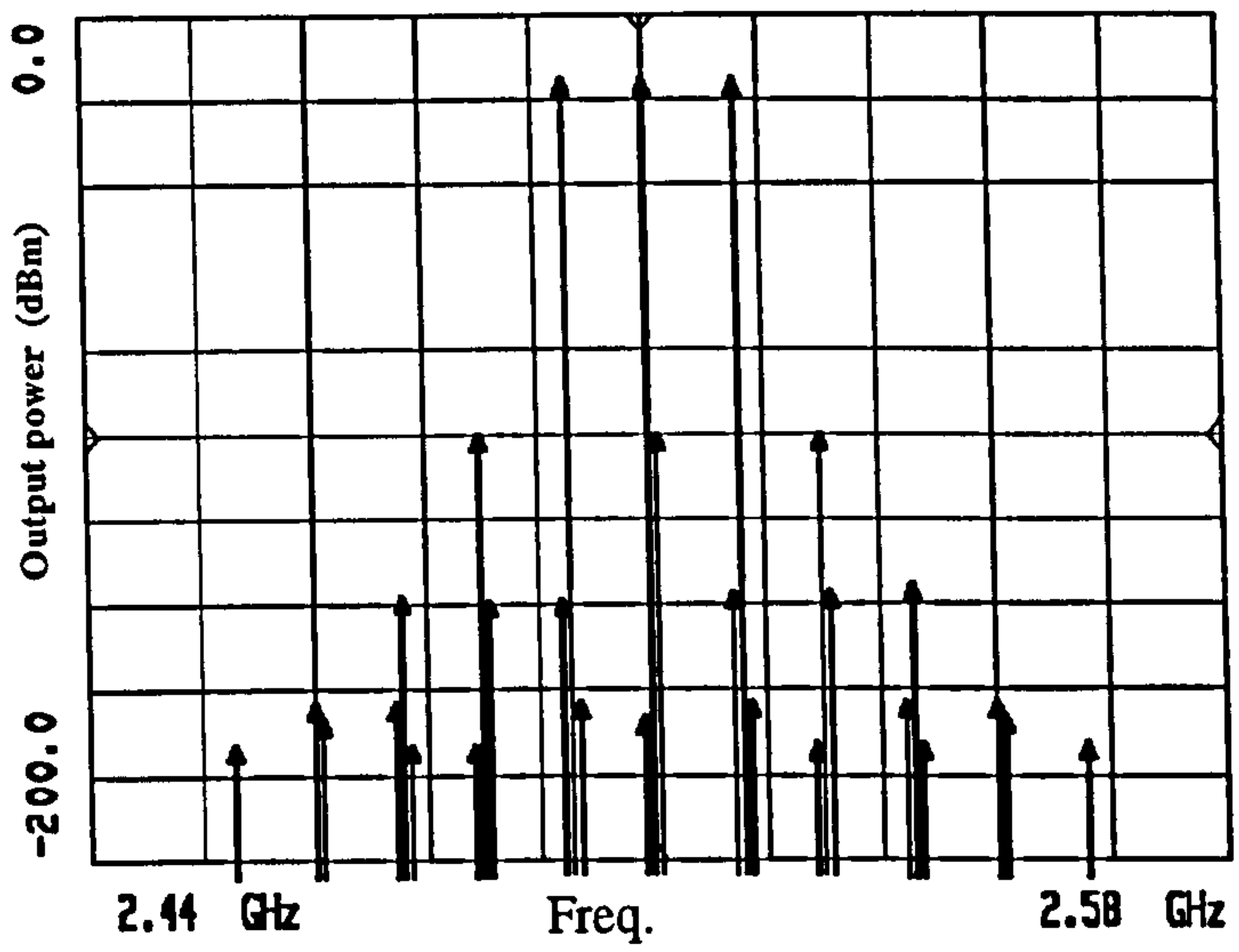

Figure 4..55: **Three-tone simulated output spectrum of amplifier after employing the technique of second harmonic injection and showing the third and fifth order intermodulation.**

The level of all IMD has not been reduced. The reduction in the third order is greater since the optimisation is performed on the high third order intermodulation. Similarly, the result of the injection of the difference frequencies, shown in figure 4.56, shows a reduction in the third order IMD and no reduction in the fifth order IMD. The use of the injection of the sum of the signals also shows no reduction in the fifth order products for the same optimum phase and amplitude (figure 4.57).

The reduction in the higher order IMD could be performed by the injection of higher order signals associated with the second harmonic signal, the difference frequency signals or the sum of the fundamental frequencies for the same amplitude and phase required for the reduction of the IMD3. The cancellation of the fifth order IMD requires a different phase and amplitude setting. The cancellation of fifth order IMD is required for a power amplifier working at saturation level or above. Since the fifth order IMD

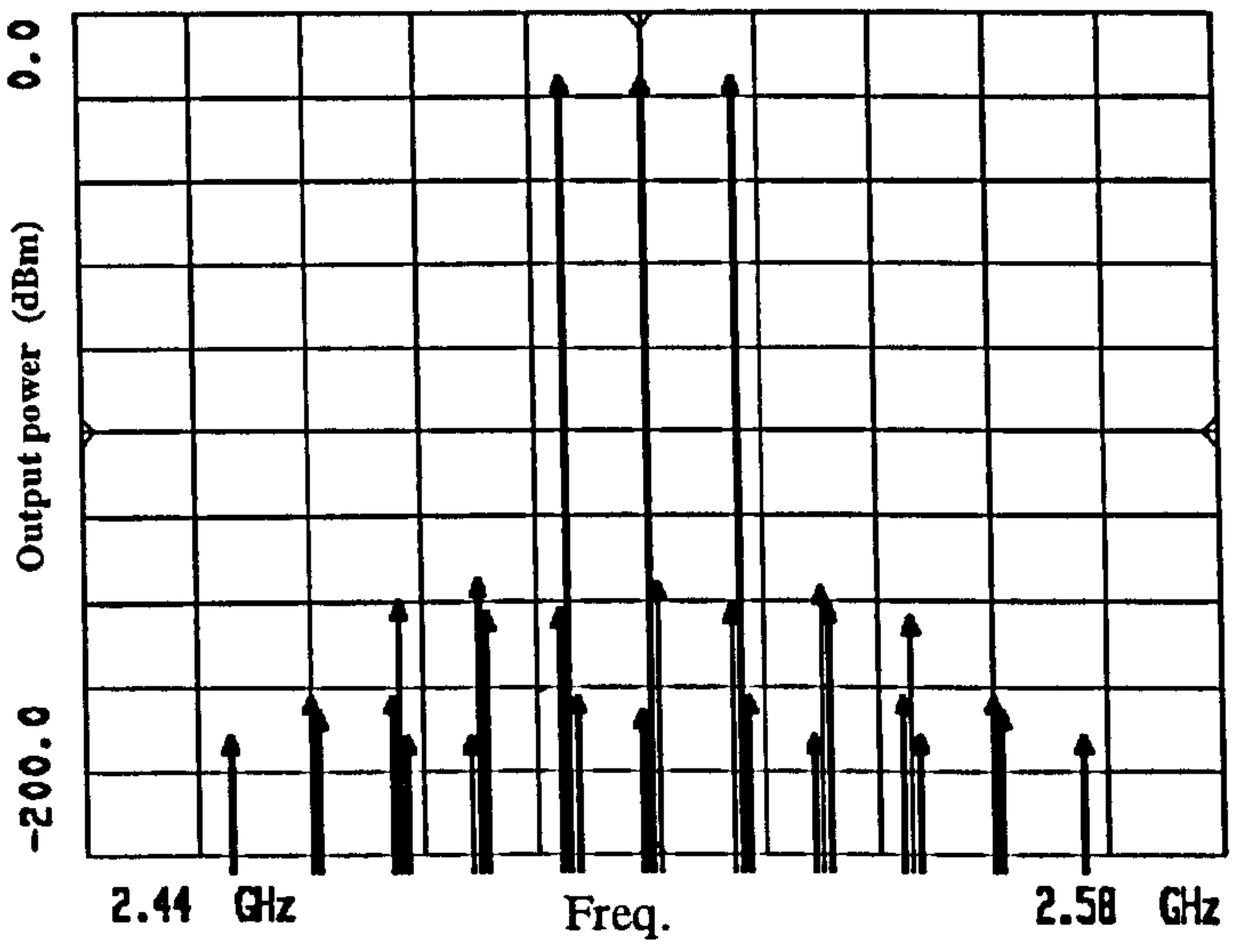

Figure 4..56: **Three-tone simulated output spectrum of amplifier after employing the technique of difference frequency injection and showing the third and fifth order intermodulation.**

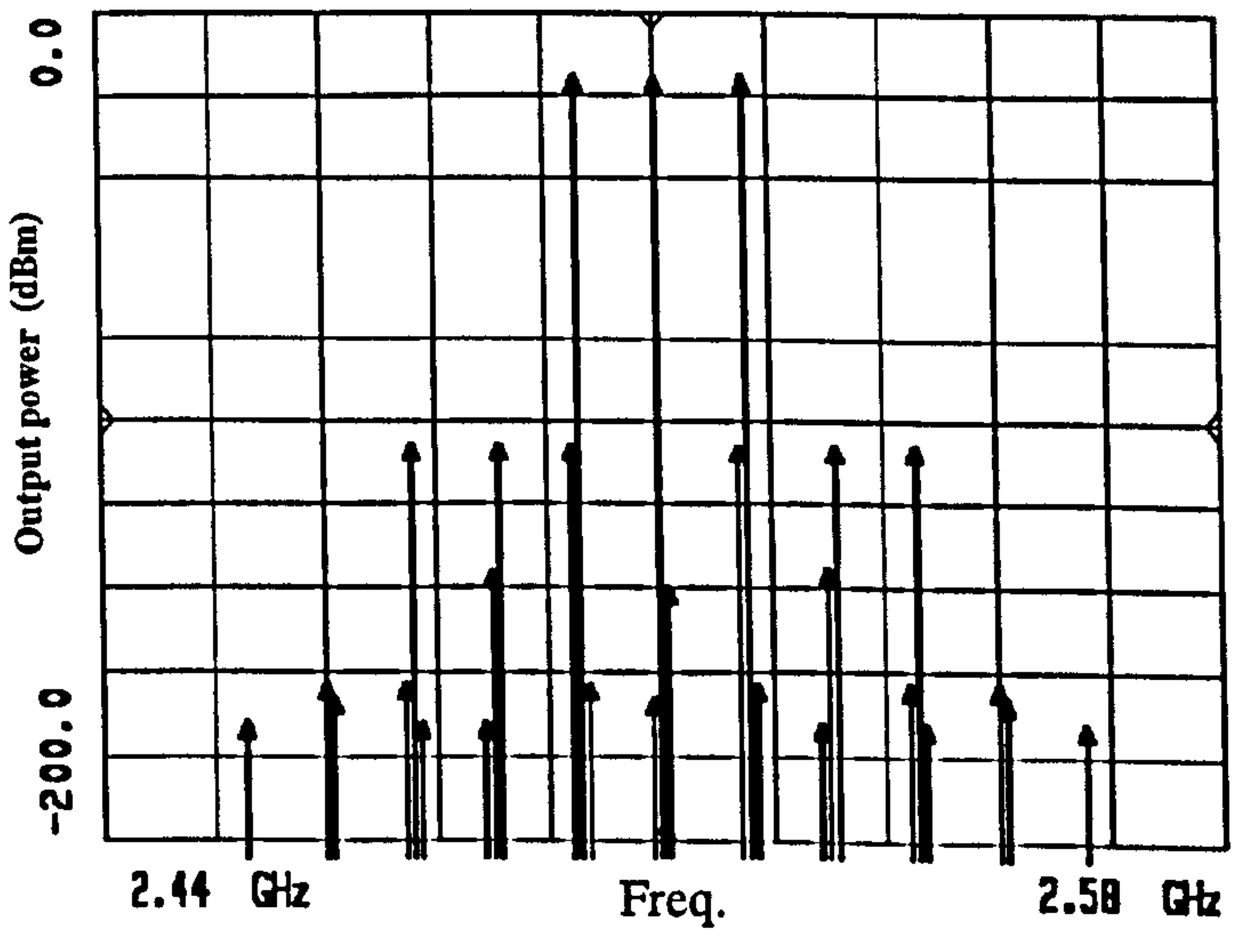

Figure 4..57: **Three-tone simulated output spectrum of amplifier after employing the technique of frequency summation injection and showing the third and fifth order intermodulation.**

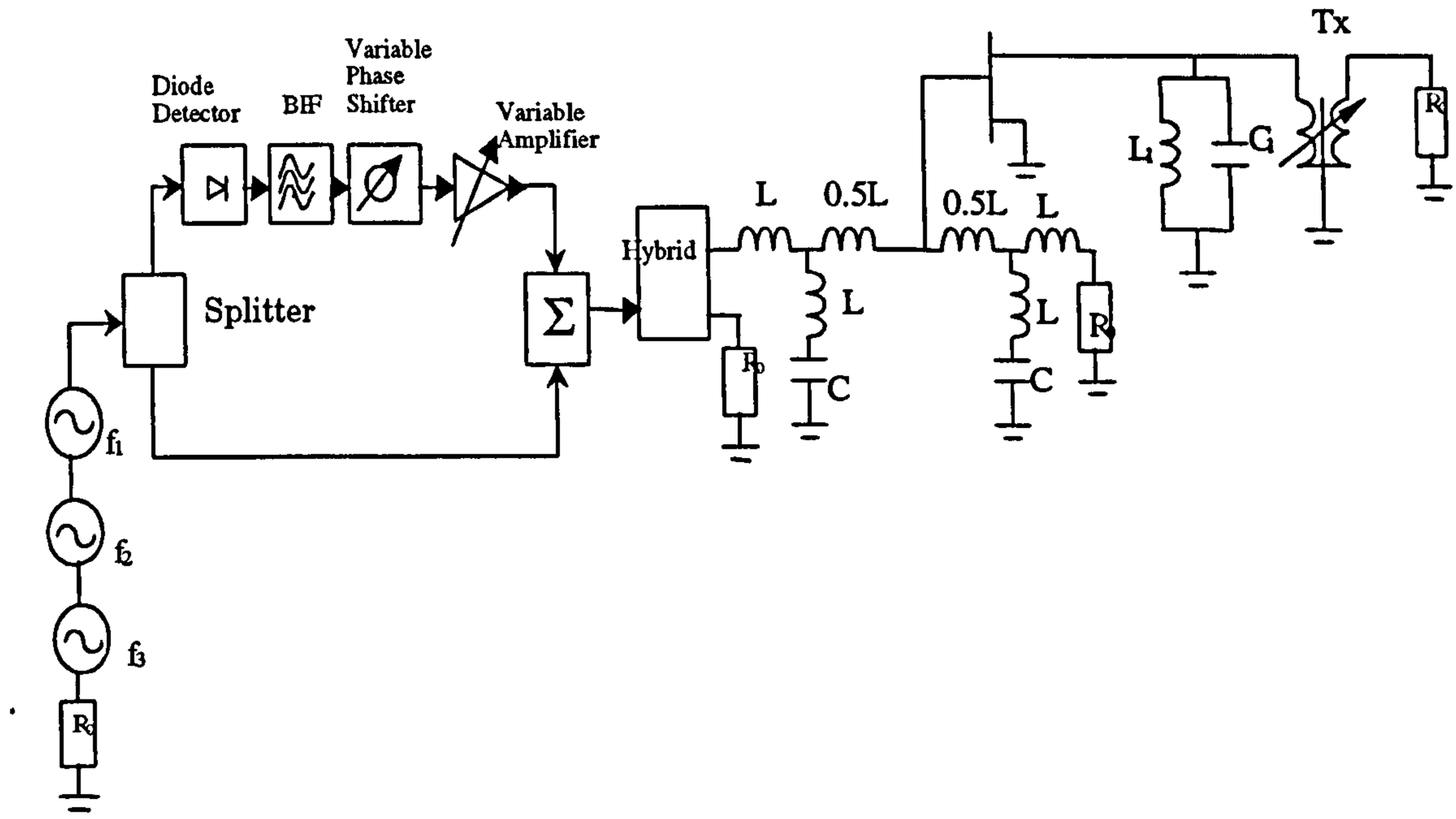

Figure 4..58: **The amplifier schematic diagram with the fundamentals and injected difference frequency predistortion configuration.**

becomes troublesome at high power level, the use of the amplifier below saturation typically requires only the cancellation of third order IMD. As a large number of IMD components are generated, it is very cumbersome to look at all IMDs. It requires a great deals of computer resources and will take quite long time. When dealing with such amount of information, it is useful to look at the adjacent channel power (ACP) instead of looking at the different IMD signals. ACP is defined as the summation of the IMDs terms in the adjacent channel. The envelope of the signal at the output of the amplifier needs to be looked at when using complex modulated signals.

4.10 ACPR Reduction by Difference Frequency Injection

As discussed previously in section 3.3, the adjacent channel power ratio (ACPR) is calculated as the power in the adjacent channel divided by the power in the channel

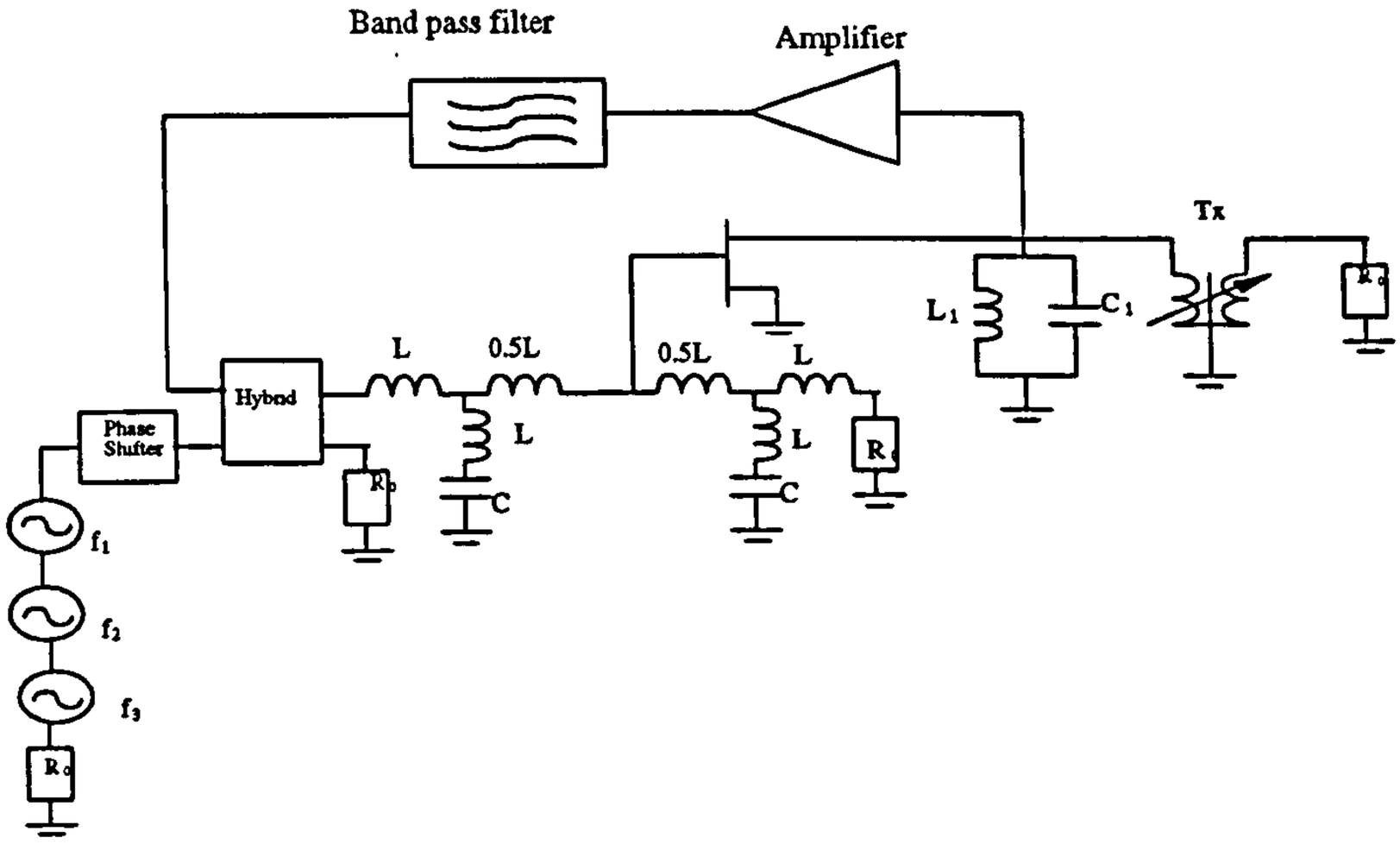

Figure 4..59: **The amplifier schematic diagram with the fundamentals and injected difference frequency feedback configuration.**

carrying the modulated signal. Various modulation schemes are used in communication systems. The test presented in this section, are based on the CDMA system used in such systems.

In order to verify the performance of the difference frequency technique, the injected signals need to be generated in a nonlinear device before being injected into the amplifier or taken at the output of the amplifier and fedback to the amplifier input. This can be achieved by the use of a predistortion circuit as shown in figure 4.58 or a feedback amplifier circuit as shown in figure 4.59. Simulation results of a predistortion circuit based on the amplifier of section 4.3 with a CDMA (IS95) input signal are presented in figure 4.59 and figure 4.60. The results show that for an input power of $0dBm$, a $7.5dB$ improvement on the ACPR by the injection of the difference frequency is obtained. The circuit of figure 4.58 requires the use of a nonlinear diode to generate the low IM signal, which are then amplified and adjusted (phase and amplitude) for

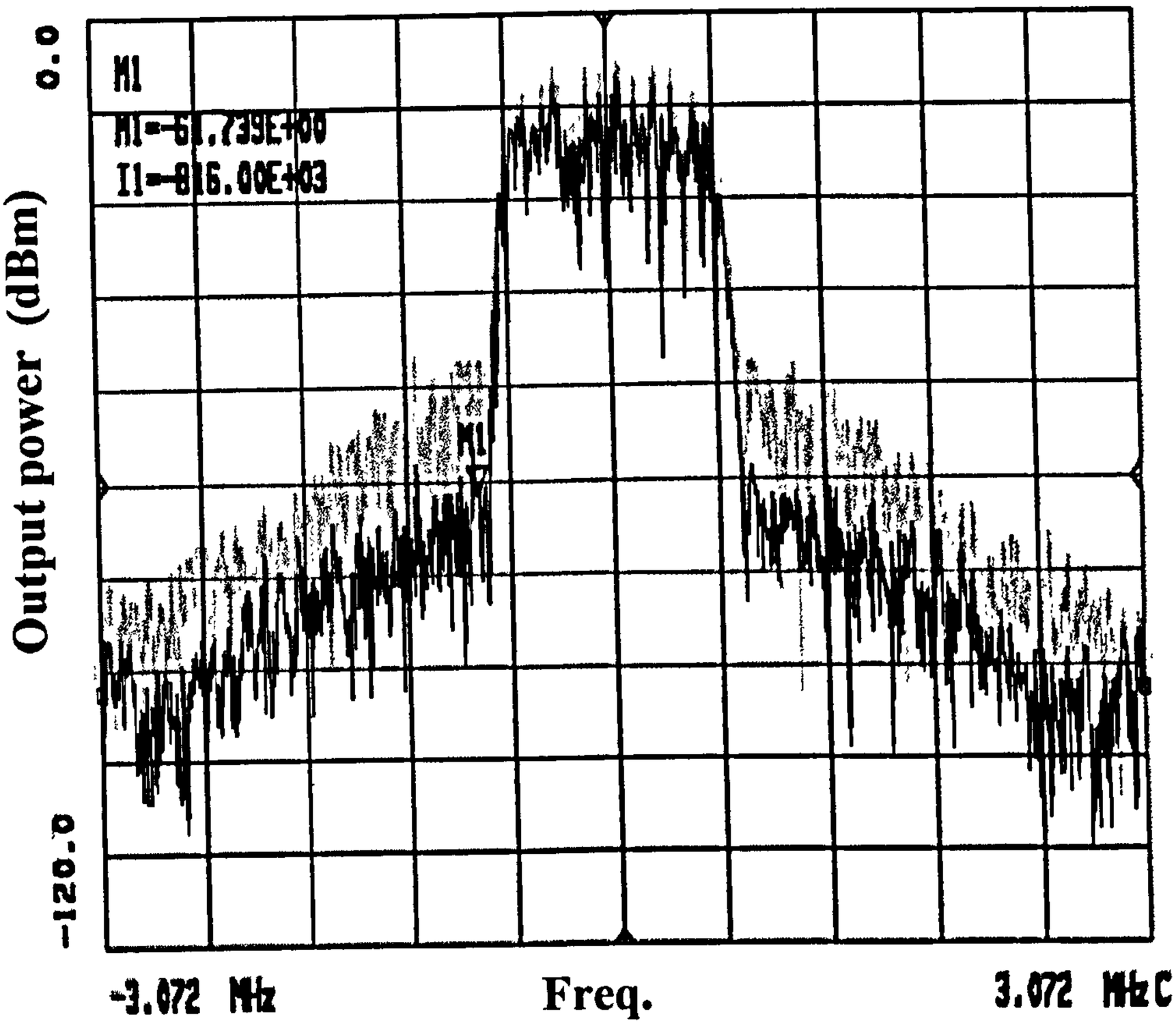

Figure 4..60: **Amplifier output spectrum of a CDMA IS95 signal with (black) and without (grey) the injection of the difference frequency signal.**

optimum ACPR reduction.

A feedback of the second harmonic causes the injection of the sum of the pairs of fundamental frequencies. Since the second harmonic signals and the sum are very close, it is difficult and impracticable to separate these signals. A combination of the two techniques was reported in the literature with a good IMD performance [73,74] although this combination was not identified explicitly.

The reduction in the fifth order IMD can be associated with higher order IMD signals generated by the injection of the difference frequency signals. The simulation

was performed with signals up to the third order terms. This limits the number of terms generated by the nonlinear process and therefore does not give a complete answer to the IMD performance associated with higher order IMD (fifth and seventh order). For higher order IMD, a combination of the injection of the second harmonic and high frequency second order signals provides the same effects on the fifth order IMD.

4.11 Summary and Discussion

Simulation of the technique of second harmonic injection was performed. The use of more than two signals is necessary to see the first and second kind of IMD3. The technique of second harmonic injection reduces only the first kinds of IMD by up to $30dB$ with the use of a common phase and amplitude of the injected second harmonic. The use of a different phase shifter and attenuator on each injected signals improves the reduction by a further $10dB$ to a optimum value of $40dB$.

This result shows that the use of this technique in a multicarrier environment will not contribute to the reduction of IMD3 or the improvement on related distortion such as inter-channel interference. Simulations of the technique of difference frequency injection show, as predicted by in theory, that it reduces both the first and second kinds of IMD3 by more than $30dB$. The reduction is achieved by using a common phase for the injected difference frequency signals. The improvement on the level of third order IM with the use of frequency summations sum of the fundamentals is achieved only on the second kind of IMD by more than $30dB$. The first kinds of IMD3 are not reduced by the injection of the sum of frequencies.

A change in the phase of the injected signal was shown to cause an increase in

the improvement on the IMD, which was greater than that obtained with the change in amplitude. The system is clearly more sensitive to phase changes than amplitude changes. The use of the single attenuator will give results which differ from those obtained by the use of more attenuators. The use of different phase shifters will cause greater reduction of the intermodulation distortion.

In the analysis, all IMD3s were reduced to the same level by the use of a common phase for all injected signals. The use of a different phase shifter for each injected signal produces an improvement on the IMD performance of the amplifier by more than $15dB$ for the different techniques presented. It was shown that the reduction of the different signals required a specific phase and amplitude setting for each signal. The injected signals need to be separated and then their phase set to the phase requirement of each signal for optimum IMD cancellation. This will require a single separate phase for cancellation of each IMD3 generated at the output.

At higher power level the reduction of the first kind of IMD3 by the injection of the sum of the fundamental signals and the second kind of IMD3 by the injection of the second harmonic signals, is caused by the large signal behaviour of the device. This result was not predicted by the theory because the theoretical work considered a weakly nonlinear device. The overall effects of combining the two techniques does however confirm the theory because all IMD3 are reduced.

4.12 Conclusion

It was found that a two-tone test of IMDs level fails to show the true amplifier IMD performance. A second set of third order IMDs is present when dealing with

more than two tones. The second kinds of IMD need to be considered since it contributes to the potentially high level of IMD. The second kind of IMDs are of the form $(f_m + f_n - f_q)$ and are $6dB$ higher than the first kind of IMD, of the form $(2f_m - f_n)$ when the input signals are of the same amplitude.

The difference frequency technique shows a reduction on all the third order intermodulation distortions. The reduction can be up to $60dB$ and sometimes above that, this is achieved with different phases and amplitudes for each IMD signal. Reduction of more than $30dB$ on all IMD was achieved. The use of different phases and amplitudes on the injected signals, improves the overall results.

The injection of second harmonic signals shows from the analysis that the second kind of IMD cannot be reduced with the same amplitude and phase settings as the first kinds. The first kinds of IMDs are reduced by more than $34dB$. However, the use of different phase setting and amplitude will improve the reduction on the first kind of IMD. The use of several phase shifters and attenuators adds to the complexity and the cost of the circuit.

The injection of the sum of the pairs of the frequencies of the fundamental signals reduces the second kind of IMD and not the first kind of IMD at low power level. At higher power level the opposite phenomenon will take place. Similar results were observed with the second harmonic injection technique. Since the injection of second harmonics and the sum of the fundamental signals reduce either the first or the second kind of IMD and their signal are very close in frequency, a combination of both techniques gives very good results. A reduction of more than $30dB$ is obtained on all IMD

In all the techniques, the use of individually adjusted phases shifters on each injected signal, rather than a single common phase shifter, improves the reduction level of IMD products by $10dB$ to $20dB$. This is due to the nonlinear effects of the amplifier, which cause a change in phase at different power levels and frequencies.

Variation of the phase of the injected signals had more impact on the third order IMD than changing the amplitude. Greater reduction was obtained with different phases whereas the amplitude required to reduce all IMD was almost the same. The use of more phase shifters is clearly required for a greater reduction of the IMD. The use of a single phase shifter is adequate in a two tone system and acceptable in a three tone system. However, for multi-tone (more than 3 tones) applications, more phase shifters are clearly required, since the phase difference between the IMDs generated by such a system will cause a phase requirement on the injected signal that can not be met by a single phase shifter as illustrated by the diagram of figure 4.26.

CHAPTER 5.

PRACTICAL PERFORMANCE OF THE DIFFERENCE FREQUENCY TECHNIQUE

5.1 Introduction

This chapter deals with the practical implementation of the difference frequency technique. A predistortion linearizer using an injection of the difference frequency technique is presented. The circuit configuration and design methodologies are described. This technique of IMD cancellation performance is then compared to the second harmonic technique which can be considered as mentioned in the previous chapter, as a combination of the second harmonic injection and the frequency summation (second order IM signal) injection techniques.

5.2 Difference Frequency Linearizer Circuit

For simplicity and practicality, a predistortion circuit is designed and tested for the reduction of IMD in order to verify the theory. The choice in the design is merely due to the availability of components and the ease of implementation of the technique.

The predistortion circuit built is shown in figure 5.1. The circuit is designed with a mini-circuit $ZL-2000$ amplifier, which is the main amplifier. The device is a broadband amplifier, which operates over a bandwidth of $10MHz$ to $2000MHz$, a typical gain of $21dB$ and gain flatness of $\pm 1.5dB$. The amplifier has a $1dB$ output compression point of $+15dBm$ for frequencies below $1GHz$ and an IP of $+25dBm$. The noise figure of the amplifier measured on a HP8970B noise figure meter, is typically $4dB$ as shown in figure 5.2. The amplifier uses a single $15V$ supply. The output power

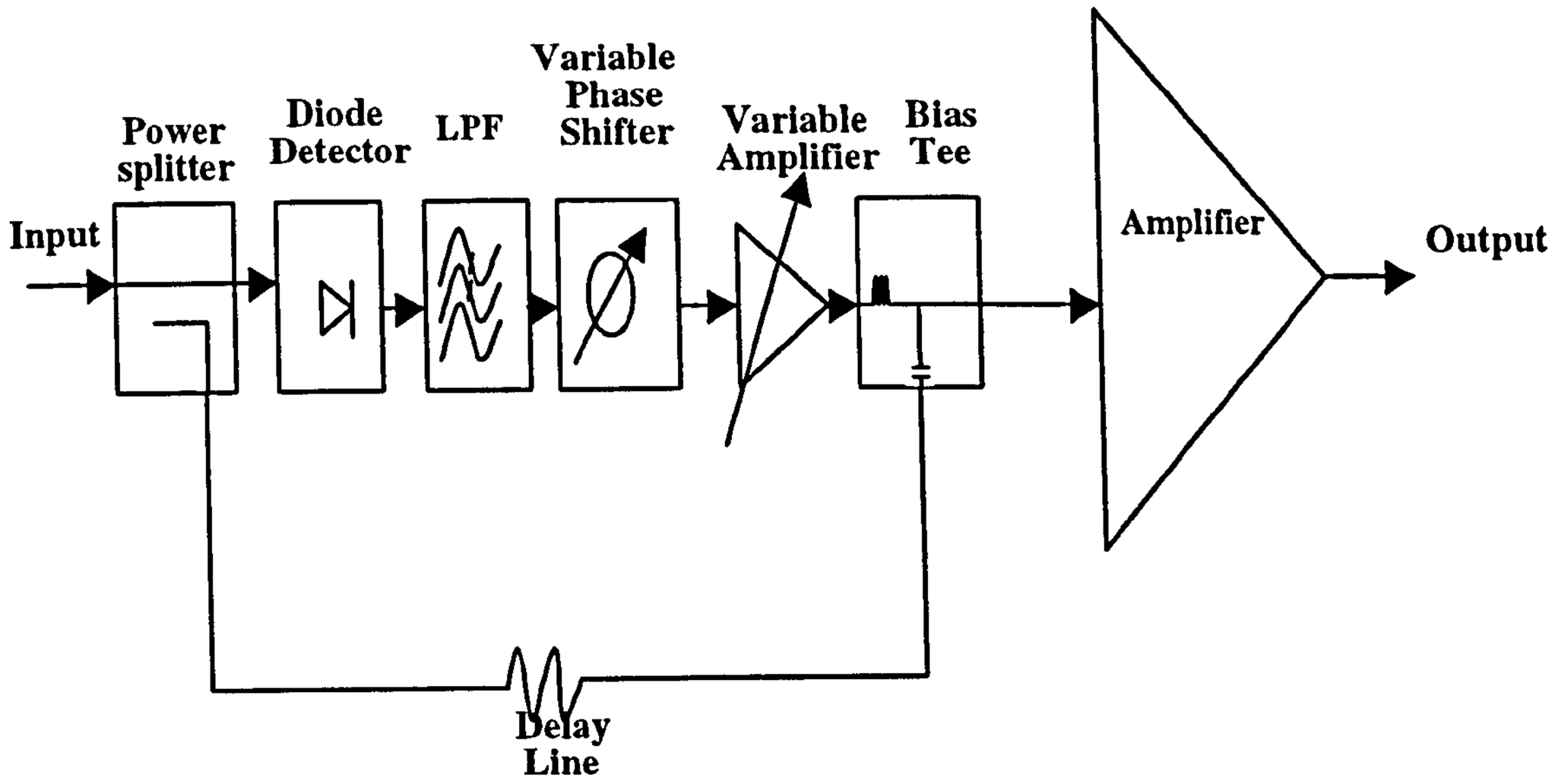

Figure 5..1: **The circuit diagram for experimental implementation of the technique at** $900MHz$**.**

variation to input power level for the frequencies of $880MHz$ and 1MHz are both tested on the amplifier and are shown in figure 5.3 and figure 5.4. It shows that the maximum output power at the frequency of $880MHz$ is about $17dBm$.

The predistortion circuit is directly connected to the input of the amplifier. The operation of the predistorter is to provide the main amplifier with the fundamental signal and the difference frequency signals. The signals at the frequencies $880MHz$ and $881MHz$ at the input of the predistorter are divided into two paths using the Mini-circuit power splitter, which provides two signals of equal amplitude, with 0° phase relationship and more than $20dB$ isolation between the output signals. The insertion loss of the power splitter is $3dB$ ($\pm 0.5dB$) between input and output ports.

The fundamental signals are passed through a delay line (main path) and fed into a bias tee circuit. The second path is used to generate the difference frequency

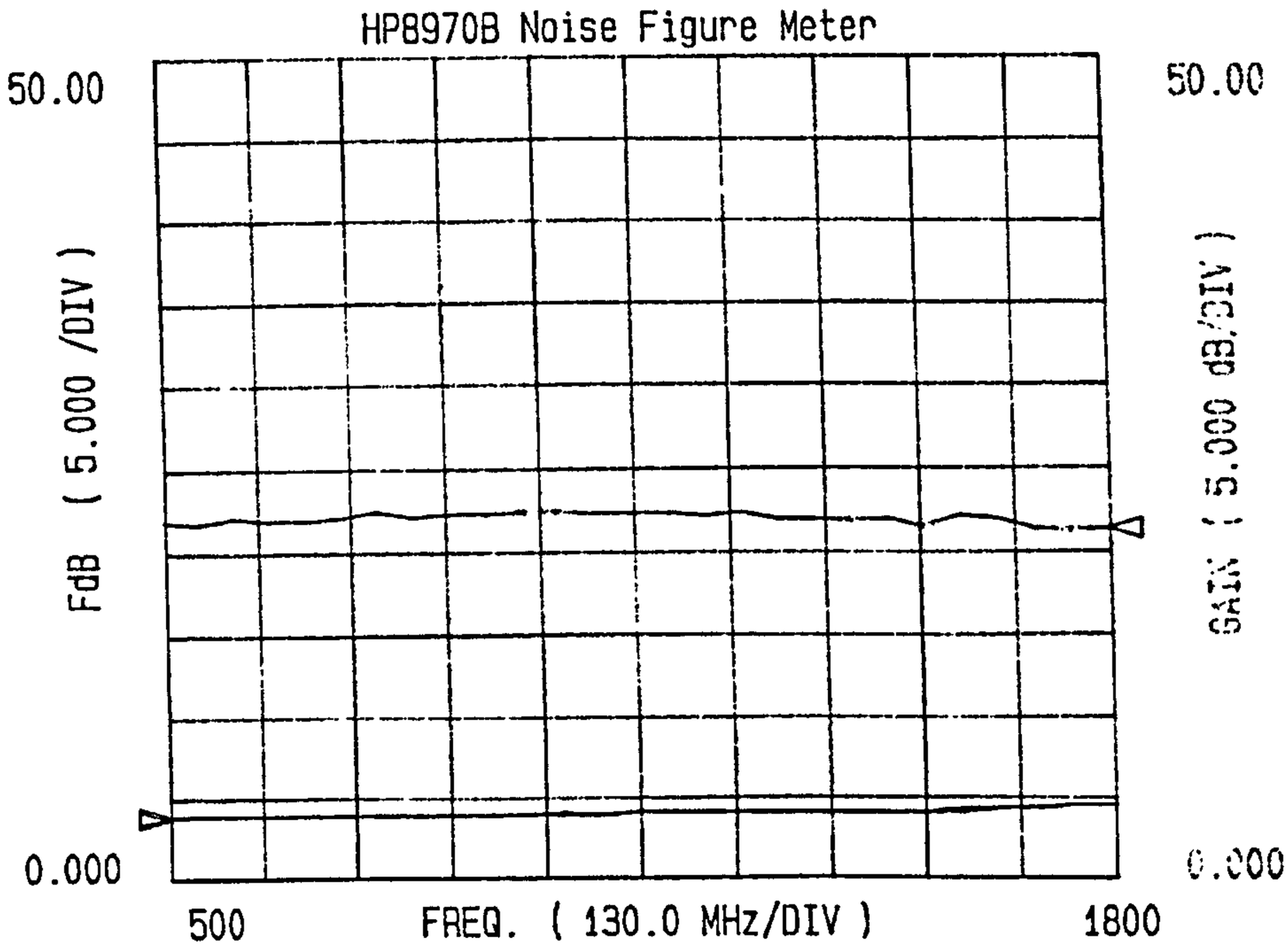

Figure 5..2: **Measured noise figure and gain of the mini-circuit ZL-200 amplifier.**

signal needed for the cancellation of third order intermodulation distortions. The signal in this path will pass through a diode detector. The diode detector being a nonlinear device will provide all the relevant intermodulation products at its output. This enables a separation of the difference frequency signals from the remaining IMD signals by the use of a low pass filter (LPF). The use of the signals at the frequencies $880MHz$ and $881MHz$ generates a difference frequency signal at the frequency $1MHz$. A Mini-circuit $BLP-300$ low pass filter with a bandwidth of $300MHz$ is used. The filter exhibits a bandpass of DC to $300MHz$ with a typical $3dB$ cut-off frequency of $297MHz$ and a return loss of $20dB$ and $40dB$ for the stop band of $410MHz$ to $550MHz$ and $550MHz$ to $1200MHz$, respectively. The maximum power rating of the device is $0.5W$. The filter cut-off the high frequency portion of the spectrum leaving only the low frequency

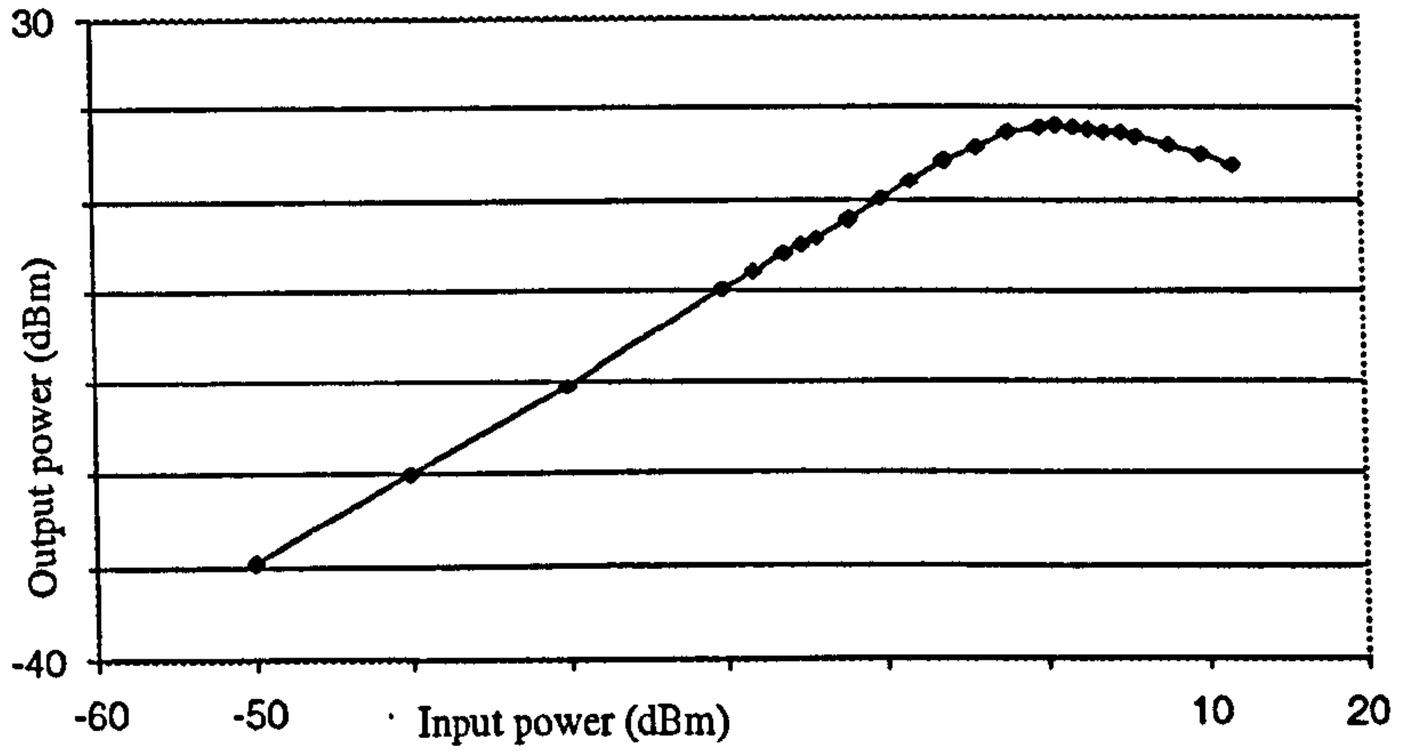

Figure 5..3: **Output power Vs input power of the ZFL 2000 amplifier used in the measurement at 880MHz.**

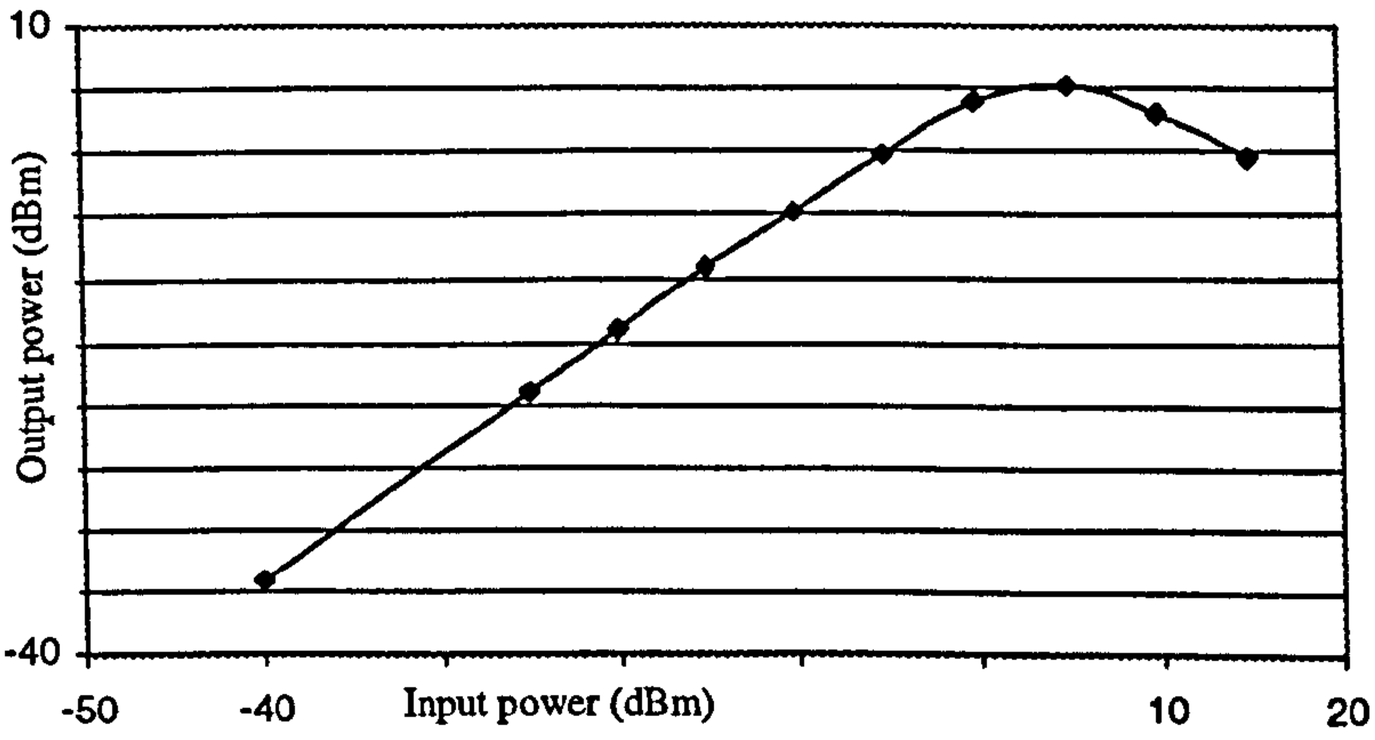

Figure 5..4: **Output power Vs input power of the ZFL 2000 amplifier used in the measurement at 1MHz.**

which contains the difference frequency signal of $1MHz$. The signal is then phase shifted with a passive phase shifter and its amplitude is adjusted using a variable low frequency amplifier. Both circuits are designed to specifications that give the best IMD performance and are described below in greater detail. The low frequency path and the main high frequency path are combined using a purpose built bias tee, the design of which is detailed below. The combined output of the bias tee is then injected into the amplifier as shown in figure 5.1.

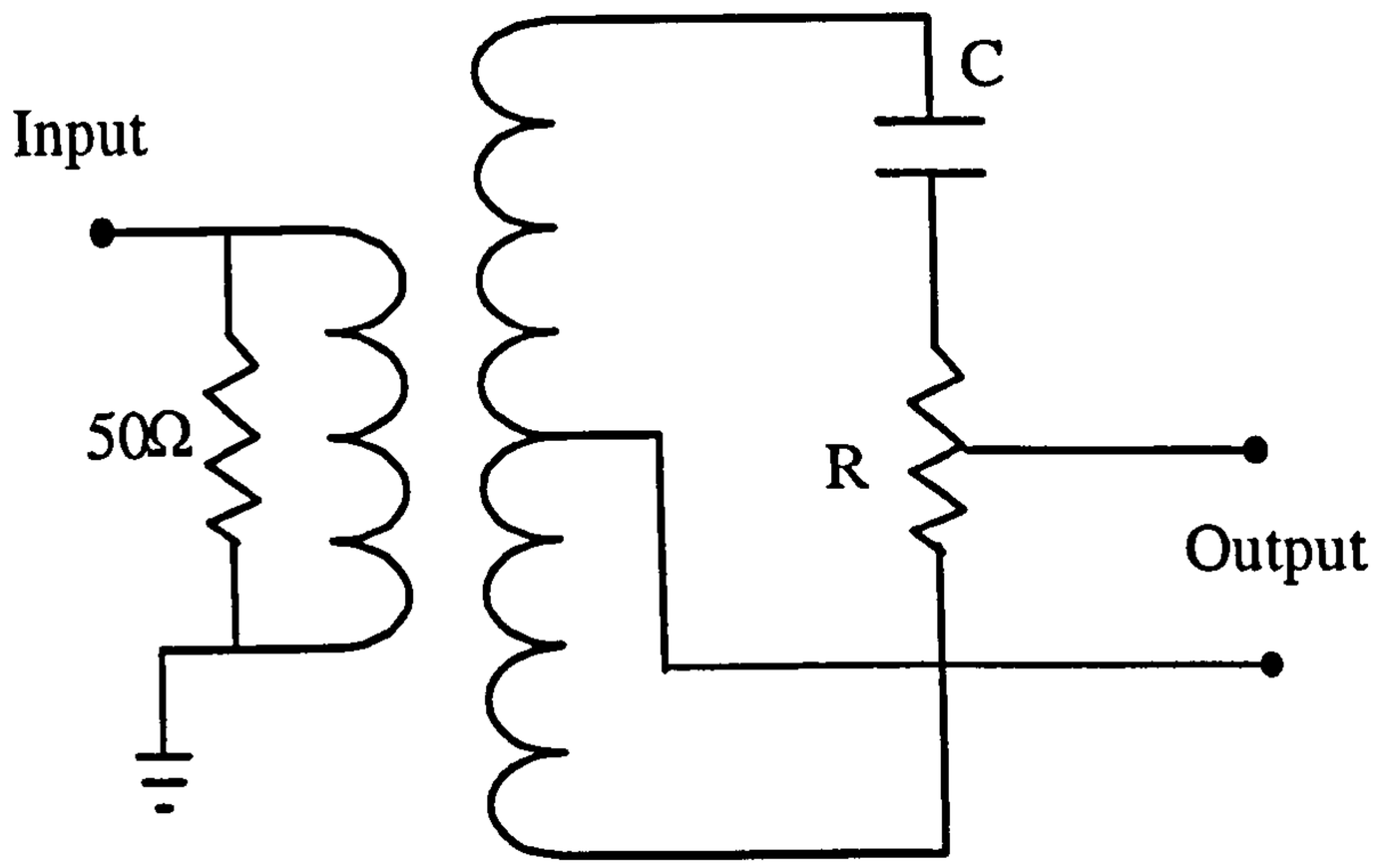

Figure 5..5: **Circuit diagram of the phase shifter.**

5.2.1 Phase Shifter Design

The phase shifter is designed to provide a defined phase shift at $1MHz$. The circuit of figure 5.5 is used to provide phase shifts between 0° and 180°. Since the operation of the device is tuned at the frequency $1MHz$, the components required to provide the phase shift at this frequency can be calculated by using a formula whereby

$$f_c = \frac{1}{2\pi RC} \tag{5..1}$$

With f_c the tuned frequency,

R and C are the output resistor and capacitor respectively.

Since $f_c = 1MHz$, if the resistance is chosen to be $R = 1k\Omega$, then $C \simeq 159pF$.

A practical value of capacitor of $220pF$ was used for the experiment after experimental test for correct operation of the phase shifter. It provides approximately 180o phase shift with zero attenuation. With the potentiometer set to a fixed value, the circuit can be treated as a phase equalizer and therefore acts as a phase corrector

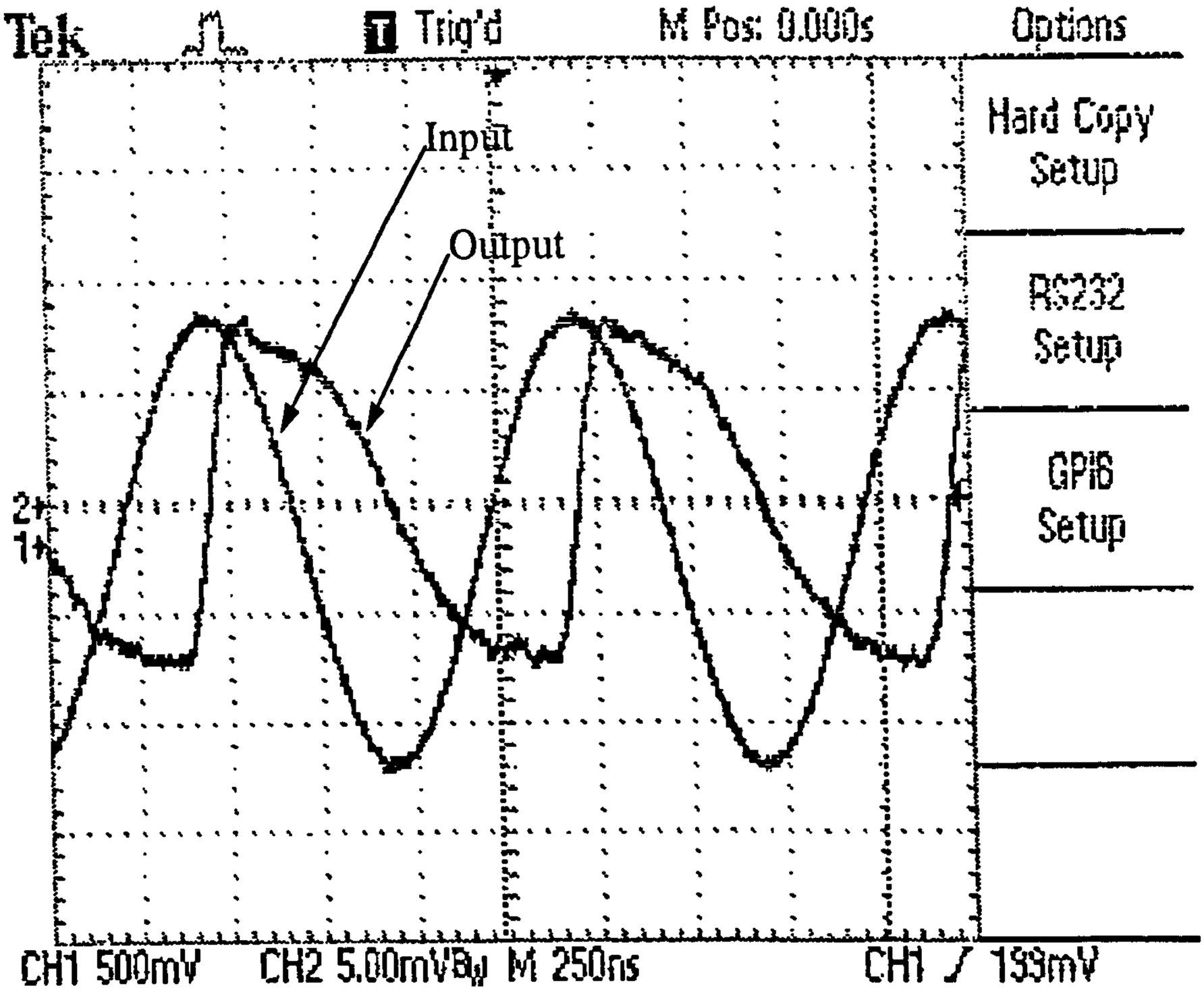

Figure 5..6: **Difference frequency signal waveform at the input and output of the phase shifter.**

without distorting the gain characteristic of the overall circuit. The waveform of the signal before and after the phase shifter can be seen in figure 5.6 where a slight distortion can be detected on the output signal which is shifted by about 90°.The distortions at the output of the phase shifter are caused by impedance mismatch in the low path circuit.

5.2.2 Low Frequency Amplifier Design

The variable amplifier was designed using the Analog Devices ultralow distortion, wide bandwidth voltage feedback Operational Amplifier $AD9631$. The device provides a low noise of $-113dBc$ at 1MHz and $-72dBc$ at $20MHz$. The third order intercept

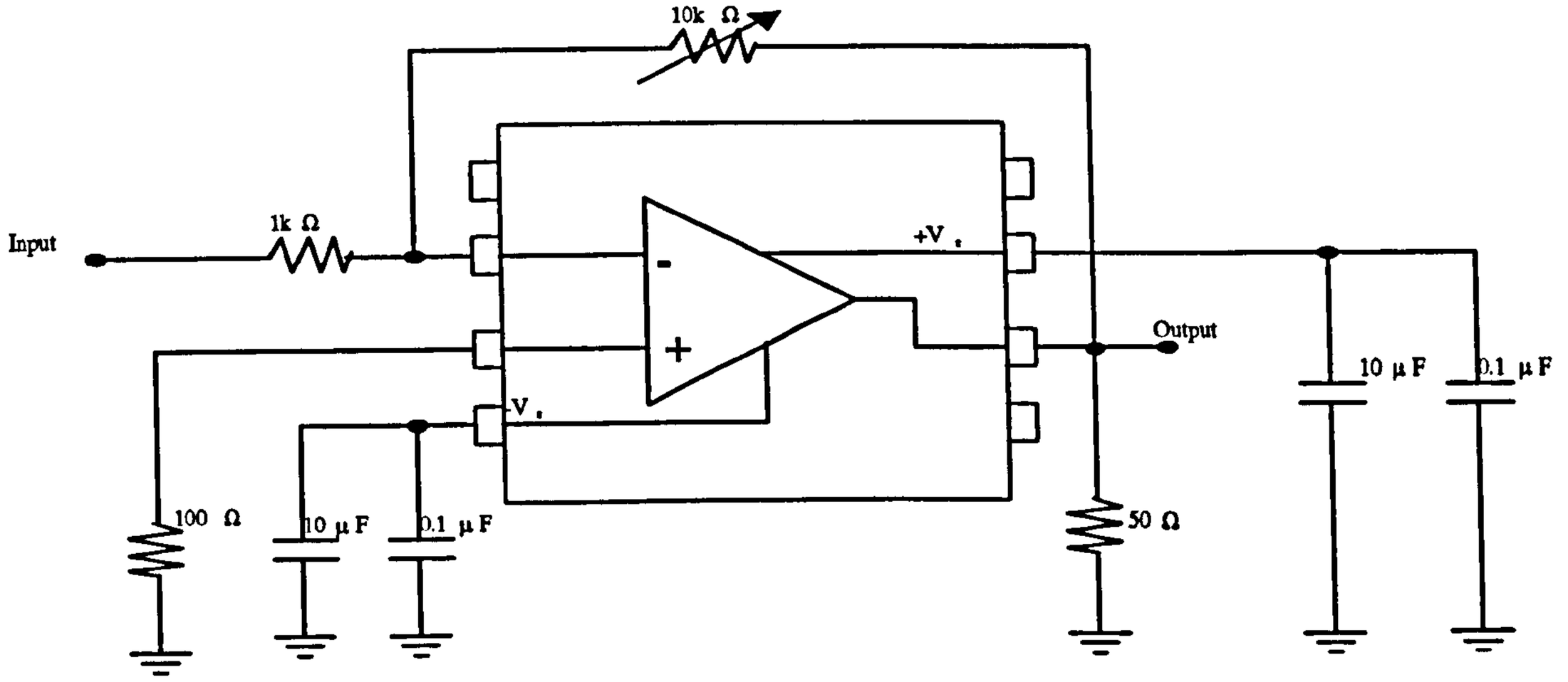

Figure 5..7: **Circuit diagram of the low frequency amplifier using an AD9631 ultralow distortion, wide bandwidth voltage feedback OP Amp.**

is $+46dBm$ at $25MHz$. It has a high input resistance of $500k\Omega$ and a low output resistance of 0.3Ω. The typical dc supply of the device is $\pm 5V$ with a quiescent current of $17mA$. The phase distortion of the device is of the order of 1.1° from DC to $100MHz$.

The inverting amplifier configuration of figure 5.7 was constructed to provide a gain of up to $20dB$ by a careful selection of R_f and R_i ($10k\Omega$ & $1k\Omega$). The value of the feedback resistor is critical for optimum dynamic performance of the amplifier. The $0.1\mu F$ and $10\mu F$ capacitors are supply decoupling capacitors.

5.2.3 Bias Tee Design

The device was designed to provide a connection to the input of the main amplifier

for the low frequency signal $(f_2 - f_1)$ on one hand and for the high frequency signals $(f_1$ & $f_2)$ on the other. The low frequency signal at $1MHz$ is injected at port 2 and is blocked from interfering with the high frequency signal at the other input port 1. The high frequency signal is injected at the input port 1 and the signal is blocked from interfering with the low frequency path at port 2.

The circuit of figure 5.8 was used to provide the required characteristics of the device. A capacitor was used as a low frequency blocking capacitor, working at frequencies up to a few megaHertz to stop the difference frequency signals on one side. The high frequency was choked using a series inductor and a shunt capacitor to prevent a feedback to the low frequency path of the predistorter.

Microstrip lines were added to the circuit, which was then optimised to achieve the desired performance. The width of the microstrip line was calculated using the Hewlett Packard LINECALC[1] software at the frequency of $880MHz$.

The substrate used was the RT/Duroid 5880 by Rogers Corporation with the following specifications:

- The relative permittivity (ε_r) is 2.2.
- The height of the substrate is $0.81mm$.
- The metal thickness is $0.025mm$.

The measured results of figure 5.9 show that the return loss between port 1 and port 2 at $880MHz$ is about $-28.92dB$. This reduces the interference caused by the

[1] LINECALC (linear calculation) is an analysis & synthesis program that calculates the elcctrical paramters of single and coupled transmission lines from physical parameters and calculates physical parameters from electrical parameters.

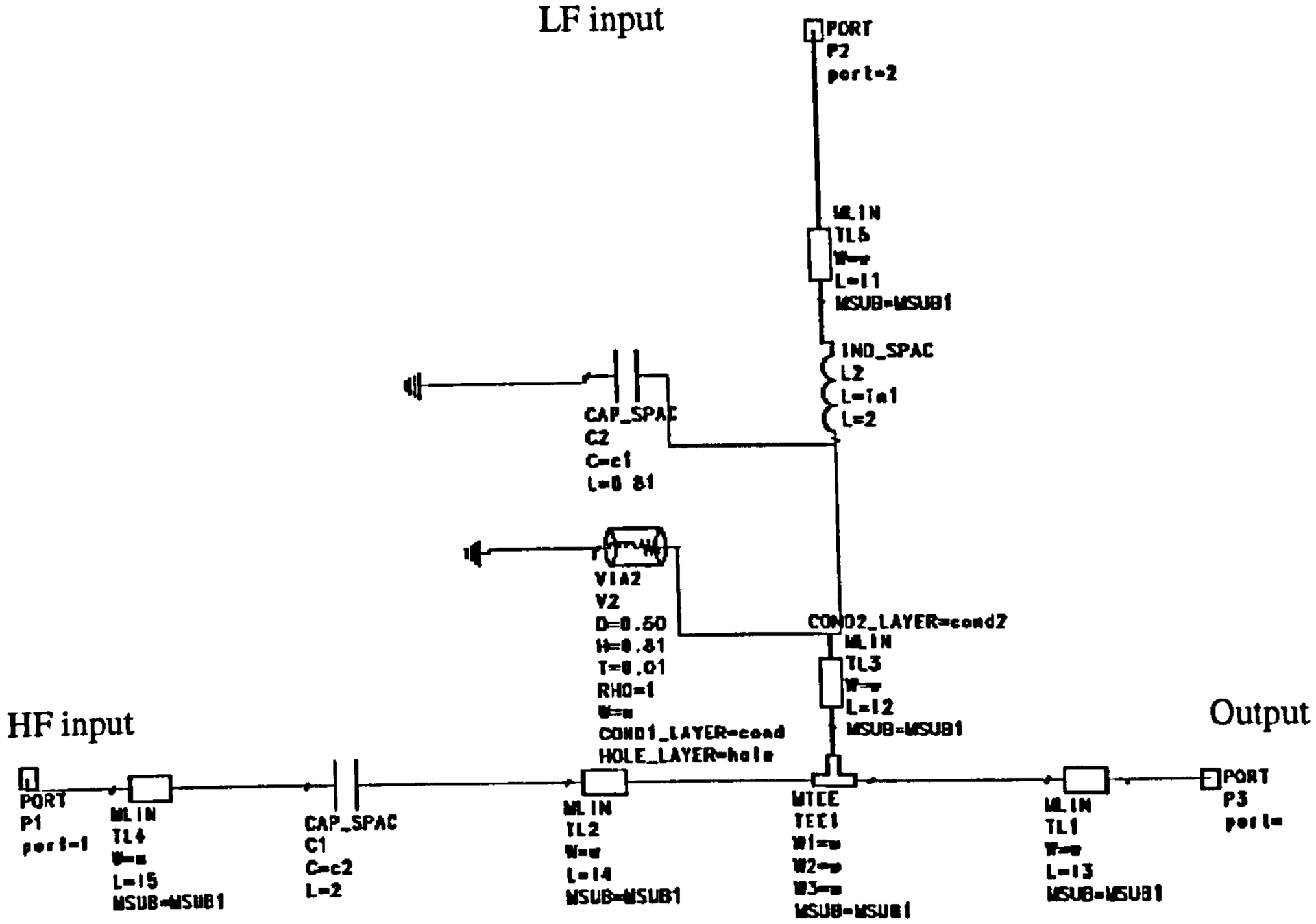

Figure 5..8: **Bias tee circuit diagram.**

high frequency in the predistorter low frequency path.

Figure 5.10 shows the return loss between the input port 2 of the difference frequency and the output. At $880MHz$ the signal is attenuated by $23dB$ and therefore allows the isolation of the high frequency. In figure 5.11, the loss between the input port 1 of the high frequency signal shows a $-1.14dB$ return loss and a greater loss at lower frequency. Measurement at $1MHz$ could not be taken on the HP8510B Network analyser used. The $1MHz$ operation was tested using a spectrum analyser by means of measuring the signal attenuation between the different ports.

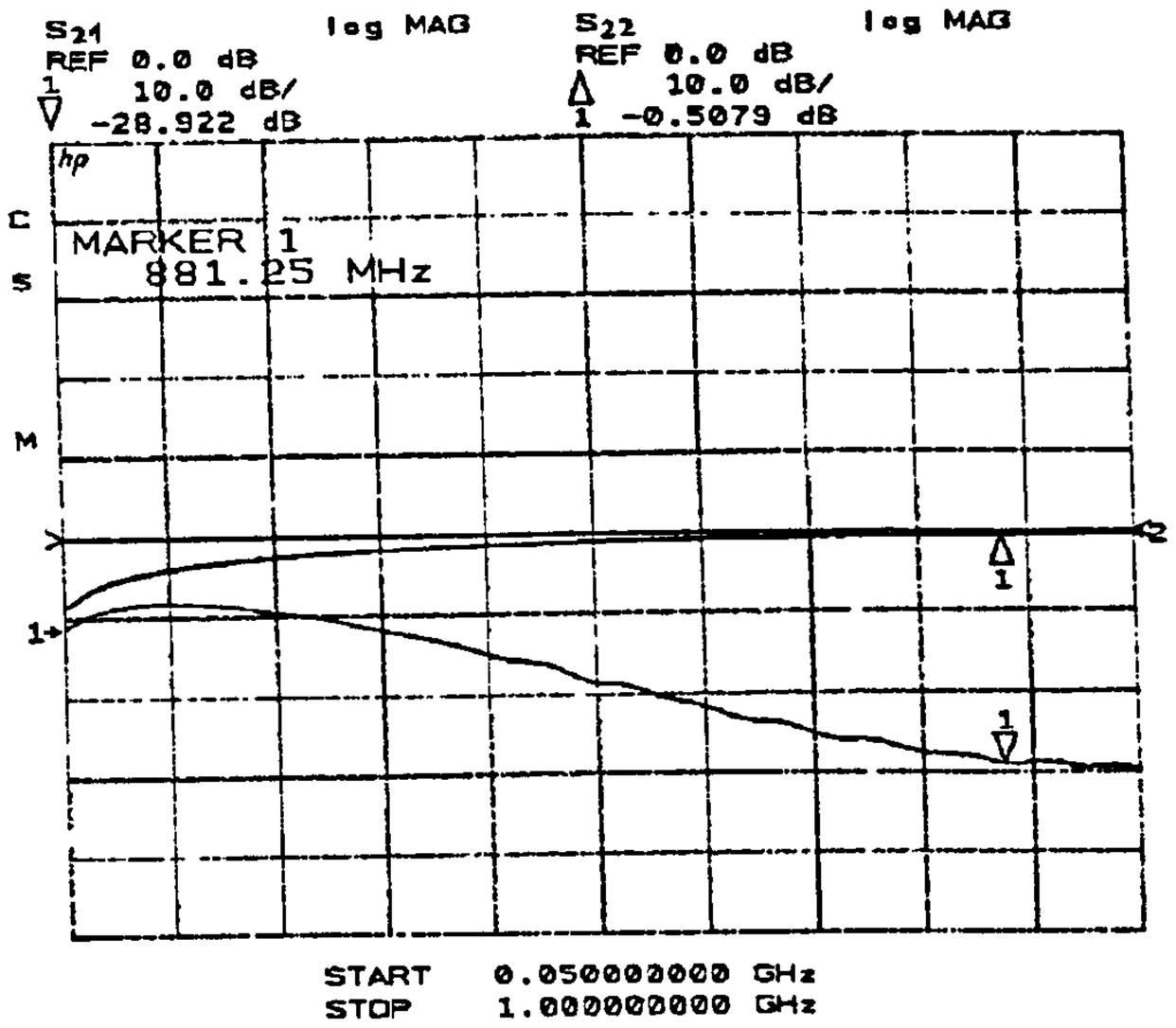

Figure 5..9: **Measured input reflection at port 2 and return loss between input port 1 and 2 of the bias tee.**

5.3 Circuit Design and Measurement.

Since this predistortion amplifier is not a compact linearizer circuit but made up of various subsystems, various precautions need to be exercised for correct operation and performance evaluation of the IMD reduction. The circuit of figure 5.12 shows the overall system with the signal generators and test equipment used for the evaluation of the performance of the system as well as the devices used to enhance the performance of the circuit.

The use of the Dorado circulator Model $C-5002$ as an isolator in the circuit prevents a complete isolation of the signal generators as this can lead to generation of IMD terms within the signal generator. An isolation was also provided before the diode detector to avoid the IMD generated in the detector being fed into the amplifier. Isolation is required between the bias tee and the main amplifier to reduce the effects

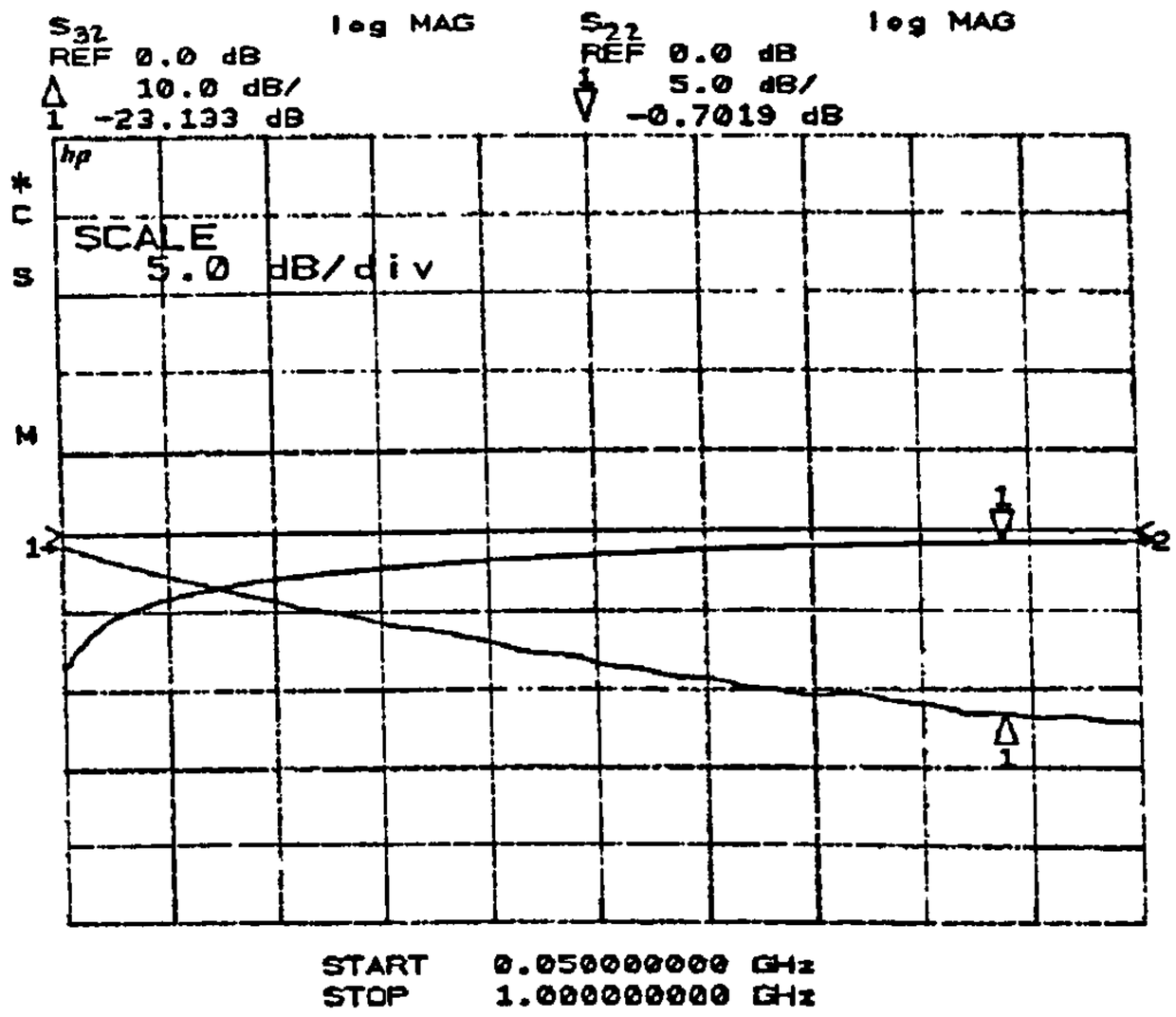

Figure 5..10: **Measured input reflection at port 2 and return loss between input port 2 and output port 3 of the bias tee.**

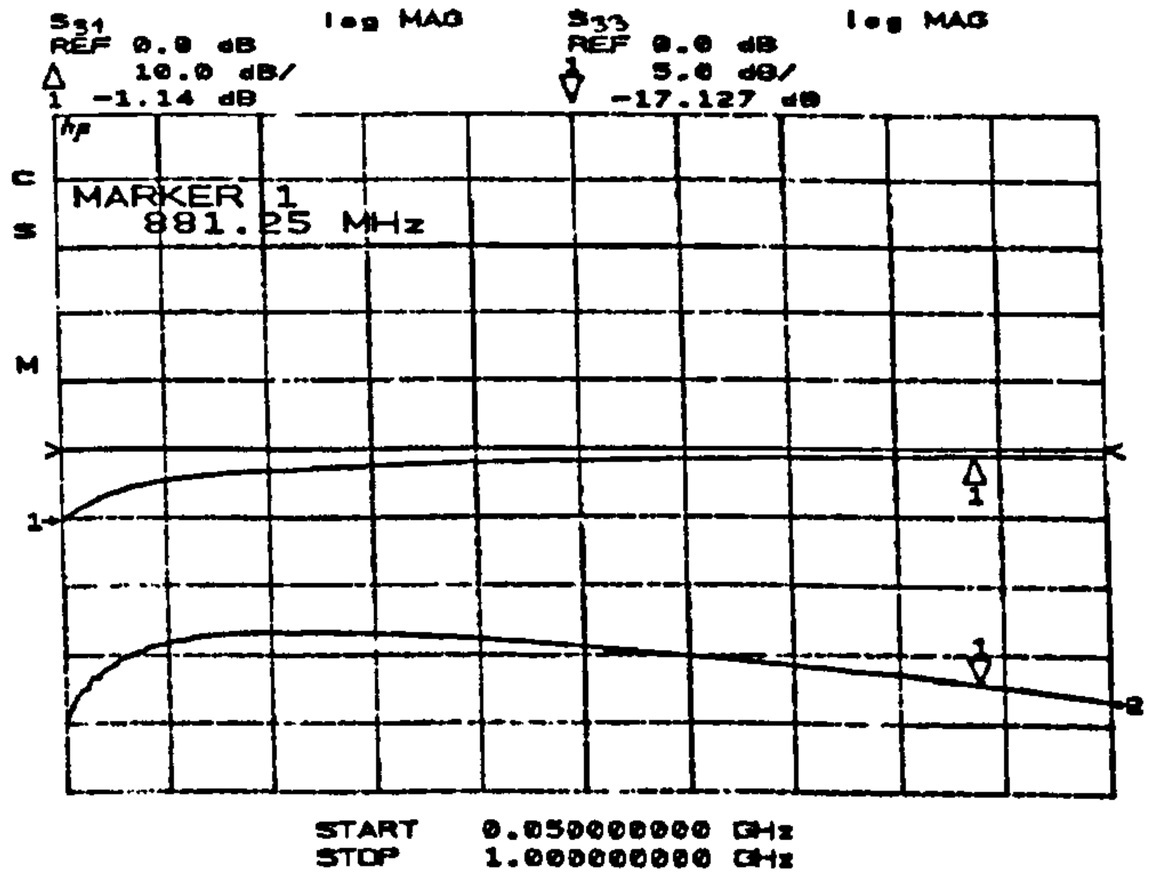

Figure 5..11: **Measured output reflection at port 3 and return loss between input port 1 and output port 3 of the bias tee.**

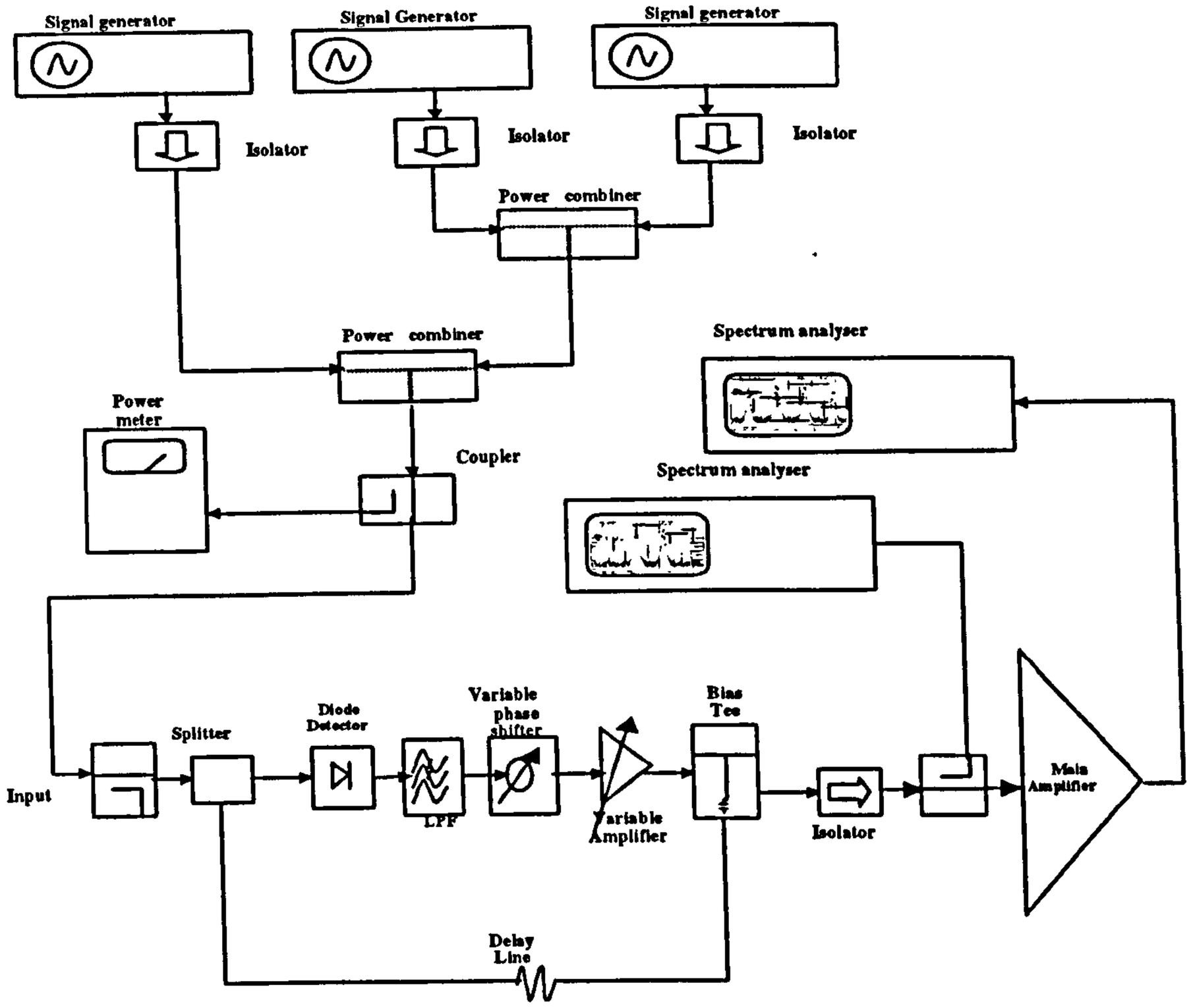

Figure 5..12: **The circuit diagram and measurement set-up for performance test of the technique at** $900MHz$.

that are caused by the distortion within the amplifier being fedback into the predistorter circuit and therefore disturbing its operation. The circulator operates in the frequency range of $820MHz$ to $960MHz$ with a minimum insertion loss of $-0.4dB$ and a minimum isolation of $-20dB$ as shown in figure 5.13. The circulator tolerates up to 8 $Watts$. An attenuator was used at the output of the low frequency variable amplifier, to enable the injected difference frequency signals to be switched on and off. Monitoring of the $1MHz$ difference signal was achieved through the used of an oscilloscope. This arrangement provided the opportunity to see the difference frequency signals before and after the phase shifter and the variable amplifier, to detect any distortions in the operation of

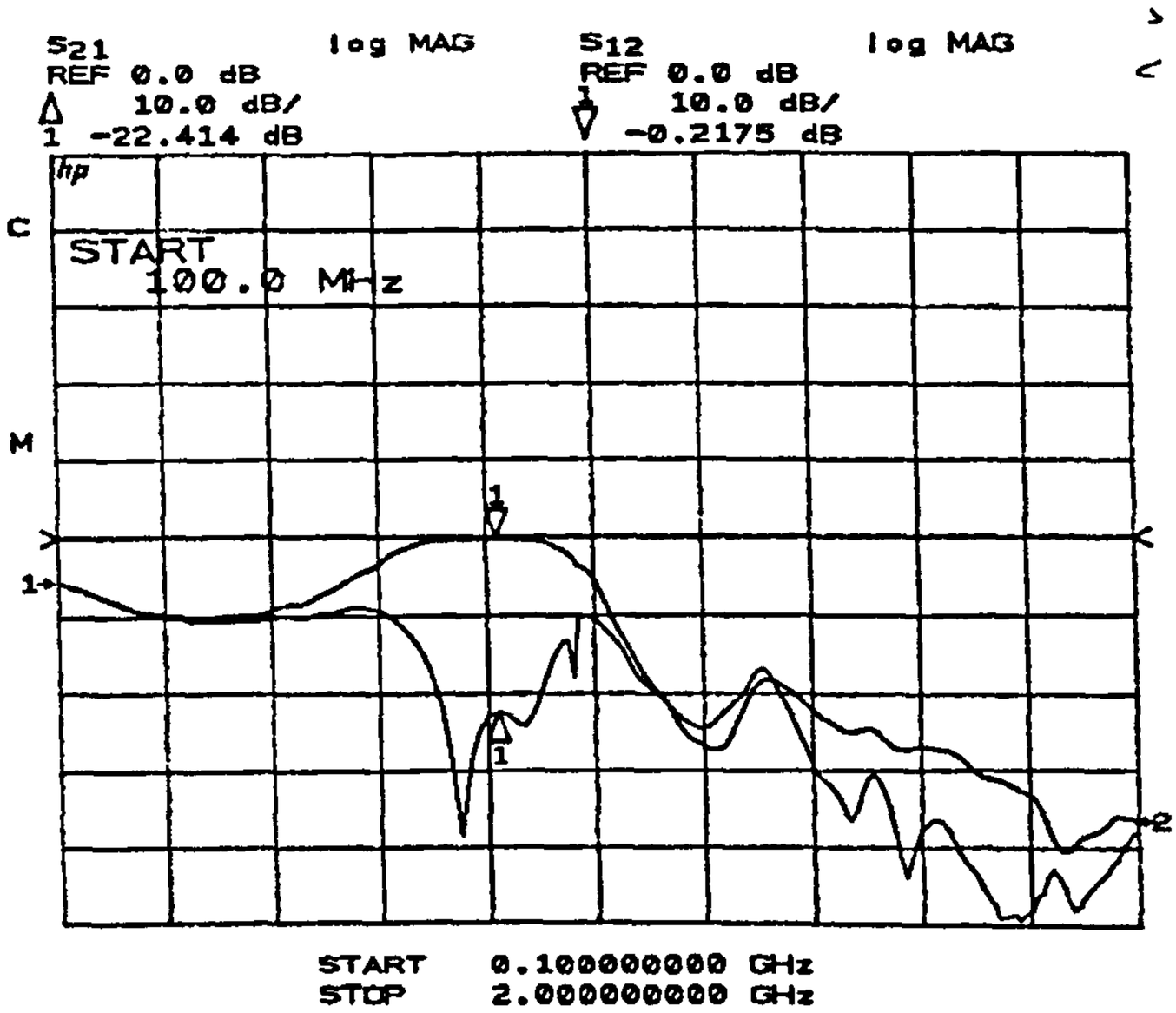

Figure 5..13: Measured input and output reflection loss of the Dorado circulator model used in the predistortion circuit set-up.

the low frequency path.

For the two-tone test, signals at the frequencies $880MHz$ and $881MHz$ were provided by a Hewlett Packard signal generator (HP8657A) and a Wavetek 2-2500A synthesised signal generator. IMD measurement were made on a Hewlett Packard HP8562A spectrum analyser.

5.4 Difference Frequency Technique Performance

The experimental investigation of the technique of difference frequency injection was performed at various frequencies with different tone spacing. The results of this investigation are hereby presented.

5.4.1 Two-Tone Test

The two-tone test was performed with two fundamental signals at the frequencies of

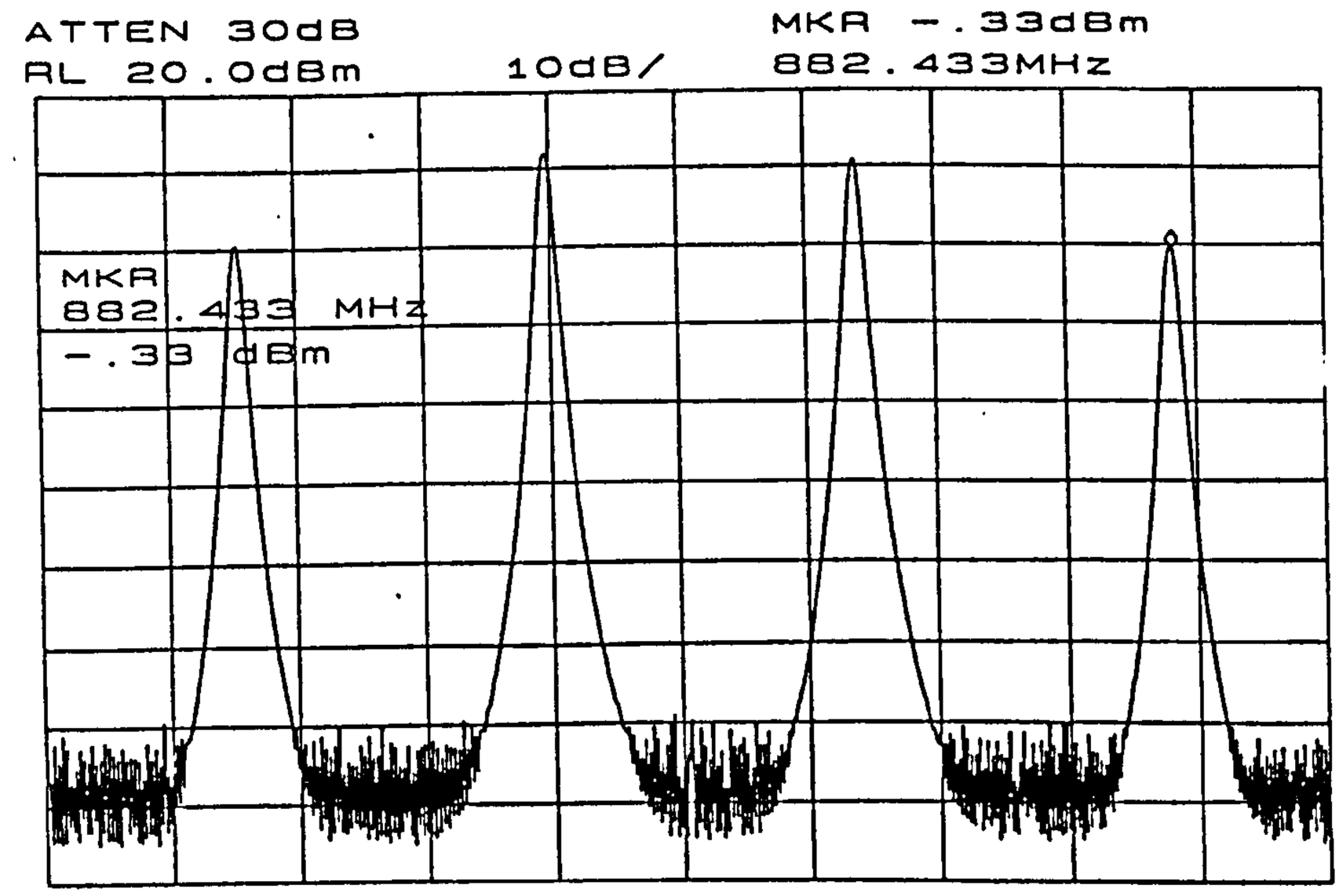

(a)

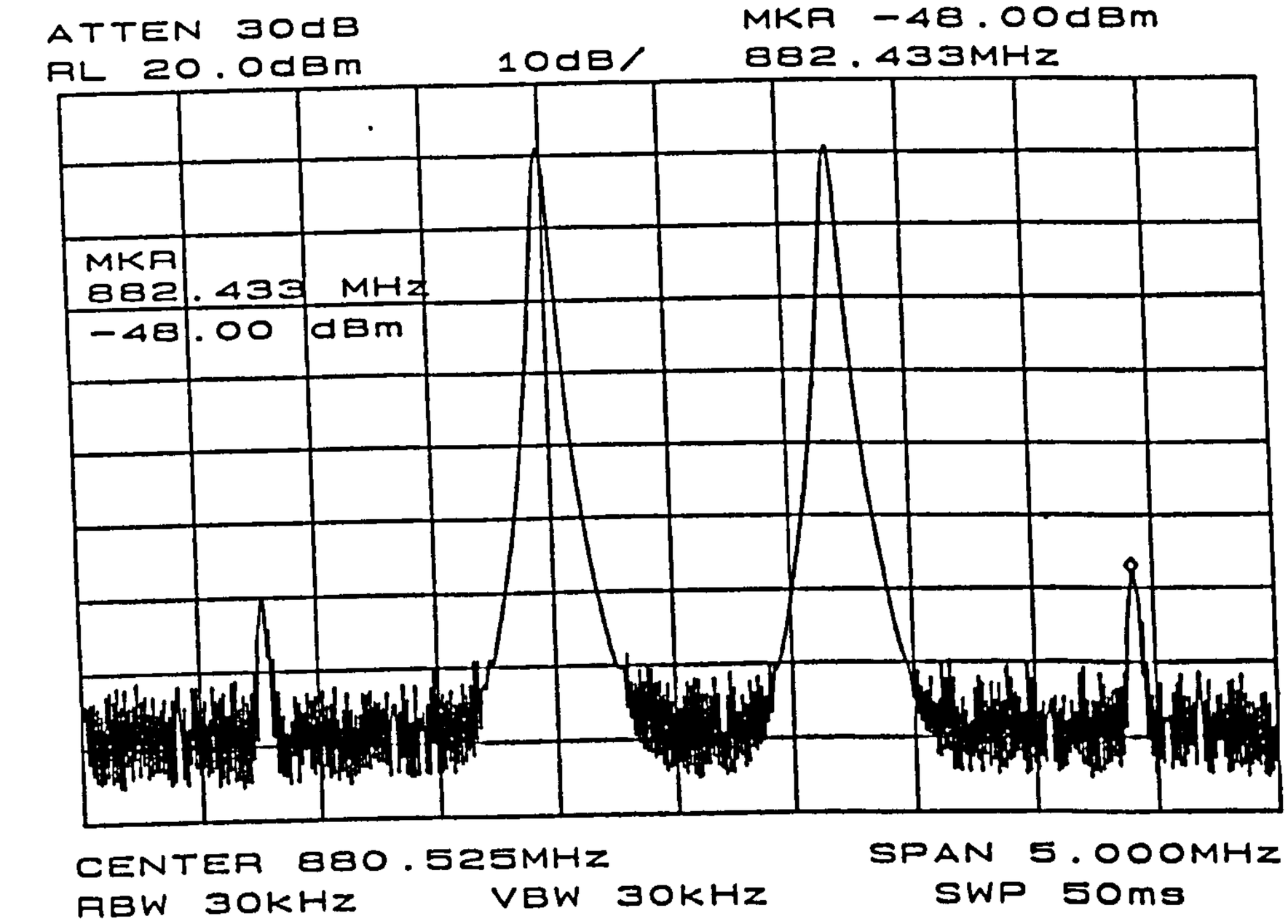

(b)

Figure 5..14: **Measured output spectrum of a 900 MHz amplifier before (a) and after (b) employing the technique for a two-tone test.**

$880MHz$ and $881MHz$. The amplifier output is shown in figure 5.14 without the injection of the difference frequency signal at $1MHz$. The output spectrum of the amplifier after the $1MHz$ signal is injected, is shown in figure 5.14, where there is a reduction of more than $47dB$ on the two third order IMD signals. The phase and amplitude of the injected signal is chosen so as to reduce simultaneously both third order IMD terms to the same level, the phase shift needed was around 90°. Greater reduction was achieved on each individual third order term by a slight change in the phase of the difference frequency signals. The input power level of the signals was $13dBm$. The input power of the difference frequency signals was $9.17dBm$. Similar results were observed at other power levels. Figure 5.15 shows that the reduction in the third order can be accompanied by a reduction in higher order IM terms. It shows a reduction of $23dB$ in the third order IM products and a $30dB$ reduction in the fifth order IM term, with the input power of the fundamentals signals at $-20dBm$. The phase and amplitude relation in the third order and fifth order has to be such that the phase shift and amplitude change applied to the injected signals cancel all IMDs, which is mostly the case. As the tone spacing is increased or reduced, if the phase and amplitude setting of the injected signals are kept constant, degradation in the level of IM is clearly noticed.

5.4.2 Three and Four-Tone Tests

For the three-tone case, again signals at various frequencies were used and different tones spacing were also investigated. The phase and amplitude of the injected signals ($f_3 - f_1$, $f_2 - f_1$ and $f_3 - f_2$) were adjusted so as to reduce all the IMD term to the same

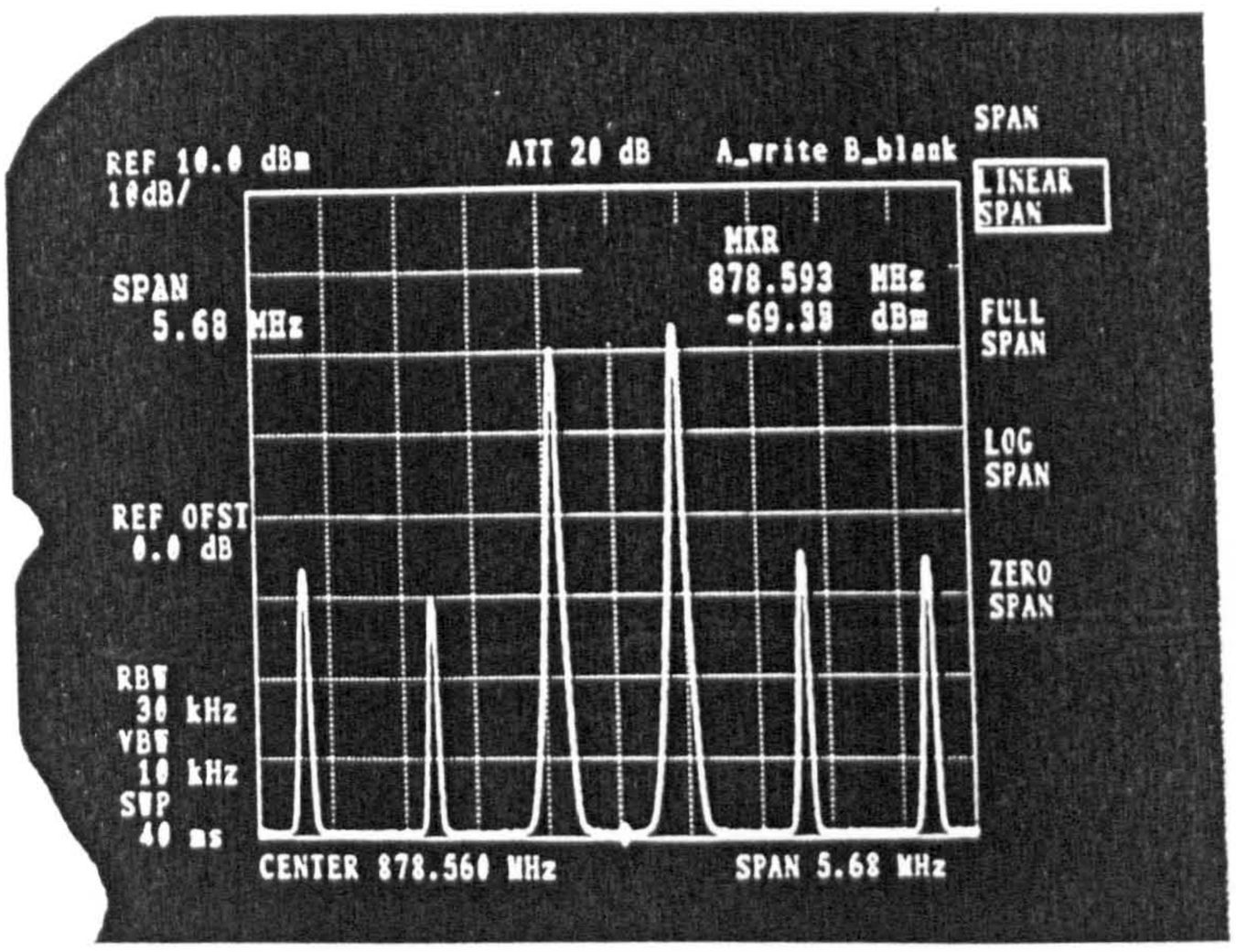

(a)

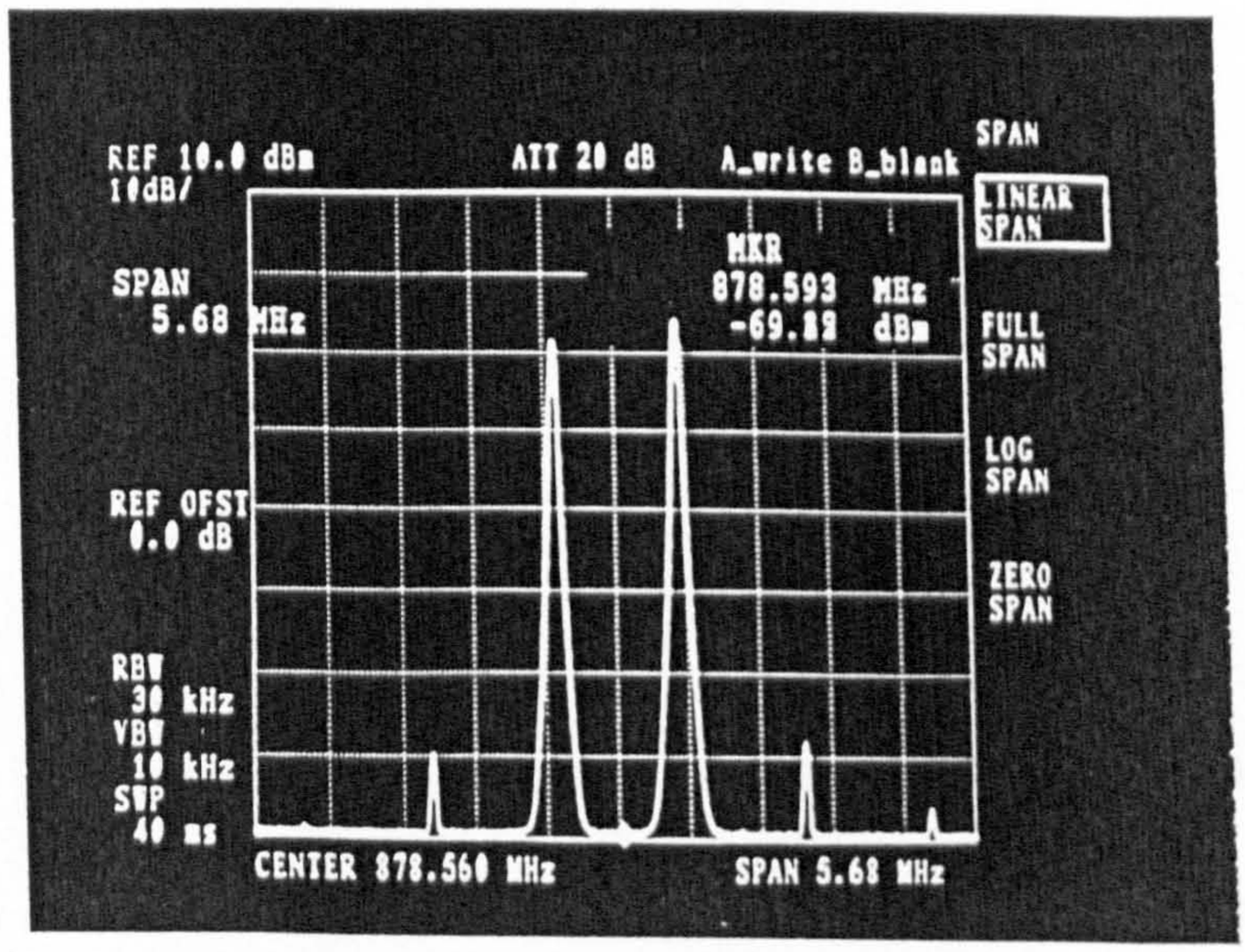

(b)

Figure 5..15: **Measured output spectrum of a** $900MHz$ **amplifier before (a) and after (b) employing the technique for a two-tone test showing the third and fifth IM.**

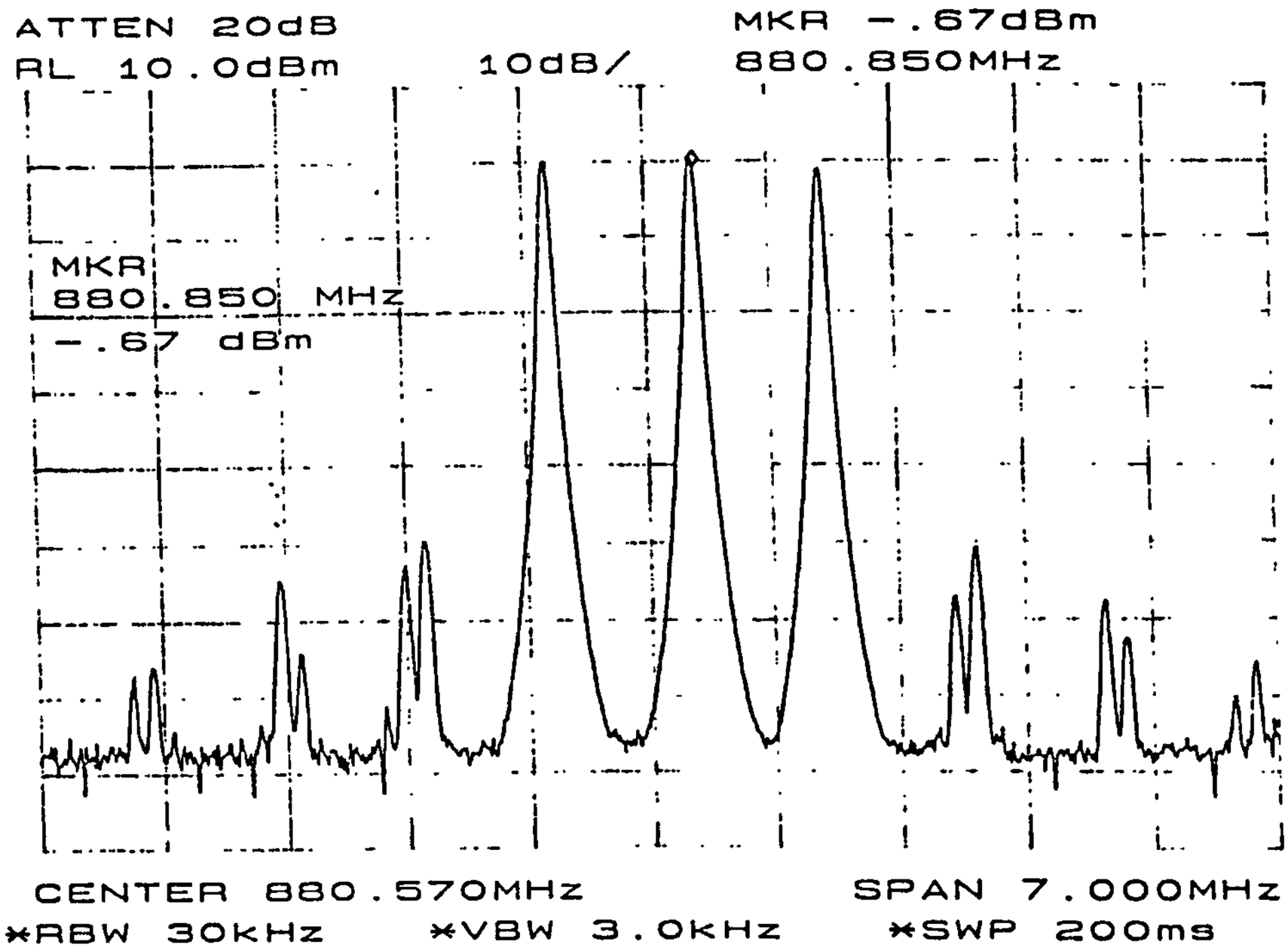

(a)

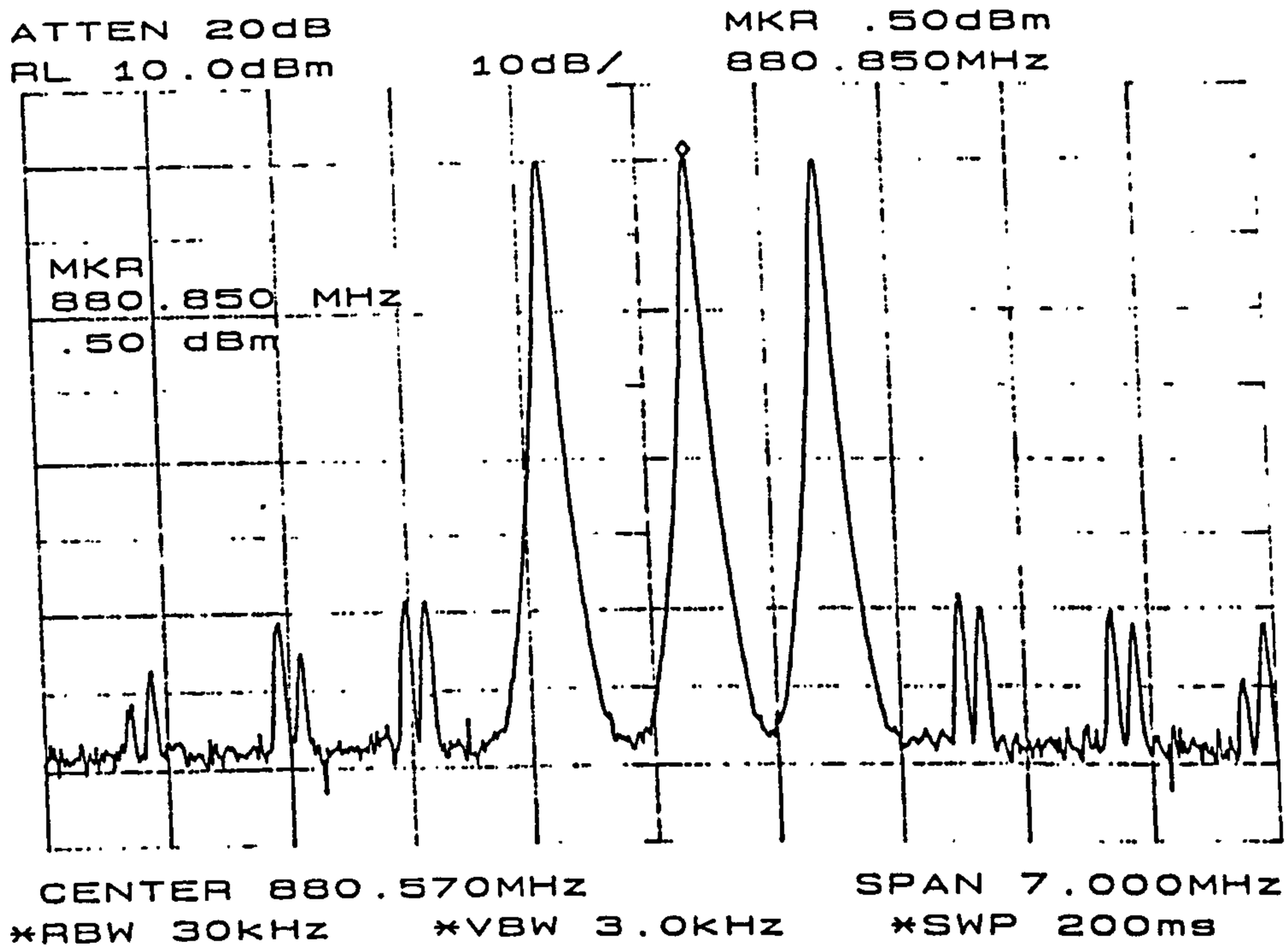

(b)

Figure 5..16: **Measured output spectrum of a 900MHz amplifier before (a) and after (b) employing the technique for a three-tone test with 1MHz tone spacing.**

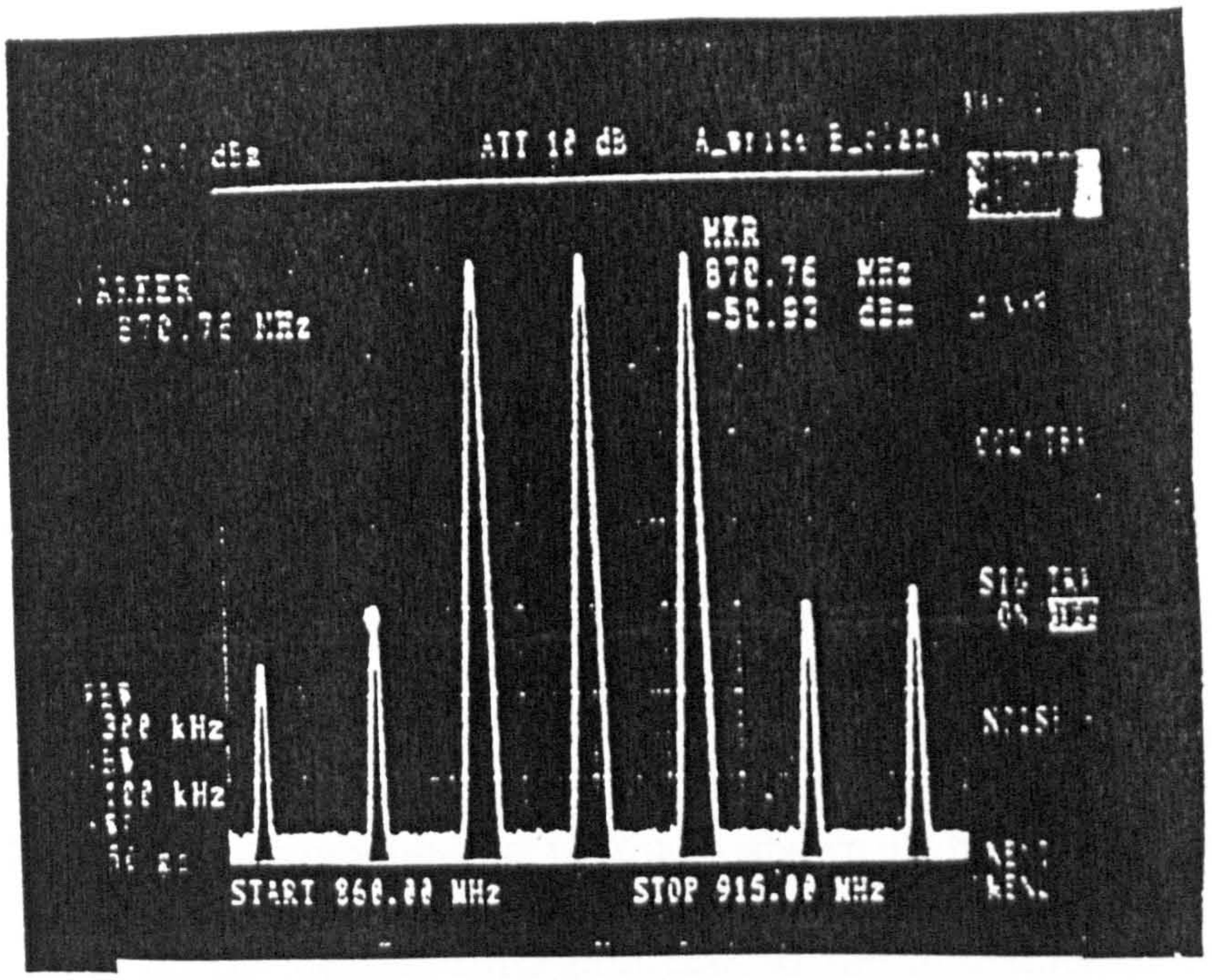

(a)

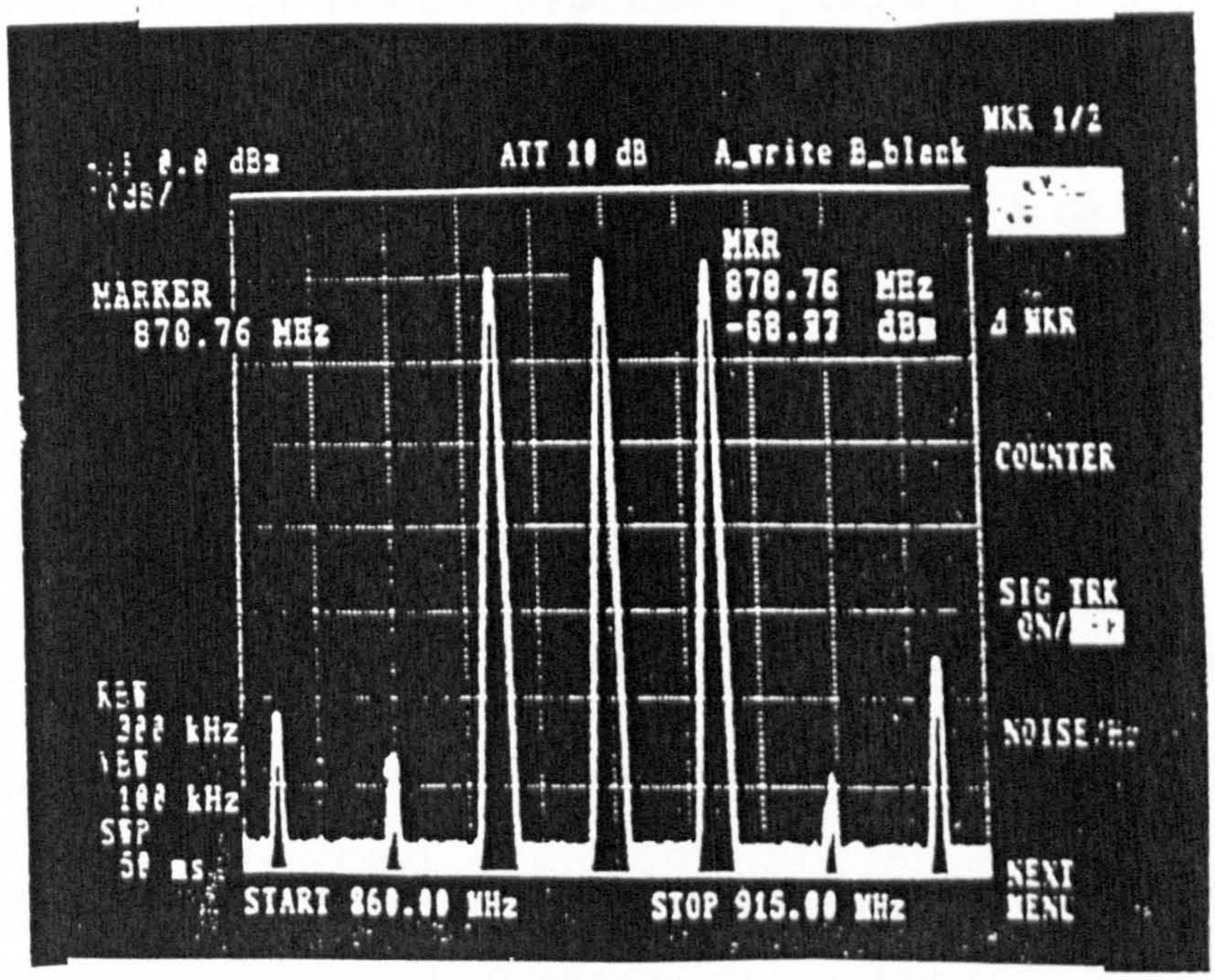

(b)

Figure 5..17: **Measured output spectrum of a 900MHz amplifier before (a) and after (b) employing the technique for a three-tone test with 7.5MHz tone spacing.**

level. Figure 5.16 shows the output spectrum before and after injection of the difference frequency signals. The input signals are at the frequencies $879.7MHz$, $880.8MHz$ and $881.7MHz$ with input powers of $-20dBm$. The level of these signals was around $-10.56dBm$.The difference frequency signals are at the frequencies $0.9MHz$, $1.1MHz$ and $2MHz$. The IMD level is reduced by about $10dB$.

The technique can give a reduction of more than $30dB$ on each individual IMD components but an overall $10dB$ was achieved on all IMD3 simultaneously. A test performed with the signals about $8MHz$ apart shows that the technique works for wider bandwidth. The intermodulation products shown in figure 5.17 were reduced by more than $15dB$ on the nearest IMD products to the fundamental and by about $10dB$ on the remaining IMD products. The input signals were arbitrarily chosen at the frequencies $878.5MHz$, $886MHz$ and $893.5MHz$ with the three difference frequency signals at the frequencies $7.5MHz$, $7.5MHz$ and $15MHz$. A $6dB$ improvement on the IMD was obtained for a four-tone system ($P_{in} = -20dBm$) with a tone spacing of $1MHz$ as shown in figure 5.18.

The above results confirmed the theory and simulation and show that the technique of difference frequency injection reduces all IMD3 in MESFET power amplifiers. The use in the three-tone case of the frequency dependent phase shifter designed for the two-tone case limited the overall result. Although the phase shifter works for the above frequency spacing ($8MHz$), in the three tone case it is required to works at both the $1MHz$ and the $2MHz$ frequencies and provide the same phase shift. This was not the case unfortunately, the phase shifter provided different phases at $1MHz$ and $2MHz$. The choice of the phase shifter designed, was driven by component availability and

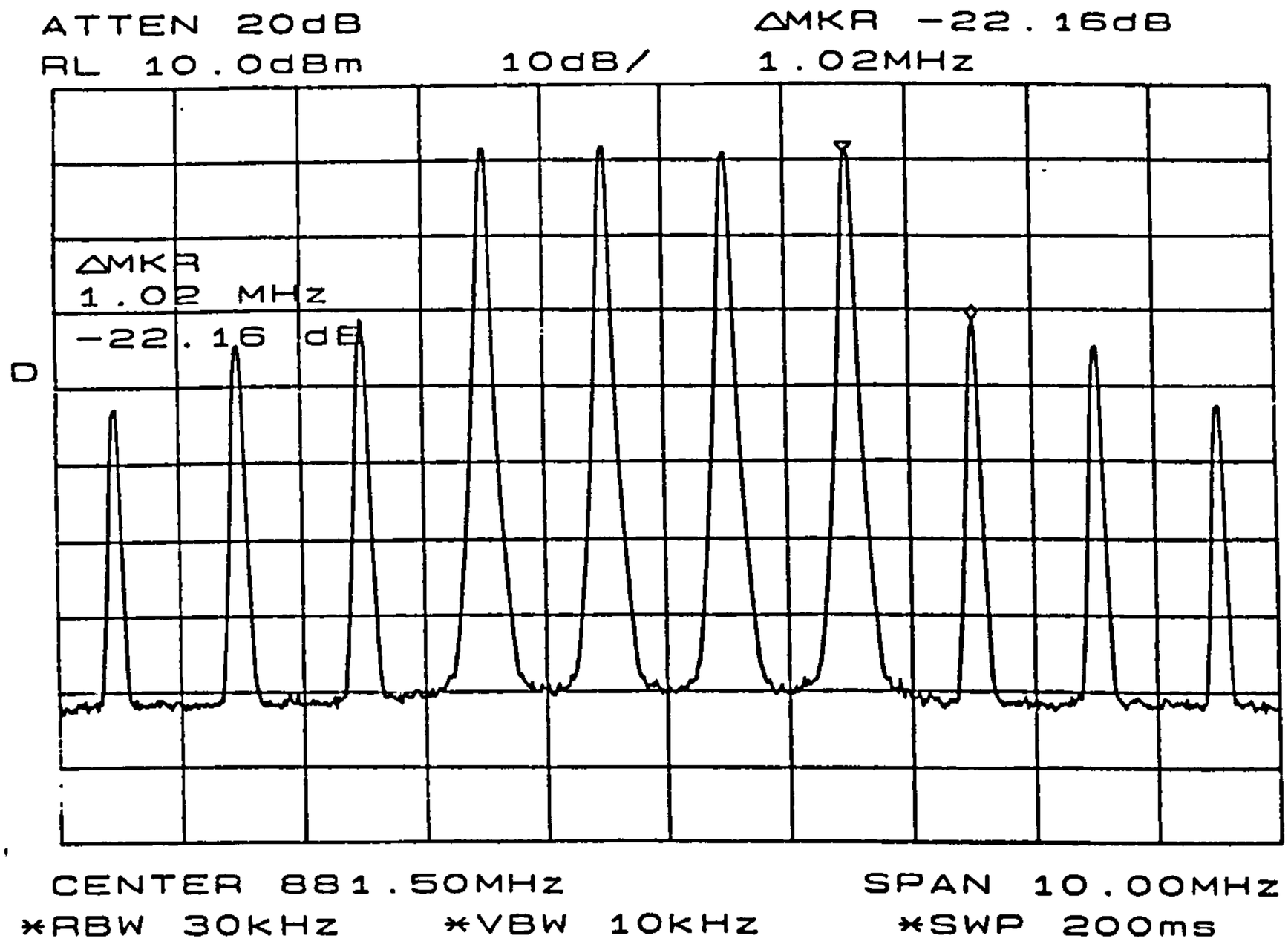

(a)

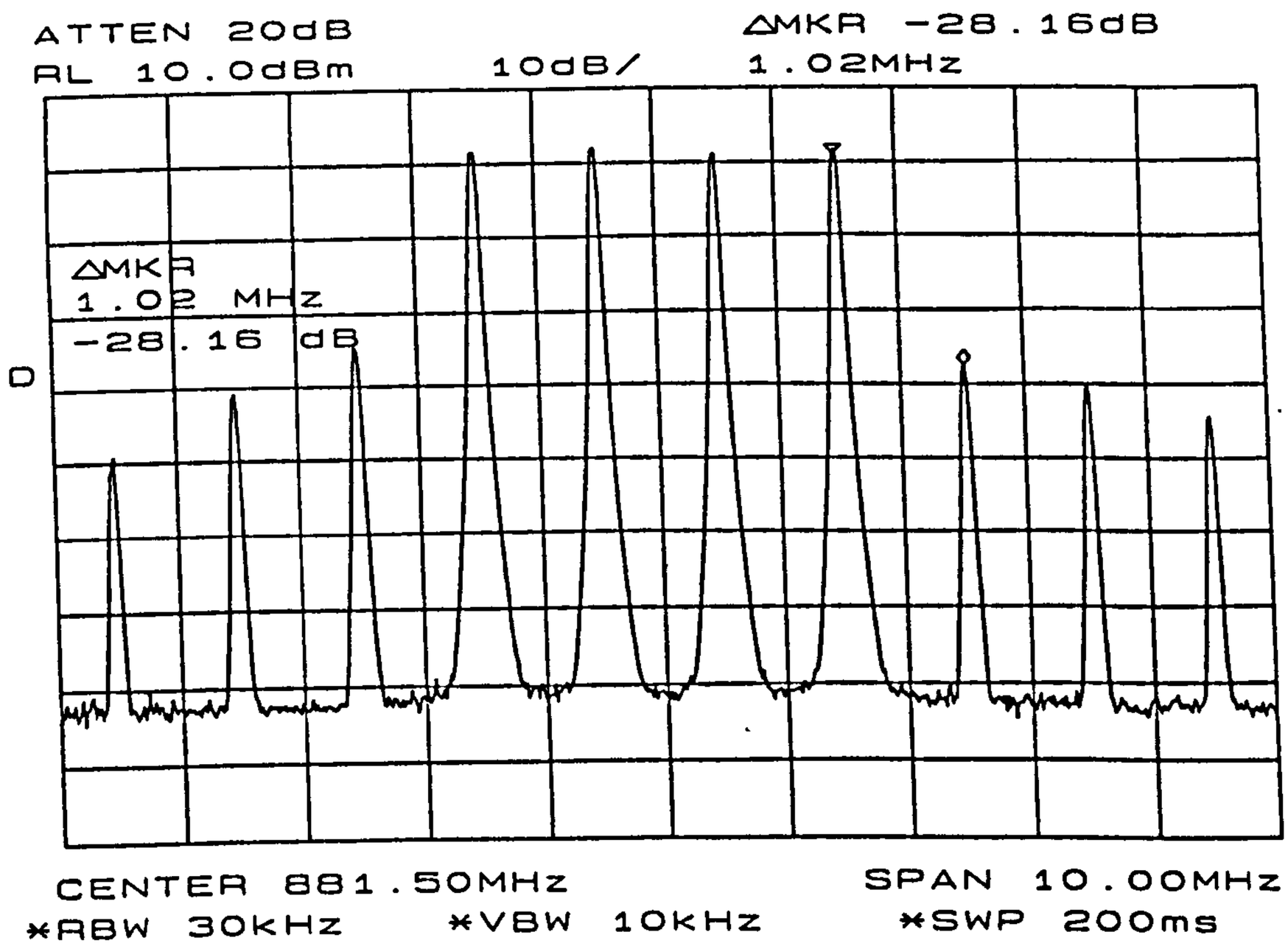

(b)

Figure 5..18: **Measured output spectrum of a 900MHz amplifier before (a) and after (b) employing the technique for a four-tone test.**

cost rather than performance. It was considered acceptable for this proof of principle exercise.

It should be noted that the limitation in the system is also engendered by various components such as the phase shifter which can produce a slight decrease in the injected signal amplitude because of its fundamental characteristics and if it is not properly matched. The low frequency variable amplifier will introduce a phase change associated with different frequencies. The phase change introduced by signals which are $1MHz$ apart differs by 3°. These different effects add to the complexity of the system and reduce the overall performance of the system. For good system performance, great control has to be exercised on the components characteristics and performance.

5.5 Performance Comparison of the Techniques

As mentioned earlier, the implementation and practical performance of a two-tone system using the second harmonic in a feedback circuit have shown that the third order IMD can be reduced by $20dB$ in a MESFET amplifier [73,74] at $500MHz$, by $43dB$ in a HBT amplifier at $830MHz$ [75] and recently in complex modulated signals[35,153]. These results have been confirmed theoretically in this thesis, however, the mechanism has been identified as a combination of the second harmonic and the sum of the fundamental frequencies. When more than two tones or complex signals are used, the resulting reduction in IMD can not be obtained by second harmonic injection alone. It requires careful control of both the second harmonic signals and the high frequency second order IM signals (the sum of the pairs of the fundamental signals).

This thesis shows that the use of the difference frequency technique gives an

improvement of around $50dB$ in a two-tone test at $880MHz$ and up to $17dB$ in a three-tone test at 880MHz in a MESFET amplifier. These results have been published [M1, M2].

5.6 Conclusions

The theory and simulation of the difference frequency technique predicted that the third order IMD level of both kinds at the output of the non-linear amplifier could be reduced. The prediction was confirmed in practice at $880MHz$ with a MESFET power amplifier and has given $50dB$ reduction in a two-tone test. The prediction in a three-tone simulation was that all third order would be reduced by $35dB$. The reduction on all IMD3 was also confirmed in practise and a reduction of $10dB$ was achieved. This rather modest result is due to effects such as amplitude modulation to phase modulation (AM/PM) and amplitude modulation to phase modulation (AM/AM) conversion occurring within the nonlinear amplifier. The practicality of the technique for amplifier linearisation was clearly shown by the linearizer circuit designed. Results show that both the difference frequency injection and the combined second harmonic and sum of the fundamental frequency injection techniques can work and reduce all IMD3 in a multicarrier amplifier. The latter required the adjustment of both techniques simultaneously for the reduction in the nonlinearities to be effective. The limitation with the difference frequency is associated with the heating effects of the transistor by the injection of a low frequency signal too close to the self-heating effects of the device [8]. This is dependent on the tone spacing as specified in the various communications applications standards

CHAPTER 6.

CONCLUSIONS AND FURTHER WORK

6.1 Introduction

This chapter summarises the work undertaken by the author. It presents the conclusions observed from the work. It shows the benefits of the IMD reduction techniques and further compares the three techniques. The limitations of the techniques are outlined and further work is suggested.

6.2 Conclusions

The primary goal of this report was to investigate the effects of the injection of multiple signals of different frequencies on the intermodulation distortion performance of power amplifiers. From the various results obtained, it is clear that a two-tone test does not show the complete intermodulation performance of a real power amplifier. Theoretical analysis shows that a two-tone test creates one single kind of third order IMD. However, it was found that third order IMD products in a multicarrier amplifier (more than 2 tones) occur through two different routes and this gives rise two different IMD3 contributions. The second kinds of intermodulation are $6dB$ higher than the first kind if the input tones have the same amplitude. In general, the highest IMD product level in a multicarrier is caused by the second kind of IMD. The first kind of IMDs are of the form $(2f_2 - f_1)$ and result from the interaction of the two input signals, whereas the second kinds are of the form $(f_1 - f_2 + f_3)$ and are the result of the interaction between three input signals.

The second harmonic injection technique was shown to reduce the first kind of

IMD3 level greatly but does not give a significant reduction of the second kind of IMD3. The difference frequency technique, however, reduces both kinds of IMD3 significantly.

The simulation results given in section 4.5 show a reduction of more than $30dB$ on all third order IMD signals. The injection of the second harmonic signals shows that the first kind of IMD3 are reduced by more than $35dB$ and no reduction is achieved on the second kinds. The difference frequency technique removed this limitation of the second harmonic injection as demonstrated by simulation results given in section 4.5. Reduction of more than 30 dB was achieved on all third order IMD signals.

The analysis included theoretical and simulated analysis of the injection of second order signal whose frequencies are the sum of pairs of the fundamental signals (frequency summation technique). The theory shows that the injection of the sum of the fundamental frequencies does not reduce the first kind of IMD3 but will reduce the second kind of IMD by more than $35dB$ as seen in the simulated amplifier IMD analysis of section 4.5. The difference frequency technique therefore achieved better results than the second harmonic injection technique or the frequency summation injection technique.

Although, a mathematical expression or a simulator can be used to evaluate the IMD performance of an amplifier, this cannot be achieved in a similar manner in practice. In practice the second harmonic and the frequency sum of the fundamental signals are very close and can not be easily separated. This means that the injection of the second harmonic will be accompanied by an injection of the sum of the pairs of the fundamental signals in practice. In the simulation (see section 4.5) the fundamental signals at the frequencies $2.5GHz$, $2.51GHz$ and $2.521GHz$ will have their second harmonics

at the frequencies $5GHz$, $5.02GHz$ and $5.042GHz$ and the sum of the fundamental signals will be at the frequencies $5.01GHz$, $5.021GHz$ and $5.031GHz$. These frequencies are very close and the signals at these frequencies can not be easily separated. The combination of these two techniques does reduce all intermodulations. It was shown that the combination of second harmonic injection and frequency summation injection techniques reduces the first and the second kind simultaneously. Contrary to previously published reports in which the injection of only second harmonic is presented as a reduction technique for intermodulation, the reduction of IMD is the result of the injection of the second harmonic of the fundamental signals and the second order IM signals whose frequencies is the sum of the pairs of the frequencies of the fundamental signals.

The use of the technique of difference frequency injection with a simulated CDMA input signal shows that a $7.6dB$ reduction in ACPR was observed (section 4.10).

As shown in section 5.4.1, a practical implementation of the difference frequency technique shows a reduction of the order of $50dB$ for a two-tone test in a MESFET power amplifier. A three-tone test gives a measured result at 880MHz, with a tone spacing of 1MHz, of more than $10dB$ reduction on all IMD3 products (see section 5.4.2).

When dealing with a three-tone test, three different frequency signals are needed to cancel all components of the intermodulation. The number of second harmonics is three and the number of frequency summation signals is also three. For n input tones, the number of difference frequency signals required to cancel all IMD3 is a number X

is such that

$$X = \frac{(n-1)n}{2} \tag{6..1}$$

The number of the second harmonic signals will be a number Y such that

$$Y = 2n \tag{6..2}$$

The number of the frequency summation signals will be a number Z such that

$$Z = \frac{(n-1)n}{2} \tag{6..3}$$

Since the second harmonic and the frequency summation techniques should be use in combination, the number of signals which must be injected, is equal to the sum of X and Y

$$X + Y = \frac{(n+3)n}{2} \tag{6..4}$$

It clearly shows that the second harmonic injection and the summation frequency injection techniques require $2n$ signals more than the difference frequency injection technique. The technique will therefore require a greater control of the amplitude and phase for adequate cancellation of the IMD3 to occur. However, the requirements of the difference technique is a lot less than with the combination of the other two techniques. The difference technique can be regarded as a superior technique.

When dealing with complex signals, the injection of either the second harmonic signal and the sum of the fundamental frequencies or the difference frequencies can be done by either an injection or a feedback of the low frequency envelope at the difference frequency or at the second order frequency.

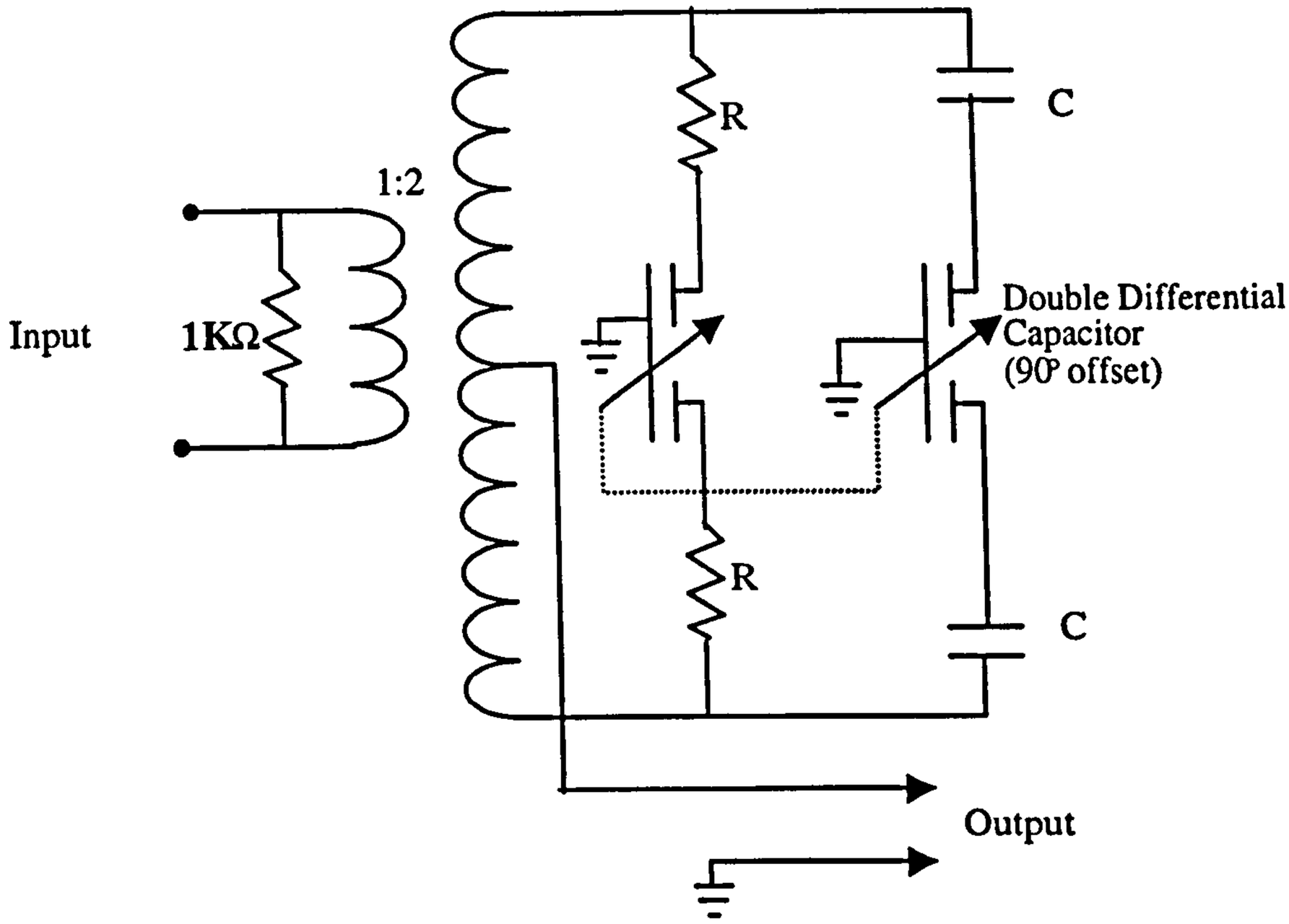

Figure 6..1: **Circuit diagram of a 360° mechanically tuned phase shifter.**

6.3 Further Work

Although various results were obtained and the investigation shows how the techniques performed. Various other parameters affecting the circuit need to be closely looked at and implementation can be performed to further enhance the performance of the technique of IMD reduction. These different aspects are indicated below.

6.3.1Frequency Independent Phase Shifter Design

In the bench test, a simple phase shifter was used for the $1MHz$ signal. The phase shifter was frequency dependent because it was designed for a signal at $1MHz$. Whilst better designs were known, the availability of the components and the cost of the system prompted the choice of the original, simpler phase shifter. While its performance was not optimal, it was better shown to be adequate for a proof of principle test.

After careful research, a better frequency independent phase shifter with improved performance was discovered [119]. The circuit is a mechanically tuned frequency independent phase shifter called a Goniometer (figure 6.1). It could potentially improve on the performance of the predistortion linearizer. Although the circuit looks fairly simple, the availability of the components for the implementation of the circuit, is not straightforward.

A simulation of the above circuit and a practical implementation of the circuit with the predistortion linearizer used previously could be investigated. The phase shifter could on the other hand be replaced by a digitally controlled phase shifter which would add to the complexity and the cost of the circuit. This improvement on the circuit performance could also be investigated.

6.3.2 Effects of Injection Technique in HBT and Related Devices

The results presented in this report are mostly related to MESFET power amplifiers. The technique can, however, be applied to various devices and amplifier architectures. The theoretical analysis shows that the reduction of intermodulation distortion will take place in a nonlinear device that has its nonlinear input-output characteristics represented by a Volterra series.

The technique can be applied to other devices using semiconductor heterojunctions, with superior noise figure and gain characteristics. Examples include the heterojunction bipolar transistor (HBT) or GaAs FET derivatives such as high electron mobility transistors (HEMTs), which are used in small signal and low noise applications. The performance of the IMD reduction techniques can also be studied on GaAs

FET amplifiers which have been enhanced by incorporated heterojunctions in some architecture areas such as indium gallium arsenide/ gallium arsenide (InGaAs/GaAs) heterojunction, indium aluminium arsenide/ Gallium Arsenide (InAlAs/GaAs) heterojunction, indium phosphide (InP).

The use of the techniques on these different devices will cancel the intermodulation but with perhaps a greater or lesser reduction figure than the $30dB$ obtained with the injection of the difference frequency or the combined second harmonic technique and frequency summation technique on a MESFET amplifier. In addition to the results obtained in this work, results recently reported on the reduction of IMD by injection of the second harmonic in HBT power amplifier were presented. Second harmonic injection into other amplifiers needs to be investigated as well as the difference frequency injection.

6.3.3 Design of a Compact Predistortion Linearizer Amplifier

This thesis shows that the technique of difference frequency injection reduces the third order intermodulation in a RF or microwave power amplifier. The performance tests for the difference frequency technique were performed using a system where by all components were individually built and tested separately for adequate characteristics and then combined to give a fully working amplifier system. The next logical step is the design of a compact amplifier where by all the different components are designed as described in chapter 5, and can be put together in a compact circuit. There are various challenges to this and they need to be assessed. Various technologies such as microstrip, slotline, and band-gap structures can be used and will engender different

results at microwave frequencies and beyond. An integrated circuit of the amplifier can also be considered.

The use of low and high frequency circuitry is one obvious challenge to the design of amplifiers using such techniques. However, it has already been shown both by simulation and practical tests that phase shifting and amplitude adjustment of the difference frequency can be done at high frequency before generation of the difference frequency. This eliminates the need for complex low frequency circuitry and reduces the size of the circuit.

6.3.4 Design of a Compact Feedback Amplifier

In a similar manner as for the design of the predistortion linearizer, a feedback amplifier using the IMD reduction techniques can be achieved. Again the use of complex low frequency devices can be eliminated by the use of high frequency devices. Phase shifting and attenuation of the amplified fundamental signals at the output can be done at higher frequency. The phase and the amplitude can then be adjusted so as to obtain the required difference frequency signals and therefore cancel the IMD. The design of such an amplifier will need to take into account the application for correct specifications of the components for amplifier stability.

6.3.5 A Predistortion Linearizer with Difference Frequency Injection Controller

A predistortion circuit which make use of a cancellation controller in the low frequency path is proposed (figure 6.2). The design is based on the linearizer circuit built in chapter 5. The circuit will improve on the IMD reduction level obtained in chapter5. The low difference frequency path is sampled, the amplitude and phase of the signals

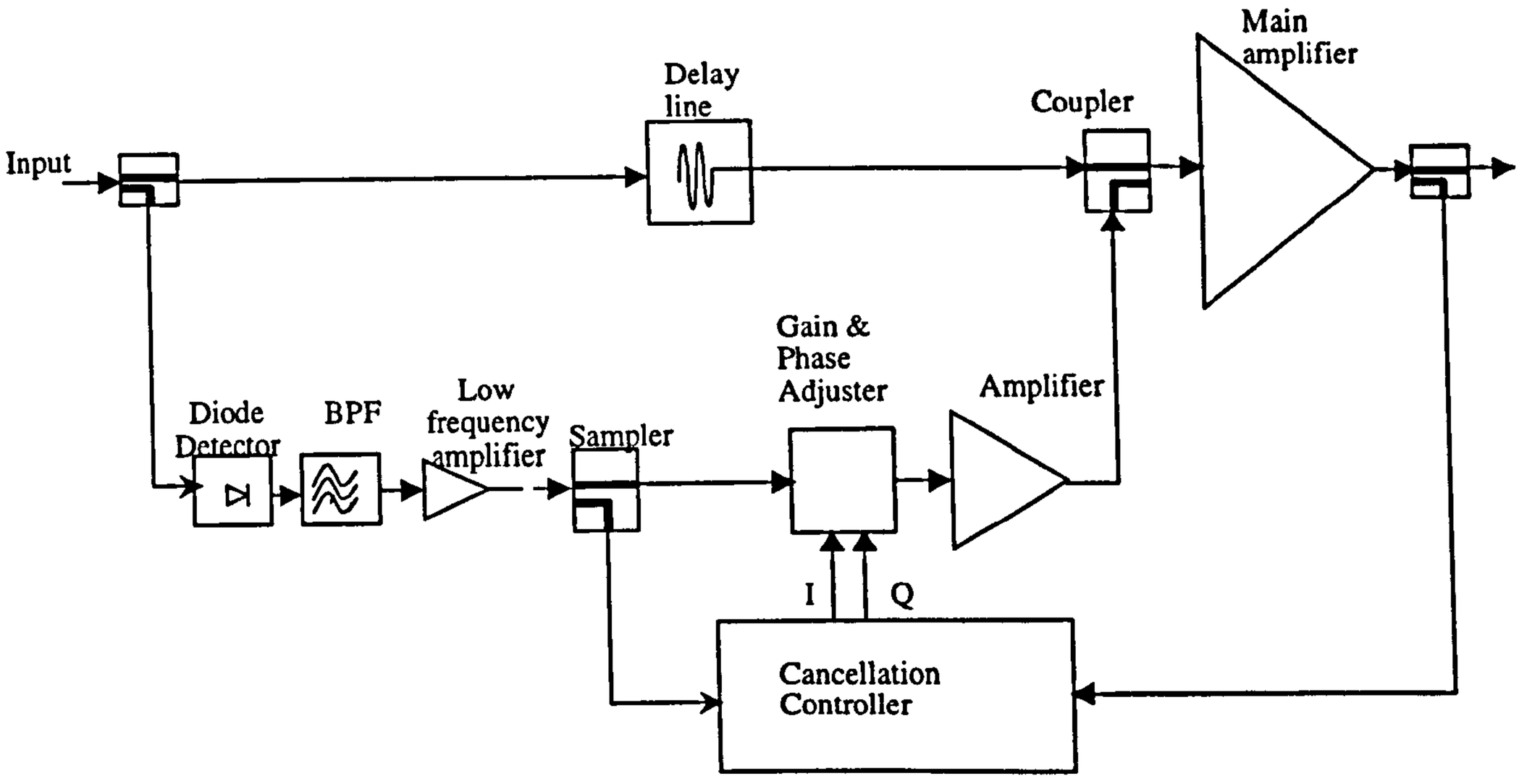

Figure 6..2: **A basic predistortion linearizer with difference frequency injection amplitude and phase controller.**

are then passed onto a cancellation controller which use this information and the output information to adjust the amplitude and the phase of the injected signals. The adjusted signals are then fed into the main amplifier with the fundamentals signals to provide lower intermodulation performance at the output of the amplifier. The cancellation controller can make use of robust DSP algorithm to provide an adequate adjustment for optimum distortion cancellation. The circuit is quite similar to the predistortion circuit of figure 5.1. It is enhanced by the improved low frequency circuit controller which work in the same manner as in the adaptive feedforward cancellation system.

APPENDIX A.

IDEAL FOUR PORT COUPLER (HYBRID.S4P FILE)

! Hybrid.s4p

! S-parameter data file for ideal 4 port 0 degree hybrid

! Symbol freq.-unit parameter-type data-format keyword impedance-ohms

GHZ S MA R 50

! freq magS11 magS11 magS12 angS12 magS13 angS13 magS14 angS14 !1st line

! magS11 magS11 magS12 angS12 magS13 angS13 magS14 angS14 !2st line

! magS11 magS11 magS12 angS12 magS13 angS13 magS14 angS14 !3st line

! magS11 magS11 magS12 angS12 magS13 angS13 magS14 angS14 !4st line

0 0 0 .707 -180 .707 -180 0 0

.707 -180 0 0 0 0 .707 -180

.707 -180 0 0 0 0 .707 -180

0 0 .707 -180 .707 -180 0 0

210 0 0 .707 -180 .707 -180 0 0

.707 -180 0 0 0 0 .707 -180

.707 -180 0 0 0 0 .707 -180

0 0 .707 -180 .707 -180 0 0

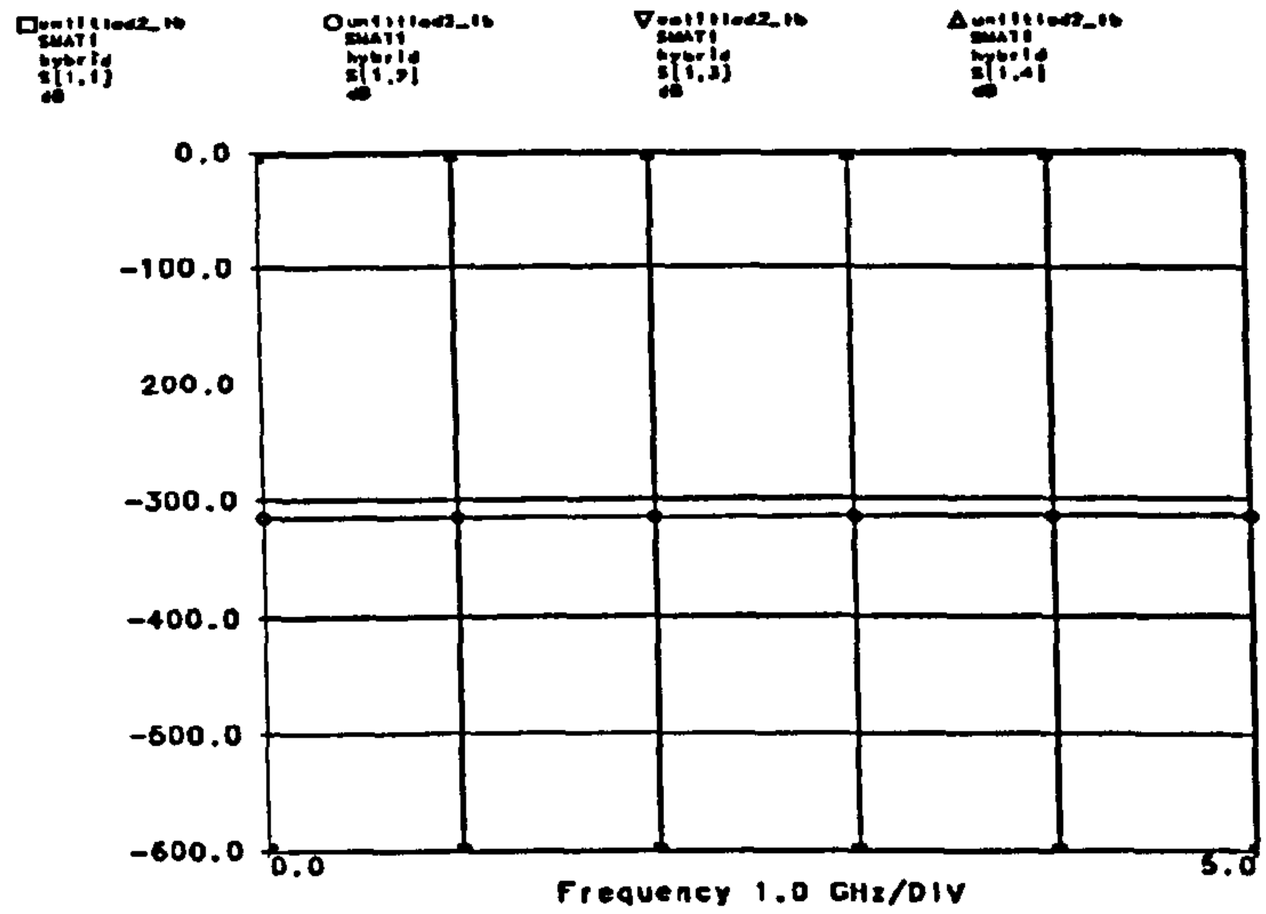

Figure A..1: **Simulated S-parameters of the hybrid coupler, showing the input reflection coefficient at port 2, the coupling between the input port 1 and 2, the return loss between input port 2 and the output port 3 and 4.**

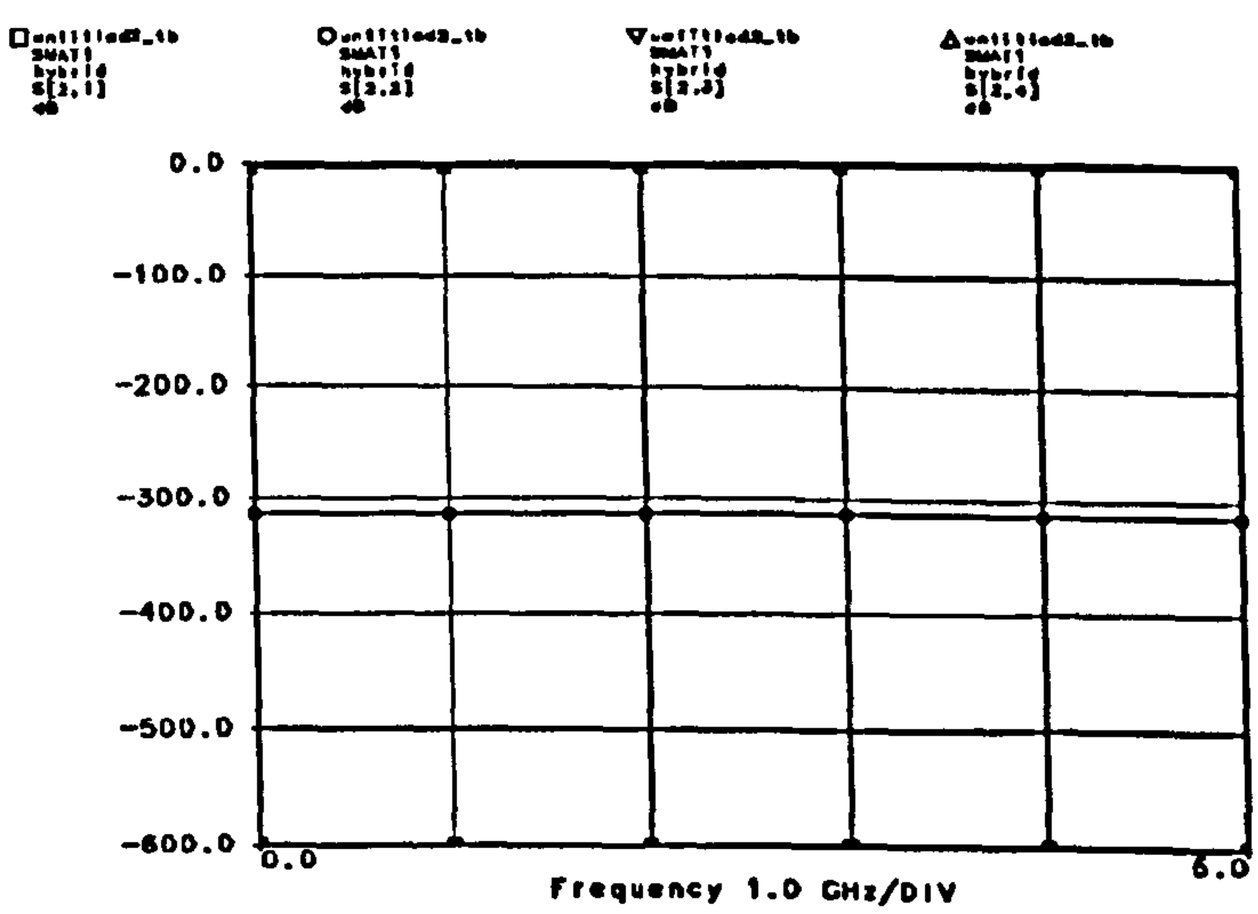

Figure A..2: **Simulated S-parameters of the hybrid coupler, showing the input reflection coefficient at port 2, the coupling between the input port 1 and 2, the return loss between input port 2 and the output port 3 and 4.**

APPENDIX B.

CALCULATION OF INTERMODULATION PRODUCTS USING A POWER SERIES EXPANSION

2.1 Power Series Analysis of a Three-Tone System without the Injected Signals

A calculation of the third order intermodulation distortions of three-tones non-linear system is performed in this section. The nonlinear system is represented by a power series expansion up to the third order, which clearly enable the calculation of all the relevant third order IMD.

The system input is made of two sinusoid signals at the frequencies ω_1, ω_2 and ω_3 with amplitudes A_{ω_1}, A_{ω_2} and A_{ω_3} respectively.

The input is

$$v_{in} = A_{\omega_1}\cos(\omega_1 t) + A_{\omega_2}\cos(\omega_2 t) + A_{\omega_3}\cos(\omega_3 t) \tag{2.11}$$

The amplifier output spectrum is calculated by using a power series expansion, such that

$$V_{out} = \sum_{n=1}^{3} g_{mn} v_{in}^{n} \tag{2.12}$$

The calculation is performed using Mathematica®[1]. The following is the input file and the output file showing all intermodulation terms at the output of the amplifier without the injection of any signals.

[1] Mathematica is a software system and computer language for the use in mathematical applications. Mathematica is a product of Wolfram Reseach, Inc. It can perform operations on functions, manipulate algebraic formulas, do calculus, produce two- and three-dimensional graphs and support high-level programming language.

- **Input file**

$$x1 = \sum_{k=1}^{3} (A_{\omega_k} \cos[\omega_k]);$$

$$Y = \sum_{n=0}^{3} (g_n (x1)^n);$$

TrigReduce[Y]
TeXSave["no.tex"]

- **Output file**

$$V_{out} = \tfrac{1}{4}(4g_0 + 4\cos[\omega_1]A_{\omega_1}g_1 + 4\cos[\omega_2]A_{\omega_2}g_1 +$$
$$4\cos[\omega_3]A_{\omega_3}g_1 + 2A_{\omega_1}^2 g_2 + 2\cos[2\omega_1]A_{\omega_1}^2 g_2 +$$
$$4\cos[\omega_1 - \omega_2]A_{\omega_1}A_{\omega_2}g_2 + 4\cos[\omega_1 + \omega_2]A_{\omega_1}A_{\omega_2}g_2 +$$
$$2A_{\omega_2}^2 g_2 + 2\cos[2\omega_2]A_{\omega_2}^2 g_2 + 4\cos[\omega_1 - \omega_3]A_{\omega_1}A_{\omega_3}g_2 +$$
$$4\cos[\omega_1 + \omega_3]A_{\omega_1}A_{\omega_3}g_2 + 4\cos[\omega_2 - \omega_3]A_{\omega_2}A_{\omega_3}g_2 +$$
$$4\cos[\omega_2 + \omega_3]A_{\omega_2}A_{\omega_3}g_2 + 2A_{\omega_3}^2 g_2 + 2\cos[2\omega_3]A_{\omega_3}^2 g_2 +$$
$$3\cos[\omega_1]A_{\omega_1}^3 g_3 + \cos[3\omega_1]A_{\omega_1}^3 g_3 + 3\cos[2\omega_1 - \omega_2]A_{\omega_1}^2 A_{\omega_2}g_3 +$$
$$6\cos[\omega_2]A_{\omega_1}^2 A_{\omega_2}g_3 + 3\cos[2\omega_1 + \omega_2]A_{\omega_1}^2 A_{\omega_2}g_3 +$$
$$6\cos[\omega_1]A_{\omega_1}A_{\omega_2}^2 g_3 + 3\cos[\omega_1 - 2\omega_2]A_{\omega_1}A_{\omega_2}^2 g_3 +$$
$$3\cos[\omega_1 + 2\omega_2]A_{\omega_1}A_{\omega_2}^2 g_3 + 3\cos[\omega_2]A_{\omega_2}^3 g_3 + \cos[3\omega_2]A_{\omega_2}^3 g_3 +$$
$$3\cos[2\omega_1 - \omega_3]A_{\omega_1}^2 A_{\omega_3}g_3 + 6\cos[\omega_3]A_{\omega_1}^2 A_{\omega_3}g_3 +$$
$$3\cos[2\omega_1 + \omega_3]A_{\omega_1}^2 A_{\omega_3}g_3 + 6\cos[\omega_1 - \omega_2 - \omega_3]A_{\omega_1}A_{\omega_2}A_{\omega_3}g_3 +$$
$$6\cos[\omega_1 + \omega_2 - \omega_3]A_{\omega_1}A_{\omega_2}A_{\omega_3}g_3 +$$
$$6\cos[\omega_1 - \omega_2 + \omega_3]A_{\omega_1}A_{\omega_2}A_{\omega_3}g_3 +$$
$$6\cos[\omega_1 + \omega_2 + \omega_3]A_{\omega_1}A_{\omega_2}A_{\omega_3}g_3 + 3\cos[2\omega_2 - \omega_3]A_{\omega_2}^2 A_{\omega_3}g_3 +$$
$$6\cos[\omega_3]A_{\omega_2}^2 A_{\omega_3}g_3 + 3\cos[2\omega_2 + \omega_3]A_{\omega_2}^2 A_{\omega_3}g_3 +$$
$$6\cos[\omega_1]A_{\omega_1}A_{\omega_3}^2 g_3 + 3\cos[\omega_1 - 2\omega_3]A_{\omega_1}A_{\omega_3}^2 g_3 +$$
$$3\cos[\omega_1 + 2\omega_3]A_{\omega_1}A_{\omega_3}^2 g_3 + 6\cos[\omega_2]A_{\omega_2}A_{\omega_3}^2 g_3 +$$
$$3\cos[\omega_2 - 2\omega_3]A_{\omega_2}A_{\omega_3}^2 g_3 + 3\cos[\omega_2 + 2\omega_3]A_{\omega_2}A_{\omega_3}^2 g_3 +$$
$$3\cos[\omega_3]A_{\omega_3}^3 g_3 + \cos[3\omega_3]A_{\omega_3}^3 g_3)$$

2.2 Power Series Analysis of a Three-Tone System with Injected Sum of the Fundamentals Frequency Signals.

The input system is made of two sinusoid signals at the frequencies ω_1, ω_2 and ω_3 with amplitudes A_{ω_1}, A_{ω_2} and A_{ω_3} respectively and the sum of the fundamental frequency signals at the frequencies $(\omega_2+\omega_1)$, $(\omega_3+\omega_1)$ and $(\omega_3+\omega_2)$ with amplitudes $A\omega_{21}$, $A\omega_{31}$ and $A\omega_{32}$ with phases $\phi\omega_{21}$, $\phi\omega_{31}$ and $\phi\omega_{32}$ respectively.

The input is

$$v_{in} = A_{\omega_1}\cos(\omega_1 t) + A_{\omega_2}\cos(\omega_2 t) + A_{\omega_3}\cos(\omega_3 t) + A\omega_{21}\cos(\omega_2+\omega_1 t+\phi\omega_{21}) + A\omega_{31}\cos(\omega_3+\omega_1 t+\phi\omega_{31}) + A\omega_{32}\cos(\omega_3+\omega_2 t+\phi\omega_{32}) \tag{2.23}$$

The amplifier output spectrum is calculated by using a power series expansion, such that

$$V_{out} = \sum_{n=1}^{3} g_{mn} v_{in}^{n} = \sum_{n=1}^{3} g_{mn}\left[\begin{array}{c} A_{\omega_1}\cos(\omega_1 t) + A_{\omega_2}\cos(\omega_2 t) + A_{\omega_3}\cos(\omega_3 t) + A\omega_{21}\cos(\omega_2+\omega_1 t+\phi\omega_{21}) \\ + A\omega_{31}\cos(\omega_3+\omega_1 t+\phi\omega_{31}) + A\omega_{32}\cos(\omega_3+\omega_2 t+\phi\omega_{32}) \end{array}\right]^{n} \tag{2.24}$$

The following is the input file and the output file calculation using Mathematica® showing all intermodulation terms at the output of the amplifier with the injected sum of the fundamental frequency signals.

- **Input file**

$x1 = (A_{\omega_{21}} \cos[\omega_2 + \omega_1 + \emptyset_{21}]) +$
$(A_{\omega_{31}} \cos[\omega_3 + \omega_1 + \emptyset_{31}]) + (A_{\omega_{32}} \cos[\omega_3 + \omega_2 + \emptyset_{32}]);$
$x2 = \sum_{k=1}^{3} (A_{\omega_k} \cos[\omega_k]);$
$Y = \sum_{n=0}^{3} (g_n (x1 + x2)^n);$
TrigReduce[Y]
TeXSave["sum.tex"]

- **Output file**

$V_{out} = \frac{1}{4}(4g_0 + 4\cos[\omega_1]A_{\omega_1}g_1 + 4\cos[\omega_2]A_{\omega_2}g_1 + 4\cos[\omega_3]A_{\omega_3}g_1 +$
$4\cos[\omega_1 + \omega_2 + \emptyset_{21}]A_{\omega_{21}}g_1 + 4\cos[\omega_1 + \omega_3 + \emptyset_{31}]A_{\omega_{31}}g_1 +$
$4\cos[\omega_2 + \omega_3 + \emptyset_{32}]A_{\omega_{32}}g_1 + 2A^2_{\omega_1}g_2 + 2\cos[2\omega_1]A^2_{\omega_1}g_2 +$
$4\cos[\omega_1 - \omega_2]A_{\omega_1}A_{\omega_2}g_2 + 4\cos[\omega_1 + \omega_2]A_{\omega_1}A_{\omega_2}g_2 +$
$2A^2_{\omega_2}g_2 + 2\cos[2\omega_2]A^2_{\omega_2}g_2 + 4\cos[\omega_1 - \omega_3]A_{\omega_1}A_{\omega_3}g_2 +$
$4\cos[\omega_1 + \omega_3]A_{\omega_1}A_{\omega_3}g_2 + 4\cos[\omega_2 - \omega_3]A_{\omega_2}A_{\omega_3}g_2 +$
$4\cos[\omega_2 + \omega_3]A_{\omega_2}A_{\omega_3}g_2 + 2A^2_{\omega_3}g_2 + 2\cos[2\omega_3]A^2_{\omega_3}g_2 +$
$4\cos[\omega_2 + \emptyset_{21}]A_{\omega_1}A_{\omega_{21}}g_2 + 4\cos[2\omega_1 + \omega_2 + \emptyset_{21}]A_{\omega_1}A_{\omega_{21}}g_2 +$
$4\cos[\omega_1 + \emptyset_{21}]A_{\omega_2}A_{\omega_{21}}g_2 + 4\cos[\omega_1 + 2\omega_2 + \emptyset_{21}]A_{\omega_2}A_{\omega_{21}}g_2 +$
$4\cos[\omega_1 + \omega_2 - \omega_3 + \emptyset_{21}]A_{\omega_3}A_{\omega_{21}}g_2 +$
$4\cos[\omega_1 + \omega_2 + \omega_3 + \emptyset_{21}]A_{\omega_3}A_{\omega_{21}}g_2 +$
$2A^2_{\omega_{21}}g_2 + 2\cos[2\omega_1 + 2\omega_2 + 2\emptyset_{21}]A^2_{\omega_{21}}g_2 +$
$4\cos[\omega_3 + \emptyset_{31}]A_{\omega_1}A_{\omega_{31}}g_2 + 4\cos[2\omega_1 + \omega_3 + \emptyset_{31}]A_{\omega_1}A_{\omega_{31}}g_2 +$
$4\cos[\omega_1 - \omega_2 + \omega_3 + \emptyset_{31}]A_{\omega_2}A_{\omega_{31}}g_2 +$
$4\cos[\omega_1 + \omega_2 + \omega_3 + \emptyset_{31}]A_{\omega_2}A_{\omega_{31}}g_2 +$
$4\cos[\omega_1 + \emptyset_{31}]A_{\omega_3}A_{\omega_{31}}g_2 + 4\cos[\omega_1 + 2\omega_3 + \emptyset_{31}]A_{\omega_3}A_{\omega_{31}}g_2 +$
$4\cos[\omega_2 - \omega_3 + \emptyset_{21} - \emptyset_{31}]A_{\omega_{21}}A_{\omega_{31}}g_2 +$
$4\cos[2\omega_1 + \omega_2 + \omega_3 + \emptyset_{21} + \emptyset_{31}]A_{\omega_{21}}A_{\omega_{31}}g_2 +$
$2A^2_{\omega_{31}}g_2 + 2\cos[2\omega_1 + 2\omega_3 + 2\emptyset_{31}]A^2_{\omega_{31}}g_2 +$
$4\cos[\omega_1 - \omega_2 - \omega_3 - \emptyset_{32}]A_{\omega_1}A_{\omega_{32}}g_2 +$
$4\cos[\omega_1 + \omega_2 + \omega_3 + \emptyset_{32}]A_{\omega_1}A_{\omega_{32}}g_2 +$
$4\cos[\omega_3 + \emptyset_{32}]A_{\omega_2}A_{\omega_{32}}g_2 + 4\cos[2\omega_2 + \omega_3 + \emptyset_{32}]A_{\omega_2}A_{\omega_{32}}g_2 +$
$4\cos[\omega_2 + \emptyset_{32}]A_{\omega_3}A_{\omega_{32}}g_2 + 4\cos[\omega_2 + 2\omega_3 + \emptyset_{32}]A_{\omega_3}A_{\omega_{32}}g_2 +$
$4\cos[\omega_1 - \omega_3 + \emptyset_{21} - \emptyset_{32}]A_{\omega_{21}}A_{\omega_{32}}g_2 +$
$4\cos[\omega_1 + 2\omega_2 + \omega_3 + \emptyset_{21} + \emptyset_{32}]A_{\omega_{21}}A_{\omega_{32}}g_2 +$
$4\cos[\omega_1 - \omega_2 + \emptyset_{31} - \emptyset_{32}]A_{\omega_{31}}A_{\omega_{32}}g_2 +$
$4\cos[\omega_1 + \omega_2 + 2\omega_3 + \emptyset_{31} + \emptyset_{32}]A_{\omega_{31}}A_{\omega_{32}}g_2 +$
$2A^2_{\omega_{32}}g_2 + 2\cos[2\omega_2 + 2\omega_3 + 2\emptyset_{32}]A^2_{\omega_{32}}g_2 +$
$3\cos[\omega_1]A^3_{\omega_1}g_3 + \cos[3\omega_1]A^3_{\omega_1}g_3 + 3\cos[2\omega_1 - \omega_2]A^2_{\omega_1}A_{\omega_2}g_3 +$
$6\cos[\omega_2]A^2_{\omega_1}A_{\omega_2}g_3 + 3\cos[2\omega_1 + \omega_2]A^2_{\omega_1}A_{\omega_2}g_3 +$
$6\cos[\omega_1]A_{\omega_1}A^2_{\omega_2}g_3 + 3\cos[\omega_1 - 2\omega_2]A_{\omega_1}A^2_{\omega_2}g_3 +$
$3\cos[\omega_1 + 2\omega_2]A_{\omega_1}A^2_{\omega_2}g_3 + 3\cos[\omega_2]A^3_{\omega_2}g_3 + \cos[3\omega_2]A^3_{\omega_2}g_3 +$
$3\cos[2\omega_1 - \omega_3]A^2_{\omega_1}A_{\omega_3}g_3 + 6\cos[\omega_3]A^2_{\omega_1}A_{\omega_3}g_3 +$
$3\cos[2\omega_1 + \omega_3]A^2_{\omega_1}A_{\omega_3}g_3 + 6\cos[\omega_1 - \omega_2 - \omega_3]A_{\omega_1}A_{\omega_2}A_{\omega_3}g_3 +$
$6\cos[\omega_1 + \omega_2 - \omega_3]A_{\omega_1}A_{\omega_2}A_{\omega_3}g_3 +$
$6\cos[\omega_1 - \omega_2 + \omega_3]A_{\omega_1}A_{\omega_2}A_{\omega_3}g_3 +$
$6\cos[\omega_1 + \omega_2 + \omega_3]A_{\omega_1}A_{\omega_2}A_{\omega_3}g_3 +$
$3\cos[2\omega_2 - \omega_3]A^2_{\omega_2}A_{\omega_3}g_3 + 6\cos[\omega_3]A^2_{\omega_2}A_{\omega_3}g_3 +$
$3\cos[2\omega_2 + \omega_3]A^2_{\omega_2}A_{\omega_3}g_3 + 6\cos[\omega_1]A_{\omega_1}A^2_{\omega_3}g_3 +$
$3\cos[\omega_1 - 2\omega_3]A_{\omega_1}A^2_{\omega_3}g_3 + 3\cos[\omega_1 + 2\omega_3]A_{\omega_1}A^2_{\omega_3}g_3 +$
$6\cos[\omega_2]A_{\omega_2}A^2_{\omega_3}g_3 + 3\cos[\omega_2 - 2\omega_3]A_{\omega_2}A^2_{\omega_3}g_3 +$
$3\cos[\omega_2 + 2\omega_3]A_{\omega_2}A^2_{\omega_3}g_3 + 3\cos[\omega_3]A^3_{\omega_3}g_3 + \cos[3\omega_3]A^3_{\omega_3}g_3 +$
$3\cos[\omega_1 - \omega_2 - \emptyset_{21}]A^2_{\omega_1}A_{\omega_{21}}g_3 + 6\cos[\omega_1 + \omega_2 + \emptyset_{21}]A^2_{\omega_1}A_{\omega_{21}}g_3 +$

$$
\begin{aligned}
&3\cos[3\omega_1+\omega_2+\emptyset_{21}]A_{\omega_1}^2A_{\omega_{21}}g_3+\\
&6\cos[\emptyset_{21}]A_{\omega_1}A_{\omega_2}A_{\omega_{21}}g_3+6\cos[2\omega_1+\emptyset_{21}]A_{\omega_1}A_{\omega_2}A_{\omega_{21}}g_3+\\
&6\cos[2\omega_2+\emptyset_{21}]A_{\omega_1}A_{\omega_2}A_{\omega_{21}}g_3+\\
&6\cos[2\omega_1+2\omega_2+\emptyset_{21}]A_{\omega_1}A_{\omega_2}A_{\omega_{21}}g_3+\\
&3\cos[\omega_1-\omega_2+\emptyset_{21}]A_{\omega_2}^2A_{\omega_{21}}g_3+6\cos[\omega_1+\omega_2+\emptyset_{21}]A_{\omega_2}^2A_{\omega_{21}}g_3+\\
&3\cos[\omega_1+3\omega_2+\emptyset_{21}]A_{\omega_2}^2A_{\omega_{21}}g_3+\\
&6\cos[\omega_2-\omega_3+\emptyset_{21}]A_{\omega_1}A_{\omega_3}A_{\omega_{21}}g_3+\\
&6\cos[2\omega_1+\omega_2-\omega_3+\emptyset_{21}]A_{\omega_1}A_{\omega_3}A_{\omega_{21}}g_3+\\
&6\cos[\omega_2+\omega_3+\emptyset_{21}]A_{\omega_1}A_{\omega_3}A_{\omega_{21}}g_3+\\
&6\cos[2\omega_1+\omega_2+\omega_3+\emptyset_{21}]A_{\omega_1}A_{\omega_3}A_{\omega_{21}}g_3+\\
&6\cos[\omega_1-\omega_3+\emptyset_{21}]A_{\omega_2}A_{\omega_3}A_{\omega_{21}}g_3+\\
&6\cos[\omega_1+2\omega_2-\omega_3+\emptyset_{21}]A_{\omega_2}A_{\omega_3}A_{\omega_{21}}g_3+\\
&6\cos[\omega_1+\omega_3+\emptyset_{21}]A_{\omega_2}A_{\omega_3}A_{\omega_{21}}g_3+6\cos[\omega_1+2\omega_2+\omega_3+\emptyset_{21}]\\
&A_{\omega_2}A_{\omega_3}A_{\omega_{21}}g_3+6\cos[\omega_1+\omega_2+\emptyset_{21}]A_{\omega_3}^2A_{\omega_{21}}g_3+\\
&3\cos[\omega_1+\omega_2-2\omega_3+\emptyset_{21}]A_{\omega_3}^2A_{\omega_{21}}g_3+\\
&3\cos[\omega_1+\omega_2+2\omega_3+\emptyset_{21}]A_{\omega_3}^2A_{\omega_{21}}g_3+\\
&6\cos[\omega_1]A_{\omega_1}A_{\omega_{21}}^2g_3+3\cos[\omega_1+2\omega_2+2\emptyset_{21}]A_{\omega_1}A_{\omega_{21}}^2g_3+\\
&3\cos[3\omega_1+2\omega_2+2\emptyset_{21}]A_{\omega_1}A_{\omega_{21}}^2g_3+\\
&6\cos[\omega_2]A_{\omega_2}A_{\omega_{21}}^2g_3+3\cos[2\omega_1+\omega_2+2\emptyset_{21}]A_{\omega_2}A_{\omega_{21}}^2g_3+\\
&3\cos[2\omega_1+3\omega_2+2\emptyset_{21}]A_{\omega_2}A_{\omega_{21}}^2g_3+\\
&6\cos[\omega_3]A_{\omega_3}A_{\omega_{21}}^2g_3+3\cos[2\omega_1+2\omega_2-\omega_3+2\emptyset_{21}]A_{\omega_3}A_{\omega_{21}}^2g_3+\\
&3\cos[2\omega_1+2\omega_2+\omega_3+2\emptyset_{21}]A_{\omega_3}A_{\omega_{21}}^2g_3+\\
&3\cos[\omega_1+\omega_2+\emptyset_{21}]A_{\omega_{21}}^3g_3+\cos[3\omega_1+3\omega_2+3\emptyset_{21}]A_{\omega_{21}}^3g_3+\\
&3\cos[\omega_1-\omega_3-\emptyset_{31}]A_{\omega_1}^2A_{\omega_{31}}g_3+6\cos[\omega_1+\omega_3+\emptyset_{31}]A_{\omega_1}^2A_{\omega_{31}}g_3+\\
&3\cos[3\omega_1+\omega_3+\emptyset_{31}]A_{\omega_1}^2A_{\omega_{31}}g_3+\\
&6\cos[\omega_2-\omega_3-\emptyset_{31}]A_{\omega_1}A_{\omega_2}A_{\omega_{31}}g_3+\\
&6\cos[2\omega_1-\omega_2+\omega_3+\emptyset_{31}]A_{\omega_1}A_{\omega_2}A_{\omega_{31}}g_3+\\
&6\cos[\omega_2+\omega_3+\emptyset_{31}]A_{\omega_1}A_{\omega_2}A_{\omega_{31}}g_3+6\cos[2\omega_1+\omega_2+\omega_3+\emptyset_{31}]\\
&A_{\omega_1}A_{\omega_2}A_{\omega_{31}}g_3+6\cos[\omega_1+\omega_3+\emptyset_{31}]A_{\omega_2}^2A_{\omega_{31}}g_3+\\
&3\cos[\omega_1-2\omega_2+\omega_3+\emptyset_{31}]A_{\omega_2}^2A_{\omega_{31}}g_3+\\
&3\cos[\omega_1+2\omega_2+\omega_3+\emptyset_{31}]A_{\omega_2}^2A_{\omega_{31}}g_3+\\
&6\cos[\emptyset_{31}]A_{\omega_1}A_{\omega_3}A_{\omega_{31}}g_3+6\cos[2\omega_1+\emptyset_{31}]A_{\omega_1}A_{\omega_3}A_{\omega_{31}}g_3+\\
&6\cos[2\omega_3+\emptyset_{31}]A_{\omega_1}A_{\omega_3}A_{\omega_{31}}g_3+\\
&6\cos[2\omega_1+2\omega_3+\emptyset_{31}]A_{\omega_1}A_{\omega_3}A_{\omega_{31}}g_3+\\
&6\cos[\omega_1-\omega_2+\emptyset_{31}]A_{\omega_2}A_{\omega_3}A_{\omega_{31}}g_3+\\
&6\cos[\omega_1+\omega_2+\emptyset_{31}]A_{\omega_2}A_{\omega_3}A_{\omega_{31}}g_3+\\
&6\cos[\omega_1-\omega_2+2\omega_3+\emptyset_{31}]A_{\omega_2}A_{\omega_3}A_{\omega_{31}}g_3+\\
&6\cos[\omega_1+\omega_2+2\omega_3+\emptyset_{31}]A_{\omega_2}A_{\omega_3}A_{\omega_{31}}g_3+\\
&3\cos[\omega_1-\omega_3+\emptyset_{31}]A_{\omega_3}^2A_{\omega_{31}}g_3+6\cos[\omega_1+\omega_3+\emptyset_{31}]A_{\omega_3}^2A_{\omega_{31}}g_3+\\
&3\cos[\omega_1+3\omega_3+\emptyset_{31}]A_{\omega_3}^2A_{\omega_{31}}g_3+\\
&6\cos[\omega_1+\omega_2-\omega_3+\emptyset_{21}-\emptyset_{31}]A_{\omega_1}A_{\omega_{21}}A_{\omega_{31}}g_3+\\
&6\cos[\omega_1-\omega_2+\omega_3-\emptyset_{21}+\emptyset_{31}]A_{\omega_1}A_{\omega_{21}}A_{\omega_{31}}g_3+\\
&6\cos[\omega_1+\omega_2+\omega_3+\emptyset_{21}+\emptyset_{31}]A_{\omega_1}A_{\omega_{21}}A_{\omega_{31}}g_3+\\
&6\cos[3\omega_1+\omega_2+\omega_3+\emptyset_{21}+\emptyset_{31}]A_{\omega_1}A_{\omega_{21}}A_{\omega_{31}}g_3+\\
&6\cos[2\omega_2-\omega_3+\emptyset_{21}-\emptyset_{31}]A_{\omega_2}A_{\omega_{21}}A_{\omega_{31}}g_3+\\
&6\cos[\omega_3-\emptyset_{21}+\emptyset_{31}]A_{\omega_2}A_{\omega_{21}}A_{\omega_{31}}g_3+\\
&6\cos[2\omega_1+\omega_3+\emptyset_{21}+\emptyset_{31}]A_{\omega_2}A_{\omega_{21}}A_{\omega_{31}}g_3+\\
&6\cos[2\omega_1+2\omega_2+\omega_3+\emptyset_{21}+\emptyset_{31}]A_{\omega_2}A_{\omega_{21}}A_{\omega_{31}}g_3+\\
&6\cos[\omega_2+\emptyset_{21}-\emptyset_{31}]A_{\omega_3}A_{\omega_{21}}A_{\omega_{31}}g_3+\\
&6\cos[\omega_2-2\omega_3+\emptyset_{21}-\emptyset_{31}]A_{\omega_3}A_{\omega_{21}}A_{\omega_{31}}g_3+\\
&6\cos[2\omega_1+\omega_2+\emptyset_{21}+\emptyset_{31}]A_{\omega_3}A_{\omega_{21}}A_{\omega_{31}}g_3+\\
&6\cos[2\omega_1+\omega_2+2\omega_3+\emptyset_{21}+\emptyset_{31}]A_{\omega_3}A_{\omega_{21}}A_{\omega_{31}}g_3+\\
&3\cos[\omega_1+2\omega_2-\omega_3+2\emptyset_{21}-\emptyset_{31}]A_{\omega_{21}}^2A_{\omega_{31}}g_3+\\
&6\cos[\omega_1+\omega_3+\emptyset_{31}]A_{\omega_{21}}^2A_{\omega_{31}}g_3+\\
&3\cos[3\omega_1+2\omega_2+\omega_3+2\emptyset_{21}+\emptyset_{31}]A_{\omega_{21}}^2A_{\omega_{31}}g_3+
\end{aligned}
$$

$$
\begin{aligned}
&6\cos[\omega_1]A_{\omega_1}A_{\omega_{31}}^2 g_3 + 3\cos[\omega_1 + 2\omega_3 + 2\emptyset_{31}]A_{\omega_1}A_{\omega_{31}}^2 g_3 + \\
&3\cos[3\omega_1 + 2\omega_3 + 2\emptyset_{31}]A_{\omega_1}A_{\omega_{31}}^2 g_3 + \\
&6\cos[\omega_2]A_{\omega_2}A_{\omega_{31}}^2 g_3 + 3\cos[2\omega_1 - \omega_2 + 2\omega_3 + 2\emptyset_{31}]A_{\omega_2}A_{\omega_{31}}^2 g_3 + \\
&3\cos[2\omega_1 + \omega_2 + 2\omega_3 + 2\emptyset_{31}]A_{\omega_2}A_{\omega_{31}}^2 g_3 + \\
&6\cos[\omega_3]A_{\omega_3}A_{\omega_{31}}^2 g_3 + 3\cos[2\omega_1 + \omega_3 + 2\emptyset_{31}]A_{\omega_3}A_{\omega_{31}}^2 g_3 + \\
&3\cos[2\omega_1 + 3\omega_3 + 2\emptyset_{31}]A_{\omega_3}A_{\omega_{31}}^2 g_3 + \\
&6\cos[\omega_1 + \omega_2 + \emptyset_{21}]A_{\omega_{21}}A_{\omega_{31}}^2 g_3 + \\
&3\cos[\omega_1 - \omega_2 + 2\omega_3 - \emptyset_{21} + 2\emptyset_{31}]A_{\omega_{21}}A_{\omega_{31}}^2 g_3 + \\
&3\cos[3\omega_1 + \omega_2 + 2\omega_3 + \emptyset_{21} + 2\emptyset_{31}]A_{\omega_{21}}A_{\omega_{31}}^2 g_3 + \\
&3\cos[\omega_1 + \omega_3 + \emptyset_{31}]A_{\omega_{31}}^3 g_3 + \cos[3\omega_1 + 3\omega_3 + 3\emptyset_{31}]A_{\omega_{31}}^3 g_3 + \\
&3\cos[2\omega_1 - \omega_2 - \omega_3 - \emptyset_{32}]A_{\omega_1}^2 A_{\omega_{32}} g_3 + \\
&6\cos[\omega_2 + \omega_3 + \emptyset_{32}]A_{\omega_1}^2 A_{\omega_{32}} g_3 + \\
&3\cos[2\omega_1 + \omega_2 + \omega_3 + \emptyset_{32}]A_{\omega_1}^2 A_{\omega_{32}} g_3 + \\
&6\cos[\omega_1 - \omega_3 - \emptyset_{32}]A_{\omega_1}A_{\omega_2}A_{\omega_{32}} g_3 + \\
&6\cos[\omega_1 - 2\omega_2 - \omega_3 - \emptyset_{32}]A_{\omega_1}A_{\omega_2}A_{\omega_{32}} g_3 + \\
&6\cos[\omega_1 + \omega_3 + \emptyset_{32}]A_{\omega_1}A_{\omega_2}A_{\omega_{32}} g_3 + \\
&6\cos[\omega_1 + 2\omega_2 + \omega_3 + \emptyset_{32}]A_{\omega_1}A_{\omega_2}A_{\omega_{32}} g_3 + \\
&3\cos[\omega_2 - \omega_3 - \emptyset_{32}]A_{\omega_2}^2 A_{\omega_{32}} g_3 + 6\cos[\omega_2 + \omega_3 + \emptyset_{32}]A_{\omega_2}^2 A_{\omega_{32}} g_3 + \\
&3\cos[3\omega_2 + \omega_3 + \emptyset_{32}]A_{\omega_2}^2 A_{\omega_{32}} g_3 + \\
&6\cos[\omega_1 - \omega_2 - \emptyset_{32}]A_{\omega_1}A_{\omega_3}A_{\omega_{32}} g_3 + \\
&6\cos[\omega_1 - \omega_2 - 2\omega_3 - \emptyset_{32}]A_{\omega_1}A_{\omega_3}A_{\omega_{32}} g_3 + \\
&6\cos[\omega_1 + \omega_2 + \emptyset_{32}]A_{\omega_1}A_{\omega_3}A_{\omega_{32}} g_3 + \\
&6\cos[\omega_1 + \omega_2 + 2\omega_3 + \emptyset_{32}]A_{\omega_1}A_{\omega_3}A_{\omega_{32}} g_3 + \\
&6\cos[\emptyset_{32}]A_{\omega_2}A_{\omega_3}A_{\omega_{32}} g_3 + 6\cos[2\omega_2 + \emptyset_{32}]A_{\omega_2}A_{\omega_3}A_{\omega_{32}} g_3 + \\
&6\cos[2\omega_3 + \emptyset_{32}]A_{\omega_2}A_{\omega_3}A_{\omega_{32}} g_3 + \\
&6\cos[2\omega_2 + 2\omega_3 + \emptyset_{32}]A_{\omega_2}A_{\omega_3}A_{\omega_{32}} g_3 + \\
&3\cos[\omega_2 - \omega_3 + \emptyset_{32}]A_{\omega_3}^2 A_{\omega_{32}} g_3 + 6\cos[\omega_2 + \omega_3 + \emptyset_{32}]A_{\omega_3}^2 A_{\omega_{32}} g_3 + \\
&3\cos[\omega_2 + 3\omega_3 + \emptyset_{32}]A_{\omega_3}^2 A_{\omega_{32}} g_3 + \\
&6\cos[2\omega_1 - \omega_3 + \emptyset_{21} - \emptyset_{32}]A_{\omega_1}A_{\omega_{21}}A_{\omega_{32}} g_3 + \\
&6\cos[\omega_3 - \emptyset_{21} + \emptyset_{32}]A_{\omega_1}A_{\omega_{21}}A_{\omega_{32}} g_3 + \\
&6\cos[2\omega_2 + \omega_3 + \emptyset_{21} + \emptyset_{32}]A_{\omega_1}A_{\omega_{21}}A_{\omega_{32}} g_3 + \\
&6\cos[2\omega_1 + 2\omega_2 + \omega_3 + \emptyset_{21} + \emptyset_{32}]A_{\omega_1}A_{\omega_{21}}A_{\omega_{32}} g_3 + \\
&6\cos[\omega_1 - \omega_2 - \omega_3 + \emptyset_{21} - \emptyset_{32}]A_{\omega_2}A_{\omega_{21}}A_{\omega_{32}} g_3 + \\
&6\cos[\omega_1 + \omega_2 - \omega_3 + \emptyset_{21} - \emptyset_{32}]A_{\omega_2}A_{\omega_{21}}A_{\omega_{32}} g_3 + \\
&6\cos[\omega_1 + \omega_2 + \omega_3 + \emptyset_{21} + \emptyset_{32}]A_{\omega_2}A_{\omega_{21}}A_{\omega_{32}} g_3 + \\
&6\cos[\omega_1 + 3\omega_2 + \omega_3 + \emptyset_{21} + \emptyset_{32}]A_{\omega_2}A_{\omega_{21}}A_{\omega_{32}} g_3 + \\
&6\cos[\omega_1 + \emptyset_{21} - \emptyset_{32}]A_{\omega_3}A_{\omega_{21}}A_{\omega_{32}} g_3 + \\
&6\cos[\omega_1 - 2\omega_3 + \emptyset_{21} - \emptyset_{32}]A_{\omega_3}A_{\omega_{21}}A_{\omega_{32}} g_3 + \\
&6\cos[\omega_1 + 2\omega_2 + \emptyset_{21} + \emptyset_{32}]A_{\omega_3}A_{\omega_{21}}A_{\omega_{32}} g_3 + \\
&6\cos[\omega_1 + 2\omega_2 + 2\omega_3 + \emptyset_{21} + \emptyset_{32}]A_{\omega_3}A_{\omega_{21}}A_{\omega_{32}} g_3 + \\
&3\cos[2\omega_1 + \omega_2 - \omega_3 + 2\emptyset_{21} - \emptyset_{32}]A_{\omega_{21}}^2 A_{\omega_{32}} g_3 + \\
&6\cos[\omega_2 + \omega_3 + \emptyset_{32}]A_{\omega_{21}}^2 A_{\omega_{32}} g_3 + \\
&3\cos[2\omega_1 + 3\omega_2 + \omega_3 + 2\emptyset_{21} + \emptyset_{32}]A_{\omega_{21}}^2 A_{\omega_{32}} g_3 + \\
&6\cos[2\omega_1 - \omega_2 + \emptyset_{31} - \emptyset_{32}]A_{\omega_1}A_{\omega_{31}}A_{\omega_{32}} g_3 + \\
&6\cos[\omega_2 - \emptyset_{31} + \emptyset_{32}]A_{\omega_1}A_{\omega_{31}}A_{\omega_{32}} g_3 + \\
&6\cos[\omega_2 + 2\omega_3 + \emptyset_{31} + \emptyset_{32}]A_{\omega_1}A_{\omega_{31}}A_{\omega_{32}} g_3 + \\
&6\cos[2\omega_1 + \omega_2 + 2\omega_3 + \emptyset_{31} + \emptyset_{32}]A_{\omega_1}A_{\omega_{31}}A_{\omega_{32}} g_3 + \\
&6\cos[\omega_1 + \emptyset_{31} - \emptyset_{32}]A_{\omega_2}A_{\omega_{31}}A_{\omega_{32}} g_3 + \\
&6\cos[\omega_1 - 2\omega_2 + \emptyset_{31} - \emptyset_{32}]A_{\omega_2}A_{\omega_{31}}A_{\omega_{32}} g_3 + \\
&6\cos[\omega_1 + 2\omega_3 + \emptyset_{31} + \emptyset_{32}]A_{\omega_2}A_{\omega_{31}}A_{\omega_{32}} g_3 + \\
&6\cos[\omega_1 + 2\omega_2 + 2\omega_3 + \emptyset_{31} + \emptyset_{32}]A_{\omega_2}A_{\omega_{31}}A_{\omega_{32}} g_3 + \\
&6\cos[\omega_1 - \omega_2 - \omega_3 + \emptyset_{31} - \emptyset_{32}]A_{\omega_3}A_{\omega_{31}}A_{\omega_{32}} g_3 + \\
&6\cos[\omega_1 - \omega_2 + \omega_3 + \emptyset_{31} - \emptyset_{32}]A_{\omega_3}A_{\omega_{31}}A_{\omega_{32}} g_3 + \\
&6\cos[\omega_1 + \omega_2 + \omega_3 + \emptyset_{31} + \emptyset_{32}]A_{\omega_3}A_{\omega_{31}}A_{\omega_{32}} g_3 + \\
&6\cos[\omega_1 + \omega_2 + 3\omega_3 + \emptyset_{31} + \emptyset_{32}]A_{\omega_3}A_{\omega_{31}}A_{\omega_{32}} g_3 + \\
&6\cos[2\omega_1 + \emptyset_{21} + \emptyset_{31} - \emptyset_{32}]A_{\omega_{21}}A_{\omega_{31}}A_{\omega_{32}} g_3 +
\end{aligned}
$$

$$
\begin{aligned}
&6\cos[2\omega_2 + \emptyset_{21} - \emptyset_{31} + \emptyset_{32}]A_{\omega_{21}}A_{\omega_{31}}A_{\omega_{32}}g_3+\\
&6\cos[2\omega_3 - \emptyset_{21} + \emptyset_{31} + \emptyset_{32}]A_{\omega_{21}}A_{\omega_{31}}A_{\omega_{32}}g_3+\\
&6\cos[2\omega_1 + 2\omega_2 + 2\omega_3 + \emptyset_{21} + \emptyset_{31} + \emptyset_{32}]A_{\omega_{21}}A_{\omega_{31}}A_{\omega_{32}}g_3+\\
&3\cos[2\omega_1 - \omega_2 + \omega_3 + 2\emptyset_{31} - \emptyset_{32}]A^2_{\omega_{31}}A_{\omega_{32}}g_3+\\
&6\cos[\omega_2 + \omega_3 + \emptyset_{32}]A^2_{\omega_{31}}A_{\omega_{32}}g_3+\\
&3\cos[2\omega_1 + \omega_2 + 3\omega_3 + 2\emptyset_{31} + \emptyset_{32}]A^2_{\omega_{31}}A_{\omega_{32}}g_3+\\
&6\cos[\omega_1]A_{\omega_1}A^2_{\omega_{32}}g_3 + 3\cos[\omega_1 - 2\omega_2 - 2\omega_3 - 2\emptyset_{32}]A_{\omega_1}A^2_{\omega_{32}}g_3+\\
&3\cos[\omega_1 + 2\omega_2 + 2\omega_3 + 2\emptyset_{32}]A_{\omega_1}A^2_{\omega_{32}}g_3+\\
&6\cos[\omega_2]A_{\omega_2}A^2_{\omega_{32}}g_3 + 3\cos[\omega_2 + 2\omega_3 + 2\emptyset_{32}]A_{\omega_2}A^2_{\omega_{32}}g_3+\\
&3\cos[3\omega_2 + 2\omega_3 + 2\emptyset_{32}]A_{\omega_2}A^2_{\omega_{32}}g_3+\\
&6\cos[\omega_3]A_{\omega_3}A^2_{\omega_{32}}g_3 + 3\cos[2\omega_2 + \omega_3 + 2\emptyset_{32}]A_{\omega_3}A^2_{\omega_{32}}g_3+\\
&3\cos[2\omega_2 + 3\omega_3 + 2\emptyset_{32}]A_{\omega_3}A^2_{\omega_{32}}g_3+\\
&6\cos[\omega_1 + \omega_2 + \emptyset_{21}]A_{\omega_{21}}A^2_{\omega_{32}}g_3+\\
&3\cos[\omega_1 - \omega_2 - 2\omega_3 + \emptyset_{21} - 2\emptyset_{32}]A_{\omega_{21}}A^2_{\omega_{32}}g_3+\\
&3\cos[\omega_1 + 3\omega_2 + 2\omega_3 + \emptyset_{21} + 2\emptyset_{32}]A_{\omega_{21}}A^2_{\omega_{32}}g_3+\\
&6\cos[\omega_1 + \omega_3 + \emptyset_{31}]A_{\omega_{31}}A^2_{\omega_{32}}g_3+\\
&3\cos[\omega_1 - 2\omega_2 - \omega_3 + \emptyset_{31} - 2\emptyset_{32}]A_{\omega_{31}}A^2_{\omega_{32}}g_3+\\
&3\cos[\omega_1 + 2\omega_2 + 3\omega_3 + \emptyset_{31} + 2\emptyset_{32}]A_{\omega_{31}}A^2_{\omega_{32}}g_3+\\
&3\cos[\omega_2 + \omega_3 + \emptyset_{32}]A^3_{\omega_{32}}g_3 + \cos[3\omega_2 + 3\omega_3 + 3\emptyset_{32}]A^3_{\omega_{32}}g_3)
\end{aligned}
$$

2.3 Power Series Analysis of a Three-Tone System with Injected Second Harmonic Signals

The system input is made of two sinusoid signals at the frequencies ω_1, ω_2 and ω_3 with amplitudes A_{ω_1}, A_{ω_2} and A_{ω_3} respectively and their second harmonic at the frequencies $(2\omega_1)$, $(2\omega_2)$ and $(2\omega_3)$ with amplitudes $A_{2\omega_1}$, $A_{2\omega_2}$ and $A_{2\omega_3}$ with phases $\phi_{2\omega_1}$, $\phi_{2\omega_2}$ and $\phi_{2\omega_3}$ respectively.

The input is

$$\begin{aligned} v_{in} = A_{\omega_1}\cos(\omega_1 t) + A_{\omega_2}\cos(\omega_2 t) + A_{\omega_3}\cos(\omega_3 t) + A_{2\omega_1}\cos(2\omega_1 t + \phi_{2\omega_1}) \\ + A_{2\omega_2}\cos(2\omega_2 + \phi_{2\omega_2}) + A_{2\omega_3}\cos(2\omega_3 + \phi_{2\omega_3}) \end{aligned} \tag{2.35}$$

The amplifier output spectrum is calculated by using a power series expansion, such that

$$V_{out} = \sum_{n=1}^{3} g_{mn} v_{in}^n$$

$$= \sum_{n=1}^{3} g_{mn} \left[\begin{aligned} v_{in} = A_{\omega_1}\cos(\omega_1 t) + A_{\omega_2}\cos(\omega_2 t) + A_{\omega_3}\cos(\omega_3 t) + A_{2\omega_1}\cos(2\omega_1 t + \phi_{2\omega_1}) \\ + A_{2\omega_2}\cos(2\omega_2 + \phi_{2\omega_2}) + A_{2\omega_3}\cos(2\omega_3 + \phi_{2\omega_3}) \end{aligned} \right]^n \tag{2.36}$$

The following is the input file and the output file calculation using Mathematica® showing all intermodulation terms at the output of the amplifier with the injection of the second harmonic signals.

•Input file

$$x1 = \sum_{k=1}^{3}(A_{\omega_k}\cos[2\omega_k + \emptyset_{2\omega_k}]);$$

$$x2 = \sum_{k=1}^{3}(A_{\omega_k}\cos[\omega_k]);$$

$$Y = \sum_{n=0}^{3}(g_n(x1+x2)^n);$$

TrigReduce[Y]
TeXSave["second.tex"]

•Output file

$$V_{out} = \tfrac{1}{4}(4g_0 + 4\cos[\omega_1]A_{\omega_1}g_1 + 4\cos[2\omega_1 + \emptyset_{2\omega_1}]A_{\omega_1}g_1 +$$
$$4\cos[\omega_2]A_{\omega_2}g_1 + 4\cos[2\omega_2 + \emptyset_{2\omega_2}]A_{\omega_2}g_1 + 4\cos[\omega_3]A_{\omega_3}g_1 +$$
$$4\cos[2\omega_3 + \emptyset_{2\omega_3}]A_{\omega_3}g_1 + 4A^2_{\omega_1}g_2 + 2\cos[2\omega_1]A^2_{\omega_1}g_2 +$$
$$4\cos[\omega_1 + \emptyset_{2\omega_1}]A^2_{\omega_1}g_2 + 4\cos[3\omega_1 + \emptyset_{2\omega_1}]A^2_{\omega_1}g_2 +$$
$$2\cos[4\omega_1 + 2\emptyset_{2\omega_1}]A^2_{\omega_1}g_2 + 4\cos[\omega_1 - \omega_2]A_{\omega_1}A_{\omega_2}g_2 +$$
$$4\cos[\omega_1 + \omega_2]A_{\omega_1}A_{\omega_2}g_2 + 4\cos[2\omega_1 - \omega_2 + \emptyset_{2\omega_1}]A_{\omega_1}A_{\omega_2}g_2 +$$
$$4\cos[2\omega_1 + \omega_2 + \emptyset_{2\omega_1}]A_{\omega_1}A_{\omega_2}g_2 +$$
$$4\cos[\omega_1 - 2\omega_2 - \emptyset_{2\omega_2}]A_{\omega_1}A_{\omega_2}g_2 +$$
$$4\cos[2\omega_1 - 2\omega_2 + \emptyset_{2\omega_1} - \emptyset_{2\omega_2}]A_{\omega_1}A_{\omega_2}g_2 +$$
$$4\cos[\omega_1 + 2\omega_2 + \emptyset_{2\omega_2}]A_{\omega_1}A_{\omega_2}g_2 +$$
$$4\cos[2\omega_1 + 2\omega_2 + \emptyset_{2\omega_1} + \emptyset_{2\omega_2}]A_{\omega_1}A_{\omega_2}g_2 +$$
$$4A^2_{\omega_2}g_2 + 2\cos[2\omega_2]A^2_{\omega_2}g_2 +$$
$$4\cos[\omega_2 + \emptyset_{2\omega_2}]A^2_{\omega_2}g_2 + 4\cos[3\omega_2 + \emptyset_{2\omega_2}]A^2_{\omega_2}g_2 +$$
$$2\cos[4\omega_2 + 2\emptyset_{2\omega_2}]A^2_{\omega_2}g_2 + 4\cos[\omega_1 - \omega_3]A_{\omega_1}A_{\omega_3}g_2 +$$
$$4\cos[\omega_1 + \omega_3]A_{\omega_1}A_{\omega_3}g_2 + 4\cos[2\omega_1 - \omega_3 + \emptyset_{2\omega_1}]A_{\omega_1}A_{\omega_3}g_2 +$$
$$4\cos[2\omega_1 + \omega_3 + \emptyset_{2\omega_1}]A_{\omega_1}A_{\omega_3}g_2 +$$
$$4\cos[\omega_1 - 2\omega_3 - \emptyset_{2\omega_3}]A_{\omega_1}A_{\omega_3}g_2 +$$
$$4\cos[2\omega_1 - 2\omega_3 + \emptyset_{2\omega_1} - \emptyset_{2\omega_3}]A_{\omega_1}A_{\omega_3}g_2 +$$
$$4\cos[\omega_1 + 2\omega_3 + \emptyset_{2\omega_3}]A_{\omega_1}A_{\omega_3}g_2 + 4\cos[2\omega_1 + 2\omega_3 + \emptyset_{2\omega_1} + \emptyset_{2\omega_3}]$$
$$A_{\omega_1}A_{\omega_3}g_2 + 4\cos[\omega_2 - \omega_3]A_{\omega_2}A_{\omega_3}g_2 +$$
$$4\cos[\omega_2 + \omega_3]A_{\omega_2}A_{\omega_3}g_2 + 4\cos[2\omega_2 - \omega_3 + \emptyset_{2\omega_2}]A_{\omega_2}A_{\omega_3}g_2 +$$
$$4\cos[2\omega_2 + \omega_3 + \emptyset_{2\omega_2}]A_{\omega_2}A_{\omega_3}g_2 +$$
$$4\cos[\omega_2 - 2\omega_3 - \emptyset_{2\omega_3}]A_{\omega_2}A_{\omega_3}g_2 +$$
$$4\cos[2\omega_2 - 2\omega_3 + \emptyset_{2\omega_2} - \emptyset_{2\omega_3}]A_{\omega_2}A_{\omega_3}g_2 +$$
$$4\cos[\omega_2 + 2\omega_3 + \emptyset_{2\omega_3}]A_{\omega_2}A_{\omega_3}g_2 +$$
$$4\cos[2\omega_2 + 2\omega_3 + \emptyset_{2\omega_2} + \emptyset_{2\omega_3}]A_{\omega_2}A_{\omega_3}g_2 +$$
$$4A^2_{\omega_3}g_2 + 2\cos[2\omega_3]A^2_{\omega_3}g_2 +$$
$$4\cos[\omega_3 + \emptyset_{2\omega_3}]A^2_{\omega_3}g_2 + 4\cos[3\omega_3 + \emptyset_{2\omega_3}]A^2_{\omega_3}g_2 +$$
$$2\cos[4\omega_3 + 2\emptyset_{2\omega_3}]A^2_{\omega_3}g_2 + 9\cos[\omega_1]A^3_{\omega_1}g_3 +$$
$$\cos[3\omega_1]A^3_{\omega_1}g_3 + 3\cos[\emptyset_{2\omega_1}]A^3_{\omega_1}g_3 + 9\cos[2\omega_1 + \emptyset_{2\omega_1}]A^3_{\omega_1}g_3 +$$
$$3\cos[4\omega_1 + \emptyset_{2\omega_1}]A^3_{\omega_1}g_3 + 3\cos[3\omega_1 + 2\emptyset_{2\omega_1}]A^3_{\omega_1}g_3 +$$
$$3\cos[5\omega_1 + 2\emptyset_{2\omega_1}]A^3_{\omega_1}g_3 + \cos[6\omega_1 + 3\emptyset_{2\omega_1}]A^3_{\omega_1}g_3 +$$
$$3\cos[2\omega_1 - \omega_2]A^2_{\omega_1}A_{\omega_2}g_3 + 12\cos[\omega_2]A^2_{\omega_1}A_{\omega_2}g_3 +$$
$$3\cos[2\omega_1 + \omega_2]A^2_{\omega_1}A_{\omega_2}g_3 + 6\cos[\omega_1 - \omega_2 + \emptyset_{2\omega_1}]A^2_{\omega_1}A_{\omega_2}g_3 +$$
$$6\cos[3\omega_1 - \omega_2 + \emptyset_{2\omega_1}]A^2_{\omega_1}A_{\omega_2}g_3 +$$
$$6\cos[\omega_1 + \omega_2 + \emptyset_{2\omega_1}]A^2_{\omega_1}A_{\omega_2}g_3 +$$
$$6\cos[3\omega_1 + \omega_2 + \emptyset_{2\omega_1}]A^2_{\omega_1}A_{\omega_2}g_3 +$$
$$3\cos[4\omega_1 - \omega_2 + 2\emptyset_{2\omega_1}]A^2_{\omega_1}A_{\omega_2}g_3 +$$
$$3\cos[4\omega_1 + \omega_2 + 2\emptyset_{2\omega_1}]A^2_{\omega_1}A_{\omega_2}g_3 +$$
$$3\cos[2\omega_1 - 2\omega_2 - \emptyset_{2\omega_2}]A^2_{\omega_1}A_{\omega_2}g_3 +$$
$$6\cos[\omega_1 - 2\omega_2 + \emptyset_{2\omega_1} - \emptyset_{2\omega_2}]A^2_{\omega_1}A_{\omega_2}g_3 +$$
$$6\cos[3\omega_1 - 2\omega_2 + \emptyset_{2\omega_1} - \emptyset_{2\omega_2}]A^2_{\omega_1}A_{\omega_2}g_3 +$$
$$3\cos[4\omega_1 - 2\omega_2 + 2\emptyset_{2\omega_1} - \emptyset_{2\omega_2}]A^2_{\omega_1}A_{\omega_2}g_3 +$$
$$12\cos[2\omega_2 + \emptyset_{2\omega_2}]A^2_{\omega_1}A_{\omega_2}g_3 +$$

$$
\begin{aligned}
&3\cos[2\omega_1+2\omega_2+\emptyset_{2\omega_2}]A_{\omega_1}^2A_{\omega_2}g_3+\\
&6\cos[\omega_1+2\omega_2+\emptyset_{2\omega_1}+\emptyset_{2\omega_2}]A_{\omega_1}^2A_{\omega_2}g_3+\\
&6\cos[3\omega_1+2\omega_2+\emptyset_{2\omega_1}+\emptyset_{2\omega_2}]A_{\omega_1}^2A_{\omega_2}g_3+\\
&3\cos[4\omega_1+2\omega_2+2\emptyset_{2\omega_1}+\emptyset_{2\omega_2}]A_{\omega_1}^2A_{\omega_2}g_3+\\
&12\cos[\omega_1]A_{\omega_1}A_{\omega_2}^2g_3+3\cos[\omega_1-2\omega_2]A_{\omega_1}A_{\omega_2}^2g_3+\\
&3\cos[\omega_1+2\omega_2]A_{\omega_1}A_{\omega_2}^2g_3+12\cos[2\omega_1+\emptyset_{2\omega_1}]A_{\omega_1}A_{\omega_2}^2g_3+\\
&3\cos[2\omega_1-2\omega_2+\emptyset_{2\omega_1}]A_{\omega_1}A_{\omega_2}^2g_3+\\
&3\cos[2\omega_1+2\omega_2+\emptyset_{2\omega_1}]A_{\omega_1}A_{\omega_2}^2g_3+\\
&3\cos[\omega_1-4\omega_2-2\emptyset_{2\omega_2}]A_{\omega_1}A_{\omega_2}^2g_3+\\
&3\cos[2\omega_1-4\omega_2+\emptyset_{2\omega_1}-2\emptyset_{2\omega_2}]A_{\omega_1}A_{\omega_2}^2g_3+\\
&6\cos[\omega_1-3\omega_2-\emptyset_{2\omega_2}]A_{\omega_1}A_{\omega_2}^2g_3+\\
&6\cos[\omega_1-\omega_2-\emptyset_{2\omega_2}]A_{\omega_1}A_{\omega_2}^2g_3+\\
&6\cos[2\omega_1-3\omega_2+\emptyset_{2\omega_1}-\emptyset_{2\omega_2}]A_{\omega_1}A_{\omega_2}^2g_3+\\
&6\cos[2\omega_1-\omega_2+\emptyset_{2\omega_1}-\emptyset_{2\omega_2}]A_{\omega_1}A_{\omega_2}^2g_3+\\
&6\cos[\omega_1+\omega_2+\emptyset_{2\omega_2}]A_{\omega_1}A_{\omega_2}^2g_3+\\
&6\cos[\omega_1+3\omega_2+\emptyset_{2\omega_2}]A_{\omega_1}A_{\omega_2}^2g_3+\\
&6\cos[2\omega_1+\omega_2+\emptyset_{2\omega_1}+\emptyset_{2\omega_2}]A_{\omega_1}A_{\omega_2}^2g_3+\\
&6\cos[2\omega_1+3\omega_2+\emptyset_{2\omega_1}+\emptyset_{2\omega_2}]A_{\omega_1}A_{\omega_2}^2g_3+\\
&3\cos[\omega_1+4\omega_2+2\emptyset_{2\omega_2}]A_{\omega_1}A_{\omega_2}^2g_3+\\
&3\cos[2\omega_1+4\omega_2+\emptyset_{2\omega_1}+2\emptyset_{2\omega_2}]A_{\omega_1}A_{\omega_2}^2g_3+9\cos[\omega_2]A_{\omega_2}^3g_3+\\
&\cos[3\omega_2]A_{\omega_2}^3g_3+3\cos[\emptyset_{2\omega_2}]A_{\omega_2}^3g_3+9\cos[2\omega_2+\emptyset_{2\omega_2}]A_{\omega_2}^3g_3+\\
&3\cos[4\omega_2+\emptyset_{2\omega_2}]A_{\omega_2}^3g_3+3\cos[3\omega_2+2\emptyset_{2\omega_2}]A_{\omega_2}^3g_3+\\
&3\cos[5\omega_2+2\emptyset_{2\omega_2}]A_{\omega_2}^3g_3+\cos[6\omega_2+3\emptyset_{2\omega_2}]A_{\omega_2}^3g_3+\\
&3\cos[2\omega_1-\omega_3]A_{\omega_1}^2A_{\omega_3}g_3+12\cos[\omega_3]A_{\omega_1}^2A_{\omega_3}g_3+\\
&3\cos[2\omega_1+\omega_3]A_{\omega_1}^2A_{\omega_3}g_3+6\cos[\omega_1-\omega_3+\emptyset_{2\omega_1}]A_{\omega_1}^2A_{\omega_3}g_3+\\
&6\cos[3\omega_1-\omega_3+\emptyset_{2\omega_1}]A_{\omega_1}^2A_{\omega_3}g_3+\\
&6\cos[\omega_1+\omega_3+\emptyset_{2\omega_1}]A_{\omega_1}^2A_{\omega_3}g_3+\\
&6\cos[3\omega_1+\omega_3+\emptyset_{2\omega_1}]A_{\omega_1}^2A_{\omega_3}g_3+\\
&3\cos[4\omega_1-\omega_3+2\emptyset_{2\omega_1}]A_{\omega_1}^2A_{\omega_3}g_3+\\
&3\cos[4\omega_1+\omega_3+2\emptyset_{2\omega_1}]A_{\omega_1}^2A_{\omega_3}g_3+\\
&3\cos[2\omega_1-2\omega_3-\emptyset_{2\omega_3}]A_{\omega_1}^2A_{\omega_3}g_3+\\
&6\cos[\omega_1-2\omega_3+\emptyset_{2\omega_1}-\emptyset_{2\omega_3}]A_{\omega_1}^2A_{\omega_3}g_3+\\
&6\cos[3\omega_1-2\omega_3+\emptyset_{2\omega_1}-\emptyset_{2\omega_3}]A_{\omega_1}^2A_{\omega_3}g_3+\\
&3\cos[4\omega_1-2\omega_3+2\emptyset_{2\omega_1}-\emptyset_{2\omega_3}]A_{\omega_1}^2A_{\omega_3}g_3+\\
&12\cos[2\omega_3+\emptyset_{2\omega_3}]A_{\omega_1}^2A_{\omega_3}g_3+\\
&3\cos[2\omega_1+2\omega_3+\emptyset_{2\omega_3}]A_{\omega_1}^2A_{\omega_3}g_3+\\
&6\cos[\omega_1+2\omega_3+\emptyset_{2\omega_1}+\emptyset_{2\omega_3}]A_{\omega_1}^2A_{\omega_3}g_3+\\
&6\cos[3\omega_1+2\omega_3+\emptyset_{2\omega_1}+\emptyset_{2\omega_3}]A_{\omega_1}^2A_{\omega_3}g_3+\\
&3\cos[4\omega_1+2\omega_3+2\emptyset_{2\omega_1}+\emptyset_{2\omega_3}]A_{\omega_1}^2A_{\omega_3}g_3+\\
&6\cos[\omega_1-\omega_2-\omega_3]A_{\omega_1}A_{\omega_2}A_{\omega_3}g_3+\\
&6\cos[\omega_1+\omega_2-\omega_3]A_{\omega_1}A_{\omega_2}A_{\omega_3}g_3+\\
&6\cos[\omega_1-\omega_2+\omega_3]A_{\omega_1}A_{\omega_2}A_{\omega_3}g_3+\\
&6\cos[\omega_1+\omega_2+\omega_3]A_{\omega_1}A_{\omega_2}A_{\omega_3}g_3+\\
&6\cos[2\omega_1-\omega_2-\omega_3+\emptyset_{2\omega_1}]A_{\omega_1}A_{\omega_2}A_{\omega_3}g_3+\\
&6\cos[2\omega_1+\omega_2-\omega_3+\emptyset_{2\omega_1}]A_{\omega_1}A_{\omega_2}A_{\omega_3}g_3+\\
&6\cos[2\omega_1-\omega_2+\omega_3+\emptyset_{2\omega_1}]A_{\omega_1}A_{\omega_2}A_{\omega_3}g_3+\\
&6\cos[2\omega_1+\omega_2+\omega_3+\emptyset_{2\omega_1}]A_{\omega_1}A_{\omega_2}A_{\omega_3}g_3+\\
&6\cos[\omega_1-2\omega_2-\omega_3-\emptyset_{2\omega_2}]A_{\omega_1}A_{\omega_2}A_{\omega_3}g_3+\\
&6\cos[\omega_1-2\omega_2+\omega_3-\emptyset_{2\omega_2}]A_{\omega_1}A_{\omega_2}A_{\omega_3}g_3+\\
&6\cos[2\omega_1-2\omega_2-\omega_3+\emptyset_{2\omega_1}-\emptyset_{2\omega_2}]A_{\omega_1}A_{\omega_2}A_{\omega_3}g_3+\\
&6\cos[2\omega_1-2\omega_2+\omega_3+\emptyset_{2\omega_1}-\emptyset_{2\omega_2}]A_{\omega_1}A_{\omega_2}A_{\omega_3}g_3+\\
&6\cos[\omega_1+2\omega_2-\omega_3+\emptyset_{2\omega_2}]A_{\omega_1}A_{\omega_2}A_{\omega_3}g_3+\\
&6\cos[\omega_1+2\omega_2+\omega_3+\emptyset_{2\omega_2}]A_{\omega_1}A_{\omega_2}A_{\omega_3}g_3+
\end{aligned}
$$

$$
\begin{aligned}
&6\cos[2\omega_1+2\omega_2-\omega_3+\emptyset_{2\omega_1}+\emptyset_{2\omega_2}]A_{\omega_1}A_{\omega_2}A_{\omega_3}g_3+\\
&6\cos[2\omega_1+2\omega_2+\omega_3+\emptyset_{2\omega_1}+\emptyset_{2\omega_2}]A_{\omega_1}A_{\omega_2}A_{\omega_3}g_3+\\
&6\cos[\omega_1-\omega_2-2\omega_3-\emptyset_{2\omega_3}]A_{\omega_1}A_{\omega_2}A_{\omega_3}g_3+\\
&6\cos[\omega_1+\omega_2-2\omega_3-\emptyset_{2\omega_3}]A_{\omega_1}A_{\omega_2}A_{\omega_3}g_3+\\
&6\cos[2\omega_1-\omega_2-2\omega_3+\emptyset_{2\omega_1}-\emptyset_{2\omega_3}]A_{\omega_1}A_{\omega_2}A_{\omega_3}g_3+\\
&6\cos[2\omega_1+\omega_2-2\omega_3+\emptyset_{2\omega_1}-\emptyset_{2\omega_3}]A_{\omega_1}A_{\omega_2}A_{\omega_3}g_3+\\
&6\cos[\omega_1-2\omega_2-2\omega_3-\emptyset_{2\omega_2}-\emptyset_{2\omega_3}]A_{\omega_1}A_{\omega_2}A_{\omega_3}g_3+\\
&6\cos[2\omega_1-2\omega_2-2\omega_3+\emptyset_{2\omega_1}-\emptyset_{2\omega_2}-\emptyset_{2\omega_3}]A_{\omega_1}A_{\omega_2}A_{\omega_3}g_3+\\
&6\cos[\omega_1+2\omega_2-2\omega_3+\emptyset_{2\omega_2}-\emptyset_{2\omega_3}]A_{\omega_1}A_{\omega_2}A_{\omega_3}g_3+\\
&6\cos[2\omega_1+2\omega_2-2\omega_3+\emptyset_{2\omega_1}+\emptyset_{2\omega_2}-\emptyset_{2\omega_3}]A_{\omega_1}A_{\omega_2}A_{\omega_3}g_3+\\
&6\cos[\omega_1-\omega_2+2\omega_3+\emptyset_{2\omega_3}]A_{\omega_1}A_{\omega_2}A_{\omega_3}g_3+\\
&6\cos[\omega_1+\omega_2+2\omega_3+\emptyset_{2\omega_3}]A_{\omega_1}A_{\omega_2}A_{\omega_3}g_3+\\
&6\cos[2\omega_1-\omega_2+2\omega_3+\emptyset_{2\omega_1}+\emptyset_{2\omega_3}]A_{\omega_1}A_{\omega_2}A_{\omega_3}g_3+\\
&6\cos[2\omega_1+\omega_2+2\omega_3+\emptyset_{2\omega_1}+\emptyset_{2\omega_3}]A_{\omega_1}A_{\omega_2}A_{\omega_3}g_3+\\
&6\cos[\omega_1-2\omega_2+2\omega_3-\emptyset_{2\omega_2}+\emptyset_{2\omega_3}]A_{\omega_1}A_{\omega_2}A_{\omega_3}g_3+\\
&6\cos[2\omega_1-2\omega_2+2\omega_3+\emptyset_{2\omega_1}-\emptyset_{2\omega_2}+\emptyset_{2\omega_3}]A_{\omega_1}A_{\omega_2}A_{\omega_3}g_3+\\
&6\cos[\omega_1+2\omega_2+2\omega_3+\emptyset_{2\omega_2}+\emptyset_{2\omega_3}]A_{\omega_1}A_{\omega_2}A_{\omega_3}g_3+\\
&6\cos[2\omega_1+2\omega_2+2\omega_3+\emptyset_{2\omega_1}+\emptyset_{2\omega_2}+\emptyset_{2\omega_3}]A_{\omega_1}A_{\omega_2}A_{\omega_3}g_3+\\
&3\cos[2\omega_2-\omega_3]A_{\omega_2}^2A_{\omega_3}g_3+12\cos[\omega_3]A_{\omega_2}^2A_{\omega_3}g_3+\\
&3\cos[2\omega_2+\omega_3]A_{\omega_2}^2A_{\omega_3}g_3+6\cos[\omega_2-\omega_3+\emptyset_{2\omega_2}]A_{\omega_2}^2A_{\omega_3}g_3+\\
&6\cos[3\omega_2-\omega_3+\emptyset_{2\omega_2}]A_{\omega_2}^2A_{\omega_3}g_3+\\
&6\cos[\omega_2+\omega_3+\emptyset_{2\omega_2}]A_{\omega_2}^2A_{\omega_3}g_3+\\
&6\cos[3\omega_2+\omega_3+\emptyset_{2\omega_2}]A_{\omega_2}^2A_{\omega_3}g_3+\\
&3\cos[4\omega_2-\omega_3+2\emptyset_{2\omega_2}]A_{\omega_2}^2A_{\omega_3}g_3+\\
&3\cos[4\omega_2+\omega_3+2\emptyset_{2\omega_2}]A_{\omega_2}^2A_{\omega_3}g_3+\\
&3\cos[2\omega_2-2\omega_3-\emptyset_{2\omega_3}]A_{\omega_2}^2A_{\omega_3}g_3+\\
&6\cos[\omega_2-2\omega_3+\emptyset_{2\omega_2}-\emptyset_{2\omega_3}]A_{\omega_2}^2A_{\omega_3}g_3+\\
&6\cos[3\omega_2-2\omega_3+\emptyset_{2\omega_2}-\emptyset_{2\omega_3}]A_{\omega_2}^2A_{\omega_3}g_3+\\
&3\cos[4\omega_2-2\omega_3+2\emptyset_{2\omega_2}-\emptyset_{2\omega_3}]A_{\omega_2}^2A_{\omega_3}g_3+\\
&12\cos[2\omega_3+\emptyset_{2\omega_3}]A_{\omega_2}^2A_{\omega_3}g_3+\\
&3\cos[2\omega_2+2\omega_3+\emptyset_{2\omega_3}]A_{\omega_2}^2A_{\omega_3}g_3+\\
&6\cos[\omega_2+2\omega_3+\emptyset_{2\omega_2}+\emptyset_{2\omega_3}]A_{\omega_2}^2A_{\omega_3}g_3+\\
&6\cos[3\omega_2+2\omega_3+\emptyset_{2\omega_2}+\emptyset_{2\omega_3}]A_{\omega_2}^2A_{\omega_3}g_3+\\
&3\cos[4\omega_2+2\omega_3+2\emptyset_{2\omega_2}+\emptyset_{2\omega_3}]A_{\omega_2}^2A_{\omega_3}g_3+\\
&12\cos[\omega_1]A_{\omega_1}A_{\omega_3}^2g_3+3\cos[\omega_1-2\omega_3]A_{\omega_1}A_{\omega_3}^2g_3+\\
&3\cos[\omega_1+2\omega_3]A_{\omega_1}A_{\omega_3}^2g_3+12\cos[2\omega_1+\emptyset_{2\omega_1}]A_{\omega_1}A_{\omega_3}^2g_3+\\
&3\cos[2\omega_1-2\omega_3+\emptyset_{2\omega_1}]A_{\omega_1}A_{\omega_3}^2g_3+\\
&3\cos[2\omega_1+2\omega_3+\emptyset_{2\omega_1}]A_{\omega_1}A_{\omega_3}^2g_3+\\
&3\cos[\omega_1-4\omega_3-2\emptyset_{2\omega_3}]A_{\omega_1}A_{\omega_3}^2g_3+\\
&3\cos[2\omega_1-4\omega_3+\emptyset_{2\omega_1}-2\emptyset_{2\omega_3}]A_{\omega_1}A_{\omega_3}^2g_3+\\
&6\cos[\omega_1-3\omega_3-\emptyset_{2\omega_3}]A_{\omega_1}A_{\omega_3}^2g_3+\\
&6\cos[\omega_1-\omega_3-\emptyset_{2\omega_3}]A_{\omega_1}A_{\omega_3}^2g_3+\\
&6\cos[2\omega_1-3\omega_3+\emptyset_{2\omega_1}-\emptyset_{2\omega_3}]A_{\omega_1}A_{\omega_3}^2g_3+\\
&6\cos[2\omega_1-\omega_3+\emptyset_{2\omega_1}-\emptyset_{2\omega_3}]A_{\omega_1}A_{\omega_3}^2g_3+\\
&6\cos[\omega_1+\omega_3+\emptyset_{2\omega_3}]A_{\omega_1}A_{\omega_3}^2g_3+\\
&6\cos[\omega_1+3\omega_3+\emptyset_{2\omega_3}]A_{\omega_1}A_{\omega_3}^2g_3+\\
&6\cos[2\omega_1+\omega_3+\emptyset_{2\omega_1}+\emptyset_{2\omega_3}]A_{\omega_1}A_{\omega_3}^2g_3+\\
&6\cos[2\omega_1+3\omega_3+\emptyset_{2\omega_1}+\emptyset_{2\omega_3}]A_{\omega_1}A_{\omega_3}^2g_3+\\
&3\cos[\omega_1+4\omega_3+2\emptyset_{2\omega_3}]A_{\omega_1}A_{\omega_3}^2g_3+\\
&3\cos[2\omega_1+4\omega_3+\emptyset_{2\omega_1}+2\emptyset_{2\omega_3}]A_{\omega_1}A_{\omega_3}^2g_3+\\
&12\cos[\omega_2]A_{\omega_2}A_{\omega_3}^2g_3+3\cos[\omega_2-2\omega_3]A_{\omega_2}A_{\omega_3}^2g_3+\\
&3\cos[\omega_2+2\omega_3]A_{\omega_2}A_{\omega_3}^2g_3+12\cos[2\omega_2+\emptyset_{2\omega_2}]A_{\omega_2}A_{\omega_3}^2g_3+\\
&3\cos[2\omega_2-2\omega_3+\emptyset_{2\omega_2}]A_{\omega_2}A_{\omega_3}^2g_3+
\end{aligned}
$$

$$
\begin{aligned}
&3\cos[2\omega_2+2\omega_3+\emptyset_{2\omega_2}]A_{\omega_2}A_{\omega_3}^2g_3+\\
&3\cos[\omega_2-4\omega_3-2\emptyset_{2\omega_3}]A_{\omega_2}A_{\omega_3}^2g_3+\\
&3\cos[2\omega_2-4\omega_3+\emptyset_{2\omega_2}-2\emptyset_{2\omega_3}]A_{\omega_2}A_{\omega_3}^2g_3+\\
&6\cos[\omega_2-3\omega_3-\emptyset_{2\omega_3}]A_{\omega_2}A_{\omega_3}^2g_3+\\
&6\cos[\omega_2-\omega_3-\emptyset_{2\omega_3}]A_{\omega_2}A_{\omega_3}^2g_3+\\
&6\cos[2\omega_2-3\omega_3+\emptyset_{2\omega_2}-\emptyset_{2\omega_3}]A_{\omega_2}A_{\omega_3}^2g_3+\\
&6\cos[2\omega_2-\omega_3+\emptyset_{2\omega_2}-\emptyset_{2\omega_3}]A_{\omega_2}A_{\omega_3}^2g_3+\\
&6\cos[\omega_2+\omega_3+\emptyset_{2\omega_3}]A_{\omega_2}A_{\omega_3}^2g_3+\\
&6\cos[\omega_2+3\omega_3+\emptyset_{2\omega_3}]A_{\omega_2}A_{\omega_3}^2g_3+\\
&6\cos[2\omega_2+\omega_3+\emptyset_{2\omega_2}+\emptyset_{2\omega_3}]A_{\omega_2}A_{\omega_3}^2g_3+\\
&6\cos[2\omega_2+3\omega_3+\emptyset_{2\omega_2}+\emptyset_{2\omega_3}]A_{\omega_2}A_{\omega_3}^2g_3+\\
&3\cos[\omega_2+4\omega_3+2\emptyset_{2\omega_3}]A_{\omega_2}A_{\omega_3}^2g_3+\\
&3\cos[2\omega_2+4\omega_3+\emptyset_{2\omega_2}+2\emptyset_{2\omega_3}]A_{\omega_2}A_{\omega_3}^2g_3+9\cos[\omega_3]A_{\omega_3}^3g_3+\\
&\cos[3\omega_3]A_{\omega_3}^3g_3+3\cos[\emptyset_{2\omega_3}]A_{\omega_3}^3g_3+9\cos[2\omega_3+\emptyset_{2\omega_3}]A_{\omega_3}^3g_3+\\
&3\cos[4\omega_3+\emptyset_{2\omega_3}]A_{\omega_3}^3g_3+3\cos[3\omega_3+2\emptyset_{2\omega_3}]A_{\omega_3}^3g_3+\\
&3\cos[5\omega_3+2\emptyset_{2\omega_3}]A_{\omega_3}^3g_3+\cos[6\omega_3+3\emptyset_{2\omega_3}]A_{\omega_3}^3g_3)
\end{aligned}
$$

2.4 Power Series Analysis of a Three-Tone System with Injected Difference Frequency Signals

The system input is made of two sinusoid signals at the frequencies $\omega 1$, $\omega 2$ and $\omega 3$ with amplitudes $A\omega 1$, $A\omega 2$ and $A\omega 3$ respectively and the difference frequency signals at the frequencies $(\omega_2 - \omega_1)$, $(\omega_3 - \omega_1)$ and $(\omega_3 - \omega_2)$ with amplitudes $A\omega_{21}$, $A\omega_{31}$ and $A\omega_{32}$ with phases $\phi\omega_{21}$, $\phi\omega_{31}$ and $\phi\omega_{32}$ respectively.

The input is

$$v_{in} = A_{\omega_1}\cos(\omega_1 t) + A_{\omega_2}\cos(\omega_2 t) + A_{\omega_3}\cos(\omega_3 t) + A\omega_{21}\cos(\omega_2 - \omega_1 t + \phi\omega_{21})$$
$$+A\omega_{21}\cos(\omega_2 - \omega_1 t + \phi\omega_{21}) + A\omega_{21}\cos(\omega_3 - \omega_1 t + \phi\omega_{21}) \tag{2.47}$$

The amplifier output spectrum is calculated by using a power series expansion, such that

$$V_{out} = \sum_{n=1}^{3} g_{mn} v_{in}^n$$
$$= \sum_{n=1}^{3} g_{mn}\left[\begin{array}{c} A_{\omega_1}\cos(\omega_1 t) + A_{\omega_2}\cos(\omega_2 t) + A_{\omega_3}\cos(\omega_3 t) + A\omega_{21}\cos(\omega_2 - \omega_1 t + \phi\omega_{21}) \\ +A\omega_{31}\cos(\omega_3 - \omega_1 t + \phi\omega_{31}) + A\omega_{32}\cos(\omega - \omega_2 t + \phi\omega_{32}) \end{array}\right]^n \tag{2.48}$$

The following is the input file and the output file calculation using Mathematica®

showing all intermodulation terms at the output of the amplifier with the injection of difference frequency signals.

• **Input file**

$x1 = (A_{\omega_{21}} \cos[\omega_2 - \omega_1 + \emptyset_{21}]) +$
$(A_{\omega_{31}} \cos[\omega_3 - \omega_1 + \emptyset_{31}]) + (A_{\omega_{32}} \cos[\omega_3 - \omega_2 + \emptyset_{32}]);$

$x2 = \sum_{k=1}^{3} (A_{\omega_k} \cos[\omega_k]);$

$Y = \sum_{n=0}^{3} (g_n (x1 + x2)^n);$

TrigReduce[Y]
TeXSave["dif.tex"]

• **Ouput file**

$V_{out} = \frac{1}{4}(4g_0 + 4\cos[\omega_1]A_{\omega_1}g_1 + 4\cos[\omega_2]A_{\omega_2}g_1 + 4\cos[\omega_3]A_{\omega_3}g_1 +$
$4\cos[\omega_1 - \omega_2 - \emptyset_{21}]A_{\omega_{21}}g_1 + 4\cos[\omega_1 - \omega_3 - \emptyset_{31}]A_{\omega_{31}}g_1 +$
$4\cos[\omega_2 - \omega_3 - \emptyset_{32}]A_{\omega_{32}}g_1 + 2A^2_{\omega_1}g_2 + 2\cos[2\omega_1]A^2_{\omega_1}g_2 +$
$4\cos[\omega_1 - \omega_2]A_{\omega_1}A_{\omega_2}g_2 + 4\cos[\omega_1 + \omega_2]A_{\omega_1}A_{\omega_2}g_2 +$
$2A^2_{\omega_2}g_2 + 2\cos[2\omega_2]A^2_{\omega_2}g_2 + 4\cos[\omega_1 - \omega_3]A_{\omega_1}A_{\omega_3}g_2 +$
$4\cos[\omega_1 + \omega_3]A_{\omega_1}A_{\omega_3}g_2 + 4\cos[\omega_2 - \omega_3]A_{\omega_2}A_{\omega_3}g_2 +$
$4\cos[\omega_2 + \omega_3]A_{\omega_2}A_{\omega_3}g_2 + 2A^2_{\omega_3}g_2 + 2\cos[2\omega_3]A^2_{\omega_3}g_2 +$
$4\cos[2\omega_1 - \omega_2 - \emptyset_{21}]A_{\omega_1}A_{\omega_{21}}g_2 + 4\cos[\omega_2 + \emptyset_{21}]A_{\omega_1}A_{\omega_{21}}g_2 +$
$4\cos[\omega_1 - \emptyset_{21}]A_{\omega_2}A_{\omega_{21}}g_2 + 4\cos[\omega_1 - 2\omega_2 - \emptyset_{21}]A_{\omega_2}A_{\omega_{21}}g_2 +$
$4\cos[\omega_1 - \omega_2 - \omega_3 - \emptyset_{21}]A_{\omega_3}A_{\omega_{21}}g_2 +$
$4\cos[\omega_1 - \omega_2 + \omega_3 - \emptyset_{21}]A_{\omega_3}A_{\omega_{21}}g_2 +$
$2A^2_{\omega_{21}}g_2 + 2\cos[2\omega_1 - 2\omega_2 - 2\emptyset_{21}]A^2_{\omega_{21}}g_2 +$
$4\cos[2\omega_1 - \omega_3 - \emptyset_{31}]A_{\omega_1}A_{\omega_{31}}g_2 +$
$4\cos[\omega_3 + \emptyset_{31}]A_{\omega_1}A_{\omega_{31}}g_2 + 4\cos[\omega_1 - \omega_2 - \omega_3 - \emptyset_{31}]A_{\omega_2}A_{\omega_{31}}g_2 +$
$4\cos[\omega_1 + \omega_2 - \omega_3 - \emptyset_{31}]A_{\omega_2}A_{\omega_{31}}g_2 +$
$4\cos[\omega_1 - \emptyset_{31}]A_{\omega_3}A_{\omega_{31}}g_2 + 4\cos[\omega_1 - 2\omega_3 - \emptyset_{31}]A_{\omega_3}A_{\omega_{31}}g_2 +$
$4\cos[2\omega_1 - \omega_2 - \omega_3 - \emptyset_{21} - \emptyset_{31}]A_{\omega_{21}}A_{\omega_{31}}g_2 +$
$4\cos[\omega_2 - \omega_3 + \emptyset_{21} - \emptyset_{31}]A_{\omega_{21}}A_{\omega_{31}}g_2 +$
$2A^2_{\omega_{31}}g_2 + 2\cos[2\omega_1 - 2\omega_3 - 2\emptyset_{31}]A^2_{\omega_{31}}g_2 +$
$4\cos[\omega_1 + \omega_2 - \omega_3 - \emptyset_{32}]A_{\omega_1}A_{\omega_{32}}g_2 +$
$4\cos[\omega_1 - \omega_2 + \omega_3 + \emptyset_{32}]A_{\omega_1}A_{\omega_{32}}g_2 +$
$4\cos[2\omega_2 - \omega_3 - \emptyset_{32}]A_{\omega_2}A_{\omega_{32}}g_2 + 4\cos[\omega_3 + \emptyset_{32}]A_{\omega_2}A_{\omega_{32}}g_2 +$
$4\cos[\omega_2 - \emptyset_{32}]A_{\omega_3}A_{\omega_{32}}g_2 + 4\cos[\omega_2 - 2\omega_3 - \emptyset_{32}]A_{\omega_3}A_{\omega_{32}}g_2 +$
$4\cos[\omega_1 - \omega_3 - \emptyset_{21} - \emptyset_{32}]A_{\omega_{21}}A_{\omega_{32}}g_2 +$
$4\cos[\omega_1 - 2\omega_2 + \omega_3 - \emptyset_{21} + \emptyset_{32}]A_{\omega_{21}}A_{\omega_{32}}g_2 +$
$4\cos[\omega_1 + \omega_2 - 2\omega_3 - \emptyset_{31} - \emptyset_{32}]A_{\omega_{31}}A_{\omega_{32}}g_2 +$
$4\cos[\omega_1 - \omega_2 - \emptyset_{31} + \emptyset_{32}]A_{\omega_{31}}A_{\omega_{32}}g_2 +$
$2A^2_{\omega_{32}}g_2 + 2\cos[2\omega_2 - 2\omega_3 - 2\emptyset_{32}]A^2_{\omega_{32}}g_2 +$
$3\cos[\omega_1]A^3_{\omega_1}g_3 + \cos[3\omega_1]A^3_{\omega_1}g_3 + 3\cos[2\omega_1 - \omega_2]A^2_{\omega_1}A_{\omega_2}g_3 +$
$6\cos[\omega_2]A^2_{\omega_1}A_{\omega_2}g_3 + 3\cos[2\omega_1 + \omega_2]A^2_{\omega_1}A_{\omega_2}g_3 +$
$6\cos[\omega_1]A_{\omega_1}A^2_{\omega_2}g_3 + 3\cos[\omega_1 - 2\omega_2]A_{\omega_1}A^2_{\omega_2}g_3 +$
$3\cos[\omega_1 + 2\omega_2]A_{\omega_1}A^2_{\omega_2}g_3 + 3\cos[\omega_2]A^3_{\omega_2}g_3 + \cos[3\omega_2]A^3_{\omega_2}g_3 +$
$3\cos[2\omega_1 - \omega_3]A^2_{\omega_1}A_{\omega_3}g_3 + 6\cos[\omega_3]A^2_{\omega_1}A_{\omega_3}g_3 +$
$3\cos[2\omega_1 + \omega_3]A^2_{\omega_1}A_{\omega_3}g_3 + 6\cos[\omega_1 - \omega_2 - \omega_3]A_{\omega_1}A_{\omega_2}A_{\omega_3}g_3 +$
$6\cos[\omega_1 + \omega_2 - \omega_3]A_{\omega_1}A_{\omega_2}A_{\omega_3}g_3 +$
$6\cos[\omega_1 - \omega_2 + \omega_3]A_{\omega_1}A_{\omega_2}A_{\omega_3}g_3 +$
$6\cos[\omega_1 + \omega_2 + \omega_3]A_{\omega_1}A_{\omega_2}A_{\omega_3}g_3 +$
$3\cos[2\omega_2 - \omega_3]A^2_{\omega_2}A_{\omega_3}g_3 + 6\cos[\omega_3]A^2_{\omega_2}A_{\omega_3}g_3 +$
$3\cos[2\omega_2 + \omega_3]A^2_{\omega_2}A_{\omega_3}g_3 + 6\cos[\omega_1]A_{\omega_1}A^2_{\omega_3}g_3 +$
$3\cos[\omega_1 - 2\omega_3]A_{\omega_1}A^2_{\omega_3}g_3 + 3\cos[\omega_1 + 2\omega_3]A_{\omega_1}A^2_{\omega_3}g_3 +$
$6\cos[\omega_2]A_{\omega_2}A^2_{\omega_3}g_3 + 3\cos[\omega_2 - 2\omega_3]A_{\omega_2}A^2_{\omega_3}g_3 +$
$3\cos[\omega_2 + 2\omega_3]A_{\omega_2}A^2_{\omega_3}g_3 + 3\cos[\omega_3]A^3_{\omega_3}g_3 +$
$\cos[3\omega_3]A^3_{\omega_3}g_3 + 6\cos[\omega_1 - \omega_2 - \emptyset_{21}]A^2_{\omega_1}A_{\omega_{21}}g_3 +$
$3\cos[3\omega_1 - \omega_2 - \emptyset_{21}]A^2_{\omega_1}A_{\omega_{21}}g_3 +$

$$3\cos[\omega_1+\omega_2+\emptyset_{21}]A_{\omega_1}^2A_{\omega_{21}}g_3+6\cos[2\omega_1-\emptyset_{21}]A_{\omega_1}A_{\omega_2}A_{\omega_{21}}g_3+$$
$$6\cos[2\omega_1-2\omega_2-\emptyset_{21}]A_{\omega_1}A_{\omega_2}A_{\omega_{21}}g_3+$$
$$6\cos[\emptyset_{21}]A_{\omega_1}A_{\omega_2}A_{\omega_{21}}g_3+6\cos[2\omega_2+\emptyset_{21}]A_{\omega_1}A_{\omega_2}A_{\omega_{21}}g_3+$$
$$3\cos[\omega_1-3\omega_2-\emptyset_{21}]A_{\omega_2}^2A_{\omega_{21}}g_3+$$
$$6\cos[\omega_1-\omega_2-\emptyset_{21}]A_{\omega_2}^2A_{\omega_{21}}g_3+3\cos[\omega_1+\omega_2-\emptyset_{21}]A_{\omega_2}^2A_{\omega_{21}}g_3+$$
$$6\cos[2\omega_1-\omega_2-\omega_3-\emptyset_{21}]A_{\omega_1}A_{\omega_3}A_{\omega_{21}}g_3+$$
$$6\cos[2\omega_1-\omega_2+\omega_3-\emptyset_{21}]A_{\omega_1}A_{\omega_3}A_{\omega_{21}}g_3+$$
$$6\cos[\omega_2-\omega_3+\emptyset_{21}]A_{\omega_1}A_{\omega_3}A_{\omega_{21}}g_3+$$
$$6\cos[\omega_2+\omega_3+\emptyset_{21}]A_{\omega_1}A_{\omega_3}A_{\omega_{21}}g_3+$$
$$6\cos[\omega_1-\omega_3-\emptyset_{21}]A_{\omega_2}A_{\omega_3}A_{\omega_{21}}g_3+$$
$$6\cos[\omega_1-2\omega_2-\omega_3-\emptyset_{21}]A_{\omega_2}A_{\omega_3}A_{\omega_{21}}g_3+$$
$$6\cos[\omega_1+\omega_3-\emptyset_{21}]A_{\omega_2}A_{\omega_3}A_{\omega_{21}}g_3+6\cos[\omega_1-2\omega_2+\omega_3-\emptyset_{21}]$$
$$A_{\omega_2}A_{\omega_3}A_{\omega_{21}}g_3+6\cos[\omega_1-\omega_2-\emptyset_{21}]A_{\omega_3}^2A_{\omega_{21}}g_3+$$
$$3\cos[\omega_1-\omega_2-2\omega_3-\emptyset_{21}]A_{\omega_3}^2A_{\omega_{21}}g_3+$$
$$3\cos[\omega_1-\omega_2+2\omega_3-\emptyset_{21}]A_{\omega_3}^2A_{\omega_{21}}g_3+$$
$$6\cos[\omega_1]A_{\omega_1}A_{\omega_{21}}^2g_3+3\cos[\omega_1-2\omega_2-2\emptyset_{21}]A_{\omega_1}A_{\omega_{21}}^2g_3+$$
$$3\cos[3\omega_1-2\omega_2-2\emptyset_{21}]A_{\omega_1}A_{\omega_{21}}^2g_3+$$
$$6\cos[\omega_2]A_{\omega_2}A_{\omega_{21}}^2g_3+3\cos[2\omega_1-3\omega_2-2\emptyset_{21}]A_{\omega_2}A_{\omega_{21}}^2g_3+$$
$$3\cos[2\omega_1-\omega_2-2\emptyset_{21}]A_{\omega_2}A_{\omega_{21}}^2g_3+$$
$$6\cos[\omega_3]A_{\omega_3}A_{\omega_{21}}^2g_3+3\cos[2\omega_1-2\omega_2-\omega_3-2\emptyset_{21}]A_{\omega_3}A_{\omega_{21}}^2g_3+$$
$$3\cos[2\omega_1-2\omega_2+\omega_3-2\emptyset_{21}]A_{\omega_3}A_{\omega_{21}}^2g_3+$$
$$\cos[3\omega_1-3\omega_2-3\emptyset_{21}]A_{\omega_{21}}^3g_3+$$
$$3\cos[\omega_1-\omega_2-\emptyset_{21}]A_{\omega_{21}}^3g_3+6\cos[\omega_1-\omega_3-\emptyset_{31}]A_{\omega_1}^2A_{\omega_{31}}g_3+$$
$$3\cos[3\omega_1-\omega_3-\emptyset_{31}]A_{\omega_1}^2A_{\omega_{31}}g_3+$$
$$3\cos[\omega_1+\omega_3+\emptyset_{31}]A_{\omega_1}^2A_{\omega_{31}}g_3+$$
$$6\cos[2\omega_1-\omega_2-\omega_3-\emptyset_{31}]A_{\omega_1}A_{\omega_2}A_{\omega_{31}}g_3+$$
$$6\cos[\omega_2-\omega_3-\emptyset_{31}]A_{\omega_1}A_{\omega_2}A_{\omega_{31}}g_3+$$
$$6\cos[2\omega_1+\omega_2-\omega_3-\emptyset_{31}]A_{\omega_1}A_{\omega_2}A_{\omega_{31}}g_3+6\cos[\omega_2+\omega_3+\emptyset_{31}]$$
$$A_{\omega_1}A_{\omega_2}A_{\omega_{31}}g_3+6\cos[\omega_1-\omega_3-\emptyset_{31}]A_{\omega_2}^2A_{\omega_{31}}g_3+$$
$$3\cos[\omega_1-2\omega_2-\omega_3-\emptyset_{31}]A_{\omega_2}^2A_{\omega_{31}}g_3+$$
$$3\cos[\omega_1+2\omega_2-\omega_3-\emptyset_{31}]A_{\omega_2}^2A_{\omega_{31}}g_3+$$
$$6\cos[2\omega_1-\emptyset_{31}]A_{\omega_1}A_{\omega_3}A_{\omega_{31}}g_3+$$
$$6\cos[2\omega_1-2\omega_3-\emptyset_{31}]A_{\omega_1}A_{\omega_3}A_{\omega_{31}}g_3+$$
$$6\cos[\emptyset_{31}]A_{\omega_1}A_{\omega_3}A_{\omega_{31}}g_3+6\cos[2\omega_3+\emptyset_{31}]A_{\omega_1}A_{\omega_3}A_{\omega_{31}}g_3+$$
$$6\cos[\omega_1-\omega_2-\emptyset_{31}]A_{\omega_2}A_{\omega_3}A_{\omega_{31}}g_3+$$
$$6\cos[\omega_1+\omega_2-\emptyset_{31}]A_{\omega_2}A_{\omega_3}A_{\omega_{31}}g_3+$$
$$6\cos[\omega_1-\omega_2-2\omega_3-\emptyset_{31}]A_{\omega_2}A_{\omega_3}A_{\omega_{31}}g_3+$$
$$6\cos[\omega_1+\omega_2-2\omega_3-\emptyset_{31}]A_{\omega_2}A_{\omega_3}A_{\omega_{31}}g_3+$$
$$3\cos[\omega_1-3\omega_3-\emptyset_{31}]A_{\omega_3}^2A_{\omega_{31}}g_3+$$
$$6\cos[\omega_1-\omega_3-\emptyset_{31}]A_{\omega_3}^2A_{\omega_{31}}g_3+3\cos[\omega_1+\omega_3-\emptyset_{31}]A_{\omega_3}^2A_{\omega_{31}}g_3+$$
$$6\cos[\omega_1-\omega_2-\omega_3-\emptyset_{21}-\emptyset_{31}]A_{\omega_1}A_{\omega_{21}}A_{\omega_{31}}g_3+$$
$$6\cos[3\omega_1-\omega_2-\omega_3-\emptyset_{21}-\emptyset_{31}]A_{\omega_1}A_{\omega_{21}}A_{\omega_{31}}g_3+$$
$$6\cos[\omega_1+\omega_2-\omega_3+\emptyset_{21}-\emptyset_{31}]A_{\omega_1}A_{\omega_{21}}A_{\omega_{31}}g_3+$$
$$6\cos[\omega_1-\omega_2+\omega_3-\emptyset_{21}+\emptyset_{31}]A_{\omega_1}A_{\omega_{21}}A_{\omega_{31}}g_3+$$
$$6\cos[2\omega_1-\omega_3-\emptyset_{21}-\emptyset_{31}]A_{\omega_2}A_{\omega_{21}}A_{\omega_{31}}g_3+$$
$$6\cos[2\omega_1-2\omega_2-\omega_3-\emptyset_{21}-\emptyset_{31}]A_{\omega_2}A_{\omega_{21}}A_{\omega_{31}}g_3+$$
$$6\cos[2\omega_2-\omega_3+\emptyset_{21}-\emptyset_{31}]A_{\omega_2}A_{\omega_{21}}A_{\omega_{31}}g_3+$$
$$6\cos[\omega_3-\emptyset_{21}+\emptyset_{31}]A_{\omega_2}A_{\omega_{21}}A_{\omega_{31}}g_3+$$
$$6\cos[2\omega_1-\omega_2-\emptyset_{21}-\emptyset_{31}]A_{\omega_3}A_{\omega_{21}}A_{\omega_{31}}g_3+$$
$$6\cos[2\omega_1-\omega_2-2\omega_3-\emptyset_{21}-\emptyset_{31}]A_{\omega_3}A_{\omega_{21}}A_{\omega_{31}}g_3+$$
$$6\cos[\omega_2+\emptyset_{21}-\emptyset_{31}]A_{\omega_3}A_{\omega_{21}}A_{\omega_{31}}g_3+6\cos[\omega_2-2\omega_3+\emptyset_{21}-\emptyset_{31}]$$
$$A_{\omega_3}A_{\omega_{21}}A_{\omega_{31}}g_3+6\cos[\omega_1-\omega_3-\emptyset_{31}]A_{\omega_{21}}^2A_{\omega_{31}}g_3+$$
$$3\cos[3\omega_1-2\omega_2-\omega_3-2\emptyset_{21}-\emptyset_{31}]A_{\omega_{21}}^2A_{\omega_{31}}g_3+$$
$$3\cos[\omega_1-2\omega_2+\omega_3-2\emptyset_{21}+\emptyset_{31}]A_{\omega_{21}}^2A_{\omega_{31}}g_3+$$
$$6\cos[\omega_1]A_{\omega_1}A_{\omega_{31}}^2g_3+3\cos[\omega_1-2\omega_3-2\emptyset_{31}]A_{\omega_1}A_{\omega_{31}}^2g_3+$$

$$
\begin{aligned}
&3\cos[3\omega_1 - 2\omega_3 - 2\emptyset_{31}]A_{\omega_1}A_{\omega_{31}}^2 g_3 + \\
&6\cos[\omega_2]A_{\omega_2}A_{\omega_{31}}^2 g_3 + 3\cos[2\omega_1 - \omega_2 - 2\omega_3 - 2\emptyset_{31}]A_{\omega_2}A_{\omega_{31}}^2 g_3 + \\
&3\cos[2\omega_1 + \omega_2 - 2\omega_3 - 2\emptyset_{31}]A_{\omega_2}A_{\omega_{31}}^2 g_3 + \\
&6\cos[\omega_3]A_{\omega_3}A_{\omega_{31}}^2 g_3 + 3\cos[2\omega_1 - 3\omega_3 - 2\emptyset_{31}]A_{\omega_3}A_{\omega_{31}}^2 g_3 + \\
&3\cos[2\omega_1 - \omega_3 - 2\emptyset_{31}]A_{\omega_3}A_{\omega_{31}}^2 g_3 + \\
&6\cos[\omega_1 - \omega_2 - \emptyset_{21}]A_{\omega_{21}}A_{\omega_{31}}^2 g_3 + \\
&3\cos[3\omega_1 - \omega_2 - 2\omega_3 - \emptyset_{21} - 2\emptyset_{31}]A_{\omega_{21}}A_{\omega_{31}}^2 g_3 + \\
&3\cos[\omega_1 + \omega_2 - 2\omega_3 + \emptyset_{21} - 2\emptyset_{31}]A_{\omega_{21}}A_{\omega_{31}}^2 g_3 + \\
&\cos[3\omega_1 - 3\omega_3 - 3\emptyset_{31}]A_{\omega_{31}}^3 g_3 + \\
&3\cos[\omega_1 - \omega_3 - \emptyset_{31}]A_{\omega_{31}}^3 g_3 + 6\cos[\omega_2 - \omega_3 - \emptyset_{32}]A_{\omega_1}^2 A_{\omega_{32}} g_3 + \\
&3\cos[2\omega_1 + \omega_2 - \omega_3 - \emptyset_{32}]A_{\omega_1}^2 A_{\omega_{32}} g_3 + \\
&3\cos[2\omega_1 - \omega_2 + \omega_3 + \emptyset_{32}]A_{\omega_1}^2 A_{\omega_{32}} g_3 + \\
&6\cos[\omega_1 - \omega_3 - \emptyset_{32}]A_{\omega_1}A_{\omega_2}A_{\omega_{32}} g_3 + \\
&6\cos[\omega_1 + 2\omega_2 - \omega_3 - \emptyset_{32}]A_{\omega_1}A_{\omega_2}A_{\omega_{32}} g_3 + \\
&6\cos[\omega_1 + \omega_3 + \emptyset_{32}]A_{\omega_1}A_{\omega_2}A_{\omega_{32}} g_3 + 6\cos[\omega_1 - 2\omega_2 + \omega_3 + \emptyset_{32}] \\
&A_{\omega_1}A_{\omega_2}A_{\omega_{32}} g_3 + 6\cos[\omega_2 - \omega_3 - \emptyset_{32}]A_{\omega_2}^2 A_{\omega_{32}} g_3 + \\
&3\cos[3\omega_2 - \omega_3 - \emptyset_{32}]A_{\omega_2}^2 A_{\omega_{32}} g_3 + \\
&3\cos[\omega_2 + \omega_3 + \emptyset_{32}]A_{\omega_2}^2 A_{\omega_{32}} g_3 + \\
&6\cos[\omega_1 + \omega_2 - \emptyset_{32}]A_{\omega_1}A_{\omega_3}A_{\omega_{32}} g_3 + \\
&6\cos[\omega_1 + \omega_2 - 2\omega_3 - \emptyset_{32}]A_{\omega_1}A_{\omega_3}A_{\omega_{32}} g_3 + \\
&6\cos[\omega_1 - \omega_2 + \emptyset_{32}]A_{\omega_1}A_{\omega_3}A_{\omega_{32}} g_3 + \\
&6\cos[\omega_1 - \omega_2 + 2\omega_3 + \emptyset_{32}]A_{\omega_1}A_{\omega_3}A_{\omega_{32}} g_3 + \\
&6\cos[2\omega_2 - \emptyset_{32}]A_{\omega_2}A_{\omega_3}A_{\omega_{32}} g_3 + \\
&6\cos[2\omega_2 - 2\omega_3 - \emptyset_{32}]A_{\omega_2}A_{\omega_3}A_{\omega_{32}} g_3 + \\
&6\cos[\emptyset_{32}]A_{\omega_2}A_{\omega_3}A_{\omega_{32}} g_3 + 6\cos[2\omega_3 + \emptyset_{32}]A_{\omega_2}A_{\omega_3}A_{\omega_{32}} g_3 + \\
&3\cos[\omega_2 - 3\omega_3 - \emptyset_{32}]A_{\omega_3}^2 A_{\omega_{32}} g_3 + \\
&6\cos[\omega_2 - \omega_3 - \emptyset_{32}]A_{\omega_3}^2 A_{\omega_{32}} g_3 + 3\cos[\omega_2 + \omega_3 - \emptyset_{32}]A_{\omega_3}^2 A_{\omega_{32}} g_3 + \\
&6\cos[2\omega_1 - \omega_3 - \emptyset_{21} - \emptyset_{32}]A_{\omega_1}A_{\omega_{21}}A_{\omega_{32}} g_3 + \\
&6\cos[2\omega_2 - \omega_3 + \emptyset_{21} - \emptyset_{32}]A_{\omega_1}A_{\omega_{21}}A_{\omega_{32}} g_3 + \\
&6\cos[2\omega_1 - 2\omega_2 + \omega_3 - \emptyset_{21} + \emptyset_{32}]A_{\omega_1}A_{\omega_{21}}A_{\omega_{32}} g_3 + \\
&6\cos[\omega_3 + \emptyset_{21} + \emptyset_{32}]A_{\omega_1}A_{\omega_{21}}A_{\omega_{32}} g_3 + \\
&6\cos[\omega_1 - \omega_2 - \omega_3 - \emptyset_{21} - \emptyset_{32}]A_{\omega_2}A_{\omega_{21}}A_{\omega_{32}} g_3 + \\
&6\cos[\omega_1 + \omega_2 - \omega_3 - \emptyset_{21} - \emptyset_{32}]A_{\omega_2}A_{\omega_{21}}A_{\omega_{32}} g_3 + \\
&6\cos[\omega_1 - 3\omega_2 + \omega_3 - \emptyset_{21} + \emptyset_{32}]A_{\omega_2}A_{\omega_{21}}A_{\omega_{32}} g_3 + \\
&6\cos[\omega_1 - \omega_2 + \omega_3 - \emptyset_{21} + \emptyset_{32}]A_{\omega_2}A_{\omega_{21}}A_{\omega_{32}} g_3 + \\
&6\cos[\omega_1 - \emptyset_{21} - \emptyset_{32}]A_{\omega_3}A_{\omega_{21}}A_{\omega_{32}} g_3 + \\
&6\cos[\omega_1 - 2\omega_3 - \emptyset_{21} - \emptyset_{32}]A_{\omega_3}A_{\omega_{21}}A_{\omega_{32}} g_3 + \\
&6\cos[\omega_1 - 2\omega_2 - \emptyset_{21} + \emptyset_{32}]A_{\omega_3}A_{\omega_{21}}A_{\omega_{32}} g_3 + \\
&6\cos[\omega_1 - 2\omega_2 + 2\omega_3 - \emptyset_{21} + \emptyset_{32}]A_{\omega_3}A_{\omega_{21}}A_{\omega_{32}} g_3 + \\
&6\cos[\omega_2 - \omega_3 - \emptyset_{32}]A_{\omega_{21}}^2 A_{\omega_{32}} g_3 + \\
&3\cos[2\omega_1 - \omega_2 - \omega_3 - 2\emptyset_{21} - \emptyset_{32}]A_{\omega_{21}}^2 A_{\omega_{32}} g_3 + \\
&3\cos[2\omega_1 - 3\omega_2 + \omega_3 - 2\emptyset_{21} + \emptyset_{32}]A_{\omega_{21}}^2 A_{\omega_{32}} g_3 + \\
&6\cos[\omega_2 - 2\omega_3 - \emptyset_{31} - \emptyset_{32}]A_{\omega_1}A_{\omega_{31}}A_{\omega_{32}} g_3 + \\
&6\cos[2\omega_1 + \omega_2 - 2\omega_3 - \emptyset_{31} - \emptyset_{32}]A_{\omega_1}A_{\omega_{31}}A_{\omega_{32}} g_3 + \\
&6\cos[\omega_2 + \emptyset_{31} - \emptyset_{32}]A_{\omega_1}A_{\omega_{31}}A_{\omega_{32}} g_3 + \\
&6\cos[2\omega_1 - \omega_2 - \emptyset_{31} + \emptyset_{32}]A_{\omega_1}A_{\omega_{31}}A_{\omega_{32}} g_3 + \\
&6\cos[\omega_1 - 2\omega_3 - \emptyset_{31} - \emptyset_{32}]A_{\omega_2}A_{\omega_{31}}A_{\omega_{32}} g_3 + \\
&6\cos[\omega_1 + 2\omega_2 - 2\omega_3 - \emptyset_{31} - \emptyset_{32}]A_{\omega_2}A_{\omega_{31}}A_{\omega_{32}} g_3 + \\
&6\cos[\omega_1 - \emptyset_{31} + \emptyset_{32}]A_{\omega_2}A_{\omega_{31}}A_{\omega_{32}} g_3 + \\
&6\cos[\omega_1 - 2\omega_2 - \emptyset_{31} + \emptyset_{32}]A_{\omega_2}A_{\omega_{31}}A_{\omega_{32}} g_3 + \\
&6\cos[\omega_1 + \omega_2 - 3\omega_3 - \emptyset_{31} - \emptyset_{32}]A_{\omega_3}A_{\omega_{31}}A_{\omega_{32}} g_3 + \\
&6\cos[\omega_1 + \omega_2 - \omega_3 - \emptyset_{31} - \emptyset_{32}]A_{\omega_3}A_{\omega_{31}}A_{\omega_{32}} g_3 + \\
&6\cos[\omega_1 - \omega_2 - \omega_3 - \emptyset_{31} + \emptyset_{32}]A_{\omega_3}A_{\omega_{31}}A_{\omega_{32}} g_3 + \\
&6\cos[\omega_1 - \omega_2 + \omega_3 - \emptyset_{31} + \emptyset_{32}]A_{\omega_3}A_{\omega_{31}}A_{\omega_{32}} g_3 + \\
&6\cos[2\omega_1 - 2\omega_3 - \emptyset_{21} - \emptyset_{31} - \emptyset_{32}]A_{\omega_{21}}A_{\omega_{31}}A_{\omega_{32}} g_3 + \\
&6\cos[2\omega_2 - 2\omega_3 + \emptyset_{21} - \emptyset_{31} - \emptyset_{32}]A_{\omega_{21}}A_{\omega_{31}}A_{\omega_{32}} g_3 +
\end{aligned}
$$

$$
\begin{aligned}
&6\cos[2\omega_1 - 2\omega_2 - \emptyset_{21} - \emptyset_{31} + \emptyset_{32}]A_{\omega_{21}}A_{\omega_{31}}A_{\omega_{32}}g_3 + \\
&6\cos[\emptyset_{21} - \emptyset_{31} + \emptyset_{32}]A_{\omega_{21}}A_{\omega_{31}}A_{\omega_{32}}g_3 + \\
&6\cos[\omega_2 - \omega_3 - \emptyset_{32}]A_{\omega_{31}}^2 A_{\omega_{32}}g_3 + \\
&3\cos[2\omega_1 + \omega_2 - 3\omega_3 - 2\emptyset_{31} - \emptyset_{32}]A_{\omega_{31}}^2 A_{\omega_{32}}g_3 + \\
&3\cos[2\omega_1 - \omega_2 - \omega_3 - 2\emptyset_{31} + \emptyset_{32}]A_{\omega_{31}}^2 A_{\omega_{32}}g_3 + \\
&6\cos[\omega_1]A_{\omega_1}A_{\omega_{32}}^2 g_3 + 3\cos[\omega_1 + 2\omega_2 - 2\omega_3 - 2\emptyset_{32}]A_{\omega_1}A_{\omega_{32}}^2 g_3 + \\
&3\cos[\omega_1 - 2\omega_2 + 2\omega_3 + 2\emptyset_{32}]A_{\omega_1}A_{\omega_{32}}^2 g_3 + \\
&6\cos[\omega_2]A_{\omega_2}A_{\omega_{32}}^2 g_3 + 3\cos[\omega_2 - 2\omega_3 - 2\emptyset_{32}]A_{\omega_2}A_{\omega_{32}}^2 g_3 + \\
&3\cos[3\omega_2 - 2\omega_3 - 2\emptyset_{32}]A_{\omega_2}A_{\omega_{32}}^2 g_3 + \\
&6\cos[\omega_3]A_{\omega_3}A_{\omega_{32}}^2 g_3 + 3\cos[2\omega_2 - 3\omega_3 - 2\emptyset_{32}]A_{\omega_3}A_{\omega_{32}}^2 g_3 + \\
&3\cos[2\omega_2 - \omega_3 - 2\emptyset_{32}]A_{\omega_3}A_{\omega_{32}}^2 g_3 + \\
&6\cos[\omega_1 - \omega_2 - \emptyset_{21}]A_{\omega_{21}}A_{\omega_{32}}^2 g_3 + \\
&3\cos[\omega_1 + \omega_2 - 2\omega_3 - \emptyset_{21} - 2\emptyset_{32}]A_{\omega_{21}}A_{\omega_{32}}^2 g_3 + \\
&3\cos[\omega_1 - 3\omega_2 + 2\omega_3 - \emptyset_{21} + 2\emptyset_{32}]A_{\omega_{21}}A_{\omega_{32}}^2 g_3 + \\
&6\cos[\omega_1 - \omega_3 - \emptyset_{31}]A_{\omega_{31}}A_{\omega_{32}}^2 g_3 + \\
&3\cos[\omega_1 + 2\omega_2 - 3\omega_3 - \emptyset_{31} - 2\emptyset_{32}]A_{\omega_{31}}A_{\omega_{32}}^2 g_3 + \\
&3\cos[\omega_1 - 2\omega_2 + \omega_3 - \emptyset_{31} + 2\emptyset_{32}]A_{\omega_{31}}A_{\omega_{32}}^2 g_3 + \\
&\cos[3\omega_2 - 3\omega_3 - 3\emptyset_{32}]A_{\omega_{32}}^3 g_3 + 3\cos[\omega_2 - \omega_3 - \emptyset_{32}]A_{\omega_{32}}^3 g_3)
\end{aligned}
$$

APPENDIX C.

OUTPUT VS INPUT POWER OF THE FUNDAMENTAL SIGNALS AND THE IMDS BEFORE AND AFTER EMPLOYING THE TECHNIQUES IN A THREE TONE TEST

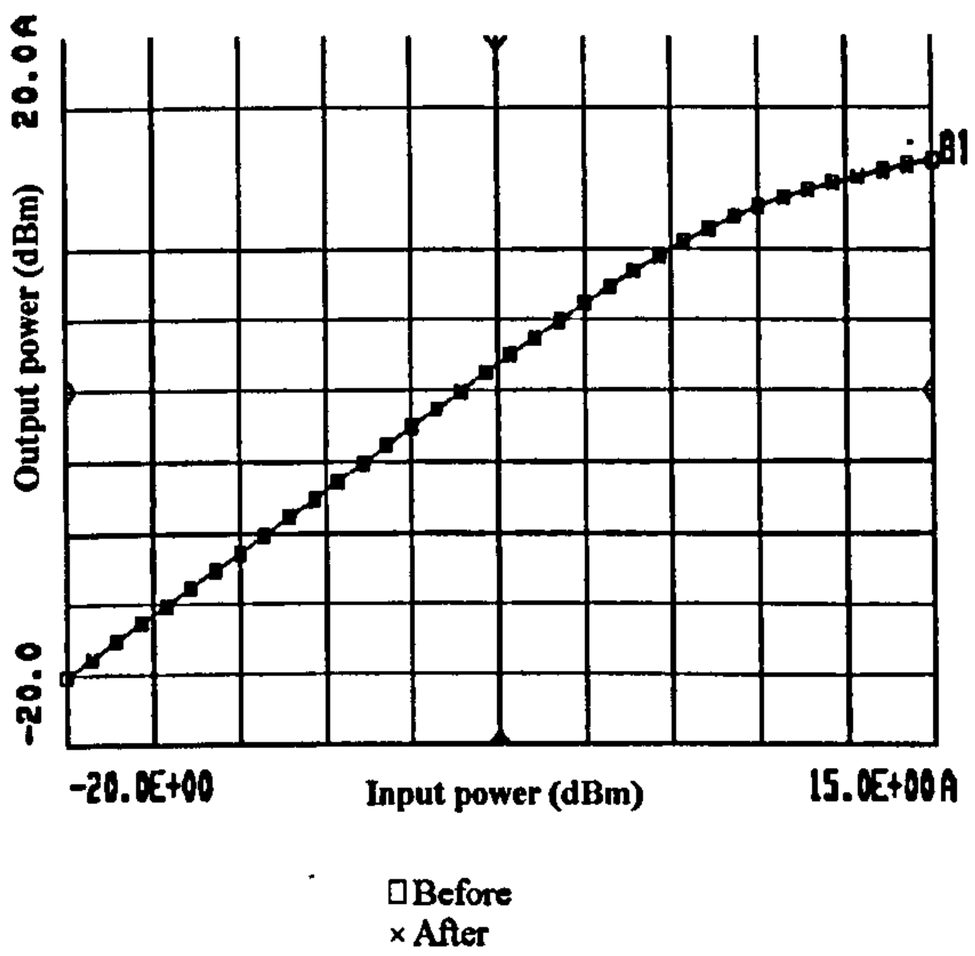

Figure C..1: **Output Vs input power of the fundamental signal (f_1) at the frequency $2.5GHz$ before and after injection of the difference frequency signals.**

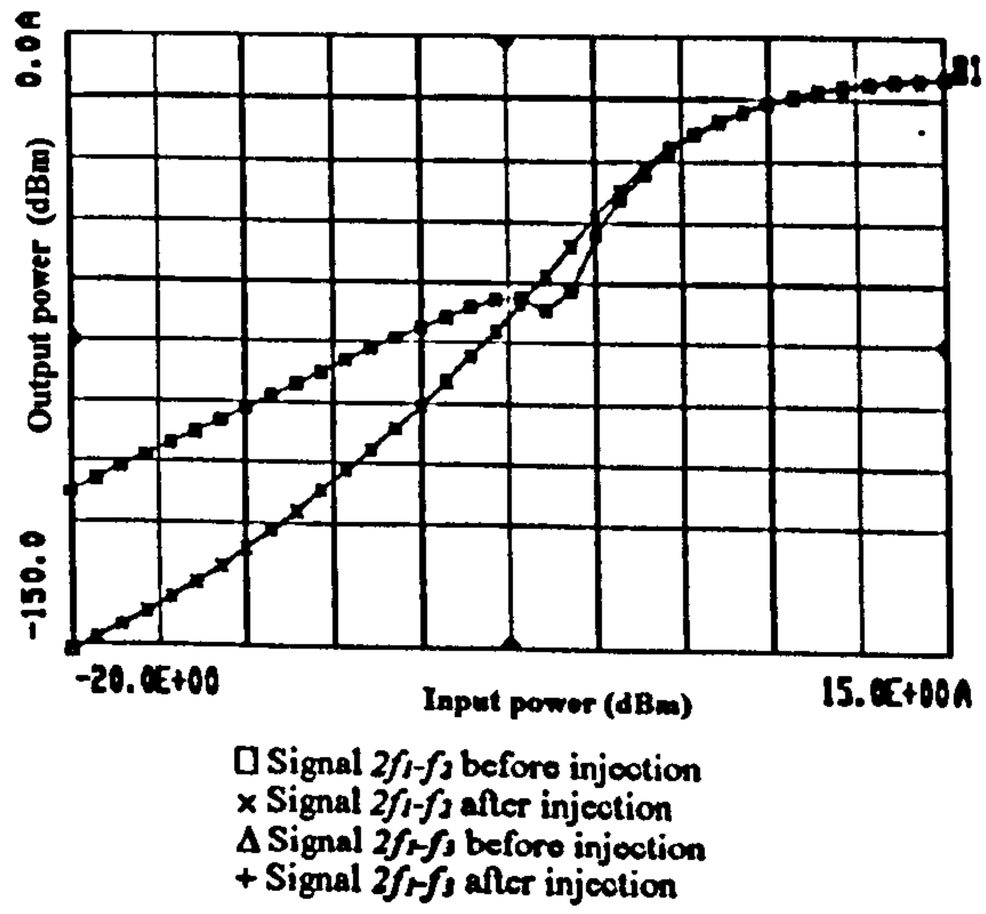

Figure C..2: **Output Vs input power of the intermodulation signals ($2f_1 - f_2$) and ($2f_1 - f_3$) at the frequencies $2.49GHz$ and $2.479GHz$ before and after injection of the difference frequency signals.**

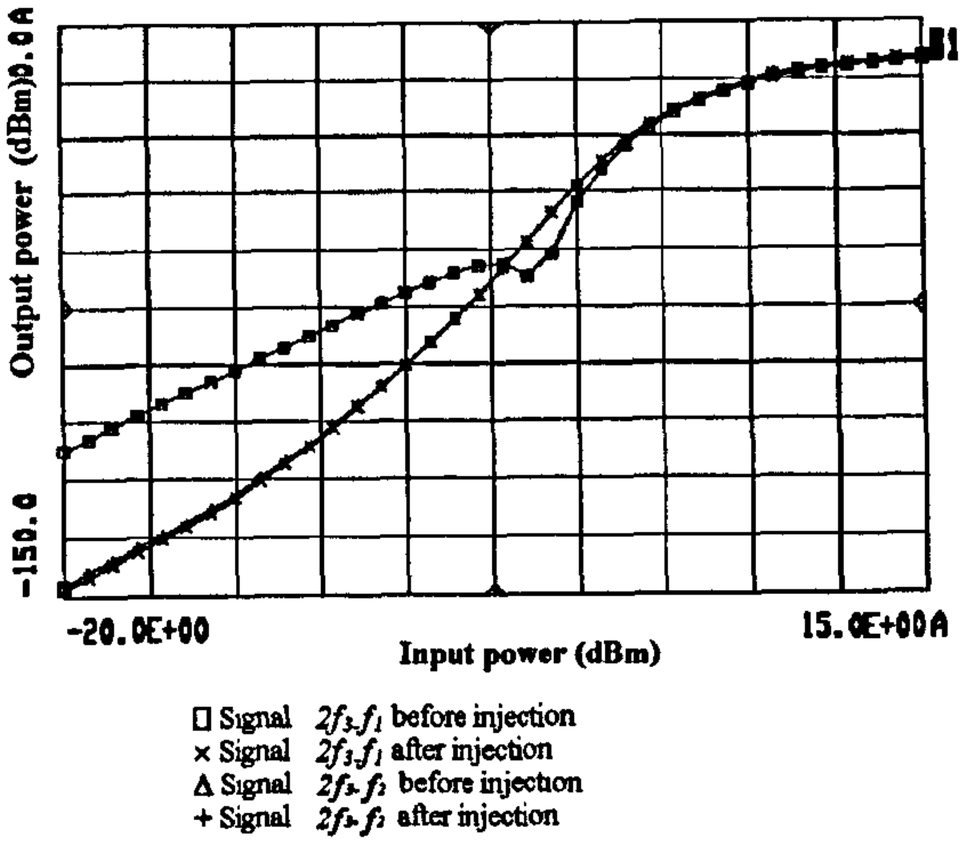

Figure C..3: **Output Vs input power of the intermodulation signal $(2f_3 - f_1)$ and $(2f_3 - f_2)$ at the frequencies $2.542GHz$ and $2.532GHz$ before and after injection of the difference frequency signals.**

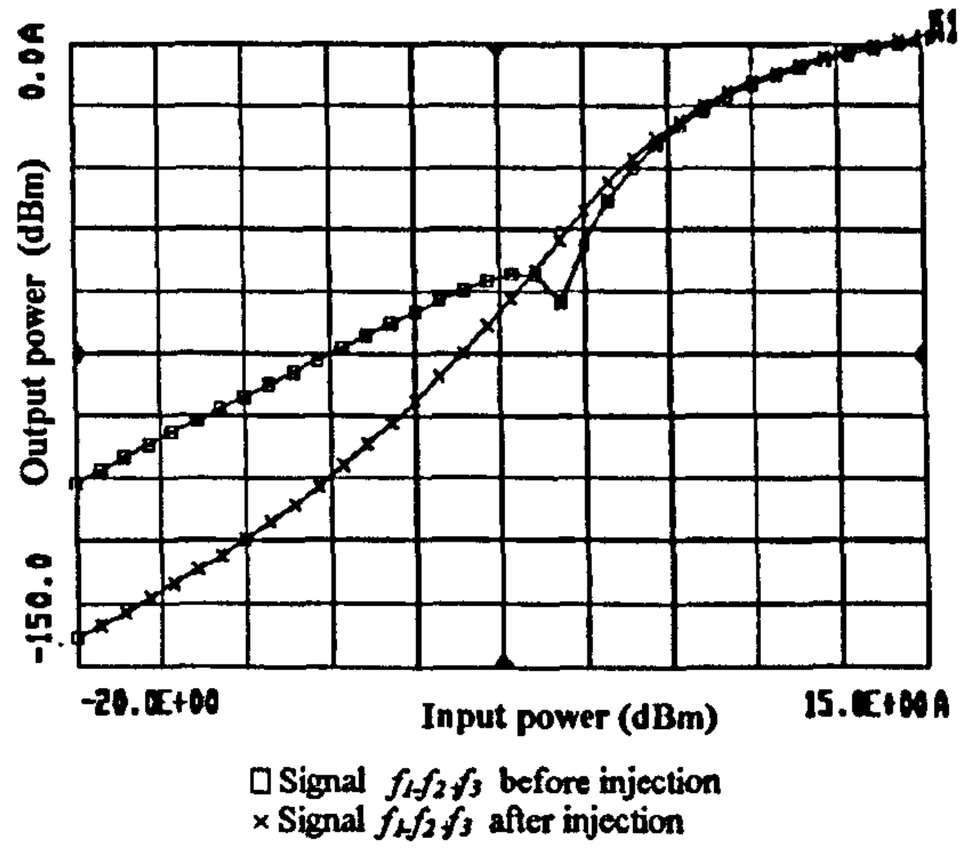

Figure C..5: **Output Vs input power of the intermodulation signal $(f_1 - f_2 + f_3)$ at the frequency $2.511GHz$ before and after injection of the difference frequency signals.**

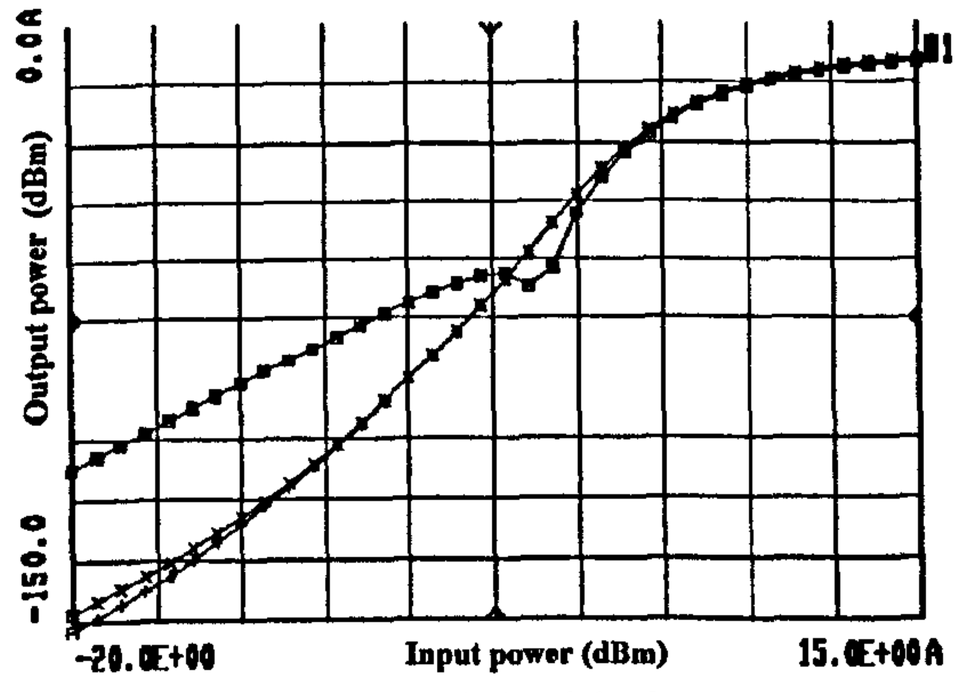

Figure C..4: **Output Vs input power of the intermodulation signals $(2f_2 - f_1)$ and $(2f_2 - f_3)$ at the frequencies$2.52GHz$ and $2.499GHz$ before and after injection of the difference frequency signals.**

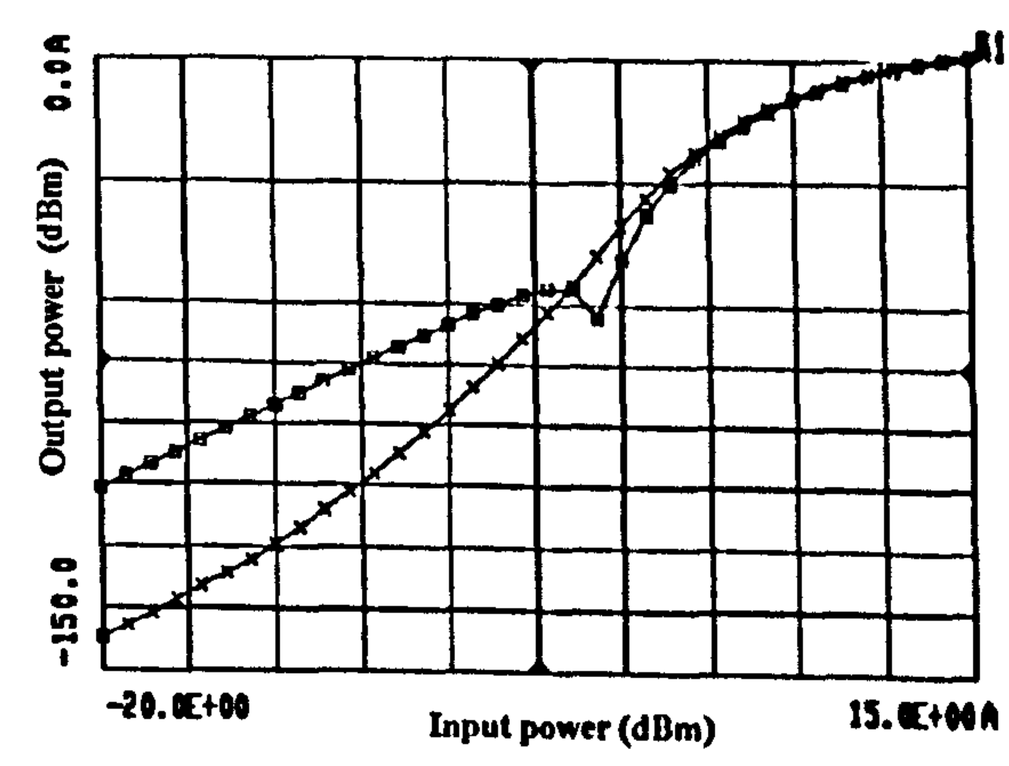

Figure C..6: **Output Vs input power of the intermodulation signal $(f_3 + f_2 - f_1)$ at the frequency $2.511GHz$ before and after injection of the difference frequency signals.**

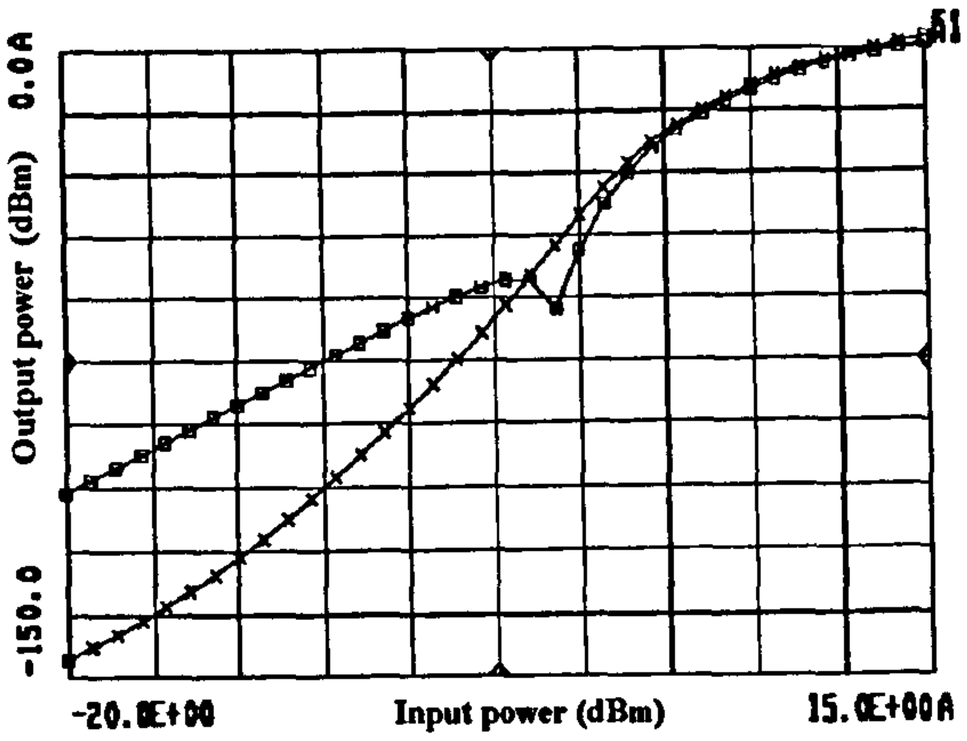

▽ Signal f_1-f_2f_3 before injection
□ Signal f_1-f_2f_3 after injection
× Signal f_1-f_2f_3 after injection

Figure C..7: **Output Vs input power of the intermodulation signal $(f_1 + f_2 - f_3)$ at the frequency $2.489GHz$ before and after injection of the difference frequency signals.**

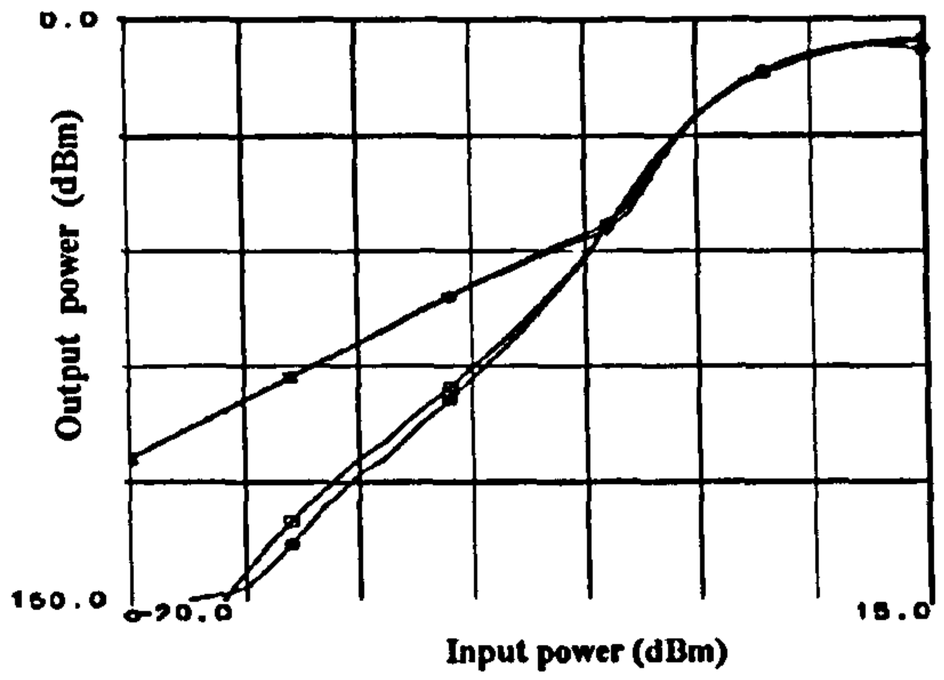

▽ Signal $2f_1$-f_2 before injection
□ Signal $2f_1$-f_2 after injection
Δ Signal $2f_2$-f_1 before injection
O Signal $2f_2$-f_1 after injection

Figure C..9: **Output Vs input power of the intermodulation signals$(2f_1 - f_2)$ and $(2f_2 - f_1)$ at the frequencies $2.49GHz$ and $2.52GHz$ before and after injection of the second harmonic signals.**

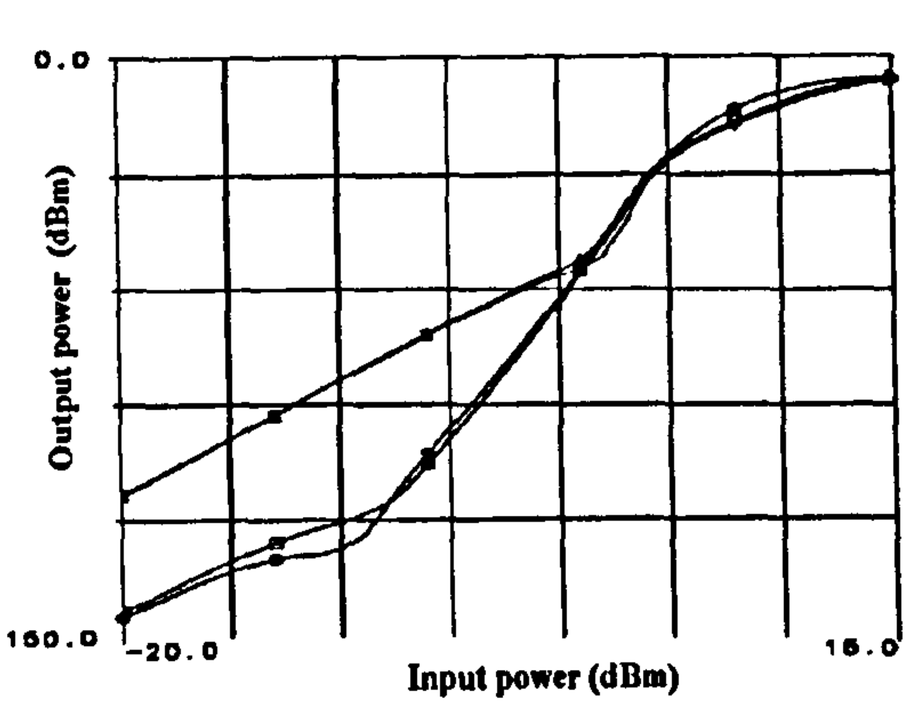

▽ Signal $2f_1$-f_3 before injection
□ Signal $2f_1$-f_3 after injection
Δ Signal $2f_3$-f_1 before injection
O Signal $2f_3$-f_1 after injection

Figure C..8: **Output Vs input power of the intermodulation signals$(2f_3 - f_1)$ and $(2f_1 - f_3)$ at the frequencies $2.479GHz$ and $2.542GHz$ before and after injection of the second harmonic signals.**

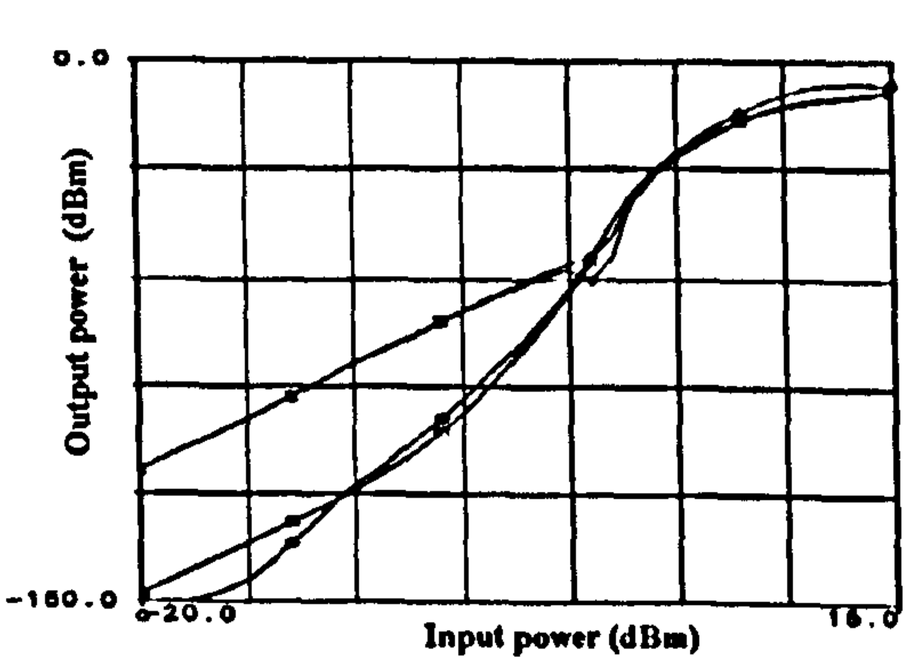

▽ Signal $2f_3$-f_2 before injection
□ Signal $2f_3$-f_2 after injection
Δ Signal $2f_2$-f_3 before injection
O Signal $2f_2$-f_3 after injection

Figure C..10: **Output Vs input power of the intermodulation signal $(2f_3 - f_2)$ and $(2f_2 - f_3)$ at the frequencies $2.532GHz$ and $2.499GHz$ before and after injection of the second harmonic signals.**

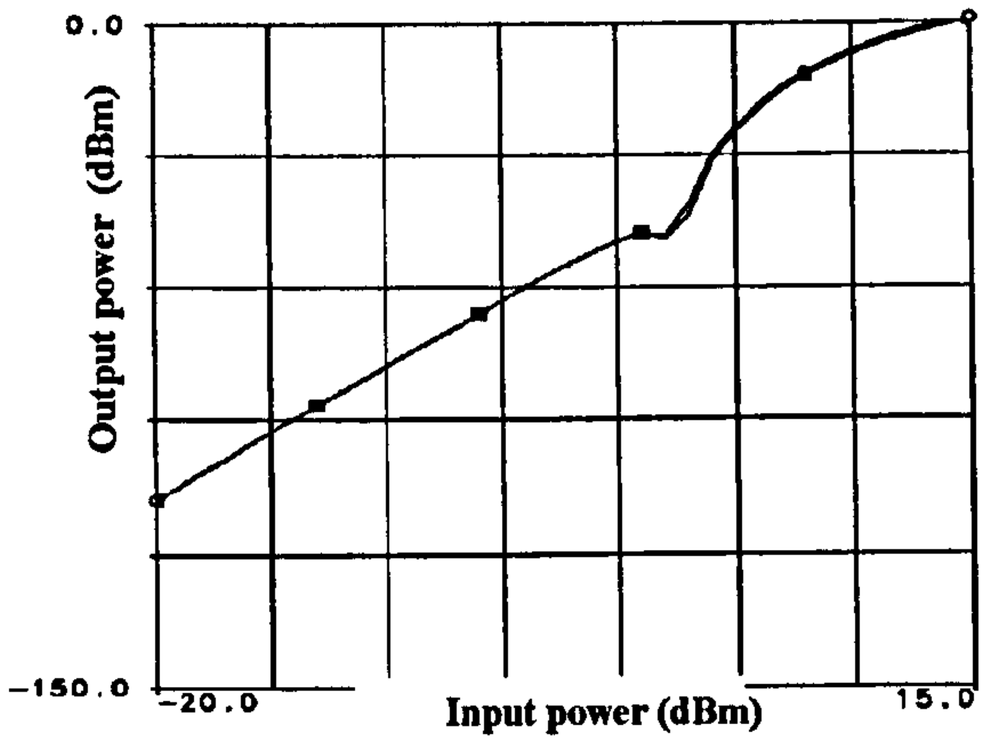

□ Signal f_1-f_2+f_3 before injection
○ Signal f_1-f_2+f_3 after injection

Figure C..11: **Output Vs input power of the intermodulation signal $(f_1 - f_2 + f_3)$ at the frequency $2.511GHz$ before and after injection of the second harmonic signals.**

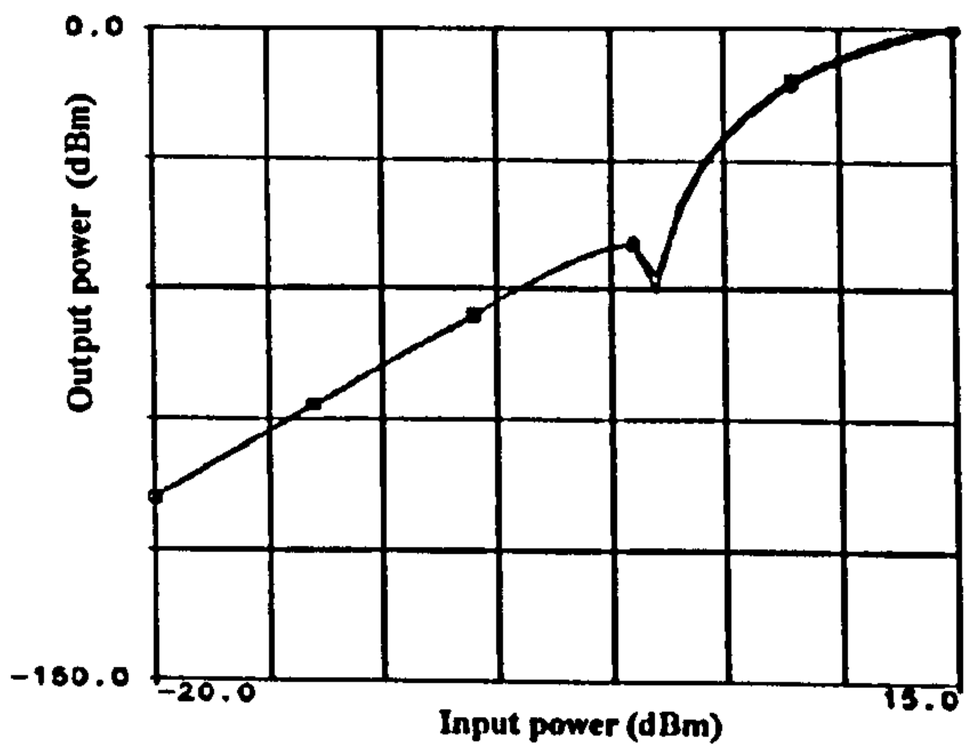

□ Signal f_3+f_2-f_1 before injection
○ Signal f_3+f_2-f_1 after injection

Figure C..13: **Output Vs input power of the intermodulation signal $(f_3 + f_2 - f_1)$ at the frequency $2.511GHz$ before and after injection of the second harmonic signals.**

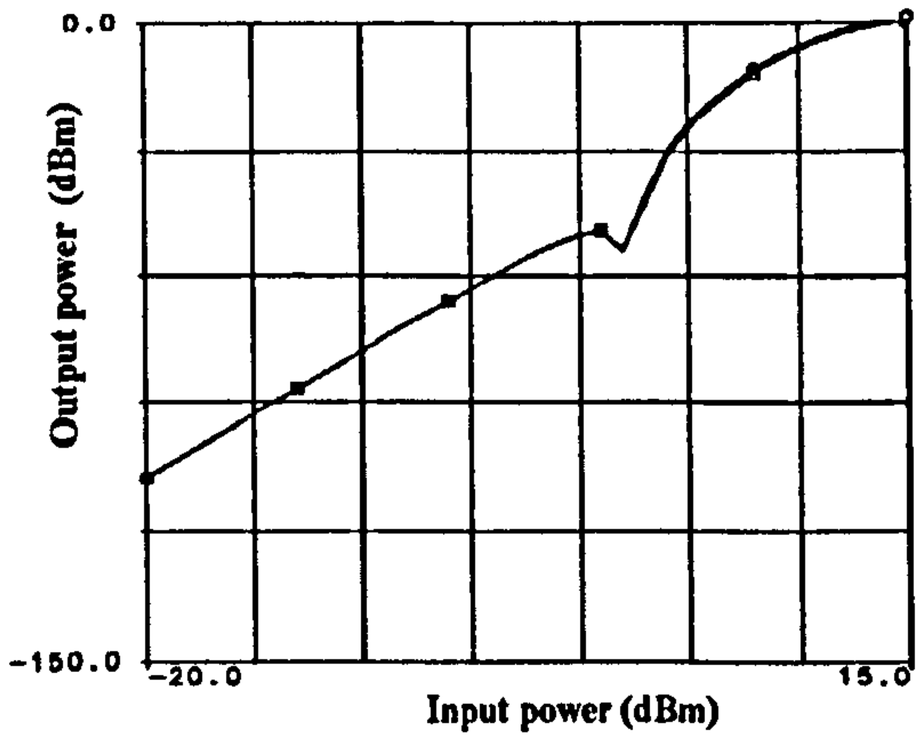

□ Signal f_1+f_2-f_3 before injection
○ Signal f_1+f_2-f_3 after injection

Figure C..12: **Output Vs input power of the intermodulation signal $(f_1 + f_2 - f_3)$ at the frequency $2.489GHz$ before and after injection of the second harmonic signals.**

APPENDIX D.

AMPLITUDE AND PHASE CHANGE EFFECTS ON THIRD ORDER IMD

4.1 Second Harmonic Injection Technique

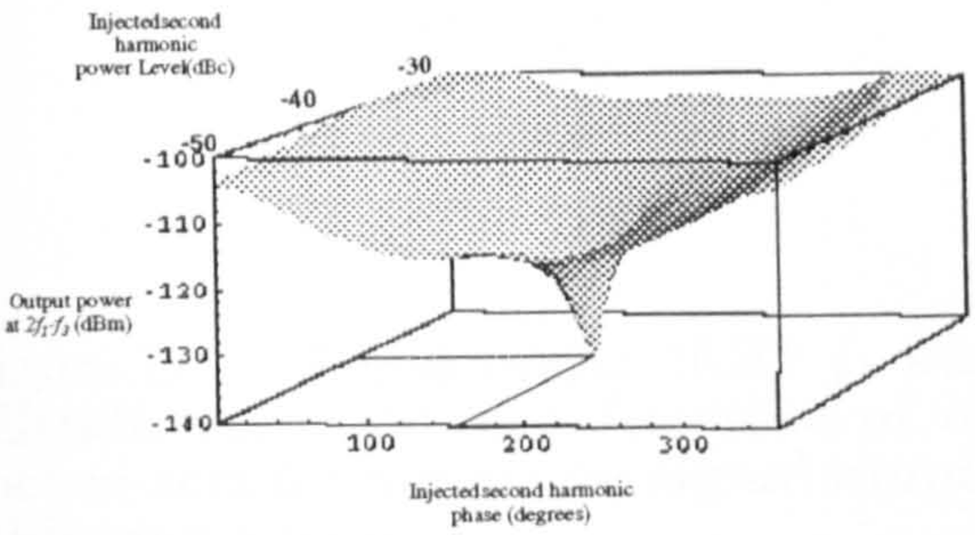

Figure D..1: **Third order IMD $(2f_1 - f_3)$ amplitude variation as a function of injected second harmonic signal amplitude and phase.**

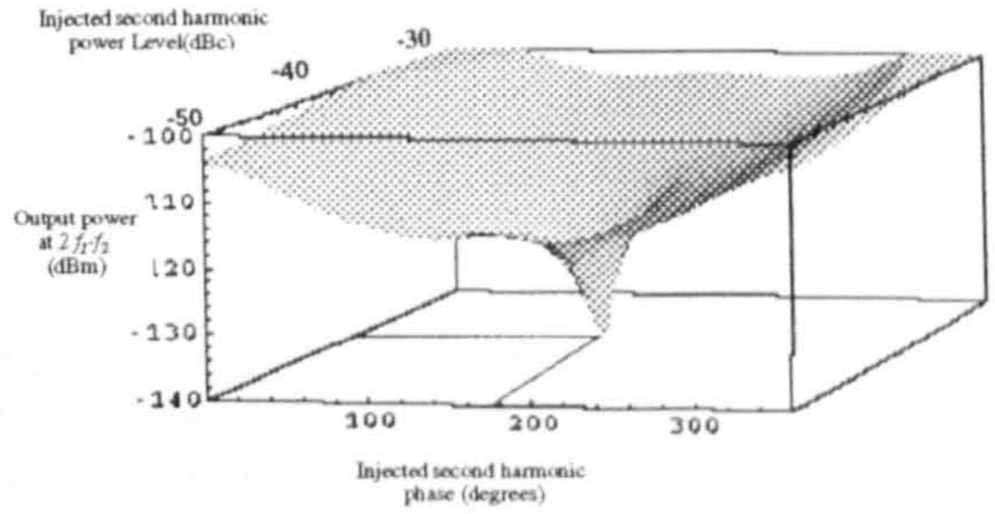

Figure D..3: **Third order IMD $(2f_1 - f_2)$ amplitude variation as a function of injected second harmonic signal amplitude and phase.**

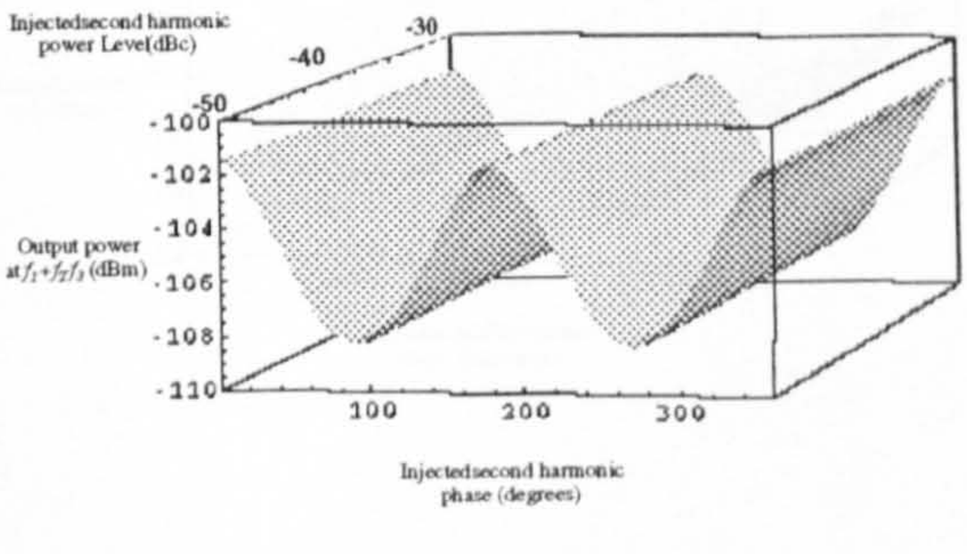

Figure D..2: **Third order IMD $(f_1 + f_2 - f_3)$ amplitude variation as a function of injected second harmonic signal amplitude and phase.**

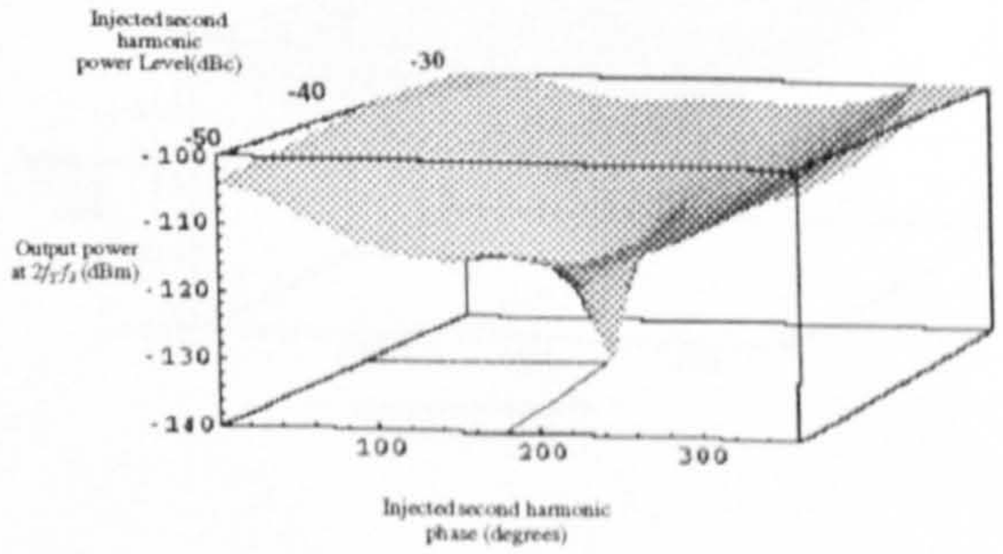

Figure D..4: **Third order IMD $(2f_2 - f_3)$amplitude variation as a function of injected second harmonic signal amplitude and phase.**

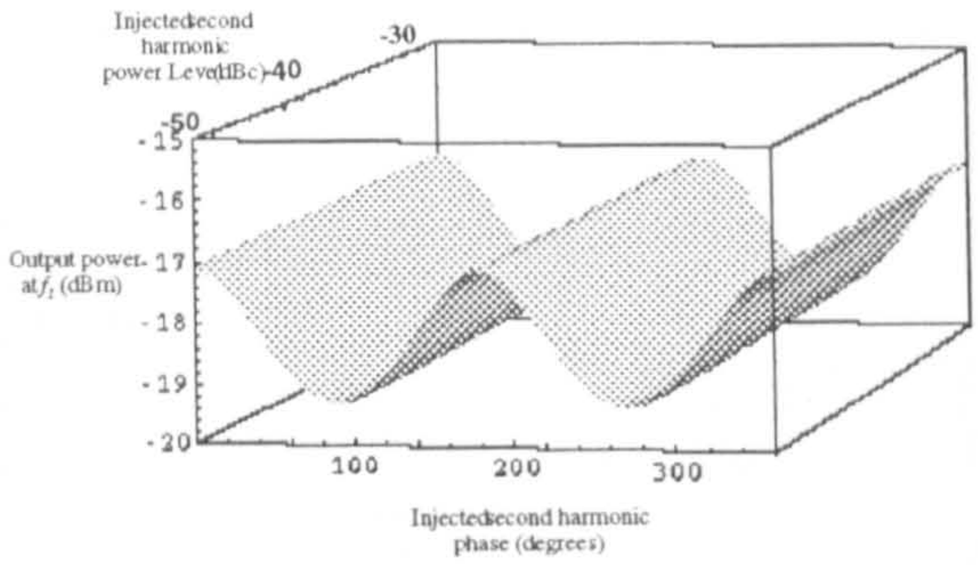

Figure D..5: **Third order IMD f_1 amplitude variation as a function of injected second harmonic signal amplitude and phase.**

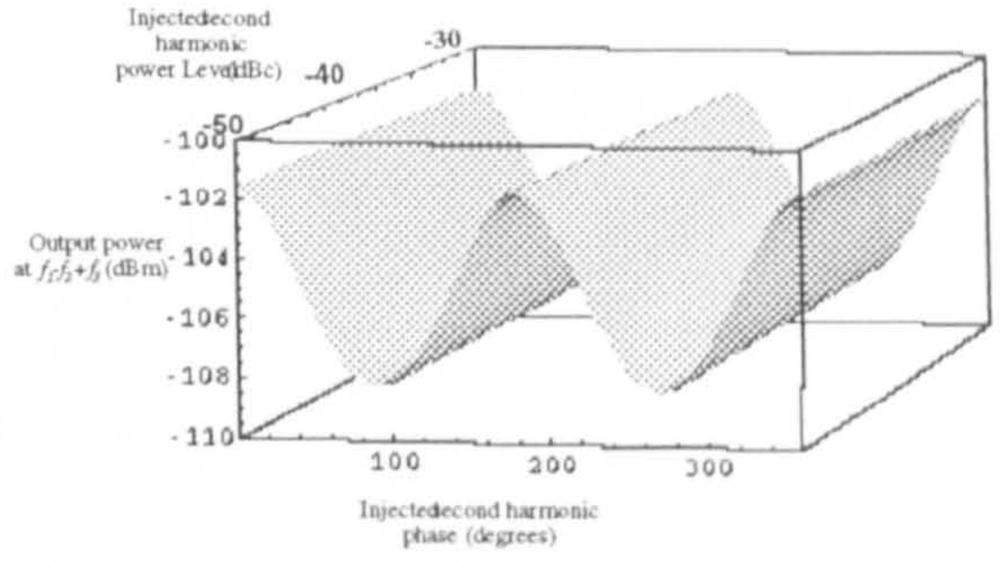

Figure D..7: **Third order IMD $(f_1 - f_2 + f_3)$ amplitude variation as a function of injected second harmonic signal amplitude and phase.**

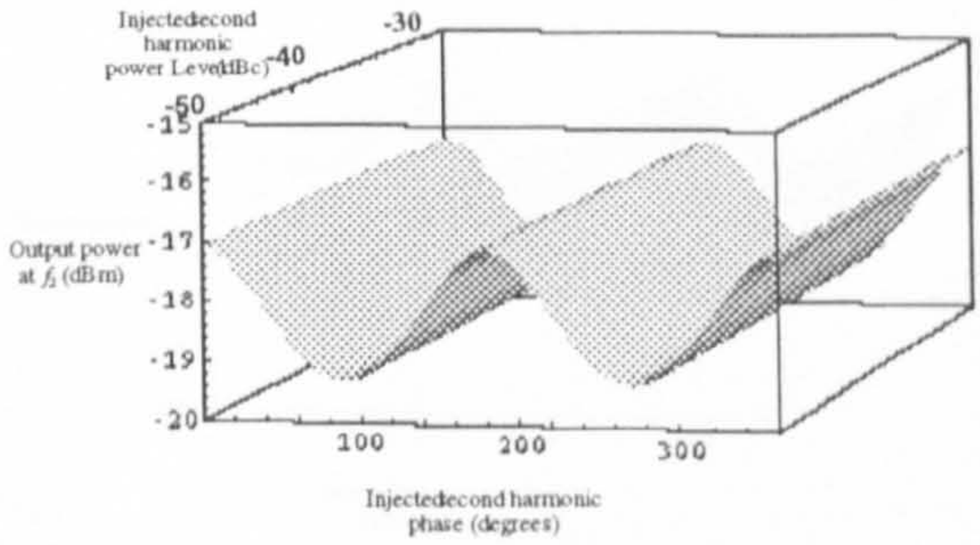

Figure D..6: **Third order IMD f_2 amplitude variation as a function of injected second harmonic signal amplitude and phase.**

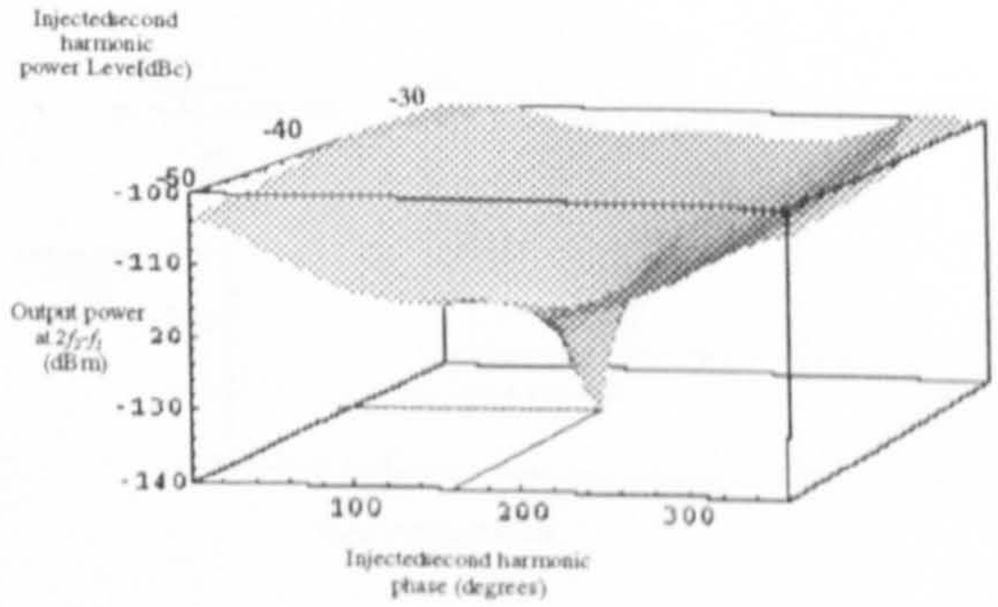

Figure D..8: **Third order IMD $(2f_2 - f_1)$ amplitude variation as a function of injected second harmonic signal amplitude and phase.**

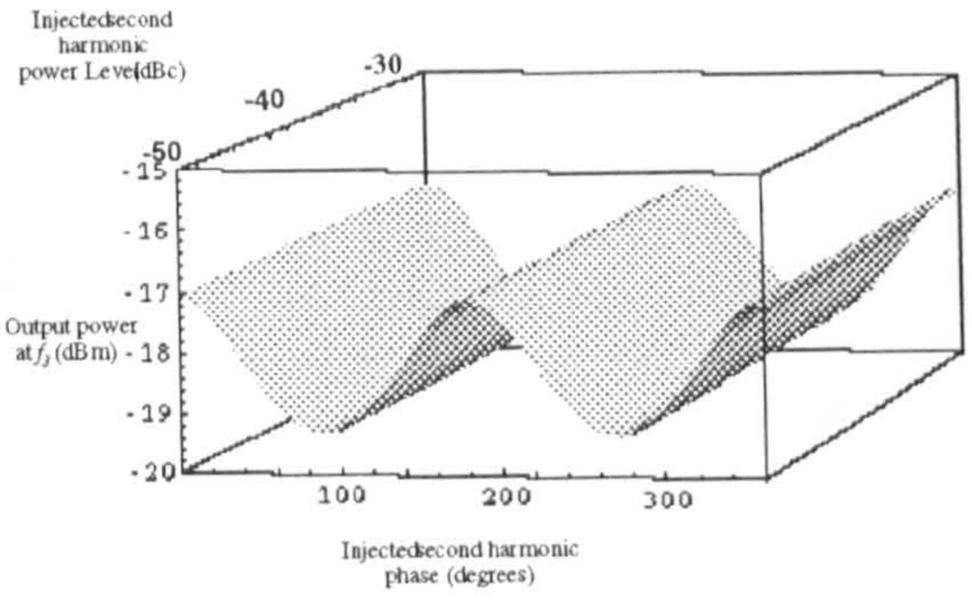

Figure D..9: **Fundamental signal f_3 amplitudevariation as a function of injected second harmonic signal amplitude and phase.**

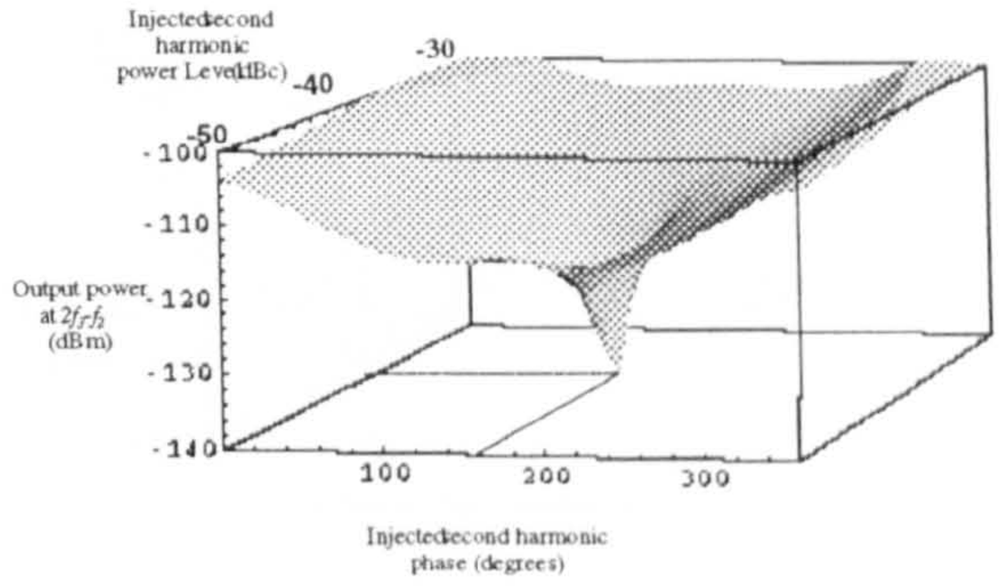

Figure D..11: **Third order IMD $(2f_3 - f_2)$ amplitude variation as a function of injected second harmonic signal amplitude and phase.**

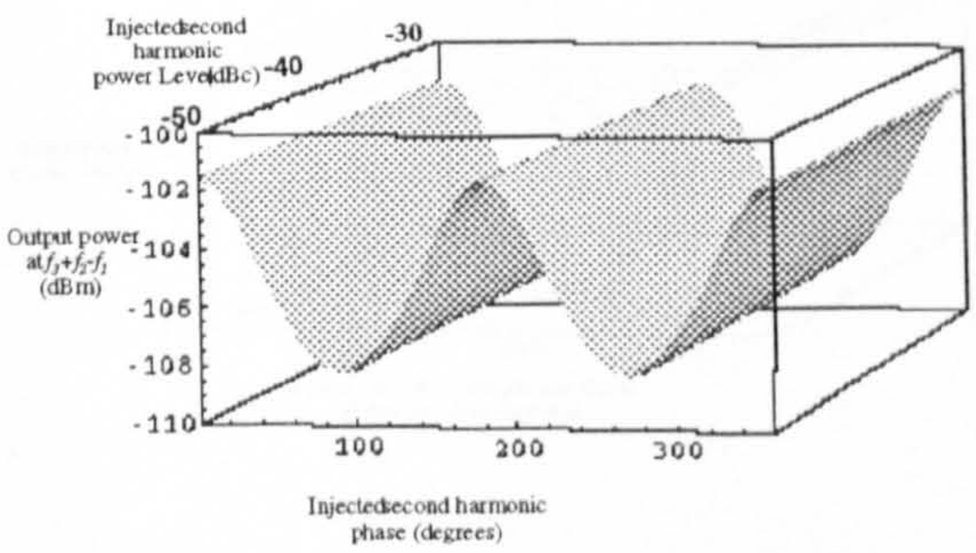

Figure D..10: **Third order IMD $(f_3 + f_2 - f_1)$ amplitude variation as a function of injected second harmonic signal amplitude and phase.**

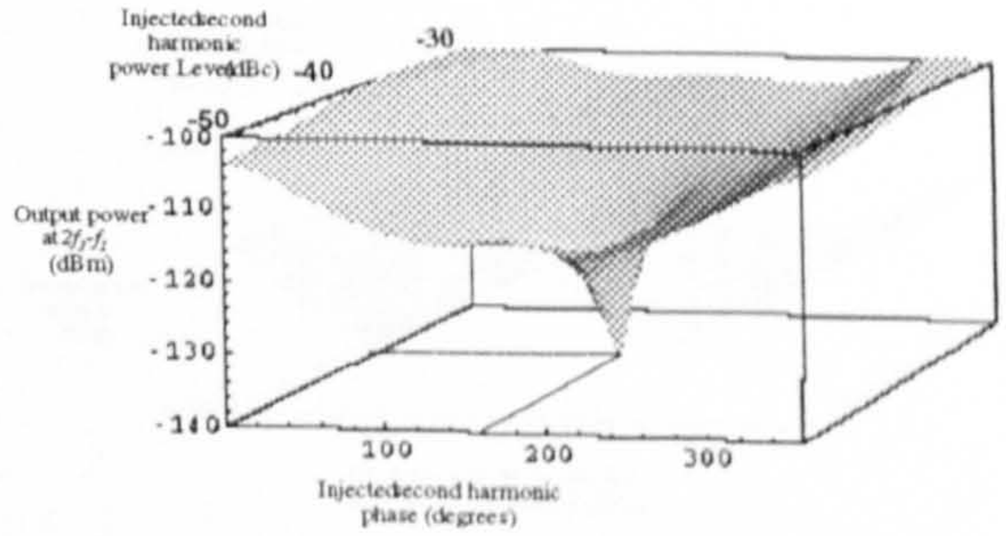

Figure D..12: **Third order IMD $(2f_3 - f_1)$ amplitude variation as a function of injected second harmonic signal amplitude and phase.**

4.2 Frequency Summation Technique

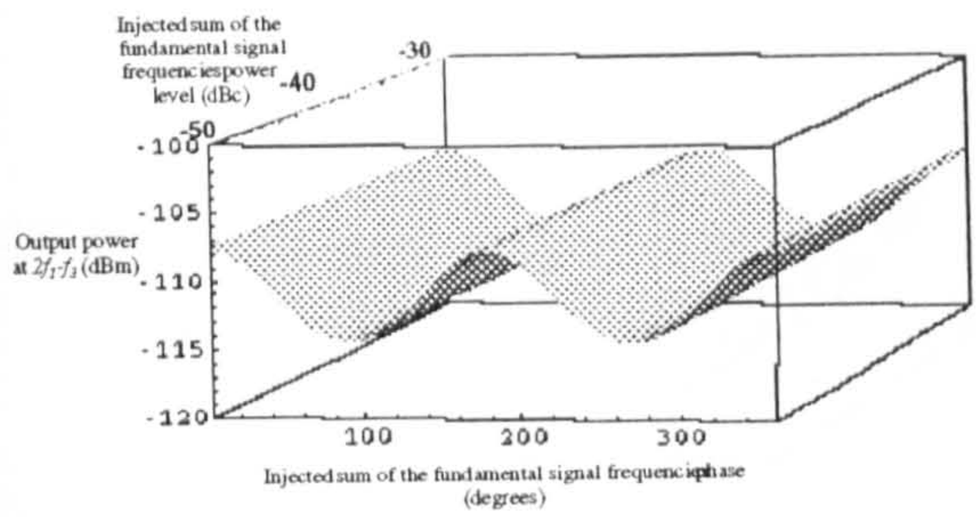

Figure D..13: **Third order IMD $(2f_1 - f_3)$amplitude variation as a function of injected sum of the fundamental signals amplitude and phase.**

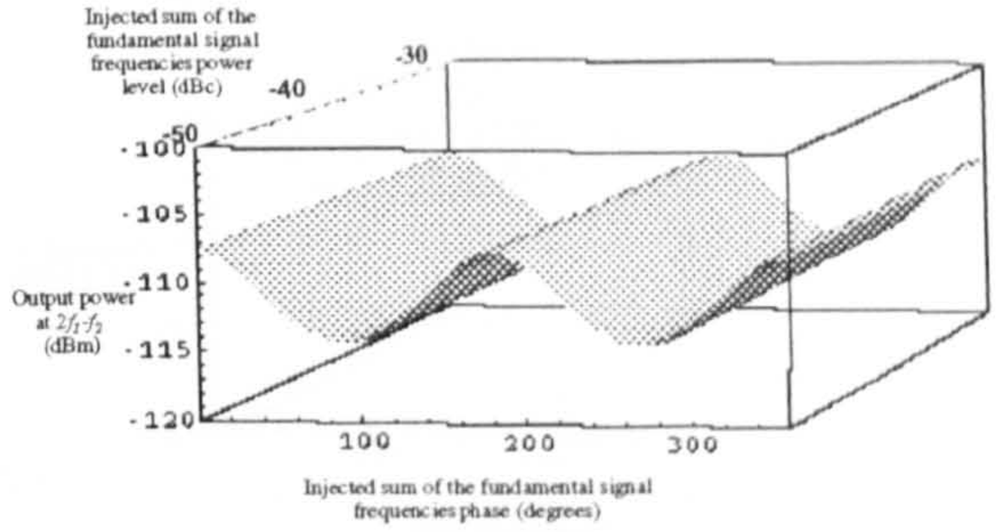

Figure D..15: **Third order IMD $(2f_1 - f_2)$ amplitude variation as a function of injected sum of the fundamental signals amplitude and phase.**

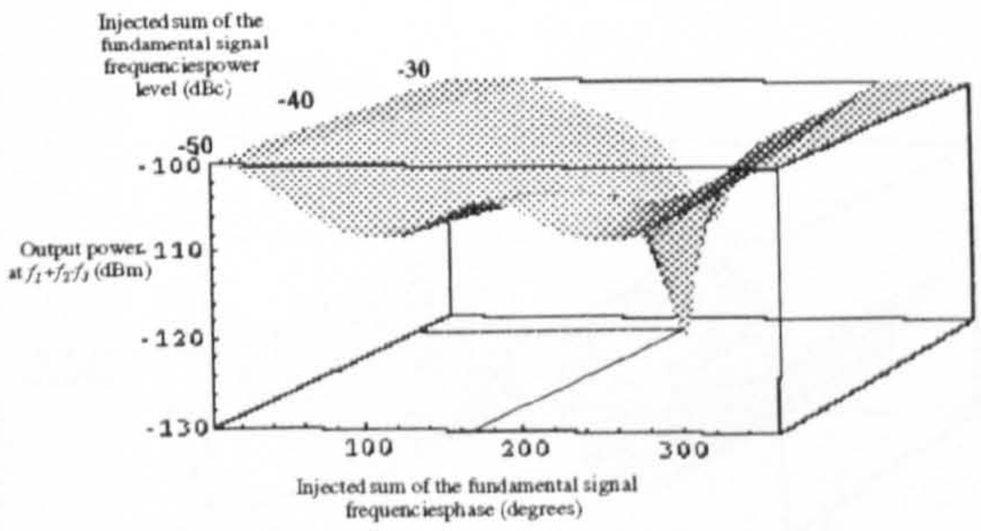

Figure D..14: **Third order IMD$(f_1 + f_2 - f_3)$ amplitude variation as a function of injected sum of the fundamental signal frequencies amplitude and phase.**

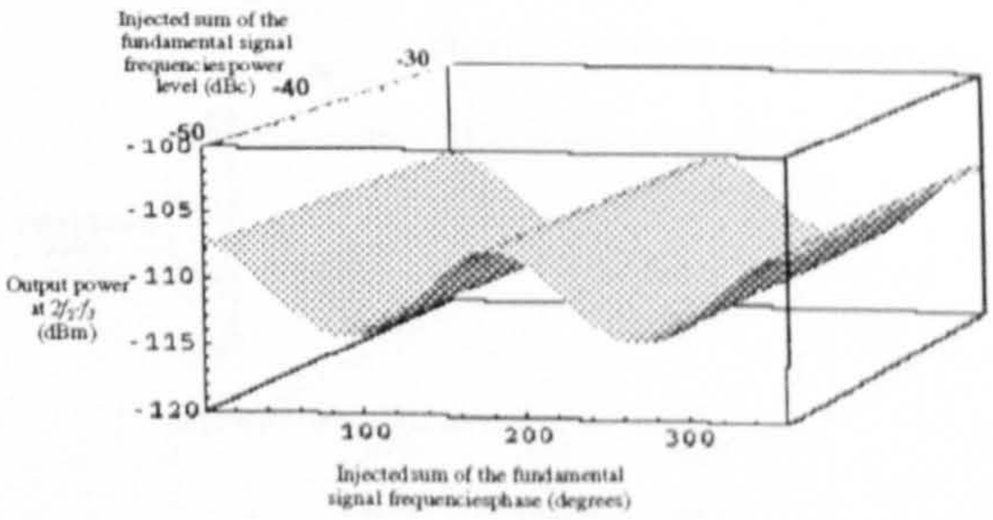

Figure D..16: **Third order IMD $(2f_2 - f_3)$ amplitude variation as a function of injected sum of the fundamental signals amplitude and phase.**

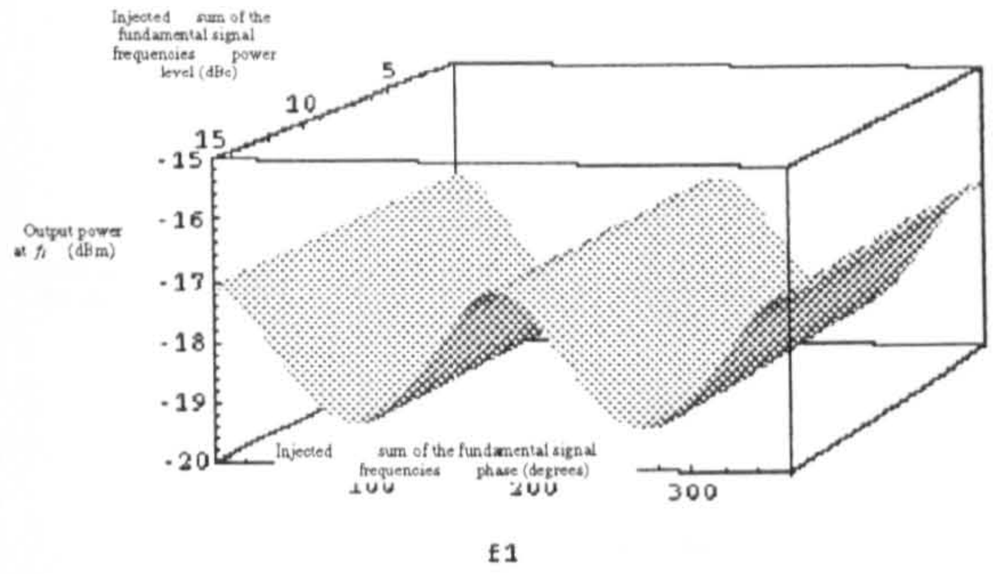

Figure D..17: **Third order IMD f_1 amplitude variation as a function of injected sum of the fundamental signals amplitude and phase.**

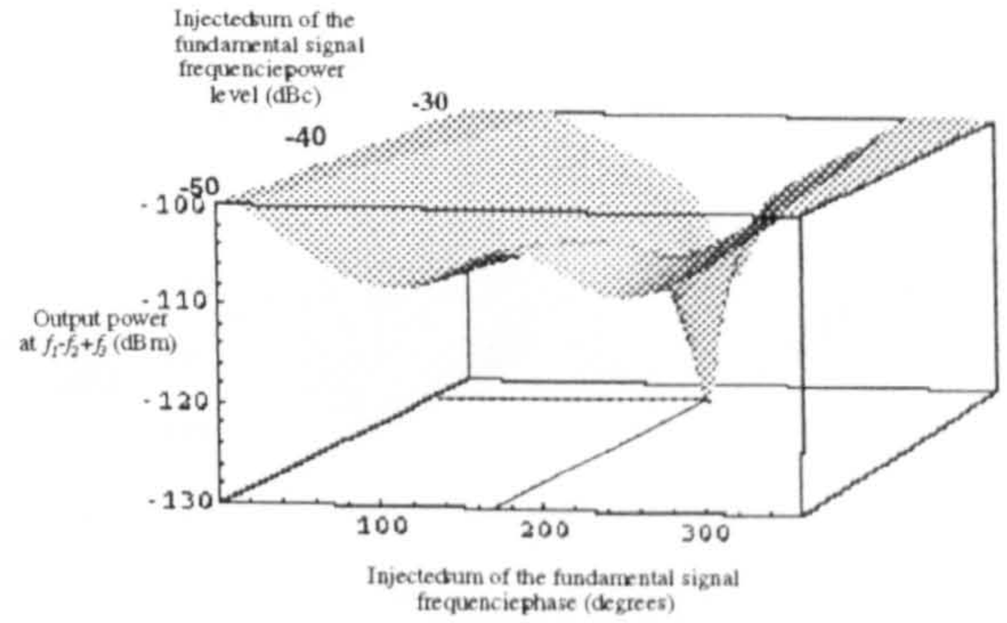

Figure D..19: **Third order IMD $(f_1 - f_2 + f_3)$ amplitude variation as a function of injected sum of the fundamental signals amplitude and phase.**

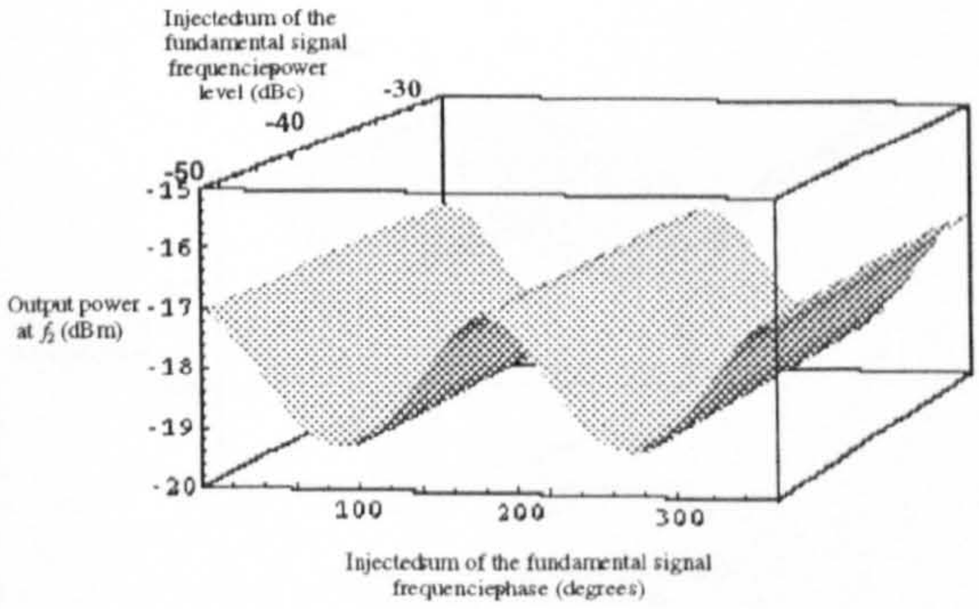

Figure D..18: **Third order IMD f_2 amplitude variation as a function of injected sum of the fundamental signals amplitude and phase.**

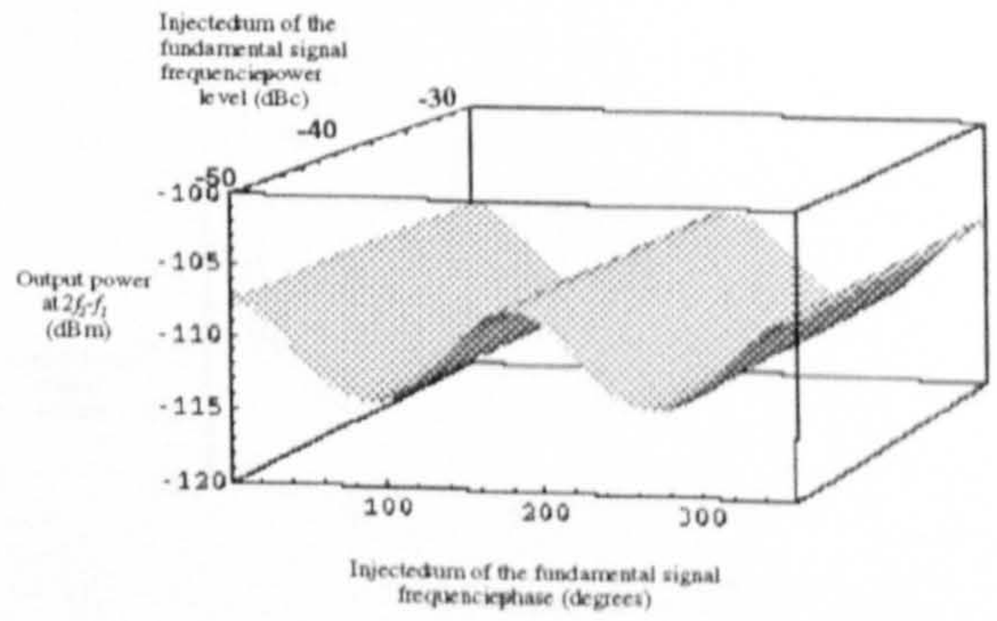

Figure D..20: **Third order IMD $(2f_2 - f_1)$ amplitude variation as a function of injected sum of the fundamental signals amplitude and phase.**

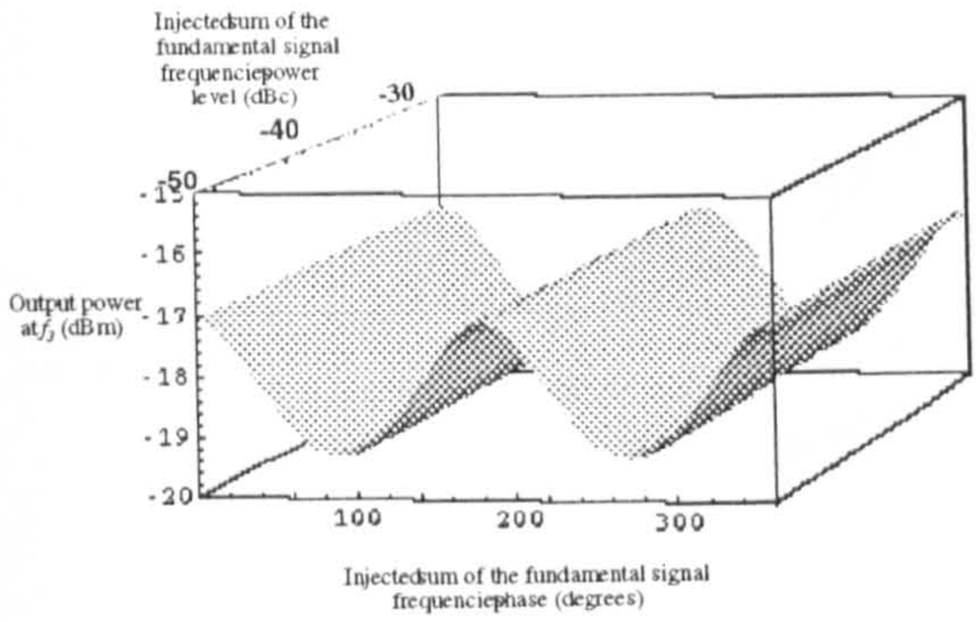

Figure D..21: **Third order IMD f_3 amplitude variation as a function of injected sum of the fundamental signals amplitude and phase.**

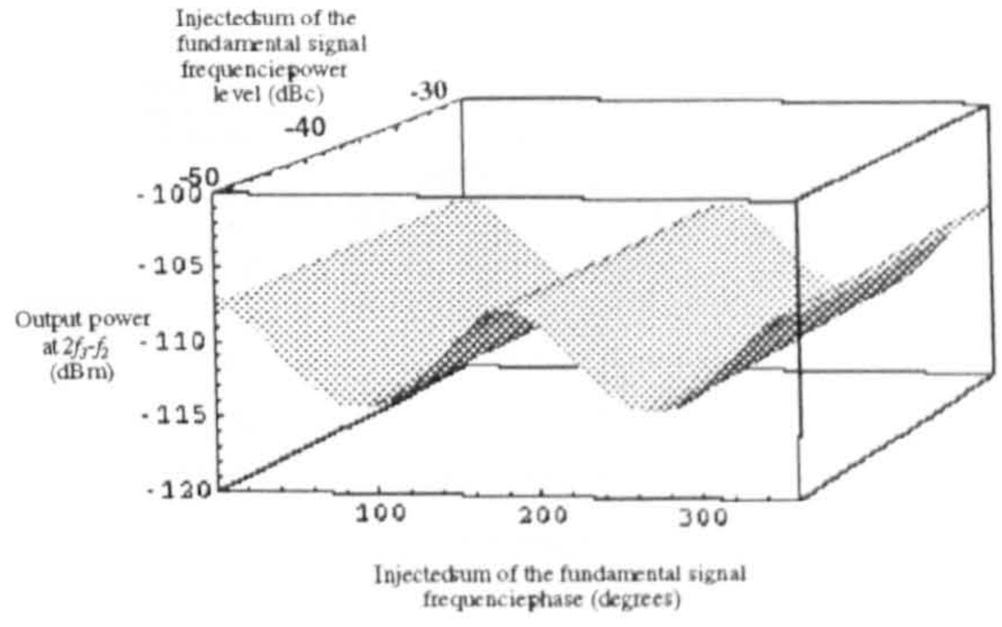

Figure D..23: **Third order IMD $(2f_3 - f_2)$ amplitude variation as a function of injected sum of the fundamental signals amplitude and phase.**

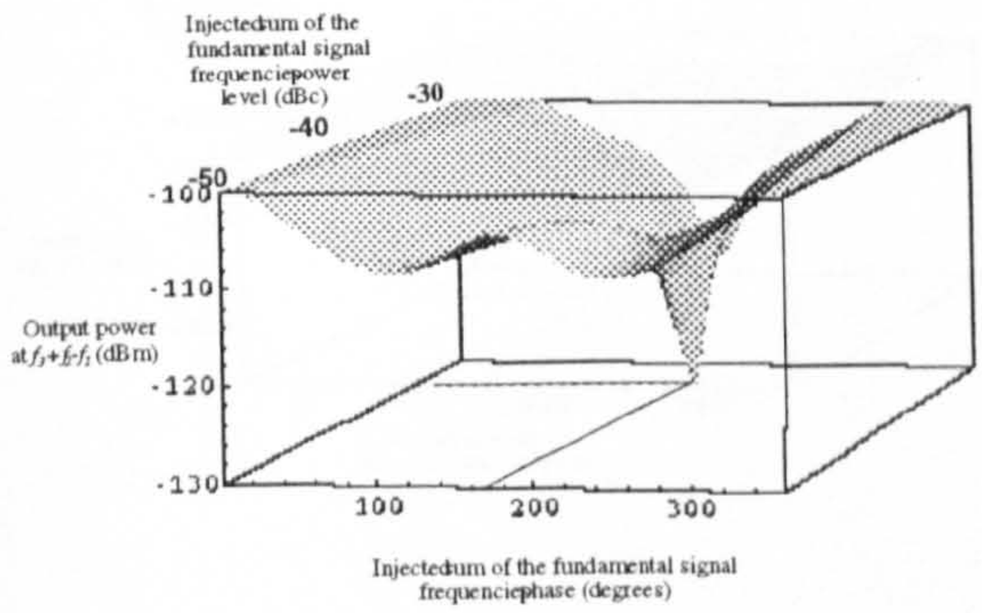

Figure D..22: **Third order IMD $(f_3 + f_2 - f_1)$ amplitude variation as a function of injected sum of the fundamental signals amplitude and phase.**

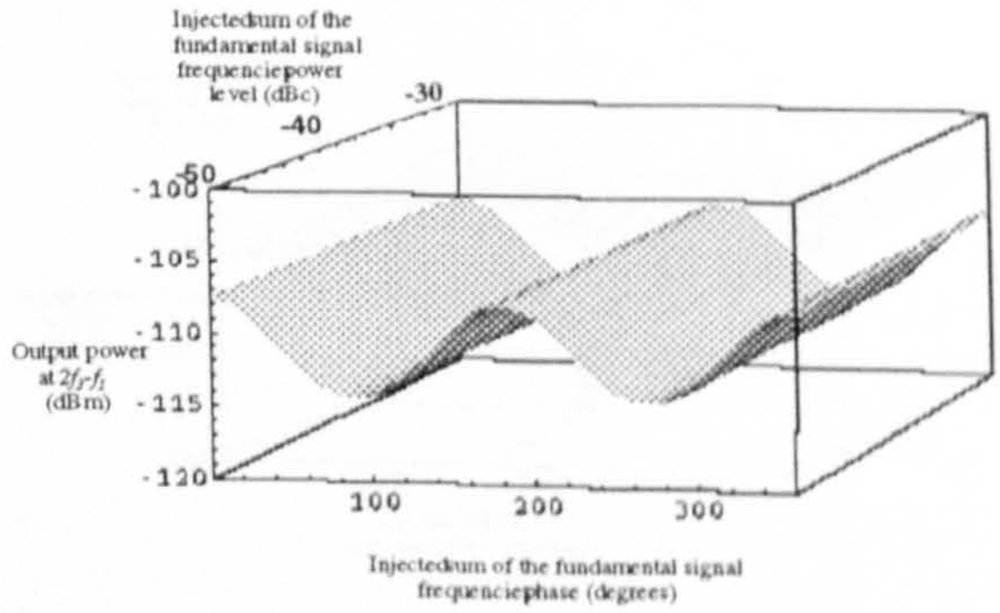

Figure D..24: **Third order IMD $(2f_3 - f_1)$amplitude variation as a function of injected sum of the fundamental signals amplitude and phase.**

4.3 Difference Frequency Technique

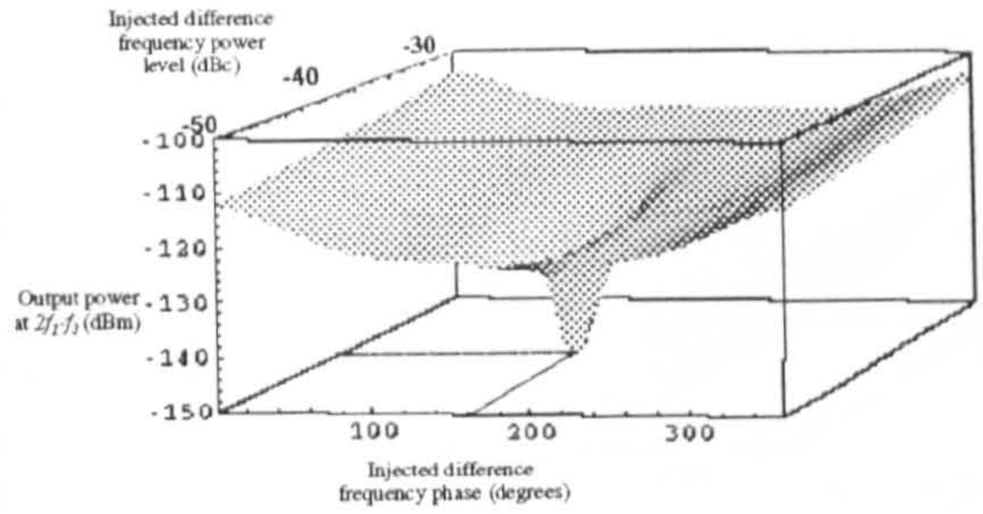

Figure D..25: **Third order IMD $(2f_1 - f_3)$ amplitude variation as a function of injected difference frequency signal amplitude and phase.**

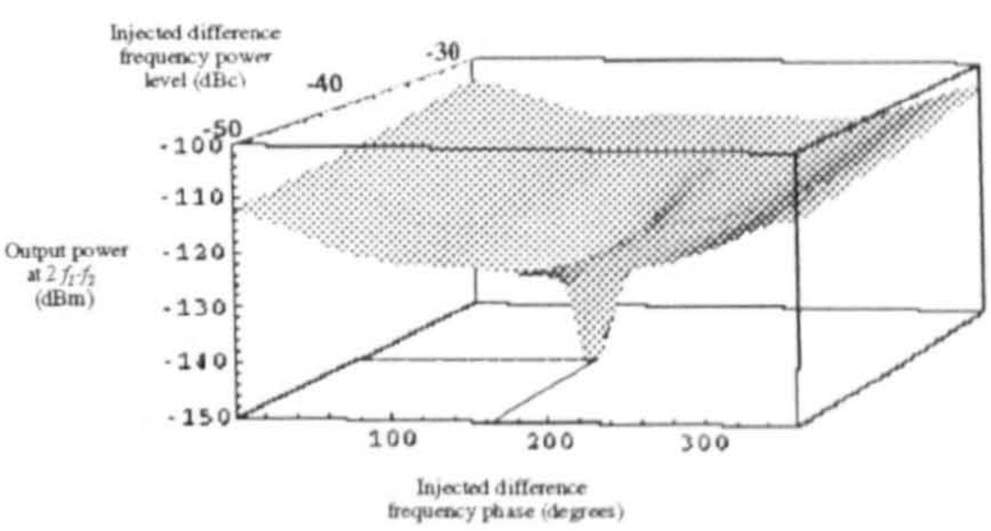

Figure D..27: **Third order IMD $(2f_1 - f_2)$ amplitude variation as a function of injected difference frequency signal amplitude and phase.**

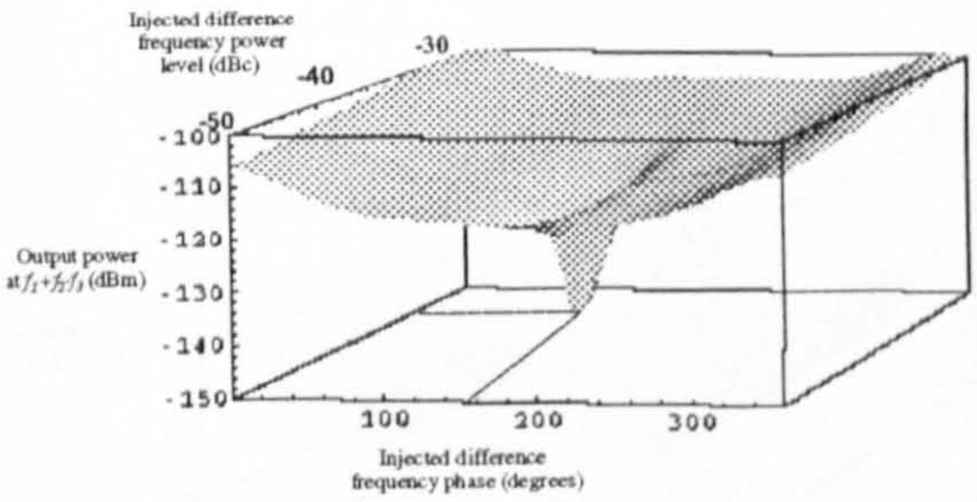

Figure D..26: **Third order IMD$(f_1 + f_2 - f_3)$amplitude variation as a function of injected difference frequency signal amplitude and phase.**

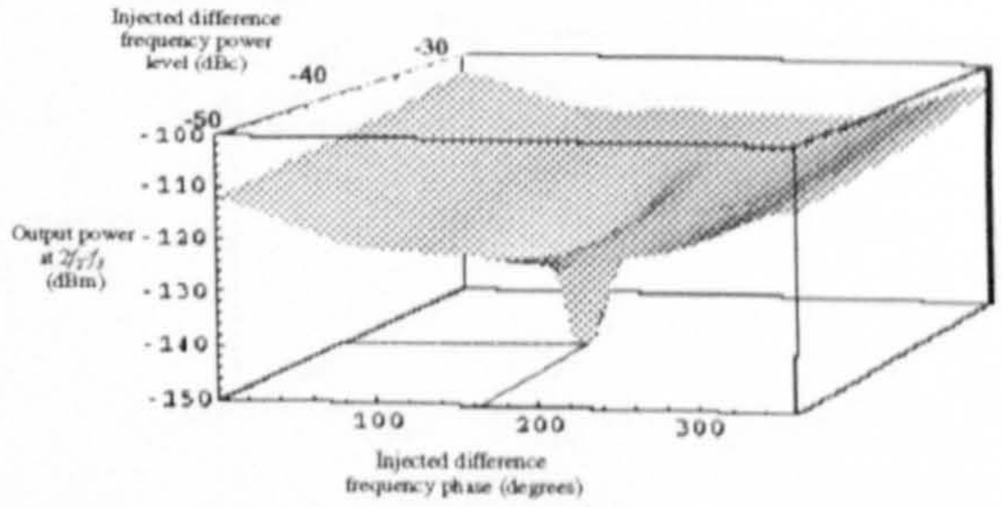

Figure D..28: **Third order IMD $(2f_2 - f_3)$ amplitude variation as a function of injected difference frequency signal amplitude and phase.**

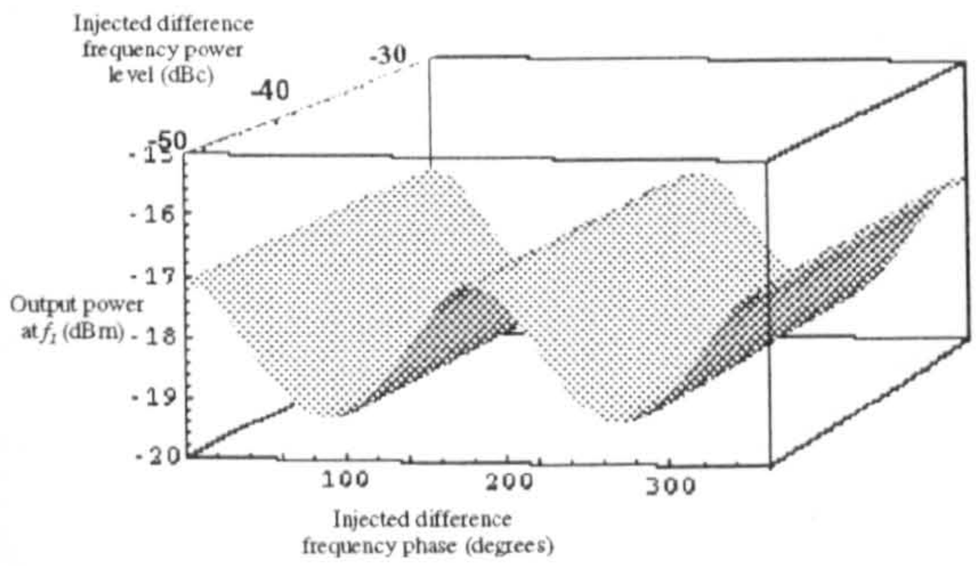

Figure D..29: **Third order IMD f_1 amplitude variation as a function of injected difference frequency signal amplitude and phase.**

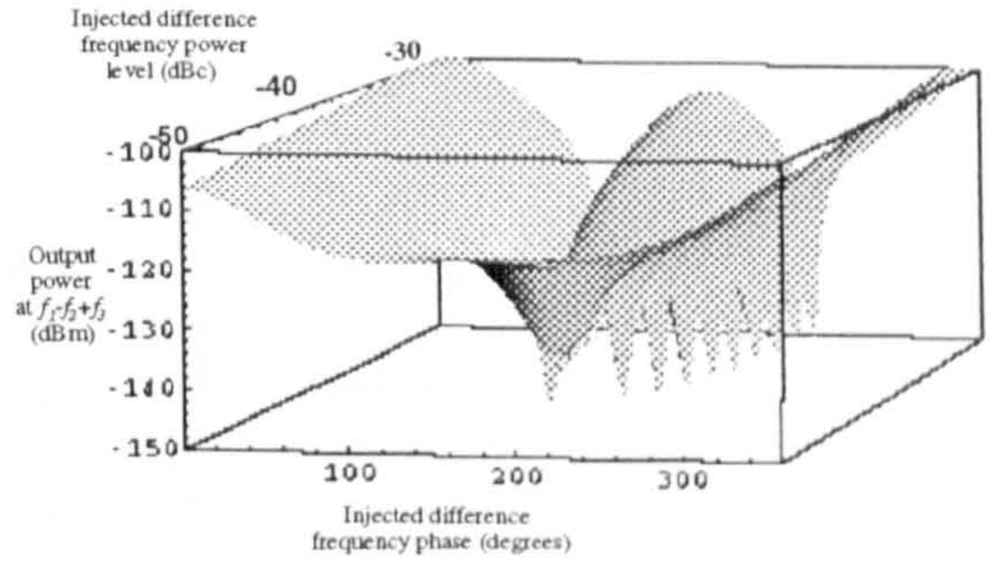

Figure D..31: **Third order IMD $(f_1 - f_2 + f_3)$ amplitude variation as a function of injected difference frequency signal amplitude and phase.**

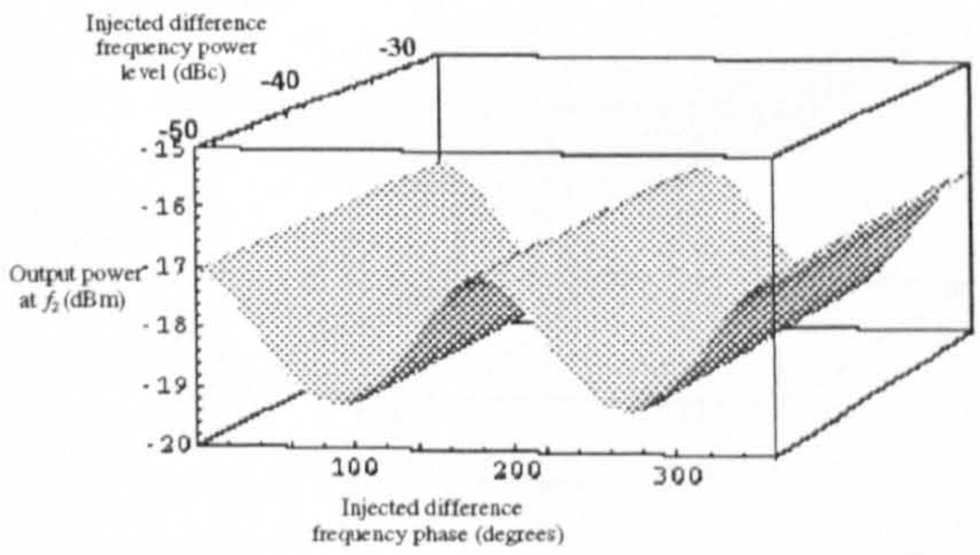

Figure D..30: **Third order IMD f_2 amplitude variation as a function of injected difference frequency signal amplitude and phase.**

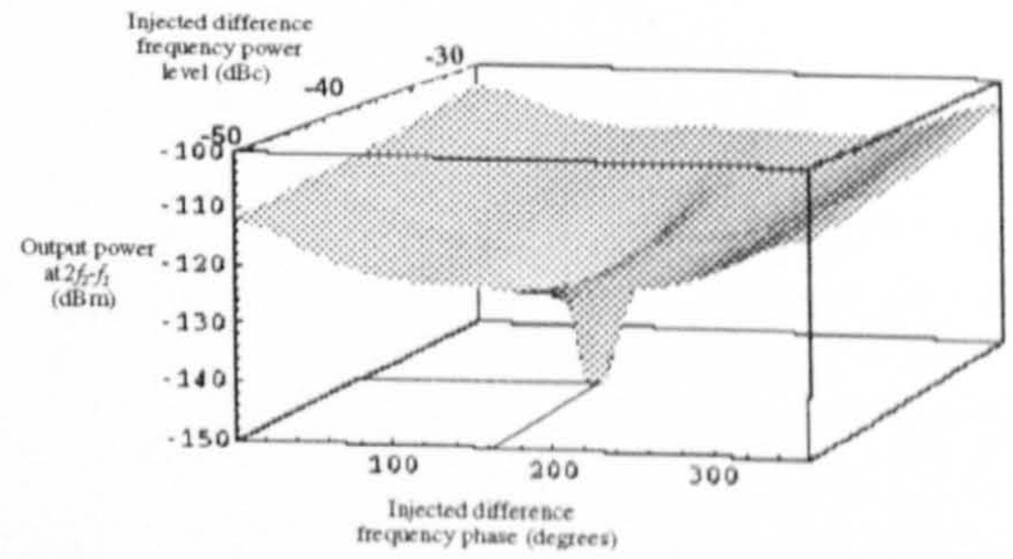

Figure D..32: **Third order IMD $(2f_2 - f_1)$ amplitude variation as a function of injected difference frequency signal amplitude and phase.**

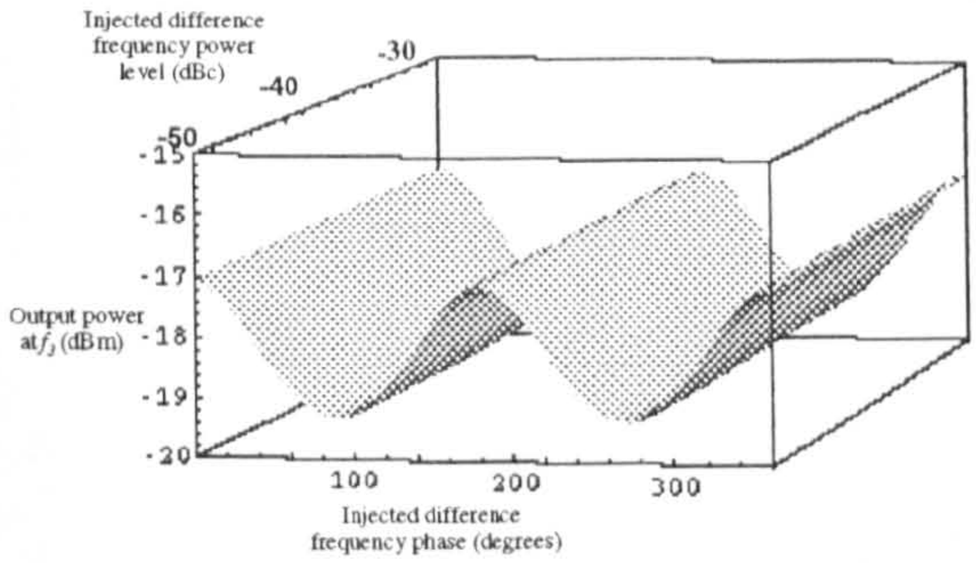

Figure D..33: **Third order IMD f_3 amplitude variation as a function of injected difference frequency signal amplitude and phase.**

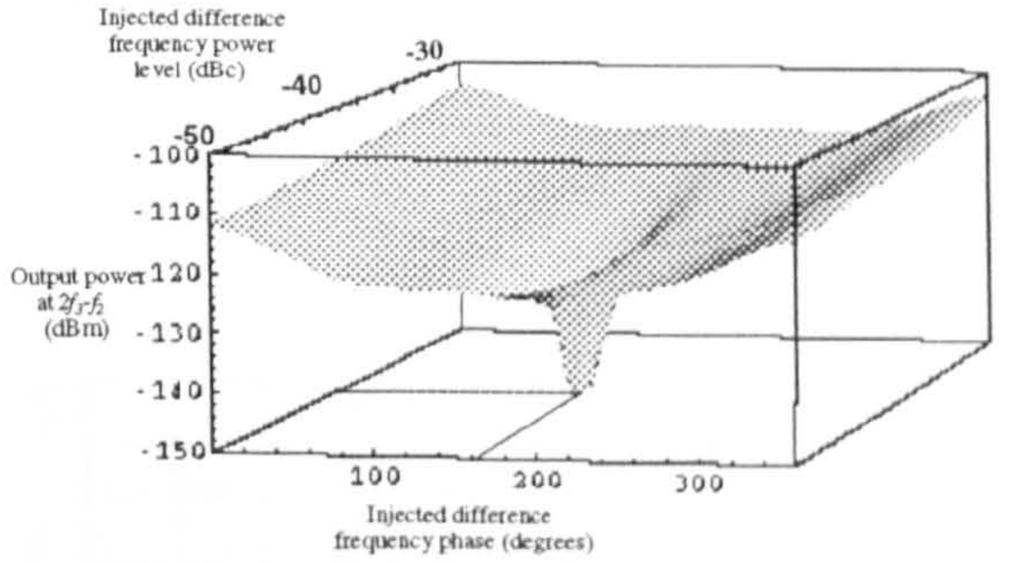

Figure D..35: **Third order IMD $(2f_3 - f_2)$ amplitude variation as a function of injected difference frequency signal amplitude and phase.**

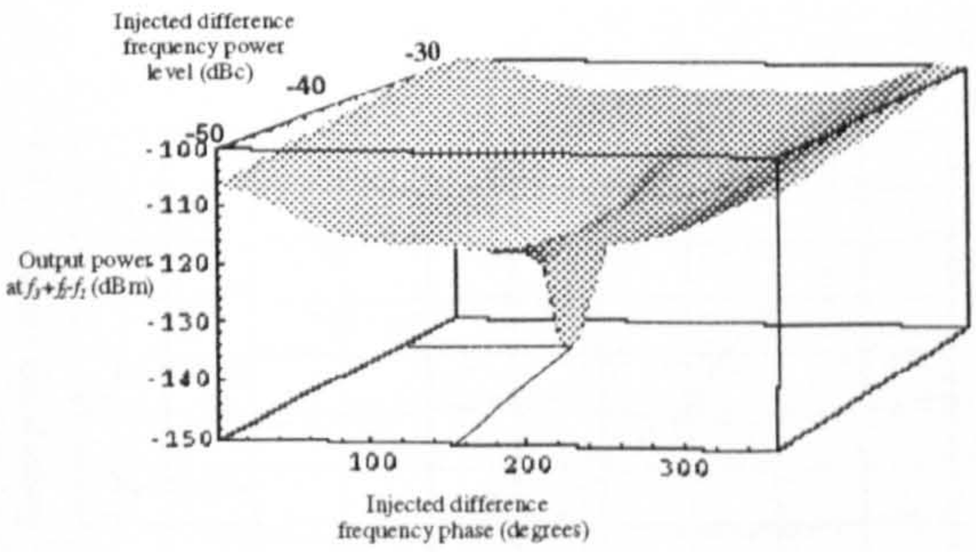

Figure D..34: **Third order IMD$(f_3 + f_2 - f_1)$ amplitude variation as a function of injected difference frequency signal amplitude and phase.**

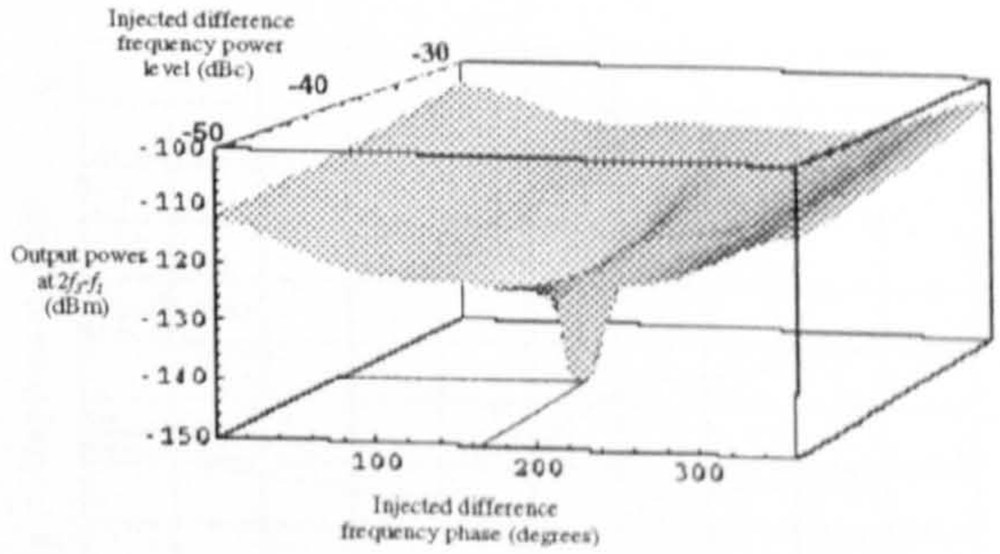

Figure D..36: **Third order IMD $(2f_3 - f_1)$ amplitude variation as a function of injected difference frequency signal amplitude and phase.**

APPENDIX E.

PHASE SENSITIVITY OF SYSTEMS

5.1 Second Harmonic Injection Technique

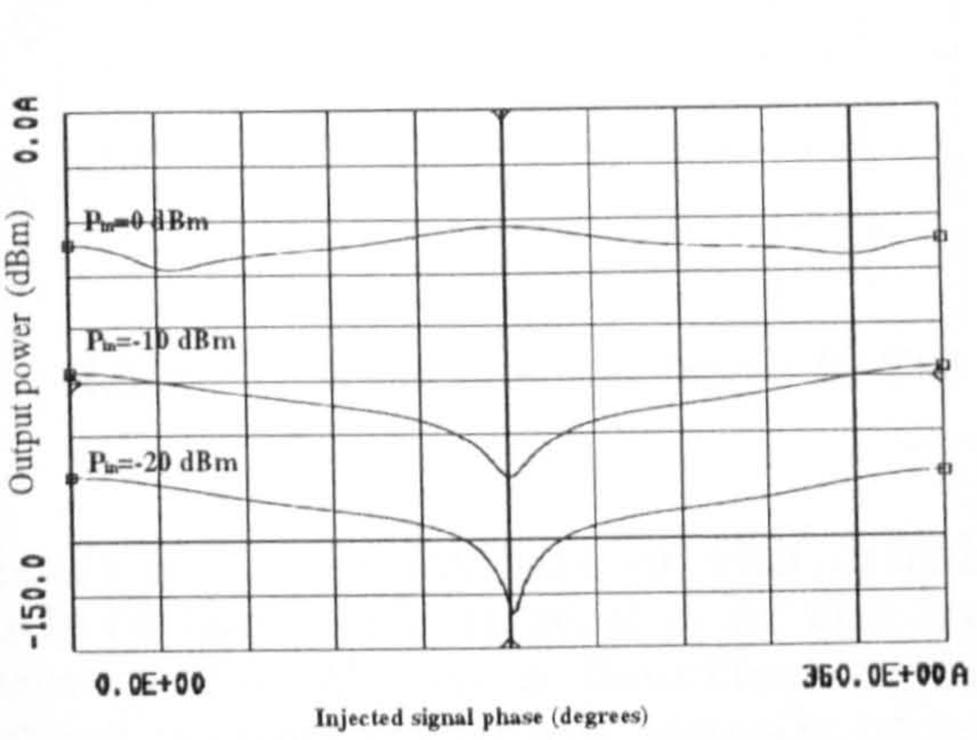

Figure E..1: **Variations in the amplitude of IM term** $(2f_1 - f_3)$ **at the frequency** $2.479GHz$ **as a function of injected second harmonic signals phase for input power levels of** $-20dBm$, $-10dBm$ **and** $0dBm$.

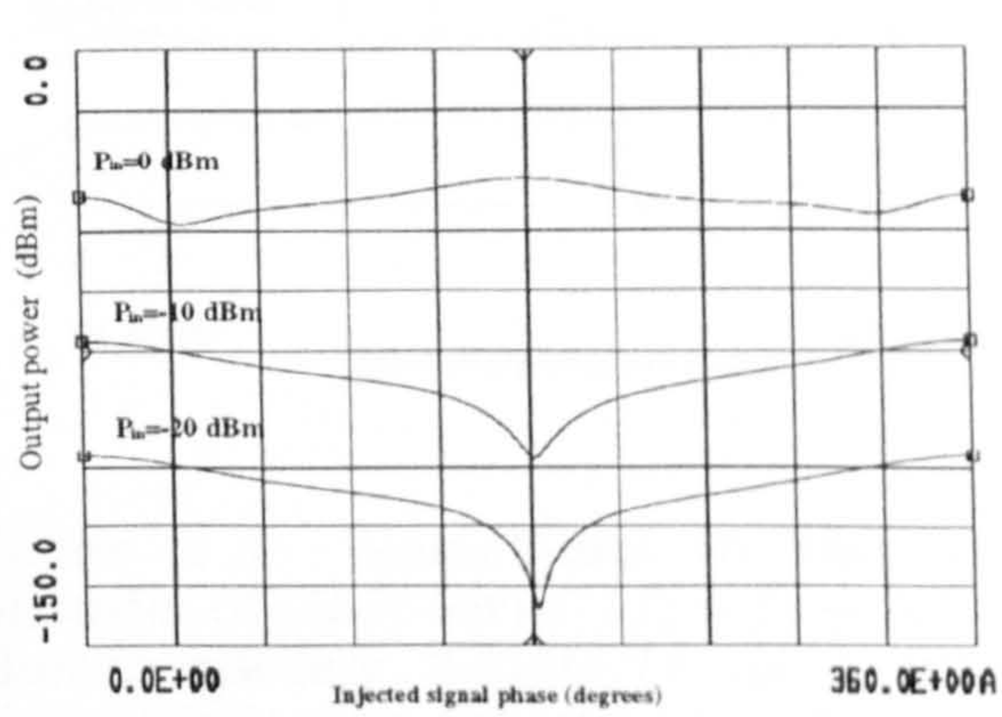

Figure E..3: **Variations in the amplitude of the fundamental** $(2f_1 - f2)$ **at the frequency** $2.49GHz$ **as a function of injected second harmonic signals phase for input power levels of** $-20dBm$, $-10dBm$ **and** $0dBm$.

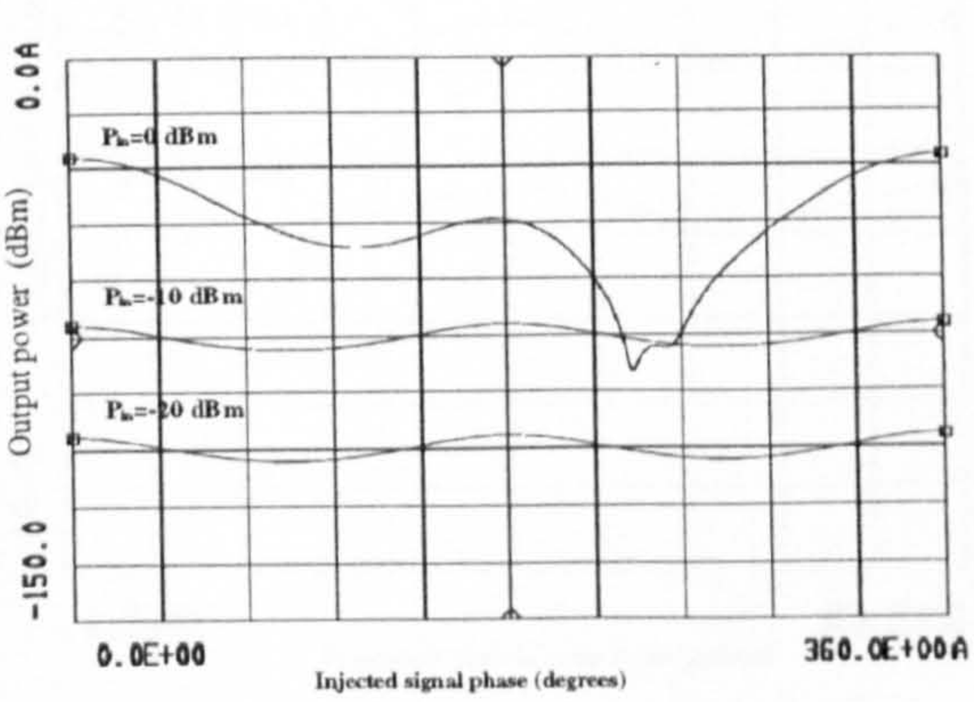

Figure E..2: **Variations in the amplitude of IM term** $(f_1 + f_2 - f_3)$ **at the frequency** $2.489GHz$ **as a function of injected second harmonic signals phase for input power levels of** $-20dBm$, $-10dBm$ **and** $0dBm$.

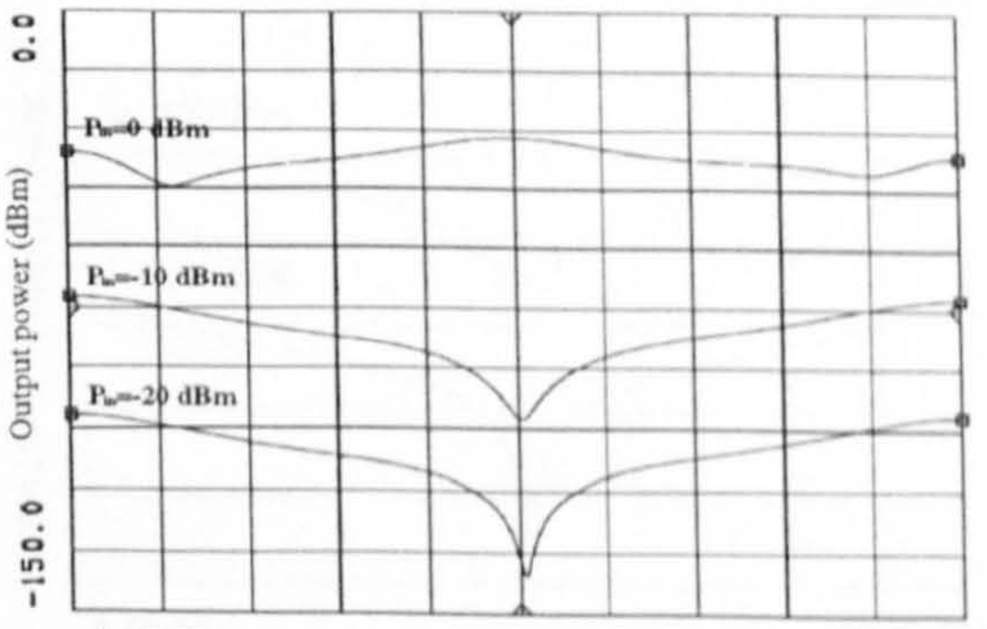

Figure E..4: **Variations in the amplitude of IM term** $(2f_2 - f_3)$ **at the frequency** $2.499GHz$ **as a function of injected second harmonic signals phase for input power levels of** $-20dBm$, $-10dBm$ **and** $0dBm$.

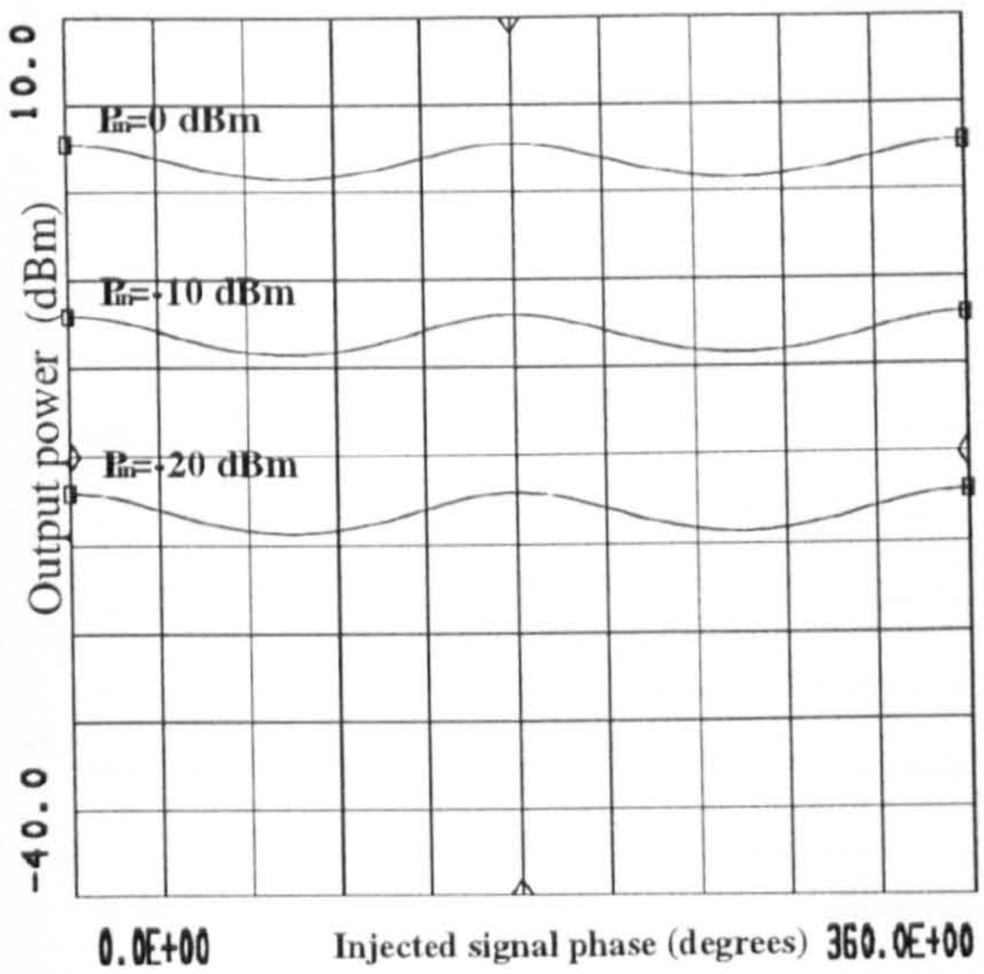

Figure E..5: **Variations in the amplitude of the fundamental f_1 at the frequency $2.5GHz$ as a function of injected second harmonic signals phase for input power levels of $-20dBm$, $-10dBm$ and $0dBm$.**

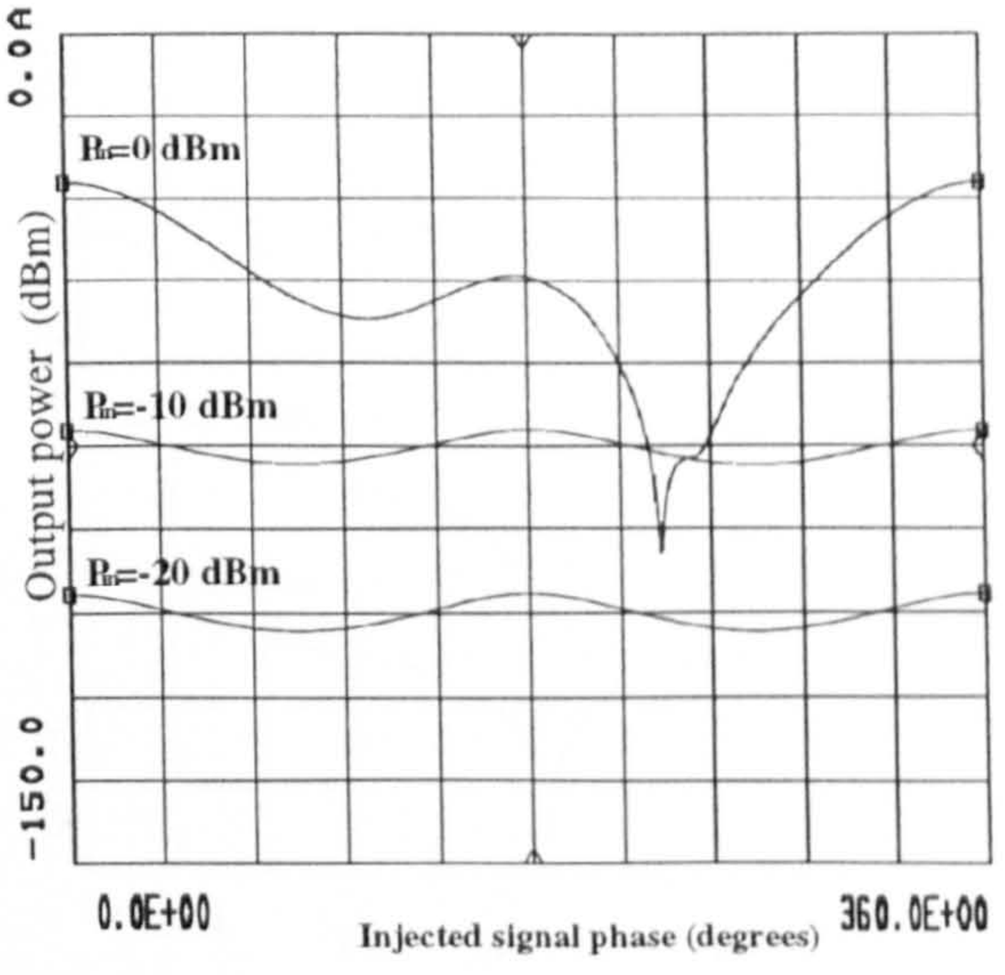

Figure E..7: **Variations in the amplitude of IM term $(f_1 - f_2 + f_3)$ at the frequency $2.511GHz$ as a function of injected second harmonic signals phase for input power levels of $-20dBm$, $-10dBm$ and $0dBm$.**

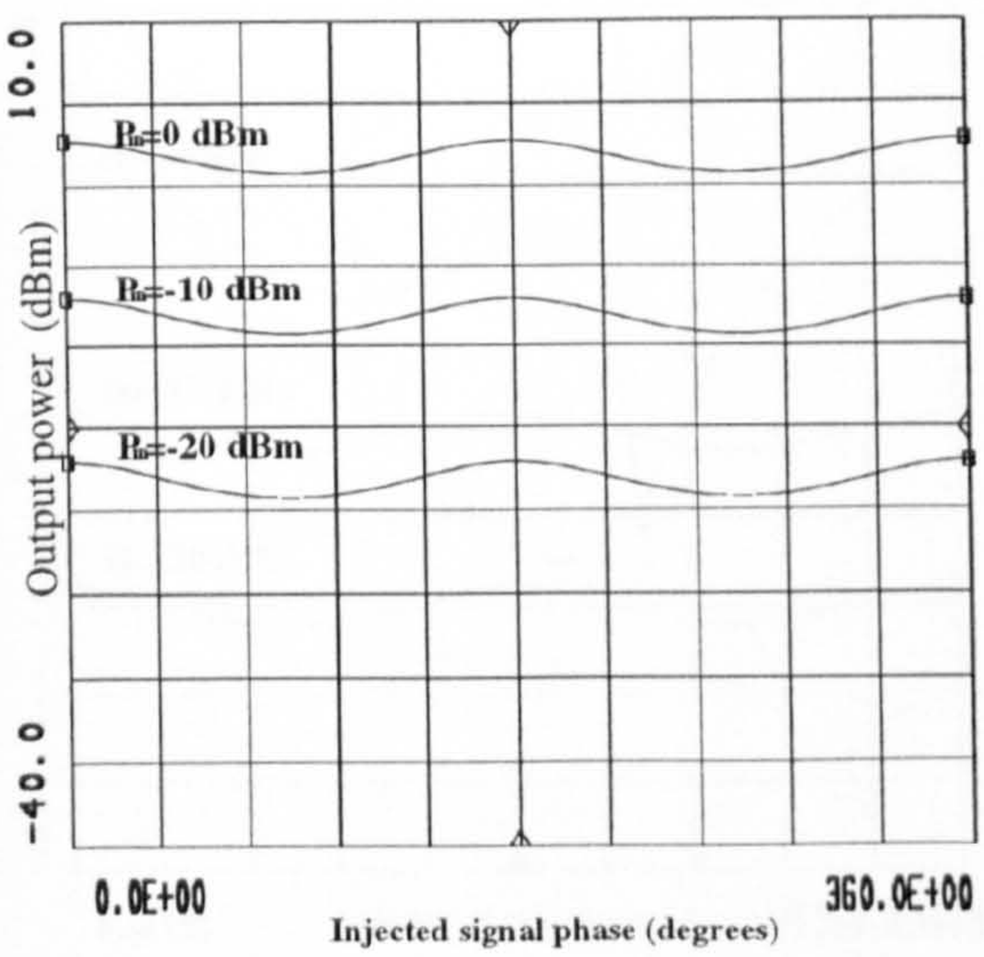

Figure E..6: **Variations in the amplitude of IM term f_2 at the frequency $2.51GHz$ as a function of injected second harmonic signals phase for input power levels of $-20dBm$, $-10dBm$ and $0dBm$.**

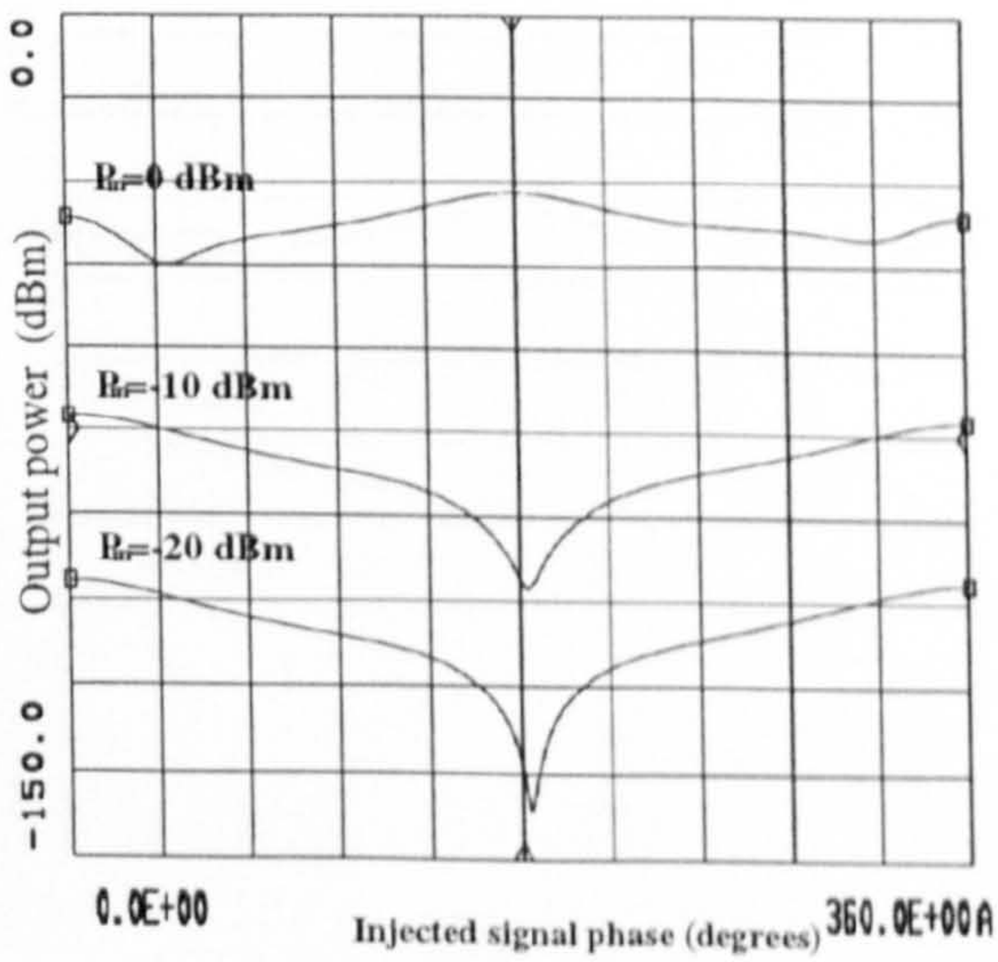

Figure E..8: **Variations in the amplitude of IM term $(2f_2 - f_1)$ at the frequency $2.52GHz$ as a function of injected second harmonic signals phase for input power levels of $-20dBm$, $-10dBm$ and $0dBm$.**

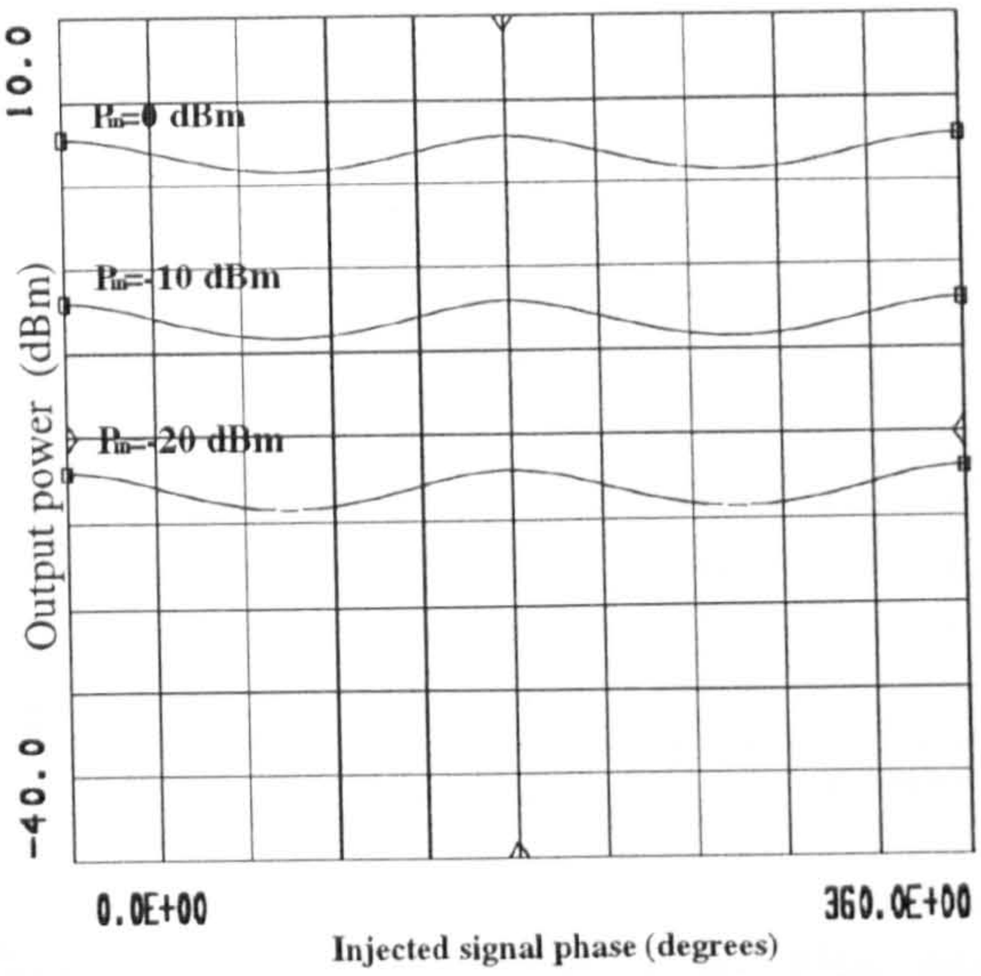

Figure E..9: **Variations in the amplitude of the fundamental f_3 at the frequency**$2.521GHz$ **as a function of injected second harmonic signals phase for input power levels of** $-20dBm$, $-10dBm$ **and** $0dBm$.

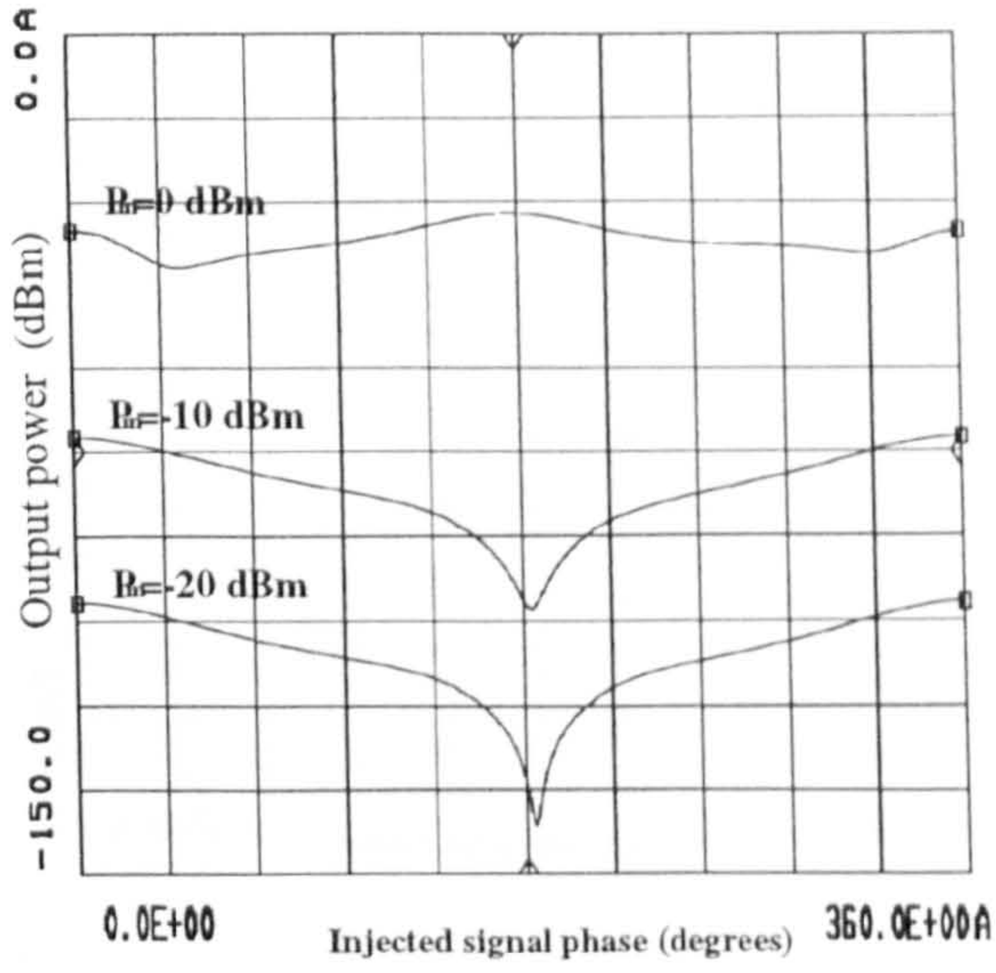

Figure E..11: **Variations in the amplitude of IM term** $(2f_3 - f_2)$ **at the frequency** $2.532GHz$ **as a function of injected second harmonic signals phase for input power levels of** $-20dBm$, $-10dBm$ **and** $0dBm$.

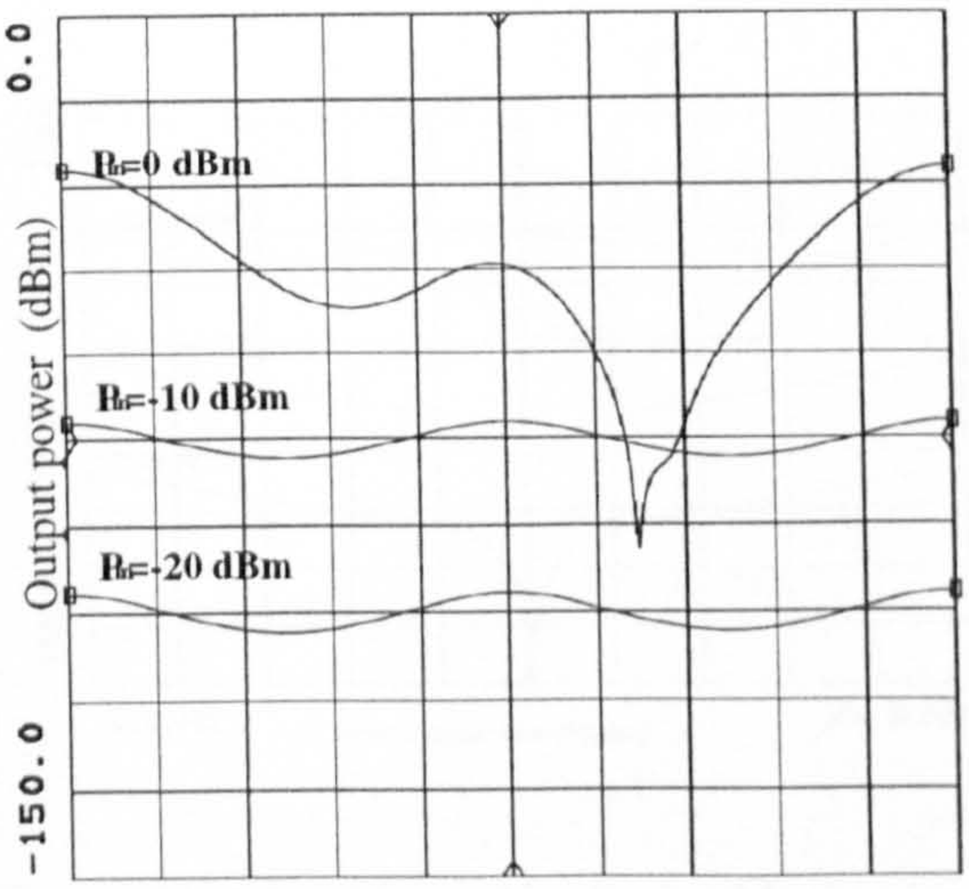

Figure E..10: **Variations in the amplitude of IM term** $(f_3 + f_2 - f_1)$ **at the frequency** $2.531GHz$ **as a function of injected second harmonic signals phase for input power levels of** $-20dBm$, $-10dBm$ **and**$0dBm$.

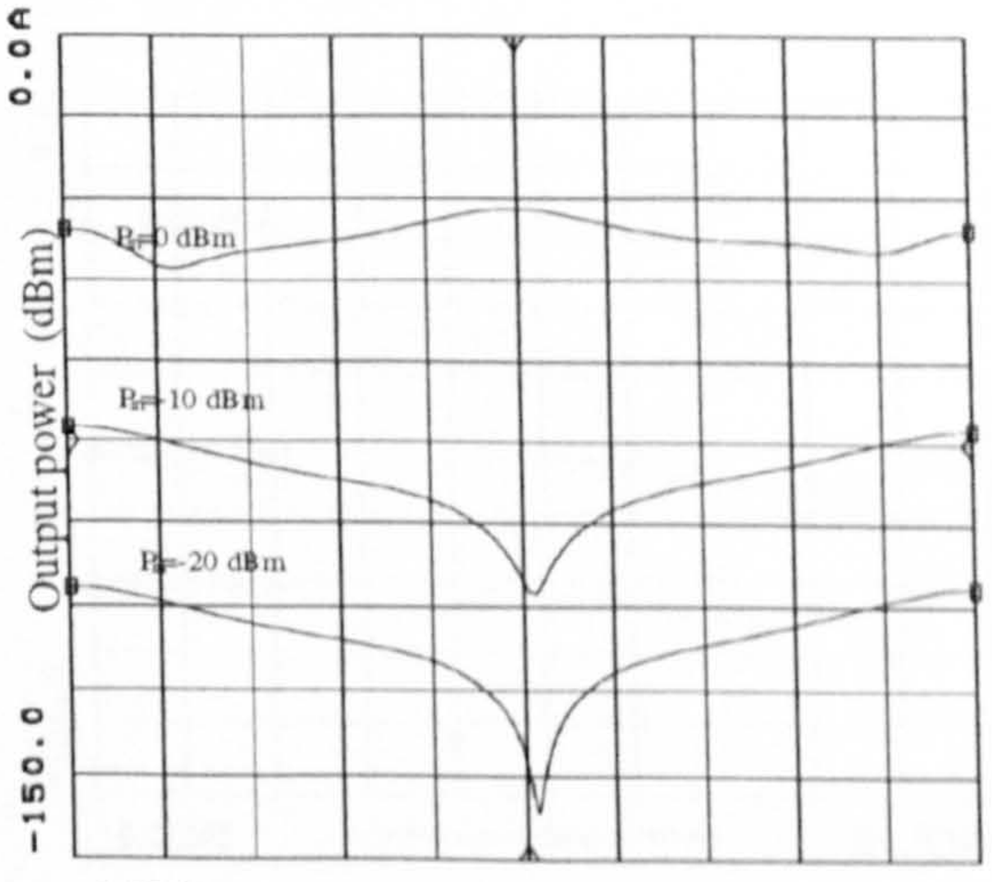

Figure E..12: **Variations in the amplitude of IM term** $(2f_3 - f_1)$ **at the frequency** $2.542GHz$ **as a function of injected second harmonic signals phase for input power levels of** $-20dBm$, $-10dBm$ **and** $0dBm$.

5.2 Frequency Summation Technique

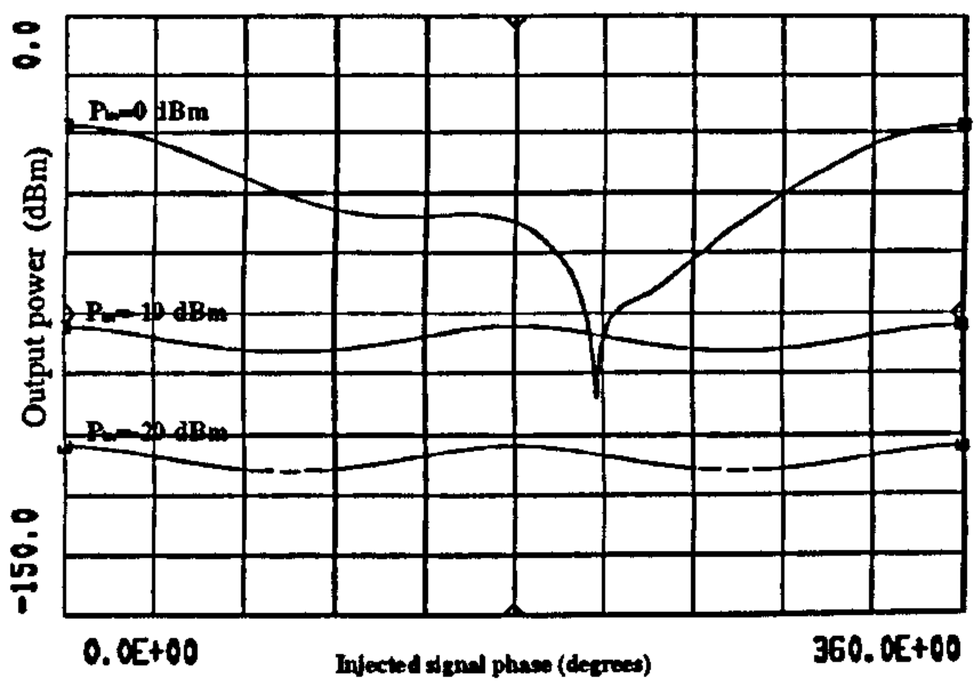

Figure E..13: **Variations in the amplitude of the IM term $(2f_1 - f_3)$ at the frequency $2.479GHz$ as a function of frequency sum of the fundamental signals phase for input power levels of $-20dBm$, $-10dBm$ and $0dBm$.**

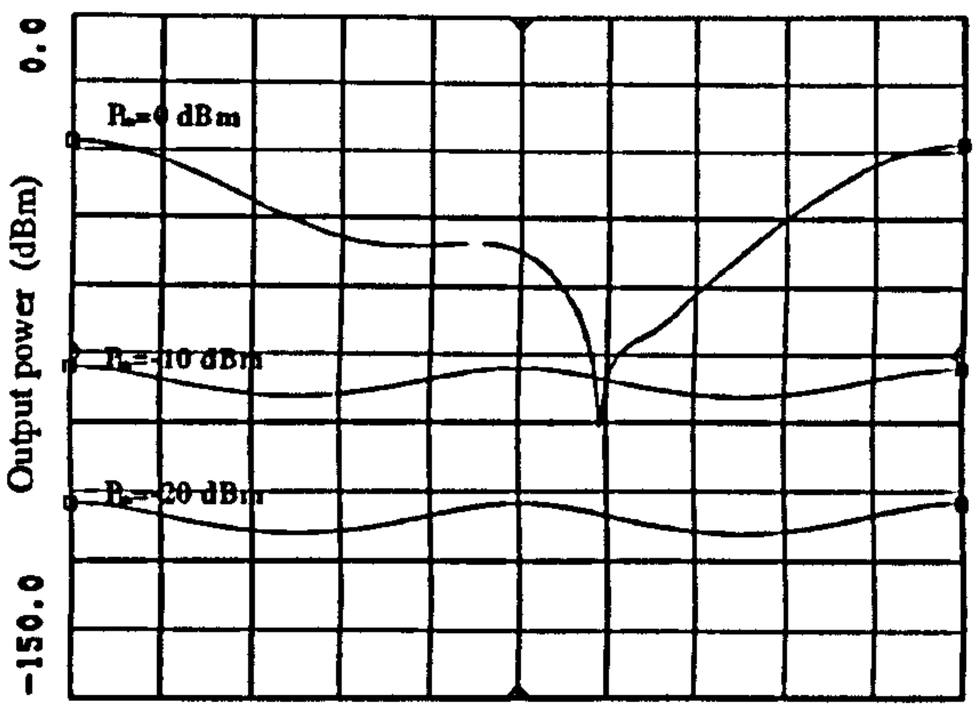

Figure E..15: **Variations in the amplitude of the IM term $(2f_1 - f_2)$ at the frequency $2.49GHz$ as a function of frequency sum of the fundamental signals phase for input power levels of $-20dBm$, $-10dBm$ and $0dBm$.**

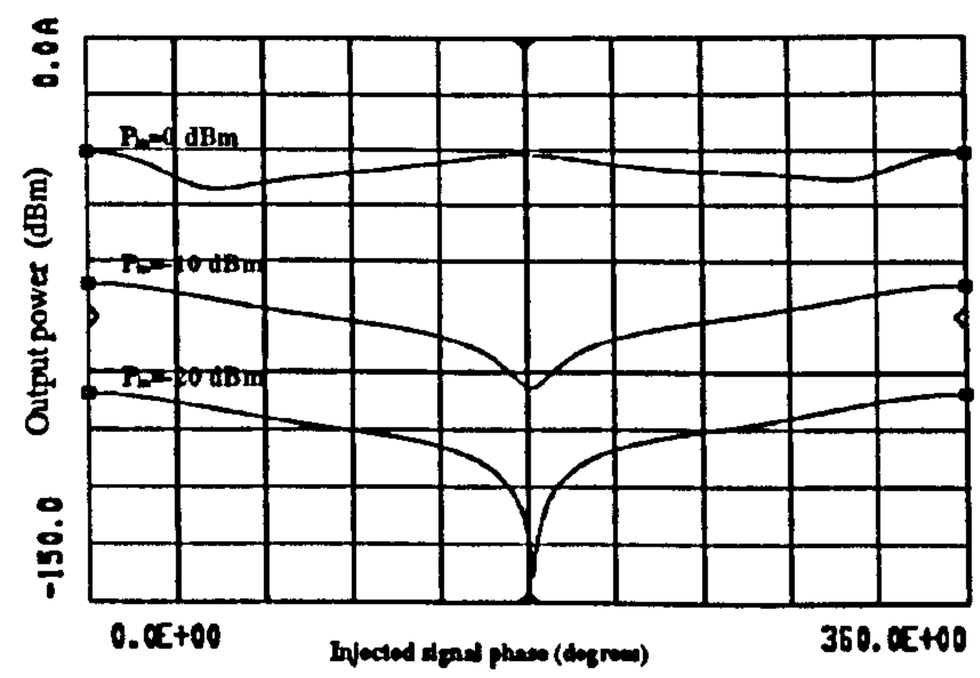

Figure E..14: **Variations in the amplitude of IM term $(f_1 + f_2 - f_3)$ at the frequency $2.489GHz$ as a function of injected frequency sum of the fundamental signals phase for input power levels of $-20dBm$, $-10dBm$ and$0dBm$.**

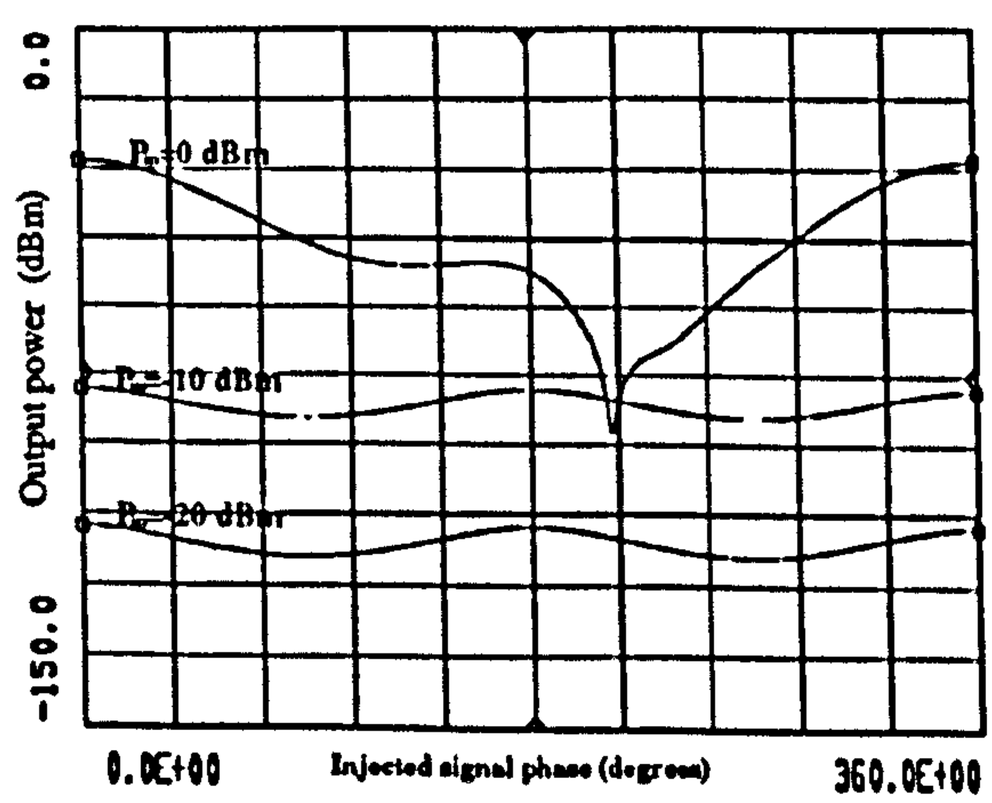

Figure E..16: **Variations in the amplitude of IM term $(2f_2 - f_3)$ at the frequency $2.499GHz$ as a function of injected frequency sum of the fundamental signals phase for input power levels of $-20dBm$, $-10dBm$ and $0dBm$.**

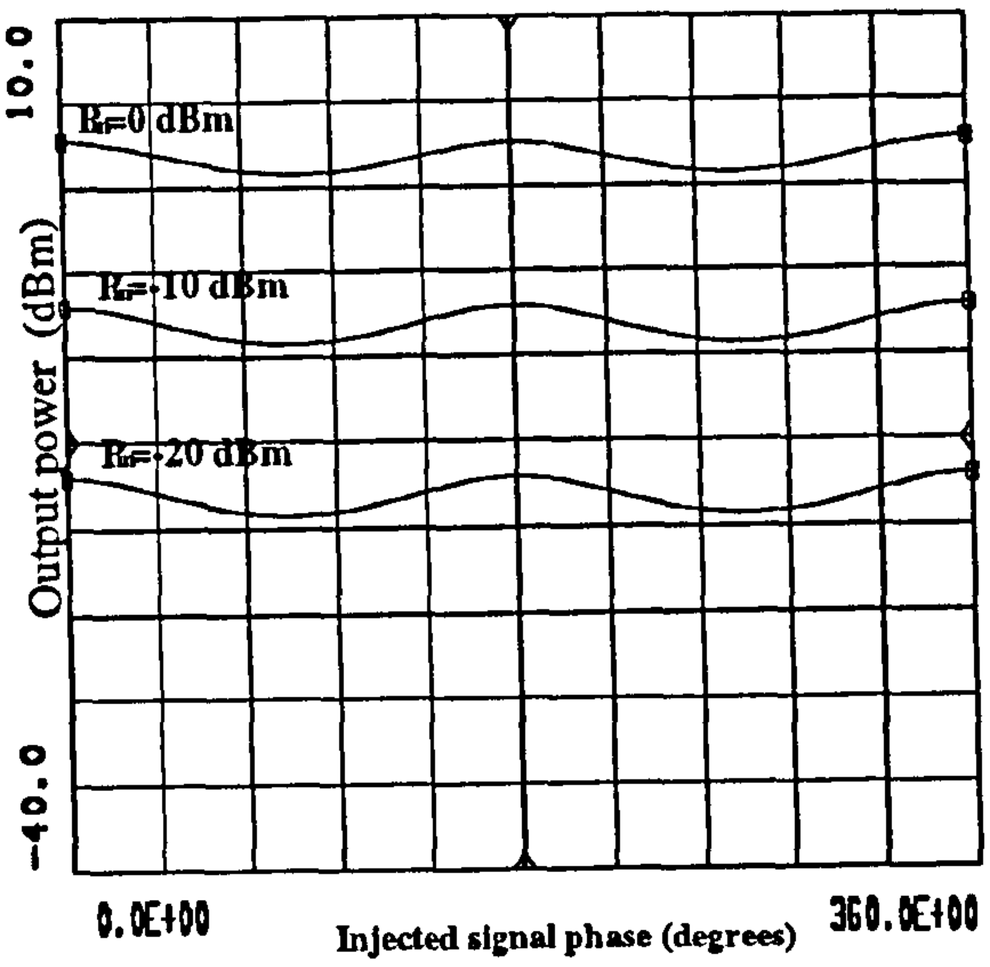

Figure E..17: **Variations in the amplitude of the fundamental f_1 at the frequency $2.5GHz$ as a function of injected frequency sum of the fundamental signals phase for input power levels of $-20dBm$, $-10dBm$ and $0dBm$.**

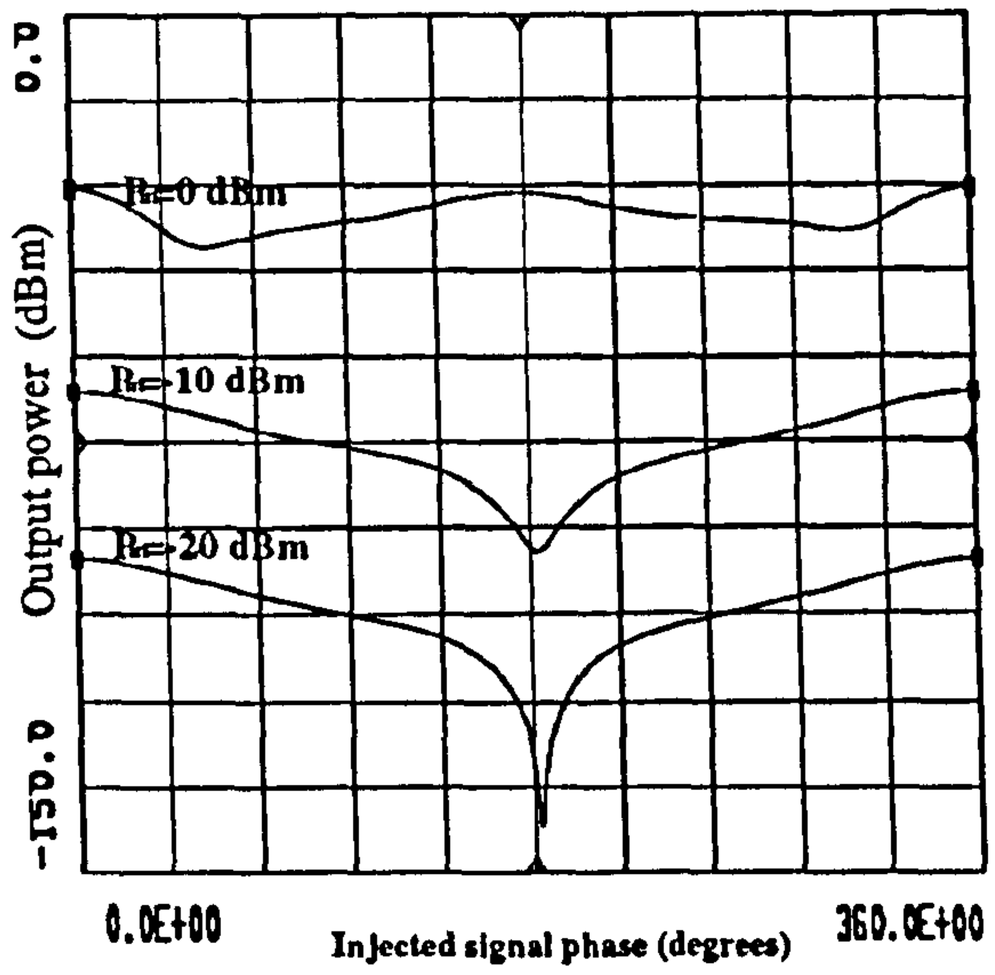

Figure E..19: **Variations in the amplitude of IM term $(f_1 - f_2 + f_3)$ at the frequency $2.511GHz$ as a function of injected frequency sum of the fundamental signals phase for input power levels of $-20dBm$, $-10dBm$ and $0dBm$.**

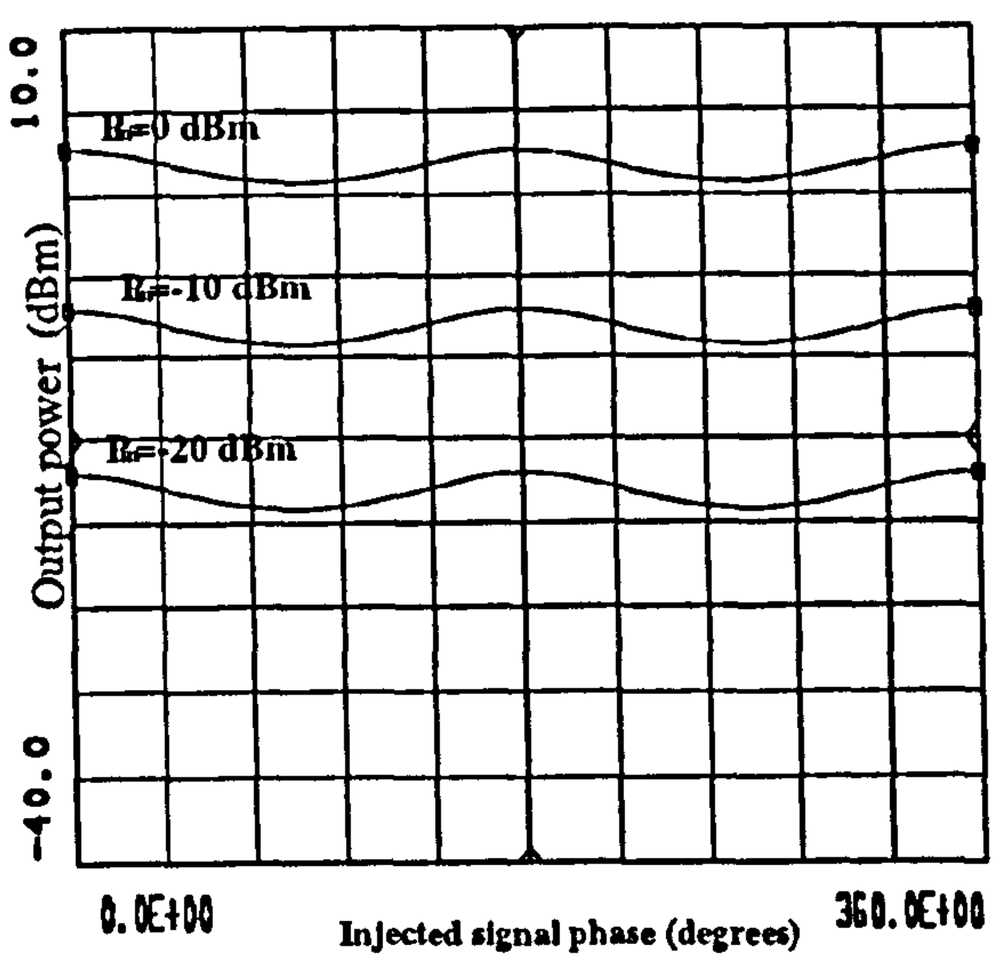

Figure E..18: **Variations in the amplitude of the fundamental f_2 at the frequency $2.51GHz$ as a function of injected frequency sum of the fundamental signals phase for input power levels of $-20dBm$, $-10dBm$ and $0dBm$.**

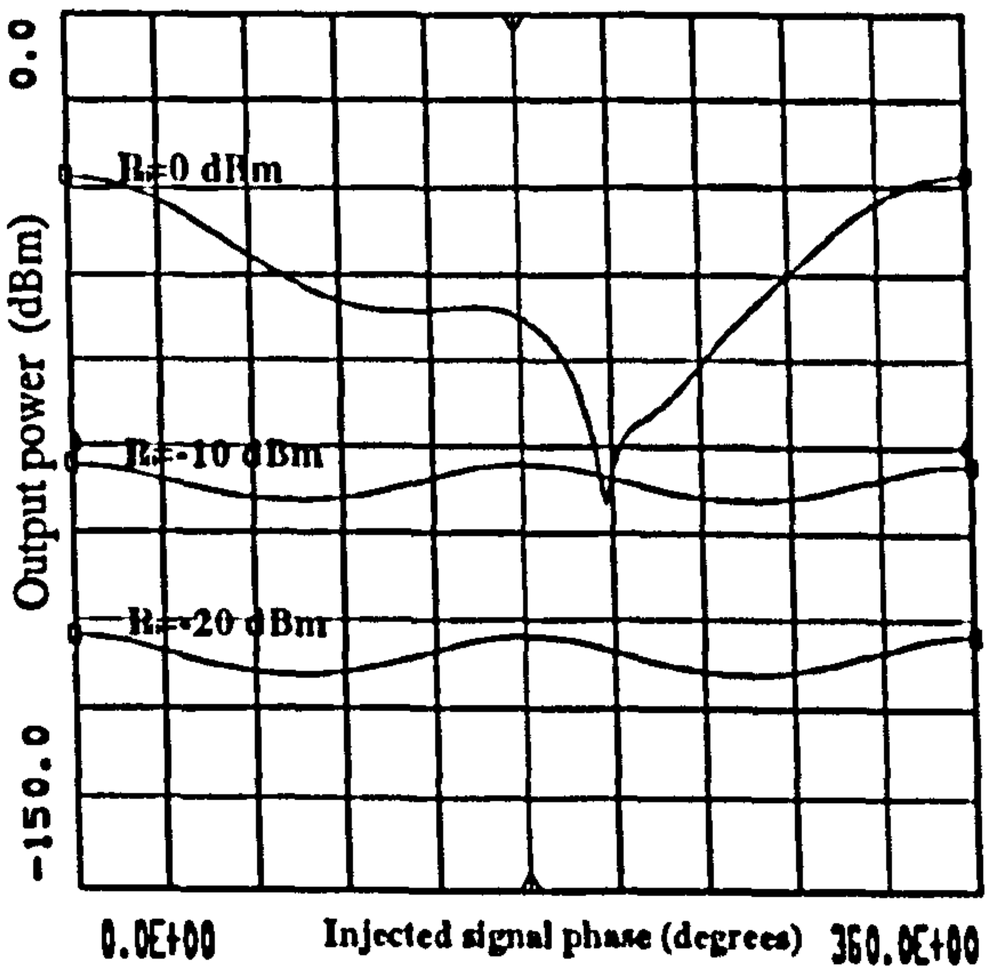

Figure E..20: **Variations in the amplitude of IM term $(2f_2 - f_1)$ at the frequency $2.52GHz$ as a function of injected frequency sum of the fundamental signals phase for input power levels of $-20dBm$, $-10dBm$ and $0dBm$.**

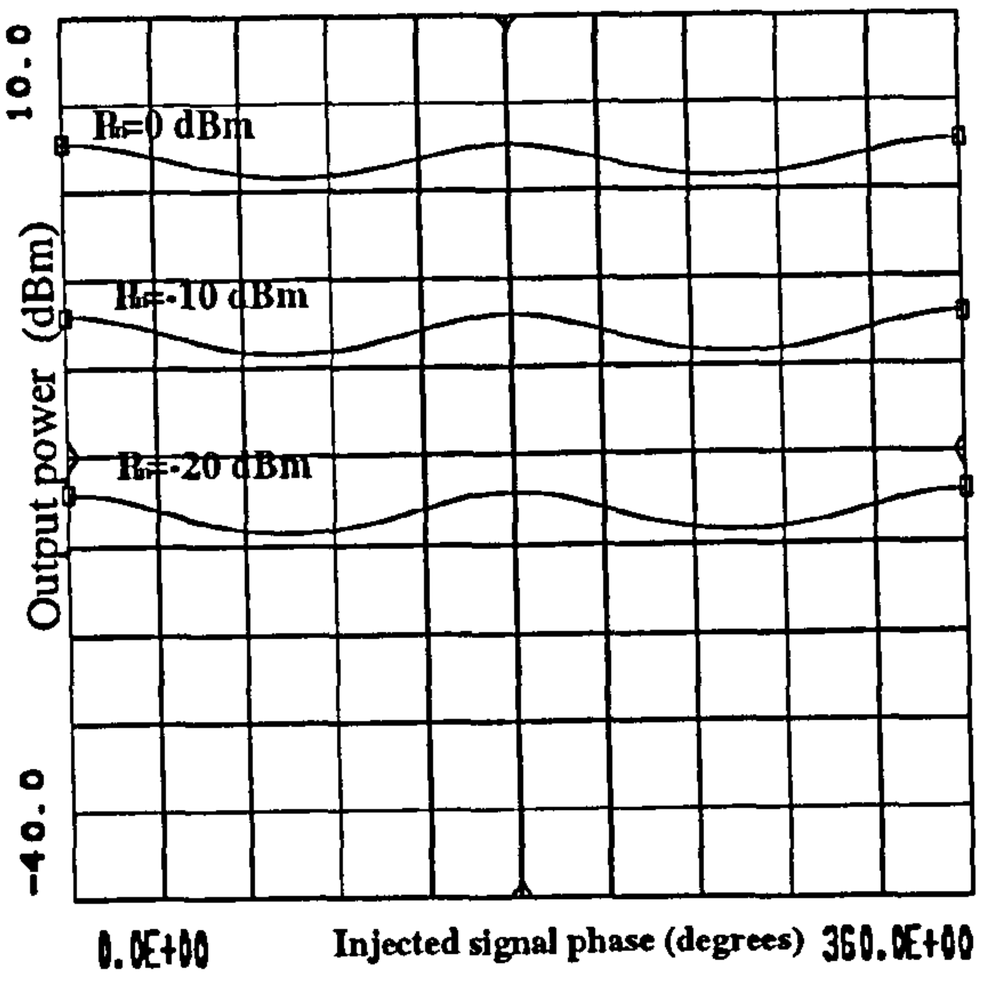

Figure E..21: Variations in the amplitude of the fundamental f_3 at the frequency $2.521GHz$ as a function of injected frequency sum of the fundamental signals phase for input power levels of $-20dBm$, $-10dBm$ and $0dBm$.

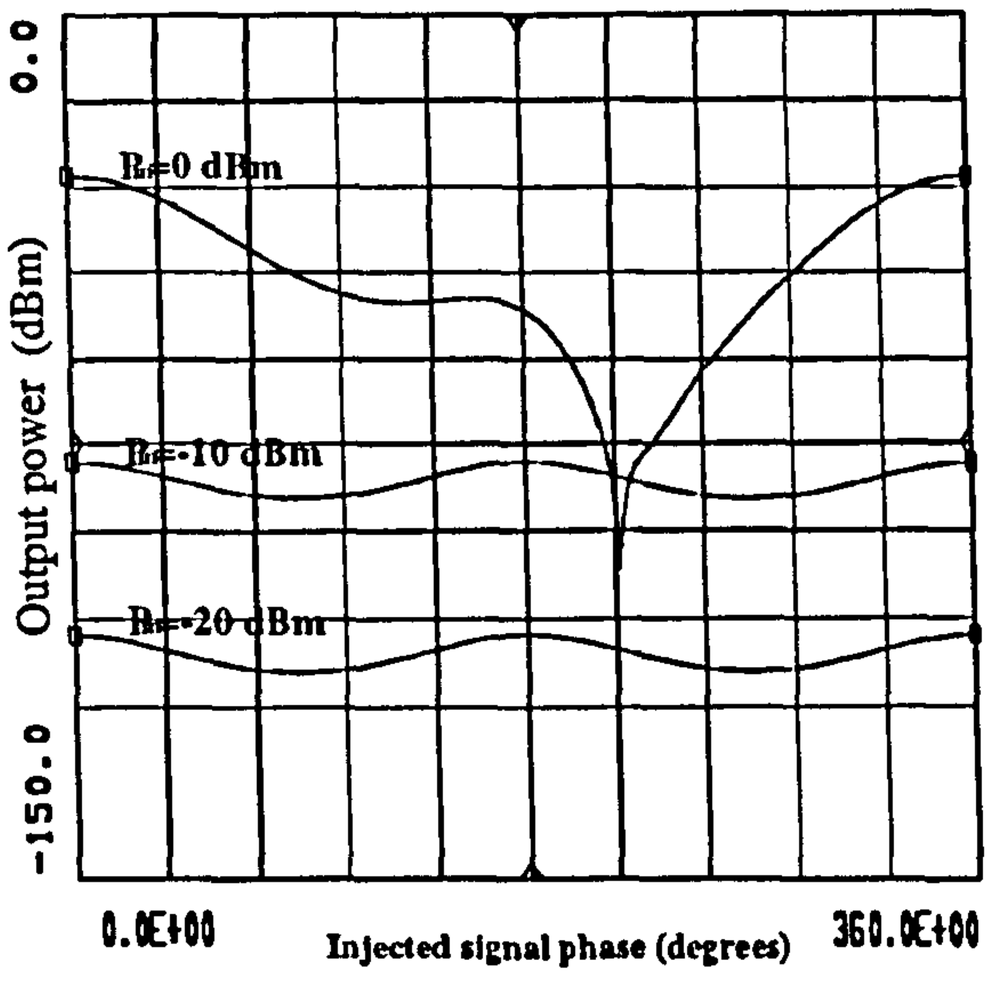

Figure E..23: Variations in the amplitude of IM term $(2f_3 - f_2)$ at the frequency $2.532GHz$as a function of injected frequency sum of the fundamental signals phase for input power levels of $-20dBm$, $-10dBm$ and $0dBm$.

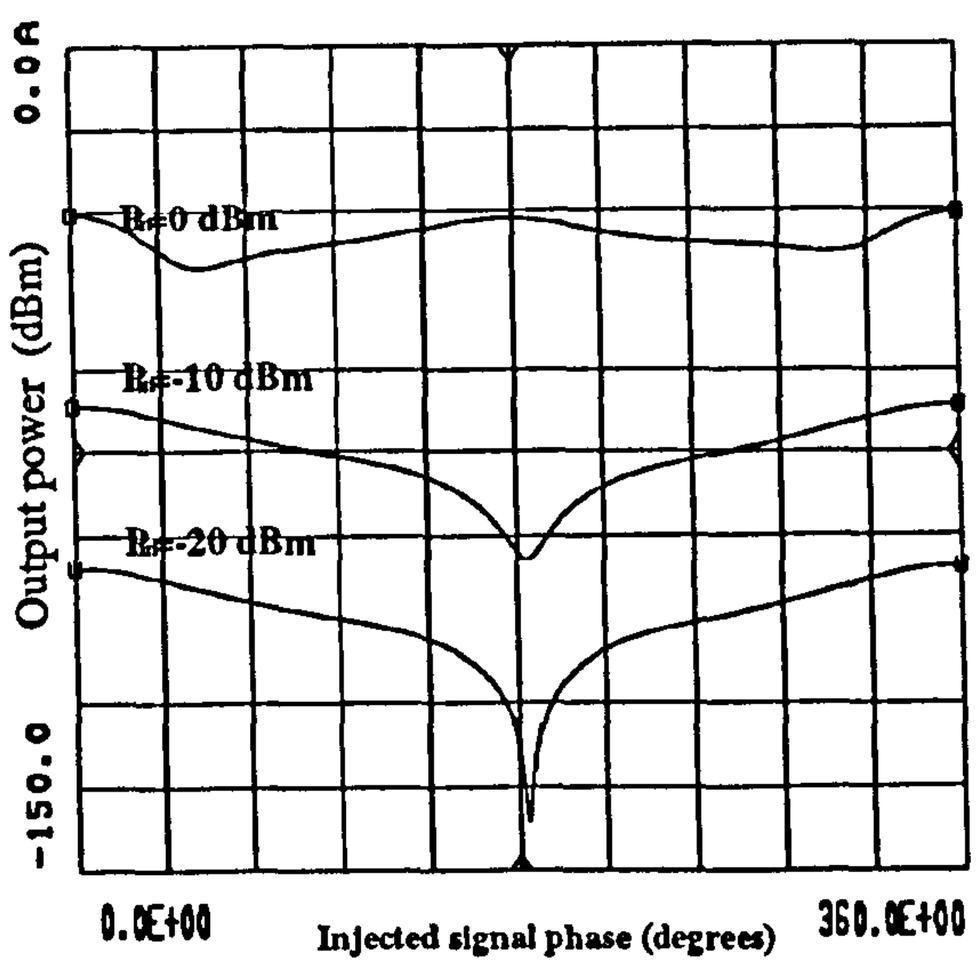

Figure E..22: Variations in the amplitude of IM term $(f_3 + f_2 - f_1)$ at the frequency $2.531GHz$ as a function of injected frequency sum of the fundamental signals phase for input power levels of $-20dBm$, $-10dBm$ and $0dBm$.

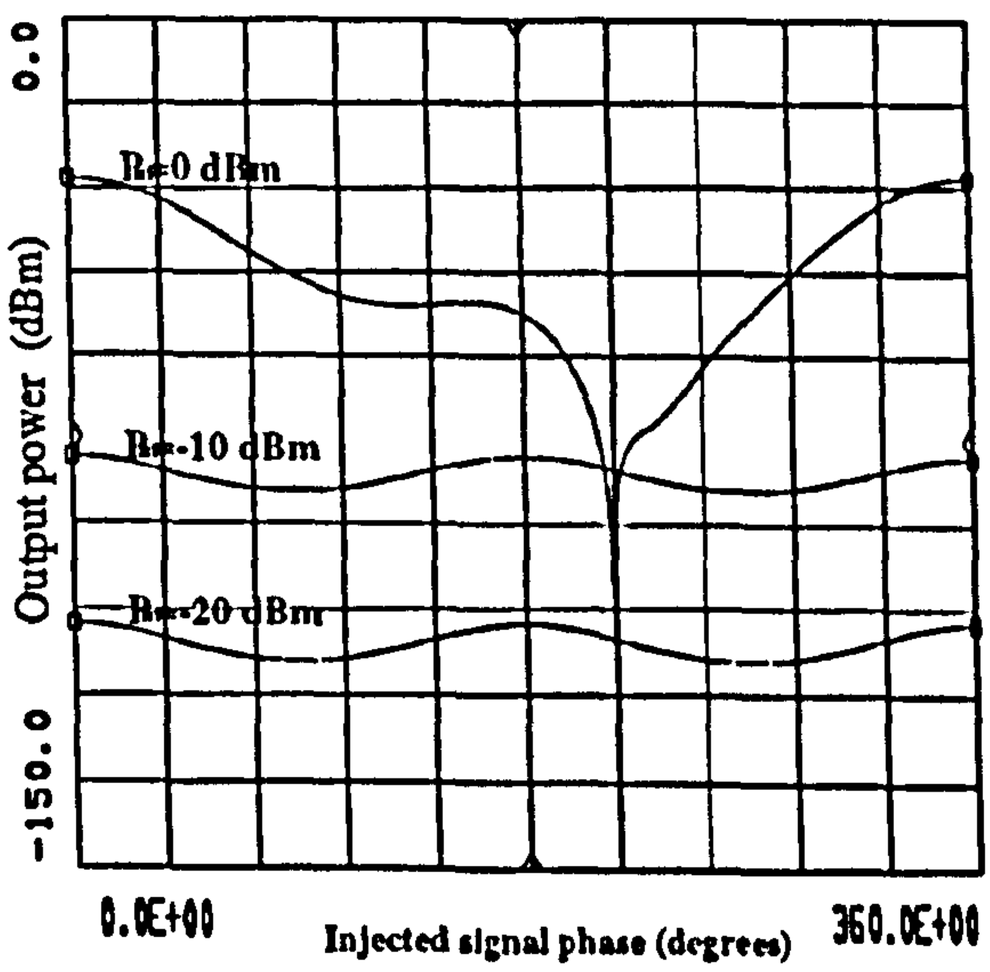

Figure E..24: Variations in the amplitude of IM term $(2f_3 - f_1)$ at the frequency $2.542GHz$ as a function of injected frequency sum of the fundamental signals phase for input power levels of $-20dBm$, $-10dBm$ and $0dBm$.

5.3 Difference Frequency Technique

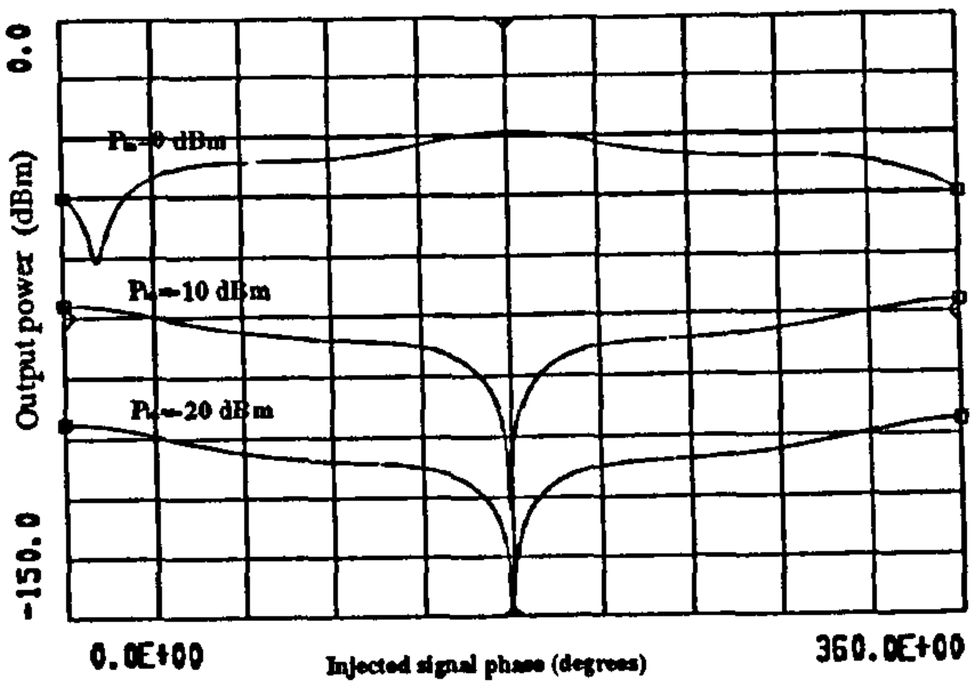

Figure E..25: **Variations in the amplitude of IM term $(2f_1 - f_3)$ at the frequency $2.479GHz$ as a function of injected difference frequency signals phase for input power levels of $-20dBm$, $-10dBm$ and $0dBm$.**

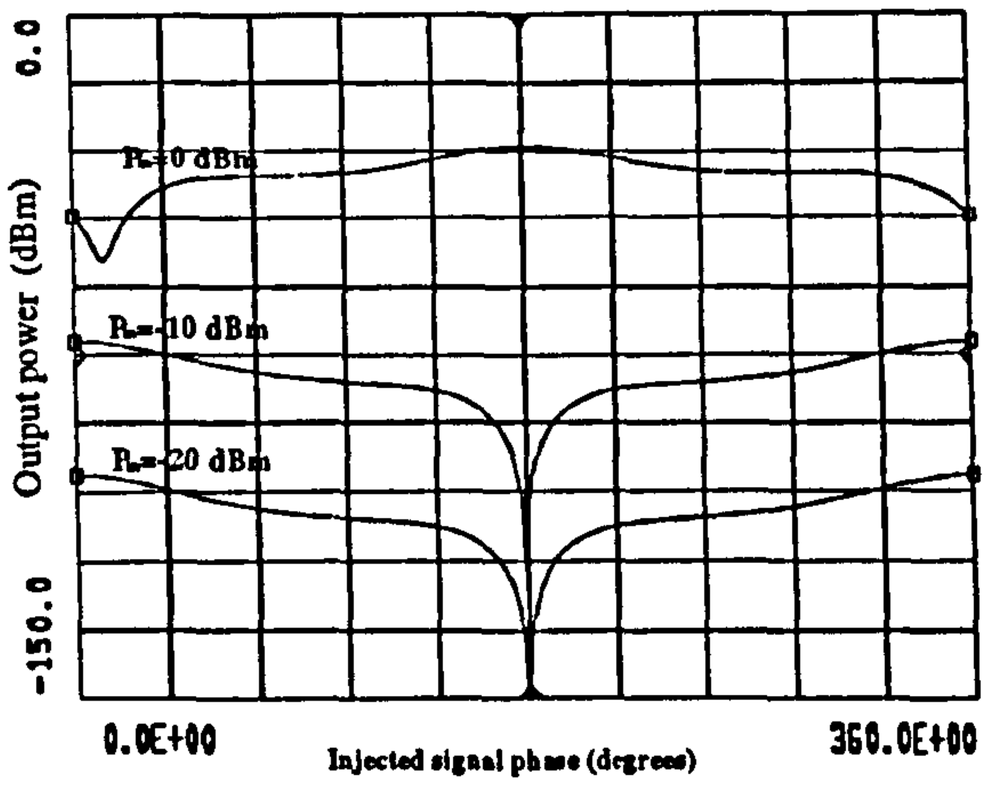

Figure E..27: **Variations in the amplitude of the fundamental$(2f_1 - f_2)$ at the frequency $2.49GHz$ as a function of injected difference frequency signals phase for input power levels of $-20dBm$, $-10dBm$ and $0dBm$.**

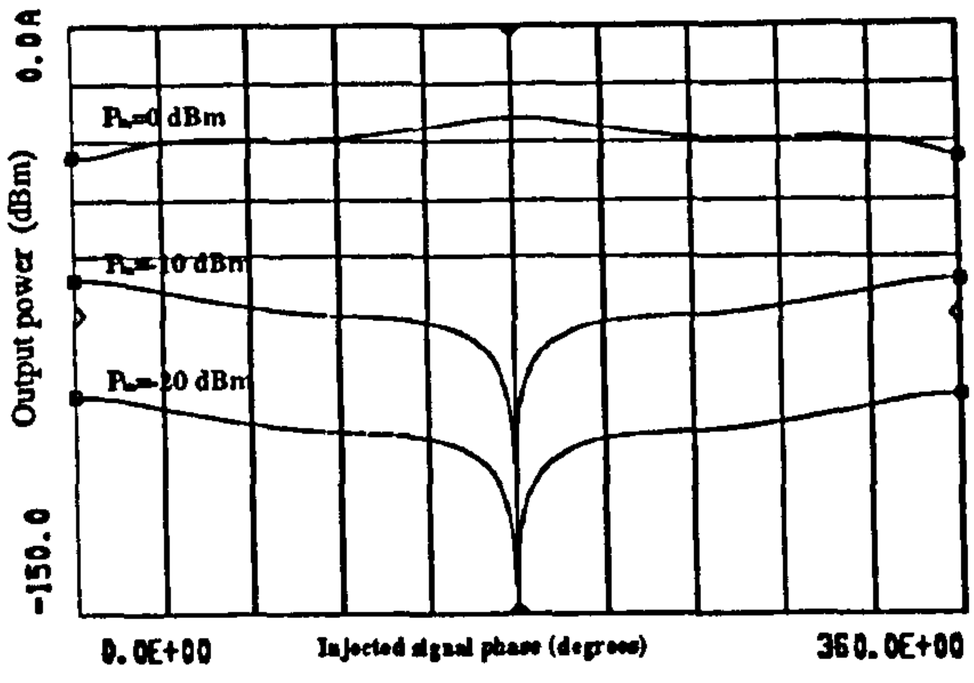

Figure E..26: **Variations in the amplitude of IM term $(f_1 + f_2 - f_3)$ at the frequency $2.489GHz$ as a function of injected difference frequency signals phase for input power levels of $-20dBm$, $-10dBm$ and $0dBm$.**

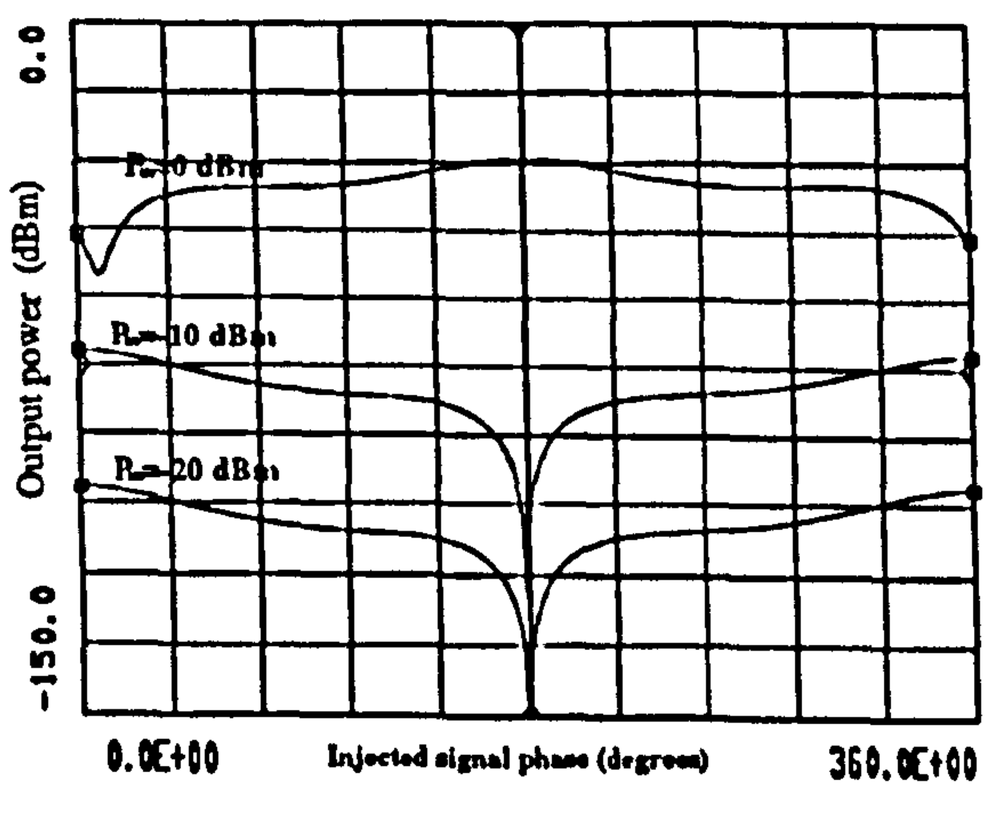

Figure E..28: **Variations in the amplitude of IM term $(2f_2 - f_3)$ at the frequency $2.499GHz$ as a function of difference frequency signals phase for input power levels of $-20dBm$, $-10dBm$ and $0dBm$.**

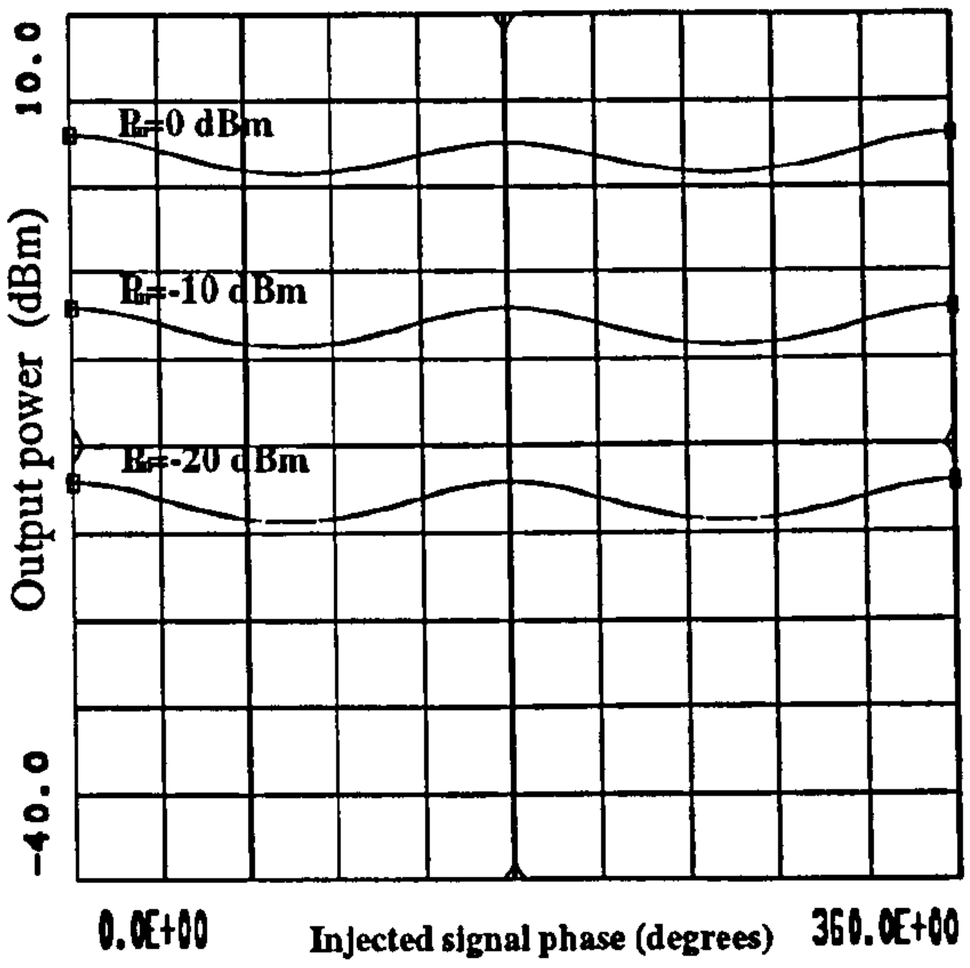

Figure E..29: **Variations in the amplitude of the fundamental f_1 at the frequency $2.5GHz$ as a function of difference frequency signals phase for input power levels of $-20dBm$, $-10dBm$ and $0dBm$.**

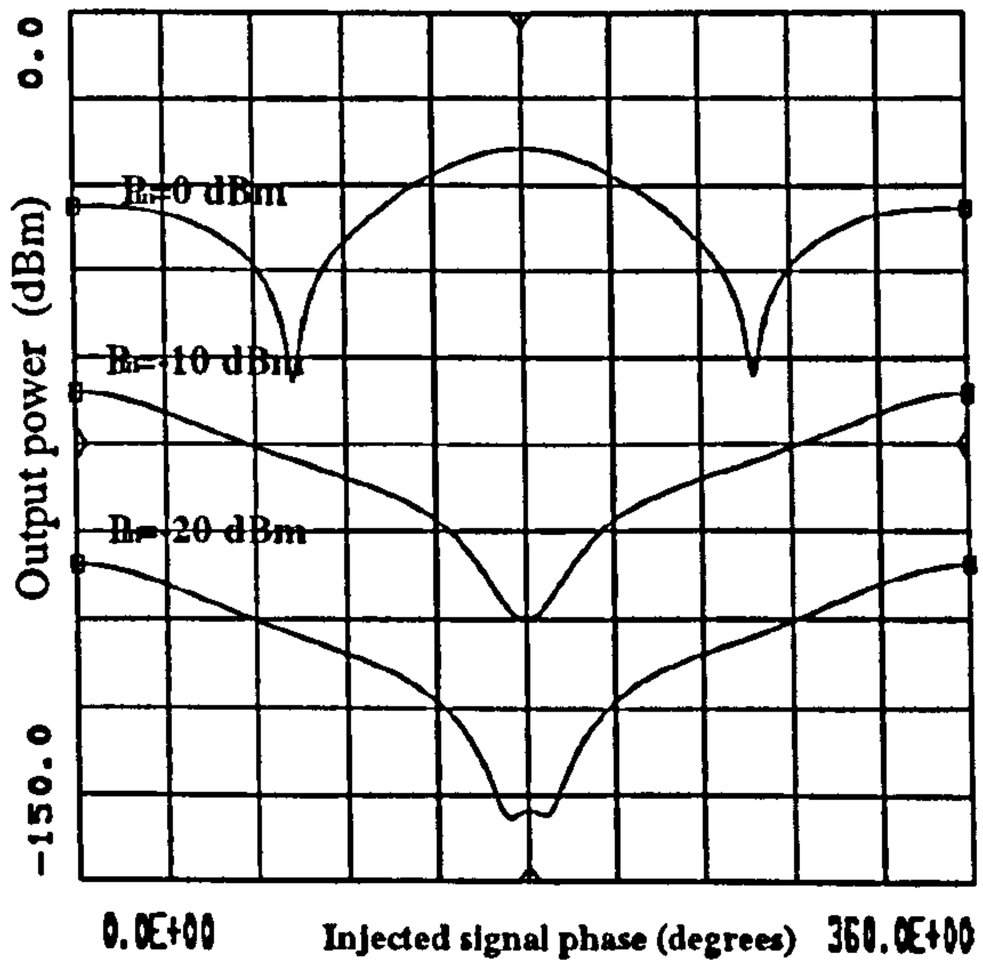

Figure E..31: **Variations in the amplitude of IM term $(f_1 - f_2 + f_3)$ at the frequency $2.511GHz$ as a function of injected difference frequency signals phase for input power levels of $-20dBm$, $-10dBm$ and $0dBm$.**

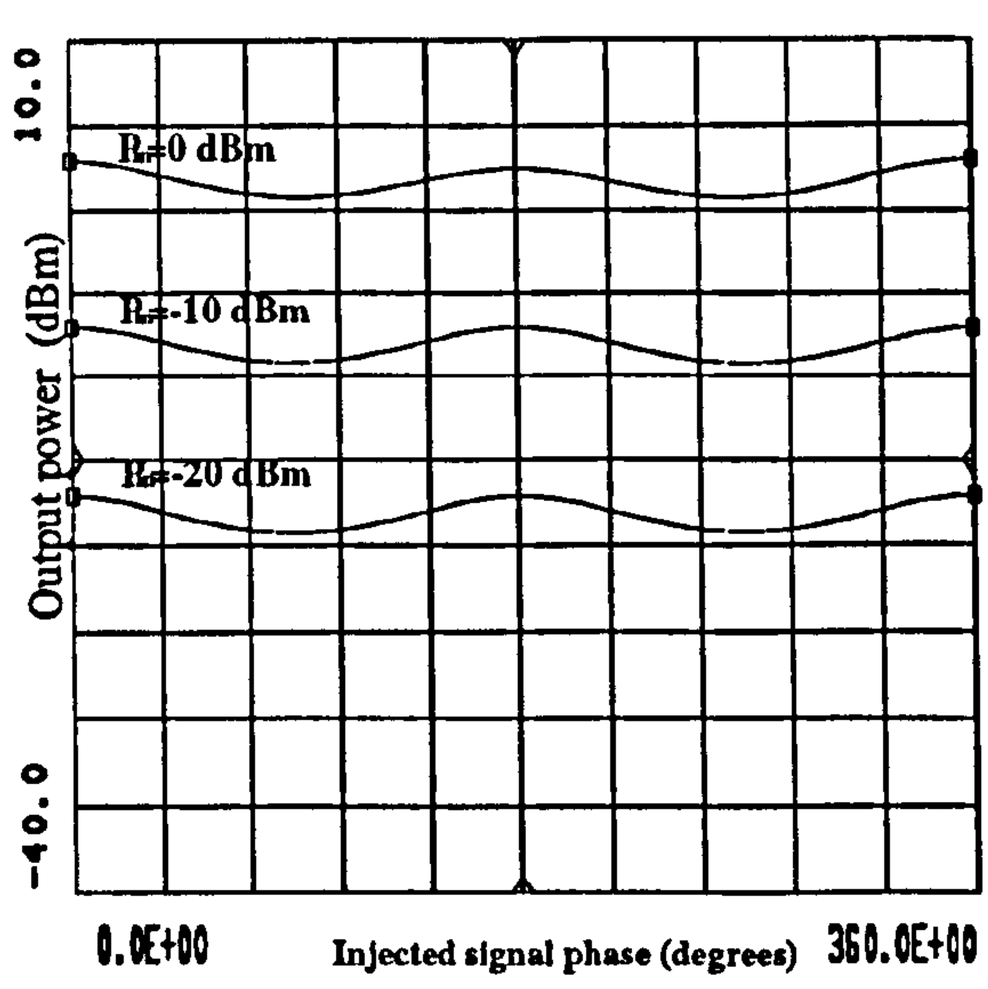

Figure E..30: **Variations in the amplitude of the fundamental f_2 at the frequency $2.51GHz$ as a function of difference frequency signals phase for input power levels of $-20dBm$, $-10dBm$ and $0dBm$.**

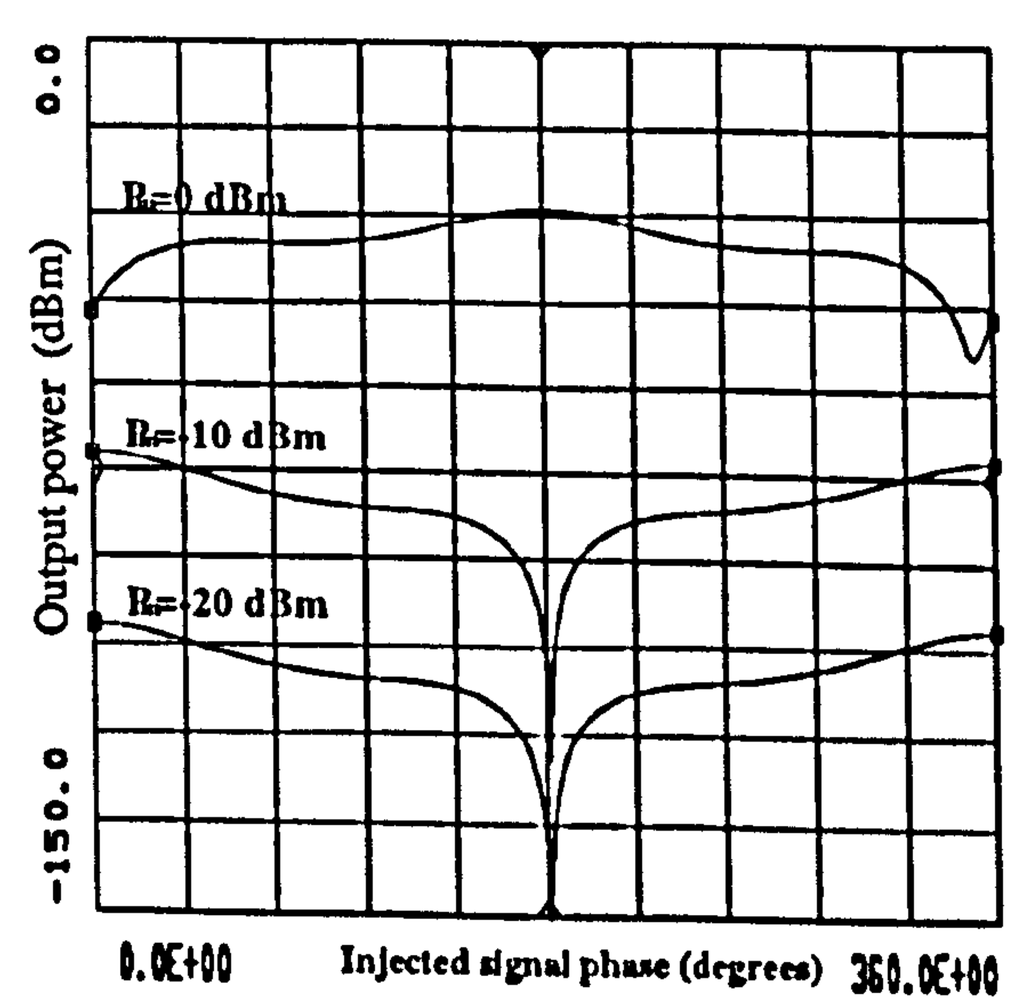

Figure E..32: **Variations in the amplitude of IM term $(2f_2 - f_1)$ at the frequency $2.52GHz$ as a function of difference frequency signals phase for input power levels of $-20dBm$, $-10dBm$ and $0dBm$.**

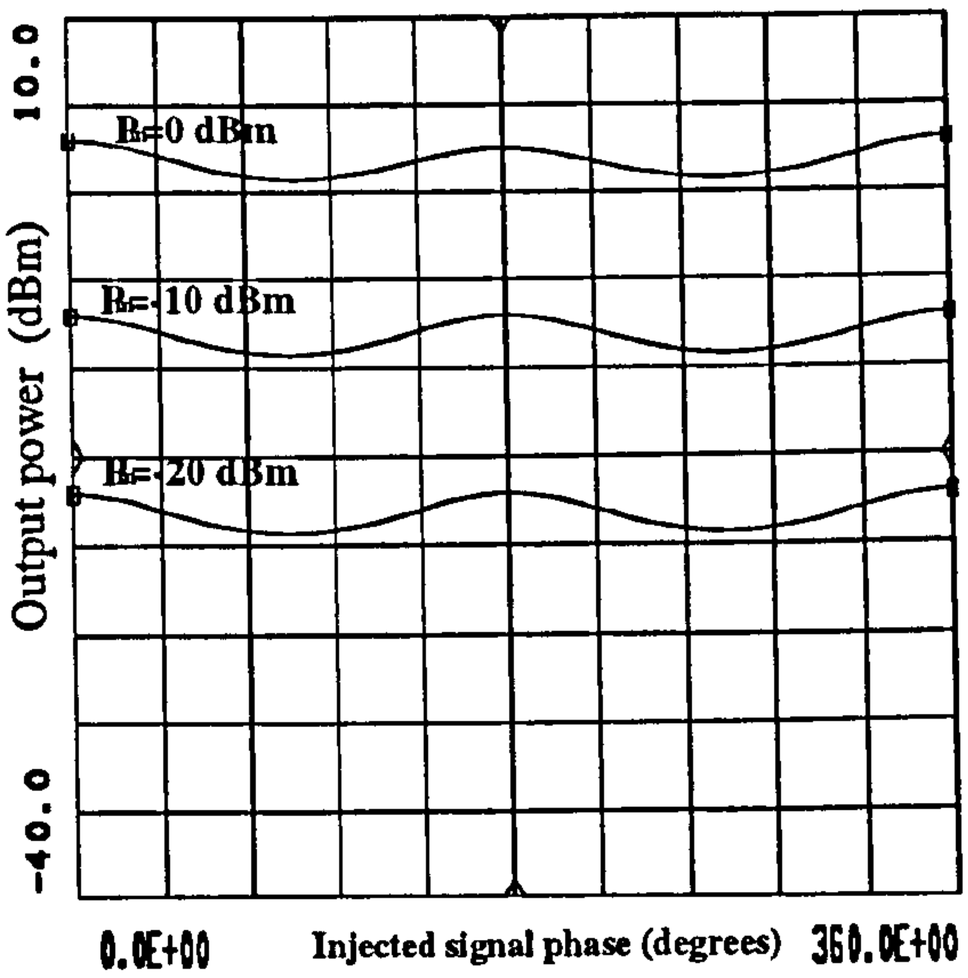

Figure E..33: Variations in the amplitude of the fundamental f_3 at the frequency $2.521GHz$ as a function of injected difference frequency signals phase for input power levels of $-20dBm$, $-10dBm$ and $0dBm$.

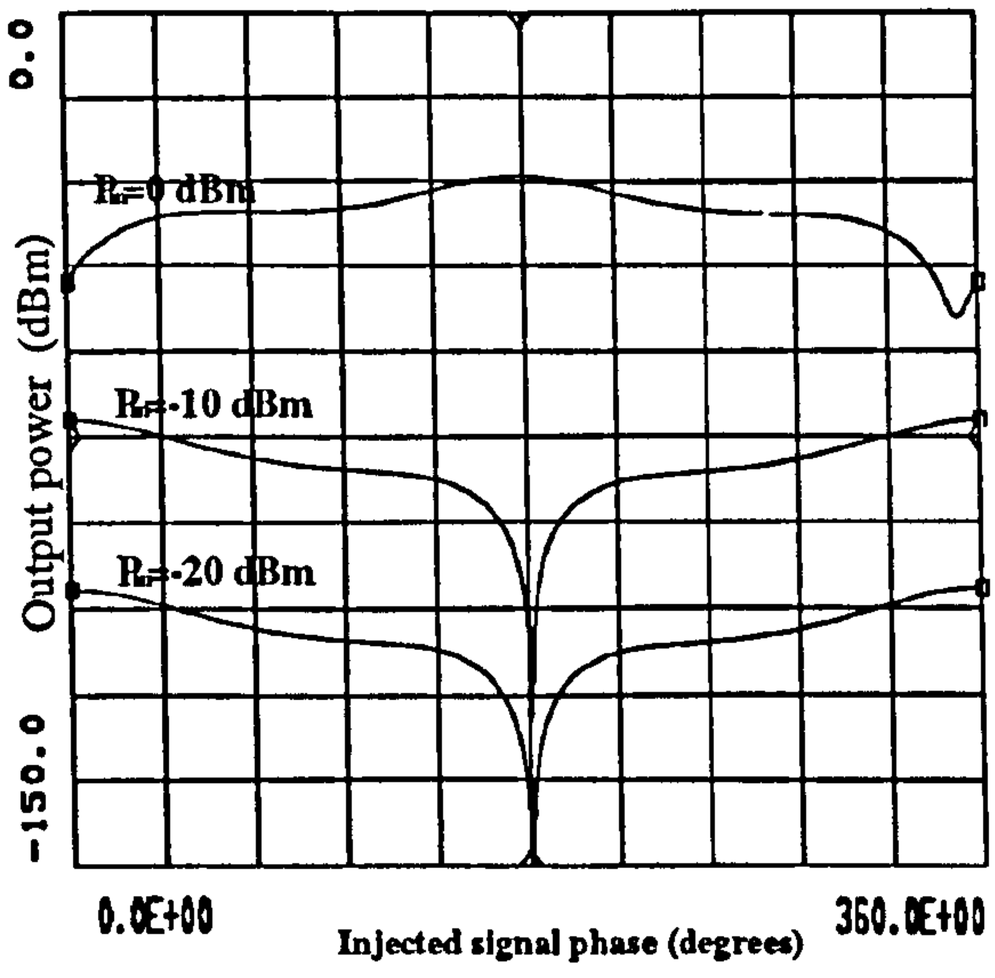

Figure E..35: Variations in the amplitude of IM term $(2f_3 - f_2)$ at the frequency $2.532GHz$ as a function of difference frequency signals phase for input power levels of $-20dBm$, $-10dBm$ and $0dBm$.

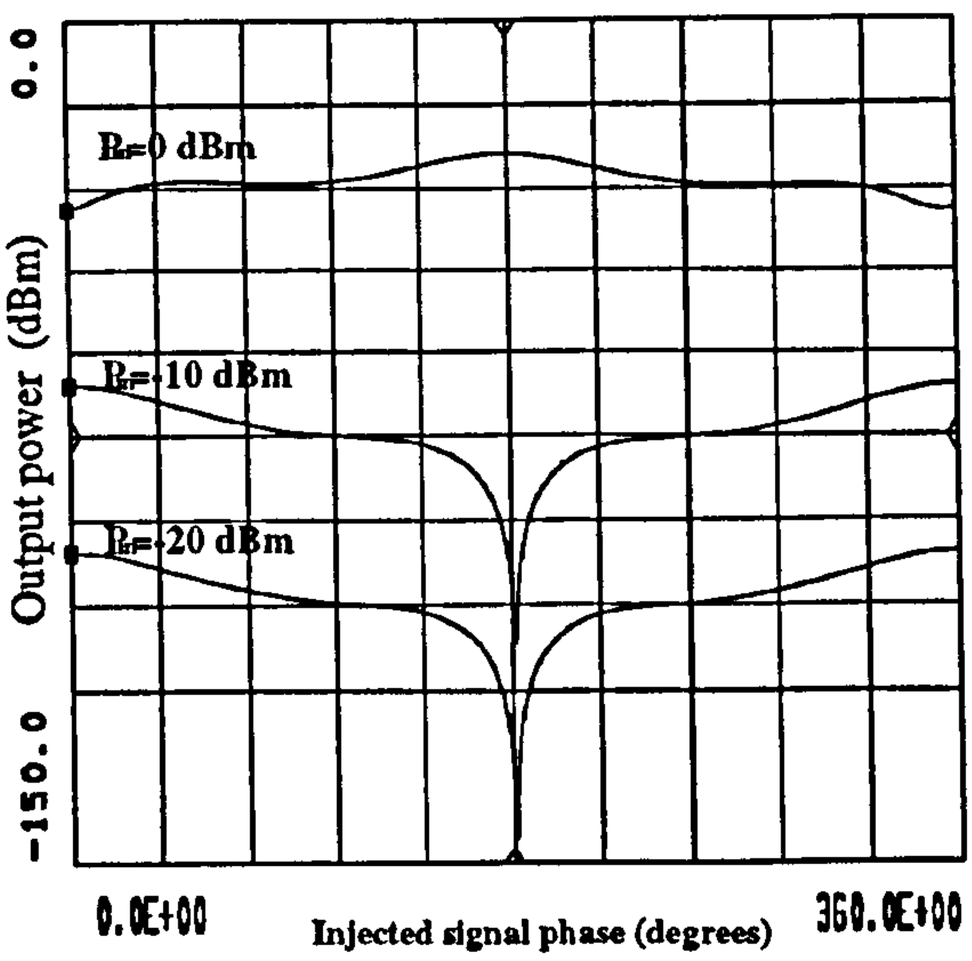

Figure E..34: Variations in the amplitude of IM term $(f_3 + f_2 - f_1)$ at the frequency $2.531GHz$ as a function of difference frequency signals phase for input power levels of $-20dBm$, $-10dBm$ and $0dBm$.

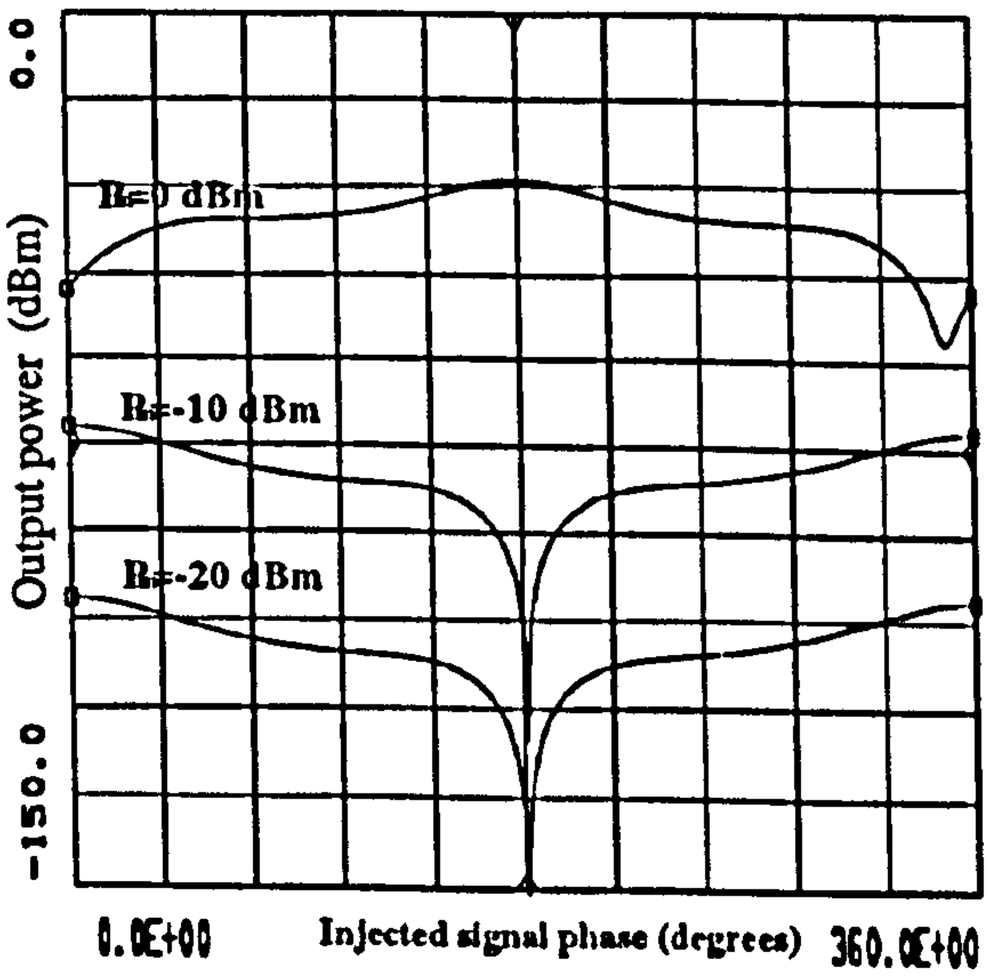

Figure E..36: Variations in the amplitude of IM term $(2f_3 - f_1)$ at the frequency $2.542GHz$ as a function of injected difference frequency signals phase for input power levels of $-20dBm$, $-10dBm$ and $0dBm$.

APPENDIX F.

AMPLITUDE SENSITIVITY OF SYSTEMS

6.1 Second Harmonic Injection Technique

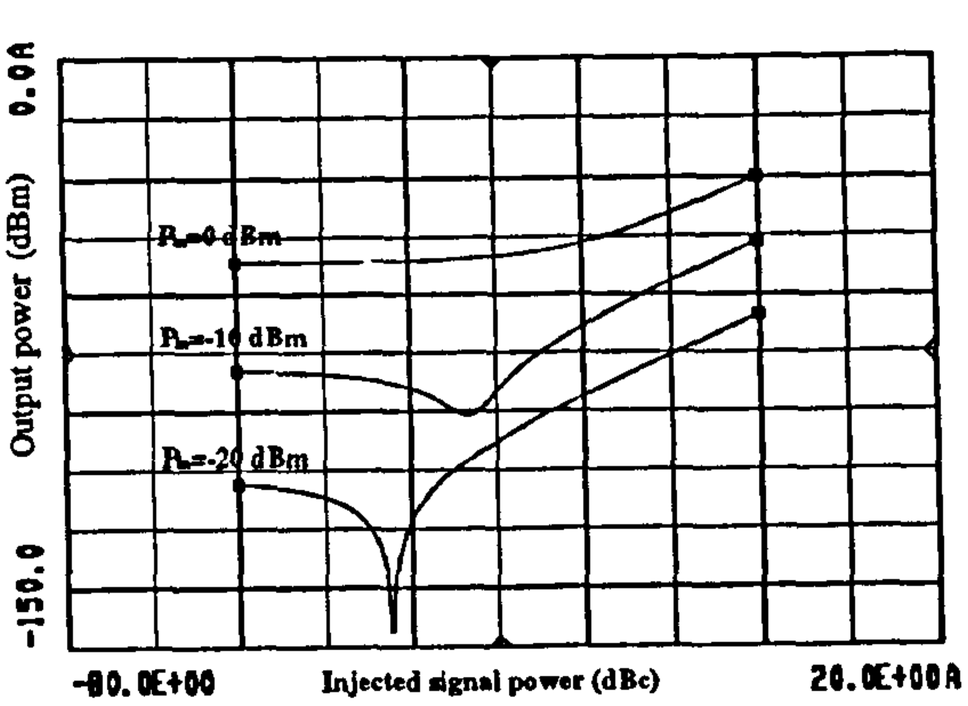

Figure F..1: **Variations in the amplitude of IM term $(2f_1 - f_3)$as a function of injected second harmonic signals amplitude for input power levels of $-20dBm$, $-10dBm$ and $0dBm$.**

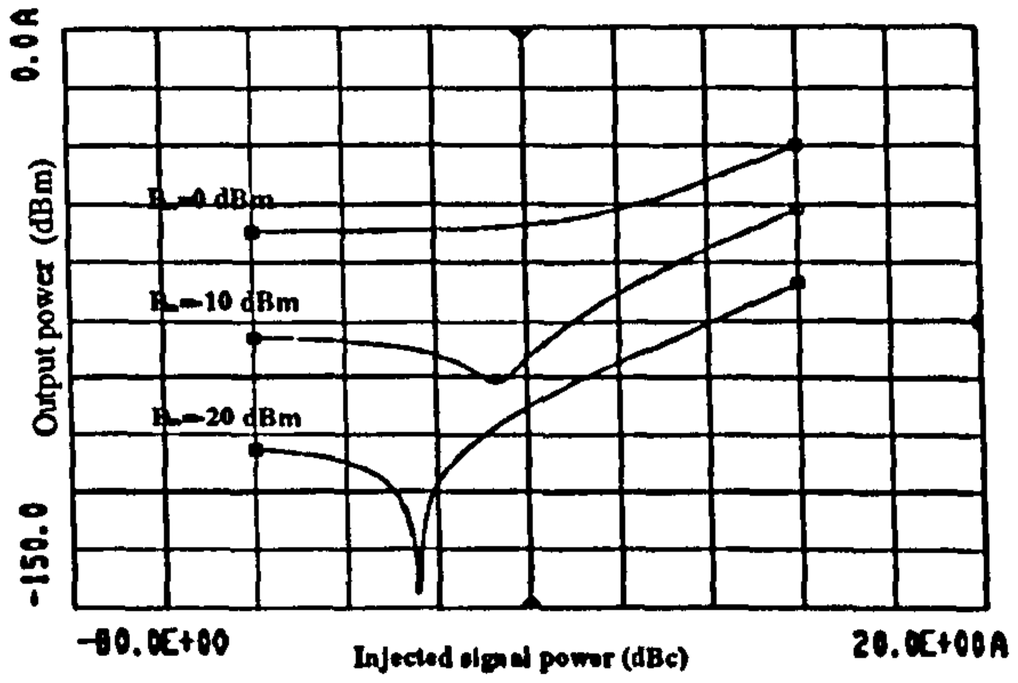

Figure F..3: **Variations in the amplitude of IM term $(2f_1 - f_2)$ as a function of injected second harmonic signals amplitude for input power levels of $-20dBm$, $-10dBm$ and $0dBm$.**

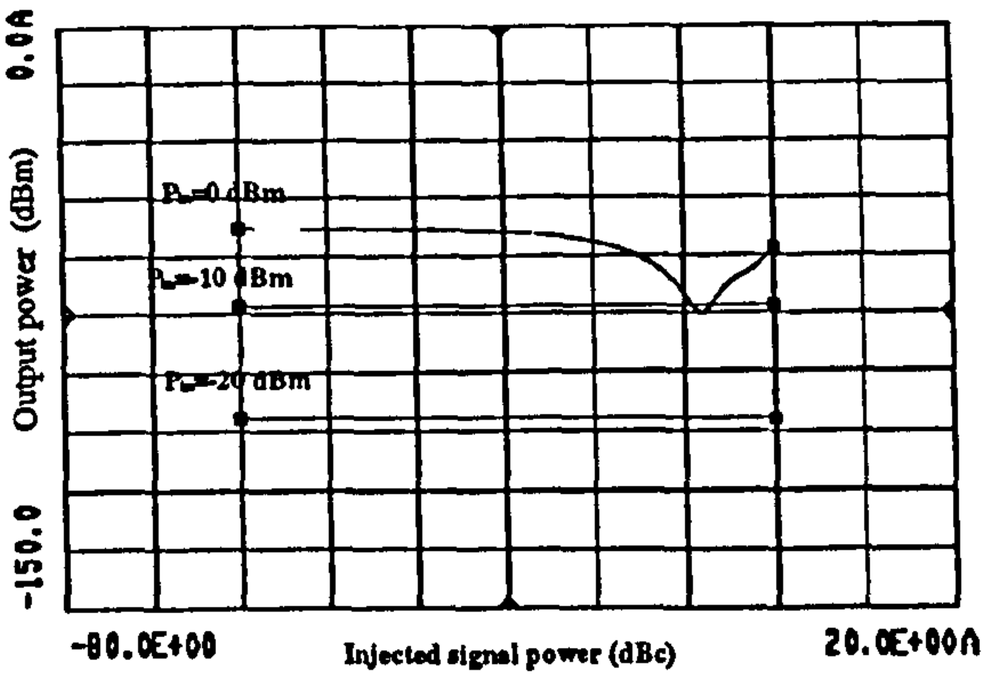

Figure F..2: **Variations in the amplitude of IM term $(f_1 + f_2 - f_3)$ as a function of injected second harmonic signals amplitude for input power levels of $-20dBm$, $-10dBm$ and $0dBm$.**

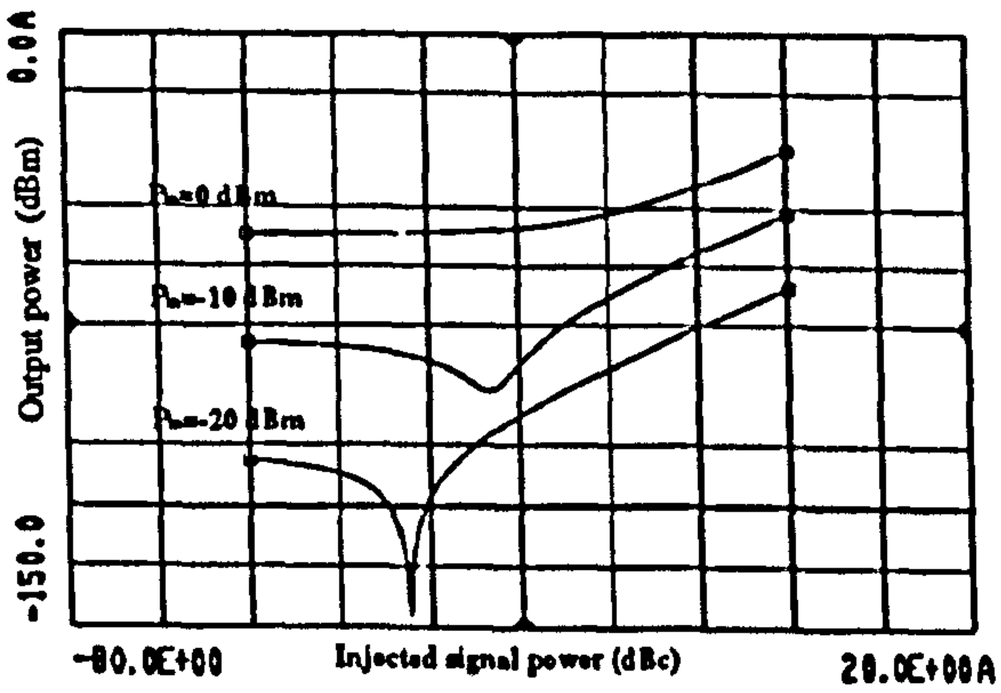

Figure F..4: **Variations in the amplitude of IM term $(2f_2 - f_3)$ as a function of injected second harmonic signals amplitude for input power levels of $-20dBm$, $-10dBm$ and $0dBm$.**

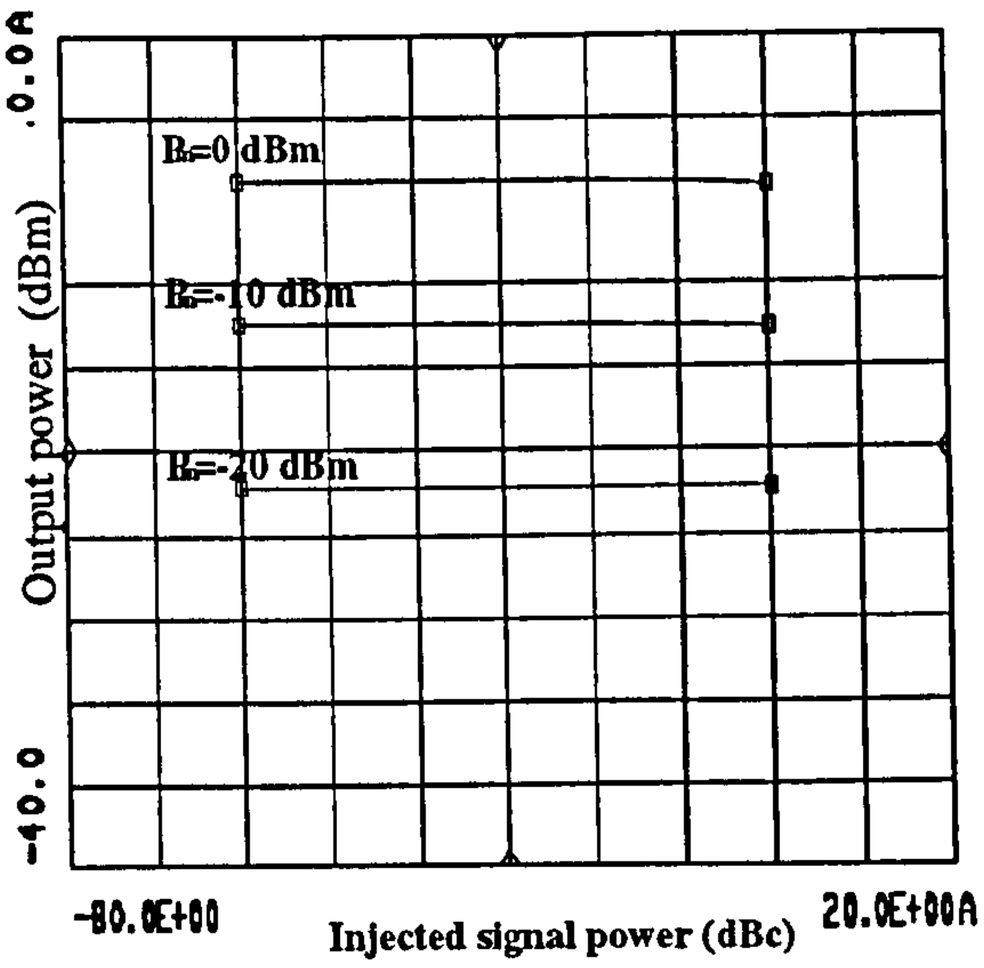

Figure F..5: **Variations in the amplitude of the fundamental signal f_1 as a function of injected second harmonic signals amplitude for input power levels of $-20dBm$, $-10dBm$ and $0dBm$.**

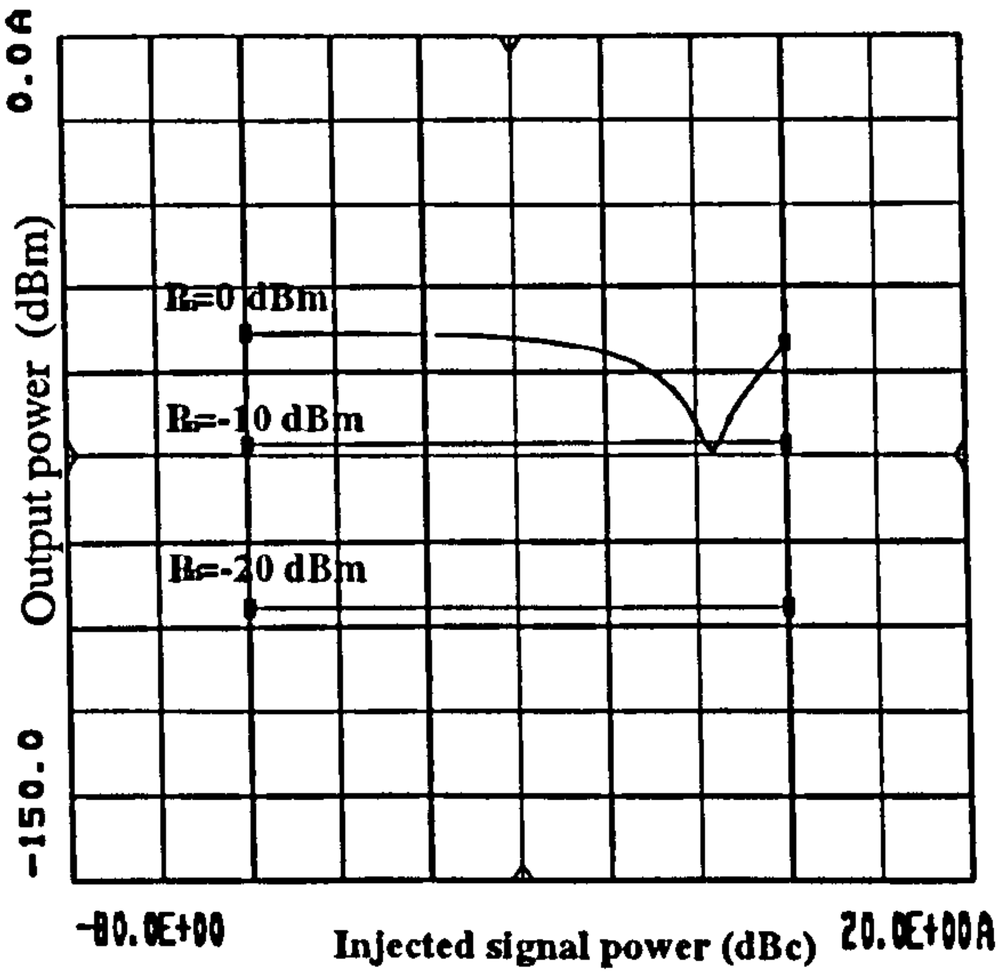

Figure F..7: **Variations in the amplitude of IM term $(f_2 - f_1 + f_3)$ as a function of injected second harmonic signals amplitude for input power levels of $-20dBm$, $-10dBm$ and $0dBm$.**

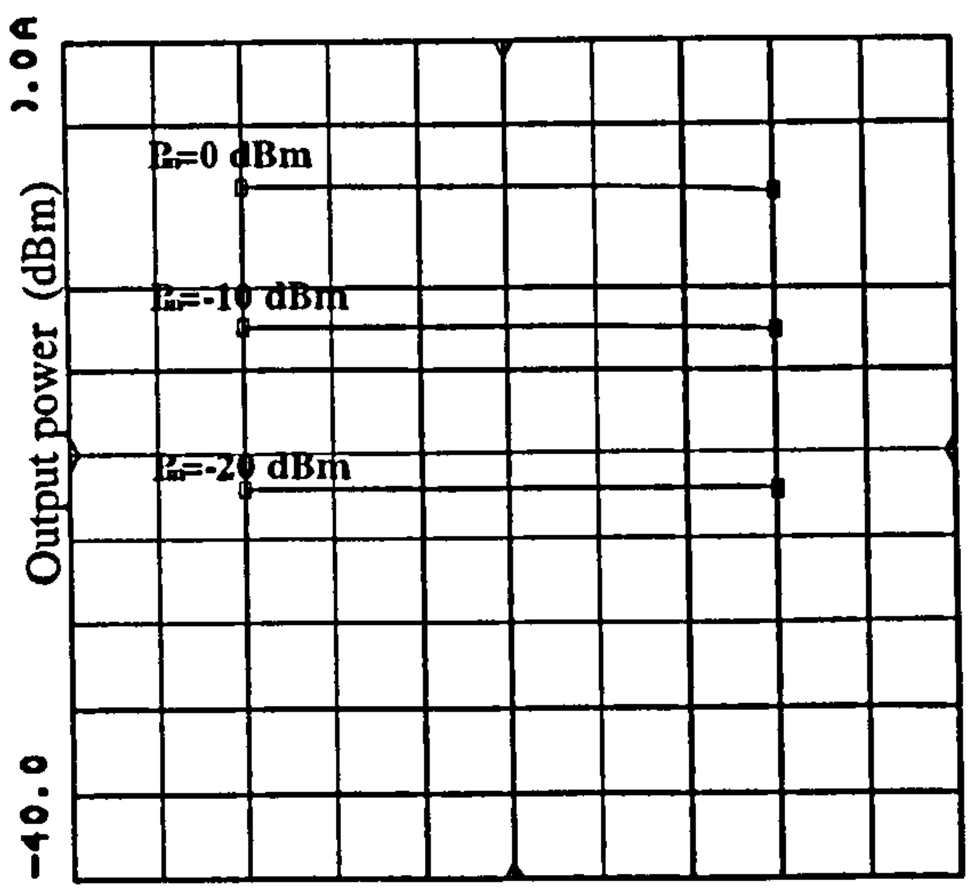

Figure F..6: **Variations in the amplitude of the fundamental signal f_2 as a function of injected second harmonic signals amplitude for input power levels of $-20dBm$, $-10dBm$ and $0dBm$.**

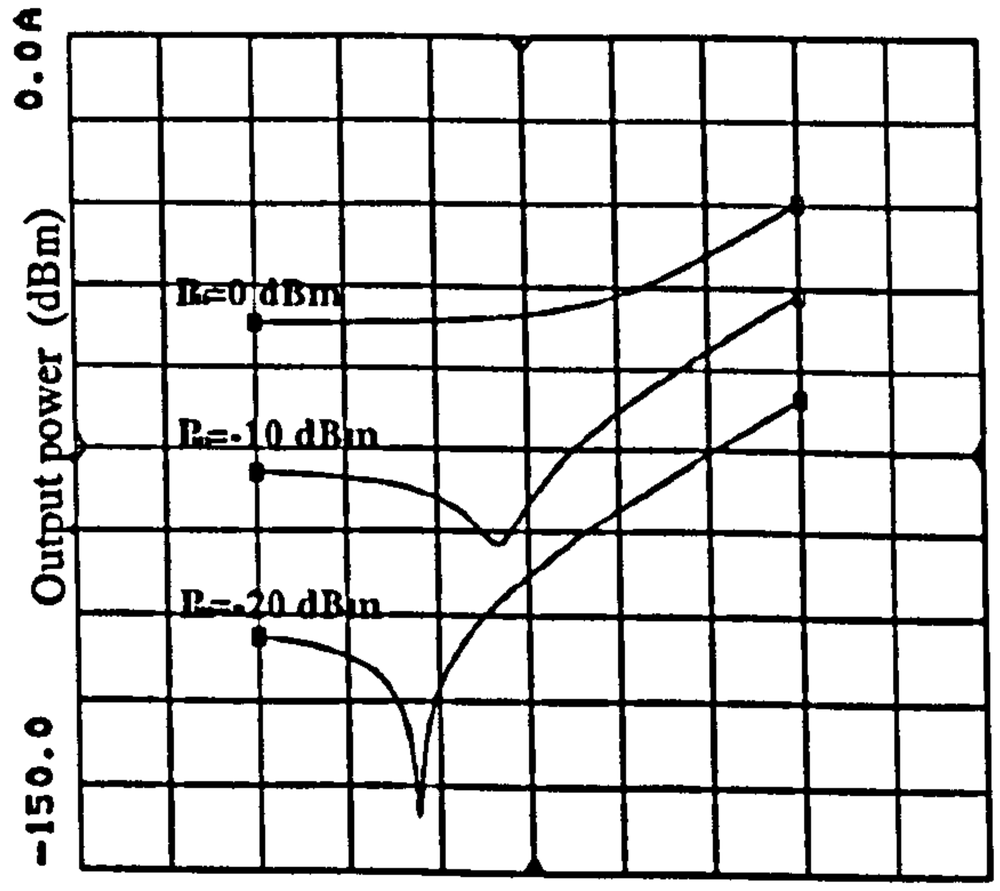

Figure F..8: **Variations in the amplitude of IM term $(2f_2 - f_1)$ as a function of injected second harmonic signals amplitude for input power levels of $-20dBm$, $-10dBm$ and $0dBm$.**

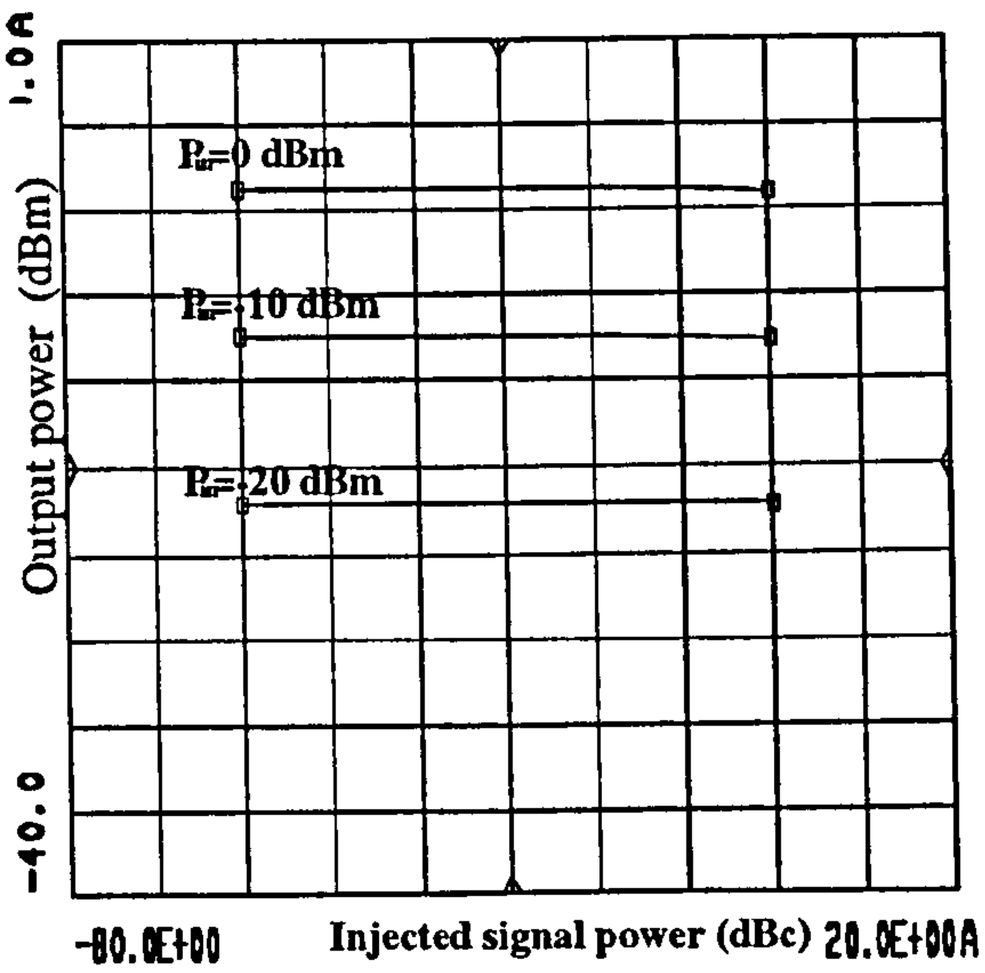

Figure F..9: **Variations in the amplitude of the fundamental signal f_3 as a function of injected second harmonic signals amplitude for input power levels of $-20dBm$, $-10dBm$ and $0dBm$.**

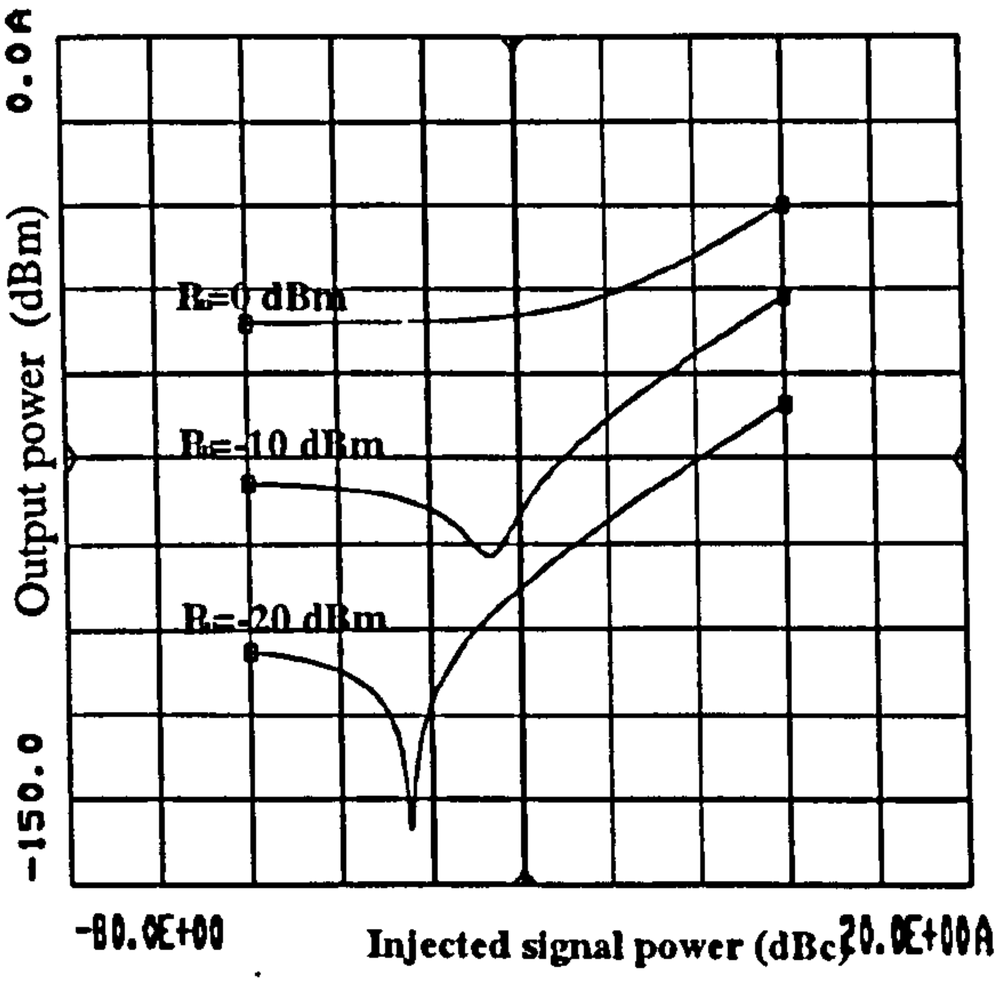

Figure F..11: **Variations in the amplitude of IM term $(2f_3 - f_2)$ as a function of injected second harmonic signals amplitude for input power levels of $-20dBm$, $-10dBm$ and $0dBm$.**

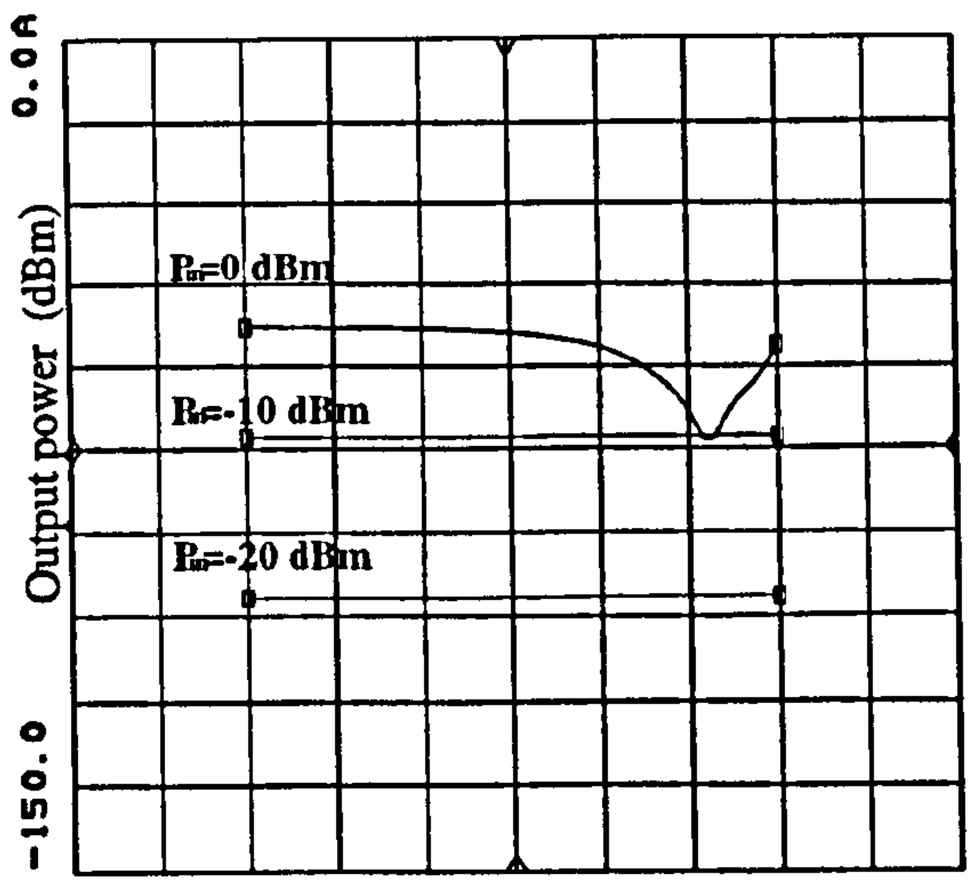

Figure F..10: **Variations in the amplitude of IM term $(f_3 + f_2 - f_1)$ as a function of injected second harmonic signals amplitude for input power levels of $-20dBm$, $-10dBm$ and $0dBm$.**

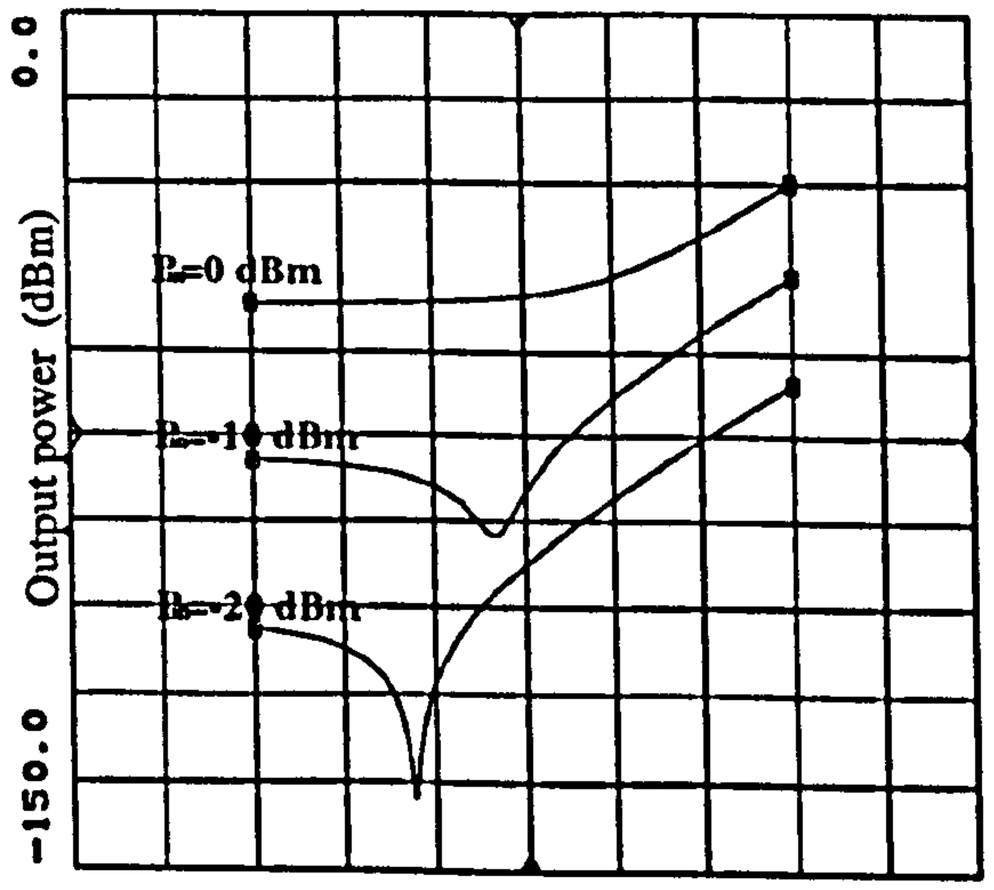

Figure F..12: **Variations in the amplitude of IM term $(2f_3 - f_1)$ as a function of injected second harmonic signals amplitude for input power levels of $-20dBm$, $-10dBm$ and $0dBm$.**

6.2 Frequency Summation Technique

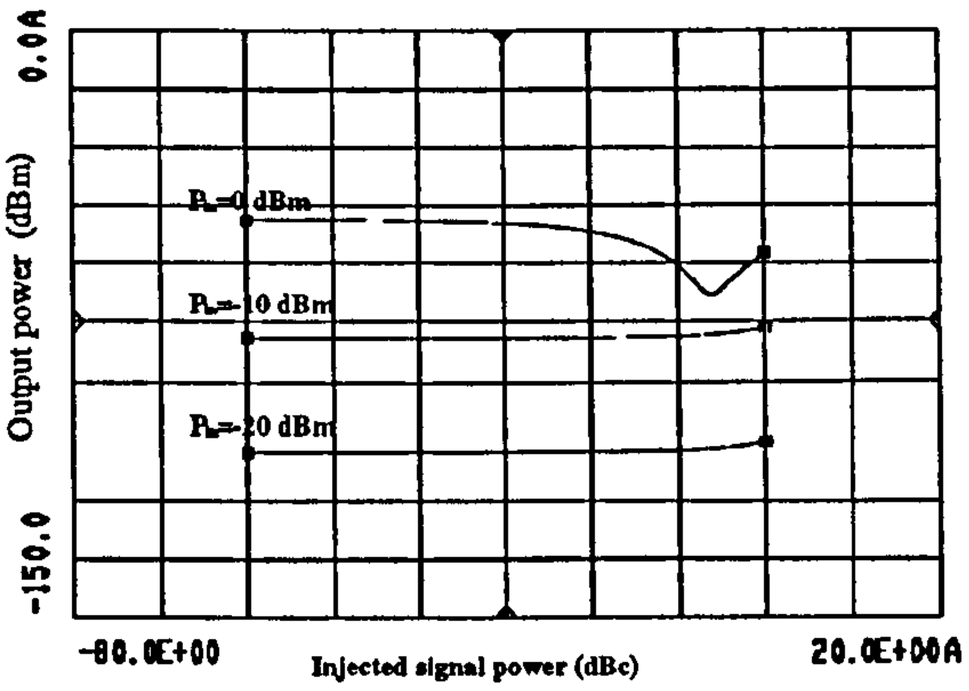

Figure F..13: **Variations in the amplitude of IM term $(2f_1 - f_3)$ as a function of the injected frequency sum of the fundamental signals amplitude for input power levels of $-20dBm$, $-10dBm$ and $0dBm$.**

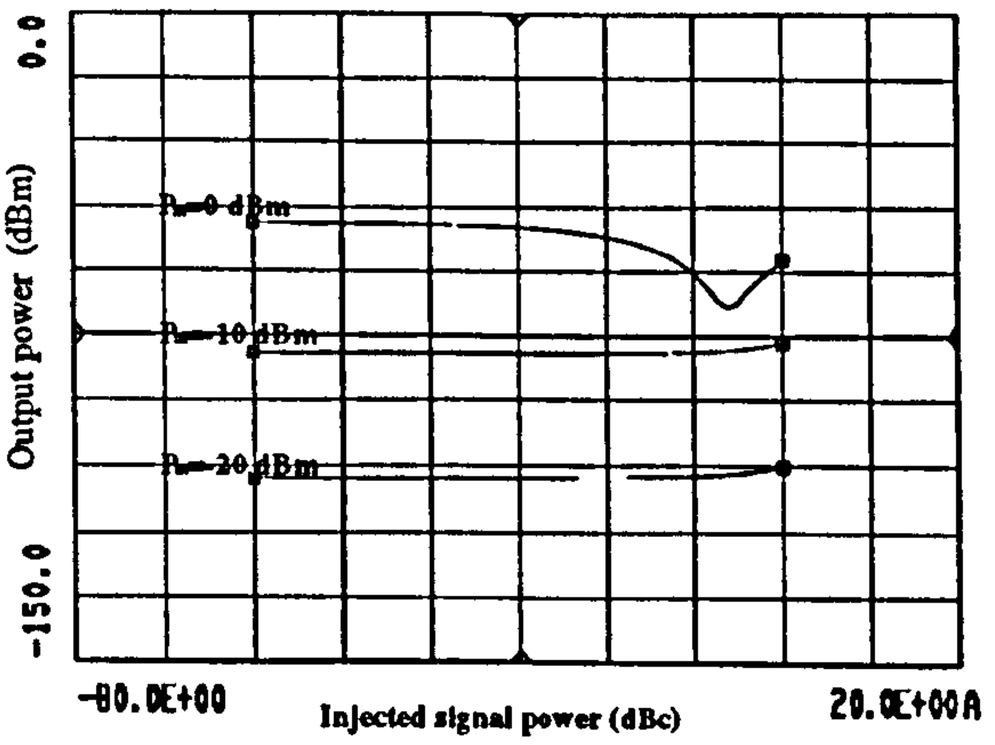

Figure F..15: **Variations in the amplitude of IM term $(2f_1 - f_2)$ as a function of the injected frequency sum of the fundamental signals amplitude for input power levels of $-20dBm$, $-10dBm$ and $0dBm$.**

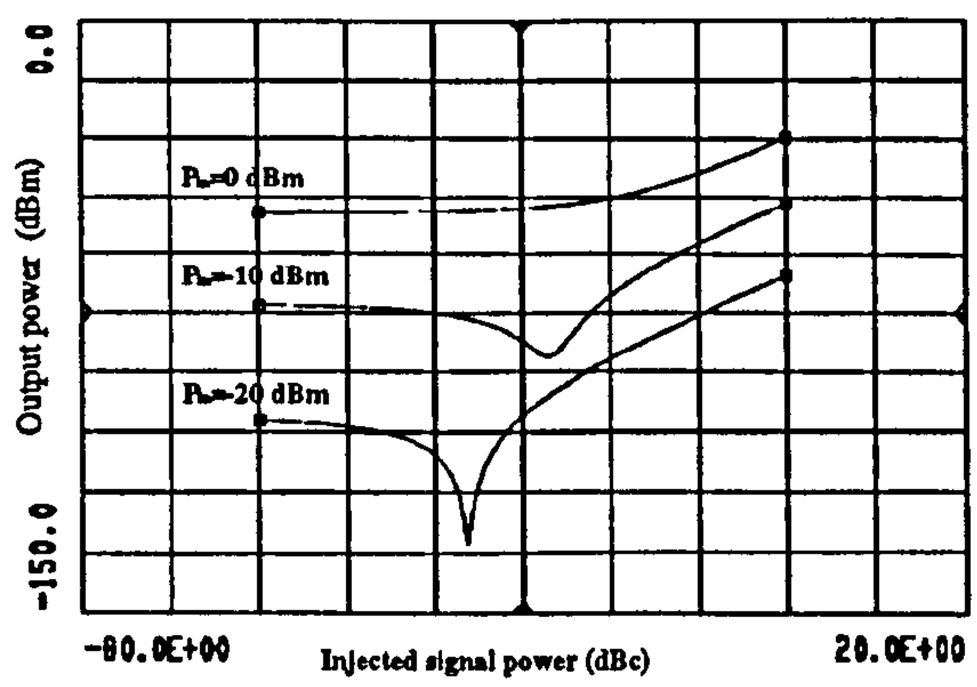

Figure F..14: **Variations in the amplitude of IM term $(f_1 + f_2 - f_3)$ as a function of the injected frequency sum of the fundamental signals amplitude for input power levels of $-20dBm$, $-10dBm$ and $0dBm$.**

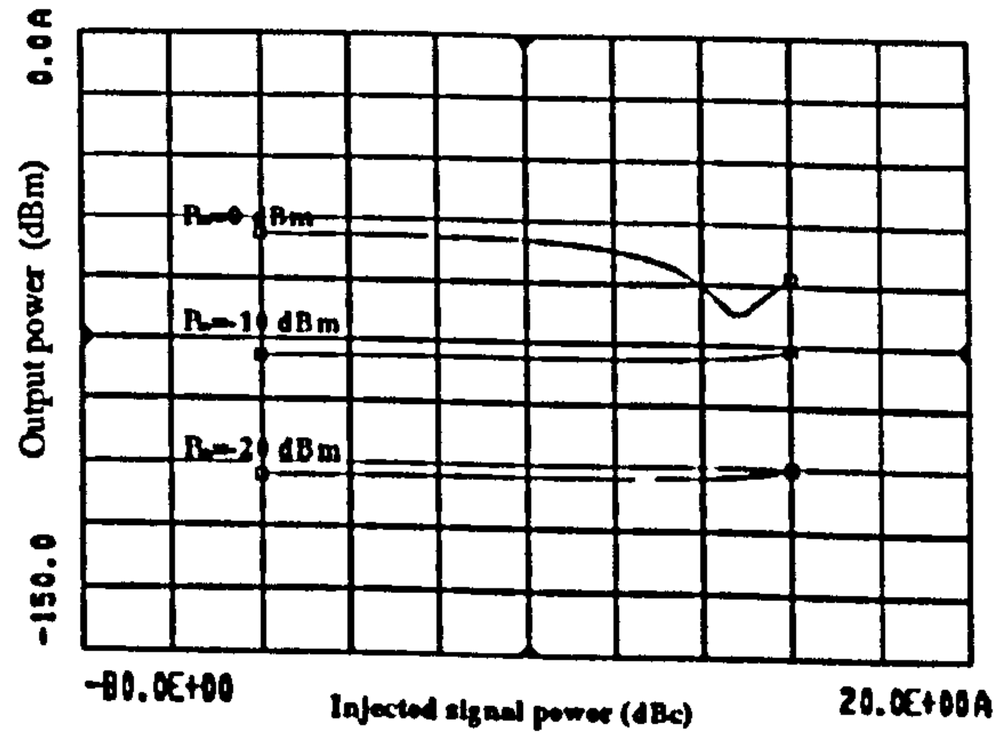

Figure F..16: **Variations in the amplitude of IM term $(2f_2 - f_3)$ as a function of the injected frequency sum of the fundamental signals amplitude for input power levels of $-20dBm$, $-10dBm$ and $0dBm$.**

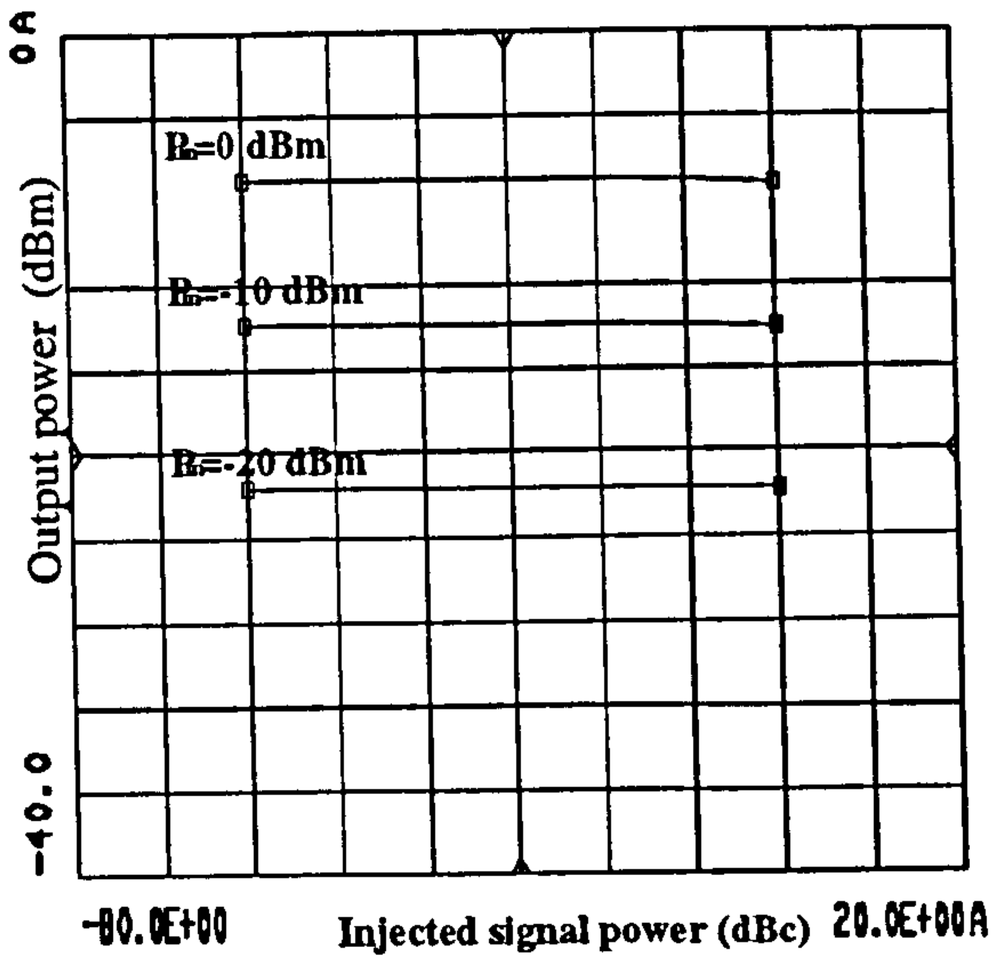

Figure F..17: Variations in the amplitude of the fundamental signal f_1 as a function of the injected frequency sum of the fundamental signals amplitude for input power levels of $-20dBm$, $-10dBm$ and $0dBm$.

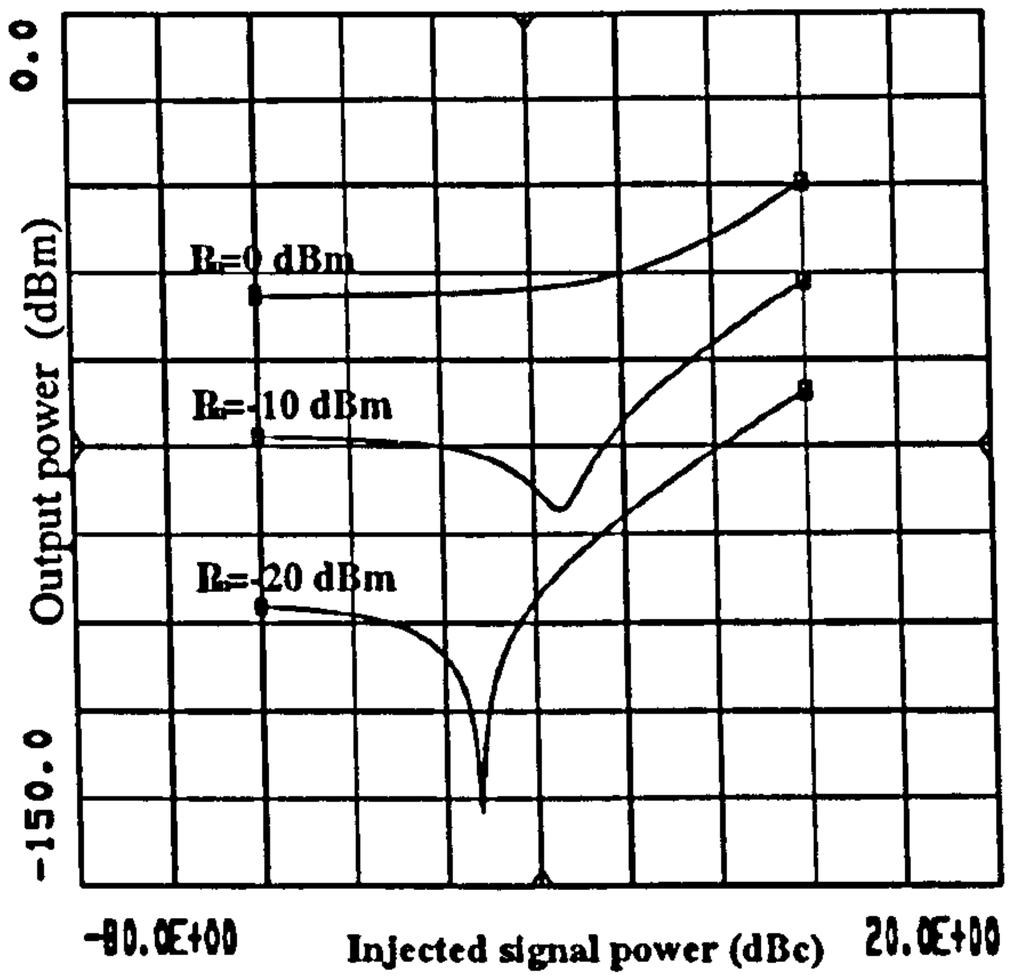

Figure F..19: Variations in the amplitude of IM term $(f_1 - f_2 + f_3)$ as a function of the injected frequency sum of the fundamental signals amplitude for input power levels of $-20dBm$, $-10dBm$ and $0dBm$.

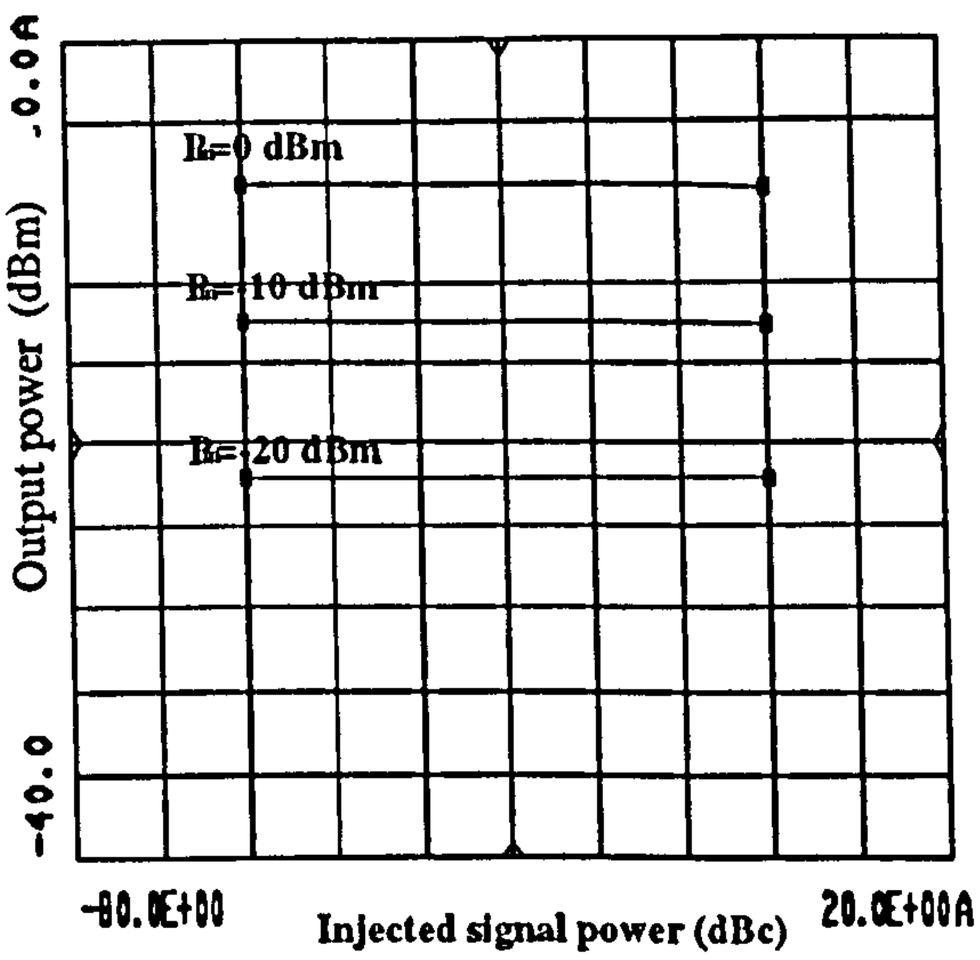

Figure F..18: Variations in the amplitude of the fundamental signal f_2 as a function of the injected frequency sum of the fundamental signals amplitude for input power levels of $-20dBm$, $-10dBm$ and $0dBm$.

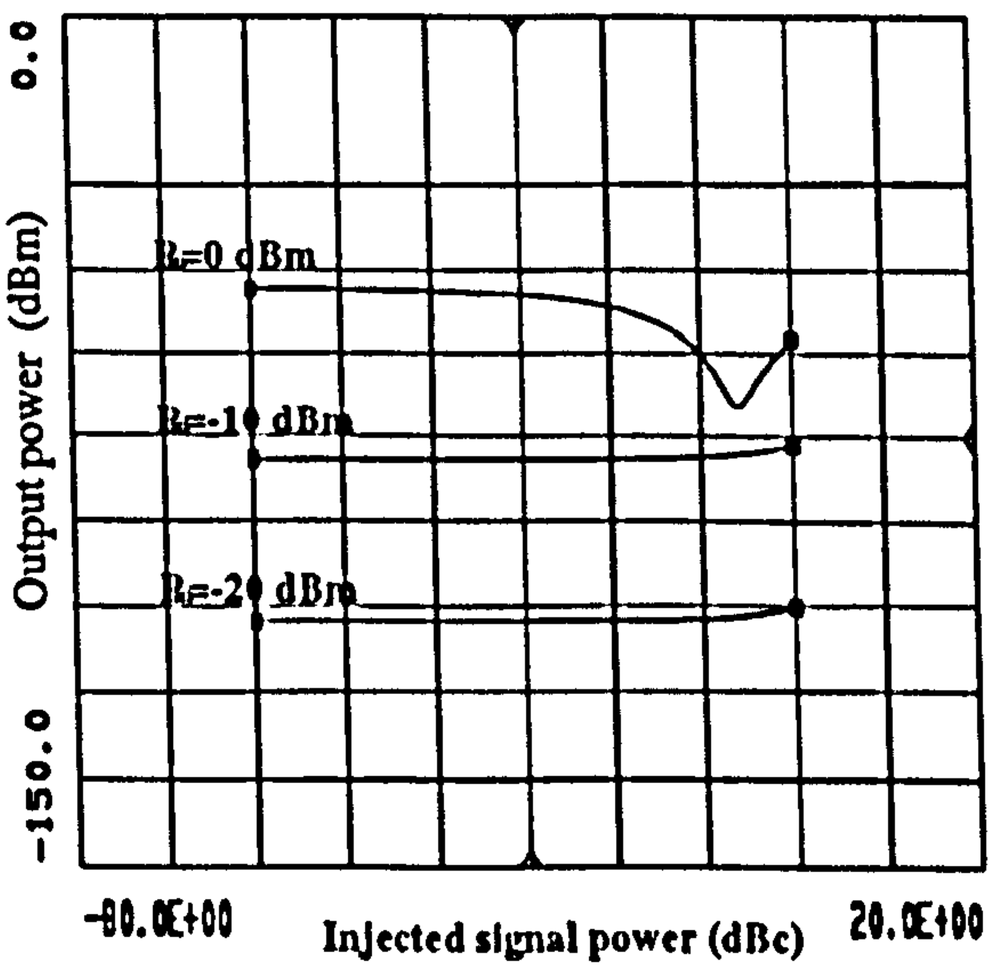

Figure F..20: Variations in the amplitude of IM term $(2f_2 - f_1)$ as a function of the injected frequency sum of the fundamental signals amplitude for input power levels of $-20dBm$, $-10dBm$ and $0dBm$.

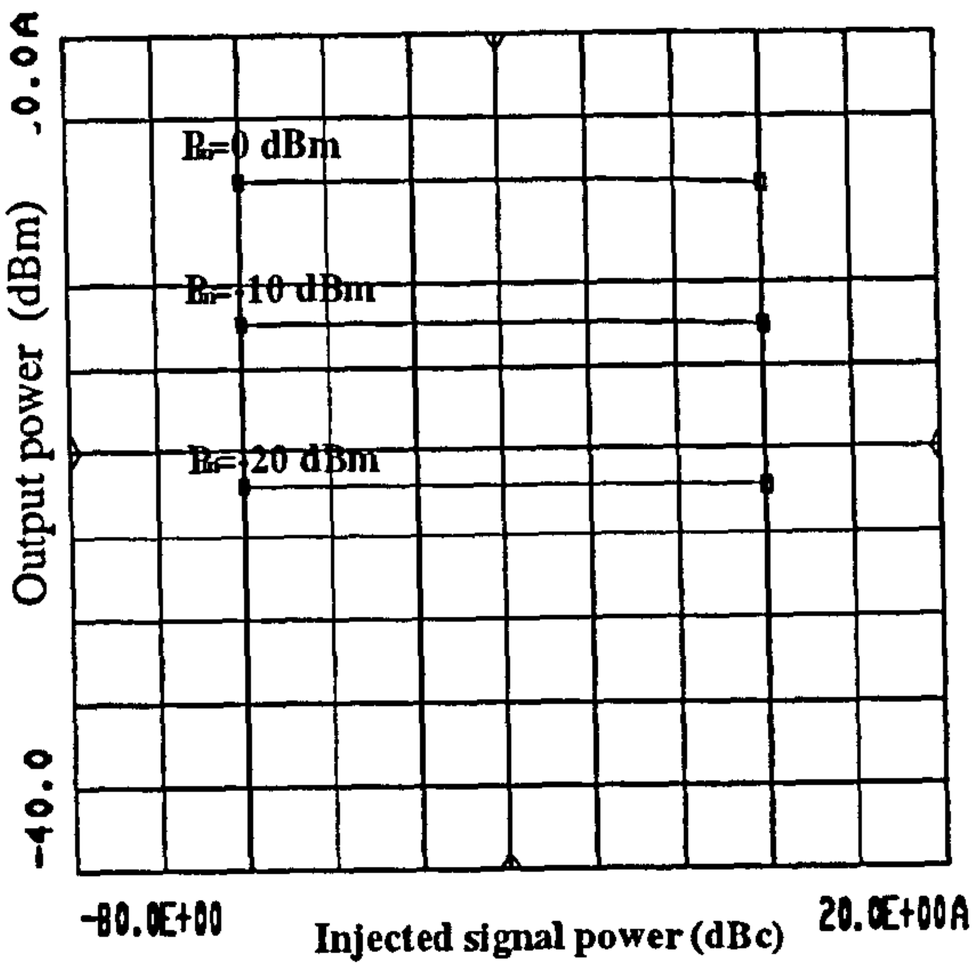

Figure F..21: Variations in the amplitude of the fundamental signal f_3 as a function of the injected frequency sum of the fundamental signals amplitude for input power levels of $-20dBm$, $-10dBm$ and $0dBm$.

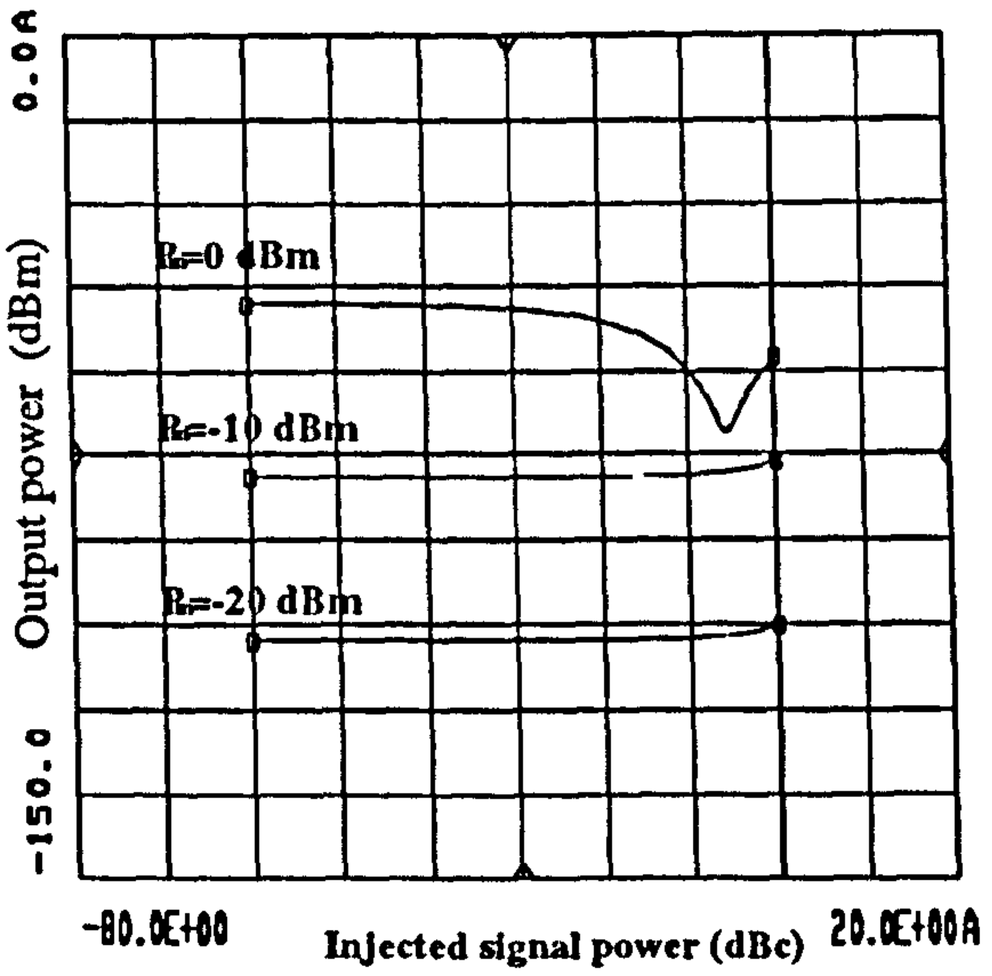

Figure F..23: Variations in the amplitude of IM term $(2f_3 - f_2)$ as a function of the injected frequency sum of the fundamental signals amplitude for input power levels of $-20dBm$, $-10dBm$ and $0dBm$.

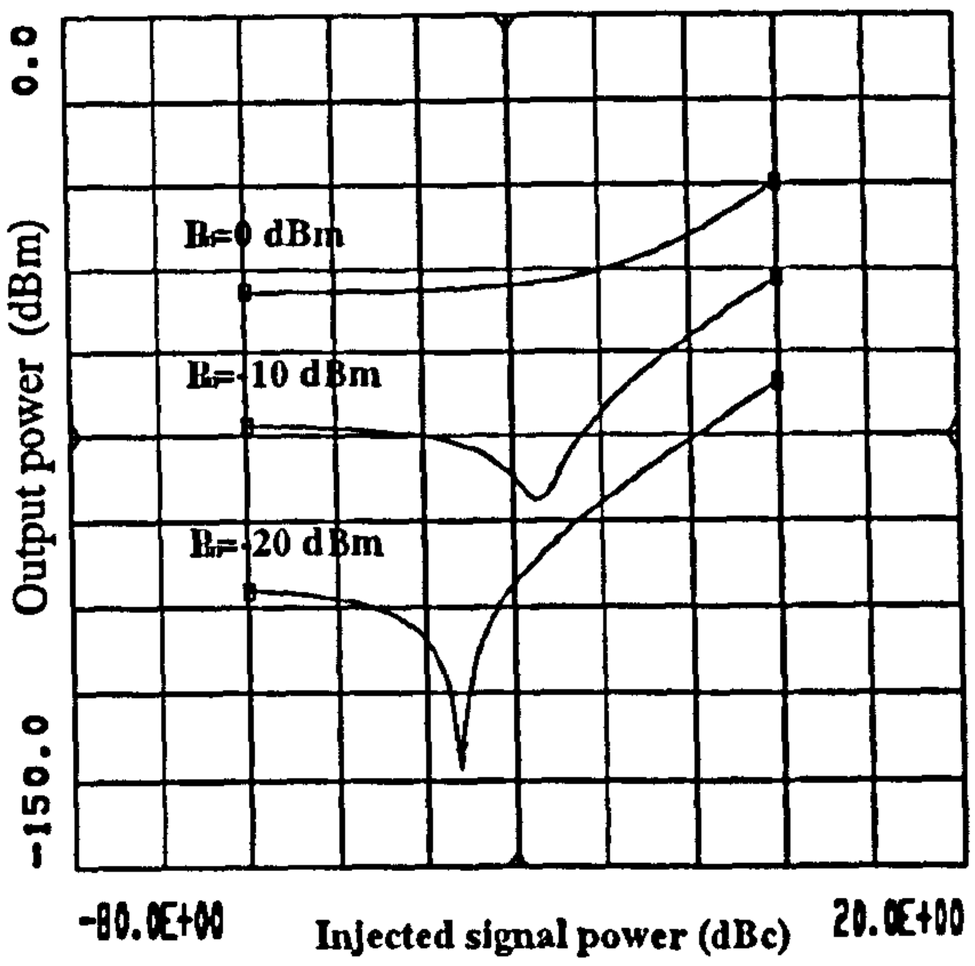

Figure F..22: Variations in the amplitude of IM term $(f_3 + f_2 - f_1)$ as a function of the injected frequency sum of the fundamental signals amplitude for input power levels of $-20dBm$, $-10dBm$ and $0dBm$.

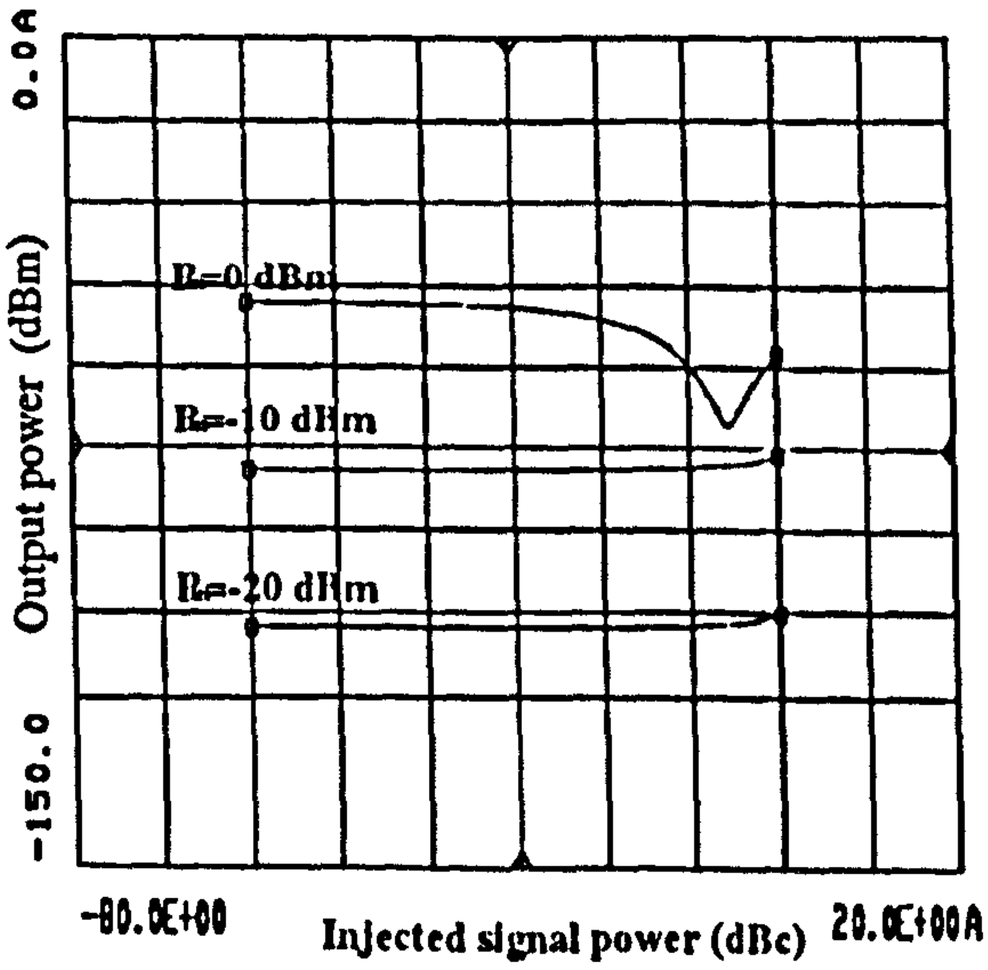

Figure F..24: Variations in the amplitude of IM term $(2f_3 - f_1)$ as a function of the injected frequency sum of the fundamental signals amplitude for input power levels of $-20dBm$, $-10dBm$ and $0dBm$.

6.3 Difference Frequency Technique

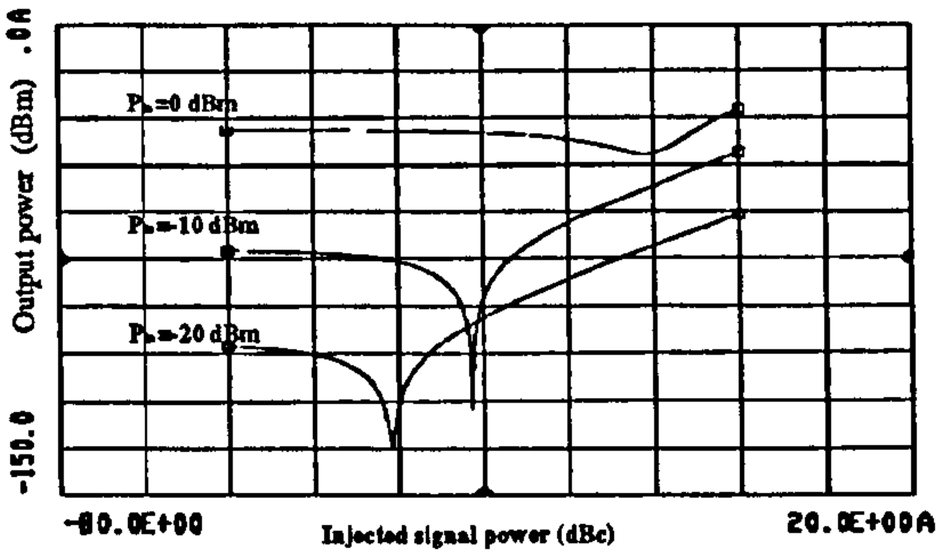

Figure F..25: **Variations in the amplitude of IM term $(2f_1 - f_3)$ as a function of injected difference frequency signals amplitude for input power levels of $-20dBm$, $-10dBm$ and $0dBm$.**

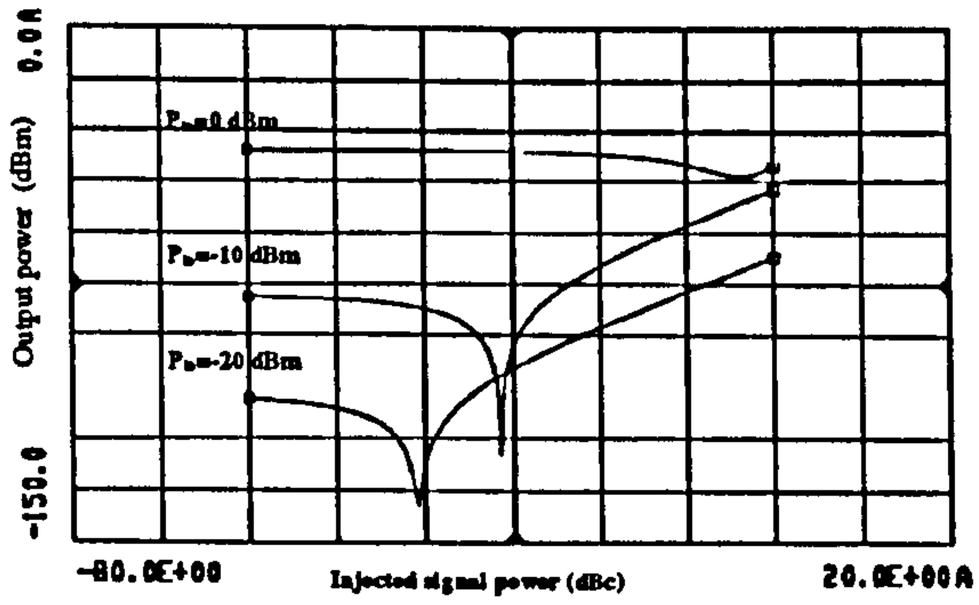

Figure F..27: **Variations in the amplitude of the IM term $(2f_1 - f_2)$ as a function of injected difference frequency signals amplitude for input power levels of $-20dBm$, $-10dBm$ and $0dBm$.**

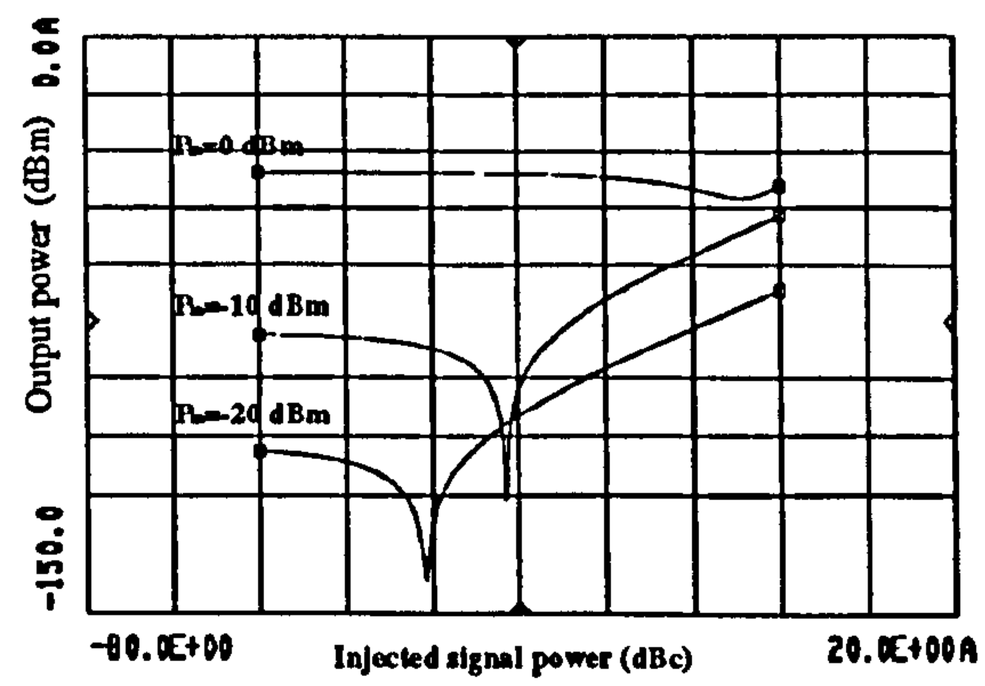

Figure F..26: **Variations in the amplitude of IM term $(f_1 + f_2 - f_3)$ as a function of injected difference frequency signals amplitude for input power levels of $-20dBm$, $-10dBm$ and $0dBm$.**

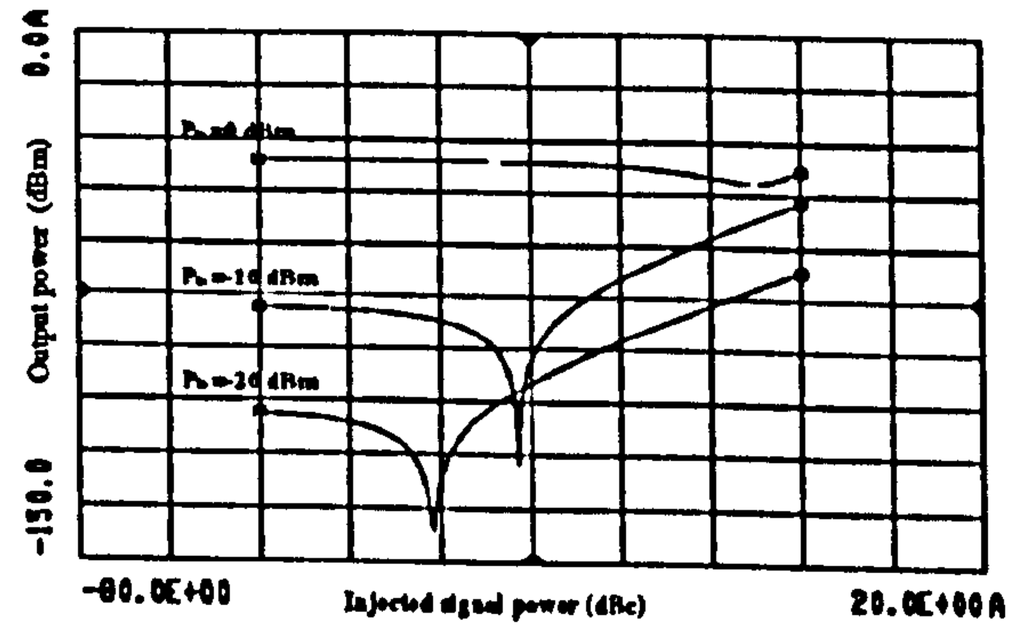

Figure F..28: **Variations in the amplitude of the IM term $(2f_2 - f_3)$ as a function of injected difference frequency signals amplitude for input power levels of $-20dBm$, $-10dBm$ and $0dBm$.**

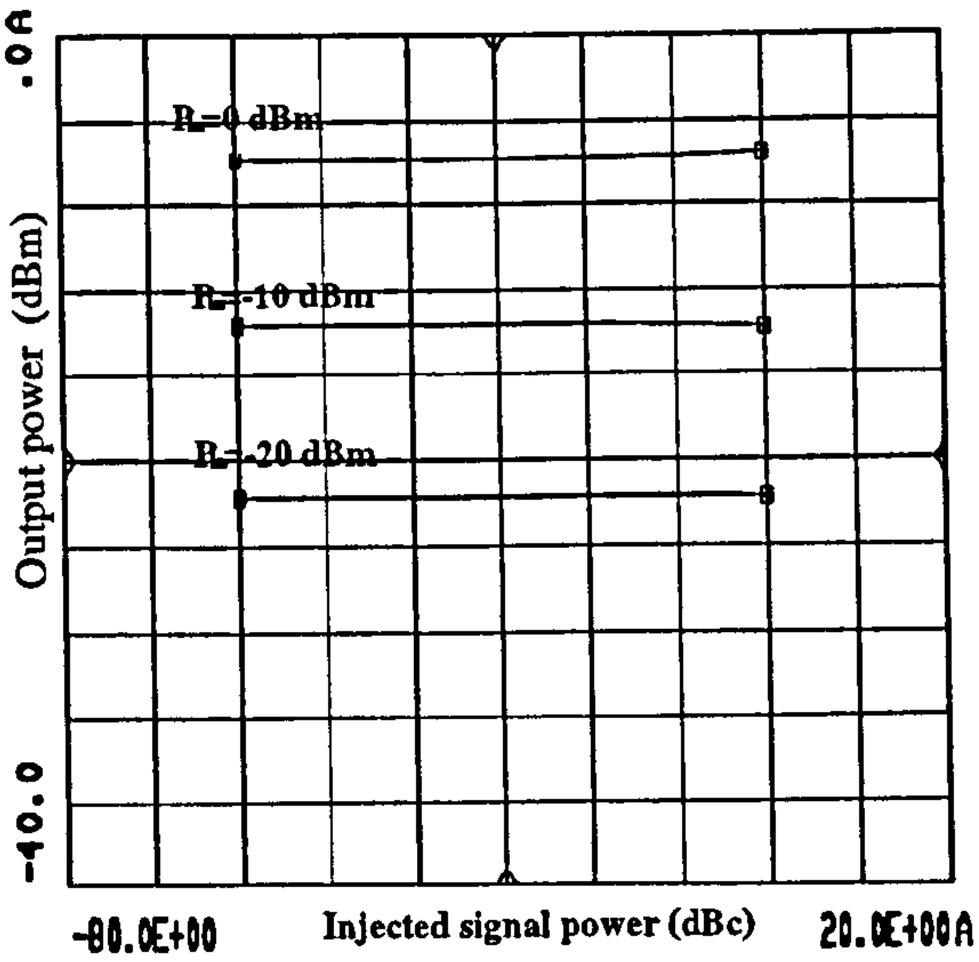

Figure F..29: **Variations in the amplitude of the fundamental signal f_1 as a function of injected difference frequency signals amplitude for input power levels of $-20dBm$, $-10dBm$ and $0dBm$.**

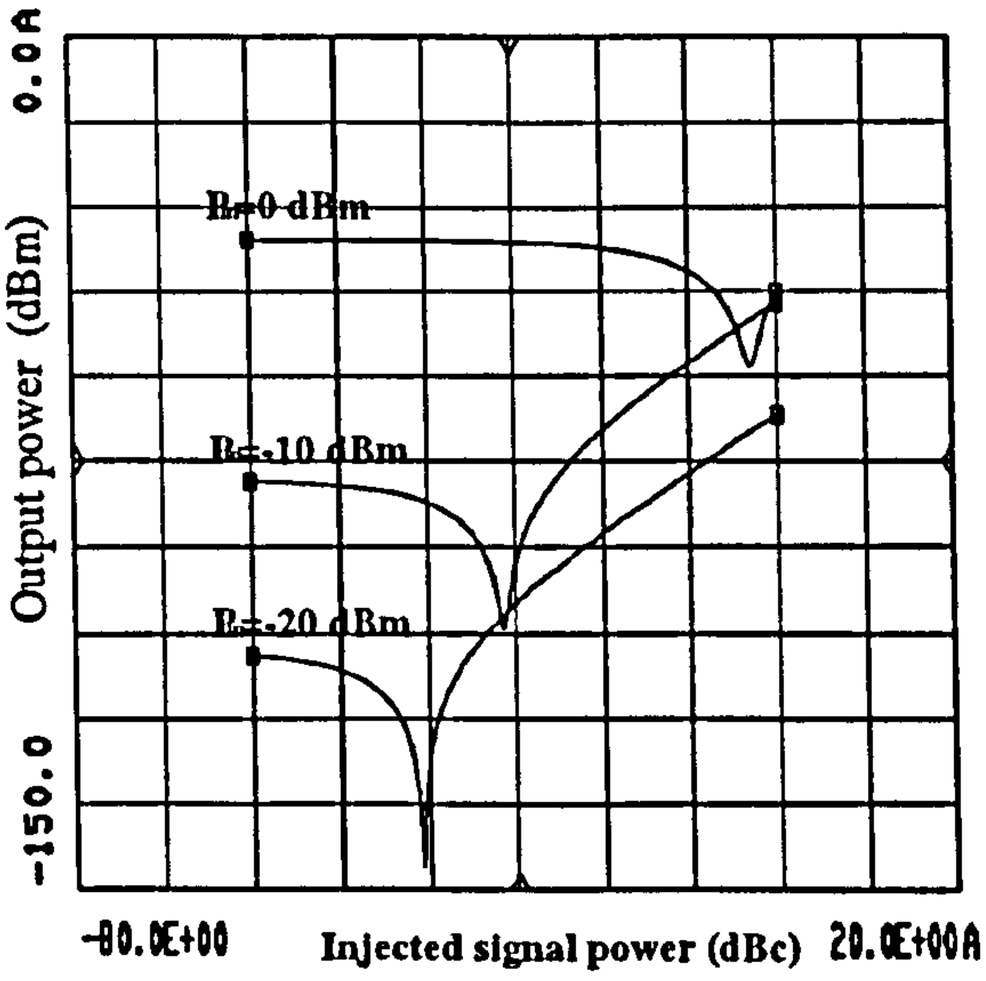

Figure F..31: **Variations in the amplitude of IM term $(f_1 - f_2 + f_3)$ as a function of injected difference frequency signals amplitude for input power levels of $-20dBm$, $-10dBm$ and$0dBm$.**

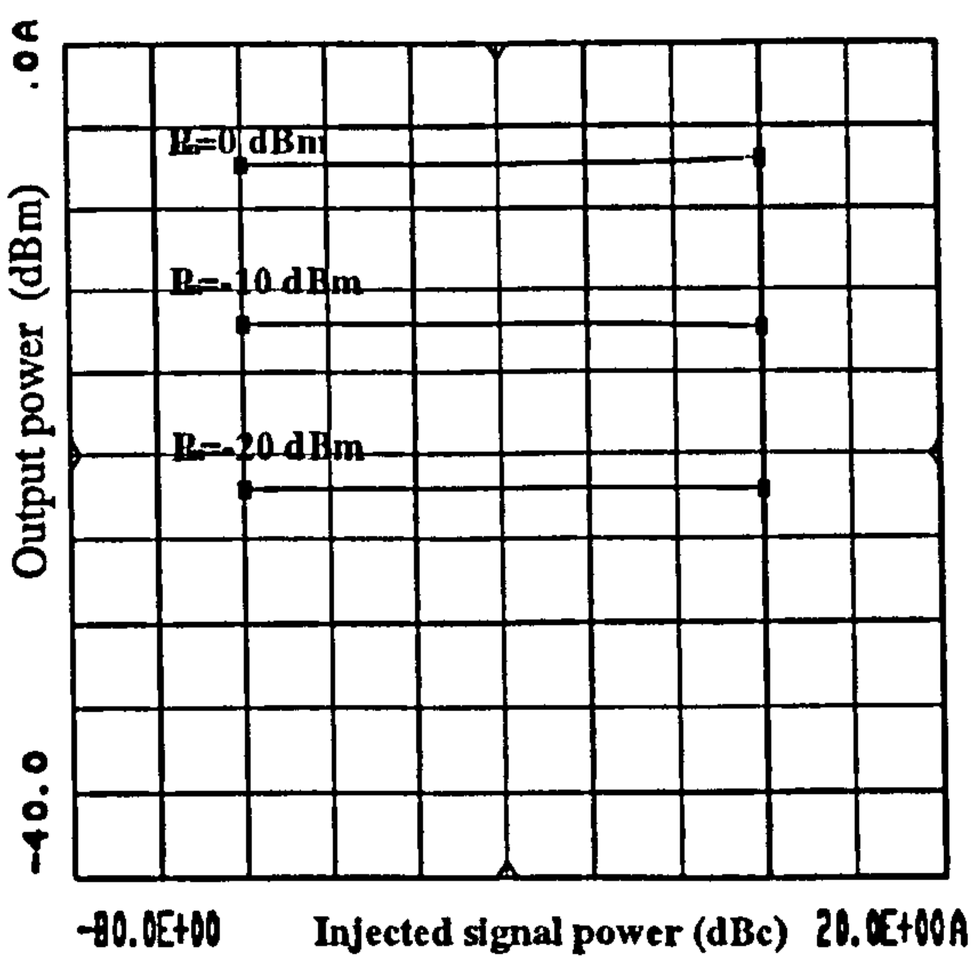

Figure F..30: **Variations in the amplitude of the fundamental signal f_2 as a function of injected difference frequency signals amplitude for input power levels of $-20dBm$, $-10dBm$ and $0dBm$.**

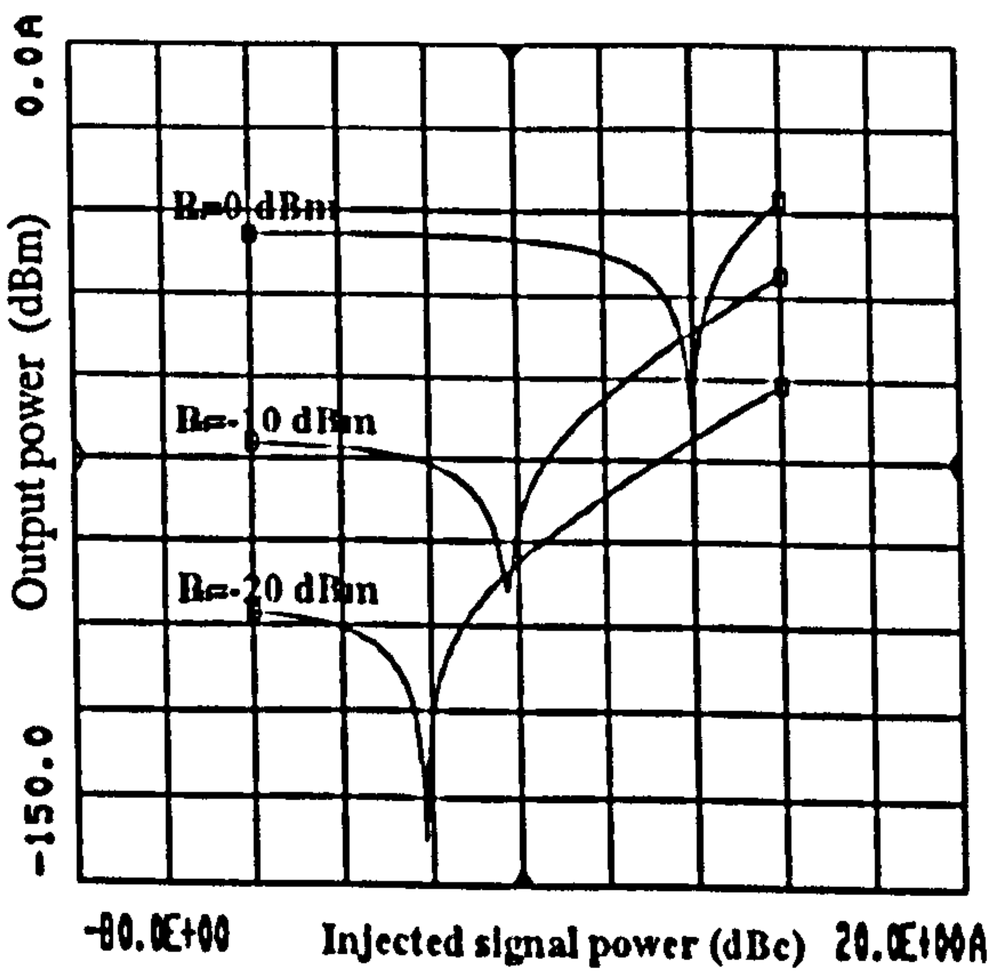

Figure F..32: **Variations in the amplitude of IM term $(2f_2 - f_1)$ as a function of injected difference frequency signals amplitude for input power levels of $-20dBm$, $-10dBm$ and $0dBm$.**

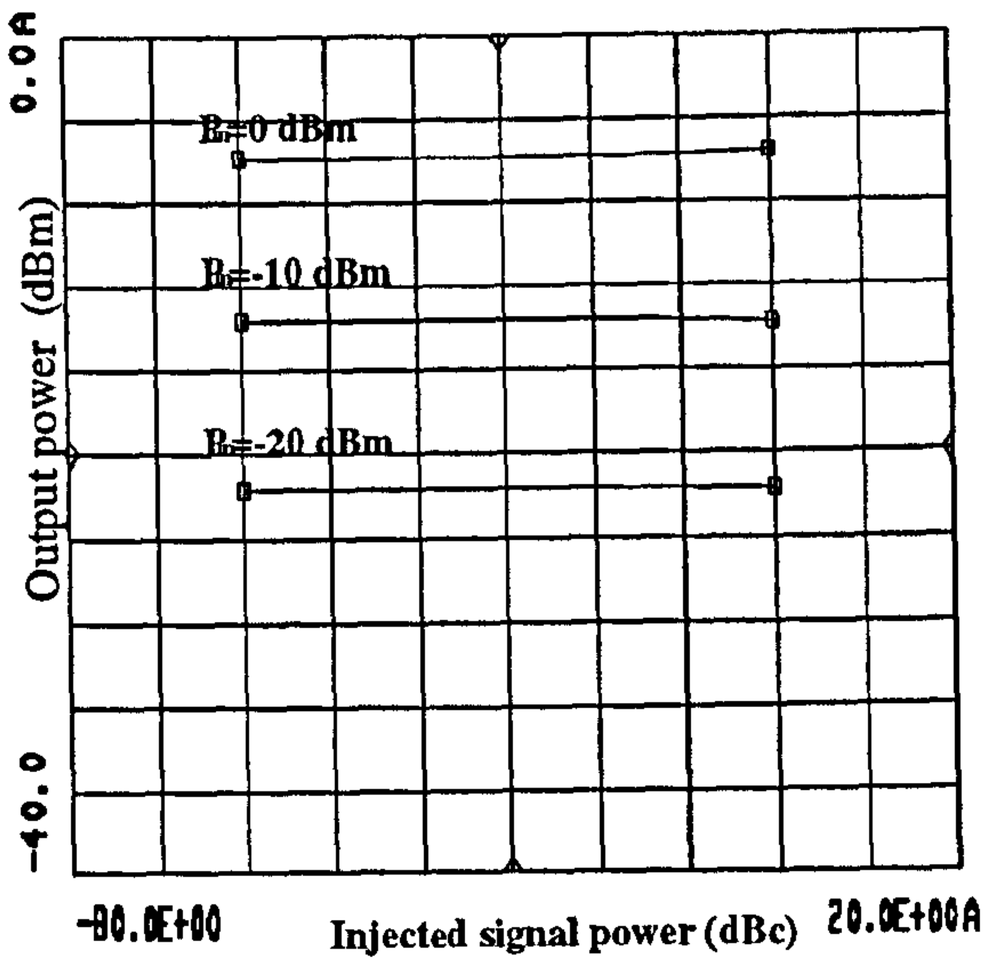

Figure F..33: Variations in the amplitude of the fundamental signal f_3 as a function of injected difference frequency signals amplitude for input power levels of $-20dBm$, $-10dBm$ and $0dBm$.

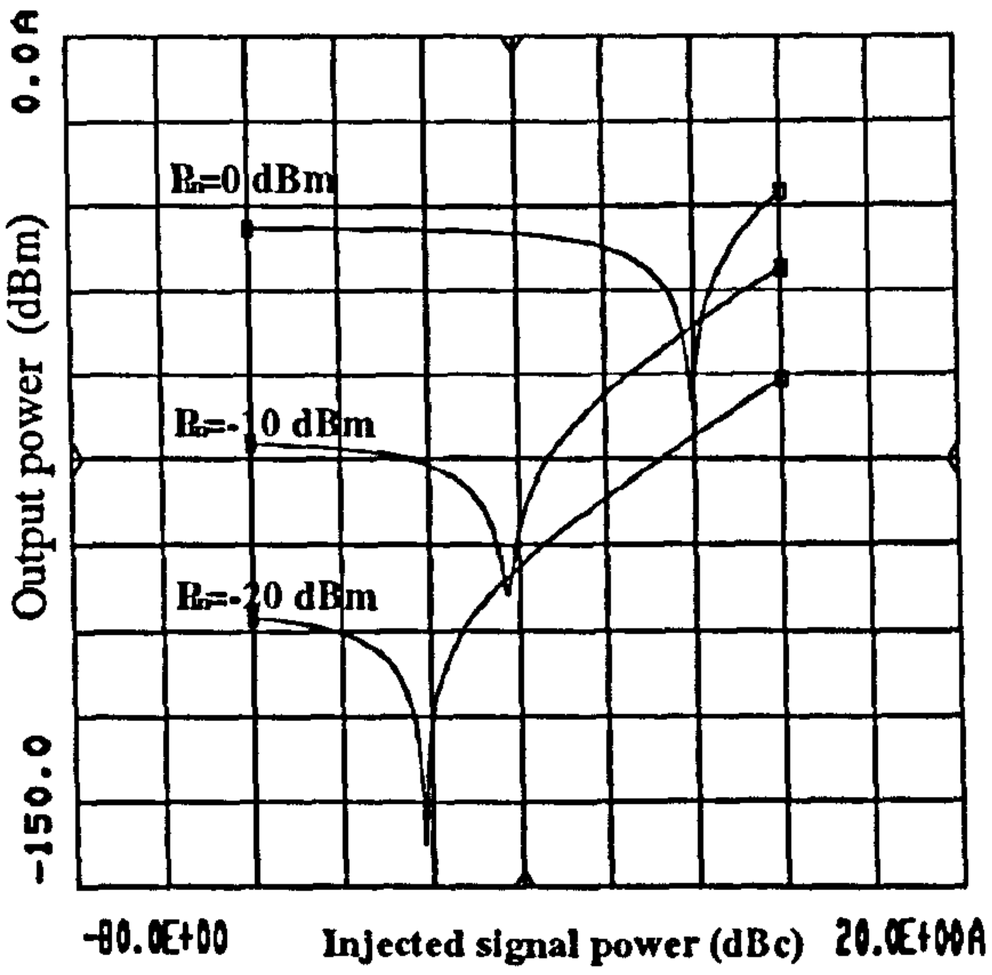

Figure F..35: Variations in the amplitude of IM term $(2f_3 - f_2)$ as a function of injected difference frequency signals amplitude for input power levels of $-20dBm$, $-10dBm$ and $0dBm$.

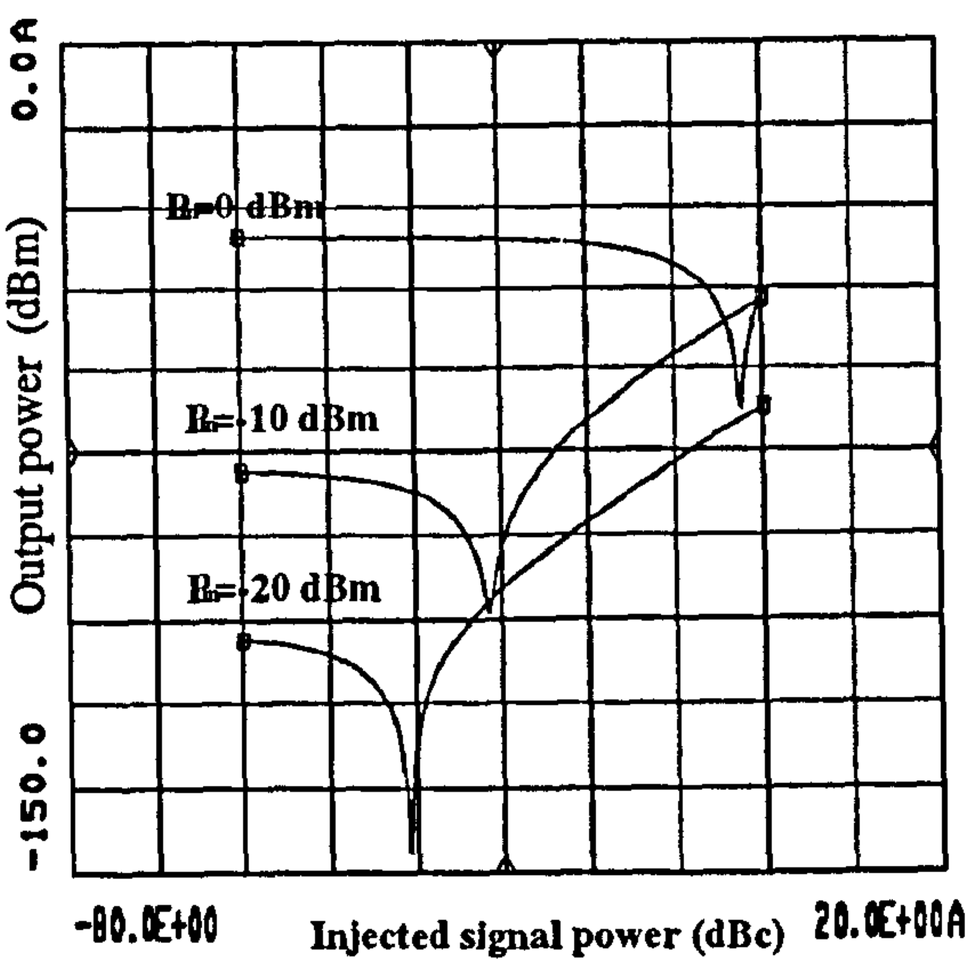

Figure F..34: Variations in the amplitude of IM term $(f_3 + f_2 - f_1)$ as a function of injected difference frequency signals amplitude for input power levels of $-20dBm$, $-10dBm$ and $0dBm$.

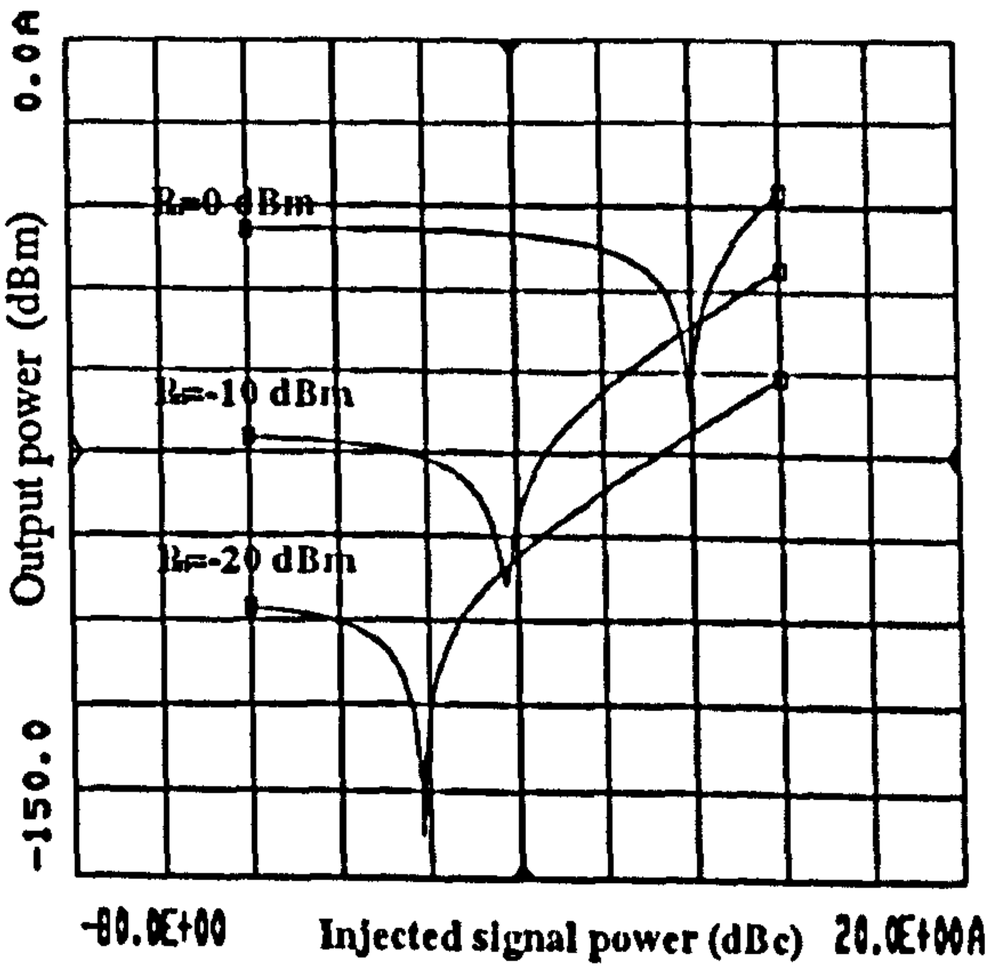

Figure F..36: Variations in the amplitude of IM term $(2f_3 - f_1)$ as a function of injected difference frequency signals amplitude for input power levels of $-20dBm$, $-10dBm$ and $0dBm$.

APPENDIX G.

CDMA IS95 SPECIFICATIONS

Code division multiple access represents the end to end wireless system and the necessary specifications that govern its operation. CDMA is a spread-spectrum technique which spreads the signal of multiple users with a unique spreading waveform assigned to users. The users are allowed simultaneous access to a shared communication channel. CDMA IS95 refers only to the air interface specification and is part of the north American digital cellular which is a collection of standards covering digital cellular systems in the united states.

IS95 Radio Specifications

Uplink (handset transmit)	$824MHz - 849MHz$
Dowlink (handset receive)	$869MHz - 894MHz$
Multiple access scheme	CDMA
Duplexing scheme	FDMA
TR/RX spacing	$45KHz$
Channel spacing	$1250KHz$
Radio channels	1000
Channel bit rate	$1.2288Mb/s$
Full rate channels per carrier	118 users/ch
Modulation	pi/4 DQPSK port base pi/4 OQPSK base mobile
Transmit power(mobile unit)	$3.0Watt$
Full speech channel bit rate	$3.7kb/s$
Cell radius (km)	$2 - 20$
Max MS power	$600mW$
Average MS power	$600mW$
Power control	BS/MS
Speech coding	QCELP

APPENDIX H.

PUBLICATIONS

[M1] M. Modeste, D. Budimir, R. Moazzam and C. S. Aitchison, "*Analysis and Practical Performance of a Difference Frequency Technique for Improving the Multi-carrier IMD Performance of RF Amplifiers*", IEEE MTT-S Digest, International Symposium on Technologies for Wireless Applications, pp. 53-56,Vancouver, Feb 1999.

[M2] M. Modeste, D. Budimir, R. Moazzam and C. S. Aitchison, " *Multicarrier IMD Performance Improvement by Difference Frequency Injection*", IEEE Postgraduate Research Conference, pp. 284-290, Manchester, January 1999.

REFERENCES CITED

1. I. J. Bahl, E. L. Griffin and C. Andricos, "*A 14W C band Power Amplifier Employing MMIC Chips*", Microwave Journal. Vol. 32, No. 5, pp. 295-303, May 1989.

2. M. Fukuta, T. Mimura, I. Tsujimura and A. Furumoto, "*Mesh Source Type Microwave Power FET*", IEEE Int. Solid State Circuit Conf. Tech. Digest, pp.84-85, 1973.

3. L. S. Napoli, R. E. Debrecht, J. J. Hughes, W. E. reichert, A. Dreeben and A. Triano, " *High Power GaAs FET Amplifier - A Multistage Structure*", IEEE Int. Solid State Circuit Conf. Tech. Digest, pp.84-85, 1973.

4. M. Mimura, T. S. Hiyamizu, T. Fujii and K. Nanbu, "*A New Field Effect Transistor With Selectively Doped GaAs/n-AlxGa1-xAs Heterojunctions*", JPn. J. Appl. Phys. Lett., Vol. 19, pp. L225-L227, May 1980.

5. P. Smith, P. C. Chao, J. Ballingall and A. Swanson, "*Microwave and Millimeter Power Amplification using Pseudomorphic HEMTs*", Microwave Journal, Vol. 33, No.5, pp. 71-86, May 1990.

6. A. Fazal and A. Gupta, "*HEMTs and HBTs: Device Fabrication and Circuits*", Artech House, 1991.

7. M. E. Kim, A. K. Oki, G. M. Gorman, D. K. Umemoto and J. B. Camou,"*GaAs Heterojunction Bipolar Transistor Device & IC technology for High Performance Analog and Microwaves Applications*", IEEE Trans. Microwave Theory and Techniques, Vol. MTT-37, pp. 1286-1303, September 1989.

8. Ke Lu, P. M. McInstosh, C. M. Snowden and R. D. Pollard, "*Low-Frequency Dispersion and Its Influence on the Intermodulation Performance of AlGaAs/GaAs HBTs*", IEEE MTT-S Digest, pp. 1373-1376, June 1996.

9. Y. Ayasli, R. L. Mozzi, J. L. Vorhans, L. D. Reynolds and R. A. Pucel, "*A Monolithic GaAs 1-13 GHz Travelling-Wave Amplifier*", IEEE Trans. Microwave Theory and Techniques, Vol. MTT-30, No7, pp. 976-981, July 1982.

10. Y. Ayasli, R. L. Mozzi, L. D. Reynolds and L. K. Hanes, "*2-20GIIz Travelling-Wave Power Amplifier*", IEEE Trans. Microwave Theory and Techniques, Vol. MTT-32, No.3, pp. 290-295, March 1984.

11. H. L. Kraus, C. W. Bostian and F. H. Raab, "*Solid State Radio Engineering*", New York: John Wiley, 1980.

12. Behzad Razavi, "*RF Microelectronics*", Prentice Hall Communications and Emerging Technologies Series, Prentice Hall, 1998.

13. N. O. Sokel and A. D. Sokel, "*Class E- A New Class of High Efficiency Tuned Single Ended Switching Power Amplifiers*", IEEE Journal of Solid State Circuits, Vol. 10, pp. 168-176, June 1975.

14. T. Sowlati et Al. "*Low Voltage High Efficiency Class E GaAs Power Amplifiers for Wireless Communications*", IEEE Journal of Solid State Circuits, Vol. 30, pp. 1074-1080, October 1995.

15. F. H. Raab, "*An Introduction to Class F Power Amplifiers*", RF Design, pp. 79-84, May 1996.

16. C. A. Liechti,"*Microwaves Field Effect Transistors-1976*", IEEE Trans. Microwave Theory and Techniques, Vol. MTT-24, pp. 279-300, June 1976.

17. C. M. Snowden, "*Semiconductor Device Modelling*", Springer-Verlag Berlin Heidelberg, 1989.

18. Peter H. Labroke, " *MMIC Design: GaAs FETS and HEMTs*", Artech House, 1993.

19. M. V. Calvo, A. D. Snider and L. P. Dunleavy, "*Resolving Capacitor Discrepancies Between Large and Small Signal FETs Models*", IEEE MTT-Symposium Digest, pp. 1251-1254, 1995.

20. W. Struble, A. Platzker, S. Nash and J. Pla, "*A New Small Signal MESFET and HEMT Model Compatible with Large Signal Modelling*", IEEE MTT-Symposium Digest, pp. 1567- 1570, 1994.

21. Ke Lu, P. Perry and T. J. Brazil, "*A New Spice Type Heterojunction Bipolar Transistor Model for DC, Microwave Small signal and Large-Signal circuit Simulation*", MTT-Symposium Digest, pp. 1579- 1582, 1994.

22. I. Corbella, J. M. Legido and G. Naval, "*Instantaneous Model of a MESFET for Use in Linear and Nonlinear Circuit Simulations*", IEEE Trans. Microwave Theory and Techniques, Vol. MTT-40, No.7, pp. 1410-1421, July 1992.

23. T. A. Winslow and R. J. Trew, "*Principles of Large-Signal MESFET Operation*", IEEE Trans. Microwave Theory and Techniques, Vol. MTT-42, No.6, pp. 935-942, June 1994.

24. G. D. Vendelin, A. M. Pavio and Ulrich L. Rhode, "*Microwave Circuit Design using Linear and Nonlinear Techniques*", John Wiley & sons, 1990.

25. D. C. Surana and j. G. Gardner, " *Computation of Mixing Coefficient for Field Effect Transistors with Non Square Law Transfer Characteristics*", Electronics letters, Vol. 6, No 13, P403-405, June 1970.

26. T. Fernandez, Y. Newport, J. M. Zamanilo A. Tozon and A. Mediavilla, "*Extracting a Bias Dependent Large Signal MESFET Model form the Pulsed I/V Measurements*", IEEE Trans. Microwave Theory and Techniques, Vol. MTT-44, No.3, pp. 372-378, June 1996.

27. J. C. Leckey, J. A. C. Steward, A. D. Patterson and M.J. Kelly, "*Nonlinear MESFET Estimation Using Harmonic Amplitude and Phase Measurements*", IEEE MTT-Symposium Digest, pp. 1563- 1566, 1994.

28. N. Constantin and F. M. Ghannouchi, "*GaAs FET's Gate Current Behaviour and Its effects on RF Performance and Reability in SSPAs*", IEEE Trans. Microwave Theory and Techniques, Vol. MTT-43, No.12, pp. 2918-2925, December 1995.

29. J. C. Pedro and J. Perez, "*An Improved MESFET Model for Prediction of Intermodulation Load-Pull Characterisation*", MTT-Symposium Digest, pp. 825-828, 1994.

30. J. C. Pedro and J. Perez, "*Accurate Simulation of GaAs MESFET's Intermodulation Distortion using a New Drain-Source Current Model*", IEEE Trans. Microwave Theory and Techniques, Vol. MTT-42, No.1, pp. 25-33, January 1994.

31. G. Passiopoulos, D. R. Webster, A. E. Parker D. G. Haigh and I. D. Robertson, " *Effect of Bias and Load on MESFET Nonlinear Characteristics*", IEE Electronics letters, pp.19-20 February 1996.

32. S. M. Sze, "Physics of Semiconductor", 2nd ed., chap 6, Wiley 1981.

33. R. Middlebrok and I. Richter, "*A Limits on the Square Law Exponent for the FET Characteristics*", Solid State Elect. , Vol. 6, pp. 542-547, 1963

34. M.S. Shur and L. F. Eastman: "*Current Voltage Characteristics, Small Signal Parameters and Switching Times of GaAs FETs*", IEEE Trans. Elect. Dev., Vol. ED-25, pp. 606-612, June 1978.

35. S. M. Li, W.S. Chan and D. Jing, "*Verification on the practicality of using the second harmonic in reducing IMD*", *Electronics Letters*, Vol. 34,No.11, pp.1097-1098, May 1998.

36. Ladbrooke P. H., "*GaAs MESFETs and HEMTs*", Peregrinus, London 1986.

37. W.R. Curtice and M. Ettenberg, " *A Nonlinear GaAs FET Model for Use in the Design of Output Circuits for Power Amplifiers*", IEEE Trans. Microwave Theory and Techniques, Vol. MTT-33, pp. 1383-1394, December 1985

38. H. Statz, P. Newman, I. W. Smith, R. A. Pucel and H. A. Haus, "*GaAs FET Device and Circuit Simulation in SPICE*", IEEE J. Solid State Circuits, Vol. ED-24, April 1989, pp.532-539.

39. W. R. Curtice,"*A MESFET Model for Use in the Design of GaAs Integrated Circuits*", IEEE Trans. Microwave Theory and Techniques, vol. MTT-28, pp. 448-456, May 1980.

40. A. Martekra and Kacprzak, "*Computer Calculation of Large Signal GaAs FET Amplifier Characteristics.*" IEEE Trans. Microwave Theory and Techniques, Vol. MTT-33, pp. 129-135, February 1985.

41. R. A. Minasian, "*Intermodulation Distortion using the Volterra Series Representation*", IEEE Trans. Microwave Theory and Techniques, Vol. MTT-28, No 1, pp. 1-8, January 1980.

42. R. Van Tuyl. and C. Lechti, "*High Speed Integrated Logic with GaAs MESFET* ", IEEE Journal Solid State Circuits Vol. sc-9, pp. 269-276, Oct 1974.

43. C. A. Mead,"*Schottky Barrier gate Field Effect Transistor*" Proc. IEEE, Vol. 54, pp. 307-308, February 1966.

44. Maeda, et Al, "*A 3.5 V, 1.3 W GaAs Power Multichip for IC Cellular Phones*", IEEE GaAs Symposium, 1983.

45. T. Quach and J. Staudinger, "*A high Efficiency Commercial GaAs MESFET Power Amplifier for PCM/CIA Application at 2.45 GHz*", IEEE GaAs Symposium, 1994.

46. E. Strid and R. Gleason, "*A DC- 12 GHz GaAs FET Distributed Amplifier*", IEEE Trans. Microwave Theory and Techniques, Vol. MTT-30, No. 7, pp. 969-975, July 1982.

47. I. Angelov, L. Bengtsson and M. Garcia, "*Extensions of the Chalmers Nonlinear HEMT and MESFET Model*", IEEE Trans. Microwave Theory and Techniques, Vol. MTT-44, No.10, pp. 1664-1674, October 1996.

48. Blakemore J. S., "*Semiconductor and Other Major Properties of Gallium Arsenide*", J. App.l. Phys., Vol. 53, pp. R123-R181, October 1982.

49. Microwave & RF Design Systems," *Designer's Task Reference: Simulating & optimizing circuit performance.*", Volume 4,No. 85150-90224, Hewlett Packard Company, 1994.

50. L. O. Chua and C. Y. Ng, " *Frequency Domain Analysis of Nonlinear Systems: General Theory*", IEEE electronic circuits and systems, Vol.3, No. 4,pp. 165-185, July 1979.

51. J. J. Bussgang, L. Erhman and J. W. Graham, "*Analysis of Nonlinear Systems with Multiple Inputs*", Proceedings of the IEEE, Vol.8, No.8, pp.1088-1119, August 1974.

52. S. Narayanan, "*Transistor Distortion Analysis Using Volterra Series Representation*", The Bell system technical Journal, pp. 991-1024, May-June 1967.

53. S. Narayanan, " *Intermodulation distortion of Cascaded Transistors*", IEEE Journal of Solid State circuits, Vol. 4, No. 3, pp. 97-106, June 1969.

54. H. B. Smets, "*Analysis and Synthesis of Nonlinear Systems*", IRE Trans. Circuits and Theory, pp.459-469, December 1960.

55. R. A. Minasian, "*Intermodulation Distortion Analysis of MESFET Amplifiers using the Volterra Series Representation*", IEEE Trans. Microwave Theory and Techniques, Vol. MTT-28, No 1, pp. 1-8, January 1980.

56. A. M. Khadar and R. H. Johnston, "*Distortion in High-Frequency FET Amplifiers*", IEEE Journal of Solid State circuits, Vol. SC-9K, pp. 180-106, August 1974.

57. S. Boyd, Y. S. Tang and L.O. Chua, "*Measuring Volterra Kernels*", IEEE Trans. Microwave Theory and Techniques, Vol. MTT-30, No. 8, pp. 571-577, August 1983.

58. M. Flies, M. Lamnabhi and F. L. Larrigue, "*An Algebraic Approach to Nonlinear Functional Expansions*", IEEE Trans. Circuits and Systems, Vol. CAS-30, No.8, pp. 554-570, August 1983.

59. S. O. Rice, "*Volterra Systems with More than One Input Port-Distortion in a Frequency Converter*", The Bell system Technical Journal, Vol. 52, No. 8, pp.1255-1270, October 1973.

60. G. L. Heither,"*Characterisation on Nonlinearities in Microwave Devices and Systems*", IEEE Trans. Microwave Theory and Techniques, Vol. MTT-21, No 12, pp. 797-805, December 1973.

61. G. W. Rhyne, M. B. Steer and B. D. Bates," *Frequency -Domain Nonlinear Circuit Analysis Using Generalised Power Series*", IEEE Trans. Microwave Theory and Techniques, Vol. MTT-36, No. 2, pp. 379-387, February 1988.

62. R. G. Sea and A. G. Vacroux,"*On the Computation of Intermodulation Products for a Power series Nonlinearity*", Proceedings of the IEEE, pp. 337-338, March 1969.

63. R. G. Sea,"*An Algebraic Formula for Amplitudes of Intermodulation Products Involving an Arbitrary Number of Frequencies*", Proceedings of the IEEE, pp. 1388-1389, March 1968.

64. S. Peng, P. J. McCleer and G. I. Haddad, "*Nonlinear Models for the Intermodulation Analysis of FET Mixers*", IEEE Trans. Microwave Theory and Techniques, Vol. MTT-43, No. 5, pp. 1037-1045, May 1995.

65. J. J. Bussgang, Ehrman L. and Graham J. W.,"*Analysis of Nonlinear Systems with Multiple Inputs*", Proceeding of the IEEE, Vol. 62, No 8, pp. 1088-1119, August 1974.

66. S. A. Maas,"*Two-Tone Intermodulation in Diode Mixers*", IEEE Trans. Microwave Theory and Techniques, Vol. MTT-35, No. 3, pp. 307-314, March 1987.

67. J. C. Fuenzalodo, O. Shimbo and W. L. Cook, "*Time- Domain analysis of Intermodulation effects caused by nonlinear amplifiers*", COMSAT Technical review, Vol. 3, No. 3, spring 1973.

68. S. Kundert, G. B. Sorkin and A. S. Vincentelli, "*Applying Harmonic Balance to Almost Periodic Circuits*", IEEE Trans. Microwave Theory and Techniques, Vol. MTT-36, No 2, pp. 366-378, February 1988.

69. J. H. Haywood and L. Chow, "*Intermodulation Distortion Analysis Using a Frequency Domain Harmonic Balance Technique*", IEEE Trans. Microwave Theory and Techniques, Vol. MTT-36, No. 8, pp. 1251-1257, August 1988.

70. W. R. Curtice, "*Nonlinear Analysis of GaAs MESFET Amplifiers, Mixers and Distributed Amplifiers Using The Harmonic Balance Technique*", IEEE Trans. Microwave Theory and Techniques, Vol. MTT-35, No. 4, pp. 441-447, April 1987.

71. V. Rizzoli, C. Cecchetti, A. Lipparni and F. Mastri, "*General-Purpose Harmonic Balance Analysis of Nonlinear Microwave Circuits under Multitones Excitation*", IEEE Trans. Microwave Theory and Techniques, Vol. MTT-36, No. 12, pp. 1650-1659, December 1988.

72. M. B. Steer and P. J. Khan, "*An Algebraic Formula for the Output of a System with Large - Signal, Multifrequency Excitation*", Proceedings of the IEEE, Vol.71, pp. 177-179, January 1983.

73. M. R. Moazzam and C. S. Aitchison, "*The reduction of Third Order Intermodulation Product in Microwave Amplifiers*", IEE Colloquium on Solid State power Amplification and Generation, Digest No. 1996/013, pp.7/1-7/5, London, January 1996.

74. M. R. Moazzam and C. S. Aitchison, "*A Low Third Order Intermodulation Amplifier with Feedback Circuitry*", IEEE MTT-S Digest, pp. 827-830, 1996.

75. F. Ali, R. Moazzam and C. S. Aitchison, "*IMD Elimination and ACPR Improvement for an 800MHz HBT MMIC Amplifier*", IEEE RFIC Symposium, pp.69-71, June 1998.

76. John L. B. Walker, " *High power GaAs FET Amplifiers*", Artech House, 1993.

77. Raymond S. Pengelly,"*Microwave Field Effect Transistors: Theory, Design and Applications.*" Research Studies Press ltd, John Wiley & Sons, 1986.

78. T.Nojima, S. Nichiki and K. Chiba, "*High Efficiency Transmitting Power Amplifiers for Portable Radio Units.*" IEICI Trans., Vol. E-74, no. 6, pp. 1563-1570, June 1991.

79. J. C. Pedro,"*MESFET Linearity Improvement by Channel Doping Control*", IEEE MTT-S Int. Microwave Symposium Digest, San Diego, pp. 1527-1530, June 1995.

80. H. Ryssel and I. Ruge, "*Ion Implantation*", John Wiley and Sons, 1986.

81. J. A. Higgins, Reidar L. Kuvas, "*Analysis and Improvement of Intermodulation Distortion in GaAs Power FETs*", IEEE Trans. Microwave Theory and Techniques, Vol. MTT-28, pp. 9-17, January 1980.

82. Jose Carlos Pedro, "*Evaluation of MESFET Nonlinear Intermodulation Distortion by channel Doping Control*", IEEE Trans. Microwave Theory and Techniques, Vol. MTT-45, No 11, pp. 1989-1997, November 1997.

83. A. Standing, " *An Active Phase and Amplitude Correction Device For Reducing IMD Produced by TWTs and Klystrons*", IEEE Conference on Earth Station Technology, London, October 1970.

84. W. Bosch and G. Gatti, "*Measurement and Simulation of Memory Effects in Predistortion Linearizers*", IEEE Trans. Microwave Theory and Techniques, Vol. MTT-37, No 12, pp. 1884-1890, December 1989.

85. M. Nakayama, K. Mori, Y. Itoh and Yasuo Mitsui, "*An Amplitude and Phase Linearizing Technique for Linear Power Amplifiers*", Microwave Journal, pp. 96-104, March 1996

86. C. Buoli, L.A. Cervi and A Abbiati, "*Quasi Pinch-Off GaAs FET Linearizer for Microwave SSPAs*", Proceedings of the 21st European Conference, pp. 1447 -1452, September 1991.

87. S. Ogura, K. Seino, T. Ono, A. Kamikokura and H. Hirose, "*Development of a Compact, Broadband FET Linearizer for Satellite Use*", IEEE MTT-S Int. Microwave Symposium Digest, pp. 1195-1198, June 1997.

88. D. Cahana, J. R. Potsukuchi and D. K. Paul, " *Linerarized Transponder Technology for Satellite Communications*", COMSAT Technical Review, Vol. 15, No. 2a, pp. 277-341, fall 1985.

89. K. Yamauchi, K. Mori, M. Nakayama, Y. Itoh, Y. mitsui and O. Ishida, "*A Novel Series Diode Linearizer for Mobile Radio Power Amplifiers*", IEEE MTT-S Int. Microwave Symposium Digest, pp. 831-834, June 1996.

90. K. Yamauchi, K. Mori, M. Nakayama, Y. mitsui and T. Takagi, "*A Microwave Miniatured Linearizer using a Parallel Diode*", IEEE MTT-S Int. Microwave Symposium Digest, pp. 1199-1202, June 1996.

91. M. Nakayama, K. Mori, K. Yamauchi, Y. Itoh and T. Takagi, "*A Novel Serie Diode Linearizer for Mobile Radio Power Amplifiers*", IEEE MTT-S Int. Microwave Symposium Digest, pp. 1451-1454, June 1995.

92. P. Kangaslahti, S. Kalajo, V. porra and P. Jukkala, " *Unlimited Bandwith TWT Predistortion Lineriazer MMICs for Ku- an Ka-Band Operation*", The European Gallium Arsenide and Related II-V Compounds Application Symposium (GaAs '98), pp. 85-88, Amsterdam 1998.

93. C. Bremenson and D. Lombard, " *Linearisation du Canal de Transmission pour un System en Acces Multiple par Repartition dans le Temps*", INTELSAT, IECE, ITE 3rd INT. Conf. On Dig. SAT. COM. proceedings, Kyoto, Japan, pp. 144 -149 , November 1975.

94. K. Madani, " *A New Active Predistortion Technique for Wideband Microwave Power Amplifier Linearisation*", MTT-s European Topical congress on Technologies for Wireless Applications, pp. 1-4, Amsterdam 1998.

95. G. Satoh and T. mizumo, "*Impact of a New TWT Linearizer upon QPSK/TDMA Transmission Performance.*", IEEE Journal On Selected Areas in COM., Vol. SAC-1, No 1, pp. 39 -43, January 1983.

96. M. Kumar and J. Whartenby, " *TWTA Linearizer using Dual Gate MESFET.*" IEEE MTT International Microwave Symposium, San-Francisco, Digest pp. 314 - 315, 1984.

97. "*Assessment of predistortion linearizer technology.*" COMSAT laboratory's Final Report for INTELSAT contract, INTEL 317, October 1983.

98. A. Egger, M. Horn, T. View, "*Broadband Linearisation of Microwave Power Amplifier*" 10th European Microwave Conference, Warsaw. Poland, Proc. pp. 89, September 1980.

99. G. Satoh, "*Linearizer for High Power TWTA.*" Trans. Int. Electron. Com., Japan, Vol. J62 -B, No 10, pp. 932-939, November 1979.

100. M. Kumar, J. C. Whartenby, H. J. Wolkstein, "*Predistortion Linearizer using GaAs Dual Gate MESFET for TWTA and SSPA used in Satellite Transponder.*", IEEE MTT, Vol. MTT-33, No 12, December 1985.

101. H. Seidel, H. R. Beurrier, Friedman A. N., "*Error Controlled High Power Linear Amplifier at VHF.*" Bell System Technology Journal, Vol. 47, No 5, pp. 651, May-June 1968.

102. N. Toshio , and Tohru K., "*Cuber Predistortion Linearizer for Relay Equipment in 800MHzz Band Land Mobile Telephone System*", IEEE Trans. Vehicular Tech., Vol. VT-34, No 4, pp. 169-177, Nov 1985.

103. J. C. Fuenzalido, "*Time Domain Analysis of IM Effects Caused by Non Linear Amplifiers*", COMSAT Technical Review, Vol. 3, No 1, pp. 89 -103, Spring 1973.

104. M. Seidel, *"A Microwave Feedforward Experiment"*, Bell System Technology Journal, Vol. 50, pp. 2879 - 2961, September 1971.

105. P. M. Bakken,"*Technical Consideration for the Linearization of High Power Amplifier in Satellite Ground Terminal.*" Space Technical Centre, The Hague, Technical Memorandum, STC- 509, 1976.

106. S. Stell, D. Scott and S. Ludvik. "*A 6-18 GHz High Dynamic Range MMIC Amplifier using a Feedforward Technique*", IEEE MTT-S Int. Microwave Symposium Digest, San Diego, pp. 911-914, June 1990.

107. R.D. Steward and F. F. Tusubira, "*Feedforward Linearization of 950 MHz Amplifiers*", IEE Proc-H, Vol. 135, pp.347-351, October 1988.

108. K. Konstantinou and D. K. Paul, "*Analysis and Design of Broadband, High Efficiency Feedforward Amplifiers*", IEEE MTT-S Int. Microwave Symposium Digest, pp. 867-870, June 1996.

109. Sang-Gee Kang, Il-Kyoo Lee and Ki-Suk Yoo, "*Analysis and Design of Feedforward Power Amplifier*", IEEE MTT-S Int. Microwave Symposium Digest, 1519-1522, June 1997.

110. A Javed, P. A. Goud and B. A. Syrett, "*Analysis of a Microwave Feedforward Amplifier using Volterra Series Representation*", IEEE Trans. Communications, pp. 355-360, March 1977.

111. R. J. Wilkinson and P. B. Kenington , "*Specification of Error Amplifiers for Use in Feedforward Transmitters*", IEE Proc-G, Vol. 139 pp. 477-481, 1992.

112. K. Konstantinou and D. K. Paul, "*Broadband Feedforward Linearization of Microwave Power Amplifiers*", IEE Colloquium on SSPA and Generation, London, pp. 23-26, January 1996.

113. R. G. Meyer, R. Eschenbach and W. M. Edgerley, "*A Wide-Band Feedforward Amplifier*", IEEE Journal of Solid State Circuits, Vol. , No.6, pp. 422-428, December 1974.

114. P.B. Kennington and David W. Bennett, "*Linear Distortion Using a Feedforward System*", IEEE Trans. Vehicular Technology, Vol. 45, No.1, February 1996.

115. Asholk Talwar, "*Noise and Distortion Reduction in Amplifier using Adaptive Cancellation*", IEEE Trans. Microwave Theory and Techniques, Vol. MTT-37, No 12, pp. 1884-1890, December 1989.

116. J. M. Holtzman,"*Nonlinear Distortion in feedback systems*", Bell System Technology Journal, Vol. 46, No 5, pp. 503-509, April 1968.

117. J. G. McRory and Johnston R. H.,"*An RF amplifier for low Intermodulation Distortion*", IEEE MTT-S Int. Microwave Symposium Digest, pp. 1741 - 1744, 1994.

118. C. Hsich and E. Strid, "*A S-Band high power feedback amplifier.*" , IEEE MTT-S International Microwave Symposium Digest, San Diego, pp. 182-184, June 1977.

119. M. J. Underhill, " *Fundamentals of Oscillator Performance*", Electronics and Communications Engineering Journal, pp.185-193, August 1992.

120. H. Yongcay, J. C. Mollier and J. Obregon, "*A New Method of Third Order Intermodulation Reduction in Non Linear Microwave System*", IEEE Trans. Microwave Theory and Techniques, Vol. MTT-34, pp. 245-250, February 1986.

121. E. Ballesteros, F. Perez and J. Perez, "*Analysis and Design of Microwave Linearised Amplifier using Active Feedback.*" , IEEE Trans. Microwave Theory and Techniques, Vol. 36, No 3, March 1988.

122. E. Ballesteros, F. Perez and J. Perez, " *Linearrization of Microwave Power Amplifier using Active Feedback*", Electronic Letters, Vol. 21, No 1, pp. 9-10, January 1988.

123. Nishikawa K. and T. Tokumitsu, "*An MMIC low-Distortion Variable Gain Amplifier using Active Feedback*", IEEE Trans. Microwave Theory and Techniques, Vol. MTT-43, No 12, pp. 2812-2816, December 1995.

124. Series IV, HPEESOF," *High Frequency Design Solutions: Designer's Task Reference*", Volume 1,No. E4605-90046, Hewlett Packard Company, 1995.

125. S. Narayanan, "*Application of Volterra Series to Intermodulation Distortion Analysis of Transistor Feedback Amplifiers.*" IEEE Trans. Circuit Theory, Vol. CT-17, No 4, pp. 518-527, Nov 1970.

126. A. E. Parker and J. B. Scott, "*Intermodulation Nulling in GaAs MESFETs*", Electronics Letters, Vol.29, No.12, pp. 1961-1962, December 1993.

127. D. R. Webster, D. G. Haigh and A. E. Parker, "*Novel Circuit Synthesis Technique Using Short Channel GaAs FETs Giving Reduced Intermodulation Distortion*", IEEE International Symposium Circuits and Systems, Seattle, pp. 1348- 1351, 1995.

128. D. R. Webster, J. B. Scott and D. Haigh, "*Control of Circuit Distortion by the Derivative Superposition Method*", IEEE Microwave and Guided Wave Letters, Vol. 6, No. 3, pp. 123-125, March 1996.

129. D. R. Webster, G. R. Ataei, A. Assenov, D. G. Haigh and I. Thayne, "*Reduction of 3rd-Order Intermodulation Distortion Through the Use of a High Pass Transmission Line Implementation of Derivative Superposition and Through the Use of Channel Doped HEMTS*", IEE Colloquium on Analogue Signal Proccssing, pp. 13/13/10, Oxford UK, 20th November 1996.

130. D. R. Webster, D. G. Haigh, J. B. Scott and A. E. Parker. "*Derivative Superposition - A Linearisation Technique for Ultra Broadband Systems*", IEE Colloquium on "Wideband Circuits, Modelling and Techniques", London, May 1996.

131. D. R. Webster, G. R. Ataei, A. E.Parker, D G Haigh, "*Developments in Linear and Non-Linear FET Circuit Design Using Derivative Superposition*", IEE Colloquium on"Analog Signal Processing, pp. 1/1-1/10, Oxford UK, October 1998.

132. G. R. Ataei, "*Low Distortion Power Amplifier Using the Derivative Superposition*", Postgraduate Research in Electronics, Photonics and Related Fields, PREP 99 Proceedings, Manchester, pp. 257-260, January 1999.

133. V. Petrovic, "*Reduction of Spurious Emission from Radio Transmitters by Means of Modulation Feedback*", IEE conf. On Radio Spectrum Conservation Techniques, pp. 44-49, 1983.

134. N. Suematsu, Y. Iyama and O. Ishida, "*A 900 MHz-Band Cartesian Feedback Type Low Distortion Transmitter Having Narrow Bandwidth Loop Filter*", Asia Pacific Conference, pp.323-327, December 1998.

135. P.K. Kenington, R. J. Wilkinson and K. J. Parisons, "*Noise Performance of Cartesian Transmitter*", IEEE Transaction on Vehicular Technology, Vol. 46, No.2, pp. 467-476, May 1997.

136. M. Bolorian and J. P. McGeehan, "*The frequency Hoped Cartesian feedback Linear Transmitter*", IEEE Transaction on Vehicular Technology, Vol. 45, No.4, pp. 688-706, November 1996.

137. V. Petrovic and W. Gosling, "*Polar loop Transmitter*", IEE Electronics Letters, Vol. 15, No. 10, pp. 286-288, May 1979.

138. A. S. Wright and W. G. Durtler, " *Experimental Performance of Adaptive Digital Linearized Power Amplifier*", IEEE Transaction on Vehicular Technology, Vol. 41, No.4, pp. 394-400, November 1992.

139. J. K. Cavers , "*Amplifier Linearisation using A Digital Predistorter with Fast Adaptation and Low Memory Requirements*", IEEE Transaction on Vehicular Technology, Vol. 39, No.4, pp. 374-382, November 1990.

140. S. P. Stapleton and F. C. Costescu, " *An Adaptive Predistorter for a Power Amplifier Based on Adjacent Channel Emissions*", IEEE Transaction on Vehicular Technology, Vol. 41, No.1, pp. 49-56, February 1992.

141. S. P. Stapleton, G. S. Kandola and K. Cavers, " *Simulation and Analysis of an Adaptive Predistorter Utilising a Complex Spectral Convolution*", IEEE Transaction on vehicular Technology, Vol. 41, No.4, pp. 49-56, November 1992.

142. M. Faulkner and M. Johanssen, " *Adaptive Linearization using Predistortion-Experimental Results*", IEEE Transaction on Vehicular Technology, Vol. 43, No.2, pp. 323-332, May 1994.

143. J. K. Cavers, "*The effects of Quadrature Modulator and Demodulator Errors on Adaptive Digital Predistorters for Amplifier Linearization*", IEEE Transaction on vehicular Technology, Vol. 46, No.2, pp. 456-466, May 1997.

144. Leonard R. Khan, " *Single-Sideband Transmission by Envelope Elimination and Restoration*", Proceedings of the IRE, pp. 803-806, July 1952.

145. Leonard R. Khan, "*Comparison of Linear Single-Sideband Transmitters with Envelope Elimination and Restoration Single-Sideband Transmitters* ", Proceedings of the IRE, pp. 1706-1712, December 1956.

146. F. H. Raab, B. E. Sigmon, R. G. Myers and R. M. Jackson, "*L-Band Transmitter using Kahn EER Technique*", IEEE Trans. Microwave Theory and Techniques, Vol. MTT-46, No 12, pp. 2220-2224, December 1998.

147. D. C. Cox, "*Linear Amplification with Nonlinear Components*", IEEE Trans. Communications, Vol. COM-22, pp. 1942-1945, December 1974.

148. A. N. D. Andrea, V. Lottici and R. Reggiannini, "*RF Power Amplifier Linearisation Through Amplitude and Phase Predistortion*", IEEE Trans. Communications, Vol. 40, No 11, pp. 1477-1484, November 1996.

149. R. C. Tupynamba and Camargo E., "*MESFET non lineriaties applied to Predistortion Linearizer design*", IEEE MTT-S digest, pp. 955-958, 1992.

150. R. Inada, H. Ogawa, S. Kitazume, P. Desoutis, "*A Compact 4 GIIz Linearizer for Space Use*" , IEEE Trans. Microwave Theory and Techniques, Vol. MTT-34, pp. 1327 - 1332, December 1986.

151. N. Imai, T. Nojima and T. Murase," *Novel Linearizer Using Balanced Circulators and Its Application to Multilevel Digital Radio Systems*" A, IEEE Trans. Microwave Theory And Techniques, Vol. 37, No 8, pp. 1237 - 1243, August 1989.

152. David Wills, "*A Control System for a Feedforward Amplifier*", Microwave Journal, pp. 22-34, April 1998.

153. D. Jing, S. M. Li, C. S. Yu and W. S. Chan "*A new linearisation method for reducing adjacent channel power in PHS amplifiers*", Asia Pacific Microwave Conference Proceedings, pp.123-127, Dec.1998.

154. C. Hsich and E. Strid," *A Feedforward S-Band MIC Amplifier System.*" IEEE J. Solid- State circuits, Vol. SC-11, No 2, pp. 271-278, April 1976.

155. Cardinal, J. S. and Fadhel M. Ghannouchi, "*A new Adaptive Double Envelope Feedback (ADEF) Linearizer for the Solid State Power Amplifiers*", IEEE Trans. Microwave Theory and Techniques, Vol. MTT-43, pp. 1508-1515, July 1995.

156. S. Narayanan, "*Application of Volterra Series to Intermodulation Analysis of Transistor Feedback Amplifiers.*" IEEE Trans. Circuit Theory, Vol. CT-17, No 4, pp. 518-527, November 1970.

157. G. Palumbo and S. Pennisi, " *Harmonic Distortion in Non-Linear Amplifier with Non-Linear Feedback*", International Journal of Circuit Theory and Applications, Vol. 26, pp.293-299, 1998.

158. J. Engberg and T. Larsen, "*Noise Theory of Linear and Nonlinear Circuits*", John Wiley and Sons, 1995

159. Walker L. B. John, "High Power GaAs FET Amplifiers", Artech House, 1993.

160. Rob Van Brunt, "Third generation wireless Test equipment Requirement", Microwave journal, pp. 23-29, October 1998.

161. J. K. Stenvenson and Achankeng Leke, "Power amplifier spectral regrowth for digital cellular and PCS applications" Microwave journal, pp. 74-92, October 1995.